THE JOURNAL OF CHEMICAL PHYSICS

VOLUME 23 NUMBER 12

DECEMBER, 1955

Published by the
AMERICAN INSTITUTE OF PHYSICS
Incorporated
Lancaster, Pa. and New York, N. Y.

THE JOURNAL OF CHEMICAL PHYSICS

BOARD OF EDITORS

CLYDE A. HUTCHISON, JR., *Editor*

Associate Editors

Term ending December 31, 1955	Term ending December 31, 1956	Term ending December 31, 1957
RICHARD M. BADGER	BRYCE CRAWFORD, JR.	JAMES R. ARNOLD
DAVID M. DENNISON	H. S. GUTOWSKY	JACOB BIGELEISEN
JOHN G. KIRKWOOD	WILLIAM N. LIPSCOMB	WALTER GORDY
G. B. KISTIAKOWSKY	ELLIOTT W. MONTROLL	ALVIN H. NIELSEN
A. W. LAWSON	GEORGE SCATCHARD	EARLE K. PLYLER
S. S. PENNER	J. W. STOUT	WAVE H. SHAFFER
ROBERT L. SCOTT	GREGORY H. WANNIER	T. F. YOUNG

THE JOURNAL OF CHEMICAL PHYSICS is published monthly by the American Institute of Physics. Its purpose is to bridge a gap between journals of physics and journals of chemistry. The artificial boundary between physics and chemistry has now been in actual fact completely eliminated, and a large and active group is engaged in research which is as much the one as the other. It is to this group that the Journal is rendering its principal service and makes its greatest appeal, both as a prompt and efficient medium for publication of research and as a convenient and carefully edited assemblage of pertinent information.

Information for Contributors

Send manuscripts to Clyde A. Hutchison, Jr., Editor, *The Journal of Chemical Physics*, Institute for Nuclear Studies, University of Chicago, Chicago 37, Illinois. Unless otherwise stated submission of a manuscript is a representation that it has been neither copyrighted, published, nor submitted for publication elsewhere. Textual material (abstract, body of the paper, tabular material, references, and figure captions) must be in English, typewritten (except mathematical expressions) double spaced with wide margins on a durable, white paper, preferably letter size. The original copy, not the carbon, should be submitted. For general style, spellings, abbreviations, and form, consult recent issues of this journal. The authors' institutions are requested to pay a publication charge of $25.00 per page which, if honored, entitles them to 100 free reprints. Instructions will be sent with galley proofs.

An abstract must accompany each article. It should be adequate as an index and as a summary.

All but the simplest mathematical expressions should be carefully printed in by hand. Be sure to distinguish between capital and small letters. Indicate clearly superscripts and subscripts by inverted carets and carets, respectively. Avoid complicated superscripts and subscripts. Avoid repetition of a complicated expression by representing it by a symbol. Identify in the margin Greek letters and unusual symbols. Use fractional exponents instead of root signs. Use the solidus (/) for fractions wherever this will save vertical space.

References should appear as footnotes, numbered consecutively. Literature citations of technical journals should be in the form indicated in the Style Manual of the American Institute of Physics and Chemical Abstracts (Chem. Abstracts 45, I-CCLV (1951)).

Tables may be typewritten on sheets separate from the running text. Each table must have a caption which will make the data in the table intelligible without reference to the text. Avoid complicated column headings.

Wherever possible figures should be planned for the width of a column (3 in.). A convenient reduction ratio is about 2:1 or 3:1. Lettering should be large enough on the original that when reduced it shall not be less than about $\frac{1}{16}$ in. (~1.5 mm). Line drawings must be in *india ink* on white paper or tracing cloth. Coordinate paper is not desirable but if used must be blue lined and the coordinate lines which are to show must be inked over. Pictures of apparatus, etc., should be glossy prints and should have maximum black and white contrast. Identify each original drawing or photograph on the back with the author's name and the figure number. Figures should be numbered consecutively. Captions should be typed on a separate sheet of paper.

A limited number of alterations in proof are unavoidable, but the cost of making extensive alterations after the article has been set in type will be charged to the author.

Proof and all correspondence concerning papers in the process of publication should be addressed to the Publication Manager, American Institute of Physics, 57 East 55 Street, New York 22, New York.

Subscription Price

	U. S. and Canada	Elsewhere
To members of the American Institute of Physics and Affiliated Societies	$12.00	$13.00
To all others	15.00	17.00

Back Number Prices

Yearly rate when complete year is available: $18.00.
Single copies: $1.75 each.

Subscriptions, renewals, and orders for single copies should be addressed to the American Institute of Physics, 57 East 55 Street, New York 22, New York.

Changes of address should be sent to the American Institute of Physics.

The Journal of Chemical Physics is published monthly at Prince and Lemon Streets, Lancaster, Pennsylvania.

Entered as second-class matter December 30, 1932, at the Post Office at Lancaster, Pa., under the Act of August 24, 1912. Acceptance for mailing at special rate of postage, provided for in paragraph (d-2), section 34.40, P. L. & R. of 1948, authorized February 3, 1933.

Copyright © 1955 by the American Institute of Physics

THE JOURNAL
OF
CHEMICAL PHYSICS

VOLUME 23, NUMBER 12 DECEMBER, 1955

Calculation of Depolarization Factors of the Raman Lines of CCl_3X Molecules

ALFONS WEBER AND SALVADOR M. FERIGLE
Spectroscopy Laboratory, Department of Physics, Illinois Institute of Technology, Chicago 16, Illinois*
(Received March 11, 1955)

The depolarization factors of the totally symmetric vibrations of CCl_3H, CCl_3D, and CCl_3Br are computed using previously derived expressions for the spur and anisotropy of the polarizability tensor. The associated normal coordinate treatment uses the Wilson *FG*-matrix technique with a general quadratic potential function. Calculated and observed depolarization factors agree well for stretching but not for the bending modes.

INTRODUCTION

In a previous paper[1] general expressions were derived for the spur and anisotropy of the derived polarizability tensor of a noncyclic polyatomic molecule. The expressions were derived in the light of Wolkenstein's[2] assumptions: (1) additivity of bond polarizabilities and their derivatives, and (2) independence of the bond polarizability with respect to the bond orientation. In this paper, we report the results for the computed depolarization factors of the totally symmetric vibrations of the molecules CCl_3H, CCl_3D, and CCl_3Br. No depolarization factors for CCl_3F and CCl_3I are reported since for the C−F and C−I bond data exist only for the polarizabilities[3] and not for the derivatives and furthermore, no reasonable data exist for the normal coordinate treatment of CCl_3I. Since the results for the asymmetric vibrations are trivial ($\rho=6/7$), calculations are done only for the totally symmetric vibrations.

NORMAL COORDINATES

As the expressions for the spur and anisotropy of the derived polarizability contain the transformation coefficients between the symmetry coordinates and the normal coordinates, a normal coordinate treatment precedes any computation of the intensities and depolarization factors of a Raman line. Using the symmetry coordinates given by Meister and Cleveland[4] for the a_1 vibrations of CCl_3X,

$$S^1=\Delta x,$$
$$S^2=3^{-\frac{1}{2}}(\Delta c_1+\Delta c_2+\Delta c_3),$$
$$S^3=6^{-\frac{1}{2}}(\Delta c_1c_2+\Delta c_1c_3+\Delta c_2c_3-\Delta c_1x-\Delta c_2x-\Delta c_3x),$$
$$S^4=6^{-\frac{1}{2}}(\Delta c_1c_2+\Delta c_1c_3+\Delta c_2c_3+\Delta c_1x+\Delta c_2x+\Delta c_3x)\equiv 0,$$

we get the F- and G-matrices for the a_1-type vibrations to be

$$F_{11}=f_x,$$
$$F_{22}=f_c+2f_c{}^c,$$
$$F_{33}=\tfrac{1}{2}(f_{cc}+2f_{cc}{}^{cc'}+2f_{cx}{}^{c'x}-2f_{cc}{}^{c'x}-4f_{cc}{}^{cx}+f_{cx}),$$
$$F_{12}=\sqrt{3}f_c{}^x,$$
$$F_{13}=3(f_{cc}{}^x-f_{cx}{}^x)/6^{\frac{1}{2}},$$
$$F_{23}=2^{-\frac{1}{2}}(f_{cc}{}^{c'}+2f_{cc}{}^c-f_{cx}{}^c-2f_{cx}{}^{c'});$$

and

$$G_{11}=1+\mu_X/\mu_C,$$
$$G_{22}=\tfrac{1}{3}+\mu_{Cl}/\mu_C,$$
$$G_{33}=(2\mu_{Cl}/\mu_C+16/3)/c^2,$$
$$G_{12}=-\sqrt{3}/3,$$
$$G_{13}=4\sqrt{3}/3c,$$
$$G_{23}=-4/3c;$$

the reciprocal of the carbon mass, μ_C has been factored out of the G-matrix. Using $m_C=12.011$, $m_H=1.0080$,

* Publication No. 113.

[1] S. M. Ferigle and A. Weber, Can. J. Phys. **32**, 799 (1954).

[2] M. Wolkenstein and M. Eliashevich, Acta Physicochim. U.R.S.S. **20**, 525 (1945).

[3] C. G. Le Fevre and R. J. W. Le Fevre, J. Chem. Soc. 1577 (1954).

[4] A. G. Meister and F. F. Cleveland, Am. J. Phys. **14**, 13 (1946). For the notation used in the present paper, see the paper by Davis, Cleveland, and Meister, J. Chem. Phys. **20**, 454 (1952).

TABLE I. Potential constants for CCl_3X molecules.[a]

Constant	Value	Constant	Value
f_h	4.8002	f_{ch}	0.92126
f_f	4.9447	$f_{ch'h}$	0.27305
f_c	3.4580	f_{cf}	1.6580
f_b	2.8976	$f_{cf'f}$	0.22068
f_{c^h}	0.0880	f_{cc}	1.1621
f_{c^f}	0.90713	$f_{cc'c}$	0.085027
f_{c^c}	0.30760	f_{bc}	1.3038
f_{b^c}	0.37782	$f_{bc'bc'}$	0.12142
f_{c^ch}	0.18601	$f_{bc'cc}$	0.13425
f_{c^cf}	0.30940	$f_{bc'cc}$	0.00000
f_{c^cc}	0.36434	$f_{cc'cf}$	0.062357
f_{c^cbc}	0.42630	$f_{cc'f'f}$	0.00000
$f_{c'ch}$	−0.16400	$f_{cc'ch}$	0.028235
$f_{c'cf}$	−0.22571	$f_{cc'h}$	0.00000
$f_{c'cc}$	−0.27281		
$f_{c'bc}$	−0.21314	$f_{hcc}-f_{hch}$ =	0.63846
f_{bbc}	0.35007	$f_{fcc}-f_{fch}$ = −	0.13733
f_{bcc}	−0.19812		

[a] Values taken from Meister's table of potential constants presented at the Ohio State Symposium, June, 1952. The constants are given in units of md/A, md/rad, md-A/rad² for bond stretching, bond-angle interaction, and angle constants, respectively. The number of significant figures is retained to give best reproduction of the observed wave numbers and to secure internal consistency in the calculations.

$m_D=2.01418$, $m_F=19.000$, $m_{Cl}=35.457$, and $m_{Br}=79.916$ amu for the atomic masses, and C−H=C−D=1.093, C−F=1.40, C−Cl=1.77, and C−Br=1.91 A for the bond distances, the totally symmetric vibrations for the CCl_3X molecules are computed by using the potential constants of Table I. The observed and computed wave numbers as well as the computed λ values are collected in Table II.[5] The coefficients of the L^{-1}-matrix are obtained by solving for each λ_m a set of simultaneous equations.[6]

$$\sum_k[(GF)_{kl}-\delta_{kl}\lambda_m](L^{-1})_k{}^m=0.$$

TABLE II. Wave numbers and λ values for the a_1-type vibrations of CCl_3X molecules.[a]

Molecule	λ_{calc}	σ_{calc}	σ_{obs}
	64.40836	3017.2K	3018.2K
CCl_3H	3.15873	668.2	667.4
	0.97499	371.2	366.4
	36.10155	2258.9	2256.3
CCl_3D	2.90787	641.1	652.1
	0.95874	368.1	365.2
	8.07060	1068.0	1068.1
CCl_3F	2.03098	535.8	535.8
	0.86913	350.5	350.5
	3.62985	716.3	716.3
CCl_3Br	1.26144	422.2	422.3
	0.43263	247.3	247.3

[a] Wave numbers are given in kaysers. The observed values are taken from Zietlow, Cleveland, and Meister (reference 16).

[5] To ease the calculations we use masses and distances expressed in amu and A, and factor μ_C out of the G-matrix since it occurs in every matrix element. If this is done we have

$$\lambda=(4\pi^2c^2m_C/N\times10^5)\sigma^2.$$

[6] E. B. Wilson, Jr., J. Chem. Phys. **7**, 1047 (1939); **9**, 76 (1941).

TABLE III. L^{-1}-matrix elements for CCl_3X molecules.

$(L^{-1})_k{}^m$	CCl_3H	CCl_3D	CCl_3F	CCl_3Br
$(L^{-1})_1{}^1$	0.943561	1.252314	2.287225	1.524653
$(L^{-1})_2{}^2$	−2.854156	−3.055558	−4.181791	5.448086
$(L^{-1})_3{}^3$	3.203420	3.274649	3.965088	5.300861
$(L^{-1})_2{}^1$	−0.003428	−0.0436608	0.247473	−1.759540
$(L^{-1})_3{}^1$	0.180680	0.266878	0.604701	0.542251
$(L^{-1})_3{}^2$	1.122293	1.062523	1.108392	0.816160
$(L^{-1})_1{}^2$	−0.299176	−0.574933	−2.538911	2.849876
$(L^{-1})_1{}^3$	−0.138867	−0.285800	−2.166797	−6.104451
$(L^{-1})_2{}^3$	4.879575	4.757723	3.854645	0.752491

TABLE IV. L-matrix elements for CCl_3X molecules.

$L_k{}^l$	CCl_3H	CCl_3D	CCl_3F	CCl_3Br
$L_1{}^1$	1.034417	0.757096	0.364592	0.289490
$L_2{}^2$	−0.215707	−0.209973	−0.181465	0.116674
$L_3{}^3$	0.190583	0.193642	0.156240	0.136429
$L_2{}^1$	−0.0626084	−0.710193	−0.0235965	0.0997089
$L_3{}^1$	−0.0358967	−0.0386647	−0.0490062	−0.0449658
$L_3{}^2$	0.0788043	0.0745816	0.0711630	0.00308101
$L_1{}^2$	−0.0568772	−0.0793751	−0.134016	−0.205746
$L_1{}^3$	0.131571	0.181401	0.329522	0.362582
$L_2{}^3$	0.325768	0.298898	0.163518	0.0982593

The L^{-1}-elements thus obtained are then normalized by multiplying by a factor K_m given by

$$K_m{}^{-1}=(\mu_C)^{\frac{1}{2}}[\sum_{kl}(L^{-1})_k{}^m(L^{-1})^m{}_lG_{kl}]^{\frac{1}{2}},$$

where G_{kl} are the G-matrix elements given above. The elements of the L-matrix are then found from the identity

$$L^{-1}G=\tilde{L}.$$

The results of the computation are collected in Tables III ond IV.

CALCULATION OF DEPOLARIZATION FACTORS

The depolarization factor ρ_k of the kth fundamental vibration is given by

$$\rho_k=6B_k{}^2/(5A_k{}^2+7B_k{}^2),$$

where A_k is the spur and B_k is the anisotropy of the derived polarizability tensor $\partial\alpha_{uv}/\partial Q^k$. The general expressions for A_k and B_k become for the case of the tetrahedral CCl_3X molecule,[1] and the set of symmetry coordinates used in this paper,

$$A_k=(\alpha_{x1}'+2\alpha_{x2}')L_k{}^1+\sqrt{3}(\alpha_{c1}'+2\alpha_{c2}')L_k{}^2$$

TABLE V. Bond polarizabilities and their derivatives.[a]

	α_{n1}	α_{n2}	α'_{n1}	α'_{n2}
C−H	0.79	0.58	1.28	0.31
C−Cl	3.67	2.08	2.82	0.68
C−Br	5.04	2.88	3.23	0.83

[a] Bond polarizabilities from Denbigh, reference 7. Derivatives of the bond polarizabilities from Wolkenstein and Eliashevich, reference 2.

TABLE VI. Depolarization factors of the totally symmetric vibrations of CCl_3X molecules.[a]

	σ_k	A_k	B_k	PR	ρ_{calc} (b)	(c)	(d)	(e)	ρ_{obs} (f)	(g)	(h)	(i)	(j)	(k)	(l)	(m)
	3017.2K	1.552	0.8321	0.25	0.22	0.2	0.22	0.31	0.32	0.4	0.32	0.20	0.24	0.38		
CCl_3H	668.2	−1.681	−0.3924	0.06	0.04	0.1	0.13	0.06	0.06	0.08	0.06	0.07	0.082	0.07		
	371.2	0.5023	−0.4814	0.48	0.41	0.2	0.22	0.18	0.22	0.18	0.22	0.19	0.19	0.25		
	2258.9	0.8639	0.4994	0.27												0.26
CCl_3D	641.1	−2.869	−0.9785	0.12												0.03
	368.1	0.4665	−0.4847	0.52												0.10
	716.3	−0.0735	0.2830	0.81					0.81					0.75	0.7	
CCl_3Br	422.2	1.333	−0.08504	0.005					0.005					0.15	0.05	
	247.3	−0.1976	−0.3615	0.71					0.71					0.57	0.35	

[a] Wave numbers σ_k are calculated values. ρ_{calc}: PR = present results; ρ_{obs}: from references c to m.
[b] See reference 2.
[c] S. Venkateswaran, Phil. Mag. **15**, 263 (1933).
[d] S. Bhagavantam, Indian J. Phys. **5**, 59 (1930).
[e] A. V. Rao, Z. Physik **97**, 154 (1935).
[f] M. de Hemptinne and J. Wouters, Nature **138**, 884 (1936).
[g] B. L. Crawford, Jr., and W. Horwitz, J. Chem. Phys. **15**, 268 (1947).
[h] J. Cabannes and A. Rousset, Ann. phys. **19**, 229 (1933).
[i] L. Simons, Soc. Sci. Fennica Commentationes Phys.-Math. **6**, No. 13 (1932).
[j] D. H. Rank, J. Opt. Soc. Am. **37**, 798 (1947).
[k] Zietlow, Cleveland, and Meister, J. Chem. Phys. **18**, 1076 (1950).
[l] M. L. Delwaulle and F. Francois, J. phys. radium **7**, 15 (1946).
[m] Madigan, Cleveland, Boyer, and Bernstein, J. Chem. Phys. **18**, 1081 (1950).

and

$$B_k=(\alpha_{x1}'-\alpha_{x2}')L_k^1-3^{-\frac{1}{2}}(\alpha_{c1}'-\alpha_{c2}')L_k^2 -4/\sqrt{3}(\alpha_{c1}-\alpha_{c2})Q_c\{2[3^{-\frac{1}{2}}(L^{-1})_1{}^k-\tfrac{1}{3}(L^{-1})_2{}^k +4/3Q_c(L^{-1})_3{}^k]\mu_C+\mu_{Cl}Q_c(L^{-1})_3{}^k\}.$$

Here α_{x1}, α_{x2} and α_{c1}, α_{c2} are the bond polarizabilities of the C−X and C−Cl bonds and the suffix 1 and 2 indicates the component of the polarizability along and perpendicular to the bond respectively. Q_c is the reciprocal of the C−Cl distance. The primes indicate differentiation with respect to the corresponding bond stretching coordinate.

We must now obtain values for the bond polarizabilities and their derivatives. The calculation of the α's and α''s from first principles is impossible since the very idea of a "bond polarizability" is an empirical one. Wolkenstein and Eliashevich[2] used for the polarizabilities of the C−H, C−Cl, and C−Br bonds the results of Denbigh's work.[7]

In order to obtain values for the derivatives of the bond polarizabilities they reversed the process of calculation by considering the α''s as unknowns and solving for them by using known depolarization factors. Table V shows the values of the bond polarizabilities and their derivatives calculated by Wolkenstein and Eliashevich.[2] The depolarization factors that were calculated using the data from Tables III, IV, and V are compared with the observed values in Table VI.

DISCUSSION

Table VI compares our calculated depolarization factors with the experimentally determined values. As can be seen, the agreement is rather good for the stretching vibrations but is very poor for the bending vibrations. As already pointed out by Wolkenstein[2] this latter discrepancy is due to the neglect in the theory of the orientational dependence of the bond polarizabilities and their derivatives during vibration. Inclusion of this dependence in the theory ought to bring about a better agreement for the bending vibrations. Of course, extra parameters would then have to be introduced which would then have to be determined experimentally.

It is to be noted that the α''s used by us are those calculated by Wolkenstein[2] who used a different set of potential constants. This slight inconsistency makes our calculated values somewhat higher than those of Wolkenstein. As the determination of the α''s depends upon the choice of the experimentally determined depolarization factors, and there is an uncertainty as to what constitutes an "accurately determined" depolarization factor, (as is evidenced by the multitude of values shown in Table VI for CCl_3H), we don't believe that this inconsistency is too critical. Although we carried out the normal coordinate treatment for CCl_3F, and report the L- and L^{-1}-matrix elements we did not attempt to compute values for the derivatives of the C−F bond polarizability since not enough precise data seem to be available.

[7] K. G. Denbigh, Trans. Faraday Soc. **36**, 936 (1940).

ACKNOWLEDGMENTS

This investigation was part of a research program which has been aided by grants from the Research Corporation and the American Academy of Arts and Sciences. The authors are grateful for this assistance.

Dielectric Dispersion of Rochelle Salt in the Microwave Region

HUMIO AKAO AND TAIZO SASAKI
Physical Institute, Faculty of Science, Osaka University, Osaka, Japan
(Received January 25, 1955)

The dielectric dispersion of rochelle salt was measured at 3000~20 000 Mc/sec using a new method. In this method $\mathcal{E}'$ and $\mathcal{E}''$ is obtained by measuring the half-power point and the shift of resonant frequency of a rectangular TE_{01} mode cavity.

These results show that the relaxation frequency of rochelle salt exists in the decimeter wave region.

INTRODUCTION

IT was expected by W. P. Mason that the clamped crystal ($y_z=0$) of rochelle salt should show dielectric dispersion in the microwave region.[1] According to the unpublished experimental result by W. A. Jager, there is no peak of dielectric constant at the wavelength 1.2 cm and over the temperature range $-40°C$ to $+26°C$ the value of $\mathcal{E}'$ is independent of temperatures.

However, we know nothing about the frequency range in which dispersion occurs and the nature of its relaxation, i.e., whether it is mono- or poly-disperse system.

We have observed the dispersion of this crystal over the region 3000~20 000 Mc/sec by the method devised by authors[2] to make the large dielectric constant measurable with sufficient accuracy.

A discussion is given of the mechanism of dispersion using the results of the measurements of the temperature and frequency dependence of $\mathcal{E}'$ and $\mathcal{E}''$.

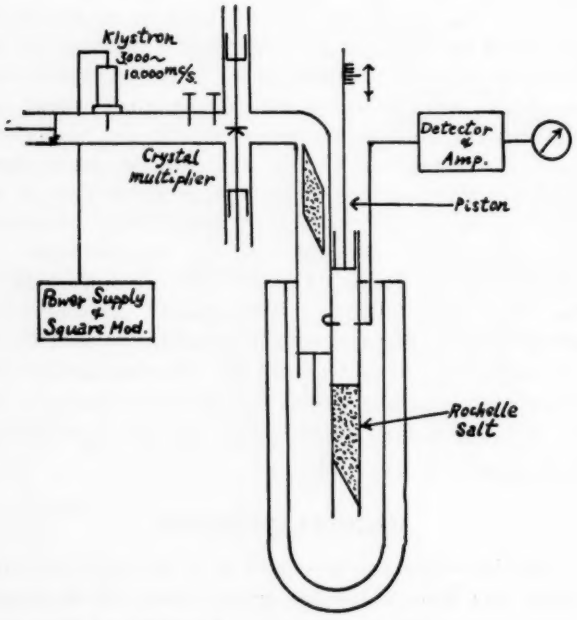

FIG. 1. Experimental apparatus.

EXPERIMENTAL METHOD

The complete dielectric constant $\mathcal{E}$ in the wave guide is given by the well-known formula

$$\mathcal{E}=\mathcal{E}_0\frac{(1/\lambda_c)^2-(\gamma/2\pi)^2}{(1/\lambda_c)^2-(\gamma_0/2\pi)^2}\equiv\mathcal{E}'-j\mathcal{E}'' \tag{1}$$

where λ_c is the cut-off wavelength of TE_{01} mode and γ_0, γ are propagation constants in the air and in the dielectrics, respectively, written as

$$\begin{aligned}\gamma_0&=j\beta_0+\alpha_0\\ \gamma&=j\beta+\alpha.\end{aligned} \tag{2}$$

The relation between the propagation constant and the characteristic impedance of the wave guide is given by

$$\gamma/\gamma_0=Z_0/Z. \tag{3}$$

Referring to Fig. 1 and Fig. 2, one end of the resonance cavity is terminated by a movable piston and the other end consists of a surface of dielectric contained in the wave guide. The length of the dielectric column is sufficient to ensure that no TE_{01} wave once transmitted into the dielectric and reflected from another surface of it can appear in the air-filled section of the cavity. Taken in the a-axis of rochelle salt, attenuation is so high that 5 cm is sufficient length for this requirement as shown later. If we have to examine a material without such a large attenuation, it is necessary to reduce the reflection from the terminating surface of the dielectric by making it of tapered shape.

The resonance cavity is excited by a probe at A and the electric field in the cavity is detected by a probe at A' (Fig. 2). If we put $l_0=\lambda_g/4$ the admittance Y

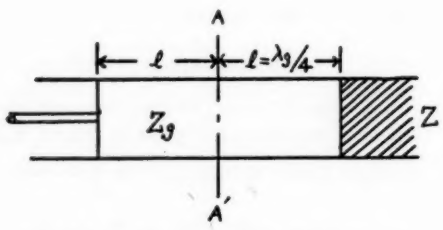

FIG. 2. Schematic diagram of the cavity.

[1] W. P. Mason, *Piezoelectric Crystals and Their Application in Ultrasonics* (D. Van Nostrand Company, Inc., New York, 1950), p. 234.
[2] H. Akao and T. Sasaki, J. Phys. Soc. Japan. 7, 361 (1952).

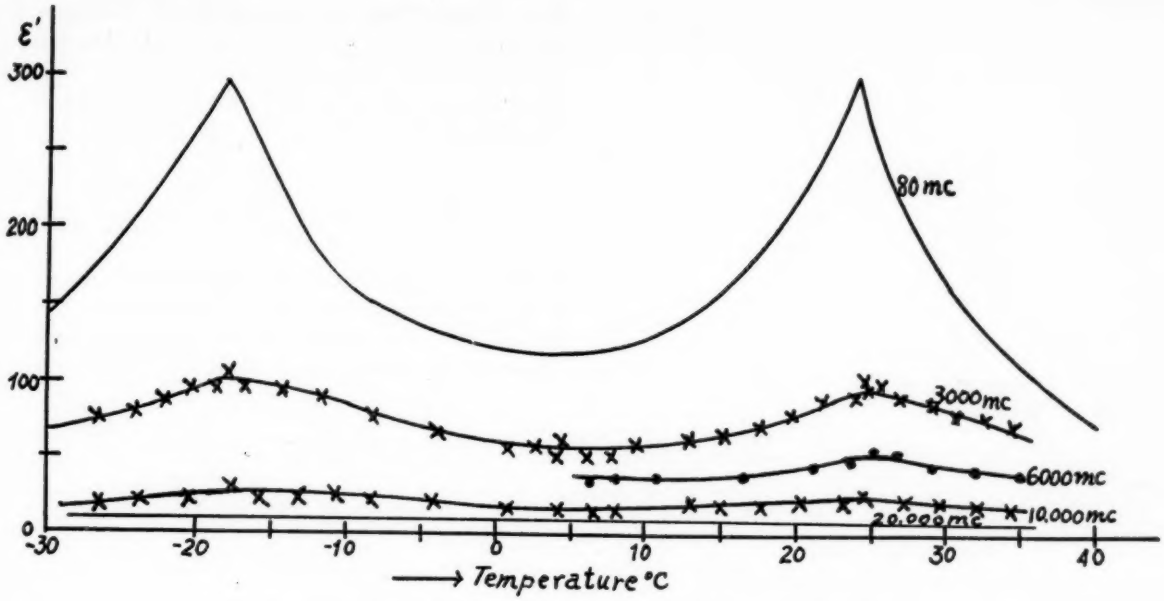

FIG. 3. Values of $\mathcal{E}'$ plotted against temperature for each frequency.

at the plane $A-A'$ in Fig. 2 is given by

$$Y=(\rightarrow Y_{A-A'})+(\leftarrow Y_{A-A'})$$

$$=\frac{1}{Z_g}\frac{Z_g\tanh\alpha_g'+Z}{Z\tanh\alpha_g'+Z_g}+\frac{1}{Z_g\tanh(\alpha_g+j\beta_g)l}, \quad (4)$$

where $\alpha_g'=\alpha_g\lambda_g/4$, and the sense of the arrows are taken as the direction seen from $A-A'$ plane. In this equation α_g and β_g are determined as the attenuation and phase constant when the characteristic impedance Z becomes zero, i.e., the resonance cavity is short-circuited at the input surface of the crystal. And when the cavity is terminated by a crystal, its impedance is calculated from the position of the piston at resonance $l_{(res)}$, half-power points $l=l_{(res)}\pm\Delta l$, α_g, and α_β. If the loss of the wave guide is negligible, as is actually the case, impedance Z is obtained from a simpler formula. $\mathcal{E}'$ and $\mathcal{E}''$ are then calculated by substituting the value of Z in (1) and (3). Recently, J. G. Powles and others[3] have proposed a similar method of measuring dielectric constants and losses by means of standing wave and have made measurements on various liquids and solids.

TABLE I. Cryatal sizes.

	10 cm		9.5 cm	5 cm		3 cm		1.5 cm
	No. 1	No. 2	No. 1	No. 1	No. 2	No. 1	No. 2	No. 1
a^{mm}	10	10	10	15	15	15	10	3
b^{mm}	70	70	70	35	35	35	20	10
c^{mm}	80	50	60	100	60	100	40	40

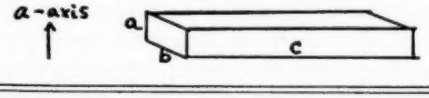

[3] J. G. Powles, J. Chem. Phys. 21, 136 (1953).

We also have tried the same method to measure the dielectric constant of rochelle salt and found that values derived by both procedure agrees fairly well at 5-cm wavelength.

EXPERIMENTAL RESULTS

Measurements were made at wavelengths 10 cm, 9.5 cm, 5 cm, and 1.5 cm. The size of crystals used in our measurements are given in Table I.

Experimental results are given in Figs. 3–7.

It is easily seen from Fig. 3 that the value of $\mathcal{E}'$ at the upper Curie point 24°C for 80 Mc/sec is about 300, but for 6000 Mc/sec it reduces about 40, showing that the relaxation time is shorter at the Curie temperature than at the other temperatures.

It must be noticed that there is no remarkable difference of relaxation time between the ferroelectric and paraelectric states, and consequently we find that spontaneous polarization has no effect on the relaxation time. We will discuss these topics later.

Figure 4 shows variation of $\mathcal{E}'$ and $\mathcal{E}''$ at 3000 Mc/sec, plotted against temperature. Accuracy in the measurements of $\mathcal{E}''$ is not as good as $\mathcal{E}'$ which contains

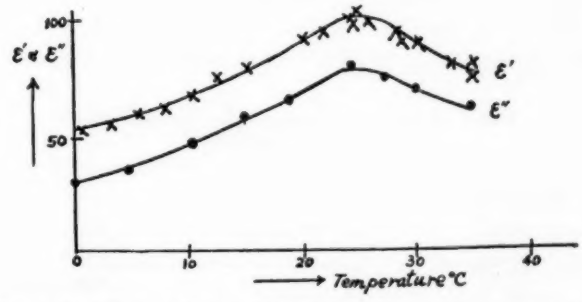

FIG. 4. Variation of $\mathcal{E}'$ and $\mathcal{E}''$ at 3000 Mc/sec *vs* temperature °C.

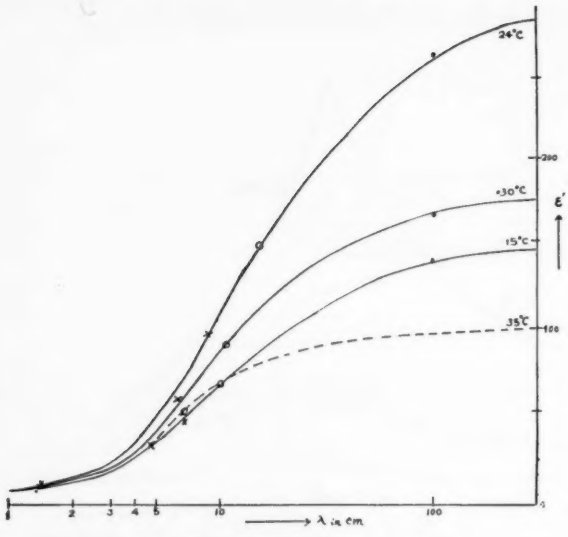

FIG. 5. $\mathcal{E}$ *vs* λ in cm.

approximately 10% error. In Fig. 5, we show variation of $\mathcal{E}'$ against the wavelength, taking temperature as the parameter. In Fig. 5 values of $\mathcal{E}'$ are plotted against temperature for each frequency listed in the foregoing and, for comparison, for two frequencies below 300 Mc/sec formerly investigated by one of the authors.

Following these results, relaxation frequencies corresponding to various temperatures are given in Table II.

Finally, so-called Cole-Cole arcs are illustrated in Fig. 6, where $\mathcal{E}'$ and $\mathcal{E}''$ are the abscissa and ordinate, respectively. Examination of this pattern shows that rochelle salt behaves as a polydisperse system instead of as a monodisperse system in the region from 15°C to 30°C, but at 35°C the arc is nearly a half-circle indicating a monodisperse system.

ON THE RELAXATION FREQUENCY

It may be correct that the anomalous dielectric properties of rochelle salt are explained by the hydrogen bond.

We assume here, as in the theory of W. P. Mason, that ferroelectric effects are caused by the translational motion of the hydrogen nucleus along the bond O——H - - - O. Since this is a bond between a water molecule and an oxygen ion, there is no reason to expect that the bond is symmetric.

Referring to the well-known structure of rochelle salt, its symmetry belongs to the orthorhombic system

TABLE II. Relaxation frequencies corresponding to various temperatures.

Temperature °C	Relaxation freq.		
15°C	3.0	10^9 cy/sec	Ferroelectric
24	2.0		Curie point
30	3.0		Paraelectric
35	4.5		Paraelectric

V_{222}. Then, there are two kinds of hydrogen bond, which are asymmetrical (region I and II). Assuming that the interactions between dipoles are only of long range, Mason's expression for the dielectric constant $\mathcal{E}$ of the clamped crystal in the paraelectric region is

$$\mathcal{E}=\mathcal{E}_\infty+\frac{(4\pi A'/\gamma)[1+\gamma(\mathcal{E}_s-1/4\pi)]}{1-A'+[j\omega e^{\Delta U/kT}/\Gamma\cosh(V/kT)]} \tag{5}$$

where Γ is a constant (in Eyring's reaction rate theory, Γ is an infrared frequency substantially equal to kT/h), ΔU the height of the potential barrier, V dissymmetry energy, and A' is a factor of the form

$$\begin{aligned} A'_{y_z=0}&=\frac{N\mu^2\gamma}{kT[1-(4\pi\nu/3)]}\left\{1-\tanh^2\frac{V}{kT}\right\} \\ A'_{Y_z=0}&=\frac{N\mu^2\gamma+(\beta^2/\alpha)}{kT[1-(4\pi\nu/3)]}\left\{1-\tanh^2\frac{V}{kT}\right\}. \end{aligned} \tag{6}$$

The factor β^2/α can be defined from the following consideration: if the crystal undergoes a shearing strain y_z, a dipole will change its orientation and the dipole energy will also be varied. Writing the energy of dipole directed to the $+a$-axis as $\mathcal{E}_+$ and to the $-a$-axis as $\mathcal{E}_-$, they are

in Region I	in Region II
$\rightarrow\mathcal{E}_+=V+\beta y_z+\gamma Z$	$\rightarrow\mathcal{E}_+=-V+\beta y_z+\gamma Z$
$\leftarrow\mathcal{E}_-=-V-(\beta y_z+\gamma Z)$	$\leftarrow\mathcal{E}_-=V-(\beta y_z+\gamma Z)$,

where β and γ are constants, V is the dissymmetry energy, and $Z=P_d/N\mu$. With the foregoing assumption, the internal energy of the crystal may be written (in the region I):

$$U^{\mathrm{I}}=N\left\{\frac{\alpha}{2}y_z^2-\beta y_z/[1-(4\pi\nu/3)]\right.$$

$$\left.\times Z^{\mathrm{I}}-\frac{N\gamma P_d}{[1-(4\pi\nu/3)]}Z^{\mathrm{I}}-\frac{\mu E}{[1-(4\pi\nu/3)]}Z^{\mathrm{I}}-V\right\}. \tag{7}$$

Another formula will be obtained similarly in the region II. Then the free energy F is written as

$$F=U^{\mathrm{I}}+U^{\mathrm{II}}-kT\log G, \tag{8}$$

where G is the number of total configurations. The spontaneous polarization is obtained by use of this free energy. As a result, the spontaneous polarization of the clamped or free crystal is applied for values of $A_{y_z=0}$ or $A_{Y_z=0}$ slightly greater than unity. Measurement of the spontaneous polarization cannot be carried out under the condition of the clamped crystal. Therefore, the clamped dielectric constant has a peak at the same temperature as the Curie point of the free crystal. Accordingly, the dispersion in the ferroelectric region cannot be obtained exactly.

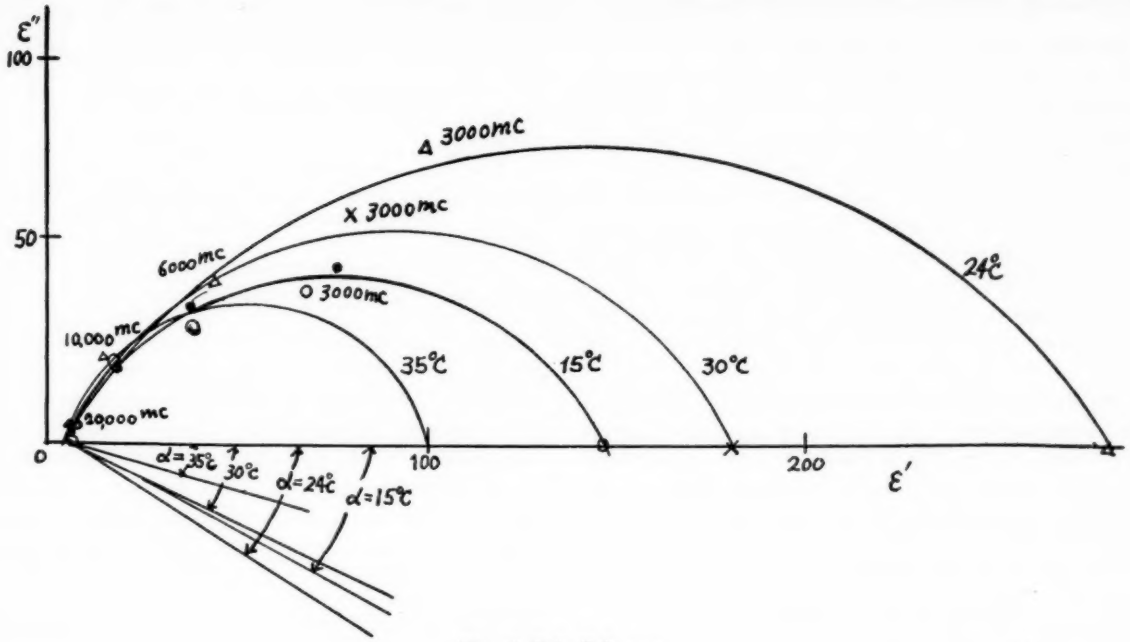

FIG. 6. Cole-Cole arcs.

If we put $\omega \to 0$, the clamped dielectric constant $\mathcal{E}_0$ is

$$\mathcal{E}_0 = \frac{(4\pi A'/\gamma)[1+\gamma(\mathcal{E}_\infty - 1/4\pi)]}{1-A'} + \mathcal{E}_\infty \tag{9}$$

and substituting this expression in (5) we have

$$\mathcal{E} - \mathcal{E}_\infty = \frac{\mathcal{E}_0 - \mathcal{E}_\infty}{1+(\mathcal{E}_0-\mathcal{E}_\infty)\, j\omega\tau'/\alpha}, \tag{10}$$

where

$$\alpha = \frac{4\pi}{\beta}\left[1+\beta\left(\frac{\mathcal{E}_0-1}{4\pi}\right)\right]A',$$

$$\tau' = \frac{h}{kT}\left\{\cosh\frac{V}{kT}\right\}^{-1} e^{\Delta U/kT},$$

and ΔU is the height of the potential barrier. Therefore, the relaxation time τ is

$$\tau = \frac{\mathcal{E}_0-\mathcal{E}_\infty}{\alpha}\,\frac{h}{kT}\,e^{\Delta U/kT}\left(\cosh\frac{V}{kT}\right)^{-1}. \tag{11}$$

TABLE III. Relaxation time calculated from Eq. (8).[a]

T°K	τ	$f_{relax}=1/2\pi\tau$
300	0.54×10^{9}	3×10^{9}
297	0.70	2.3
290	0.475	3.35
280	0.35	4.54 } for reference
270	0.415	3.84 }
260	0.815	1.95 }
255	1.54	1.03
250	0.99	1.60
240	0.49	3.25

[a] $\Delta U = 1.800$ cal/mole.

Then we can plot the relaxation frequency against temperature, putting in $\mathcal{E}_0$ the observed clamped dielectric constant and giving appropriate values for A', etc. The results are shown in Table III.

Figure 7 shows these values of relaxation frequencies together with the results given in Fig. 5. They agree qualitatively in that the relaxation time has a maximum at the Curie point and shows no remarkable changes at the other temperature. We have assumed the value of ΔU to be 1600 cal/mole, which might be a reasonable value for hydrogen nuclei to go over a potential barrier, though it might be small compared with the activation energy for dipole rotation.

Here, $\mathcal{E}'$ and $\mathcal{E}''$ are given by the formulas:

$$\mathcal{E}' - \mathcal{E}_\infty = \frac{\mathcal{E}_0-\mathcal{E}_\infty}{1+(\mathcal{E}_0-\mathcal{E}_\infty)^2\omega^2 l^2}$$

$$\mathcal{E}'' = \frac{(\mathcal{E}_0-\mathcal{E}_\infty)^2\omega l}{1+(\mathcal{E}_0-\mathcal{E}_\infty)^2\omega^2 l^2}, \quad \mathcal{E} = \mathcal{E}' + j\mathcal{E}'', \tag{12}$$

where we can expect dispersion of the Debye type.

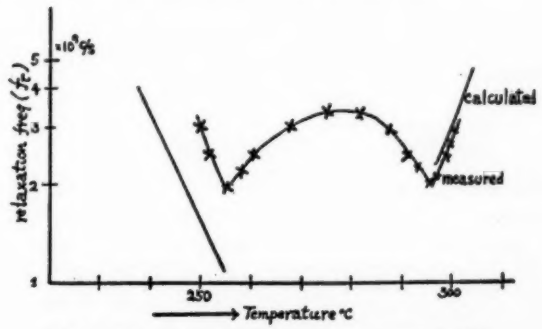

FIG. 7. Relaxation frequency *vs* temperature °K.

DISCUSSION ON THE EXPERIMENTAL RESULTS

It has been frequently discussed whether the ferroelectricity of $BaTiO_3$ and KH_2PO_4 is the result of the long-range force of dipole-dipole interaction or whether it should be treated as the valence problem of ionic displacement of the short-range type. We may ask the same question of the mechanism of polarization of rochelle salt. If the assumption of pure short-range effect, as J. C. Slater had applied to the KH_2PO_4, is applied to rochelle salt, the hydrogen nucleus H^+ needs to rotate around the oxygen. Since the activation energy for this process is very high, it is not likely to happen.

Accordingly, the interaction between the hydrogen bonds is assumed to be almost entirely due to long-range forces. Then, modifying Mason's theory and taking into account short range effect, the following expressions for the molecular fields are obtained.[4]

$$\left.\begin{aligned} F_1 &= E+\gamma_1 P_{d1}+\gamma_2 P_{d2} \\ F_2 &= E+\gamma_1 P_{d2}+\gamma_2 P_{d1} \end{aligned}\right\}. \tag{12}$$

F_1, F_2 are the internal fields and P_{d1}, P_{d2} the polarization in the region I or II, respectively.

After some simple calculations we get

$$P_0=P_{01}+P_{02}=\frac{(\mu/kT)E_0\{A+B+(2\mu\gamma_2/kT)\}}{AB}, \tag{13}$$

where

$$E=E_0e^{j\omega t}, \quad P_{d1}=P_{s1}+P_{01}, \quad P_{d2}=P_{s2}+P_{02}$$

(P_s is the spontaneous polarization)

$$A=1-\frac{\mu}{kT}\gamma_1+\frac{j\omega e^{\Delta U/kT}}{\Gamma\cosh(V/kT)\cosh(\mu/kT)(\gamma_1P_{s1}+\gamma_2P_{s2})},$$

$$B=1-\frac{\mu}{kT}\gamma_1+\frac{j\omega e^{\Delta U/kT}}{\Gamma\cosh(V/kT)\cosh(\mu/kT)(\gamma_1P_{s2}+\gamma_2P_{s1})}.$$

In the case for which γ_1 is equal to γ_2 or the spontaneous polarization is zero, the dispersion is of the monodispersion type, while on the ferroelectric region, it becomes the polydispersion type.

According to our measurement, the dispersion curve is not monodisperse both in the ferro- and paraelectric regions. This fact means that long-range interaction alone cannot describe the dipole interaction in this case.

However, since it was impossible to obtain the exact theory including short-range interaction, we cannot give any discussion on the shape of the dispersion.

CONCLUSION

(1) The dielectric loss of rochelle salt is at a maximum at a wavelength of about 10 cm. The temperature dependency of the relaxation frequency was explained by modified Mason's theory.

(2) The dispersion curve did not show monodisperse characteristics.

[4] T. Mitsui, at the meeting of the Physical Society of Japan, April, 1953.

THE JOURNAL OF CHEMICAL PHYSICS VOLUME 23, NUMBER 12 DECEMBER, 1955

Direct Production of Spectroscopic Specimens from Single Crystals by Controlled Growth from a Vapor

SOLOMON ZWERDLING* AND RALPH S. HALFORD
Department of Chemistry, Columbia University, New York 27, New York
(Received July 26, 1954)

Studies of anisotropic infrared absorption demand quite thin sections of single crystals, having relatively large cross section parallel with one of the few spectroscopically significant planes. This article describes the principles of design, the construction, and the successful operation with benzene of an apparatus for producing such specimens of single crystals. The method involves gradual introduction of vapor into an enclosed space, supporting a gradient of temperature and having the shape desired for the specimen, until self-nucleation occurs in a small vicinity of the colder pole of temperature. Processes of attrition among the nuclei ensue automatically and instantaneously, resulting in the survival of only those that become attached to the confining wall with a most favored orientation, an orientation that can be selected to some degree by factors of design and operation. Thereafter, vapor issuing into the enclosure accretes upon the few surviving nuclei until these seeds coalesce and develop to fill the entire volume available. The method promises to be especially useful for producing and investigating crystals that exist only at low temperatures.

INTRODUCTION

THE anisotropic spectral absorption that can be anticipated for many molecular crystals constitutes a rich, largely untapped store of unique information concerning both intramolecular and intermolecular processes. The general locations of absorbed spectral frequencies have their origins primarily within the molecules, whereas the anisotropy, contributions to the intensity, and a multiplet structure of absorptions are consequences of intermolecular interactions.[1] Recent literature furnishes evidence[2–7] of a quickening interest in the study of absorption anisotropy.

A formidable obstacle to rapid progress is the procurement of specimens meeting all of the stringent requirements for a significant observation.

Information that is to be accorded quantitative significance should be obtained with a single crystal in parallel radiation, incident normally upon a face that is parallel to one of certain crystallographic planes (usually 100, 001, and 010 except in monoclinic and triclinic systems where proper planes exist but cannot be specified a priori at this time and may vary with the frequency of the radiation[2]). The natural absorptivities of most substances will necessitate the use of quite thin sections, ranging downwards from a few hundred microns, while the optical apertures of suitable instruments at places where they furnish approximately parallel radiation will demand at least one dimension in the magnitude of 1 cm to be contained in the cross section.

The most fruitful investigations in the area of intermolecular processes for some time to come, moreover, will be ones conducted with anisotropic crystals composed of small molecules whose spectra have been observed and interpreted thoroughly while these constituents exist as vapors. Substances meeting this specification in most cases exist as crystals only at extremely low temperatures. Obvious difficulties seem to preclude any attempt with such substances at the production of large crystals to be sectioned and mounted subsequently for observation.

Devices such as the microilluminator,[8] which permits observations to be conducted with tiny crystals that come to hand more readily, or the production of specimens in the form of masses of oriented microcrystals yield results that are unsuitable for any of the more refined aspects of interpretation. It is our opinion, based upon accumulated experience in these laboratories, that these devices should be avoided whenever it is at all possible to do so.

In the present article we shall describe the design, construction and operation of an apparatus that circumvents most of the aforementioned difficulties. This apparatus should be generally useful for the direct production, from a vapor, of a single crystal in the form of a thin section having any desired thickness and any desired area of cross section, and with a favorable probability that the cross section will be parallel to a crystallographic plane having spectroscopic significance. Moreover, the apparatus is amenable, in principle, to modifications aimed at producing cross sections parallel with other crystallographic planes.

PRINCIPLES GOVERNING DESIGN

The initial rate of condensation of a supersaturated vapor is determined by the rate of generation of nuclei, an extraordinarily sensitive function[9,10] of both the

* Present Address: Lincoln Laboratories, Massachusetts Institute of Technology, Cambridge 39, Massachusetts.

[1] H. Winston and R. S. Halford, J. Chem. Phys. **17**, 607 (1949).
[2] R. Newman and R. S. Halford, J. Chem. Phys. **18**, 1276 (1950).
[3] J. Mann and H. W. Thompson, Nature, **160**, 17 (1947); Proc. Roy. Soc. (London) **A192**, 489 (1948).
[4] D. A. Crooks, Nature, **160**, 17 (1947).
[5] (a) A. Elliot and E. J. Ambrose, Nature, **159**, 641 (1947); (b) Elliot, Ambrose, and Temple, J. Chem. Phys. **16**, 877 (1948).
[6] G. C. Pimentel and A. L. McClellan, J. Chem. Phys. **20**, 270 (1952).
[7] A. V. Jones and G. B. B. M. Sutherland, Nature, **160**, 567 (1947). These are merely a few examples from a rapidly growing literature.
[8] Barer, Cole, and Thompson, Nature, **163**, 198 (1949).
[9] R. Becker and W. Döring, Ann. Phys. **24**, 719 (1935).
[10] M. Volmer and A. Weber, Z. Phys. Chem. **119**, 277 (1926).

temperature and pressure of the vapor. This function is so sensitive that the rate is virtually negligible until the attainment of a critical degree of supersaturation, where the rate accelerates practically discontinuously to very high velocities.

If a condensible vapor leaks gradually into an initially evacuated enclosure it will merely accumulate therein until the slowly increasing pressure corresponds to the critical degree of supersaturation, whereupon nuclei will suddenly appear with great velocity. If the walls of the enclosure include two contrasting poles of temperature with a steady flow of heat between them, a resulting thermal gradient in the vapor will cause the critical degree of supersaturation to be attained first only in a small neighborhood of the colder pole. When nuclei can appear, they will do so first only at this place. Moreover, if the rate of introduction of new molecules is sufficiently gradual, the production of only a small number of nuclei in the one critical neighborhood will lower the pressure sufficiently at that point and elsewhere so that further nucleation will become virtually impossible. The process of condensation will proceed rapidly thereafter, however, by the accretion of molecules upon the few nuclei that have been formed. The rate of accretion will be governed initially by the rate of dissipation of the large amount of heat that is delivered to each growing nucleus by the molecules condensing upon it. Heat dissipation will be greatly facilitated for some small fraction of the nuclei which become attached to the walls of the container, and especially so for ones that become attached at the colder pole. Even here some nuclei are able to grow faster than others if the condensed phase is anisotropic because their axis of maximum heat conductivity is along the shortest distance between the growing surface and the underlying one from which the heat can be rapidly removed. If the supporting surface is also anisotropic, in the sense of possessing an isothermal line along with a line of heat flow perpendicular to it, then, among the nuclei that are most favorably attached and most favorably oriented for heat dissipation, there will be some whose further aspect of orientation in the plane parallel to the supporting surface will enable them to grow still more rapidly than others. Thus on account of the three selective factors that we have mentioned above (and there are doubtless others as well) only a compounded fraction of a tiny number of nuclei formed initially will be destined to grow at superior rates until, finally, only these few similarly oriented seeds will attain a visible size.

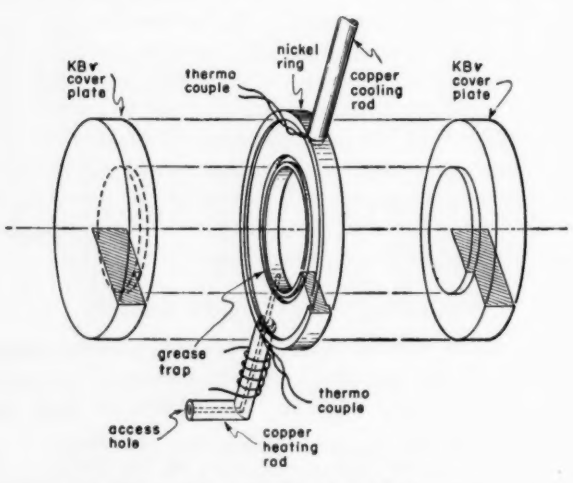

FIG. 1. The crystallization chamber.

A superiority of size attained through superior rate of growth corresponds also to attainment of a condition of greater thermodynamical stability. If the initial supersaturation is indeed effectively relieved during the competitive processes described above, the less fortunate smaller nuclei should disappear during the subsequent approach to thermodynamical equilibrium. Although the equilibrium state could be attained with certainty only in a closed system left undisturbed for an infinite period of time, nevertheless, if the rate of introduction of new material into an open system is slow compared with the natural rate of approach to equilibrium in the closed one, it is highly probable that the open system will also contain in due time only one or, at most, a few similarly oriented seeds.

For the present purposes it is immaterial whether there be but one or, instead, some number of similarly oriented seeds which coalesce as they grow to produce a single mass of uniformly oriented crystalline material. As vapor issues continuously thereafter into the enclosure, the single crystal specimen will enlarge steadily with its growing surface terminating always on isothermal lines in the walls of the container. If the vapor issues through an orifice at the warmer pole of temperature, the entire enclosure can be filled completely with a uniformly oriented crystalline specimen whose size, shape and orientation are determined by properties of its container.

The resulting crystalline specimen should have its axis of maximum heat conductivity lying nearly parallel with the line connecting the poles of temperature and often the remaining principal axes of heat conduction will have orientations determined by the arrangement of isothermal lines in the walls of the container at the colder pole. For those crystallographic systems where all ellipsoids representing physical properties must have their principal axes always along the same, symmetry-fixed directions[2] the planes defined by pairs of the principal axes for heat conduction are also the spectroscopically significant planes.

It is thus possible by proper arrangement of heat flow in a suitably designed structure to produce directly a thin, uniformly oriented, crystalline specimen having large cross section parallel with a spectroscopically significant crystallographic plane and parallel also with transparent walls of the container. The container and its contents can be transported to the working space of a spectrometer where the spectroscopic observations can be conducted with the crystalline specimen *in situ*.

The structure that we have devised to incorporate these principles is described in the next section.

DESCRIPTION OF APPARATUS

The crystallization chamber is shown schematically in Fig. 1.

A nickel ring, having outer and inner radii of 25 and 10 mm, respectively, about 3 mm thick, carries two soldered copper rods, one solid and one hollow, extending outward in opposite directions along the same diameter. The solid copper rod serves to establish thermal contact with a refrigerator which both supports the weight of the assembled chamber and defines in the nickel ring a colder pole of temperature. The hollow copper rod attached opposite has its inner opening continuous with a matching hole drilled radially through the nickel ring and also supports a heater. The hollow copper rod thus can define a warmer pole of temperature in the nickel ring and provides a connection between the interior of the crystallization chamber and an external vacuum system. The faces of the nickel ring were finished carefully on a lathe before being ground and lapped to flatness.

KBr cover plates, cut carefully on a lathe to leave protruding plugs as shown in Fig. 1, are provided with supporting shoulders lapped against the corresponding faces of the nickel ring. The plugs should fit quite snugly inside the nickel ring when the shouldering salt rests upon the nickel. The elevations of the protruding plugs above their supporting shoulders should both be machined carefully so that the gap between the two opposed faces will correspond to the desired thickness of the crystalline specimen. The finished salt covers are attached to the faces of the nickel ring with a thin layer of light grease, to support their weight and to seal off the interior of the crystallization chamber.

The method of creating a thin space by means of plugs protruding into a thick metallic ring was adopted for several reasons. The thick ring produces a desirably rugged structure that easily permits accurate control of dimensions. It makes easy the creation of a properly located, strong connection between the chamber and an external vacuum system, while also, on account of its large buffering capacity and large surface of contact with the heat exchangers at poles, it affords excellent regulation of heat flow on the inner surface of the ring.

Nickel was employed primarily because its comparatively mediocre heat conductivity permits establishment of the desired temperature distribution with more economical consumption of refrigerant. It also combines a desirable degree of hardness with easy machinability.

An alkali halide crystal was chosen in preference to other transparent materials because its relative rigidity again contributes to the extablishment and maintenence of accurate dimensions, and because it retains its excellent optical properties at all temperatures.

Grease was selected for effecting a seal between salt and metal because its easy deformability accommodates the large change of relative dimensions between salt and metal as the structure is cooled and protects the fragile alkali halide crystals from breakage. Also, it is simple to use.

Certain details of construction are significant and are shown in Fig. 1. These include (1) a shallow trench scored in each face of the nickel ring, concentric with and close to the inner circumference, for the purpose of trapping and preventing excess grease from entering the crystallization chamber, (2) an enlargement of thickness at the outer periphery of the ring to receive larger copper rods thereby improving heat exchange, (3) sections of the copper rods having reduced diameters and penetrating into the nickel ring to provide both greater mechanical strength and more precise definition of the poles of temperature on the surface of the crystallization chamber, (4) two copper-constantan thermocouples soldered onto circumference of the ring at points where it made contact with each of the copper rods, and (5) a heater of nichrome wire wound around the hollow copper rod adjacent to the nickel ring.

The auxiliary apparatus (Fig. 2), including a refrigerator articulated with an evacuated housing, provides thermal insulation and prevents accumulation of condensible constituents from the atmosphere.

The refrigerator is a silvered, modified dewar vessel whose inner wall penetrates through the outer one at the bottom and then terminates in a Kovar metal cup. A long, hollow copper cylinder provided with numerous vanes extends upward into the open interior of the dewar through a perforation in the Kovar cup to which

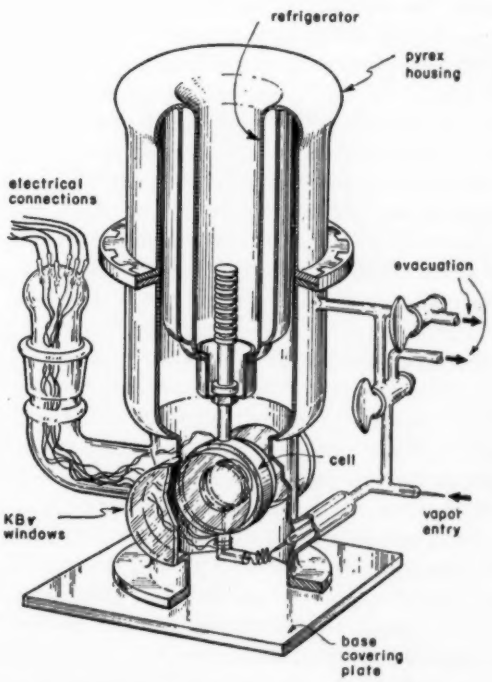

FIG. 2. Cutaway view of housing with crystallization chamber in place. Lower, three-way stopcock, drawn incorrectly, should be hollow-bore type.

it is firmly sealed by means of solder. This hollow cylinder is open only at the bottom end, the one exterior to the dewar, where it terminates in a split ring chuck. The solid copper rod attached to the nickel ring fits snugly into the interior of the hollow cylinder and penetrates well up into the interior of the dewar, where its receptacle is bathed by refrigerant. After the rod is worked into place it can be secured firmly by tightening the nut of the chuck.

The glass walls of the dewar vessel become continuous at its top with the wall of a coaxial cylindrical housing which extends downward, surrounding the dewar vessel, and is open at its bottom. The crystallization chamber can be inserted and withdrawn through this opening, which terminates in a thick flange that is sealed with grease against a ground glass covering plate to effect a closure of the envelope.

The envelope is reduced in diameter below the bottom of the dewar vessel in order to permit the attachment of four side arms within a limited space.

One arm, shown at the left in Fig. 2, is closed just above a tapered ground glass joint. The closed end holds a number of hollow Kovar tubes sealed with solder, carrying electrical leads to the thermocouples and heater. The wires are long to accommodate withdrawal of the crystallization chamber through the opening at the bottom of the envelope and the excess lengths of wire are stored in this side arm whenever the chamber is in position inside the envelope.

A short side arm, shown at the right in Fig. 2 just above the flange, is penetrated at its end by a length of glass capillary tubing. The portion of this tubing interior to the envelope terminates in a length of Kovar tubing to which the hollow copper rod carried by the nickel ring can be connected through a flexible coil of seamless brass tubing, soldered at both of its ends. The coil can be disconnected from the Kovar tubing but remain attached to the hollow copper rod, permitting the nickel ring to be withdrawn without encountering any obstructions. The portion of the glass capillary tubing exterior to the side arm extends into the cross arm of an inverted T made also of glass capillary tubing. The vertical arm of the T terminates at a hollow bore three way stopcock (shown incorrectly in Fig. 2), while the other end of the cross arm terminates in another length of Kovar tubing to receive the capillary leak from the vapor reservoir. Capillary tubing is used throughout this region in order to minimize the amount of vapor on the low pressure side of the leak. The vertical arm of the T continues above the stopcock as ordinary tubing terminating in a cross arm which toward its left re-enters the envelope and toward its right carries a stopcock and a spherical ground glass joint for attachment to a pump. A connection to the hollow bore of the three-way stopcock extends horizontally toward the rear and after turning again toward the right terminates in another spherical ground glass joint, likewise intended for attachment to the vacuum system. This latter orifice can be used alternatively to evacuate either the interior of the crystallization chamber or, exterior to it, the interior of the glass envelope, but not both at the same time. The alternative connection between the interior of the envelope and the vacuum line is included so that it might be possible to pump upon both regions simultaneously. Spherical joints provide a convenient flexibility for attaching a cumbersome system to a stationary line.

Two other side arms extend toward front and back, respectively, in the view shown as Fig. 2. These identical, side arms are short cylinders whose diameters match the nickel ring and both terminate in ground glass flanges where they are closed by attachment of salt windows that permit transit of the radiation beam. During assembly of the whole structure the nickel ring is arranged so that the cross section of the crystallization chamber is parallel with these external windows.

The capillary leak whereby vapor can be admitted from an external reservoir into the crystallization chamber is not shown in Fig. 2, although it forms an integral part of the structure depicted there. To gain mechanical flexibility the leak was formed from a 40-cm length of annealed stainless steel capillary tubing having a bore diameter of about 0.1 mm. One end of this metal capillary is attached permanently, by means of solder and an appropriate brass adapter, to the Kovar receptacle shown at the lower right, exterior to the housing and below the stopcock in Fig. 2. The other end of the steel tubing terminates again in a Kovar connector sealed into a length of glass tubing. This length of glass tubing must connect somehow with the vapor reservoir. If it carries first a stopcock and then a tapered ground glass joint, the leak can be closed after the crystal has been grown and then disconnected from the reservoir to produce, along with the structure in Fig. 2, a separate unit having a high degree of portability. Alternatively, the disconnection can be made beyond the reservoir but then the reservoir is included in the separate unit and there is some sacrifice of portability.

The rate of vapor flow through the capillary leak is governed according to well known laws by the pressure of vapor in the reservoir along with the dimensions of the metal capillary. For the particular capillary described above both calculations and actual calibrations indicate that, in the absence of condensation, the times required for the pressure in the crystallization chamber to attain one half the magnitude of the pressure in the reservoir would be of the order of one minute and ten minutes for reservoir pressures of the order of 10 mm and 1 mm, respectively, varying in inverse proportion with the reservoir pressure. Times of this order should be ample to allow a high probability of approach to conditions of thermodynamic equilibrium among the seeds that survive the various competitive processes, described in an earlier section, taking place subsequent to nucleation. Pertinent theoretical considerations indicate that the crucial events initiated by the attainment of a

critical degree of supersaturation should be completed probably within some small fraction of one second.

The dimensions of the unit illustrated in Fig. 2, especially the ones from front to back in the view shown there, were adjusted during construction so that the structure would fit between the housings of a Perkin-Elmer Model 12*B* Infrared Spectrometer. The horizontal equatorial plane of the crystallization chamber should be positioned in its envelope during assembly so that it will contain the optic axis of the spectrometer when the bottom closure plate of the envelope rests upon the bed of the optical instrument.

METHOD OF OPERATION

The completely assembled apparatus is connected to the vacuum line by means of the spherical joint leading to the hollow bore of the three-way stopcock and to the vapor reservoir through the permanently attached capillary leak, with this latter connection temporarily closed at some convenient point on the high pressure side of the leak. The three-way stopcock is manipulated first to evacuate the interior of the crystallization chamber along with the attached capillary leak up to the point of its temporary closure. When suitable tests have indicated that this region of the apparatus maintains a good vacuum, the stopcock is turned next to evacuate the interior of the jacket surrounding the crystallization chamber. After establishing that a steady static vacuum can be maintained also in this portion of the apparatus, refrigerant is added slowly to the dewar vessel. Next, a regulated variable voltage supply is connected to the heater and adjusted to produce some selected difference between the temperatures registered by the two thermocouples. When the temperatures have become steady, the three way stopcock is turned to connect the pump once more with the interior of the crystallization chamber and the reservoir is opened to the capillary leak. After a few seconds allowed for final flushing of the leak, the three way stopcock is turned to isolate the apparatus from the vacuum system. The apparatus is left undisturbed thereafter, except for occasional replenishment of the refrigerant until, usually after some hours, it can be decided either (1) that the pressure of the vapor in the reservior was not sufficiently high to cause nucleation or (2) that the developing crystal does or does not exhibit satisfactory uniformity of orientation.

Detection and inspection of the growing crystal is acomplished by viewing it between crossed sheets of polaroid, arranged so that they can be rotated together while looking toward an intense source of parallel light.

The quality of the growing crystal is judged by the uniformity and sharpness of the extinction which it exhibits at some orientation of the pair of crossed polaroids.

In the event of an unsatisfactory outcome the offending specimen, if any, can be pumped out in preparation for making a new attempt with either an altered distribution of temperature in the crystallization chamber or an altered rate of admission of vapor, which latter is controlled by adjustment of the pressure in the reservoir.

If the outcome is an acceptable cyrstalline specimen the portable unit can then be transported to other places where orientation of the crystal can be further studied with suitable instruments, if these are available, and finally to the spectrometer.

CRYSTALLIZATION OF BENZENE, AN EXAMPLE OF PERFORMANCE

As an example of performance we shall describe briefly now our experience with the production of a uniformly oriented, thin section of crystalline benzene.

In preparation for the crystallization of benzene, windows were machined as shown in Fig. 1, from disks of KBr so that when both were in place on the metal ring the gap between the faces of the two protruding plugs would be 0.1 mm. The finished windows were attached to the ring with a thin layer of light grade Celvacene stopcock grease, satisfactory for work at temperatures as low as $-80°$C.

The refrigerator was charged with a mush formed from solid CO_2 and liquid trichloroethylene, replenished occasionally as needed. The temperatures produced in this way, observed at poles on the outer periphery of the nickel ring, were about $-75°$ and $-65°$C at top and bottom, respectively, when no current was flowing in the heater.

Benzene vapor was supplied from a small portable reservoir containing a quantity of purified[11] liquid benzene, exhaustively degassed. The reservoir remained permanently attached to the capillary leak, through which the flow of vapor could be regulated or even effectively stopped by suitable adjustment of the temperature of liquid benzene. The reservoir was immersed in a mush formed with solid CO_2 and trichloroethylene during preliminary operations until such time as it was desired to initiate the flow of vapor.

A search program, consisting of observations upon the qualities of partially completed specimens produced with different temperature distributions and different rates of vapor feed, indicated that it would be advantageous to create a temperature difference of approximately 25°C between the two thermocouples and to accomplish the nucleation with a minimal pressure in the reservoir, although the rate of feed could be increased greatly after a visible seed had become well established. With this information at hand a procedure was then devised to give optimum results, taking into account the desirability of producing the final specimen as rapidly as possible without undue sacrifice of its quality. The heater current was regulated prior to at-

[11] The benzene, purified by the method of A. I. Vogel, *Practical Organic Chemistry* (Longmans Green and Company, New York, 1948), p. 171, method 1, was furnished by Dr. Harold L. Greenwald and was part of the same sample used by him in his study of the variation with temperature of induced absorption in liquid benzene.

tempting nucleation until the temperatures indicated by the upper and lower thermocouples were about −60° and −35°C, respectively. These temperatures were maintained steadily without further adjustments throughout the entire period of production.

The vapor feed was regulated by transferring the reservoir from its refrigerating mush to the interior of a small dewar flask containing water at 0°C, which was then permitted to warm slowly to room temperature, thereby producing gradually accelerating flow of vapor into the crystallization chamber.

The crystal first became visible as a single seed some fifteen minutes after the benzene in the reservoir had liquefied. We should remark that this point of origin for measuring times is not thought to have any special significance. The crystal when first noticed was so small that is appeared merely as a tiny pin point of light in the dark field created by the crossed sheets of polaroid. It was located in the cell at the position of lowest temperature, and had two sharp extinction axes at angles of approximately 30° and approximately 120° measured clockwise from the horizontal.[12] Subsequent growth occured at first primarily along the supporting metal surface, symmetrically with respect to the vertical diameter of the cell, until the seed had acquired the shape of a small crescent some several millimeters from point to point. Further deposition then caused the crystal to develop a horizontal lower edge which thereafter appeared to move slowly downward until the chamber was completely filled.

Growth was completed, that is, all available space in the chamber appeared to be filled at the end of approximately fifteen hours.

Examination of the completed specimen with parallel light striking the cell windows obliquely indicated that the crystal was in intimate contact nearly everywhere with the inner rocksalt surfaces, thus reducing scattering and interference effects that might complicate measurement of its absorption spectra. It appeared colorless and transparent when viewed with transmitted parallel light. The finished specimen exhibited a cross-sectional area of approximately 300 sq mm while its thickness was approximately 0.1 mm. The extinction axes remained essentially those of the original seed.

The orientation of the crystallographic axes in the finished specimen was deduced from observations of its anisotropic infrared absorption, observations which we report in a separate article.[13] Details of the absorption and anisotropy observed independently at different frequencies indicate consistently that our specimen of the biaxial orthorhombic crystal[14] of benzene had its *b*-axis normal to the cross section while that cross section contained the *a*-axis passing through it at an angle of 30° and the *c*-axis at an angle of 120°, both measured clockwise from the horizontal; that is, the cross section or our specimen was parallel with the (010) plane.

Similarly gratifying results can be expected for other substances in the greater proportion of cases, with respect to both uniformity and suitability of orientation. Further experiments conducted in these laboratories by Mr. Murray Gershenzon and Miss Esther Krikorian with equipment constructed according to the same principles have produced successful outcomes easily in four cases out of five.

[12] The temperature gradient is singular, or approximately so, in the vicinity of the colder pole of our apparatus. Presumably for this reason it is our experience that the extinction axes of crystals produced therein are always rotated somewhat from the vertical, horizontal relationship.

[13] S. Zwerdling and R. S. Halford, J. Chem. Phys. **23**, 2221 (1955).

[14] E. G. Cox, Proc. Roy. Soc. (London) **135A**, 491 (1932).

Motions of Molecules in Condensed Systems. IX. Infrared Absorption Anisotropy and Induced Molecular Motion in a Single Crystal of Benzene

SOLOMON ZWERDLING* AND RALPH S. HALFORD
Department of Chemistry, Columbia University, New York 27, New York
(Received July 26, 1954)

Infrared absorption spectra were observed with radiation polarized linearly along each of the two extinction axes contained in a thin cross section from a single crystal of benzene grown especially for this purpose. The spectra indicate consistently that the cross section was the 010 plane, that they record separately the absorptions polarized along the *a*-axis and the *c*-axis, respectively. The anisotropies of the induced absorptions exhibited by five fundamental molecular vibrations (ones that appear only in spectra for condensed phases) are all quite similar and may even be identical. It thus appears that the induced motions, superimposed upon the several intrinsic ones by the perturbing intermolecular interactions, have a property of similarity independent of the differing natures of the intrinsic motions that are being perturbed.

INTRODUCTION

IN its condensed phases, either liquid or solid, benzene exhibits new components of infrared absorption in addition to those characteristic frequencies which are absorbed as well by the vapor. These added frequencies are characteristic of molecular vibrations that occur similarly in all three phases but are forbidden to appear in the spectrum for the vapor by selection rules originating in the rich fund of symmetry possessed by the isolated molecule. In the condensed phases absorption is induced by perturbations of these intrinsically non-absorbing motions, perturbations associated with intermolecular interactions.

The intensities of the induced absorptions in liquid or solid benzene are quite appreciable, an aspect of perturbation that stands in marked contrast with the almost negligible changes induced in the frequencies of the perturbed motions. The magnitudes and in a crystal the directional characteristics of the intensities of induced absorption, along with their conceivable variations from motion to motion, evidently are all both sensitive and significant manifestations of the detailed nature of intermolecular interactions and of their resulting disturbances of the intrinsic patterns of molecular motions.

In this article we shall describe and discuss the results of an investigation of the anisotropy of absorption in one significant cross section, identified as the 010 plane, from a single crystal of benzene.

The results indicate that the induced motions, superimposed upon the several intrinsic ones by the perturbing intermolecular interactions, have a property of similarity, perhaps even identity, independent of the differing natures of the intrinsic motions that are being perturbed.

The infrared absorption spectrum for solid benzene was first studied systematically by Halford and Schaeffer[1] who compared it with spectra for liquid and vapor for the purpose of demonstrating that a consistent interpretation could be given to spectra for all three phases in terms of a single set of molecular motions, subject to weak perturbations, governed by appropriate symmetry considerations. Their work was repeated in part by Mair and Hornig[2] who employed superior instrumentation, extended the observations with solid to lower temperatures, and achieved a more detailed identification of frequencies absorbed with specified molecular motions. Mair and Hornig develop in their paper, with aid from voluminous prior work to which they refer, a seemingly incontrovertible and complete assignment of frequencies to the several symmetry species for normal modes of vibration in the isolated molecule of benzene.

Throughout these earlier studies the focus of interest was directed toward the motions of a single molecule, either isolated or imagined to be slightly perturbed by weak interactions with an environment that was unspecified except for a certain characteristic symmetry.

Anisotropy of absorption, with which we are to be concerned in the present article, demands for its proper interpretation a consideration of the absorbing motion as a property of the entire crystal, a motion involving all of its constituent molecules.

In a molecular crystal a normal mode of vibration can be visualized as one wherein all molecules execute identical motions, with identical frequencies but with characteristic differences from place to place in the phase of that motion. The common molecular motion will be occurring with a certain characteristic arrangement of phases for the several molecules in one unit cell, the same arrangement of *relative* phases prevailing in every unit cell, accompanied by definite, additional increments of phase between adjacent unit cells. This description for a normal mode can be developed simply from the transformation properties[3] of the classical motions under the symmetry operations contained in the crystallographic space group.

The admissible increments of phase between adjacent

* Present address: Lincoln Laboratories, Massachusetts Institute of Technology, Cambridge 39, Massachusetts.

[1] R. S. Halford and O. A. Schaeffer, J. Chem. Phys. **14**, 141 (1946).

[2] R. D. Mair and D. F. Hornig. J. Chem. Phys. **17**, 1236 (1949).

[3] H. Winston and R. S. Halford, J. Chem. Phys. **17**, 607 (1949).

unit cells are fixed[3] by the translational symmetry of the crystal and among the host of these possibilities, which are as numerous in an ideal crystal as are its unit cells, optical excitations are mostly prohibited by a strict selection rule. According to this rule, originating in the translational symmetry of the crystal, optical excitation will be possible for a mode only when the wave envelope of its phase progressions connecting adjacent unit cells matches in its wave number the wave of the exciting radiation while both the mechanical motion and the exciting radiation have approximately identical frequencies of oscillation. A motion that is excitable under this rule will resemble very closely, when the wave length is long compared with the dimensions of one unit cell, one wherein all unit cells move exactly in phase. For simplicity we can adopt this approximation which then permits us to describe[3] the resulting excitation entirely in terms of the motion occurring within a single unit cell.

The relative phases for the common motion being executed by the several identical molecules within one unit cell are fixed[3] by the special symmetry of the crystal, described by the factor group of the crystallographic space group, and are restricted[3] always to a number of possibilities equal exactly to the number of occupants of the unit cell whenever these occupants are all equivalent under the operations of the factor group. The characteristic directions for resultant vectorial properties, such as the transitory electric moment, when summed over the phases of all occupants in one unit cell will always either parallel crystallographic axes or (in monoclinic and triclinic crystals) define directions having crystallographic significance no matter what are the molecular orientations within this frame of reference. Whenever the number of equivalent molecules in one unit cell exceeds three, the resultant vectorial properties for some patterns of phase will sum to zero and in the infrared spectrum additional selection rules will operate. These special selection rules and more generally other properties of the coupled motions occurring within one unit cell can be derived[3] in a formal way from mathematical considerations of symmetry. The process will be illustrated in the course of our interpretation of the absorption anisotropy observed with the single crystal of benzene.

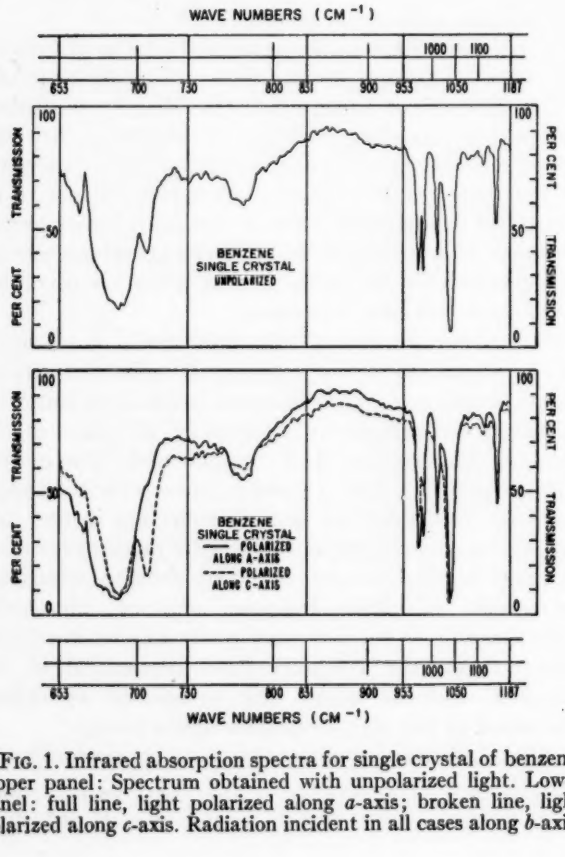

FIG. 1. Infrared absorption spectra for single crystal of benzene. Upper panel: Spectrum obtained with unpolarized light. Lower panel: full line, light polarized along *a*-axis; broken line, light polarized along *c*-axis. Radiation incident in all cases along *b*-axis.

MATERIALS, APPARATUS, AND TECHNIQUES

The single crystal of benzene, having thickness of about 0.1 millimeter and cross section of about 300 square millimeters, was produced by controlled growth from the vapor phase in an apparatus designed especially for that purpose and also to permit subsequent spectroscopic observations with the crystal *in situ*. The apparatus and the production of the single crystal used in the present investigation have both been described[4] in a separate article.

The spectra were recorded automatically with a modified[5] Perkin-Elmer, Model 12B, Infrared Spectrograph. In the present instance the instrument was used as a single beam device. After performing in duplicate the series of observations with the single crystal in differently polarized and unpolarized light, it was removed from the light path by allowing the otherwise undisturbed crystallization chamber to warm up while the crystal was being pumped out. The empty crystallization chamber was then cooled again and, when the prior temperature distribution had been reestablished, the necessary photometric blanks were recorded with all procedures and variables of operation corresponding as exactly as possible to the earlier ones. Source power consumption was monitored and maintained steady at all times. Predetermined optimum slit-width schedules were carefully executed.

The slit widths needed for unpolarized light were about one-half as large as the widths used when light was polarized along the *c*-axis, while the ones used for light polarized along the *a*-axis were about 90% of the widths required for light polarized along the *c*-axis. With unpolarized light the slit widths used were uniformly about 0.85 times the ones reported elsewhere[5] for double beam operation of our instrument.

The percental transmittances for the crystal were

[4] S. Zwerdling and R. S. Halford, J. Chem. Phys. **23**, 2215 (1955).

[5] A. Savitsky and R. S. Halford, Rev. Sci. Instr. **21**, 203 (1950).

computed from the pairs of corresponding observations at intervals varying from 15 cm^{-1} in the high-frequency region where dispersion is poor to 1 cm^{-1} in the low-frequency range, with even closer spacings for the significant absorptions.

Polarized infrared radiation was produced with an AgCl pile[6] constructed at some sacrifice of aperture so that it could be inserted in place of the entrance window of the monochromator housing. The polarizer was aligned in one case so that the electric vector of the resulting polarized radiation would be parallel with one of the extinction axes for visible light contained in the cross section of the crystal and in the other case it was rotated by 90° to bring the electric vector into congruence with the second extinction axis.

The extinction axes for visible light (symmetry fixed and thus independent of wavelength in this orthorhombic crystal) were located in the cross section prior to situating the crystal on the spectrometer by examining the crystal between crossed sheets of polaroid in an intense beam of approximately parallel, white light.

The identifications as crystallographic axes of the two extinction axes will be deduced presently in the subsequent discussion of the observed spectra.

RESULTS OF MEASUREMENTS

The polarized and unpolarized infrared absorption spectra for a benzene single crystal grown in the manner previously described[4] are presented in Figs. 1 and 2. All measurements were made with the rock-salt prism. The spectra were prepared as calculated from the sample and reference determinations without correction for random noise or scattering. The latter effect appeared to be small, as expected from the high transparency of the crystal in visible light.

The resolution in the unpolarized spectrum was quite clearly better than that in either polarized one, due to the narrower slit widths used as a consequence of the increased aperture and radiation intensity available when the polarizer was not in the light beam. The observed lines are for the most part extremely sharp, so sharp that their natural widths cannot be observed with our spectrometer

The absorption frequencies clearly indicated, together with their apparent relative intensities, are presented in Table I. Separate listings are given for the two polarized and the unpolarized spectra measured. The intensities are expressed as an estimate on an arbitrary scale increasing integrally from 1 to 10. The limits of uncertainty in the frequencies reported, arising from the plotting of the spectra and interpolation from the calibration curve for the rock-salt prism, are shown in Table II. The uncertainty limits vary with the spectral region due to changes in scanning and recorder-chart speeds, as well as in the dispersion of the prism. The assignments of the frequencies to molecular motions and their species under the operations of the molecular point group D_{6h} are taken from the paper by Mair and Hornig.[2] Absorptions in the region above 3100 cm^{-1} are not reported in the table since the very low dispersion of the prism in this region makes frequency determination too uncertain. Such absorptions correspond to combination bands, since there are no benzene fundamentals above 3100 cm^{-1}.

The spectra as presented describe the benzene crystal absorptions at a temperature determined from the thermocouple readings to lie in the range −65°C to −55°C. The reference determinations were made with the empty cell at the same temperature used for the sample determinations.

INTERPRETATION OF RESULTS

The isolated benzene molecule is planar with the symmetry of the point group D_{6h}. The thirty molecular normal modes of vibration produce[7] twenty different frequencies of which ten are doubly degenerate. These modes are associated with the irreducible representations of D_{6h} in the manner: $2A_{1g}+A_{2g}+A_{2u}+2B_{1u}+2B_{2g}+2B_{2u}+4E_{2g}+2E_{2u}+E_{1g}+3E_{1u}$.

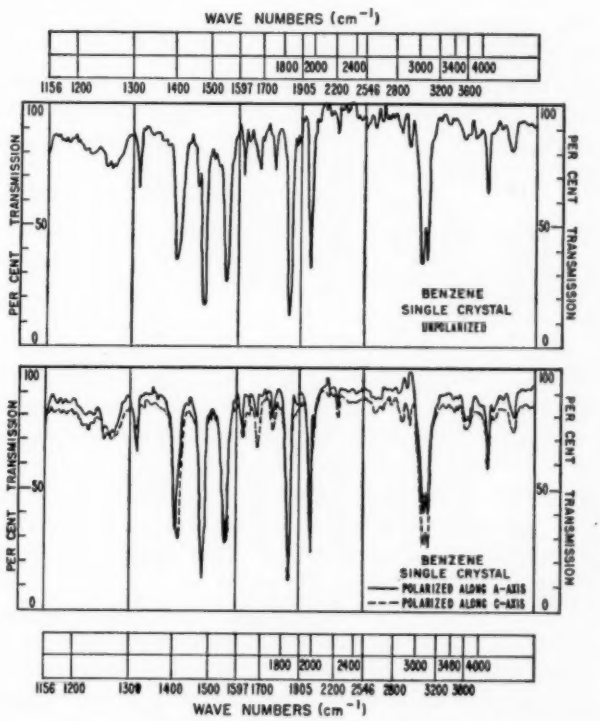

FIG. 2. Infrared absorption spectra for single crystal of benzene (continued from Fig. 1). Upper panel: Spectrum obtained with unpolarized light. Lower panel: full line, light polarized along *a*-axis; broken line, light polarized along *c*-axis. Radiation incident in all cases along *b*-axis.

[6] R. Newman and R. S. Halford, Rev. Sci. Instr. **19**, 270 (1948).

[7] E. B. Wilson, Jr., Phys. Rev. **45**, 706 (1934). The normal modes are depicted graphically by G. Herzberg, *Infrared and Raman Spectra of Polyatomic Molecules* (D. Van Nostrand Company, Inc., New York, 1945), p. 118 with a key on p. 363 to Wilson's notation, also ours.

TABLE I. Absorption frequencies.

Frequency[a] cm^{-1} M. & H.	Relative[a] intensity	Assignment[a]	D_{6h} species[a]	Polarized a-axis cm^{-1}	Relative intensity	Polarized c-axis cm^{-1}	Relative intensity	Unpolarized cm^{-1}	Relative intensity
3030		ν_{18} in res.	E_{1u}	3049		3033		3042	
3086	ms	with $\nu_{19}+\nu_8$	E_{1u}	3088	6	3081	8	3085	7
2647	ww	$\nu_{19}+\nu_9$	E_{1u}	2708					
2610	ww	$\nu_{12}+\nu_8$	E_{1u}	to		2680		2680	
2588	ww	$\nu_{17}+\nu_8$	A_{2u}	2582	2	2624	2	2624	2
2210	mw	$\nu_{20}+\nu_9$	E_{1u}	2210	3	2208	3	2210	3
2012	w	$\nu_{16}+\nu_8$	A_{2u}	~2008	1	~2008	1	~2008	1
1973									
1980	s	$\nu_{17}+\nu_5$	E_{1u}	1981	7	1981	8	1981	7
1828									
1836	s	$\nu_{17}+\nu_{10}$	E_{1u}	1834	8	1834	9	1834	9
1754	mw	$\nu_{15}+\nu_6$	E_{1u}	1755	3	1755	4	1759	4
1680									
1685	mw	$\nu_{17}+\nu_4$	E_{1u}	1685	3	1680	5	1685	5
1644	mw	$\nu_{20}+\nu_6$	E_{1u}	1650	1	1644	1	1644	1
1618	mw	$\nu_{12}+\nu_6$	E_{1u}	1625	4	1625	4	1621	4
1547									
1555	ms	$\nu_{11}+\nu_{10}$	E_{1u}	1550	8	1554	8	1550	8
1478	s	ν_{19}	E_{1u}	1478	9	1478	9	1478	9
1470	w	$\nu_{19}(C^{13}C_5^{12}H_6)$	...	~1463	1	~1463	1	~1463	2
1402									
~1412	ms	$\nu_{16}+\nu_5$	E_{1u}	1404	7	1408	8	1404	8
1311	w	ν_{14}	B_{2u}	1315	6	1315	3	1315	6
1275				1285		1290		1292	
1265	mw	$\nu_{16}+\nu_{10}$	E_{1u}	to	5	to	5	to	5
1255				1246		1238		1235	
1245									
1147	mw	ν_{15}	B_{2u}	1149	7	1147	5	1148	7
1109	ww	$\nu_{16}+\nu_4$	E_{1u}	1113	2	1112	2	1112	2
1117									
1036	s	ν_{20}	E_{1u}	1038	9	1034	10	1037	10
1010	mw	ν_{12}	B_{1u}	1011	7	1010	6	1013	7
984				986	7	985	4	986	7
975	mw	ν_{17}	E_{2u}	978	8	976	6	978	7
770	mw	ν_{11}+ger. lat. modes	...	772 (783–757)	5	773 (784–759)	5	773 (783–758)	5
702	ww	...	...	~704	1	704	5	705	3
687	s	ν_{11}	A_{2u}	688	10	689	9	688	9

[a] See reference 2.

Only the modes belonging to A_{2u} and E_{1u} may be infrared active, so that only four different fundamental frequencies may absorb directly in the spectrum for the vapor. Since the molecule has a center of symmetry, the first overtones of the fundamental frequencies as well as binary summation and difference bands between those frequencies whose modes belong both to the ungerade, or both to the gerade representations are forbidden. However, summations and differences between two frequencies, one of which corresponds to a gerade, and the other to an ungerade mode may be active if the resulting motion belongs to A_{2u} or E_{1u}

TABLE II. Limits of error in frequency determination.

Frequency range, cm^{-1}	Error, cm^{-1}
3200–2800	±9
2800–2400	±7
2400–2000	±7
2000–1800	±5
1800–1600	±4
1600–1400	±2.5
1400–1200	±2.3
1200–1000	±2.0
1000– 800	±1.6
800– 600	±1.0

of D_{6h}. These symmetry selection rules furnish a basis for the interpretation of the infrared absorption spectrum of benzene vapor and are the point of departure for a comparative interpretation of the crystal spectra.

For understanding of the absorption spectrum of solid benzene, a consultation of the crystallographic space group is necessary. Cox[8] found that the unit cell has the factor group symmetry of V_h^{15} (orthorhombic bipyramidal) and contains four molecules located at centers of symmetry. He also found the crystal to be highly birefringent. The arrangement of the molecules in the unit cell is pseudo-face-centered, since if the center of one molecule is placed at the unit cell corner, the centers of the other three occur at the face centers although their orientations are not all the same. Cox concluded that the most satisfactory structure appeared to be one in which the planes of the rings were approximately parallel to the b-axis and made an angle of about forty degrees with the c-axis. A projection of the unit cell upon the (010) plane is presented in Fig. 3. The shaded molecules lie at a depth $b/2$ below the plane of the others. The b-axis is, of course, perpendicular to the plane shown.

The benzene molecules occupy crystallographic sites with symmetry C_i. A comparison of the character tables for D_{6h} and C_i discloses[9] that each degenerate mode in the isolated molecule is split into two nondegenerate molecular motions in the crystal. The fifteen, now distinct normal modes associated with the gerade representations of D_{6h} together with the lattice modes of rotatory origin belong to the A_g representation of C_i, while the fifteen, now distinct normal modes associated with the ungerade representations of D_{6h} together with the lattice modes of translatory origin belong to the A_u representation of C_i, which is its only infrared activity representation. Consequently, the molecular normal modes and combinations belonging to the B_{1u}, B_{2u}, and E_{2u} representations of D_{6h} acquire induced activity under C_i in the crystal. These selection rules govern the infrared activity of solid benzene within the site group approximation,[9] an approximation that corresponds to perturbation of an isolated molecule by a static field.

[8] E. G. Cox, Proc. Roy. Soc. (London) **A135**, 491 (1932).
[9] R. S. Halford, J. Chem. Phys. **14**, 8 (1946).

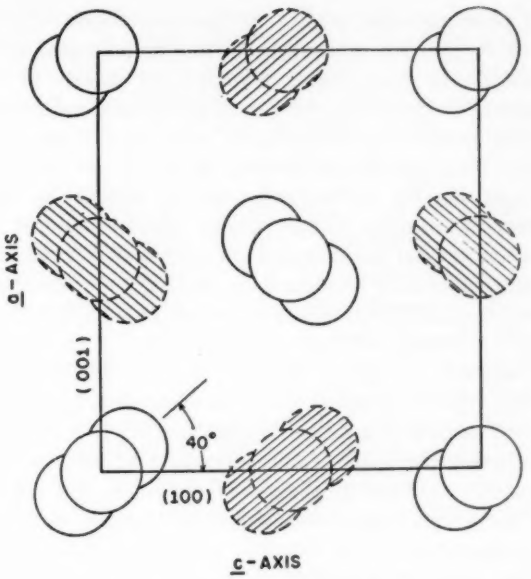

FIG. 3. Crystal structure[8] of benzene projected onto 010 plane.

In the final analysis[3] the coupling between the four molecules in one unit cell of benzene will result in four types of crystal modes for each molecular mode. This conclusion is derived formally from the correlation between the irreducible representations of the D_{6h} point group of the isolated molecule, those of the C_i site group in the crystal, and those of the V_h^{15} factor group. The last is isomorphous with the point group V_h and so has the same character table.

Of the four types of crystal modes produced by coupling, only the three belonging to B_{1u}, B_{2u}, and B_{3u} of V_h^{15} (factor) may be infrared active, each of these developing a resultant dipole moment oscillation for the whole unit cell along a different one of the three crystallographic axes. These characteristics of the coupled motions are simply connected with their respective transformation properties under the several operations contained in the factor group. The latter contains the identity, three screw axes, and three glide planes in addition to a center of inversion (on which a molecule lies). Those operations of the factor group which are not in its site subgroup C_i are applied in turn to the transitory dipole moment vector of the mode in question after it has been placed upon the site of one molecule in the unit cell. The vector is thereby carried to the molecules on the other three equivalent sites. The pertinent, nonequivalent collections of the transformation of the original vector under each one of these selected operations may be obtained in turn from the matrices of those irreducible representations of the factor group which are correlated with the irreducible representation of the site group possessing the mode concerned. Since for benzene all infrared active modes in the crystal belong to A_u of C_i, which is correlated with A_u, B_{1u}, B_{2u}, and B_{3u} of V_h^{15} (factor),

four nonequivalent sets of vectors are obtained. Each set of vectors has a resultant, the one belonging to A_u of the factor group being zero for any mode. The resultants for the other three sets will give the direction, always along a crystallographic axis, of the transitory dipole moment accompanying each of the three remaining crystal oscillations derived from the same molecular motion. Thus, there should be for the benzene crystal an infrared active triplet for each ungerade molecular mode, each member of the triplet absorbing selectively along a different unit cell axis.

In accordance with these predictions, if radiation is propagated through a benzene crystal parallel to one of the crystallographic axes, as expected for a well-chosen section of a single crystal, only two of the three members of the triplet can be observed. Moreover, if the radiation is polarized along first one, then the other of the two crystallographic axes at right angles to the one of propagation, each member of the residual doublet can be observed separately.

The relative intensities of the two perpendicularly polarized absorptions will depend in the lowest order of approximation only upon the arrangement of the molecules in the crystal, but in higher orders also upon their interactions with each other.

For some of the observed absorptions, the ones that are allowed in the spectrum of the isolated molecule, there is a large intrinsic dipole moment oscillation accompanying the molecular vibration and, for these absorptions, the lowest order of approximation may suffice for a discussion of their intensities. In this approximation, the intrinsic moment only is considered and, from its known orientation in the molecule and the known orientation of the molecules in the unit cell, the relative magnitudes of the resultant dipole moment for each member of the triplet can be predicted

In the higher orders of approximation, there must be added to the intrinsic dipole moment oscillation in each molecule an induced one, arising from the perturbation of the motion in the crystal field. For those observed absorptions which are allowed only in the crystal, there are no intrinsic moments, only induced ones, and the higher orders of approximation are necessarily required. In the present state of the theory, induced moments cannot be predicted and it will be of interest presently to examine the data to see what can be learned about them.

The A_{2u} and E_{1u} modes under D_{6h} which possess intrinsic moments will be treated first in the approximation that ignores induced ones. In this way, the orientation of the benzene single crystal section that was grown can be identified.

The molecular modes belonging to A_{2u} under D_{6h} (out-of-plane modes) will develop intrinsic transitory moments along the crystallographic a axis and c axis, but not along the b-axis. According to Fig. 3 the intrinsic moment for out-of-plane motion must oscillate perpendicular to b. This inability to develop b-axis moments intrinsically arises from the accidental organization of the unit cell and not from a strict symmetry selection rule. Moreover, the a-axis moments should be somewhat larger than the corresponding c-axis moments.

For an observation with plane polarized radiation propagated along the b axis, absorptions originating in A_{2u} under D_{6h} are permitted for orientations of the electric vector parallel to both the a axis and the c axis. On the other hand, if polarized radiation were propagated instead along the a axis or the c axis, absorption would not occur when the electric vector was parallel to the b axis, and would have a maximum when parallel to the companion axis of extinction in the cross section.

The ν_{11} fundamental at 688 cm^{-1} in the crystal furnishes the only suitable frequency for making this test. This frequency is absorbed in both of the observed polarized spectra with absorption intensities that are approximately equal, but the one for the first polarizer orientation used is somewhat greater than the one for the second. Consequently, the conclusion follows that the light beam, which was perpendicular to the crystal face, was also parallel to the b axis, or nearly so, and furthermore, that the electric vector for the first polarizer orientation was parallel to the a axis, and for the second orientation, parallel to the c axis.

The same orientation of crystallographic axes can be identified alternatively by a consideration of absorptions originating with the species E_{1u} of D_{6h}. The intrinsic moments associated with these doubly degenerate motions of the isolated molecule will lie always in the molecular plane. When the degeneracy of molecular motion is removed by the static crystal field corresponding to the site group C_i this will result, under the approximation that considers only intrinsic moments, in the fixing of two unique directions in the molecular plane. It is obvious from the unit cell structure shown in Fig. 3 that one member of this site group doublet will develop its intrinsic moment along a direction parallel with the crystallographic b axis. The other member of the pair, now a distinct local motion, will have its intrinsic moment perpendicular to the b-axis but still contained in the molecular plane, that is, projecting upon both the a and c axes with a slightly larger component in the direction of c.

Each member of a static field or site group doublet will be further split in principle into a quadruplet of distinct unit cell motions having three potentially absorbing members, as explained previously, by coupling of motions within a unit cell. However, in this approximation that considers intrinsic moments only, one of these absorbing triplets evidently will have all of its intensity concentrated in its b-branch with null branches along both a and c while the other triplet will have its intensity distributed between its a- and c-branches with a null branch along b. To the approximation we are considering, therefore, in the crystal spectrum the end result originating from a degenerate molecular motion

belonging to E_{1u} of D_{6h} will be a singlet absorbing along b separated by a static field splitting from a correlation field doublet whose branches absorb, respectively, along a and c. As before, this result arises from the accidental organization of the unit cell along with the approximation we are making and not from any strict, symmetry founded rule.

Static field splitting is comparatively much larger than that caused by the correlation field. The former leads to separations that can be resolved whereas the latter does not.

Mair and Hornig observed[2] four examples of static field splitting among absorptions originating with E_{1u} of D_{6h}, all within the spectral region from 1400 to 2000 cm^{-1}, in their unpolarized spectra for benzene frozen from the liquid phase. The average spacing for these four examples was 8 cm^{-1}.

The spectrum obtained with our single crystal in unpolarized light, under conditions of observation that are demonstrably adequate to resolve the spacings reported by Mair and Hornig, shows only single branches of absorption at every one of the four, corresponding places. This significant point of difference between their spectra and ours is readily explicable only if the radiation was incident upon our single crystal along a direction paralleling its b axis.

The conclusion substantiates in part the earlier identification of orientation for our single crystal. Absorptions originating both in A_{2u} and E_{1u} of D_{6h} indicate alike that the b-axis was perpendicular to the cross section. It remains now to examine the examples of E_{1u} absorptions with the aim of deducing from them the relative orientations of the a and c axes in the cross section of our specimen.

The significant examples of absorptions which unquestionably originate with motions belonging to E_{1u} of D_{6h} include the three fundamentals at 1037, 1478, and 3063 along with combinations at 1404, 1550, 1834, and 1981 cm^{-1}. To these cases we might add another combination that interacts with the fundamental at 3063 through Fermi resonance to produce the two peaks actually observed at 3042 and 3085 cm^{-1}. In all seven or eight of these instances we are now obliged by prior conclusions to attribute the observed absorptions to unresolved correlation field doublets containing branches along a and c with the slightly greater intensity expected to appear in the c direction. In all of these instances the apparent absorption intensity for what we have called the second polarizer orientation is at least equal and in five or six instances it is in fact unquestionably greater than the intensity registered with the polarizer in the first orientation. The two exceptions where the intensities appear to be approximately equal along both directions are at 1478 and 1550 cm^{-1}. Since the intensities for the two directions are not expected to be greatly different at best in the approximation that we are considering the comparison of observations will be somewhat sensitive both to the induced moments and to variations of line width that we have been neglecting. A clear preponderance of cases without flat contradictions is as much as we have any right to expect. We conclude accordingly that the c axis of our crystal was aligned with the electric vector of the radiation when the polarizer was in its so called second orientation. This is precisely the same conclusion that we deduced earlier from the characteristics of the A_{2u} absorption.

Finally, we should add for corroboration that if the b axis were contained in the cross section along with either a or c we would then be obliged to expect a much greater disparity in the intensities of E_{1u} absorptions along the two directions. This would be true because in the approximation that considers intrinsic moments only, one member of the static field doublet has its total intensity concentrated along b whereas the other member has an equal total intensity distributed almost equally between a and c.

Thus, from the foregoing discussions and the known orientation of the polarizer, it is now determined consistently by several independent considerations that, within close limits, the b axis of the crystal was parallel to the spectrometer light beam, and the a axis and c axis of the crystal made angles with the horizontal of thirty and one hundred twenty degrees, respectively, measured clockwise from the horizontal.

The order of approximation upon which this determination is based may fail for any intrinsic moment mode if the magnitude of its transitory moment and that of its added induced crystal moment are alike and their directions different. Inspection of the data in Figs. 1 and 2 shows that the observed absorptions just used to establish the orientation of the crystal are much more intense than others which arise from induced moments only, and thus invites confidence in these conclusions derived from that approximation which ignores induced moments compared to intrinsic ones.

The remaining absorptions of interest, ones which possess no intrinsic moment since they are associated with modes belonging to the other ungerade representations of D_{6h} forbidden in the spectrum of the vapor, need to be considered in a higher order of approximation that includes induced moments.

These induced absorptions may be used to obtain information as to the nature of the crystal perturbation of the molecular symmetry and motion. It is possible to represent the perturbation as an induced, transitory dipole moment vector for each corresponding mode. This vector might be the same for all modes, or have only the same direction or magnitude for each of them, or be completely different for every one. The orientation and magnitude of this perturbation moment with respect to the crystallographic axes would be revealed for each such mode if a complete set of three polarized spectra could be measured. In the present work, only one crystal orientation was available, so that the determination is limited to assessing the two com-

ponents of each perturbation moment upon those crystallographic axes parallel to the polarized electric vectors of the radiations used for the measurements.

The absorptions in question and their D_{6h} origin are the following fundamentals: (1) a doublet for ν_{17} at 978 cm^{-1} and 986 cm^{-1} derived from E_{2u}, (2) a singlet for ν_{12} at 1011 cm^{-1} derived from B_{1u}, (3) a singlet for ν_{15} at 1148 cm_{-1} derived from B_{2u}, and (4) a singlet for ν_{14} at 1315 cm^{-1} also derived from B_{2u}. For all of these frequencies, the absorption intensity is observed to be markedly greater in the spectrum polarized along the a axis than in the one polarized along the c axis. This circumstance leads to the very interesting conclusion that the perturbation moment which enables the corresponding modes to become infrared active is, in every case, more nearly parallel to the a-axis than the c-axis. Although complete information as to the exact orientation in the crystal of the transitory moment vectors associated with each of these frequencies could not be obtained, the results indicate the possibility that such vectors may be parallel, or nearly so.[10]

Two more ungerade molecular normal modes have been reported to produce active fundamentals in the crystal with the following frequencies: (1) a singlet for ν_{13} at 3070 cm^{-1} derived from B_{1u}, nearly masked by a resonance multiplet from 3042 cm^{-1} to 3085 cm^{-1} and (2) a doublet for ν_{16} at 405 cm^{-1} and 415 cm^{-1} derived from E_{2u}, at the far end of the vibrational infrared region. Neither of these absorptions were detected as such in this research. The latter has been assigned,[2] however, as a contributor together with the $\nu_5(B_{2g})$ fundamental to a moderately strong E_{1u} summation band at 1404 cm^{-1}.

In conclusion, several additional features of the spectra merit special mention. The incompletely resolved pair of absorptions at 978 and 986 cm^{-1} furnish the only instance where a pair of motions degenerate in the isolated molecule but rendered distinct by the static field can both be observed to absorb in the crystallographic cross section under examination. These absorptions are derived from the doubly degenerate ν_{17} belonging to E_{2u} of D_{6h}, a pair of out-of-plane motions. The unique observation arises from the circumstance that the absorptions are wholly induced with comparable intensities and anisotropies, so that the two correlation field triplets are highly similar, permitting two branches to be observed from each in the one crystallographic cross section. On the other hand, as described earlier, the intrinsic absorption associated with degenerate pairs belonging to E_{1u} of D_{6h} is concentrated differently in certain branches only of each triplet with the result that the intense intrinsic absorption in the two observable branches of one triplet masks the weaker induced absorption in the corresponding branches of the other and only one triplet can be seen distinctly.

Another feature is the weak but well-resolved absorption at 1463 cm^{-1} on the low-frequency side of the ν_{19} band at 1478 cm^{-1} in the unpolarized spectrum. This absorption appears as a very weak shoulder at the same place in the polarized spectra. It has been interpreted[2] alternatively as the partially suppressed b axis component of ν_{19}, or as the ν_{19}-like vibration of $C^{13}C_5^{12}H_6$.

Finally, the absorption for ν_{11} at 688 cm^{-1} shows an interesting structure on its broad envelope. In the spectrum polarized along the c axis, a well-resolved peak occurs at 704 cm^{-1}. In the spectrum polarized along the a-axis, there is an increased width for the fundamental, and the satellite absorption has become very weak. In the unpolarized spectrum, there is a resolved peak at 705 cm^{-1} which is weaker than the corresponding absorption in the first spectrum mentioned above. Structural features on the low-frequency side of the minimum are not reliable because of high, variable concentrations of CO_2 issuing from the refrigerator. The interpretation of these absorptions lying so close in frequency to the fundamental is uncertain, but it seems highly probable that they involve combinations of the fundamental molecular motion with lattice modes.

Further inquiry into the exact degree of similarity among induced motions is precluded by the sensitivity of apparent intensities to variations in the unknown widths of the narrow lines which characterize the spectrum of crystalline benzene.

[10] We are indebted for the suggestion of this possibility to Dr. R. M. Hexter, who reached a similar conclusion in a study of the infrared absorption anisotropy in crystals of naphthalene and related molecules. R. M. Hexter, dissertation, Columbia University, 1952 (article in preparation).

Ionization of Strong Electrolytes. IV. Nuclear Magnetic Resonance and Dissociation of Trifluoroacetic Acid

G. C. Hood, O. Redlich, and C. A. Reilly
Shell Development Company, Emeryville, California

(Received February 18, 1955)

Proton and fluorine magnetic resonance of trifluoroacetic acid in water reflects the influence of electrolytic dissociation below a mole fraction 0.5 and of hydration above 0.5. The dissociation constant is estimated to be 1.8.

PREVIOUS investigations[1,2] of nitric and perchloric acids have shown that proton magnetic resonance can be used for the determination of the degree of dissociation of strong acids. Measurements have now been extended to trifluoroacetic acid as an example of a moderately strong acid.

Experimental details and calculations have been described previously. The fluorine resonance was measured at 40 Mc/sec. The trifluoroacetic acid was purified by distillation through a ten-plate Oldershaw column.

The results are shown in Tables I and II. The stoichiometric mole fraction p of the hydrogen in H_3O^+ on a hydrogen basis is given by the mole fraction x of the acid according to $p=3x/(2-x)$. The bulk magnetic susceptibility correction g was determined by a nuclear resonance method.[2,3] The corrected proton resonance shift s, referred to water, and the fluorine shift S, referred to the pure acid, are expressed in units of 10^{-6} of the total magnetic field strength.

The dependence of the shifts on the composition of the solution (Figs. 1 and 2) is very similar to that of nitric acid. There are clear breaks in the slopes at the equimolal solution ($p=1$ or $x=0.5$). It is obvious to interpret the shape of the curves below the break points as caused by incomplete dissociation. The straight lines above the break points indicate an equilibrium between monomer hydrate and dimer.

Degrees of dissociation α have been computed from the proton shift s according to

$$s/p=\alpha s_1+(1-\alpha)s_2. \quad (1)$$

TABLE I. Proton shift in trifluoroacetic acid.

Moles per liter c	p	Susceptibility correction g	Resonance shift Series I s	Resonance shift Series II s	Degree of dissociation α	$\log(a/c)$
2.10	0.066	0.01	0.56	0.53	0.623	−0.063
4.00	0.148	0.02	0.94	0.93	0.411	+0.298
6.00	0.273	0.04	1.50	1.42	0.304	+0.670
8.01	0.472	0.07	1.87	1.85	0.142	...
10.01	0.835	0.12	2.33	2.50	0.026	...
10.59	1.007	0.15	...	2.67	0.000	...
11.47	1.376	0.22	...	3.46	...	...
12.00	1.716	0.26	3.87	3.98	...	...
12.44	2.105	0.30	...	4.55	...	...
12.91	2.616	0.34	...	5.72	...	...
13.06	3.000	0.37	6.37	6.29	...	...

TABLE II. Fluorine shift in trifluoroacetic acid.

Moles per liter c	Susceptibility correction g	Resonance shift S
2.10	−0.35	2.30
4.00	−0.34	1.77
6.00	−0.33	1.38
8.01	−0.30	0.94
10.01	−0.25	0.04
10.59	−0.21	0.29
11.47	−0.14	0.28
12.00	−0.10	0.02
12.44	−0.07	0.42
12.91	−0.02	0.12
13.06	0.00	0.00

TABLE III. Trifluoroacetic acid activity coefficients.

m	c	γ	$\log(a/c)$
0.1	0.100	0.80	−1.193
1.0	0.926	0.63	−0.369
2.0	1.732	0.56	−0.144
3.0	2.436	0.52	+0.002
5.0	3.614	0.49	+0.228
6.5	4.339	0.49	+0.367

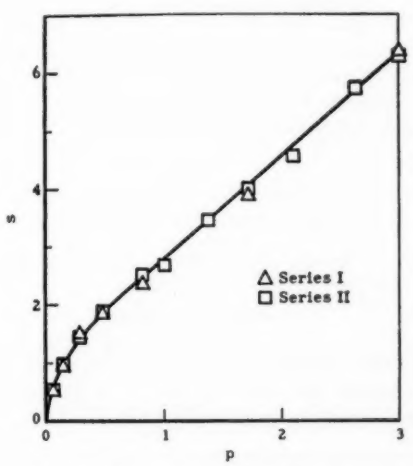

FIG. 1. Observed proton shift.

[1] H. S. Gutowsky and A. Saika, J. Chem. Phys. **21**, 1688 (1953).
[2] Hood, Redlich, and Reilly, J. Chem. Phys. **22**, 2067 (1954).
[3] Reilly, McConnell, and Meisenheimer, Phys. Rev. **98**, 264 (A) (1955).

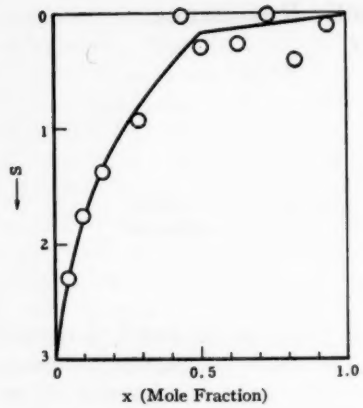

FIG. 2. Observed fluorine shift.

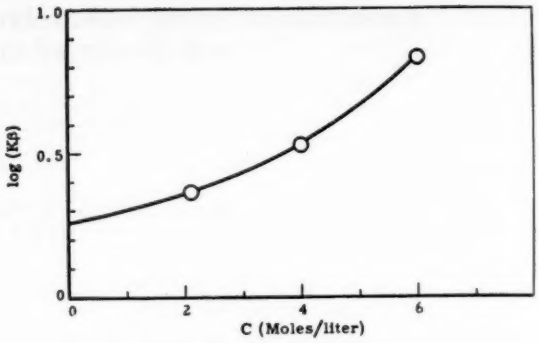

FIG. 3. Dissociation constant.

The shift $s_1=11.62$ of the hydrogen ion was known[2] from nitric and hydrochloric acids. The shift s_2 of the undissociated acid was assumed to be the value observed for the equimolal solution. The curve for the fluorine shift S below $x=0.5$ (Fig. 2) was calculated according to

$$S_3-S=x[\alpha S_1+2(1-\alpha)S_2] \qquad (2)$$

with the empirical coefficients $S_1=20.40$; $S_2=2.75$; $S_3=2.94$.

The activity coefficients γ (Table III) and activities a were computed from freezing points.[4] The dissociation constant $K=1.8$ is obtained by extrapolation of log $K\beta$ (Fig. 3) where β is the true activity coefficient of the undissociated acid. It is not surprising[5] that for an acid as strong as trifluoroacetic acid the value computed from conductivities[6] and Ostwald's dilution law, namely, $K=0.588$, is much too low.

[4] H. H. Cady and G. H. Cady, J. Am. Chem. Soc. **76**, 915 (1954).
[5] See O. Redlich, Chem. Revs. **39**, 333 (1946).
[6] A. L. Henne and C. T. Fox, J. Am. Chem. Soc. **73**, 2323 (1951).

THE JOURNAL OF CHEMICAL PHYSICS VOLUME 23, NUMBER 12 DECEMBER, 1955

Theory of Internal Over-All Rotational Interactions. II. Hamiltonian for the Nonrigid Internal Rotor

DANIEL KIVELSON*†
Research Laboratory of Electronics and Department of Physics, Massachusetts Institute of Technology, Cambridge, Massachusetts
(Received January 7, 1955)

An approximate Hamiltonian for a nonrigid internal rotor has been derived. The potential energy has been expanded in a Taylor's series in the displacement coordinates and in a Fourier series in the angle of internal rotation θ. The Hamiltonian was transformed by a contact transformation, and a second-order Hamiltonian in which vibrations and rotations have been separated has been obtained. The Hamiltonian consists of terms which constitute the usual rigid internal rotational problem, of centrifugal distortion terms involving both over-all and internal angular momentum, and of terms that arise because of the repulsive nature of the barrier. These repulsive terms enter as a single term, $2JF_v(m|1-\cos 3\theta|m)$, in the expression for the rotational transitions of symmetric rotors, where J is the total angular momentum quantum number and m is the pseudo-quantum number for internal rotation. The repulsive constant, F_v, is given by the relation

$$F_v=-\Sigma_i^{\frac{1}{2}}[B_{xx}^{(i)}+B_{yy}^{(i)}]a_i^{(1)},$$

where $B_{xx}^{(i)}+B_{yy}^{(i)}$ is the derivative of the rigid rotor rotational constant with respect to the ith symmetry coordinate, and $a_i^{(1)}$ is one-half the displacement of the equilibrium position of the ith internal coordinate in going from $\theta=0$ to $\theta=\pi/3$.

The dependence of the barrier height upon the vibrational motion has also been studied.

INTRODUCTION

IN a recent paper,[1] which will be designated as I, the interactions of internal with over-all rotations were considered for symmetric rotors. This interaction in symmetric rotors arises only through the interactions of both rotational motions with the vibrations of the molecule. The frequencies of the over-all, internal rotational transitions for symmetric rotors were given by the relation

$$\nu=2J[B_v+F_v(m|1-\cos N\theta|m)+G_v(m|\mathbf{\Pi}^2|m)+L_v(m|\mathbf{\Pi}|m)K], \qquad (1)$$

where B_v, F_v, G_v, and L_v are independent of the over-all

* This work was supported in part by the Signal Corps; the Office of Scientific Research, Air Research and Development Command; and the Office of Naval Research.
† Present address: Department of Chemistry, University of California, Los Angeles 24, California.
[1] D. Kivelson, J. Chem. Phys. **22**, 1733 (1954).

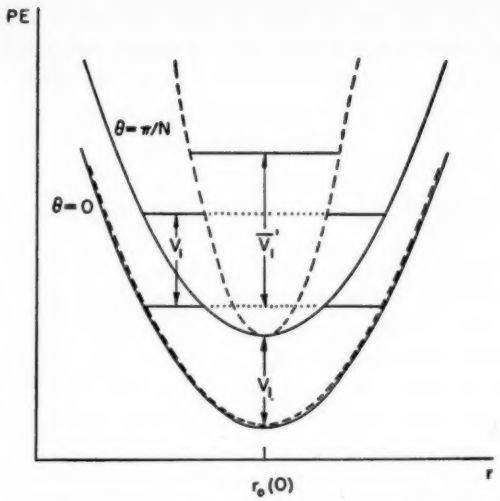

FIG. 1. Dependence of potentials upon θ with $r_0(\theta)\equiv r_0(0)$. The solid lines give the potential shape for an internal rotor in which the force constants do not change; the broken lines, for one in which the force constants depend upon θ. $\bar{V}_1' = V_1 + \Sigma\beta_{ij}^{(1)}K_{ij} \times\langle\delta r_i\delta r_j\rangle$.

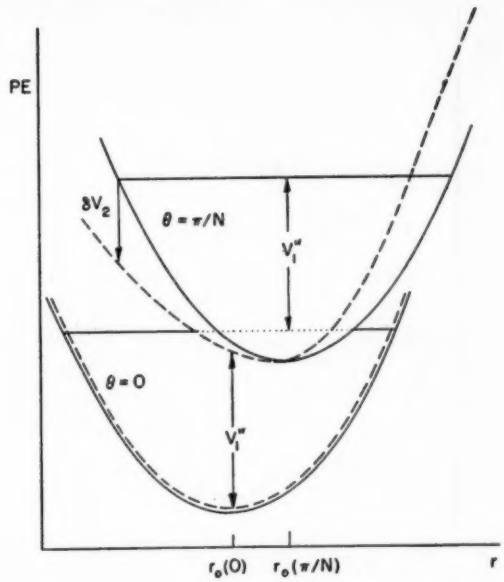

FIG. 2. Dependence of potentials and equilibrium configuration upon θ. Solid lines give potentials assuming harmonic oscillators; broken lines, for case in which the potential is distorted. $V_1'' = V_1 - 2\Sigma K_{ij}a_i^{(1)}a_j^{(1)}$; $\delta V_2 \equiv 2\Sigma K_{ij}a_j(\delta r_i)_{\min}$.

rotational quantum numbers J and K and of the internal rotational pseudo-quantum number m. B_v is the usual rigid rotor rotational constant; G_v and L_v are centrifugal distortion terms that were discussed in I; F_v is a parameter that arises from the mutual repulsion of the two functional groups that rotate with respect to each other; **II** is the internal angular momentum; and θ is the angle of internal rotation. Equation (1) was applied to methyl silane. It provided a satisfactory explanation of the microwave spectrum of this substance.

The parameter F_v depends upon the nature of the forces constituting the barrier to internal rotation. A satisfactory theory of the hindering potential should yield values of F_v in agreement with those observed experimentally. In this paper the explicit dependence of F_v upon the hindering potential will be obtained, although a study of the exact nature of this potential is beyond the scope of the present investigation.

NATURE OF THE POTENTIAL

As a zeroth-order approximation to the internal rotational problem one can consider a rotating molecule that is rigid except for internal rotation, the "rigid internal rotor." One can assume a sinusoidal potential barrier of the form $\frac{1}{2}V_1(1-\cos N\theta)$, where V_1 is a constant.[2] The next approximation assumes that the molecule may vibrate, and that these vibrations are independent of the internal rotational angle θ.[3] The potentials for a given normal vibration[4] under these conditions are shown, greatly exaggerated, by the solid curves in Fig. 1. If only one vibrational mode is considered, the barrier height V_1 is the difference between the potential minima at $\theta=0$ and at $\theta=\pi/N$, or the difference between a given vibrational level at these two values of θ. One can then add the condition that the potentials for the normal vibrations depend upon θ. This is illustrated by the broken lines in Fig. 1. The effective barrier height is now altered since it is the difference between a given vibrational level at $\theta=0$ and at $\theta=\pi/N$. One must next allow the equilibrium positions to vary with θ as shown in Fig. 2. Finally the nonsinusoidal nature of the barrier must be considered. The complete problem may be called the problem of the nonrigid internal rotor.

The origin of these effects may be explained by assuming that the bonding forces within each functional group are localized and reasonably independent of the forces within the other group except for an additional electrostatic repulsion between the two functional groups.[5] A typical potential, neglecting this electrostatic interaction, is shown by the lowest curve in Fig. 3. At $\theta=0$, the staggered position, the charges distributed over the bonds in one functional group are farthest away from the charges on the other group. The potential arising from the repulsion of these charges is shown by the solid "electrostatic" line in Fig. 3. At $\theta=\pi/N$, the eclipse position, the charges are closest and the repulsion greatest. This is shown by the broken "electro-

[2] H. H. Nielsen, Phys. Rev. **40**, 445 (1932). This potential is valid only for internal rotors in which one of the rotating groups is a symmetric rotor.

[3] It is assumed that the torsional (hindered internal rotational) mode is a normal mode and thus independent of the other normal modes in a first approximation. If the torsional motion is not a normal mode, the treatment in this paper is not quite correct. It is almost correct for CH_3OH.

[4] Vibrations, or normal modes, will refer to all normal vibrations other than torsional oscillations.

[5] E. N. Lassettre and L. B. Dean, Jr., J. Chem. Phys. **17**, 317 (1949).

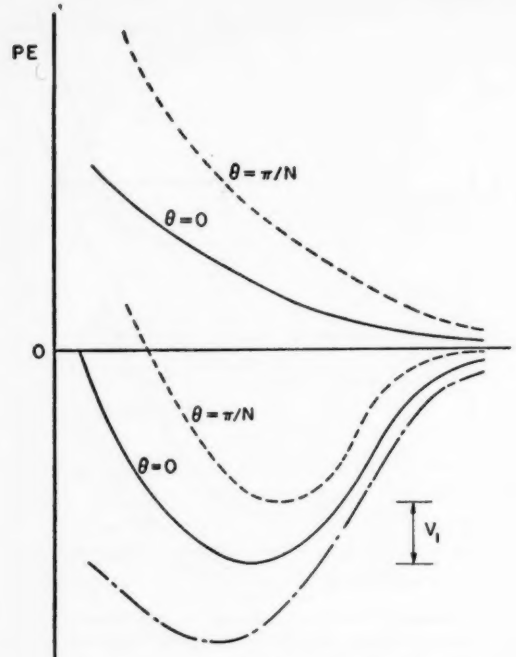

FIG. 3. Composition of potential functions. The lowest curve is the potential in which the mutual interactions of the two groups have been neglected; the upper two are electrostatic repulsive potentials; the middle two are the resultant potentials. Solid lines give potentials at $\theta=0$; broken one at $\theta=\pi/N$ (exaggerated).

static" curve in Fig. 3. The resultant potentials for these two extreme cases are also shown in Fig. 3. This picture of the potential barrier gives at least a possible qualitative explanation of the effects discussed and is the basis of some calculations carried out in the appendix. However, the following analysis is more general and does not depend upon this model.

EXPANSION OF THE POTENTIAL

The potential for the nonrigid internal rotor is a function of the angle of internal rotation, θ, as well as of the internal coordinates, r_i. The usual assumption that this potential can be expanded in terms of a Taylor's series in r_i about the equilibrium position r_{0i} will be made. It will also be assumed that the θ dependence can be expressed in terms of a rapidly converging Fourier series. If the discussion is limited to rotors that are symmetrical about $\theta=0$ and have a period of $2\pi/N$ in θ, the Fourier expansion can be developed in terms of $\cos N\theta$, or for convenience, in terms of $(1-\cos N\theta)$. If the ith internal displacement coordinate is given by the relation

$$\delta r_i = r_i - r_{0i}, \tag{2}$$

the potential may be written as

$$P.E.=\sum_n \sum_{ijk}[A^{(n)}+A_i^{(n)}\delta r_i+A_{ij}^{(n)}\delta r_i\delta r_j + A_{ijk}^{(n)}\delta r_i\delta r_j\delta r_k+\cdots](1-\cos nN\theta)+V_v+V_{va} \tag{3}$$

where the A's are parameters that are independent of δr_i and of θ. At $\theta=0$ the potential energy reduces to the usual form for the vibrational problem, that is, to V_v+V_{va}, where

$$V_v=V_0+\tfrac{1}{2}\sum_{ij}K_{ij}\delta r_i\delta r_j \tag{4}$$

$$V_{va}=\tfrac{1}{2}\sum K_{ijk}\delta r_i\delta r_j\delta r_k+\tfrac{1}{2}\sum K_{ijkl}\delta r_i\delta r_j\delta r_k\delta r_l+\cdots. \tag{5}$$

V_v is the harmonic potential, while V_{va} accounts for the nonharmonicity of the problem. V_0 is just a constant term that does not affect the results and so it will be dropped. Comparison of Eqs. (4) and (5) with Eq. (3) indicates that $A_i^{(0)}$ vanishes and that $A^{(0)}$ can be dropped. This comparison also yields values for the remaining A's for which $n=0$.

For the sake of the perturbation calculations that are to be carried out below it is necessary to arrange the terms in orders of some parameter λ. It will be postulated that the order of the term can be determined by adding $(2n-2)$ to the number of subscripts on the A's. The calculations in this paper will be carried out to second order. In the appendix some order-of-magnitude calculations are given to help justify this assignment of orders.

In order to get the problem into convenient form the following substitutions may be made:

$$A^{(n)}=\tfrac{1}{2}V_n \tag{6}$$

$$A_i^{(n)}=\sum_j K_{ij}a_j^{(n)} \tag{7}$$

$$A_{ij}^{(n)}=\tfrac{1}{2}\beta_{ij}^{(n)}K_{ij}. \tag{8}$$

V_n, $a_i^{(n)}$, $\beta_{ij}^{(n)}$ are independent of δr_i and θ. The potential energy may be written as the sum of the "pure" vibrational energy, V_v+V_{va}, plus the internal rotational potential energy, V_{int}, where to second order

$$V_{\text{int}}=\tfrac{1}{2}\sum[V_1+\lambda 2K_{ij}a_i^{(1)}\delta r_j + \lambda^2\beta_{ij}^{(1)}K_{ij}\delta r_i\delta r_j](1-\cos N\theta) + \lambda^2\tfrac{1}{2}V_2(1-\cos 2N\theta). \tag{9}$$

The λ's have been inserted to indicate the order of each term, but they will be set equal to unity in the final results. In Eqs. (4) and (5) the terms in K_{ij}, K_{ijk}, K_{ijkl}, are of order λ^0, λ^1, λ^2, respectively.

If the zeroth-order terms are considerably larger than all higher-order terms, an approximate physical interpretation of $a_i^{(1)}$ may be obtained. At $\theta=0$ the equilibrium configuration of the molecule occurs when the coordinate r_i has the value r_{0i}. At any other value of θ it is readily seen that the molecular "equilibrium" configuration occurs approximately at $r_{0i}+a_i^{(1)}\times(1-\cos N\theta)$. Thus the shift in the "equilibrium" value of r_i in going from $\theta=0$ to $\theta=\pi/N$ is $2a_i^{(1)}$. The other constants appearing in Eq. (9) will be discussed in the following.

EXPANSION OF THE ROTATIONAL HAMILTONIAN

The Hamiltonian for the present problem may be written as[6]

$$\mathbf{H}(\theta)=\mathbf{H}_v+V_{va}+\mathbf{H}_R+\mathbf{T}_I+V_{\text{int}}, \tag{10}$$

where $\mathbf{H}_v$ is the Hamiltonian for harmonic oscillations, that is, the one with potential energy V_v; $\mathbf{H}_R$ is the Hamiltonian corresponding to over-all rotations, while $\mathbf{T}_I$ represents the kinetic energy of internal rotation.

$\mathbf{H}_R$ may be expanded in terms of displacements from vibrational equilibrium. Thus,

$$\begin{aligned}\mathbf{H}_R=\sum B_{\alpha\beta}\mathbf{P}_\alpha\mathbf{P}_\beta&=\sum B_{\alpha\beta}{}^{(0)}\mathbf{P}_\alpha\mathbf{P}_\beta\\&+\lambda\sum B_{\alpha\beta}{}^{(i)}\delta r_i\mathbf{P}_\alpha\mathbf{P}_\beta\\&+\lambda^2\tfrac{1}{2}\sum B_{\alpha\beta}{}^{(ij)}\delta r_i\delta r_j\mathbf{P}_\alpha\mathbf{P}_\beta+\cdots.\end{aligned} \tag{11}$$

Except for constant factors, $B_{\alpha\beta}$ is closely related to the $\alpha\beta$ component of the instantaneous inverse inertia tensor.[7] $B_{\alpha\beta}{}^{(0)}$ is the equilibrium value of $B_{\alpha\beta}$; $B_{\alpha\beta}{}^{(i)}$ and $B_{\alpha\beta}{}^{(ij)}$ are the first and second derivatives, respectively, with respect to δr_i and δr_j evaluated at equilibrium. For molecules without an axis of symmetry, $B_{\alpha\beta}{}^{(0)}$ differs slightly from the value of the equilibrium inverse inertia tensor. This difference is discussed in the following paper which will be referred to as III.[8]

$\mathbf{T}_I$ may be treated in a similar manner. The expression for $\mathbf{T}_I$ derived in III is

$$\begin{aligned}\mathbf{T}_I=\sum\{B_\alpha\mathbf{P}_\alpha,\mathbf{\Pi}\}+B_\pi\mathbf{\Pi}^2&=\sum\{B_\alpha{}^{(0)}\mathbf{P}_\alpha,\mathbf{\Pi}\}+B_\pi{}^{(0)}\mathbf{\Pi}^2\\&+\lambda\sum\{B_\alpha{}^{(i)}\mathbf{P}_\alpha,\mathbf{\Pi}\}\delta r_i+\lambda\sum B_\pi{}^{(i)}\delta r_i\mathbf{\Pi}^2+\cdots.\end{aligned} \tag{12}$$

The B_α's and B_π, as well as the definition of the internal angular momentum $\mathbf{\Pi}$, are given in III. $\{\mathbf{A},\mathbf{B}\}$ represents the symmetrized product $\mathbf{AB}+\mathbf{BA}$.

SOLUTION

$\mathbf{H}(\theta)$ can be written in the form

$$\mathbf{H}(\theta)=\mathbf{H}_0+\lambda\mathbf{H}_1+\lambda^2\mathbf{H}_2, \tag{13}$$

where the various components of each term in this equation have been described in the foregoing. The vibrational and rotational parts of this Hamiltonian can be separated by means of a Van Vleck perturbation.[9] The results to second order are

$$\begin{aligned}(v|\mathbf{H}(\theta)|v)=(v|\mathbf{H}_0|v)&+\lambda(v|\mathbf{H}_1|v)\\&+\lambda^2(v|\mathbf{H}_2|v)+\lambda^2\sum_{v'}{}'(v|\mathbf{H}_1|v')^2/h\nu_{vv'},\end{aligned} \tag{13a}$$

where v represents the vth harmonic oscillator functions and

$$h\nu_{vv'}=W_v-W_{v'}, \tag{14}$$

where W_v is the energy corresponding to the vth harmonic oscillator state and $v'\neq v$.

The terms in this transformed Hamiltonian that are independent of θ and of $\mathbf{\Pi}$ constitute the usual vibration-rotation Hamiltonian described by Wilson and Howard[6] and are given by the formula

$$\mathbf{H}_{vr}=\mathbf{W}_v+\langle\mathbf{H}\rangle_R+\sum_{v'}{}'(v|\mathbf{H}_R|v')^2/h\nu_{vv'}, \tag{15}$$

where $\mathbf{W}_v$ is the pure vibrational energy including anharmonic terms, $\langle\mathbf{H}\rangle_R$ is the usual effective rigid rotor Hamiltonian in a given vibrational state.[10] The last term in Eq. (15) is a centrifugal distortion term that can be evaluated by previously discussed methods.[11] The terms in the Hamiltonian given by Eq. (13) that are independent of θ but depend upon $\mathbf{\Pi}$ may be written as

$$\begin{aligned}\mathbf{H}_{vI}=\langle\mathbf{T}\rangle_I+\sum_{v'}{}'[(v|\mathbf{H}_R+\mathbf{T}_I|v')^2&\\-(v|\mathbf{H}_R|v')^2]/h\nu_{vv'}.&\end{aligned} \tag{16}$$

$\mathbf{T}_I$ is the effective internal rotational kinetic energy corresponding to $\langle\mathbf{H}\rangle_R$. The last term in Eq. (16) is acentrifugal distortion term that can be treated as described in III.

The remaining terms in the general Hamiltonian all involve θ explicitly. It is useful to note the relation

$$-\tfrac{1}{2}(K^{-1})_{ij}=\sum_{v'}{}'(v|\delta r_i|v')(v'|\delta r_j|v)/h\nu_{vv'}, \tag{17}$$

where $(K^{-1})_{ij}$ is an element of the inverse matrix of K_{ij}. The terms in θ that do not contain any B's constitute the effective potential hindering internal rotation, $\bar{V}_{\text{int}}$. These terms are

$$\begin{aligned}\bar{V}_{\text{int}}&=\tfrac{1}{2}\sum[V_1+\beta_{ij}{}^{(1)}K_{ij}(v|\delta r_i\delta r_j|v)\\&\quad-3K_{ijk}a_k{}^{(1)}(v|\delta r_i\delta r_j|v)-2a_i{}^{(1)}a_j{}^{(1)}](1-\cos N\theta)\\&\quad+\tfrac{1}{2}\sum[V_2+\tfrac{1}{2}a_i{}^{(1)}a_j{}^{(1)}](1-\cos 2N\theta)\\&=\tfrac{1}{2}\bar{V}_1(1-\cos N\theta)+\tfrac{1}{2}\bar{V}_2(1-\cos 2N\theta).\end{aligned} \tag{18}$$

It will be helpful at this point to consider the nature of this effective "hindering" barrier. The $(1-\cos 2N\theta)$ term accounts for deviation of the barrier from a sinusoidal form. This term should ordinarily be quite small.[12]

[6] This Hamiltonian is a generalization of the one given by E. B. Wilson, Jr., and J. B. Howard, J. Chem. Phys. 4, 260 (1936). Terms that include the effects of Coriolis force have been neglected, since, to the order discussed here, they will not affect the interactions between over-all and internal rotations.

[7] $B_{\alpha\beta}$ differs slightly from the instantaneous inverse inertia tensor even in the problem not involving internal rotation for it includes a contribution due to Coriolis interactions. See reference 6.

[8] D. Kivelson, J. Chem. Phys. **23**, 2236 (1955). Hereinafter called III.

[9] E. C. Kemble, *The Fundamental Principles of Quantum Mechanics* (McGraw-Hill Book Company, Inc., New York, 1937), p. 394. See also reference 6.

[10] H. H. Nielsen, Revs. Modern Phys. **23**, 90 (1951). $\langle\mathbf{H}\rangle_R$ also contains some effects of Coriolis interactions.

[11] E. B. Wilson, Jr., J. Chem. Phys. **5**, 617 (1937). D. Kivelson and E. B. Wilson, Jr., J. Chem. Phys. **21**, 1229 (1953).

[12] K. B. Pitzer and J. L. Hollenberg, J. Am. Chem. Soc. **75**, 2123 (1953).

The sinusoidal barrier is dependent upon the vibrational coordinates. The effect of the $K_{ij}\beta_{ij}^{(1)}$ terms on the potential barrier is shown in Fig. 1. The effective barrier height is altered because the vibrational levels in the two θ positions are not at equal heights above the potential minimum. The $K_{ij}\beta_{ij}^{(1)}$ terms could also be interpreted as corrections to the harmonic vibrational potential resulting from interactions between vibrations and internal rotations. Some approximate calculations on the order of magnitude of this effect are given in the Appendix. The $K_{ij}a_j^{(1)}\delta r_i$ terms that enter into the potential in Eq. (9) contribute to the effective barrier only in third order except for the constant $a_i^{(1)}a_j^{(1)}$ terms. The effect of these terms is shown in Fig. 2. The barrier is altered because, even if the vibrational well is harmonic at $\theta=0$, it will deviate slightly from harmonicity at $\theta=\pi/N$. For example, at the minimum value of δr_i, $(\delta r_i)_{\min}$, the barrier is depressed by an amount labeled δV_2 in Fig. 2.

Finally one must consider the terms in the Hamiltonian that involve both the B's and θ. By combining Eqs. (9), (11), (12), and (17) in the manner prescribed by Eq. (13a) one obtains

$$\mathbf{H}_{IR}=-\sum B_{\alpha\beta}^{(i)}a_i^{(1)}\mathbf{P}_\alpha\mathbf{P}_\beta(1-\cos N\theta)-\tfrac{1}{2}\sum B_\alpha^{(i)}a_i^{(1)}\{\{\mathbf{P}_\alpha,\mathbf{\Pi}\},(1-\cos N\theta)\}-\tfrac{1}{2}\sum B_\pi^{(i)}a_i^{(1)}\{\mathbf{\Pi}^2,1-\cos N\theta\}. \quad (19)$$

Neglecting the pure vibrational terms, the Hamiltonian for the nonrigid internal rotor may be written as

$$\mathbf{H}=\langle\mathbf{H}\rangle_R+\langle\mathbf{T}\rangle_I+\tfrac{1}{2}\bar{V}_1(1-\cos N\theta)+\tfrac{1}{2}\bar{V}_2(1-\cos 2N\theta)-\sum B_{\alpha\beta}^{(i)}a_i^{(1)}\mathbf{P}_\alpha\mathbf{P}_\beta(1-\cos N\theta)-\tfrac{1}{2}\sum B_\alpha^{(i)}a_i^{(1)}\times\{\{\mathbf{P}_\alpha,\mathbf{\Pi}\},(1-\cos N\theta)\}-\tfrac{1}{2}\sum B_\pi^{(i)}a_i^{(1)}\{\mathbf{\Pi}^2,1-\cos N\theta\}+\sum_{v'}{}'(v|\mathbf{H}_R+\mathbf{T}_I|v')^2/h\nu_{vv'}. \quad (20)$$

The first three terms in the Hamiltonian constitute the usual rigid internal rotor problem. The fourth term accounts for the nonsinusoidal nature of the barrier. The next three terms arise from the interaction of internal with over-all rotations because of the repulsive nature of the barrier. These terms are attributable to the changes in the equilibrium configuration with changes in θ. They give rise to a pulsating motion closely correlated to changes in θ. The last term is also an interaction term that results from centrifugal distortion effects.

The parameters $\sum_i B_{\alpha\beta}^{(i)}a_i^{(1)}$ can be evaluated from rotational data. The quantity $B_{\alpha\beta}^{(i)}$ can be evaluated from geometric considerations. Thus, certain relations between the $a_i^{(1)}$'s can be obtained. These $a_i^{(1)}$'s depend upon the repulsive forces constituting the barrier to internal rotation and so should be an aid in determining these forces or at least should serve as a check on any theory of internal rotation.

SYMMETRIC ROTORS

When dealing with symmetric rotors Eq. (20) can be evaluated in the JKm basis as was done in I. Applying the selection rules $\Delta J=1$, $\Delta K=0$, $\Delta m=0$, one obtains an equation of the form of Eq. (1) for the frequencies of the rotational transitions. By comparison it is seen that the repulsive constant F_v is given by the relation

$$F_v=-\sum_i\tfrac{1}{2}[B_{xx}^{(i)}+B_{yy}^{(i)}]a_i^{(1)}. \quad (21)$$

Since the potential energy must be invariant under the symmetry operations of the point group to which the molecule belongs, it is useful to transform from internal displacement to symmetry coordinates.[13] It is then seen that the δr_j that enters in the $K_{ij}a_i^{(1)}\delta r_j\times(1-\cos N\theta)$ term in Eq. (9) must belong to a totally symmetric species. Since the potential constants K_{ij} connect only symmetry coordinates belonging to the same species, the $B_{\alpha\beta}^{(i)}$'s that enter into Eq. (20) represent derivatives of $B_{\alpha\beta}$ with respect to a totally symmetric coordinate δr_i. This greatly reduces the number of $a_i^{(1)}$'s that need be considered. For a symmetric rotor of C_{3v} symmetry, the $B_{xx}^{(i)}$ and $B_{yy}^{(i)}$ that enter into Eq. (21) refer to derivatives with respect to coordinates belonging only to the A_1 species.

ACKNOWLEDGMENTS

Many thanks are due my wife, Margaret G. Kivelson, for her criticism and advice.

APPENDIX

On the basis of the model discussed in the second section[5] and illustrated in Fig. 3, rough calculations can be made to estimate the orders of magnitude of $a_i^{(1)}$ and $\beta_{ij}^{(1)}$. According to this picture, the potential energy, neglecting the interaction energy between the two functional groups that rotate with respect to each other, may be written as a function f of the internal coordinates. This energy is represented by the lowest curve in Fig. 3. It is then assumed that the interaction energy is electrostatic in nature and can be represented by a general multipole interaction expansion, that is, by $\sum_{l,m,n}S_{lm}^{(n)}/R_{lm}(\theta,r)^n$ where $S_{lm}^{(n)}$ is equal to the product of the two interacting multipoles on the lth and mth bonds times an orientation factor; R_{lm} is the distance between the interacting multipoles on the lth and mth bonds, and r stands for all the internal coordinates. n is equal to $n'+n''+1$ where the two interacting multipoles are of order n' and n''. Thus, the second lowest curve in Fig. 3, the potential function at $\theta=0$, can be expressed as

$$f+\sum S_{lm}^{(n)}(0,r)/R_{lm}(0,r)^n=V_0+\tfrac{1}{2}\sum K_{ij}\delta r_i\delta r_j+\cdots. \quad (A1)$$

[13] J. B. Howard and E. B. Wilson, Jr., J. Chem. Phys. 2, 620 (1934).

TABLE I. Order-of-magnitude calculations on methyl silane. $V_0=550$ cm^{-1}; $n=5$.

Internal displacement	$K_{kk}\times10^5$ dynes/cm	$R^{-1}(\partial R/\partial r_k)$ A^{0-1}	$(\partial^2 R/\partial r_k^2)$ A^{0-1}	$a_k^{(1)}$ A^0	$-B_{zz}^{(k)}a_k^{(1)}/(n+1)$ Mc/sec[a]	$a_k^{(1)}/\langle\delta r_k\rangle$[d]	$\beta_{kk}^{(1)}$
δr_{CH}	5.04[b]	0.0416	0.086	−0.00028	−0.061	0.003	−0.00013
$r_{CH}\delta\theta_{HCH}$	0.461[b]	0.174	−0.0408	−0.013	−4.03	0.069	0.016
δr_{SiH}	2.84[b]	0.0696	0.0754	−0.00080	−0.172	0.010	0.00007
$r_{SiH}\delta\theta_{HSiH}$	0.184[b]	0.174	−0.0513	−0.030	−5.60	0.148	0.040
δr_{CSi}	4[c]	0.364	0	−0.003	−3.46	0.066	0.0065

[a] The sum of this column $=F_v=-13.2(n+1)$.
[b] G. Herzberg, *Infrared and Raman Spectra* (D. Van Nostrand Company, Inc., New York, 1949), p. 182.
[c] Interpolated value.
[d] Based on root-mean-square displacements for CH_4 and SiH_4 as given by Herzberg, and upon an estimated value for the displacement of the CSi bond.

The third lowest curve in Fig. 3, the potential curve at $\theta=\pi/N$, can be expressed as

$$\dot{f}+\sum S_{lm}^{(n)}(\pi/N,r)/R_{lm}(\pi/N,r)^n = V_0+V_1+\sum 2K_{ij}\delta r_i a_j^{(1)} +\tfrac{1}{2}\sum K_{ij}\delta r_i\delta r_j+\sum\beta_{ij}^{(1)}K_{ij}\delta r_i\delta r_j+\cdots \quad \text{(A2)}$$

[see Eq. (9)]. For the present order-of-magnitude calculations it will be assumed that the interaction potential can be adequately represented by the aid of only one distance R, that the corresponding S is unchanged in going from $\theta=0$ to $\theta=\pi/N$ and so may be treated as a constant. Furthermore, it will be assumed that the variation in R in going from $\theta=0$ to $\theta=\pi/N$ is small. And, finally, all the off-diagonal elements of K_{ij} will be neglected. With these rather drastic approximations one obtains

$$V_1=Sn\Delta R/R_0^{n+1}, \quad \text{(A3)}$$

where R_0 is the equilibrium value of R at $\theta=0$, and ΔR is the change in R in going from $\theta=0$ to $\theta=\pi/N$. Furthermore,

$$a_k^{(1)}=-\tfrac{1}{2}(V_1/K_{kk})(n+1)(\partial R/\partial r_k) \quad \text{(A4)}$$

$$\beta_{kk}^{(1)}=\tfrac{1}{2}(V_1/K_{kk})(n+1) \times[(n+2)R_0^{-2}(\partial R/\partial r_k)^2-R_0^{-1}(\partial^2 R/\partial r_k^2)]. \quad \text{(A5)}$$

These two equations have been used to carry out some very crude calculations on methyl silane. The summary of these computations is given in Table I. V_1 for methyl silane was taken as 550 cm^{-1}. The distance R was taken to be approximately the distance from the center of a CH bond to the center of the nearest SiH bond. The derivatives of R were evaluated in a very rough fashion. Since the sum of the entries in column six, of the table should yield F_v and since F_v for methyl silane has been found experimentally to be −65.3 Mc/sec, it is seen that n should be about 4. This value of n indicates that the interaction is probably primarily dipole-quadrupole or quadrupole-quadrupole, or a combination of both. More precise computations would be required to distinguish the exact nature of the interaction. The present numerical work at least indicates that the theory predicts the right order of magnitude for the parameter F_v.

The displacement $a_k^{(1)}$ should be compared to the root-mean-square displacement of r_k, $\langle\delta r_k\rangle$.

$$\langle\delta r_k\rangle=(h\bar{\nu}_k c/K_{kk})^{\frac{1}{2}}(v_k+\tfrac{1}{2})^{\frac{1}{2}}, \quad \text{(A6)}$$

where $\bar{\nu}_k$ is the kth vibrational frequency in wave numbers and v_k is the kth vibrational quantum number. Values of $\langle\delta r_k\rangle$ were calculated for the corresponding displacements in CH_4 and SiH_4, and an estimate was made for the $\langle\delta r_{CSi}\rangle$ coordinate. With these values of $\langle\delta r_k\rangle$, the quantities $a_k^{(1)}/\langle\delta r_k\rangle$ and $\beta_{kk}^{(1)}$ were evaluated and entered in Table I. n was taken as 5 for these entries. Comparison of the last two columns in Table I indicates that the arrangement of orders in Eq. (9) is reasonable.

Theory of Internal Over-All Rotational Interactions. III. Nonrigid Asymmetric Rotors

DANIEL KIVELSON*†
Research Laboratory of Electronics and Department of Physics, Massachusetts Institute of Technology, Cambridge, Massachusetts
(Received January 7, 1955)

The theory of the interactions of hindered internal rotation with over-all rotations is extended to include nonrigid asymmetric rotors. The interdependence of hindered internal rotation and vibrations and their effect upon the vibrational energy levels is considered. The theory is developed analogously to the theory developed for symmetric rotors in a previous paper. An approximate over-all internal rotational wave function of the form $1/(2\pi)^{\frac{1}{2}} \exp[i(\mathbf{P}_z I_{z2}/I_z - \tau)]\Phi_\tau$ is discussed, where Φ_τ is the wave function that diagonalizes the rigid rotor Hamiltonian and τ is an integer.

While the general energy relation involves too many parameters to compute or to fit empirically, certain special cases are discussed. In particular for the $0_{00} \rightarrow 1_{01}$ transition of the CH_3NO_2 type of molecule one has

$$\nu(0_{00} \rightarrow 1_{01}) = (1_{01}|\langle \mathbf{H} \rangle_R|1_{01})[1 + F_1(m|1-\cos 3\theta|m) + G_2(m|\mathbf{\Pi}^2|m)] + 2G_3(m|\mathbf{\Pi}^2|m) + 2F_2(m|1-\cos 3\theta|m),$$

where $(1_{01}|\langle \mathbf{H} \rangle_R|1_{01})$ is the rigid rotor energy for the 1_{01} level, θ is the angle of internal rotation, $\mathbf{\Pi}$ is the internal angular momentum, m indicates a given internal rotational level, and the F's and G's are constants which can be evaluated from a knowledge of the vibrational characteristics of the molecule and of the forces that constitute the hindering barrier to internal rotation.

INTRODUCTION

IN this paper, the theory of the nonrigid internal asymmetric rotor will be considered in much the same way as the corresponding symmetric rotor was considered in a previous paper.[1] In rigid internal symmetric rotors, that is, in symmetric rotors where the only degree of internal freedom is that of internal rotation, the internal and the over-all rotational Hamiltonians are separable except for an interrelation resulting from the imposition of boundary conditions.[2] This boundary condition introduces a dependence upon K, the quantum number corresponding to the component of total angular momentum along the figure axis, into the internal rotational energy. The over-all rotational spectrum is unaffected by this interrelation and would be the same as that of a rigid rotor were it not for the fact that molecules are nonrigid internal rotors. The internal and the over-all rotational motions can interact with the other internal motions of the molecule, that is, with the vibrations, and by means of the vibrations the two rotational motions can interact with each other. This vibrational interaction gives rise to centrifugal distortion terms in the energy and to terms that account for the repulsion of the constituent groups as they pass through the hindering barrier.

In asymmetric rotors the problem is considerably more complicated. The two rotational motions are no longer separable, even in the limit of a rigid internal rotor. The rigid internal rotor has been discussed by several authors[3] and will be treated in a new way below. The problem of the nonrigid asymmetric rotor has not been previously considered and will be the principal subject of this paper. The interactions of the rotations by means of the vibrations, although smaller than the direct interactions of the rotational motions that occur even in the rigid internal rotor, are not negligible. This can be seen in symmetric rotors where the latter is the only interaction present.

The existing treatments of the rigid internal asymmetric rotors are not suited for the consideration of a nonrigid internal rotor. Therefore, the first half of this paper will be devoted to a new method of obtaining the energy levels for the rigid internal rotor. Since the general asymmetric rotor is very difficult to treat, it will be advantageous to start with a special case and then to extend it.

RIGID INTERNAL SEMISYMMETRIC ROTORS

A semisymmetric rotor will be defined as a molecule with two constituent groups, one of which is a symmetric rotor (CH_3), in which the figure axis of the symmetric rotor group is a principal axis of the molecule. CH_3NO_2 is such a molecule. This class of molecules has the property that the principal axes of the molecule are simultaneously the principal axes of each constituent group. If the subscript 2 refers to the symmetric rotor group (CH_3) and 1 refers to the other group (NO_2), the kinetic energy may be written as

$$2T = \sum_{i=1}^{2} [I_{xi}\omega_{xi}^2 + I_{yi}\omega_{yi}^2 + I_{zi}\omega_{zi}^2], \qquad (1)$$

where $\mathbf{I}_1$ and $\mathbf{I}_2$ are the inertia tensors of the two constituent groups, $\boldsymbol{\omega}_i$ is the angular velocity, and the

* This work was supported in part by the Signal Corps; the Office of Scientific Research, Air Research and Development Command; and the Office of Naval Research.

† Present address: Department of Chemistry, University of California, Los Angeles, California.

[1] D. Kivelson, J. Chem. Phys. **22**, 1733 (1954). This paper will be referred to as I.

[2] J. S. Koehler and D. M. Dennison, Phys. Rev. **57**, 1006 (1940).

[3] (a) D. G. Burkhard and D. M. Dennison, Phys. Rev. **84**, 408 (1951). (b) Wilson, Lin, and Lide, J. Chem. Phys. **23**, 136 (1955). (c) D. G. Burkhard, J. Chem. Phys. **21**, 1541 (1953).

axes are the principal axes of the molecule; that is, the coordinate system with the z axis along the axis of internal rotation (C−N bond) and the x and y axes fixed in the nonsymmetric rotor group (NO_2). The molecule has only one degree of internal rotational freedom, the motion about the z-axis. Thus,

$$\begin{aligned}\omega_{x1}&=\omega_{x2}=\omega_x,\\ \omega_{y1}&=\omega_{y2}=\omega_y.\end{aligned}\tag{2}$$

Using

$$\mathbf{I}=\mathbf{I}_1+\mathbf{I}_2,\tag{3}$$

one can re-express the kinetic energy as

$$2T=I_x\omega_x^2+I_y\omega_y^2+I_{z1}\omega_{z1}^2+I_{z2}\omega_{z2}^2.\tag{4}$$

If γ_1 is the angle of rotation about the z-axis of group 1, and γ_2 is the corresponding angle for group 2, then ω_x and ω_y are functions of γ_1 since the principal axes move with group 1. ω_{z1} and ω_{z2} are functions of $\dot{\gamma}_1$ and $\dot{\gamma}_2$, respectively.[4] Let

$$\omega_z=\omega_{z1}I_{z1}/I_z+\omega_{z2}I_{z2}/I_z,\tag{5}$$

$$\omega_\theta=\omega_{z2}-\omega_{z1}.\tag{6}$$

This corresponds to the substitutions of angles.

$$\gamma=\gamma_1 I_{z1}/I_z+\gamma_2 I_{z2}/I_z,\tag{7}$$

$$\theta=\gamma_2-\gamma_1.\tag{8}$$

If these substitutions are made, the kinetic energy may be rewritten as

$$\begin{aligned}2T&=[I_x\omega_x^2+I_y\omega_y^2+I_z\omega_z^2]+\omega_\theta^2 I_{z1}I_{z2}/I_z\\ &=2T_R(\gamma-\theta I_{z2}/I_z)+2T_I.\end{aligned}\tag{9}$$

All the components of the inertia tensor are independent of the rotational angles. T_R is the kinetic energy corresponding to a pseudo-rigid rotor, while T_I corresponds to the kinetic energy of internal rotation. ω_x and ω_y are functions of $(\gamma-\theta I_{z2}/I_z)$. Thus the kinetic energy T_R depends upon the angle θ, the angle of internal rotation. If $\theta\equiv 0$, $T_R(\gamma)$ is the kinetic energy of a rigid rotor in which γ is the angle of rotation about the z axis.

By the usual transformations, Eqs. (9) become

$$\begin{aligned}2\mathbf{H}&=[\mathbf{P}_x^2/I_x+\mathbf{P}_y^2/I_y+\mathbf{P}_z^2/I_z]+\boldsymbol{\Pi}^2 I_z/I_{z1}I_{z2}\\ &=2\mathbf{H}_R(\gamma-\theta I_{z2}/I_z)+2\mathbf{H}_I,\end{aligned}\tag{10}$$

where $\mathbf{H}_R$ is the Hamiltonian of a pseudo-rigid rotor; $\mathbf{H}_I$ is the Hamiltonian of internal rotation; $\mathbf{P}_x$, $\mathbf{P}_y$, and $\mathbf{P}_z$ are components of total angular momentum conjugate to ω_x, ω_y, and ω_z, respectively; and $\boldsymbol{\Pi}$ is the internal angular momentum and is conjugate to ω_θ. $\mathbf{P}_x$ and $\mathbf{P}_y$ are functions of $(\gamma-\theta I_{z2}/I_z)$. If $\theta\equiv 0$, $\mathbf{H}_R(\gamma)$ becomes the rigid rotor Hamiltonian.

The two Hamiltonians are thus separable except for the dependence of $\mathbf{H}_R$ on θ, and for the interrelation resulting from boundary conditions. The boundary conditions may be inferred from the relation

$$\boldsymbol{\Pi}=-\mathbf{P}_z I_{z2}/I_z+\mathbf{p}_{z2},\tag{11}$$

where $\mathbf{p}_{z2}$ is conjugate to ω_{z2}. In units of $\hbar$ one has

$$\begin{aligned}\mathbf{P}_z&=-i(\partial/\partial\gamma)_\theta,\\ \mathbf{p}_{z2}&=-i(\partial/\partial\gamma_2)_{\gamma 1},\\ \boldsymbol{\Pi}&=-i(\partial/\partial\theta)_\gamma.\end{aligned}\tag{12}$$

There are several ways of obtaining a solution to Eq. (10).[3] In the present work, the approach should be one in which the basis functions afford the best separation of internal from over-all rotational motions yielding, at the same time, good approximations to the true wave functions. Furthermore, they should easily be adaptable to the problem of hindered internal rotation. A suitable basis function that includes both the effects of internal rotation and of the asymmetry of the molecule is

$$\Psi_{r\tau}=(2\pi)^{-\frac{1}{2}}\exp[i(-\mathbf{P}_z I_{z2}/I_z+\tau)\theta]\Phi_r,\tag{13}$$

where τ is an integer, Φ_r is an eigenfunction corresponding to the usual rigid rotor Hamiltonian, $\mathbf{H}_R(\gamma)$, and r represents the rigid rotor quantum numbers J and $K_{-1}K_1$;[5] τ is the quantum number that represents the z-component of angular momentum of the symmetric rotor group. It is clear that for a symmetric rotor this basis function reduces to the wave function

$$\Psi_{JK\tau}=(2\pi)^{-\frac{1}{2}}\exp[i(-KI_{z2}/I_z+\tau)\theta]\Phi_{JK}\tag{14}$$

given by Koehler and Dennison.[2]

The wave function in Eq. (13) must be treated with caution because of the operator in the exponent. First consider the matrix elements of $\mathbf{H}_R(\gamma-\theta I_{z2}/I_z)$ in this basis.

$$\begin{aligned}&(r'\tau'|\mathbf{H}_R(\gamma-\theta I_{z2}/I_z)|r\tau)\\ &=(2\pi)^{-1}\int\Phi_{r'}^*\{\exp[+i\theta\mathbf{P}_z I_{z2}/I_z]\\ &\quad\times\mathbf{H}_R(\gamma-\theta I_{z2}/I_z)\exp[-i\theta\mathbf{P}_z I_{z2}/I_z]\}\Phi_r\\ &\quad\times\exp[i(\tau-\tau')]dv.\end{aligned}\tag{15}$$

The expression in brackets on the right-hand side of this equation is just $\mathbf{H}_R(\gamma-\theta I_{z2}/I_z+\theta I_{z2}/I_z)$.[6] Thus if $W_R(r)$ is the usual rigid rotor energy,

$$(r'\tau'|\mathbf{H}_R(\gamma-\theta I_{z2}/I_z)|r\tau)=W_R(r)\delta_{r'r}\delta_{\tau'\tau}.\tag{16}$$

In this basis, the rigid rotor part is independent of θ and is diagonal in both r and τ.

[4] See, for example, H. Margenau and G. M. Murphy, *The Mathematics of Physics and Chemistry* (D. Van Nostrand Company, Inc., New York, 1943), p. 275.

[5] King, Hainer, and Cross, J. Chem. Phys. **11**, 27 (1943).

[6] This is just a form of Taylor's theorem that states that $\exp[-\alpha(\partial/\partial x)]f(x)\exp[\alpha(\partial/\partial x)]=f(x+\alpha)$ provided $\partial\alpha/\partial x=0$.

Now consider the matrix elements of $\mathbf{H}_I$ in this basis.

$$(\tau'\tau'|\mathbf{H}_I|\tau\tau)=-\tfrac{1}{2}(I_z/I_{z1}I_{z2})\int\Psi_{\tau'\tau'}^*\frac{\partial^2}{\partial\theta^2}\Psi_{\tau\tau}dv$$
$$=\tfrac{1}{2}(I_z/I_{z1}I_{z2})(\tau'|(\mathbf{P}_zI_{z2}/I_z-\tau)^2|\tau)\delta_{\tau\tau'}$$
$$=\tfrac{1}{2}(I_z/I_{z1}I_{z2})S_{\tau\tau'\tau}\delta_{\tau\tau'}. \quad (17)$$

Here $\mathbf{H}_I$ is diagonal in τ but not in τ. If the molecule is not too asymmetric, the $(\tau'|\mathbf{H}_I|\tau)$ elements will be small if $\tau'\neq\tau$, and so $\Psi_{\tau\tau}$ will be a good approximation to the true wave function. If a more accurate value of the energy or a more exact wave function is desired, it may be obtained from Eqs. (16) and (17) by a perturbation calculation. $S_{\tau\tau'\tau}$ is defined by Eq. (17); it will be useful in considering other aspects of the problem.

$W_R(\tau)$ may be evaluated by the methods described by King, Hainer, and Cross.[5] $(\tau|\mathbf{P}_z^2|\tau)$ may be obtained by the special techniques described by Kivelson and Wilson.[7] $(\tau|\mathbf{P}_z|\tau)$ may be handled by the scheme described in Appendix III.

The situation of primary interest is the one of hindered internal rotation in which the hindering barrier takes on the form $(1/2)V_0(1-\cos N\theta)$, where V_0 is the barrier height. Then the Hamiltonian may be written as

$$\mathbf{H}=\mathbf{H}_R(\gamma-\theta I_{z2}/I_z)+\tfrac{1}{2}\mathbf{\Pi}^2I_z/I_{z1}I_{z2}+\tfrac{1}{2}V_1(1-\cos N\theta)$$
$$=\mathbf{H}_R(\gamma-\theta I_{z2}/I_z)+\mathbf{H}_I. \quad (18)$$

In the $\Psi_{\tau\tau}$ basis, $\mathbf{H}_R$ is diagonal in both τ and τ, $\mathbf{\Pi}^2$ is diagonal in τ but not in τ, while the potential is diagonal in τ but not in τ. Thus the Hamiltonian is not diagonal in either τ or τ. The exact wave function could be obtained by a perturbation calculation that accounted for the nondiagonal terms in both τ and τ. However, if the asymmetry is large and the barrier low, the off-diagonal terms in τ will be small and $\sum_\tau b_\tau(\tau)\Psi_{\tau\tau}$ will be a good basis function where the b's are chosen so that the matrix has off-diagonal terms only in τ. In the present discussion, interest will be focused on the reverse situation in which the asymmetry is not too large and the barrier is quite high. This means that the off-diagonal terms in τ will be important, while the off-diagonal elements in τ will be relatively insignificant. It is also assumed that the limiting symmetric rotor has its unique axis along the axis of internal rotation. A suitable basis function for this case is

$$\mathrm{X}_{m\tau}=\sum_\tau a(m)_{\tau\tau}\Psi_{\tau\tau}, \quad (19)$$

where m is a pseudo-quantum number replacing τ. For a given τ, $\mathrm{X}_{m\tau}$ diagonalizes the Hamiltonian of Eq. (18). If $W_m(\tau)$ is given by

$$W_m(\tau)=(m\tau|\mathbf{H}|m\tau), \quad (20)$$

one can evaluate $a(m)_{\tau\tau}$ by considering the following integral:

$$\int\Psi_{\tau'\tau}^*[\mathbf{H}-W_m(\tau)]\mathrm{X}_{m\tau}dv=0$$
$$=[W_R(\tau)+\tfrac{1}{2}V_1-W_m(\tau)]a(m)_{\tau\tau}+\tfrac{1}{2}(I_z/I_{z1}I_{z2})(\tau|(\mathbf{P}_zI_{z2}/I_z-\tau)^2|\tau)a(m)_{\tau\tau}-\tfrac{1}{4}V_0[a(m)_{\tau,\tau'+N}+a(m)_{\tau,\tau'-N}]. \quad (21)$$

If one now defines

$$R_{m\tau}=2(I_{z1}I_{z2}/I_z)\{W_m(\tau)-W_R(\tau)-V_1/2\}, \quad (22)$$
$$\alpha=\tfrac{1}{2}(I_{z1}I_{z2}/I_z)V_1, \quad (23)$$

Eq. (21) can be rewritten as

$$[a(m)_{\tau,\tau-N}+a(m)_{\tau,\tau+N}]\alpha/\{R_{m\tau}-S_{\tau\tau}\}+a(m)_{\tau,\tau}=0, \quad (24)$$

where $S_{\tau\tau}$ is given in Eq. (17). This is analogous to Eq. (9) given by Koehler and Dennison.[2] The solution of this set of equations proceeds in the manner described by these authors. Using the continued fraction procedures they give, one may evaluate the coefficients $a(m)_{\tau\tau}$.

If the off-diagonal terms in τ are small, $\mathrm{X}_{m\tau}$ is a good approximation to the true wave function. If a better solution for the energy or for the wave functions is required, $\mathrm{X}_{m\tau}$ may be used as a basis function and a Van Vleck perturbation[8] applied.

For computational purposes it is probably simpler to use the procedures and basis functions given by the authors of reference 3. However, the wave function $\mathrm{X}_{m\tau}$ is particularly well adapted for the study of the interactions of internal and over-all rotations with the vibrations of a molecule. It is relatively simple and includes both the effects of hindered internal rotation and of asymmetry. Furthermore, it comes close to separating the internal from the over-all rotational motion, a desirable feature in treating vibrational interactions. Of course, the two motions are not truly separable and $\mathrm{X}_{m\tau}$ is just an approximation to the true wave function.

RIGID INTERNAL SEMIASYMMETRIC ROTORS

The work of the preceding section may be extended to somewhat more asymmetric molecules. A semiasymmetric rotor may be defined as a molecule with two constituent groups, of which one is a symmetric rotor (CH_3) and the other is not. The figure axis of the symmetric rotor group may be considered the internal rotation axis, but it is not a principal axis of the entire molecule. CH_3OH and CH_3NH_2 are such molecules. This class of molecules has the property, in common with semisymmetric rotors, that the principal axes are

[7] D. Kivelson and E. B. Wilson, Jr., J. Chem. Phys. **20**, 1575 (1952).

[8] See, for example, E. C. Kemble, *The Fundamental Principles of Quantum Mechanics* (McGraw-Hill Book Company, Inc., New York, 1937), p. 238.

embedded in the nonsymmetric rotor group. Let the subscript 2 refer to the symmetric rotor group (CH_3) and 1 refer to the other group (OH).

For such a molecule, one can choose a coordinate system in which the origin is at the center of mass of the entire molecule, the z axis is parallel to the figure axis of group 2 (CH_3), and the axes are embedded in the group 1 (OH) part of the molecule. The axes can be taken so that I_{xy}, the product of inertia for the entire molecule, is equal to zero. Using a notation similar to that of the preceding section, one has

$$2T=I_x\omega_x^2+I_y\omega_y^2+I_z\omega_z^2+2I_{xz}\omega_x\omega_y +2I_{xz}\omega_x\omega_z+2I_{yz}\omega_y\omega_z-2I_{yz}I_{z2}I_z^{-1}\omega_y\omega_\theta -2I_{xz}I_{z2}I_z^{-1}\omega_x\omega_\theta+\omega_\theta^2I_{z1}I_{z2}I_z^{-1}. \quad (25)$$

I_{z2} is the zz-component of the inertia tensor of the CH_3 group taken about the symmetry axis of the group, while $I_{z1}=I_z-I_{z2}$.

Proceeding exactly as in the preceding section one obtains the Hamiltonian for internal and over-all rotation[3a]:

$$\mathbf{H}=\mathfrak{H}_R(\gamma-\theta I_{z2}/I_z)+\mathfrak{H}_I(\gamma-\theta I_{z2}/I_z), \quad (26)$$

$$\mathfrak{H}_R=\sum_{\alpha,\beta} B_{\alpha\beta}\mathbf{P}_\alpha'\mathbf{P}_\beta', \quad (27)$$

$$\mathfrak{H}_I=\sum B_\alpha\{\mathbf{P}_\alpha',\mathbf{\Pi}\}+B_\tau\mathbf{\Pi}^2+\tfrac{1}{2}V_1(1-\cos N\theta). \quad (28)$$

$\{,\}$ represents a symmetrized product. The coefficients are independent of the rotational coordinates and are discussed in Appendix I. $\mathbf{P}_x'$ and $\mathbf{P}_y'$ are functions of $(\gamma-\theta I_{z2}/I_z)$. The prime indicates that they are not taken with respect to the principal axes of the molecule but with respect to the coordinate system described above. $\mathfrak{H}_R(\gamma-\theta I_{z2}/I_z)$ is the Hamiltonian for a pseudo-rigid rotor as in the preceding section; that is, it reduces to the Hamiltonian of a true rigid rotor when $\theta\equiv 0$. However, the rigid rotor represented by $\mathfrak{H}_R(\gamma)$ is not the correct rigid rotor Hamiltonian for the molecule under consideration since the coefficients $B_{\alpha\beta}$ are slightly different than they would be for an ordinary rigid rotor (see Appendix I). If $\mathbf{H}_R(\gamma)$ is the usual rigid rotor Hamiltonian, Eq. (26) can be rewritten as

$$\mathbf{H}=\mathbf{H}_R(\gamma-\theta I_{z2}/I_z)+\mathbf{H}_I(\gamma-\theta I_{z2}/I_z) =\mathbf{H}_R(\gamma-\theta I_{z2}/I_z)+[\mathfrak{H}_R-\mathbf{H}_R+\mathfrak{H}_I]. \quad (29)$$

However, Eq. (26) is the more useful of the two equations.

By arguments analogous to those used for the semisymmetric rotor, one finds that a suitable basis function for treating the Hamiltonian in Eq. (26) is

$$\mathrm{X}_{rm}'=\sum_\tau a(m)_{r\tau}\Psi_{r\tau}'=(2\pi)^{-\frac{1}{2}}\sum_\tau a(m)_{r\tau} \times\exp[i(-\mathbf{P}_z'I_{z2}/I_z+\tau)\theta]\Phi_r', \quad (30)$$

where τ is an integer, Φ_r' is the eigenfunction corresponding to $\mathfrak{H}_R(\gamma)$, and r stands for the quantum numbers J and $K_{-1}K_1$[5] for a rigid rotor represented by $\mathfrak{H}_R(\gamma)$; m and $a(m)_{r\tau}$ are defined in the previous section. It should be noted that if Φ_r' is obtained by the procedures of King, Hainer, and Cross[5] it is referred to the principal axis system while $\mathbf{P}_z'$ in the exponent is directed along the internal rotation axis and not along a molecular principal axis. Thus $\mathbf{P}_z'$ must be re-expressed in terms of components of angular momentum directed along principal axes. This will be discussed below.

The matrix elements of the Hamiltonian in the basis represented by X_{rm}' can be obtained in the same manner as for the semisymmetric rotor. Thus,

$$(rm|\mathfrak{H}_R(\gamma-\theta I_{z2}/I_z)|rm)=\mathfrak{W}_R(r)\delta_{rr'}\delta_{\tau\tau'}\delta_{mm'}, \quad (31)$$

where $\mathfrak{W}_R(r)$ is the eigenvalue corresponding to $\mathfrak{H}_R(\gamma)$. And, by the same procedures employed for the semisymmetric rotor, one obtains[9]

$$\int\Psi_{r'\tau'}{}'^*[\mathfrak{H}_I-\tfrac{1}{2}V_1(1-\cos N\theta)]\Psi_{r\tau}'dv =B_\tau(r'|(\mathbf{P}_z'I_{z2}/I_z-\tau)^2|r)\delta_{rr'} +\sum_\alpha(r'|\{\mathbf{P}_\alpha',\mathbf{P}_z'\}|r)B_\alpha I_{z2}/I_z\delta_{rr'} -2\tau\delta_{rr'}\sum_\alpha(r'|B_\alpha\mathbf{P}_\alpha'|r) =L_{Sr\tau'\tau}\delta_{r'r}. \quad (32)$$

The coefficients $a(m)_{r\tau}$ and the rotational energy may again be obtained from Eq. (24) provided $S_{r\tau}$ is defined as in Eq. (32) and

$$\alpha=V_1/4B_\tau, \quad (33)$$

$$R_{mr}=4\{W_m(r)-\mathfrak{W}_R(r)-V_1/2\}. \quad (34)$$

This problem[3(a)] is solved in the same way as the corresponding problem for the semisymmetric rotor and the same comments hold concerning its validity and its applicability. The only additional difficulty arises because $S_{r\tau}$ may now be difficult to evaluate. The operators $\mathbf{P}_x'$, $\mathbf{P}_y'$, and $\mathbf{P}_z'$ appearing there must be referred to the "principal axis" system[10]; that is, they must be expressed as a linear combination of a new set of angular momenta directed along the "principal axis" system. The transformation coefficients may be easily obtained for any molecule.

GENERAL RIGID INTERNAL ASYMMETRIC ROTORS

The general asymmetric rotor is much more difficult to treat than the previous cases,[3(b)] and will not be solved here. A coordinate system may be chosen so that it passes through the center of mass of the

[9] $(rm\,|\,f(\gamma-\theta I_{z2}/I_z)rm)=(r\tau\,|\,f(\gamma-I_{z2}\theta/I_z)\,|\,r\tau)=(r\,|\,f(\gamma)\,|\,r)$. Thus it is not necessary to specify where f is a function of $(\gamma-\theta I_{z2}/I_z)$ or just a function of γ.

[10] These are not the true principal axes of the equivalent rigid rotor since $B_{\alpha\beta}$ etc., are not the components of the inverse inertia tensor of the true rigid rotor. These axes may, however, often be close to the true principal axes. (See Appendix I.)

molecule, the z axis is parallel to the axis of internal rotation, and the axes are fixed in one of the two asymmetric functional groups composing the molecule, e.g., group 1. The kinetic energy then takes on a form similar to that of the energy in Eq. (25). However, the components of the inertia tensor may be functions of θ. The Hamiltonian has the same form as the one in Eq. (26) except for the fact that the coefficients may depend upon θ and that the hindering potential barrier need no longer be symmetric. The wave function given in Eq. (30) is a suitable basis function, but the energy matrix elements are far more complicated. For example,

$$\int \mathrm{X}_{rm}'^{*}\mathfrak{H}_R(\gamma-\theta I_{z2}/I_z,\theta)\mathrm{X}_{rm}'dv$$

$$=(2\pi)^{-1}\sum_{\tau,\tau'}a(m)_{r'\tau'}^{*}a(m)_{r\tau}$$

$$\times\int\Phi_r'^{*}\mathfrak{H}_R(\gamma,\theta)\Phi_r'e^{-i(\tau'-\tau)\theta}dv. \quad (35)$$

Thus $\mathfrak{H}_R$ is no longer diagonal in τ.

NONRIGID SEMISYMMETRIC INTERNAL ROTORS

In the preceding paper,[11] (henceforth referred to as II), the Hamiltonian for a nonrigid internal rotor was discussed in some detail and transformed into an approximate Hamiltonian which can be treated by standard methods. The treatment in II assumes that the torsional motion, in the limit of high barriers, is a normal mode of the molecule. Thus the results in II are strictly valid only for symmetric and semisymmetric rotors. However, the formulas obtained in II should hold fairly well for some semiasymmetric rotors such as CH_3OH.

The present analysis will start with Eq. (20) in II:

$$\mathbf{H}=\langle\mathbf{H}\rangle_R+\langle\mathbf{T}_I\rangle+\tfrac{1}{2}\bar{V}_1(1-\cos N\theta)$$
$$+\tfrac{1}{2}\bar{V}_2(1-\cos 2N\theta)-\sum B_{\alpha\beta}^{(i)}a_i^{(1)}\mathbf{P}_\alpha\mathbf{P}_\beta(1-\cos N\theta)$$
$$-\tfrac{1}{2}\sum B_\alpha^{(i)}a_i^{(1)}\{\{\mathbf{P}_\alpha,\mathbf{\Pi}\},(1-\cos N\theta)\}$$
$$-\tfrac{1}{2}\sum B_\pi^{(i)}a_i^{(1)}\{\mathbf{\Pi}^2,1-\cos N\theta\}$$
$$+\sum_{v'}{}'(v|\mathbf{H}_R+\mathbf{T}_I|v')^2/h\nu_{vv'}. \quad (36)$$

In this equation $\mathbf{H}_R$ represents the instantaneous over-all rotational Hamiltonian at $\theta=0$; $\mathbf{T}_I$ is the corresponding kinetic energy for internal rotation. The V's are barrier heights that depend upon the vibrations of the molecule. The expectation value of an operator in a given vibrational state is represented by a bar over the operator or by angular brackets surrounding it. $B_{\alpha\beta}^{(i)}$ is the derivative of $B_{\alpha\beta}$ with respect to the ith internal displacement coordinate evaluated at equilibrium. $B_\alpha^{(i)}$ and $B_\pi^{(i)}$ are defined in a similar way. $a_i^{(1)}$ is one-half the difference between the equilibrium value of the ith internal coordinate at $\theta=0$ and its value at $\theta=\pi/N$. $\sum v'$ means the sum over all harmonic vibrational states v' with the restriction that $v'\neq v$. These terms are discussed in detail in II.

$\langle\mathbf{T}\rangle_I+\langle\mathbf{H}\rangle_R+\frac{1}{2}\langle\mathbf{V}\rangle_1(1-\cos N\theta)$ are the rigid sinusoidal internal over-all rotational terms in the Hamiltonian.[12] These will be the zeroth-order terms to the present problem and all other terms will be treated as perturbations. These zeroth-order terms have been discussed in previous sections.

If R represents the basis that diagonalizes the zeroth-order terms, the energy corresponding to the Hamiltonian in Eq. (36) may be approximated to first order by evaluating the RR element of $\mathbf{H}$. But since the correction terms are small, they may be evaluated instead in the rm basis mentioned above, that is, in terms of the basis functions X_{rm}. The energy is thus

$$E=(R|\langle\mathbf{H}\rangle_I+\langle\mathbf{H}\rangle_R|R)+\tfrac{1}{2}\langle\mathbf{V}\rangle_2(rm|1-\cos 2N\theta|rm)$$
$$+\sum_{\alpha,\beta}F_{\alpha\beta}(rm|\mathbf{P}_\alpha\mathbf{P}_\beta(1-\cos N\theta)/rm)$$
$$+\sum_{\alpha}F_\alpha(rm|\{\mathbf{P}_\alpha(1-\cos N\theta),\mathbf{\Pi}\}|rm)$$
$$+F_\pi(rm|\{\mathbf{\Pi}^2,1-\cos N\theta\}|rm)$$
$$+(rm|\sum_{v'}{}'(v|\mathbf{H}_R+\mathbf{T}_I|v')^2/h\nu_{vv'}|rm). \quad (37)$$

The F's may be determined by comparison of Eq. (37) with Eq. (36); the F's are independent of the rotational quantum numbers. The first term in Eq. (37) is the rigid sinusoidal internal rotational term; the second term is a correction that helps account for the non-sinusoidal nature of the barrier; the last term accounts for centrifugal distortion and will be discussed below. The remaining terms depend upon the nature of the repulsive forces constituting the hindering barrier, and the manner in which the equilibrium configuration and the potential constants depend upon θ.

The last term on the right of Eq. (37) splits into three subterms: one of order $\mathbf{H}_R^2$ which is just the usual semirigid rotor centrifugal distortion term that has been treated previously[7]; one in $\mathbf{T}_1^2$ which is a centrifugal distortion term for "pure" internal rotation; and one in $\{\mathbf{T}_I,\mathbf{H}_R\}$ which is an interaction centrifugal distortion term, that is, a contribution to the energy resulting from centrifugal distortion effects that involve the interactions of internal with over-all rotations. These terms will involve a great many coefficients which can be computed from a knowledge of the vibrational modes. The application of suitable approximations reduces the

[11] D. Kivelson, J. Chem. Phys. **23**, 2230 (1955). This paper will be referred to as II.

[12] E. B. Wilson, Jr., and J. B. Howard, J. Chem. Phys. **4**, 260 (1936).

number of such constants, but the number will still be large, as one can easily see by noting that the ordinary centrifugal distortion terms alone have seven such independent parameters.[7]

To evaluate the last sum in Eq. (37) one has to work with matrix elements of the form $(v|\mathbf{T}_I+\mathbf{H}_R|v')$. This means that $\mathbf{H}_R+\mathbf{T}_I$ must be expressed as a function of the vibrational coordinates, that is, of the normal coordinates. If these vibrations are excited, the molecule may be distorted so that it is no longer a semisymmetric rotor but a general asymmetric rotor. In this instance, as was shown above, it is more convenient to write the Hamiltonian in the form $\mathfrak{H}_R+\mathfrak{T}_I$. [See Eqs. (27) and (28).][13] The ensuing terms in $\mathfrak{H}_R^2$, $\mathfrak{T}_I^2$, $\{\mathfrak{H}_R,\mathfrak{T}_I\}$ have slightly different physical interpretations from those given above since the various centrifugal distortion effects will now be slightly intermingled. The appropriate expressions for $\mathfrak{T}_I$ and $\mathfrak{H}_R$ for the general asymmetric rotor have the same form as those given in Eqs. (27) and (28) except that the coefficients are now functions of both the vibrational coordinates and of the angle of internal rotation θ. $\mathbf{P}_x$ and $\mathbf{P}_y$ are functions of $\gamma-\theta I_{xz}/I_x$. The dependence of the coefficients $B_{\alpha\beta}$, B_α, B_π upon θ will be neglected since it will enter only as a correction to the terms under consideration which are correction terms themselves.

The term of order $\mathfrak{H}_R^2$ arising from Eq. (37) is seen to be almost the usual centrifugal distortion term and can be treated by the approximation methods of reference 7. These terms are all of order $\mathbf{P}^4$. In the work below all terms of order $\mathbf{P}^4$ will be grouped together with the $\mathfrak{H}_R^2$ terms. This will not change the form of the $\mathfrak{H}_R^2$ terms, but will give the various coefficients different meanings. Explicit expressions for the $\mathfrak{H}_R^2$ plus other $\mathbf{P}^4$ terms may be obtained from reference 7 provided the seven independent parameters involved are altered appropriately. These constants can, in principle, be calculated from vibrational data,[14] but this is usually not feasible.

The sums $\sum'(v|\mathfrak{T}_I|v')^2/h\nu_{vv'}$ and $\sum'(v|\mathfrak{T}_I|v')\times(v'|\mathfrak{H}_R|v)/h\nu_{vv'}$ will involve many different terms. A simplification may be made if one looks at the structure of the entire Hamiltonian in a symmetric rotor basis. There will be real $(K|\mathbf{H}|K\pm 2n)$ elements in the energy matrix where $n=0, 1, 2$, as well as imaginary $(K|\mathbf{H}|K\pm j)$ elements where $j=1, 2, 3, 4$. As shown in a previous paper[15] the latter set of terms enters in higher order than does the former, and so may be neglected to the degree of accuracy required here. Terms of the form $\mathbf{P}_z$, $\mathbf{P}_y$, $\mathbf{P}_i\mathbf{P}_j$ where $i\neq j$, $\mathbf{P}_i\mathbf{P}_i\mathbf{P}_j$ where $j\neq z$, $\mathbf{P}_i\mathbf{P}_j\mathbf{P}_k$ where $i\neq j\neq k$, and $\mathbf{P}_i\mathbf{P}_j\mathbf{P}_k\mathbf{P}_l$ where at least one of the subscripts is unique, have imaginary elements and so can be discarded. Since $\mathbf{\Pi}$ is not a function of $\mathbf{P}_x$ or $\mathbf{P}_y$ (see Eq. (11).) One can write the following:

$$\sum_{v'}'(rm|(v|\mathfrak{T}_I|v')^2/h\nu_{vv'}|rm)$$
$$=(rm|[U_1\mathbf{\Pi}^4+\sum_\alpha U_\alpha\{\mathbf{P}_\alpha,\mathbf{\Pi}\}^2$$
$$+U_2\{\mathbf{\Pi}^2,\{\mathbf{\Pi},\mathbf{P}_z\}\}]|rm), \quad (38)$$

$$\sum_{v'}'(rm|\{(v|\mathfrak{T}_I|v'),(v'|\mathfrak{H}_I|v)\}/h\nu_{vv'}|rm)$$
$$=(rm|\sum_\alpha[U_{\alpha z}\{\{\mathbf{P}_\alpha,\mathbf{P}_z\},\{\mathbf{P}_\alpha,\mathbf{\Pi}\}\}$$
$$+U_{\alpha\pi}\{\mathbf{P}_\alpha^2,\mathbf{\Pi}^2\}+U_{\alpha\alpha}\{\mathbf{P}_\alpha^2,\{\mathbf{\Pi},\mathbf{P}_z\}\}]|rm), \quad (39)$$

where the U's are independent of all rotational motion. U_1 is given by the relation

$$U_1=\sum_{v'}'(v|B_\pi|v')(v'|B_\pi|v)/h\nu_{vv'}, \quad (40)$$

and the other U's are defined in a similar way on the basis of Eqs. (27), (28), and (37). The other correction terms in Eq. (37) may be simplified on the basis of the same approximations. Thus there will be a reduction in the number of terms involving F's since only those that include $F_{\alpha\alpha}$, F_z, and F_π need be retained.

The U's may be calculated, in principle, from the infrared vibrational data by the methods of reference 14. The calculations required to obtain the U's are lengthy; so, if possible, these parameters should be obtained empirically.

The matrix elements occurring in Eqs. (38) and (39) have been re-expressed in Appendix II. As mentioned above, all terms of order $\mathbf{P}^4$ will be combined with the so-called "ordinary" centrifugal distortion terms which have been evaluated elsewhere. Thus, making use of the various approximations and simplifications described above and in the Appendix, one can rewrite Eq. (37) as:

$$\begin{aligned}E=&(R|\langle\mathbf{H}\rangle_I+\langle\mathbf{H}\rangle_R|R)+\tfrac{1}{2}\bar{V}_2(rm|1-\cos 2N\theta|rm)\\&+[F_1(r|\langle\mathbf{H}\rangle_R|r)+F_2J(J+1)\\&+F_3(r|\mathbf{P}_z^2|r)](rm|1-\cos N\theta|rm)\\&+F_4(rm|\{\mathbf{P}_z\mathbf{\Pi},1-\cos N\theta\}|rm)\\&+F_5(rm|\{\mathbf{\Pi}^2,1-\cos N\theta\}|rm)+G_1(rm|\mathbf{\Pi}^4|rm)\\&+[G_2(r|\langle\mathbf{H}\rangle_R|r)+G_3J(J+1)+G_4(r|\mathbf{P}_z^2|r)]t^2\\&+L_1(r|\mathbf{P}_z|r)t^3+[L_2(r|\mathbf{P}_z^2|r)(r|\mathbf{P}_z|r)\\&+L_3J(J+1)(r|\mathbf{P}_z|r)+L_4(r|\mathbf{P}_z^3|r)+L_5(r|\mathbf{P}_z|r)]t\\&+\text{"ordinary centrifugal distortion terms,"} \quad (41)\end{aligned}$$

where

$$t^k=\sum_\tau a(m)_{\tau\tau}{}^*a(m)_{\tau\tau}\tau^k \quad (42)$$

and t is evaluated in Appendix II. The constants F_i, G_i, and L_i appearing in this equation are independent of the rotational quantum numbers. The first term is the energy for a rigid internal rotor with a sinusoidal barrier. This term involves five important molecular parameters, I_x, I_y, I_z, I_{z2}, and the effective sinusoidal

[13] $\mathfrak{T}_I$ is the kinetic energy part of $\mathfrak{H}_I$.
[14] D. Kivelson and E. B. Wilson, Jr., J. Chem. Phys. **21**, 1229 (1953).
[15] See reference 7, p. 1576.

barrier height $\bar{V}_1$. The second term is a correction for the nonsinusoidal nature of the hindering barrier. The terms in G_i and L_i are centrifugal distortion terms that depend upon internal rotation. The G_i's and L_i's are linear combinations of the U's already defined, and so can be obtained from a knowledge of the normal vibrations. However, in most cases it is not feasible to calculate these parameters, and so they must be treated as empirically adjustable parameters. The "ordinary centrifugal distortion terms" involve seven linearly independent constants that have been discussed elsewhere.[14] The terms in F_i are more difficult to evaluate since they depend more critically upon the exact nature of the repulsive barrier.[11] These terms are analogous to the F_v that appears in the relation for symmetric rotors.[1,11] The various matrix elements appearing in Eq. (41) are treated in Appendix III.

SPECIAL CASES

If the G_i's and L_i's in Eq. (41) are not calculated from vibrational data, the formula for the energy contains too many adjustable parameters to be useful in spectroscopic analysis. However, in certain special cases and under conditions where additional approximations may be made, the equation may be greatly simplified.

The simplest case is, of course, that of a symmetric rotor. If the transition frequencies are computed from Eq. (41), making use of the symmetric rotor selection rules $\Delta J=1$, $\Delta K=0$, $\Delta m=0$, then the resulting expression is of the form

$$\begin{aligned}\nu=&2J[B_v+(B_vF_1+F_2)(m|1-\cos N\theta|m)\\&+(B_vG_2+G_3)(m|\,\Pi^2|m)\\&+\{B_vL_2+L_3-2(I_{z2}/I_z)(B_vG_2+G_3)\}K(m|\,\Pi|m)]\\=&2J[B_v+F_v(m|1-\cos N\theta|m)+G_v(m|\,\Pi^2|m)\\&+L_vK(m|\,\Pi|m)],\end{aligned}\quad(43)$$

where B_v is the rigid rotor rotational constant. This is the result obtained in I [see II, Eq. (21).] Terms of the form $2JK^2$ have been neglected.

Equation (41) also takes on a particularly simple form for the $0_{00}\rightarrow 1_{01}$ transition for a semisymmetric rotor, e.g., CH_3NO_2. The approximate wave function takes on the form

$$X_{rm}=(2\pi)^{-\frac{1}{2}}\sum_\tau a(m)_{r\tau}\Phi_\tau\exp[i\tau\theta]\quad(44)$$

for both the 0_{00} and the 1_{01} states. With the aid of this wave function and Eq. (41), the transition frequencies may be obtained. Thus

$$\begin{aligned}\nu(0_{00}\rightarrow 1_{01})=&(1_{01}|\langle\mathbf{H}\rangle_R|1_{01})[1+F_1(m|1-\cos N\theta|m)\\&+G_2(m|\,\Pi^2|m)]+2G_3(m|\,\Pi^2|m)\\&+2F_2(m|1-\cos N\theta|m),\end{aligned}\quad(45)$$

where the selection rule, $\Delta m=0$ has been used. This simple relation does not hold in any other case.

The correction terms in Eq. (41) are of two main types: centrifugal distortion contributions and corrections arising because of the dependence of the vibrations upon the angle of internal rotation. The latter terms are given by the terms including $a_i^{(1)}$, that is, by those with coefficients F_i in Eq. (41). One can think of these terms as arising from the mutual repulsion of the two functional groups as they pass through the potential barrier. For low J-lines where the barrier is fairly high and centrifugal distortion constants small, the repulsion effect will be dominant. This is borne out by the results on CH_3SiH_3.[1] Thus one might expect to get fairly satisfactory results on low J-lines by considering the repulsion effect and neglecting all the centrifugal distortion effects. The correction terms would then be given by the F_i-terms in Eq. (41). Besides the parameters I_x, I_y, I_z, I_{z2}, and $\bar{V}_1$ that enter into the nonvibrating internal rotational problem, the present approximation introduces the new parameters F_1 through F_5.

This approximation is not always satisfactory for although the centrifugal distortion terms are small, they are probably not completely negligible (see methyl silane). One could make rough calculations and discard some of the centrifugal distortion terms while retaining the more important ones. Or, in some cases, one might evaluate these distortion terms in the symmetric rotor limit.

INTERACTIONS FOR SEMIASYMMETRIC ROTORS

In semiasymmetric rotors, the torsional mode does not necessarily correspond to a normal mode and so may not be separable from the other vibrations. However, to the extent that internal rotation may be treated as a normal mode, the general arguments for semiasymmetric rotors follow exactly those for semisymmetric rotors. However, it must be remembered that X_{rm} is now determined by Eq. (24) along with Eqs. (32) through (34), and that $\mathbf{P}_i$ must then be rotated.‡

ACKNOWLEDGMENT

I should like to thank my wife, Margaret G. Kivelson, for her valuable comments and useful suggestions.

APPENDIX I

The components of the angular momentum may be obtained from Eq. (25). Typical angular momentum components are

$$\begin{aligned}\mathbf{P}_\alpha&=\partial T/\partial\omega_\alpha=I_\alpha\omega_\alpha+I_{\alpha\beta}\omega_\beta+I_{\alpha z}\omega_z+A_{\alpha z}\omega_\theta/I_z,\\\mathbf{P}_z&=\partial T/\partial\omega_z=I_{xz}\omega_x+I_{yz}\omega_y+I_z\omega_z,\\\Pi&=\partial T/\partial\omega_\theta=A_{xz}\omega_z/I_z+A_{yz}\omega_y/I_z+I_{z1}I_{z2}\omega_\theta/I_z,\end{aligned}$$

where $\alpha=x,\ y$; $\beta=x,\ y$; and $\alpha\neq\beta$ and $A_{\alpha z}=-I_{z2}I_{\alpha z}$. It should be noted that in the limit of a rigid rotor, that is, when $\omega_\theta=0$, the internal angular momen-

‡ *Footnote added in proof.*—At the Spectroscopy Symposium held in June, 1955 at the Ohio State University, Hecht and Dennison reported a similar theory which they applied to CH_3OH.

tum $\mathbf{\Pi}$ does not go to zero. In this limit $\mathbf{\Pi}$ is no longer an independent momentum but depends linearly upon $\mathbf{P}_x$, $\mathbf{P}_y$, and $\mathbf{P}_z$.

Carrying out the substitutions of the angular velocities in terms of the angular momenta, one obtains the following expressions for the various coefficients in Eqs. (27) and (28):

$$2B_{aa}\Delta=(I_\beta I_z-I_{\beta z}^2)-A_{\beta z}^2/I_{z1}I_{z2},$$

$$2B_{zz}\Delta=(I_xI_y-I_{xy}^2)-(A_{xz}^2I_y-2A_{xz}A_{yz}I_{xy}+A_{yz}^2I_x)/I_xI_{z1}I_{z2},$$

$$2B_{xy}\Delta=I_{xz}I_{yz}-I_{xy}I_z+A_{xz}A_{yz}/I_{z1}I_{z2},$$

$$2B_{\alpha z}\Delta=I_{xy}I_{\beta z}-I_\beta I_{\alpha z}+(A_{\beta z}I_{\alpha z}-A_{\alpha z}I_{\beta z})A_{\beta z}/I_xI_{z1}I_{z2},$$

$$2B_\alpha\Delta=[A_{\alpha z}(I_{\beta z}^2-I_\beta I_z)+A_{\beta z}(I_{xy}I_z-I_{xz}I_{yz})]/I_{z1}I_{z2},$$

$$2B_z\Delta=[A_{yz}(I_{yz}I_x-I_{xz}I_{xy})+A_{xz}(I_{xz}I_y-I_{yz}I_{xy}]/I_{z1}I_{z2},$$

$$2B_\tau\Delta=[I_z(I_xI_y-I_{xy}^2)-I_{xz}^2I_y+2I_{xy}I_{yz}I_{xz}-I_{yz}^2I_x]I_z/I_xI_{z1}I_{z2},$$

where α and β stand for x and y, $\alpha\neq\beta$, and

$$\Delta=I_z(I_xI_y-I_{xy}^2)-I_{xz}^2I_y+2I_{xy}I_{yz}I_{xz}-I_{yz}^2I_x+[A_{xz}^2(I_yI_z-I_{yz}^2)-A_{yz}^2(I_xI_z-I_{xz}^2)]/I_xI_{z1}I_{z2}.$$

The coefficients $B_{\alpha\beta}$ are not precisely the components of the inverse inertia tensor of a rigid rotor because of the presence of the A_{xz} and A_{yz} terms. In semisymmetric rotors, A_{xz} and A_{yz} vanish, and the $B_{\alpha\beta}$'s become the inverse inertia tensor components of a rigid rotor, while $2B_\tau$ becomes $I_z/I_{z1}I_{z2}$, and B_x, B_y, and B_z vanish. Since I_{yz} and I_{xz} are zero here, $B_{\alpha\beta}$ vanishes if $\alpha\neq\beta$. Thus Eq. (26) reduces to Eq. (10).

APPENDIX II

The various matrix elements appearing in Eqs. (38) and (39) may be evaluated by the methods discussed here. Many of the terms are of the form $(rm|\mathbf{P}_\alpha^n,\mathbf{\Pi}^k\}|rm)$, where n and k are integers. In the semisymmetric rotor basis this becomes

$$\sum_\tau\int\phi_\tau^*\{\mathbf{P}_\alpha^n,(-\mathbf{P}_zI_{z2}/I_z+\tau)^k a(m)_{\tau\tau}^*a(m)_{\tau\tau}\Phi_\tau dv.$$

If $\mathbf{P}_\alpha$ is $\mathbf{P}_x$ or $\mathbf{P}_y$, it is a function of $\gamma-\theta I_{z2}/I_z$, but the dependence upon θ is eliminated in this expression.[6,9] The typical term in the foregoing expression is

$$\sum_\tau\int\Phi_\tau^*\{\mathbf{P}_\alpha^n,(\mathbf{P}_zI_{z2}/I_z)^{k-k'}\tau^{k'}\}a(m)_{\tau\tau}^*a(m)_{\tau\tau}\Phi_\tau dv=t^{k'}(r|\{\mathbf{P}_\alpha^n,(\mathbf{P}_zI_{z2}/I_z)^{k-k'}\}|r),$$

where k' is an integer, $k'\leqslant k$, and where

$$t^{k'}=\sum_\tau a(m)_{\tau\tau}^*a(m)_{\tau\tau}\tau^{k'}.$$

In particular,

$$t=(I_{z2}/I_z)(r|\mathbf{P}_z|r)-(rm|\mathbf{\Pi}|rm),$$

$$t^2=(rm|\mathbf{\Pi}^2|rm)-(I_{z2}/I_z)^2(r|\mathbf{P}_z^2|r)+2(I_{z2}/I_z)(r|\mathbf{P}_z|r)t,$$

$$t^3=-(rm|\mathbf{\Pi}^3|rm)+3(I_{z2}/I_z)(r|\mathbf{P}_z|r)t^2-3(I_{z2}/I_z)^2(r|\mathbf{P}_z^2|r)t+(I_{z2}/I_z)^3(r|\mathbf{P}_z^3|r).$$

Several simplifications are now possible. By using the commutation rules for the components of angular momentum along the body-fixed axes[16] one can write the following useful identities:

$$(rm|\{\mathbf{P}_x,\mathbf{\Pi}\}^2|rm)=(I_{z2}/I_z)^2(rm|\{\mathbf{P}_z,\mathbf{P}_x\}^2|rm)+4(rm|\mathbf{P}_x^2|rm)t^2-4(I_{z2}/I_z)(rm|\{\mathbf{P}_x^2,\mathbf{P}_z\}|rm)t+2(I_{z2}/I_z)(rm|\mathbf{P}_z|rm)t,$$

$$(rm|\{\{\mathbf{P}_x,\mathbf{P}_z\},\{\mathbf{P}_x,\mathbf{\Pi}\}\}|rm)=2(rm|\{\mathbf{P}_x,\mathbf{P}_z\}^2|rm)(I_{z2}/I_z)-4(rm|\{\mathbf{P}_x^2,\mathbf{P}_z\}|rm)t+2(rm|\mathbf{P}_z|rm)t,$$

$$(rm|\{\mathbf{P}_x^2,\mathbf{\Pi}^2\}|rm)=(I_{z2}/I_z)^2(rm|\{\mathbf{P}_x^2,\mathbf{P}_z^2\}|rm)-2(I_{z2}/I_z)(rm|\{\mathbf{P}_x^2,\mathbf{P}_z\}|rm)t+2(rm|\mathbf{P}_x^2|rm)t^2,$$

$$(rm|\{\mathbf{P}_x^2,\{\mathbf{\Pi},\mathbf{P}_z\}\}|rm)=(I_{z2}/I_z)(rm|\{\mathbf{P}_x^2,\mathbf{P}_z^2\}|rm)-2(rm|\{\mathbf{P}_x^2,\mathbf{P}_z\}|rm)t.$$

These equations are also valid if y or z is exchanged for x. These terms can be altered still further by the use of the following relations:

$$\mathbf{P}^2=\mathbf{P}_x^2+\mathbf{P}_y^2+\mathbf{P}_z^2=J(J+1),$$

$$W_R=(r|\langle\mathbf{H}\rangle_R|r)=\tfrac{1}{2}(r|\mathbf{P}_x^2/I_x+\mathbf{P}_y^2/I_y+\mathbf{P}_z^2/I_z|r),$$

$$(r|\{\langle\mathbf{H}\rangle_R,\mathbf{P}_z\}|r)=2W_R(r|\mathbf{P}_z|r).$$

By means of these relations Eq. (37) may be written as Eq. (41).

APPENDIX III

The matrix elements appearing in Eq. (41) may be evaluated by various techniques. $(r|\mathbf{H}_R|r)$ may be evaluated by standard methods.[5] The procedures for obtaining $(r|\mathbf{P}_z^2|r)$ have been discussed in reference 7. $(r|\mathbf{P}_z|r)$ may be treated in the same manner with the difference that the Π_n in reference 7 is to be replaced by $(-1)^\gamma K$ where γ is defined by King, Hainer, and Cross[5] and is equal to 0 or 1. γ characterizes the symmetry species of the energy levels. To obtain $(r|\mathbf{P}_z^3|r)$, Π_n is replaced by $(-1)^\gamma K^3$.

$(rm|\mathbf{\Pi}^k|rm)$, where k is an integer, may be evaluated by the techniques given in I, provided it is assumed that the wave function X_{rm} diagonalizes the Hamiltonian $\langle\mathbf{H}\rangle_R+\langle\mathbf{H}\rangle_I$. For a semisymmetric rotor, $(rm|(3n+\tau-\mathbf{P}_zI_{z2}/I_z)^k|rm)$ replaces the $(3n+\tau+\sigma)^k$ appearing in the symmetric rotor formulas in I. The evaluation of $(rm|1-\cos N\theta|rm)$ proceeds as in I with the same assumptions as above. The other matrix elements in $\cos N\theta$ can also be obtained as described in I.

[16] O. Klein, Z. Physik 58, 730 (1929).

On the Determination of Absolute Intensities from Single- and Multiple-Path Absorption Measurements*

S. S. PENNER AND H. AROESTE
Daniel and Florence Guggenheim Jet Propulsion Center, California Institute of Technology, Pasadena, California

(Received January 31, 1955)

The physical principles involved in conventional absolute intensity measurements are reviewed. Experimental difficulties rule out the use of extrapolation techniques for some spectral transitions. For this reason it is of interest to re-examine the possibility of using total absorption measurements, in conjunction with the curves of growth, for making intensity estimates. Extrapolation methods yield results which are independent of spectral line shape. Use of the curves of growth, on the other hand, implies the assumption that the line contour can be described by combined Doppler and Lorentz broadening.

The curves of growth permit a unique correlation between total absorption and f-value either for spectral lines with pure Doppler broadening or for pure collision broadening. Furthermore, a simple experimental procedure can be devised for estimating both the absolute intensity and the spectral line profile on the basis of single-path and multiple-path absorption measurements. The suggested procedure involves absorption measurements for optical densities (path lengths) under conditions in which the integrated fractional absorption is a relatively sensitive function of spectral line shape. Representative calculations referring to utilization of the proposed method have been carried out for spectral lines belonging to the $^2\Sigma \rightarrow {}^2\Pi$ transitions, (0,0)-band, of OH, and also for lines belonging to the fundamental vibration-rotation spectrum of CO.

I. INTRODUCTION

THE difficulties inherent in quantitative measurements of intensities are well-known to spectroscopists.

For absolute intensity estimates on isolated spectral lines in ultraviolet spectra probably the most widely used procedure involves measurement of the integrated fractional absorption, followed by attempts at estimating f-values through the use of the curves of growth.[1] If accurate measurements can be made for sufficiently small optical densities, unambiguous interpretation of the results is possible since the fractional absorption is independent of spectral line-shape.[2] Less satisfactory is the type of interpretation used, for example, in the determination of absolute f-values for lines belonging to $^2\Sigma \rightarrow {}^2\Pi$ transitions of OH.[3,4] In this case the integrated fractional absorption depends upon both line shape and absolute intensity. Consequently, fitting of observed data to theoretical curves for relative intensities involves such doubtful assumptions as uniform line shape for all of the measured lines, relative intensity estimates which neglect vibration-rotation interactions, etc. It is evident that a more satisfactory approach for conditions corresponding to nonlinear portions of the curves of growth must involve two independent measurements for each spectral line in order to determine the two unknowns involved, *viz.*, line shape and f-value. This suggested procedure is applicable to all spectral lines which are adequately described by combined Doppler and Lorentz broadening, irrespective of the spectral region in which the lines under study occur.

Reliable infrared intensity measurements for entire vibration-rotation bands can be carried out by judicious use of extrapolation techniques[5] combined with suitable methods for pressure broadening.[6] Since the experimental conditions required for intensity estimates are sometimes difficult to meet, particularly for diatomic molecules, use of the procedure based on the curves of growth is indicated in some cases.

There are two basic assumptions involved in the use of the curves of growth for line shape and intensity estimates. These are: (1) the spectral lines under study have a contour which is described adequately by a representation based on Lorentz and Doppler broadening; (2) the measured integrated fractional absorption is substantially independent of experimental slit width. There is experimental evidence that the first assumption is often a useful empirical rule in the sense that observed experimental data can be made to fit a simplified spectral line contour, although the actual line shape may not correspond exactly to the Doppler-Lorentz broadening formula.[7] It is easily shown[8,9] that

* Supported by the Office of Naval Research under Contract Nonr-220(03), NR 015 401. A preliminary account of this work was presented at a "Stellar Atmospheres Conference," Indiana University, Bloomington, Indiana, September 30 to October 2, 1954.

[1] E. M. F. van der Held, Z. Physik **70**, 508 (1931); S. S. Penner and R. W. Kavanagh, J. Opt. Soc. Am. **43**, 385 (1953).

[2] R. B. King and D. C. Stockbarger, Astrophys. J. **91**, 488 (1940); **95**, 78 (1942).

[3] O. Oldenberg and F. F. Rieke, J. Chem. Phys. **6**, 439 (1938); R. J. Dwyer and O. Oldenberg, *ibid.* **12**, 351 (1944).

[4] P. J. Dyne, Technical Report No. 12, Contract Nonr-220(03), NR 015 210, California Institute of Technology, Pasadena, November, 1953.

[5] E. B. Wilson, Jr., and A. J. Wells, J. Chem. Phys. **14**, 578 (1946).

[6] S. S. Penner and D. Weber, J. Chem. Phys. **19**, 807, 817, 974 (1951).

[7] For discussions of spectral line shape see, for example, H. Margenau and W. W. Watson, Revs. Modern Phys. **8**, 22 (1936); J. H. Van Vleck and V. F. Weisskopf, *ibid.* **17**, 227 (1945); P. W. Anderson, Phys. Rev. **76**, 647 (1949).

[8] Nielsen, Thornton, and Dale, Revs. Modern Phys. **16**, 307 (1944).

[9] C. R. De Prima and S. S. Penner, J. Chem. Phys. **23**, 775 (1955).

the second statement is correct, in principle; errors resulting from lack of experimental sensitivity will be discussed in a subsequent publication.

In Sec. II we present a brief review of the physical principles involved in the use of extrapolation techniques for absolute intensity measurements. Absolute intensity and line-shape estimates through the curves of growth are considered in Sec. III. Application of the proposed procedure to $^2\Sigma \rightarrow {}^2\Pi$ transitions of OH, (0,0)-band, is described in Sec. IV. Representative calculations for spectral lines belonging to the fundamental vibration-rotation band of CO are given in Sec. V.

II. EXTRAPOLATION TECHNIQUES FOR ABSOLUTE INTENSITY MEASUREMENTS

The fractional absorption, $A(\omega)$, and the fractional transmission, $T(\omega)$, are related through the expression

$$A(\omega)=1-T(\omega). \tag{1}$$

If $P(\omega)$ is the spectral absorption coefficient at the wave number ω and X equals the optical density, then

$$\int_{\omega_1}^{\omega_2} A(\omega)d\omega=\int_{\omega_1}^{\omega_2}\{1-\exp[-P(\omega)X]\}d\omega \tag{2}$$

independently of the experimental slit function, provided the integration interval from ω_1 to ω_2 exceeds the wave-number range, for which $P(\omega)$ vanishes, by the experimental slit width $\Delta\omega^*$ on either side.[9,10] It should be noted also that the validity of Eq. (2) does not depend on the functional form of $P(\omega)$ provided $P(\omega)$ vanishes for $\omega \leq \omega_1+\Delta\omega^*$ and for $\omega_2-\Delta\omega^* \leq \omega$. From Eq. (2) is is apparent that

$$S_K=\int_{\omega_1}^{\omega_2} P(\omega)d\omega=\lim_{X\to 0}\left[(1/X)\int_{\omega_1}^{\omega_2} A(\omega)d\omega\right] \tag{3}$$

where S_K represents the integrated intensity of the spectral line under study whose center is assumed to lie at the wave number ω_K. The validity of Eq. (3) for all slit functions and line shapes forms the basis of extrapolation methods for the determination of absolute intensities.[5,6,11,12] Extrapolation methods will fail to yield reliable results only if $\int_{\omega_1}^{\omega_2} A(\omega)d\omega$ is not estimated correctly at very low optical densities because of lack of intrumental sensitivity. In this case the limiting curvature of a plot of $\int_{\omega_1}^{\omega_2} A(\omega)d\omega$ *vs* X is not defined properly, and extrapolation to $X=0$ leads to an erroneous estimate for S_K.

Significant absolute intensity estimates are obtained also if the experimental slit width is small compared to the line width.[6] Under these conditions $P(\omega)$ is measured directly and

$$S_K=\int_{\omega_1}^{\omega_2} P(\omega)d\omega=-\frac{1}{X}\int_{\omega_1}^{\omega_2}[\ln T(\omega)]d\omega \tag{4}$$

defines the integrated intensity. Experimental conditions justifying the use of Eq. (4) can be approached at elevated pressures. In practice a combination of pressure broadening and extrapolation to zero optical pathlength leads to the most desirable results.[6]

It is apparent from the preceding considerations that there is a need for methods of obtaining reliable intensity estimates under conditions where pressure broadening and/or extrapolation to zero optical pathlength is not feasible. For this reason we propose to re-examine the use of the curves of growth for the interpretation of integrated fractional absorption measurements, particularly under conditions in which the measured results are a sensitive function of the line-shape parameter.

III. USE OF THE CURVES OF GROWTH FOR ABSOLUTE INTENSITY AND LINE-SHAPE MEASUREMENTS

The integrated fractional absorption is again determined through Eq. (2) while the integrated intensity S_K is defined in Eq. (4). If the spectral line under study had a pure Doppler contour the (maximum) absorption coefficient at the line center would be

$$P_K'=(S_K/\omega_K)(mc^2/2\pi kT)^{\frac{1}{2}} \tag{5}$$

where m is the mass of the radiating molecule, c equals the velocity of light, k equals the Boltzmann constant, and T is the absolute temperature. A spectral line with combined Doppler, collision, and natural line broadening is described conveniently by the parameter

$$a=(b_N+b_C)(\ln 2)^{\frac{1}{2}}/b_D, \tag{6}$$

where b_N, b_C, and b_D denote, respectively, the natural half-width, the half-width resulting from collision (Lorentz) broadening, and the half-width produced by Doppler broadening.[13]

The spectral absorption coefficient $P(\omega)$ entering into Eq. (2) is a linear function of P_K' and depends also on the line-shape parameter a. In the conventional curves of growth $A(\ln 2)^{\frac{1}{2}}/2b_D$ is plotted as a function of $P_K'X$ with a treated as a variable parameter,[1] where

$$(\ln 2)^{\frac{1}{2}}/b_D=(1/\omega_K)(mc^2/2kT)^{\frac{1}{2}}.$$

Let A_1 and A_2 represent, respectively, the total fractional absorption for the K'th spectral line if the optical pathlengths have the values X_1 and X_2, respectively. It is then a simple matter to obtain A_1 and A_2 as functions of $P_K'X_1$ and a for known values of X_2/X_1 through use of the curves of growth. Alternately, the ratio A_2/A_1 can be represented as a function of $P_K'X_1$

[10] The experimental slit width $\Delta\omega^*$ is defined by the condition that the slit function $g(|\omega'-\omega|,b,c)$ vanishes for $|\omega'-\omega| \geq \Delta\omega^*$ where $g(|\omega'-\omega|,b,c)$ determines the contributions to the measured intensity, when the instrument is set at the wave number ω, resulting from the wave number ω'.

[11] D. G. Bourgin, Phys. Rev. **29**, 794 (1927); **32**, 237 (1928).

[12] Thorndike, Wells, and Wilson, J. Chem. Phys. **15**, 157 (1947).

[13] The half-width is defined as the wave-number range for which $P(\omega)$ is greater than or equal to one-half of the spectral absorption coefficient at the line center.

and a, as has been done in a previous publication for the special case $X_2/X_1 = 2$.[14]

From the measured values of A_1 and A_2 and the known ratio X_2/X_1 we can construct two curves relating a to $P_K'X_1$. The applicable values of a and $P_K'X_1$ for the absorbing system correspond to the intersection of the two curves of a *vs* $P_K'X_1$. Finally, since X_1 is known from the partial pressure of absorbing gas and from the length of the gas absorption cell, P_K' itself is determined. The integrated intensity S_K may now be calculated from Eq. (5). Alternately, the dimensionless oscillator strength f_K associated with the K'th line is given through the expression

$$S_K = 2.379\times10^7(273.1/T)f_K(N_l/N_T) \times[1-\exp(-hc\omega_K/kT)] \quad (7)$$

where N_l/N_T represents the fraction of the total number of absorbing molecules in the lower state for the transition or transitions giving rise to the line with quantum number K, and h is Planck's constant.

If experimental measurements are made for a series of spectral lines belonging to a given electronic transition or vibration-rotation band, and if the relative intensities can be calculated theoretically, a simple experimental check is available for the consistency of the data as well as for the correctness of the relative intensity calculations. Thus

$$S_K = \frac{8\pi^3 N_T}{3hcQ}\omega_K g_u(q_K)^2[\exp(-E_l/kT)] \times[1-\exp(-hc\omega_K/kT)] \quad (8)$$

where Q is the total partition function, g_u equals the statistical weight of the upper state involved in the transition giving rise to the K'th spectral line, $(q_K)^2$ is the square of the matrix element for the transition under study, and E_l is the lower energy level of the absorbing (ground) state. From Eqs. (5) and (8) it is easily shown[15] that

$$P_K'\frac{3hcQ}{8\pi^3 N_T}\left(\frac{2\pi kT}{mc^2}\right)^{\frac{1}{2}}[\exp(E_l/kT)][g_u(q_K)^2]^{-1} = 1. \quad (9)$$

A plot of the left-hand side of Eq. (9) as a function of K would be expected to show systematic deviations from unity if, for example, significant vibration-rotation interactions had been neglected in the calculation of $g_u(q_K)^2$. Alternately, if correct theoretical values are available for $g_u(q_K)^2$, then consistency of the experimental data can be verified by showing that $\ln[S_K/g_u(q_K)^2]$ is a linear function of E_l with slope equal to $-1/kT$.

[14] S. S. Penner, J. Chem. Phys. **21**, 686 (1953).

[15] The factor $[1-\exp(-hc\omega_K/kT)]$ is practically equal to unity at all reasonable temperatures for absorption experiments in the visible and infrared regions of the spectrum.

IV. INTENSITY ESTIMATES ON SPECTRAL LINES BELONGING TO $^2\Sigma \rightarrow {}^2\Pi$ TRANSITIONS OF OH, (0,0)-BAND

We proceed to examine the required experimental conditions for an accurate redetermination of f-values for spectral lines belonging to $^2\Sigma \rightarrow {}^2\Pi$ transitions, (0,0)-band, of OH, using in our calculations for the determination of suitable experimental conditions the absolute intensity estimates of Oldenberg and Rieke[3]; the argument remains substantially unchanged if Dyne's f-values are employed.

Consider an absorption experiment in a 50-cm long cell on the OH formed in a mixture consisting initially of two parts of H_2O and one part of O_2 at atmospheric pressure. Equilibrium calculations at 1300°K show that $X = 1.185\times10^{-3}$ cm-atmos.[16] According to Oldenberg and Rieke[3,4] the f-value for the $Q_1(K=6)$ line is

$$f = 3.17\times10^{-4}S_J/(2J+1) \quad (10)$$

where the rotational line strength $S_J = 50.6$ if vibration-rotation interactions are neglected,[17] and $2J+1$ (with $J = K+\frac{1}{2}$) is the statistical weight of the lower energy level involved in the given transition.

The use of Eqs. (5), (7), and (10) and introduction of appropriate numerical values shows that $P_K' = 1.64\times10^3$ cm^{-1}–atmos^{-1} for the $Q_1(6)$ line. Hence $\log(10.6P_K'X) \simeq 1.30$ would represent the abscissa of the curves of growth. This numerical value, together with the line-shape parameter a determines A_1. For the sake of argument we assume $a=1$. A triple-path experiment for the same value of a and $\log(10.6P_K'X)$ increased by log 3 corresponds to the value of A_2. In practice A_1 and A_2 are determined with a and $P_K'X$ unknown. In Fig. 1 we show a plot of the possible values of a as a function of $P_K'X$ for a measured value of $A_1(\ln 2)^{\frac{1}{2}}/2b_D = 1.35$; this curve is seen to intersect the a *vs* $P_K'X$ curve corresponding to the value $A_2(\ln 2)^{\frac{1}{2}}/2b_D = 3.00$ for a triple-path experiment at $a=1$ and $\log(10.6P_K'X) = 1.30$. Reference to Fig. 1 shows that both a and $P_K'X$ can be determined with acceptable accuracy as long as the true values are roughly the same as those assumed in the present illustrative calculations. In other words, the use of single- and triple-path absorption measurements on OH in a 50 cm long tube at 1300°K appears to be a promising experiment for a redetermination of the f-value, provided (1) the spectral line shape is described by combined Doppler and Lorentz broadening, and (2) adequate experimental sensitivity is obtained.

A single measurement of integrated fractional absorption would determine $P_K'X$ if a is either very nearly zero or else very large (say $a>10$). Alternately, if

[16] This result is based on the thermodynamic functions prepared by the National Bureau of Standards and listed in "Tables of Selected Values of Chemical Thermodynamic Properties," Series I, Volume I, 1947–1949.

[17] G. H. Dieke and H. M. Crosswhite, Bumblebee Series Report No. 87, The Johns Hopkins University, Baltimore, November, 1948.

sufficient experimental sensitivity can be obtained to determine the integrated fractional absorption for $\log(10.6P_K'X)$ less than about 0.5, then $P_K'X$ is roughly determined independently of the absolute value of a.

V. INTENSITY ESTIMATES ON SPECTRAL LINES BELONGING TO THE FUNDAMENTAL VIBRATION-ROTATION BAND OF CO

The nonlinear parts of the curves of growth may also be used, in principle, to determine infrared intensities and the line-shape parameter a for lines with Doppler and Lorentz broadening. A graph similar to the one shown in Fig. 1 applies under suitable experimental conditions.

For CO at 300°K the integrated intensity for the rotational line $J=6\rightarrow J=7$ belonging to the fundamental vibration-rotation band ($n=0\rightarrow n=1$) is found to have the value $S_{6\rightarrow 7}^{0\rightarrow 1}=9.98$ cm^{-2}-atmos^{-1}.[6,18,19] The center of this spectral line occurs at 2169 cm^{-1}.

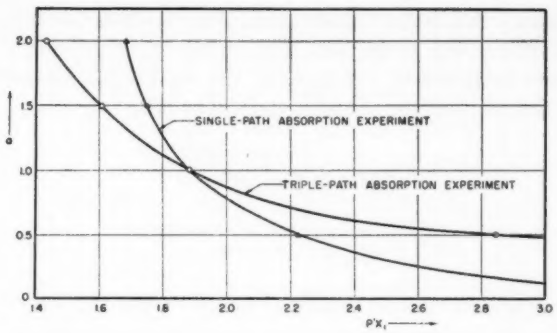

FIG. 1. Illustrative plot indicating the interpretation of single-path and triple-path absorption experiments for $a=1$ and $P'X_1=1.88$.

Therefore $P_K'=1.85\times10^3$ cm^{-1}-atmos^{-1}. For $X_1=10^{-3}$ cm-atmos, $\log(10.6P'X)\simeq1.3$ and, if $a\simeq1$, Fig. 1 applies again for $X_2=3\times10^{-3}$ cm-atmos. If the collision half-width for CO at 300°K and atmospheric pressure[20] is 0.065 cm^{-1}, then $a\simeq1$ at a total pressure of about 0.05 atmos. It is of interest to note that $a\simeq20$ at atmospheric pressure and room temperature for CO.

[18] "Wave Number and Intensity Tables for Carbon Monoxide," Contract Nonr-220(03), NR 015 210, California Institute of Technology, Pasadena, September 1952.

[19] J. R. Oppenheimer, Proc. Cambridge Phil. Soc. **23**, 327 (1926); R. C. Herman and R. F. Wallis, J. Chem. Phys. **23**, 637 (1955).

[20] S. S. Penner and D. Weber, J. Chem. Phys. **19**, 1361 (1951); **21**, 1503 (1953).

THE JOURNAL OF CHEMICAL PHYSICS VOLUME 23, NUMBER 12 DECEMBER, 1955

Diffusion Coefficients of Fatty Acids and Monobasic Phosphoric Acids in *n*-Decane

J. R. WHITE
Socony-Vacuum Laboratories (A Division of Socony-Vacuum Oil Co., Inc.), Research and Development Department, Paulsboro, New Jersey

(Received February 28, 1955)

Diffusion coefficients of the series of even-numbered fatty acids from C_6 to C_{18}, of three dialkyl phosphoric acids, and of 2-ethylhexoic and benzoic acids have been measured in dilute solutions in *n*-decane at 30°C. Gravity mixed diaphragm cells have been employed in making the measurements. The Stokes-Einstein hydrodynamic relationship adjusted by an empirical coefficient represents the magnitude and variation of diffusion coefficients in the series of fatty acids if corrections are made for solute association and nonsphericity. The unmodified Stokes-Einstein equation predicts diffusion coefficients lower than those measured by approximately a factor of two.

LITTLE information exists that relates the diffusion coefficients in a series of materials to a systematic change in molecular structure in the series. Of particular industrial interest are hydrocarbon solutions of alcohols, acids, and soaps. These may range from true solutions exhibiting little association to micellar structures with solute apparent molecular weights in the tens of thousands. In addition to providing information on structure, diffusion coefficients may relate transport rates with concentration gradients in hydrocarbon oils not subject to mechanical mixing. Quasi-static oil layers are encountered at surfaces where rheological considerations require that mechanical flow diminish to zero. With these considerations in mind the diffusion coefficients of a series of typical acids of interest in a selected hydrocarbon oil, decane, have been measured at 30°C; these include the even numbered fatty acids from C_6 to C_{18}, three monobacic phosphoric acids, benzoic acid and 2-ethylhexoic acid.

DIFFUSION THEORY

The Stokes-Einstein equation as modified by Perrin[1] for an elongated ellipsoidal geometry of the diffusate molecule has been widely applied to systems where the diffusate molecule is large compared with the solvent molecule:

$$D=\frac{kT}{6\pi\eta(3/4\pi)^{\frac{1}{3}}}(N/V)^{\frac{1}{3}}\cdot f, \qquad (1)$$

[1] F. Perrin, J. phys. radium **7**, 1 (1936).

where V is a molar volume and f is a frictional coefficient for ellipsoidal molecules. For elongated ellipsoids f is given in terms of the ratio of the equatorial semi-axis of the ellipsoid to the semi-axis of revolution, b/a,

$$f=\frac{(b/a)\ln\dfrac{1+\{1-(b/a)^2\}^{\frac{1}{2}}}{(b/a)}}{\{1-(b/a)^2\}^{\frac{1}{2}}}. \qquad (2)$$

This equation is in essential accord with the premise that the solvent is a viscous continuum, through which the diffusate is driven by osmotic forces, and which exerts a purely viscous drag on the diffusate molecule. When the solvent and diffusate molecule are made to approach each other in molecular size, relations differing from this hydrodynamic analog may be anticipated; and indeed it has been observed that Eq. (1) predicts diffusion coefficients generally smaller than those observed.[2,3] The nature of the deviations from (1) and the range of molecular sizes over which these may occur have not been fully investigated. Rather the approach has been to acknowledge the inapplicability of 1 for systems of nearly equal solvent and solute molecular volume and to consider the diffusion process of solvent, solute cooperative nature.

The transition state relationship derived by Stearn, Irish, and Eyring[4]

$$D=\frac{\lambda^2}{v_f^{\frac{1}{2}}}\left(\frac{kT}{2\pi m}\right)^{\frac{1}{2}}\exp\left(-\frac{\Delta E_{\text{vap}}}{rRT}\right), \qquad (3)$$

where λ is the distance between successive equilibrium positions of a molecule generally taken as $(V/N)^{\frac{1}{3}}$, m is the reduced mass of diffusate and solvent molecules and v_f is a free volume estimated by

$$v_f^{\frac{1}{2}}=\frac{sRTV^{\frac{1}{3}}}{N^{\frac{1}{3}}\Delta E_{\text{vap}}} \qquad (4)$$

has frequently been employed in calculating absolute diffusion rates. As employed, r has been taken as 3 to 5, assuming that the activation energy for diffusion is one-third to one-fifth the energy for evaporation, ΔE_{vap}, and s has been assigned a value of 2 for cubical packing. For interdiffusion in concentrated solutions, molecule number averages of the respective quantities, $v_f^{\frac{1}{2}}$, λ, and ΔE_{vap} have been employed. For dilute solutions in a single solvent the quantities $v_f^{\frac{1}{2}}$, λ, and ΔE_{vap} have been taken as those of the solvent alone. When treated in this latter manner, computed diffusion coefficients within a homologous series of solutes in the same solvent vary inversely with the square root of the reduced molecule masses.

Other relations of a semi-empirical nature have been employed in correlating diffusion coefficient data in nonionic systems. Trevoy and Drickamer[5] have successfully applied Arnold's[6] equation to equal mole per cent mixtures of pure hydrocarbons. Wilke[7] has organized available data around a correlation coefficient, $F(=T/D\eta)$ and a solvent factor, ϕ, and has observed that, for nonhighly ionized systems in water and other solvents, as solute molecular volumes increase diffusion coefficients tend to become proportional to the cube root of these molecular volumes and approach values computed by the Stokes-Einstein equation for large spherical molecules.

DIAPHRAGM CELL TECHNIQUES: PHENOMENOLOGY

Gordon[8] has comprehensively reviewed diaphragm cell techniques for the measurement of diffusion coefficients and the sources of error inherent therein. The work of Harned and Nuttall[9] precisely relating the differential diffusion coefficients of water solutions of potassium chloride to concentration and temperature, when combined with the integral calibration technique of Gordon, permits calibration of diaphragm cells in terms of a potassium chloride standard without analytical approximation.

When applied to the determination of diffusion coefficients, the diaphragm cell technique yields integral diffusion coefficients over the concentration range measured. For the very dilute solutions here reported these coefficients are not likely far removed from differential coefficients for an ideal system.

CHOICE OF SYSTEMS AND APPARATUS

Gravity mixed diaphragm cells, Fig. 1, have been used for the measurements. Uncertainty in the measured diffusion coefficients due to error in the volume calibration of the cells is in practice entirely negligible. The volume of the outer compartment will remain constant if the specific volume of the solution is linear in concentration over the range studied. This condition should be adequately satisfied for dilute hydrocarbon systems.

Concentration homogeneity on both sides of the diaphragm is intended to be secured by density stirring. With reproducible technique any possible contribution to the cell calibration constant from stagnant layers immediately adjacent to the diaphragm becomes constant. These possible stagnant layers although shown to be reproducible for the calibrating solution are not with certainty a negligible contributor in the effective diaphragm geometry as Stokes[10] has demonstrated by comparing stirred cells with density mixed cells. To

[2] L. Onsager, Ann. N. Y. Acad. Sci. **46**, 241 (1943).
[3] A. Polson, J. Phys. & Colloid Chem. **54**, 649 (1950).
[4] Stearn, Irish, and Eyring, J. Phys. Chem. **44**, 981 (1940).
[5] D. J. Trevoy, and H. G. Drickamer, J. Chem. Phys. **17**, 1117 (1949).
[6] J. H. Arnold, J. Am. Chem. Soc. **52**, 3937 (1930).
[7] C. R. Wilke, Chem. Eng. Progr. **45**, 218 (1949).
[8] A. R. Gordon, Ann. N. Y. Acad. Sci. **46**, 285 (1943).
[9] H. S. Harned, and R. L. Nuttall, J. Am. Chem. Soc. **71**, 1460–3 (1949).
[10] R. H. Stokes, J. Am. Chem. Soc. **72**, 763 (1950).

minimize the possible effects of incomplete density mixing and consequent stagnant layers, the physical properties of density and viscosity which govern the implied existence and reproducibility of such layers have been made as nearly alike for calibrating solutions and the measured solutions as feasible. The viscosity of the solvent phase, decane, is 0.00796 poise at 30°C; the viscosity of water is 0.00801 poise. Density differences between solution and solvent are generally less for the decane solutions than for the calibrating standard.

Barnes[11] has shown rigorously that the assumption of a steady state process in the diaphragm is valid if the ratio of the pore volume in the diaphragm to the upper or lower compartment volume is small compared with unity. This condition has been satisfied by choosing cell pore volumes of 0.1 ml for compartment volumes of 18 to 40 ml.

Corning M sintered disks were employed as the cell diaphragms. Hartley and Runnicles,[12] in seeking to avoid streamlined flow, have studied the suitability of different Jena glasses in cell design. Corning M sintered glass is roughly intermediate in pore diameter between the two Jena grades (G-4 and G-3) for which streamlined flow was found to be entirely absent (G-4) and detectable (G-3). The reproducibility of cell constants in the measurements with Corning M glass suggests that streamlined flow is not an important source of error with this glass. Finer pore diameter glasses can be satisfactory in this respect but choice of such glasses reduce the effective pore area to pore length ratios and increase the experiment time. Finer pore glasses also increase the possibility that some diffusate transport may occur as sufrace transport.

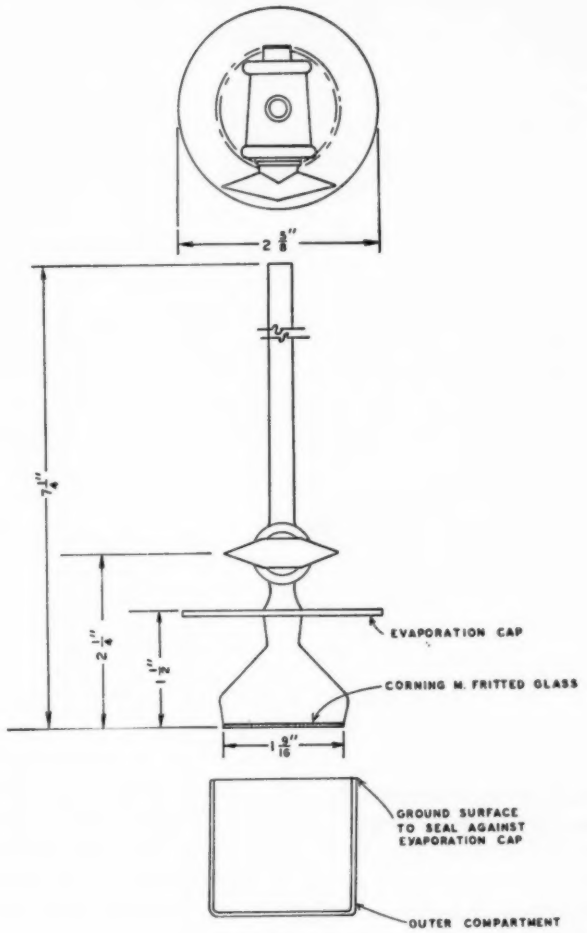

FIG. 1.

EXPERIMENTAL

1. General Method

The general methods of cell manipulation for cells of this type have been described.[8] In this series of measurements the cells were brought to thermal equilibrium in shock-mounted air-jacketed compartments immersed in a water thermostat maintained at 30.03±0.02°C. Cells and solutions were adjusted to approximately this temperature externally and then allowed to equilibrate for four hours. Preliminary diffusion periods were employed to establish a uniform concentration gradient within the diaphragm. These periods extended from four hours for the calibrating KCl solutions to 15 hours for decane solutions of the higher molecular weight acids. Variations of 50% in these times made no differences in the diffusion coefficients. Two preliminary diffusion periods were compared with a single preliminary period; differences were not observed. At the close of the preliminary diffusion, solutions were allowed to diffuse into pure solvent for measurement times up to 64 hours, depending on the magnitude of the coefficient. The cells were then disassembled and both compartments and the diaphragm contents were analyzed by electrometric titration.

2. Materials

Commercially available *n*-decane solvent was purified by vacuum redistillation from solid potassium hydroxide immediately before use. The purified material possessed a melting point of $-27\pm2°$, a refractive index (25°) of 1.4120, and a density (30°) of 0.722. The comparable accepted values[13] are $M.P.=29.66$, $n_d^{25}=1.40967$ and $d^{20}=0.722_4$. Each lot of decane was titrated immediately after distillation to ascertain freedom from acidic constituents. Storage tests under conditions of the diffusion experiments revealed that measurable acidic constituents did not form for periods up to 60 hours and were just detectable at 100 hours.

Eastman-Kodak high purity grade fatty acids were recrystallized from absolute alcohol until equivalent weights (by titration) corresponded with formula

[11] C. Barnes, Physics **5**, 4 (1934).

[12] G. S. Hartley, and D. F. Runnicles, Proc. Roy. Soc. (London) **A168**, 401 (1938).

[13] *Selected Values of Physical and Thermodynamic Properties of Hydrocarbons and Related Compounds* (Carnegie Press, Pittsburgh, 1953).

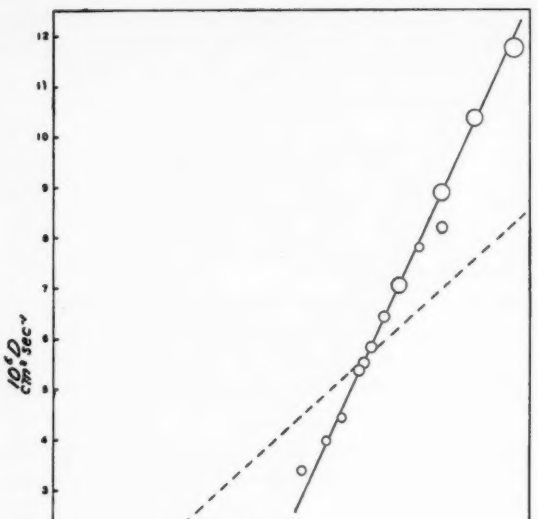

FIG. 2. Diffusion coefficients acids in decane 30.0°C.

weights to within 1%. Titration curves revealed only mono-basic characteristics. The oleic and benzoic acids were C.P. grade reagents similarly characterized by titration. The di-*n*-decyl phosphoric, di-lauryl phosphoric, and di-(octadecene-8) phosphoric acids were prepared as alcohol, phosphorous pentoxide reaction products and were multiply fractionally recrystallized from acetone and ethanol to yield materials whose phosphorous content (within 0.3%) and equivalent weight (within 0.5%) corresponded to that by formula. The principal impurities in these materials were di-esters of traces of higher and lower alcohols. In addition, the mono-ester constituted a small (3%) impurity in the di-(octadecene 8) phosphoric acid and could not be separated by recrystallization. 2-Ethyl hexoic acid was a redistilled commercial product.

EXPERIMENTAL RESULTS

The diffusion equation for a diaphragm cell can be written

$$d\ln\Delta C+\beta D dt=0,$$

where ΔC is the concentration difference across the diaphragm and β is the cell constant. This equation has been integrated for the calibrating KCl solution employing differential diffusion coefficients varying in concentration as given by Harned and Nuttall. Three separate cells have yielded the constants, β, in Table I. These cells have then been employed to measure the diffusion coefficients of the acids in decane given in Table II. These latter coefficients are integral coefficients in the concentration range up to 0.02 molal.

TABLE I. Diaphragm cell calibration, KCL standard.

Cell	β	No. of det'ns.	Av. dev.
A	0.92_3	4	0.003
B	0.77_0	8	0.007
C	0.448	7	0.005

From the data of Dorinson, McCorkle, and Ralston[14] the liquid molar volumes of the fatty acids have been estimated at 30°C. The molar volume of oleic acid has been measured by Keffler and McLean.[15] The liquid molar volumes of the phosphate esters have been estimated from the volumes of the lower members of the series[16] by determining the volume increment to be added per CH_2 group and making this addition the requisite number of times, subtracting 10 ml for each double bond. For the carboxylic acids,

$$V_1\simeq 24.5+16.95(n)$$

and for the phosphate esters

$$V_1\simeq 132.8+33.3(n-2)$$

where n is the number of carbon atoms per alkyl chain. The molar volume of 2-ethyl hexoic acid has been measured as 162.6 ml at 30°C.

From the above estimates the quantity $(N/V_1)^{\frac{1}{3}}$ has been computed and is given in Table II.

On Fig. 2 the diffusion coefficients are plotted against $(N/V_1)^{\frac{1}{3}}$. The dependence upon this volume property expected from the Stokes-Einstein relationship is evident. This relationship, Eq. (1), for spherical molecules of volume V_1/N is shown as a dashed line.

Figure 3 is a plot of the diffusion coefficients against the inverse square root of the reduced solute, solvent

TABLE II. Diffusion coefficients; acids in decane 30.0° C.

Acid	Cell	$10^6 D$	No. of det'ns.	$10^6\Delta D$[a]	$10^{-7}(N/V_1)^{\frac{1}{3}}$
Benzoic	*A,B*	11.75	4	0.18	1.83[b]
Caproic	*B,C*	10.38	4	0.14	1.68
2-Ethyl hexoic	*A,B*	8.17	2	0.10	1.55
Caprylic	*B,C*	8.88	4	0.14	1.55
Capric	*B,C*	7.77	4	0.04	1.46
Lauric	*A,B,C*	7.04	5	0.15	1.38
Myristic	*B,C*	6.41	4	0.05	1.32
Palmitic	*A*	5.80	2	0.01	1.27
Stearic	*A,B*	5.33	2	0.06	1.22
Oleic	*A,B*	5.50	3	0.03	1.24
di-*n*-decyl Phosphoric	*A,B*	4.40	6	0.04	1.15
di-lauryl Phosphoric	*B*	3.95	3	0.06	1.09
di-(octadecene-8) Phosphoric	*A*	3.35	4	0.04	0.98

[a] Average deviation.
[b] Based on density of crystal.

[14] Dorinson, McCorkel, and Ralston, J. Am. Chem. Soc. 64, 2739 (1942).
[15] L. Keffler, and J. H. McLean, J. Soc. Chem. Ind. (London) 54, 178 (1935).
[16] I. Heilbron, *Dictionary of Organic Compounds* (Oxford University Press, New York, 1953), Vol. IV.

molecule masses. The transition state Eq. (3) with constants evaluated in the manner of Stearn, Irish, and Eyring is represented by the broken curve for values of the parameter, r, of 2.75. This parameter value results from application of rate theory to obtain the free energy of activation for viscous flow of the solvent, decane.[17] Parameter values as large as 5 result in computed diffusion coefficients which are over an order of magnitude larger than those observed. More consideration of the quantities approximated in employing this relationship appears necessary if closer correspondence is to be secured.

The effective volume properties of fatty acids may be markedly altered by association. Infrared examination of certain carboxylic acids in carbon tetrachloride has revealed that these acids are largely associated into dimers,[18] even at concentrations as low as 0.02 molal. Cryoscopic measurements in cyclohexane have demonstrated that this dimeric structure is predominant in a saturated hydrocarbon at concentrations as low as 0.01 molal and should be included in the molecular volumes employed in diffusion relationships.

The fatty acids depart significantly from a spherical configuration, particularly when the dimeric structure is adopted. In an attempt to estimate the friction drag

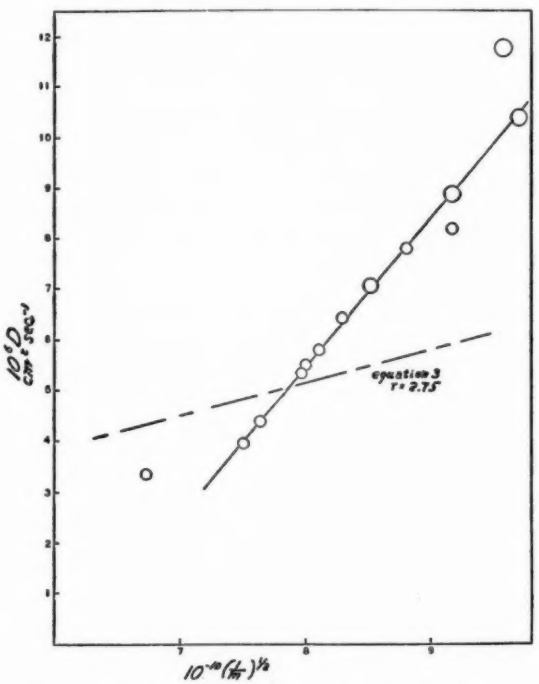

FIG. 3. Diffusion coefficients acids in decane 30.0°C.

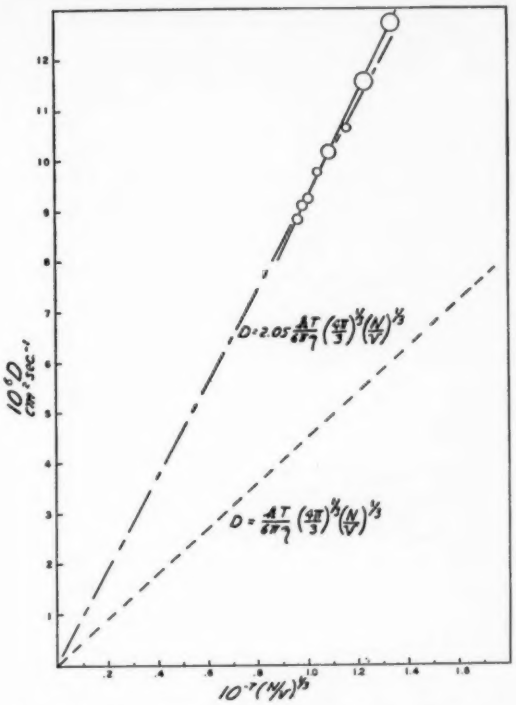

FIG. 4. Diffusion coefficients corrected to a sphere of volume equal to $2V_1/N$.

factors of Eq. (2), Taylor-Hirschfelder models of the acids have been constructed in a stretched dimeric configuration employing a carboxyl-carboxyl spacing equal to that of the known spacing of the acetic acid dimer.[19] These models have been regarded as approximate elongated ellipsoids. Axis ratios, b/a, have been scaled from the models. From these ratios and Eq. (2) the diffusion coefficients of fatty acids have been corrected to those of spheres of the same volumes as the acid dimers (taken as $2V_1/N$).

The diffusion coefficients of the fatty acids corrected as above are plotted on Fig. 4 and are compared with the Stokes-Einstein Eq. (1) shown as a dashed curve and the Stokes-Einstein equation adjusted by an empirical factor of 2.05 shown as a broken line. The corrected coefficients are higher than those predicted by the equation by this factor of about 2.

In view of the obvious approximations involved in the above, physical significance cannot be attached to this factor. Its adoption, however, results in a semi-empirical representation of the diffusion coefficients of the fatty acids over a range of molecular sizes where departures from the Stokes-Einstein relationship have been generally observed.

[17] Moore, Gibbs, and Eyring, J. Phys. Chem. **57**, 172 (1953).
[18] A. E. Martin, Nature **166**, 474 (1950).
[19] L. Pauling, and L. O. Brockway, Proc. Natl. Acad. Sci. U. S. **20**, 336 (1934).

Thermal Diffusion in Polymer Solutions*

A. H. EMERY, JR., AND H. G. DRICKAMER
Department of Chemistry and Chemical Engineering, University of Illinois, Urbana, Illinois
(Received February 7, 1955)

Thermal diffusion measurements have been made on a series of solutions of polystyrene as follows: (1) Five molecular weights (10 000 to 336 000) in toluene; (2) 136 000 molecular weight in o-xylene, styrene, ethyl benzene, dioxane, and pyridine; (3) Styrene dimer in toluene and styrene; measurements were also made on some binary monomeric mixtures.

The thermodynamic property $X\partial\mu/\partial X$ describes adequately the concentration dependence of the thermal diffusion ratio α. It appears that that portion of the motion of the polystyrene molecule in dilute and somewhat concentrated solutions which is segmental involves 10–13 chain atoms in the moving segment. The results seem consistent with Kauzmann and Eyring's picture for motion of long chain molecules.

IN previous papers[1–3] a theory for thermal diffusion in liquids has been developed. It is of interest to apply the theory to polymer solutions as these provide a rather special test of the theory.

The only known previous work on thermal diffusion in polymer solutions is that of Debye and Bueche,[4] who measured separations in the thermo-gravitational column for polystyrene solutions. Their results are not directly comparable to ours, since they used the column and we used the single cell in which the enriching thermal currents are absent. Comparisons are complicated by the enormous concentration dependence of α and the large values of α observed in polymer solutions.

Data were here obtained on a series of fractionated polystyrene cuts in toluene. The average molecular weights of the cuts were 10 000, 50 000, 136 000, 304 000, and 336 000. The polystyrene cuts were furnished by the Dow Chemical Company. Results were also obtained for the 136 000 molecular weight cut in styrene, o-xylene, ethyl benzene, pyridine, and dioxane. Data were obtained in the concentration range $\frac{1}{2}\%$ to 5% in most solvents. Some data were also obtained on binary mixtures of the solvents and for binary mixtures of a dimer of styrene with solvent. The toluene, xylene, and ethyl benzene were Phillips Petroleum pure grade. The dioxane and pyridine were Eastman's best product redistilled. The styrene monomer and dimers were furnished by Dow Chemical Company. Pertinent properties are listed in Table I.

The defining equation for the thermal diffusion ratio for binary mixtures used in this work is:

$$\mathbf{J}_1=-\rho D\left[\text{grad}X_1-\alpha X_1(1-X_1)\frac{1}{T}\text{grad}T\right] \quad (1)$$

where $\mathbf{J}_1$ = flux of component 1, ρ = density, D = diffusion coefficient, X_i = mole fraction of component i, T = absolute temperature. The steady-state solution is

$$\ln\left(\frac{X_1}{1-X_1}\right)_H\left(\frac{1-X_1}{X_1}\right)_c=\alpha\ln\frac{T_H}{T_c}. \quad (2)$$

The sign convention used is that α is positive if the polymer goes to the hot wall.

Our theory (3) gives the following equation for α in a binary mixture:

$$\alpha=\frac{M_1V_2+M_2V_1}{2\bar{M}}\frac{[(\Delta U_2^{\neq}/V_2)-(\Delta U_1^{\neq}/V_1)]}{X_1(\partial M_1/\partial X_1)} \quad (3)$$

where M_i = molecular weight of component i, V_i = molar volume of component i, $\Delta U_i^{\neq}$ = activation energy for viscous flow per mole of component i, X_i = mole fraction of component i, $M=X_1M_1+X_2M_2$. For the polymer solutions it is useful to modify this equation somewhat. Let

$$V_p/V_s=m, \quad (4)$$

$$M_p/M_s=w, \quad (5)$$

where the subscripts p and s refer to polymer and solvent, respectively. Then

$$M_sV_p+M_pV_s=M_sV_s(m+w) \quad (6)$$

and

$$X_sM_s+X_pM_p=M_s(X_s+wX_p). \quad (7)$$

In the low concentration range

$$X_p\cong\frac{\varphi_p}{m} \quad (8)$$

where φ_p is the volume fraction polymer and, since m is of the same order of magnitude as w,

$$X_sM_s+X_pM_p=M_s(X_s+\varphi_p)\cong M_s \quad (9)$$

where the last part of Eq. (9) holds because we are dealing always with dilute polymer solutions.

* This work was supported in part by the U. S. Atomic Energy Commission.

[1] W. M. Rutherford and H. G. Drickamer, J. Chem. Phys. **22**, 1157 (1954).

[2] E. L. Dougherty, Jr., and H. G. Drickamer, J. Chem. Phys. **23**, 295 (1955).

[3] E. L. Dougherty, Jr., and H. G. Drickamer, J. Phys. Chem. (to be published).

[4] B. Debye and A. M. Bueche, *High Polymer Physics* (Chemical Publishing Company, Brooklyn, 1948), pp. 497–527.

Then Eq. (3) can be written

$$\alpha_p=\frac{(m+w)\left(\Delta U_s^{\neq}-\dfrac{\Delta U_p^{\neq}}{m}\right)}{2X_p(\partial M_p/\partial X_p)}. \tag{10}$$

It is convenient to write this in the form

$$\alpha_p=\frac{\alpha_0 RT}{X_p(\partial M_p/\partial X_p)} \tag{11}$$

$$\alpha_0=\frac{(m+w)\left(\Delta U_s^{\neq}-\dfrac{\Delta U_p^{\neq}}{m}\right)}{2RT}, \tag{12}$$

where α_0 (the thermal diffusion ratio at infinite dilution) is independent of concentration. It is then possible to discuss the theory, and the agreement between theory and experiment, from the standpoint of α_0 and concentration dependence separately.

The derivation of Eq. (3) depends upon the assumption that the molecules exchange position in such manner that one volume of component 1 is replaced by one volume of component 2. In this work all of the solvents used, as well as the dimer and polymer consisted of ring structures with relatively small side chains. It is interesting to consider a modification of our assumption wherein one ring is replaced by one ring of the other component rather than a volume for volume replacement. Then Eq. (3) becomes

$$\alpha=\frac{M_1r_1+M_2r_2}{2\bar{M}}\,\frac{\left(\dfrac{\Delta U_2^{\neq}}{r_2}-\dfrac{\Delta U_1^{\neq}}{r_1}\right)}{X_1(\partial_1 M/\partial X_1)}, \tag{13}$$

where r_i = number of rings in component i. The application of Eq. (13) will be discussed in the following.

EVALUATION OF α_0

Since activation energies for self-diffusion for the pure solvents were not available, the activation energies for viscous flow were used. These were either obtained from the literature or measured in this laboratory.

Equation (3), developed and proved for low molecular weight materials previously,[3] was derived from an equation involving the quantity of energy per mole required to remove a molecule of component i from a region. This energy term was related to the activation energy for diffusion, $\Delta V^{\neq}$, which, due to the nature of the derivation, must also be energy per mole. However, since molecular motion in pure polymers is segmental, activation energies measured experimentally, $\Delta U_c^{\neq}$, are energy per segment, and it is necessary to take this into account in evaluating $\Delta V_p^{\neq}$. Let n_c be the number of segments per molecule. Then

$$\Delta U_p^{\neq}=n_c\Delta U_c^{\neq}. \tag{14}$$

If we introduce N_c, the number of chain atoms in a moving segment, for polystyrene

$$N_c=\frac{M_p}{52n_c}. \tag{15}$$

Then, since the polymer molecular weight can be written $M_p=mV_s\rho_p$ where ρ_p is the density of bulk polymer,

$$N_c=\frac{mV_s\rho_p}{52n_c}. \tag{16}$$

The equation for α_0 can now be written:

$$\alpha_0=\frac{(m+w)\left(\Delta U_s^{\neq}-\dfrac{V_s\rho_p}{52N_c}\Delta U_c^{\neq}\right)}{2RT}. \tag{17}$$

To calculate α_0 it is necessary to evaluate the activation energies of the solvent molecules and the moving element of polymer molecule in solution. For ordinary organic mixtures these are assumed to be activation energies for viscous flow of the pure liquids. This assumption is probably quite satisfactory if the heat of mixing is not excessive. It can be shown that the activation energy of a mixture is a linear function of that of the pure components under these circumstances. It is therefore possible to evaluate the activation energies of the pure components from those of a series of mixtures by extrapolating to 100% solvent on one hand and 100% polymer on the other.

Spencer and coworkers[5,6] have obtained activation energies for viscous flow for mixtures of polystyrene and isopropyl benzene, both in the liquid and gel region.

TABLE I. Properties of solvents and dimer.

Liquid	M	$V^{25°}$	$\Delta U^{\neq}$	$\frac{\Delta U^{\neq}}{V}$	μ'
Toluene	92.1	107.0	1880	17.6	0.44
O-xylene	106.2	121.2[a]	2200	18.1	0.427
Ethyl benzene	106.2	123.1	2040	16.6	0.424
Styrene	104.1	115.4[b]	1880[d]	16.3	0.424
Dioxane	88.1	85.3[c]	2650[c]	31.1	0.465
Pyridine	79.1	80.9	2330	28.8	0.464
Dimer	236.3	240[f]	4500[f]	18.7	···

All values of density not otherwise labelled were taken from International Critical Tables. All values of $\Delta V^{\neq}$ not otherwise labeled calculated from data in the Handbook of Chem. and Phys.
All values of μ' were taken from Boyer and Spencer.[8]
[a] L. Massart, Bull. Soc. Chim. Belg. 45, 76 (1936).
[b] R. Boundy and R. Boyer, *Styrene, its Polymers, Co-polymers, and Derivatives* (Reinhold Publishing Corporation, New York, 1952).
[c] J. Regeoffe, Rev. Prod. Chim. 42, 229 (1939).
[d] A. Edwards, and C. F. Ronilla, Ind. Eng. Chem. 36, 1038 (1944).
[e] H. Hartman, Z. Physik. Chem. A191, 197 (1942).
[f] This laboratory—unpublished data.

[5] R. S. Spencer and J. L. Williams, J. Colloid Sci. 2, 117 (1947).
[6] R. S. Spencer and R. E. Dillon, J. Colloid Sci. 4, 241 (1949).

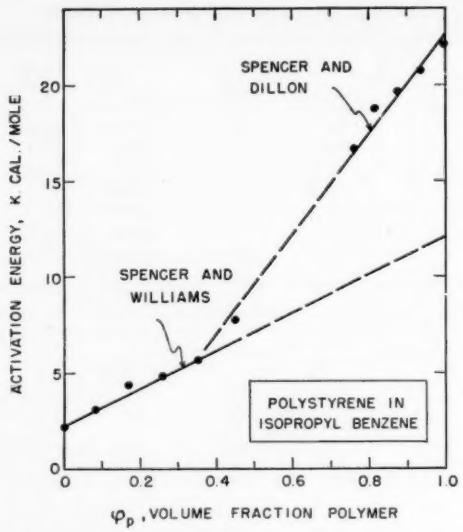
SPENCER AND DILLON
SPENCER AND WILLIAMS
POLYSTYRENE IN ISOPROPYL BENZENE
ACTIVATION ENERGY, K. CAL. / MOLE
φ_p, VOLUME FRACTION POLYMER

FIG. 1. Activation energies for viscous flow—polystyrene in isopropyl benzene.

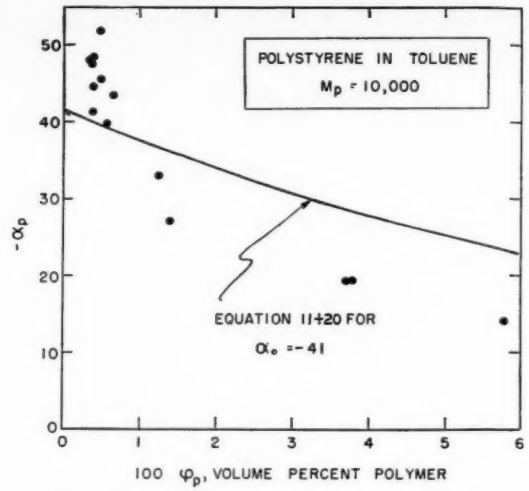

FIG. 3. Thermal diffusion ratio *vs* composition—polystyrene in toluene $M_p = 10\,000$.

These are plotted in Fig. 1 against volume fraction polymer. The data give two straight lines extrapolating approximately to 23 kcal for the gel and to 12 kcal for the liquid at 100% polymer. It would appear that the mechanism of motion is different for the liquid than for the gel. Since we are interested in motion in the dilute region, it appears not unreasonable to assume that 12 kcal per mole is the activation energy for motion of the moving segment of polymer in dilute solution.

In the lowest concentration range, a polymer molecule moves through the solvent essentially as a unit, and the activation energies measured in this range are close to that of the pure solvent. As the concentration is increased, the separate polymer molecules begin to be less independent of each other, and molecular entanglements occur, the extent of which can be appreciable even at concentrations less than 10%. When this condition exists, the mode of motion of the polymer molecule must be partially segmental, since in order to move a molecule must not only displace itself with respect to the solvent, but must cope with entanglements with other molecules. As the concentration is further increased, the mode of motion must become more and more segmental, until in the case of pure polymer it is almost entirely segmental. Thus segmental movement may play a part in the motion of the molecule even at low concentrations, and the term N_e appearing in Eq. (17) is the number of chain atoms in the segment of the polymer molecule active in that portion of the motion which is segmental, in the low concentration range. Further data by Spencer and Williams[5] on polystyrene-ethyl benzene extrapolate to 10.5 kcal.

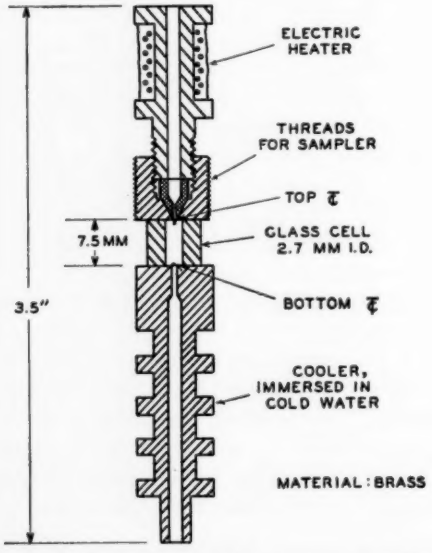

FIG. 2. Thermal diffusion cell for polymer solutions.

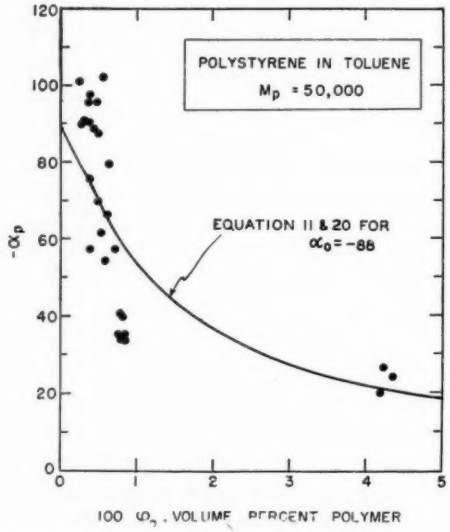

FIG. 4. Thermal diffusion ratio *vs* composition—polystyrene in toluene $M_p = 50\,000$.

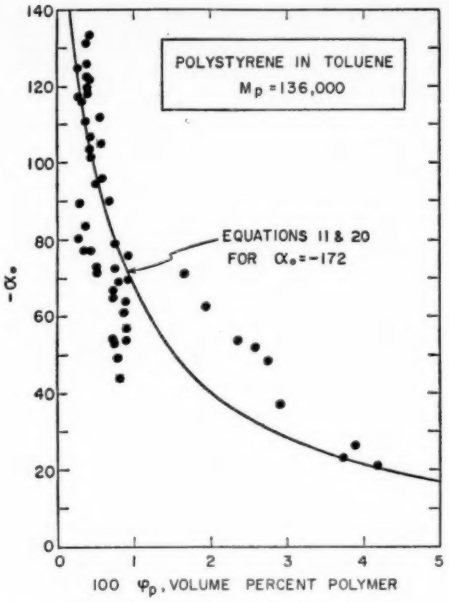

FIG. 5. Thermal diffusion ratio *vs* composition—polystyrene in toluene $M_p=136\,000$.

Data by Ferry[7] for polystyrene in xylene extrapolate to 13.5 kcal. An average value of 12 kcal was used in our calculations.

EVALUATION OF $X\frac{\partial M}{\partial X}$

The denominator of Eq. (11) contains the term

$$X_p\frac{\partial M_p}{\partial X_p}=X_s\frac{\partial M_s}{\partial X_s}. \tag{18}$$

For polymer solutions, this can be evaluated from the equation for the partial molar free energy of solvent:

$$\Delta F_s=RT\left[\ln(1-\varphi_p)+\left(1-\frac{1}{m}\right)\varphi_p+\mu'\varphi_p^2\right] \tag{19}$$

in which μ' is the empirical polymer-solvent interaction

TABLE II. Number of chain atoms N_c in a moving segment at low concentrations—polystyrene in toluene.

$\Delta U_c^{\neq}=12\,000$ cal/segment
$\rho_p=1.051$ g/cc
$\Delta U_s^{\neq}=1880$ cal/mole
$V_s=107$ cc/mole
$M_s=92.1$ g/mole

M_p	m	w	N_c
10 000	89	109	12.2
50 000	444	543	13.1
136 000	1210	1480	13.3
304 000	2700	3300	13.4
338 000	3000	3670	13.4

[7] J. D. Ferry, J. Am. Chem. Soc. 64, 1330 (1942).

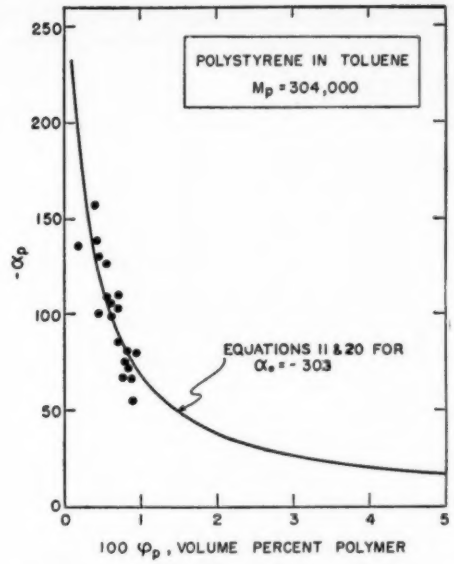

FIG. 6. Thermal diffusion ratio *vs* composition—polystyrene in toluene $M_p=304\,000$.

constant. Thus

$$X_p\frac{\partial M_p}{\partial X_p}=RT(1-\varphi_p)^2[1+2m(\tfrac{1}{2}-\mu')\varphi_p+m\varphi_p^2]. \tag{20}$$

Values of μ' for polystyrene in all the solvents of concern here have been determined by Boyer and Spencer[8] by swelling measurements of polystyrene samples gelled by the addition of small quantities of divinylbenzene.

EQUIPMENT AND PROCEDURE

The apparatus in which the thermal diffusion measurements were made, shown in Fig. 2, was essentially a column of liquid 2.7 mm in diameter contained

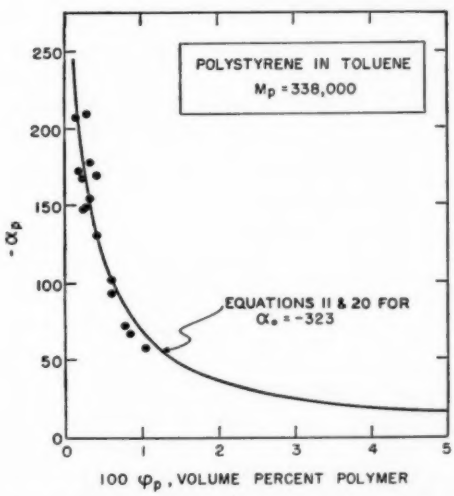

FIG. 7. Thermal diffusion ratio *vs* composition—polystyrene in toluene $M_p=338\,000$.

[8] R. F. Boyer and R. S. Spencer, J. Polymer Sci. 3, 97 (1948).

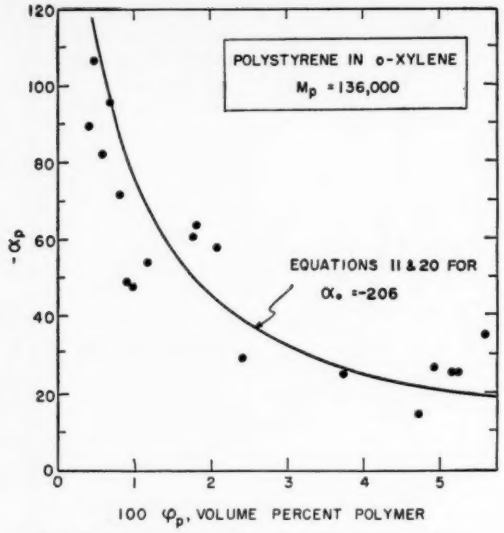

FIG. 8. Thermal diffusion ratio *vs* composition—polystyrene in O-xylene $M_p = 136\,000$.

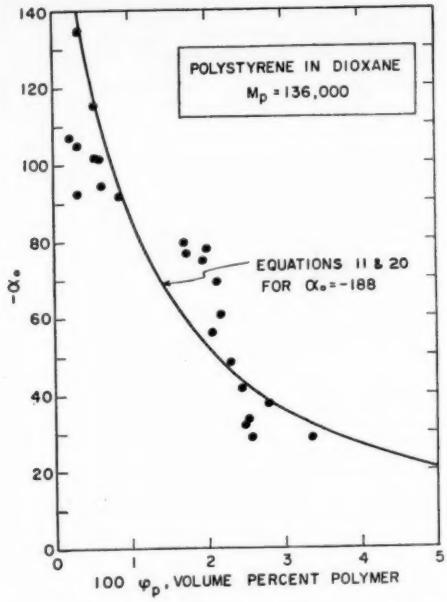

FIG. 10. Thermal diffusion ratio *vs* composition—polystyrene in dioxane $M_p = 136\,000$.

in a glass tube 8 mm long. Cylindrical brass pieces were fastened to either end of the tube with soft solder, using platinum alloy paste to make bond between the solder and glass. The top brass piece was fitted with machined threads on the inside to accommodate the thermocouple, embedded in a small conical plug, and the electrical heater. The outside of the top piece was threaded to hold a sampling device which allowed a hypodermic needle to be lowered to any particular distance in the cell. The bottom brass piece was equipped with fins to enhance the heat transfer to the cold water in which it was immersed. A thermocouple was soft soldered into the top of this piece to measure the temperature at the bottom of the column of liquid.

To determine the concentration of polystyrene a sample was drawn into a capillary tube of calibrated diameter. The volume of sample was determined by measuring the length of liquid column in the tube. The sample was deposited on a previously tared dish made of aluminum foil. The solvent was evaporated to dryness and the polymer concentration determined by weighing on a quartz helix microbalance (Microchemical Specialties, Berkeley, California) equipped with a microscope. The results were reproducible to about a microgram. Five or six samples were normally taken from a run and the concentration gradient could thus be established along the tube.

The temperature difference across the cell was controlled at 12°C with a Brown recording controller. Measurements of temperature were made at intervals. The average temperature was maintained at 25°±1°C. By running for various lengths of time we could

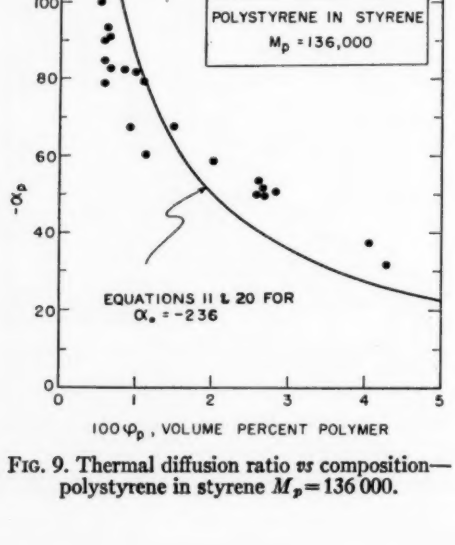

FIG. 9. Thermal diffusion ratio *vs* composition—polystyrene in styrene $M_p = 136\,000$.

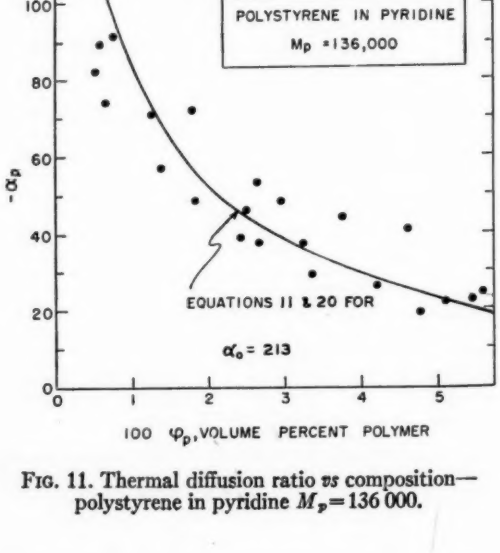

FIG. 11. Thermal diffusion ratio *vs* composition—polystyrene in pyridine $M_p = 136\,000$.

TABLE III. Calculation of number of chain atoms in a moving segment, N_c, at low concentrations. Polystyrene of $M_p=136\,000$ in various solvents.

$\Delta U_c^{\neq}=12\,000$ cal/segment
$\rho_p=1.051$ g/cc
$V_p=1307$

Solvent	$-\alpha_0$	M_s	$V_s^{25°}$	$\Delta U_s^{\neq}$	m	w	N_c Eq. (17)	N_c Eq. (13)
Toluene	172	92.1	107.0	1880	1210	1480	13.3	12.3
O-xylene	206	106.2	121.2	2200	1067	1280	12.8	10.5
Ethyl benzene	232	106.2	123.1	2040	1050	1280	13.9	11.2
Styrene	236	104.1	115.4	1880	1120	1307	14.1	12.1
Dioxane	188	88.1	85.3	2650	1517	1544	7.6	8.8
Pyridine	213	79.1	80.9	2330	1600	1720	8.2	10.0

established definitely that the steady state was approached. The longest runs were about 15 days.

For binary mixtures of solvents some runs were made on the above setup and some were also made on a two chamber cell previously described.[9] The results checked well.

This open column cell is, of course, unsatisfactory if the denser component concentrates at the hot wall. This did not occur in any of our polymer solutions.

Pertinent physical data on the solvents and on the dimer are listed in Table I. The properties of the dimer were obtained in this laboratory. The viscosities were obtained in an Ostwald-Cannon-Fenske viscometer in a temperature bath controlled to ±0.01°C.

DISCUSSION OF RESULTS

It is convenient to discuss first the data for the various molecular weights of polymer in toluene. In Figs. 3–7 the experimental points are shown compared with a plot for Eq. (11) and (20) using the value of α_0 which gave the best fit. It appears that the concentration dependence is predicted quite well by Eq. (20) in all cases except the lowest molecular weight. Probably the failure is caused by a slight molecular weight dependence of μ', here ignored.

If the curves from Figs. 3–7 are superimposed one finds that, while a large separation by molecular weight is predicted at zero concentration, this separation decreases rapidly with increasing concentration, and above 3% polymer virtually no separation among polymer fractions is to be expected.

From the values of α_0 obtained above and Eq. (17) it is possible to calculate N_c, the number of chain atoms in a moving segment characteristic of that part of molecular motion in the low concentration range which is segmental. The values are shown in Table II. It appears that $N_c=13$ essentially independent of molecular weight.

Kauzmann and Eyring[10] in their study of pure paraffins in viscous flow estimate a limiting value for N_c of 20–25 at high molecular weights. From Fig. 1 it can be seen that the activation energy for pure polymer in gel is about twice the value in liquid extrapolated to pure polymer. One might expect that this would double the value of N_c. Our results are then consistent with the findings of Kauzmann and Eyring.

[9] Saxton, Dougherty, and Drickamer, J. Chem. Phys. **22**, 1166 (1954).

[10] W. J. Kauzmann and H. R. Eyring, J. Am. Chem. Soc. **62**, 3113 (1940).

TABLE IV. Monomer-monomer and monomer-dimer data.

System (a)	(b)	X_a	α_{exp}	$\alpha_{calculated}$ Eq. (3)	$\alpha_{calculated}$ Eq. (13)
Styrene	Toluene	0.2	0.0	+0.13	0.0
		0.5	0.5	+0.13	0.0
Styrene	Dioxane	0.5	+0.75	+2.5	+1.30
Styrene	Pyridine	0.5	+1.0	+2.0	+0.81
Dimer	Toluene	0.2	−1.3	−0.37	−1.08
		0.5	−1.0	−0.27	−0.80
Dimer	Styrene	0.2	−1.3	−0.81	−1.06
		0.5	−1.0	−0.62	−0.82

Component (a) concentrated at the hot wall when there was any separation.

As was done previously, the experimental results for polystyrene in the various solvents were fitted using the best empirical value of α_0. The comparisons are shown in Figs. 8–11 for all systems except ethyl benzene, where only a very few points were obtained. It seems that the concentration dependence of α_p is reasonably well predicted by Eqs. (11) and (20).

In Table III are shown the values of N_c as calculated from Eq. (17) and from Eq. (13), where it is assumed that one ring replaces another in motion rather than one volume replacing another as in Eq. (17).

It appears that the moving segment is the same for all molecules containing a benzene ring, but somewhat lower for dioxane and pyridine. If one assumes that one ring replaces another the spread in values of N_c is much smaller and only dioxane is out of line.

In Table IV are shown the results for monomer-monomer and monomer-dimer systems. The results are compared with the values calculated from Eqs. (3) and (13), assuming $X\partial\mu/\partial X=RT$. It can be seen that Eq. (13) which assumes one ring replaces another in motion gives better results in all cases.

It appears, then, that in motion of ring molecules motion takes place with one ring replacing another in motion and, in the case of polystyrene, with a moving segment of 10–12 chain atoms.

The authors would like to acknowledge the advice and cooperation of Lu Ho Tung in the early stages of the work.

The Dow Chemical Company kindly supplied the samples of fractionated polystyrene and of styrene monomer and dimer.

A.H.E. would like to express his gratitude for the Shell Oil Company Fellowship which he held for one year, and for the Dow Chemical Company Fellowship which he held for one year.

Heat Capacity of Erbium from 15 to 320°K*

R. E. Skochdopole, Maurice Griffel, and F. H. Spedding
Institute for Atomic Research and Department of Chemistry, Iowa State College, Ames, Iowa

(Received February 16, 1955)

The heat capacity of erbium has been measured over the range 15 to 320°K and the thermodynamic functions have been calculated. Three maxima have been observed which occur at 19.9°K, 53.5°K, and 84°K. The two at the lower temperatures show a dependence on the thermal history of the sample, and this dependence was investigated. A correlation of the various contributions to the entropy at room temperature has been made and extended to the other rare earth metals.

INTRODUCTION

ALTHOUGH erbium was first identified in 1842 there has, until recently, not been available a sufficient quantity of the pure metal in a form required for a variety of investigations. For example, the noteworthy work of Klemm and Bommer[1] on the paramagnetic susceptibility and crystal structure was carried out on an intimate mixture of erbium and KCl obtained by reduction of anhydrous $ErCl_3$ with potassium. Their x-ray results were essentially confirmed and extended by Banister, Legvold, and Spedding[2]; erbium is hexagonal close packed over the range of 40 to 300°K and does not appear to undergo any abrupt changes in this interval. From the value of the Weiss constant θ in the Curie-Weiss law Klemm and Bommer suggested that erbium would be ferromagnetic at 40°K, a prediction which was emphasized by Néel.[3] Elliott, Legvold, and Spedding[4] have in fact found that the magnetic susceptibility becomes field dependent at 56±5°K and that erbium is apparently ferromagnetic below 20°K. Between these temperatures the field dependence becomes more pronounced as the temperature is reduced. The same authors have extended[5] their measurements and find that between 65 and 80°K the susceptibility is almost independent of temperature and exhibits a slight maximum at 80°K. Koehler and Wollan[6] have invesgigated the neutron diffraction and find a definite ferromagnetism at 4°K while in the range from 4 to 78°K there appears evidence of magnetic ordering which is difficult to interpret. Legvold *et al.*[7] found a change in the temperature coefficient of the resistivity at 80°K while Kevane, Legvold, and Spedding,[8] working in the interval from 20°K to room temperature, found no anomaly in the Hall coefficient.

Thus from about 80 down to 4°K there exists a variety of effects, as yet uncorrelated, which are likely to be associated with changes in the internal energy. We have now carried out an investigation of the heat capacity from 15 to 320°K and the results, which are quite unusual, are the subject of this communication.

EXPERIMENTAL

Procedures for the ion exchange separation of erbium and for the reduction of the anhydrous fluoride with calcium have been described previously.[9,10] Because of relatively high vapor pressure of erbium at its melting point, the recasting of the several buttons of erbium obtained by batch reduction and the accompanying distillation of the excess calcium was done in an atmosphere of argon. After the tantalum crucible was machined off, the sample was in the form of a right circular cylinder 7.5 cm high and 3.1 cm in diameter. It weighed 429.58 g≡2.5680 g atoms. A spectrographic analysis showed it to contain less than 0.01% of Ca, Mg, Si, or Y. Other rare earths, iron and tantalum were not detected. A method of analysis for oxygen and nitrogen was not available to us and it should be remarked that small amounts of these elements were almost certainly present.

The sample presented an excellent appearance since it was composed of large crystals, many of which were about 4 mm on an edge. A typical part of the sample was machined off and positioned in a Norelco x-ray spectrometer. No change was detected in the patterns of the reflections taken at room temperature before and after cooling to liquid nitrogen temperatures.

The adiabatic calorimeter and the experimental method were essentially the same as those previously employed.[11] However, since it was anticipated that erbium might show the same behavior as did gadolinium[12] in being able to maintain relatively large

* Taken in part from a dissertation submitted June, 1954, by R. E. Skochdopole in partial fulfillment of the requirements for the degree of Doctor of Philosophy.

[1] W. Klemm and H. Bommer, Z. anorg. u. allgem. Chem. **231**, 138 (1937).

[2] Banister, Legvold, and Spedding, Phys. Rev. **94**, 1140 (1954).

[3] L. Néel, Z. Elektrochem. **45**, 378 (1939).

[4] J. F. Elliott, Ph.D. Thesis, Iowa State College, 1953. Also Elliott, Legvold, and Spedding, U. S. Atomic Energy Commission Report ISC-378, June 1953.

[5] S. Legvold (private communication).

[6] W. C. Koehler and E. D. Wollan, U. S. Atomic Energy Commission Report ORNL-1620, December 1953.

[7] Legvold, Spedding, Barson, and Elliott, Revs. Modern Phys. **25**, 129 (1953).

[8] Kevane, Legvold, and Spedding, Phys. Rev. **91**, 1372 (1953).

[9] F. H. Spedding and J. E. Powell, U. S. Atomic Energy Commission Report ISC-349, May 1953.

[10] A. H. Daane and F. H. Spedding, J. Electrochem. Soc. **100**, 442 (1953).

[11] M. Griffel and R. E. Skochdopole, J. Am. Chem. Soc. **75**, 5250 (1953).

[12] Griffel, Skochdopole, and Spedding, Phys. Rev. **93**, 657 (1954).

thermal gradients during heating periods, the erbium cylinder was placed in a gold-plated copper can. The cylinder had a hole machined along its axis so that it fitted snugly over the re-entrant well of the can. We shall later refer to the assembly of can plus sample as "the block." The re-entrant well housed the thermometer; thermal contact was aided by a small amount of Apiezon T grease around the thermometer and by helium exchange gas within the can. The heater, having a resistance of 170 ohms, was formed from No. 38 constantan wire noninductively wound on the erbium itself and lacquered in place with G.E. adhesive No. 7031. Connection with the outside was made by two leads of No. 38 copper wire brought through a small Stupakoff seal. This arrangement effectively reduced superheating of the can during a heating period. The block required from 5 to 8 minutes to reach equilibrium after heatings as compared to the 10 or 12 required for gadolinium.

The heat capacity of the block assembly with a thin-walled copper tube substituted for the sample was measured separately and the heat capacity of the erbium obtained by subtraction. The thermochemical calorie is taken as 4.1840 abs. joules; the ice point is taken as 273.16°K. The temperature scale is that of the National Bureau of Standards.

TABLE I. Heat capacity of erbium, cal deg^{-1} (g atom)$^{-1}$; atomic weight = 167.28; 0°C = 273.16°K.

T°K	C_p	T°K	C_p
5	0.059[a]	160	6.253
10	0.474[a]	170	6.306
15	1.600		
20	5.020		
25	3.733	180	6.371
		190	6.422
		200	6.461
30	4.602		
35	5.515		
40	5.737	210	6.494
45	6.278	220	6.520
50	6.778		
		230	6.546
55	6.918	240	6.567
60	6.911	250	6.591
65	7.136		
70	7.348		
75	7.550	260	6.618
		270	6.648
		273.16	6.656
80	7.775		
85	7.710		
90	5.889	280	6.673
95	5.877	290	6.701
100	5.884	298.16	6.716
110	5.948	300	6.718
120	6.022	310	6.742
		320	6.757
130	6.088		
140	6.148		
150	6.207		

[a] These values were obtained from the extrapolation between 15° and 0°K.

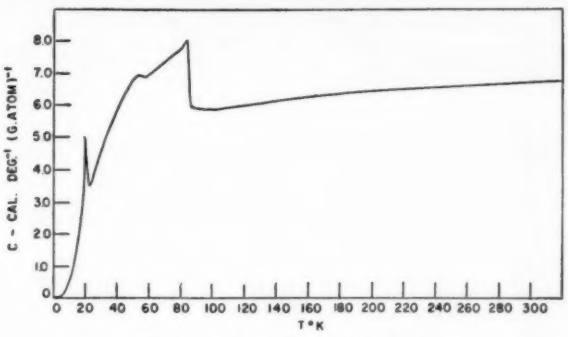

FIG. 1. Heat capacity of erbium.

RESULTS

The results of our measurements are given in Table I. These values were taken from a large smoothed curve of the form shown in Fig. 1 and for which the experimental values had been corrected for nonlinearity. Because of thermal hysteresis effects which erbium exhibits it was necessary to make 17 series of measurements. These are enumerated in the Appendix. For those intervals in which the heat capacity was subject to hysteresis the highest values were used in constructing the smoothed curve; these were obtained in the series having the lowest initial temperatures. Values from the smoothed curve were also used in the calculation of the thermodynamic functions given in Table II. With the exception of a few isolated cases, the experimental values did not deviate from the smooth curve by more than 0.1% and in approximately 85% of the cases they did not deviate by more than 0.05%. Because of the decreasing sensitivity of the thermometer the accuracy is limited to 2% below 20°K and 0.3% at 30°K. In In Table II we have estimated the error in $S^0_{298.16}$ as ±0.15 eu. Of this, 0.02 arises from uncertainty in the heat capacity values above 25°K, and 0.03 eu from uncertainty in the measurements on the lower peak. Near 15°K it appeared that the curve was of the form $C_p = AT^3$, with $A = 4.74 \times 10^{-4}$ and this equation was used in the estimation of the entropy at 15°K. This extrapolation may result in an error of 0.1 eu. In any case our lowest temperatures are too high to permit an evaluation of the separate contributions of the lattice vibrations and of the electrons to the heat capacity.

DISCUSSION

In contrast to gadolinium which showed only one well-defined peak at the Curie temperature, erbium exhibits three maxima. The heat capacity in the neighborhood of the 84° maximum is quite reproducible and is not subject to hysteresis. As is shown by the measurements of Series 4 the heat capacity is continuous throughout the maximum and for an interval of about 1.2° at the very peak the curve is almost flat.

The second maximum at 53.5±0.3°K, as shown in Fig. 2, exhibits a dependence on past thermal history of the sample, i.e., upon the temperature to which the

TABLE II. Thermodynamic functions of erbium cal deg^{-1} (g atom)$^{-1}$.

T°K	S^0	$\frac{H^0-H_0^0}{T}$	$\frac{F^0-H_0^0}{T}$
15	0.533	0.400	0.133
25	2.128	1.506	0.622
40	4.371	2.706	1.665
60	7.023	3.988	3.035
80	9.130	4.804	4.326
100	10.582	5.123	5.459
150	13.030	5.407	7.623
200	14.849	5.617	9.232
250	16.306	5.785	10.521
273.16	16.892	5.856	11.036
298.16	17.48±0.15	5.914±0.060	11.56±0.12
300	17.520	5.918	11.602
320	17.955	5.964	11.991

sample has been cooled prior to a series of measurements. However, the heat capacity seems completely reproducible when the sample is first cooled to 23.5°K.

The heat capacity in the region of the third maximum at 19.9±0.3°K is shown in Fig. 3, which indicates that the entropy change associated with the hump becomes greater, the lower the temperature to which the sample is cooled. Unfortunately, it was not practicable to maintain the sample below 20°K for sustained periods and so no thorough study was made of the effect of this variable upon the shape of the maximum. From the data that were taken it appears that the peak height and shape depend only on the temperature to which the sample is cooled before measurements are started. In none of these measurements was there any evidence of a thermal drift which, if occurring, would be indicative of a phase transition.

The temperatures of the maxima in the heat-capacity curve correspond to those at which one or more of the other physical properties of erbium exhibit anomalous behaviors. The maximum at 84°K corresponds roughly to the temperature of 80°K at which the temperature coefficient of the resistivity changes,[7] at which the slight maximum in the paramagnetic susceptibility was found,[5] and at which neutron diffraction indicates a magnetic transition. As yet it has not been possible to interpret the data in terms of any model of antiferromagnetic order. The maximum is not as steep on the left as it is in the typical antiferromagnetics $NiCl_2$[13] and MnF_2.[14] This may be due to an overlap of the effects associated with the maximum at 53.5°K. A review of the properties of erbium, so far established, suggests nothing that would explain this latter maximum.

The maximum at 19.9°K probably corresponds to the onset of the ferromagnetism found[6] by the neutron diffraction results at 4.2°K. It may be noted that Elliott *et al.* did not experimentally determine the ferromagnetic Curie temperature of erbium. Rather, they assumed a law of corresponding states to be valid for Er and Dy and on the basis of an extrapolated Curie temperature of 92°K for Dy predicted that for Er to be 29°K. According to Koehler and Wollan an incipient ferromagnetic ordering is evident at as high as 35°K and becomes more pronounced as the temperature is decreased.

The fact that the magnetic heat capacity is considerable over the entire interval investigated below 90°K is evidence of the absence of a completed antiferromagnetic ordering. This might indicate why it has not been possible to derive a model thereof from the neutron diffraction results.

Guillaud[15] hypothesized a transition from a ferromagnetic to an antiferromagnetic state in MnAs and found an accompanying maximum in the heat capacity. This would be analogous to our lowest maximum. Since his work did not extend above the antiferromagnetic region no quantitative treatment was possible and the degree of ordering was not discussed.

In our earlier work[12] on gadolinium we considered the measured heat capacity C_p to be a sum of several contributing factors:

$$C_p=C_q+C_m+C_e+\delta c, \tag{1}$$

in which C_q, C_m, and C_e are respectively the lattice, the magnetic and the electronic contributions and δc, the dilation term, is the difference between the heat capacities at constant pressure and at constant volume. A corresponding decomposition was made for the entropies. Because in the case of erbium the temperature ranges of the anomalous contributions overlap it is impossible to evaluate these effects for each of the maxima separately although it is possible to estimate the combined entropy change associated with all three.

We first calculate S_q under the assumption that C_q may be represented by a single Debye curve. Since we cannot infer the value of θ_D from our measurements we approximate θ_D by a linear extrapolation† of the θ_D

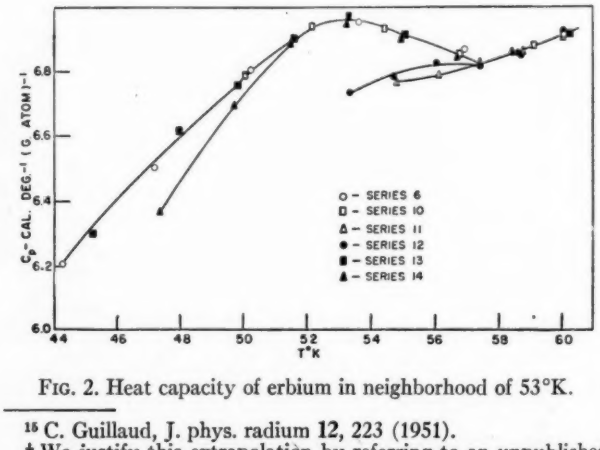

FIG. 2. Heat capacity of erbium in neighborhood of 53°K.

[13] R. H. Busey and W. F. Giauque, J. Am. Chem. Soc. **74**, 4443 (1952).

[14] J. W. Stout and H. E. Adams, J. Am. Chem. Soc. **64**, 1535 (1942).

[15] C. Guillaud, J. phys. radium **12**, 223 (1951).

† We justify this extrapolation by referring to an unpublished preliminary investigation by C. E. Carlson and J. F. Smith at the Ames Laboratory of the sound velocities in some rare earth metals. They found θ_D values of 162 for La, 176 for Gd, 180 for

values of 132°K for La and 152°K for Gd and obtain $\theta_D=163$°K.

From a table [16] of entropy *vs* θ_D/T we find the lattice contribution to the heat capacity to be $S_q=11.63$ eu at 300°K.

The dilatation correction δc at 25°C was estimated to be 0.037 cal deg^{-1} (g atom)$^{-1}$ using the usual thermodynamic formula. The required value of volume compressibility was taken from the work of Bridgman[17] to be 2.46×10^{-6} cm^2/kg. Measurements[18] on the linear expansion coefficient from 100–300°K give a value 26.7×10^{-6} deg^{-1} for the coefficient of volume expansion at room temperature and a slightly smaller value at lower temperatures, while x-ray data of Banister[2] give a similar value down to 100°K and zero below that temperature. A density of 9.020 g/cc can also be inferred from the x-ray data. For other temperatures δc may be approximated by means of the equation of Lindemann and Nernst: $\delta c=AC_q^2T$. This leads to an entropy contribution of 0.03 eu at 300°K. We may assume that the electronic contribution varies linearly with temperature and until accurate measurements at lower temperatures are available we further assume that the coefficient for erbium is the same as that for lanthanum,[19] namely, 1.6×10^{-3}. The corresponding entropy contribution at 300°K is 0.48 eu. Hence by use of Eq. (1) the magnetic entropy at 300°K is calculated to be 5.38 eu.

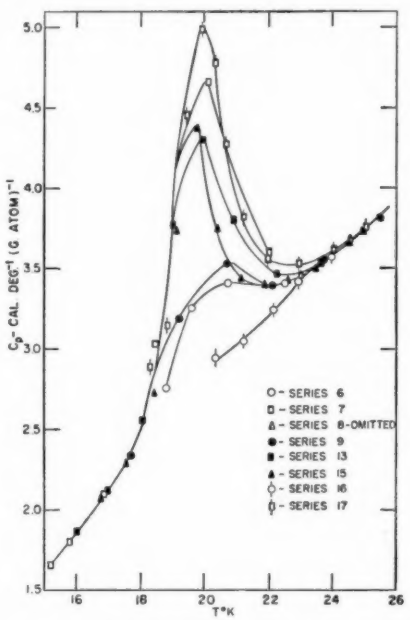

FIG. 3. Heat capacity of erbium in neighborhood of 20°K.

TABLE III. Predicted and experimental values of $S°_{300}$ for the rare earth metals.

Element	θ_D	S_q+S_e eu	J[a]	$R\ln(2J+1)$ eu	Pre. S	Exp S
La	132	13.35	0	0	13.35	13.64[b]
Ce	135	13.22	5/2	3.56	16.78	16.68[b]
Pr	138	13.09	4	4.37	17.46	17.49[b]
Nd	141	12.96	9/2	4.58	17.54	17.54[b]
Pm	143	12.88	4	4.37	17.25	···
Sm	146	12.76	5/2	3.56	16.32	···
Eu	···	···	7/2	4.13	···	···
Gd	152	12.52	7/2	4.13	16.65	15.83
Tb	155	12.40	6	5.10	17.50	···
Dy	158	12.29	15/2	5.51	17.80	···
Ho	161	12.18	8	5.63	17.81	···
Er	163	12.11	15/2	5.51	17.62	17.52
Tm	166	12.00	6	5.10	17.10	···
Yb	···	···	0	0	···	···
Lu	172	11.79	0	0	11.79	···

[a] The total angular momentum quantum number of the tripositive ion, except for europium and ytterbium where J is for the dipositive ion.
[b] These experimental values of S were obtained from reference 19.

A theoretical value of the magnetic entropy may be obtained by regarding the atoms in the metal to be tripositive and in the same spectroscopic state as that of the free ion, namely, $^4I_{15/2}$. The valence electrons are regarded as not contributing to the magnetic moment. At 0°K all of the atoms would be in the lowest energy state of the possible $(2J+1)$ or 16 states, and at sufficiently high temperatures the distribution among these states will be random. The entropy change associated with the disordering is $R\ln16$ or 5.510 eu which is seen to agree splendidly with the "experimental" value 5.38 eu. It is usual at a juncture such as this to remark that the agreement is somewhat fortuitous.‡

Nevertheless we are encouraged to predict the entropies at 300°K of the other rare earth metals using exactly analogous reasoning. We again assume a linear variation of θ_D and regard the contribution of δc as negligible. The electronic contribution is taken throughout as constant and equal to $1.6\times10^{-3}\ T$ cal deg^{-1} (g atom)$^{-1}$. The magnetic contribution is again calculated on the assumption that the atoms exist as tripositive ions and that any contribution to the entropy by the valence electrons is found in C_e. At 0°K each ion is assumed to exist in the lowest of the $2J+1$ possible states and at 300°K the distribution is assumed to be random.

Dy, and 190 for Er. It is well known that values of θ_D obtained by different methods need not necessarily agree so that the divergence of the absolute values is not alarming. Since the θ_D values were of interest mainly for the prediction of thermal properties it is logical to use θ_D values obtained from thermal measurements and to make use of the sound velocity work only in so far as it indicates the linear variation of θ_D with atomic number.

[16] Landolt-Bornstein, *Physikalische-Chemische Tabellen*, Erste Ergänzungsband, (Verlag Julius Springer, Berlin, Germany, 1927), p. 707.

[17] P. W. Bridgman, Proc. Am. Acad. Arts Sci. **83**, 1 (1954).

[18] Barson, Legvold, and Spedding, U. S. Atomic Energy Commission, ISC-424; also F. Barson, M. S. thesis, Iowa State College, 1953.

[19] Parkinson, Simon, and Spedding, Proc. Roy. Soc. (London) **A207**, 137 (1951).

‡ It will be noted that whereas at 300°K $C_q+C_e+\delta c$ would be expected to constitute the complete heat capacity, C_p, their sum falls short of the experimental value by about 0.3 cal deg^{-1} (g atom)$^{-1}$. While this indicates that our estimates of C_q or C_e or both are low over practically the entire interval from 150 to 300°K, the associated entropy would be only about 0.2 eu so that our general arguments are not appreciably affected.

TABLE IV. Experimental values of C_p for erbium, cal deg^{-1} (g atom)$^{-1}$; atomic weight = 167.28; 0°C = 273.16°K.

Mean T (°K)	Approx. ΔT	C_p
	Series 1.	
59.62	3.26	6.884
62.83	3.17	7.032
65.96	3.01	7.179
69.01	3.01	7.310
72.01	2.95	7.428
74.93	2.89	7.547
77.79	2.83	7.674
80.59	2.77	7.805
83.33	2.71	7.978
86.30	3.22	6.453
89.63	3.45	5.893
93.07	3.43	5.878
96.49	3.41	5.880
98.90	3.39	5.883
102.27	3.35	5.921
105.61	3.34	5.910
108.93	3.31	5.943
112.23	3.28	5.970
115.50	3.26	5.995
119.23	4.22	6.015
123.43	4.19	6.048
127.59	4.14	6.080
131.71	4.11	6.099
135.81	4.08	6.123
139.87	4.05	6.147
143.91	4.02	6.173
147.92	4.00	6.196
152.27	3.97	6.222
156.23	3.96	6.225
160.18	3.94	6.245
164.10	3.92	6.254
168.02	3.91	6.261
171.91	3.88	6.304
175.77	3.85	6.336
179.61	3.83	6.370
183.43	3.81	6.390
187.67	4.80	6.416
192.44	4.78	6.439
197.20	4.76	6.454
201.94	4.74	6.469
206.66	4.72	6.491
211.35	4.70	6.495
216.04	4.69	6.511
220.70	4.67	6.521
227.87	4.63	6.539
232.49	4.62	6.542
237.08	4.60	6.559
241.66	4.59	6.572
246.23	4.58	6.579
250.78	4.56	6.597
255.31	4.55	6.607
259.84	4.54	6.606
264.34	4.52	6.629
268.83	4.51	6.648
273.30	4.50	6.645
277.77	4.48	6.673
282.03	4.10	6.675
286.27	4.46	6.687
290.69	4.45	6.702
295.09	4.44	6.715
299.49	4.43	6.724

Mean T (°K)	Approx. ΔT	C_p
	Series 2.	
60.82	2.36	6.944
63.57	3.14	7.069
66.66	3.06	7.209
69.68	2.99	7.312
72.38	2.40	7.442
74.84	2.51	7.573
77.06	1.94	7.639
78.82	1.59	7.724
80.26	1.31	7.782
81.44	1.04	7.863
82.47	1.03	7.926
83.49	1.02	8.001
84.50	1.02	7.978
85.60	1.17	6.744
86.82	1.28	6.010
88.11	1.30	5.921
89.41	1.30	5.892
90.87	1.62	5.886
92.65	1.94	5.877
94.59	1.93	5.877
96.51	1.93	5.877
	Series 3.	
142.55	4.00	6.159
146.53	3.97	6.183
150.49	3.95	6.210
154.43	3.93	6.227
158.34	3.91	6.240
162.23	3.89	6.262
166.11	3.87	6.280
169.97	3.85	6.306
173.81	3.83	6.329
177.62	3.81	6.361
	Series 4.	
83.27	0.16	7.990
83.47	0.16	8.008
83.58	0.16	8.006
83.74	0.16	8.006
83.90	0.16	8.007
84.05	0.16	8.007
84.21	0.16	8.008
84.37	0.16	8.007
84.52	0.16	8.006
84.68	0.16	8.005
84.84	0.16	7.887
85.00	0.16	7.719
85.16	0.17	7.450
85.33	0.17	7.109
85.51	0.18	6.751
	Series 5.	
297.12	4.75	6.713
301.86	4.74	6.721
306.59	4.73	6.730
311.29	4.72	6.743
315.98	4.71	6.757
320.66	4.70	6.758
325.32	4.69	6.771
	Series 6.	
18.84	0.58	2.745
19.67	0.73	3.239
20.75	1.45	3.405
22.53	2.12	3.403
24.57	1.96	3.664

Mean T (°K)	Approx. ΔT	C_p
	Series 6.—*Continued.*	
26.98	2.86	4.134
29.69	2.58	4.564
32.49	3.00	4.853
35.38	2.78	5.201
38.33	3.11	5.548
41.34	2.91	5.887
44.28	2.98	6.207
47.19	2.82	6.505
50.27	3.35	6.803
53.63	3.26	6.953
56.98	3.26	6.869
60.08	3.21	6.916
	Series 7.	
15.21	0.38	1.647
15.79	0.78	1.796
16.93	1.51	2.095
18.48	1.58	3.020
20.01	1.54	4.658
22.01	2.47	3.590
	Series 8.	
18.90	0.64	2.967
19.65	0.87	3.955
20.54	0.95	3.604
21.59	1.15	3.691
23.00	1.47	3.454
24.56	1.64	3.662
26.50	2.24	4.015
28.62	2.01	4.470
	Series 9.	
17.75	1.41	2.334
19.23	1.56	3.181
20.71	1.40	3.519
22.13	1.45	3.389
23.76	1.80	3.548
25.49	1.67	3.809
	Series 10.	
24.19	1.80	3.544
26.29	2.41	3.967
50.07	1.91	6.787
52.19	2.33	6.940
54.46	2.31	6.935
56.82	2.32	6.853
59.13	2.30	6.883
61.41	2.26	6.974
63.65	2.22	7.072
	Series 11.	
54.81	1.36	6.770
56.15	1.34	6.786
57.48	1.32	6.824
58.80	1.31	6.859
60.10	1.30	6.911
61.40	1.29	6.966
	Series 12.	
53.35	1.38	6.735
54.72	1.37	6.783
56.08	1.35	6.826
57.44	1.35	6.816
58.78	1.34	6.863
60.11	1.32	6.922
61.42	1.31	6.970
62.72	1.29	7.034

Mean T (°K)	Approx. ΔT	C_p
	Series 13.	
16.01	0.98	1.859
17.03	1.08	2.118
18.09	1.07	2.550
19.04	0.87	3.763
19.93	0.95	4.300
20.94	1.29	3.801
22.27	1.40	3.461
23.65	1.37	3.538
24.98	1.29	3.730
27.16	3.09	4.168
30.42	3.43	4.642
34.01	3.76	5.039
37.61	3.44	5.464
41.34	4.03	5.885
45.22	3.73	6.301
48.01	1.86	6.622
49.84	1.80	6.762
51.61	1.76	6.904
53.36	1.73	6.972
55.09	1.74	6.916
56.83	1.74	6.853
58.57	1.73	6.865
60.29	1.71	6.923
	Series 14.	
47.36	2.88	6.369
49.71	1.82	6.693
51.50	1.76	6.883
53.25	1.74	6.952
54.99	1.74	6.906
56.73	1.74	6.849
58.47	1.73	6.860
	Series 15.	
16.79	0.76	2.062
17.60	0.86	2.268
18.46	0.86	2.724
19.16	0.53	3.725
19.77	0.71	4.363
20.46	0.67	3.741
21.15	0.72	3.433
21.87	0.73	3.393
22.60	0.72	3.407
23.48	1.05	3.500
24.51	1.01	3.649
	Series 16.	
20.39	0.86	2.934
21.23	0.81	3.041
22.02	0.76	3.234
22.94	1.08	3.416
24.00	1.03	3.570
18.34	0.50	2.896
18.88	0.57	3.313
19.44	0.56	4.452
19.92	0.42	4.977
20.34	0.35	4.770
	Series 17.	
20.70	0.39	4.261
21.22	0.67	3.815
21.99	0.89	3.545
22.98	1.08	3.519
24.04	1.05	3.608
25.06	1.01	3.751

In the cases of europium, ytterbium, and possibly samarium, these assumptions might well be inadequate. In their salts the first two elements are known to exist preferentially in the divalent state with the $4f$ shell, respectively, half-filled and completely filled and samarium shows a similar tendency. This is presumed to carry over into the metals, the atoms possessing the same electron core as the dipositive ions. The looser binding in the case of the dipositive ions should result in smaller θ_D values and correspondingly larger lattice contributions to the heat capacity and entropy at any temperature. Both Eu^{++} and Gd^{+++} have the same spectroscopic state, $^8S_{7/2}$, and would thus have the same magnetic entropy. Because of its larger lattice entropy the total entropy of europium at 300°K would be expected to be greater than either of its neighbors, samarium and gadolinium. In the case of ytterbium the spectroscopic state of the divalent ion is $^1S_0$ and there would be no magnetic contribution to the entropy. The total entropy at room temperature would be larger than that of the nonmagnetic lutetium because of the undetermined larger lattice entropy. The results of these considerations are given in Table III. There seems to be an excellent agreement between the experimental and the calculated values. The one exception is gadolinium, but this would not be expected to agree at 300°K. A part of the magnetic contribution still remains above this temperature and this might well account for the discrepancy of 0.9 eu between the predicted and experimental values at 300°K.

Experimental measurement of the heat capacity of lutetium from 1 to 300°K would provide a test of the assumptions made with respect to both θ_D and the electronic heat capacity. Should eventual experimental data for dysprosium (which we are about to investigate) confirm the predicted entropy value our confidence in the adequacy of our assumptions would be greatly strengthened.

An extension of this work should include measurements on erbium in the range from 1 to 25°K and a more thorough investigation of the 19.9°K maximum. There is apparently a large magnetic contribution to the heat capacity at 15°K which may reasonably be considered to extend below this temperature. Another interesting extension would be a study of the heat capacity in a magnetic field from 1 to 90°K. Further measurements on single crystals of erbium to determine the remanent magnetization and the anisotropy might clear up some of the vagueness which now surrounds the existence and temperature region of a ferromagnetic state.

ACKNOWLEDGMENTS

We wish to thank Dr. Jack Powell who prepared the rare earth salts, Mr. David Dennison who prepared the metal, and Mr. Lloyd Hanson who helped in the measurements and calculations. We have also had the benefit of discussions with Professors R. E. Rundle and J. M. Keller, to whom we express our appreciation.

APPENDIX

Table IV lists the seventeen series of measurements in chronological order. The thermal history of the sample previous to each series of measurements is given in Table V.

TABLE V. Thermal history of erbium during measurements.

Series no.	Temp. of sample previous to measurement	Initial temp. of series
1	295°K	58.0°K
2	295	59.7
3	295	140.6
4	295	83.2
5	295	294.8
6	295	17.3
7	62	15.0
8	25[a]	18.6
9	29.7	17.0
10	26.3	23.4[b]
11	295	54.1
12	295	52.7
13	295	15.5
14	61.1	45.9
15	28[c]	16.4
16	25	19.9
17	295	10.0[d]

[a] The block was first cooled to 17.5, but inadvertently was allowed to warm to 25° before recooling to 18.6°K.
[b] Two determinations were made at liquid hydrogen temperatures, and the refrigerant exahusted, so the block was warmed to 49.1°K and the series continued with solid nitrogen as refrigerant.
[c] The block was allowed to warm from 18° to 28°K before recooling to 16.4°.
[d] The block was cooled to 10°K, but the liquid helium was exhausted and the first measurements were started at 18.1°K.

Statistical Mechanics of Isotopic Systems with Small Quantum Corrections. I. General Considerations and the Rule of the Geometric Mean*

JACOB BIGELEISEN
Chemistry Department, Brookhaven National Laboratory, Upton, New York
(Received February 21, 1955)

It is shown that the differences in the thermodynamic properties of isotopic molecules subject to small quantum effects ($u^2/24$ law) depend on the difference in the reciprocal masses of the atoms in the molecule and are, therefore, independent of all masses except of those atoms isotopically substituted. This theorem provides a rigorous proof of the rule of the geometric mean for gaseous molecules. It is shown that the partition function ratio for a pair of double-labeled molecules, e.g., $N^{15}D_3/N^{15}H_3$ is equal to the ratio for the single-labeled pair $N^{14}D_3/N^{14}H_3$. The application of the $u^2/24$ law to isotopic isomer equilibria is pointed out.

INTRODUCTION AND SCOPE OF THE METHOD

It has been shown by Bigeleisen and Mayer[1] that the ratio of partition functions or the difference in free energy of formation of a pair of isotopic molecules in the ideal gas state can be expressed as a simple function of the masses of the isotopic atoms, the symmetry numbers of the molecules, and the vibrational frequencies of the isotopic molecules. The extension to the other thermodynamic properties, i.e., entropy, enthalpy, and heat capacity, has been given by Bigeleisen.[2] At high temperatures or when the quantum effects are small, the deviation of the ratio of partition functions for a pair of isotopic molecules from the classical ratio follows the $u^2/24$ law, where $u\equiv(hc\nu/k\mathrm{T})$.† One finds

$$s/s'f=1+\frac{1}{24}(hc/k\mathrm{T})^2\sum_i(\nu_i'^2-\nu_i^2), \tag{1}$$

$$\frac{F^0-F^{0\prime}}{R\mathrm{T}}=-\tfrac{3}{2}\sum_i\ln m_i/m_i'+\ln s/s'-\frac{1}{24}(hc/k\mathrm{T})^2\sum_i(\nu_i'^2-\nu_i^2), \tag{2}$$

$$\frac{S^0-S^{0\prime}}{R}=\tfrac{3}{2}\sum_i\ln m_i/m_i'+\ln s'/s-\frac{1}{24}(hc/k\mathrm{T})^2\sum_i(\nu_i'^2-\nu_i^2), \tag{3}$$

$$\frac{H^0-H^{0\prime}}{R\mathrm{T}}=-\frac{1}{12}(hc/k\mathrm{T})^2\sum_i(\nu_i'^2-\nu_i^2), \tag{4}$$

$$\frac{C_p{}^0-C_p{}^{0\prime}}{R}=\frac{1}{12}(hc/k\mathrm{T})^2\sum_i(\nu_i'^2-\nu_i^2). \tag{5}$$

The quantities above have been defined previously.[1,2] It is significant to note that F^0, S^0, H^0, and Cp^0 used in Eqs. (2) to (5) are the total quantities [see Eqs. (3) to (6) in reference 2].

It has been shown by Herzfeld and Teller[3] that the partition function of any system, Q, at high temperature can be written

$$Q=Q_{cl}\left\{1-\frac{1}{24}(\hbar/k\mathrm{T})^2\left\langle\sum_i\frac{1}{m_i}\frac{\partial^2V}{\partial X_i^2}\right\rangle_{Av}\right\}, \tag{6}$$

where V is the potential energy, m_i is the mass of the particle, and Q_{cl} is the classical partition function. This expansion of the ratio of the quantum mechanical to classical partition functions in terms of $(\hbar/k\mathrm{T})^2$ is based on Wigner's[4] modification of the classical probability of a distribution in coordinate space. The extension of Wigner's distribution function to systems with many degrees of freedom by Mayer and Band[5] extends the validity of Herzfeld and Teller's expansion of the partition function ratio to such systems. On forming the ratio of partition functions for a pair of isotopic systems from (6) and recalling the definition of

$$f=\frac{Q}{Q'}\pi\left(\frac{m_i'}{m_i}\right)^{\frac{1}{2}}$$

one obtains

$$s/s'f=1+\frac{1}{24}(\hbar/k\mathrm{T})^2\left\langle\sum_i\left(\frac{1}{m_i'}-\frac{1}{m_i}\right)\frac{\partial^2V}{\partial X_i^2}\right\rangle_{Av}. \tag{7}$$

This expression reduces to Eq. (1) for harmonic forces. Equations (1) to (5) can therefore be generalized to include systems of many degrees of freedom and anharmonic forces. We shall concern ourselves entirely with the harmonic approximation.

We write the Hamiltonian in the form

$$H=\sum_i^{3nN}P_i^2/2m_i+\tfrac{1}{2}\sum_i^{3nN}\sum_j^{3nN}a_{ij}X_iX_j, \tag{8}$$

where P_i, m_i, and X_i are respectively the momenta, masses, and the Cartesian coordinates of the atoms in the system, n is the number of atoms per molecule, N is Loschmidt's number, and the a_{ij}'s are the harmonic force constants. The secular equation for the frequencies,

* Research carried out under the auspices of the U. S. Atomic Energy Commission.

[1] J. Bigeleisen and M. G. Mayer, J. Chem. Phys. **15**, 261 (1947).
[2] J. Bigeleisen, J. Chem. Phys. **21**, 1333 (1953).

† Throughout this paper we use the following notation for quantities associated with the frequency: ν, frequency in cm^{-1}; ν_c, frequency in radians sec^{-1}; $\omega=2\pi\nu c$, frequency in cycles sec^{-1}; and $\lambda=\omega^2$.

[3] K. F. Herzfeld and E. Teller, Phys. Rev. **54**, 912 (1938).
[4] E. Wigner, Phys. Rev. **40**, 749 (1932).
[5] J. E. Mayer and W. Band, J. Chem. Phys. **15**, 141 (1947).

as shown previously,[1] leads to

$$4\pi^2 \sum_i^{3nN} (\nu_i'^2-\nu_i^2)=\sum_i^{3nN}\left(\frac{1}{m_i'}-\frac{1}{m_i}\right)a_{ii}. \quad (9)$$

One obtains then

$$s/s'f=\left[1+\frac{1}{24}(\hbar c/kT)^2\sum_i^{3nN}\left(\frac{1}{m_i'}-\frac{1}{m_i}\right)a_{ii}\right]^{1/N}, \quad (10)$$

$$\frac{F^0-F^{0\prime}}{RT}=-\tfrac{3}{2}\sum_i^n \ln m_i/m_i'+\ln s/s' -\frac{1}{24N}(\hbar c/kT)^2\sum_i^{3nN}\left(\frac{1}{m_i'}-\frac{1}{m_i}\right)a_{ii}, \quad (11)$$

$$\frac{S^0-S^{0\prime}}{R}=\tfrac{3}{2}\sum_i^n \ln m_i/m_i'+\ln s'/s -\frac{1}{24N}(\hbar c/kT)^2\sum_i^{3nN}\left(\frac{1}{m_i'}-\frac{1}{m_i}\right)a_{ii}, \quad (12)$$

$$\frac{H^0-H^{0\prime}}{RT}=-\frac{1}{12N}(\hbar c/kT)^2\sum_i^{3nN}\left(\frac{1}{m_i'}-\frac{1}{m_i}\right)a_{ii}, \quad (13)$$

$$\frac{C_p^0-C_p^{0\prime}}{R}=\frac{1}{12N}(\hbar c/kT)^2\sum_i^{3nN}\left(\frac{1}{m_i'}-\frac{1}{m_i}\right)a_{ii}. \quad (14)$$

Equations (10) to (14) show that at high temperatures the differences in the thermodynamic properties of two isotopic systems are a function of the masses of the isotopic atoms, m_i and m_i', and the symmetry numbers. The masses of any other type of atoms in the system have no effect whatsoever on the differences in the thermodynamic properties of the systems containing isotopes of mass m_i and m_i'. Of course, the differences do depend on the chemical species through the force constants a_{ii}. At low temperatures, where one has to use the complete expression for the partition function ratio, this conclusion is no longer valid. Nevertheless, this theorem, although restricted to the high temperature approximation, is still one of wide applicability. Bigeleisen and Mayer have given one application of the theorem, namely the partition function ratio of molecules of the type XY_n and $X'Y_n$. They find

$$f=1+\frac{1}{24}(\hbar c/kT)^2\left(\frac{m_x-m_{x'}}{m_x m_{x'}}\right)(a_{11}{}^{xx}+a_{11}{}^{yy}+a_{11}{}^{zz}), \quad (15)$$

where m_x and $m_{x'}$ are the masses of X and X', respectively, and $a_{11}{}^{xx}$, $a_{11}{}^{yy}$, and $a_{11}{}^{zz}$ are the force constants corresponding to the displacement of X or X' in the x, y, and z directions.

USE OF THE TRACE

It is worthwhile to point out explicitly a general application of the method of the trace to the difference in the thermodynamic properties of isotopic molecules. Through the use of Cartesian coordinates, we arrive at Eqs. (10) to (14) which involve the force constants corresponding to these coordinates and the masses m_i' and m_i of the isotopic atoms. In general the vibrations of polyatomic molecules are analyzed in terms of symmetry coordinates. The solutions of the secular equation in this case always involve equations in the trace

$$\sum^{3n-6}\lambda_i=f(a_{ij},m_1,m_2,\cdots m_n). \quad (16)$$

Individual solutions for molecules of different symmetry types and different force fields are given in texts on molecular vibrations. The trace provides a convenient and simple method of evaluating the differences in the thermodynamic properties of isotopic molecules when the $u^2/24$ law holds. It avoids the necessity for explicit solutions for the shifts in the individual frequencies. One has

$$s/s'f=1+\frac{1}{24}(\hbar/kT)^2\sum^{3n-6}(\lambda_i'-\lambda_i). \quad (17)$$

In the application of this method all of the frequencies must be sufficiently low to obey the $u^2/24$ law.

RULE OF THE GEOMETRIC MEAN

It is a well-known empirical fact that the vapor pressures of the mixed isotopic molecule $XY_{n-z}Y_z'$ can be represented in terms of the vapor pressures of the isotopically pure species XY_n and XY_n' by the relation

$$P_{XY_{n-z}}{}^n=P_{XY_n}{}^{(n-z)}P_{XY_n'}{}^z. \quad (18)$$

Similarly one finds that the equilibrium constants for isotopic disproportionation equilibria

$$nXY_{n-z}Y_z'=(n-z)XY_n+zXY_n' \quad (19)$$

are practically identical to the classical value, which is just the quotient of the symmetry numbers raised to the appropriate powers. These two rules are known as the rule of the geometric mean. Examples of the vapor-pressure relationship are the vapor pressures of H_2, HD, and D_2, and H_2O, HDO, and D_2O. For the isotopic disproportionation equilibria the rule is sufficiently widespread that Urey,[6] for example, tabulates $(CO_3{}^{18=}/CO_3{}^{16=})^{\frac{1}{3}}$ and utilizes this ratio for $O^{16}-O^{18}$ exchange equilibria at low abundances of O^{18}, where the principal $CO_3^=$ species containing O^{18} is $CO_2{}^{16}O^{18=}$. Even for the reaction $H_2O+D_2O=2HDO$, the equilibrium constant at room temperature, $K=3.96$, is close to the statistical value, 4, while $s/s'f$ is equal to 12.5. We shall now show that the rule of the geometric mean is an exact one for systems which obey the $u^2/24$ law. At present we shall restrict ourselves to the gaseous disproportionation equilibria. In a later paper of this series we shall return to the thermodynamics of phase equilibria.

[6] H. C. Urey, J. Chem. Soc. 1947, 562.

For reaction (19)

$$\frac{\Delta F^0}{RT}=\frac{(n-z)F^0_{XY_n}+zF^0_{XY_n'}-nF^0_{XY_{n-z}Y_z'}}{RT}, \quad (20)$$

$$\frac{\Delta F^0}{RT}=\frac{1}{RT}[(n-z)(F^0_{XY_n}-F^0_{XY_{n-z}Y_z'}) -z(F^0_{XY_{n-z}Y_z'}-F^0_{XY_n'})]. \quad (21)$$

Substitution of Eq. (11) into (21) and recalling that for gaseous equilibria

$$1/N\sum_i^{3nN}\left(\frac{1}{m_i'}-\frac{1}{m_i}\right)a_{ii}=\sum_i^{3n}\left(\frac{1}{m_i'}-\frac{1}{m_i}\right)a_{ii} \quad (22)$$

we obtain

$$\Delta F^0/RT=\ln s_{XY_n}{}^{(n-z)}s_{XY_n'}{}^{z}/s_{XY_{n-z}Y_z'}{}^{n}, \quad (23)$$

$$\Delta F^0/RT=n\ln s_{XY_n}/s_{XY_{n-z}Y_z'}, \quad (24)$$

$$\frac{\Delta S^0}{R}=-n\ln s_{XY_n}/s_{XY_{n-z}Y_z'}, \quad (25)$$

$$\Delta H^0=\Delta C_p{}^0=0. \quad (26)$$

This is the rule of the geometric mean. It is a direct statistical mechanical consequence of the $u^2/24$ law and the fact that difference in the sums of the squares of the frequencies of isotopic molecules depends only on the masses of the isotopic atoms and on no other masses. The latter theorem, as applied to isotopic disproportionation equilibria, has been stated explicitly as the sum rule by Decius and Wilson[7] and by Sverdlov.[8]

It is interesting to note that the total entropy of the mixed molecule $XY_{n-z}Y_z'$ can be calculated from the entropies of the isotopically pure species XY_n and XY_n' by a simple correction for the change in the symmetry number. At low temperature, for the case of the homonuclear diatomic molecule, it has been shown that apart from the small rotational correction[9]

$$\frac{2S_{AA'}{}^0-S_{A'A'}{}^0-S_{AA}{}^0}{R} =2\ln 2+\ln(m_A+m_{A'})-\tfrac{1}{2}\ln 4m_Am_{A'}. \quad (27)$$

Since the sum rule is an exact one for molecules with a harmonic potential, any deviations from the rule of the geometric mean result from the limitations of the $u^2/24$ law and the small corrections to $s/s'f$ from anharmonicity. The $u^2/24$ law is a very good approximation up to $u=2$. At higher values of u, the deviations become very large. Nevertheless, empirically, one finds the rule of the geometric mean holds over a much larger range of values of u. This is a statistical mechanical consequence of the empirical sum rules found by Bernstein and Pullin.[10] They find, for instance, a linear sum rule for a series of deuterocarbons

$$\sum_i \nu_i(C_mH_n)-\nu_i(C_mD_n)\simeq n\sum \nu_i(C_mH_n) -\nu_i(C_mH_{n-1}D). \quad (28)$$

Simple considerations show that Eq. (28) can never be an equality. In the special case of the linear XY_2 molecules, the approximate relationship has been shown to hold when $(m_y-m_y')/m_y$ is small.[11] In the case where u is large and Δu is small, $s/s'f$ is given by the $G(u)$ formula[1]

$$s/s'f=1+\sum_i G(u_i)\Delta u_i. \quad (29)$$

At large u, $G(u)$ varies slowly with u and, therefore, Eqs. (28) and (29) plus rules in $\sum_i 1/\nu_i$ lead to an approximate rule of the geometric mean. Such a rule cannot at this time be considered a general one, but rather an empirical one which can be shown to be approximately true in several cases. The greatest deviations are expected where the $G(u)$ formula is not applicable, and thus one finds for

$$H_2+D_2=2HD \quad (30)$$

$K=(4)(0.81)$ at room temperature.

PARTITION FUNCTIONS FOR ISOTOPICALLY DOUBLE-LABELED MOLECULES

In addition to the sum rule which leads to the rule of the geometric mean, Decius and Wilson have also stated another sum rule from Eq. (9) explicitly. That is, for example,

$$\sum \nu_i{}^2(N^{15}H_3)+\sum \nu_i{}^2(N^{14}D_3) =\sum \nu_i{}^2(N^{14}H_3)+\sum \nu_i{}^2(N^{15}D_3). \quad (31)$$

This rule can also be extended to include two or more isotopes of the same element. For example

$$\sum \nu_i{}^2(HTO)+\sum \nu_i{}^2(HDO) =\sum \nu_i{}^2(DTO)+\sum \nu_i{}^2(H_2O). \quad (32)$$

At temperatures where these molecules obey the $u^2/24$ law

$$s/s'f(N^{15}D_3/N^{15}H_3)=s/s'f(N^{14}D_3/N^{14}H_3), \quad (33)$$

$$s/s'f(DTO/HTO)=s/s'f(HDO/H_2O). \quad (34)$$

Thus to a good approximation the partition function ratio of a pair of isotopically double-labeled molecules is equal to the corresponding ratio of the single-labeled species. Again this rule has a larger range of validity than the $u^2/24$ law. For instance at 298°K the left-hand side of Eq. (34) is equal to 17.0, while the right-hand side is 16.4. Apart from the partition functions of the isotopic H_2 molecules, which are well known, and in

[7] J. C. Decius and E. B. Wilson, Jr., J. Chem. Phys. **19**, 1409 (1951).
[8] L. M. Sverdlov, Doklady Akad. Nauk. S.S.S.R. **78**, 1115 (1951).
[9] See reference 2, Eqs. (27) and (28).
[10] H. J. Bernstein and A. D. E. Pullin, J. Chem. Phys. **21**, 2188 (1953).
[11] E. O. Salant and J. E. Rosenthal, Phys. Rev. **42**, 812 (1932).

those cases where high accuracy is required, these rules will suffice for the calculation of the thermodynamic properties of the double-labeled molecules. The free energy, entropy, enthalpy, and heat capacity changes for reactions involving double-labeled species, can be derived from the $s/s'f$ relationship and give equations similar to Eqs. (24) to (26).

ISOTOPIC ISOMERS

The theorem that differences in the thermodynamic properties of isotopic molecules (for small quantum corrections) are independent of the masses of all the atoms in the molecule, except those which have isotopic substitution, is of considerable use in making approximate estimates of equilibria involving isotopic isomers. The general equation for an isotopic isomer equilibrium is

$$AXYA'=A'XYA, \tag{35}$$

where X and Y need not be monatomic groups. Then from Eqs. (10) to (14), one finds, in the case of gaseous molecules

$$K=1+\frac{1}{24}(\hbar c/k\mathrm{T})^2\sum^{3}\left(\frac{1}{m_{A'}}-\frac{1}{m_A}\right)\times(a_{ii}(Y-A)-a_{ii}(X-A)), \tag{36}$$

$$\frac{\Delta F^0}{RT}=-\frac{1}{24}(\hbar c/k\mathrm{T})^2\sum^{3}\left(\frac{1}{m_{A'}}-\frac{1}{m_A}\right)\times(a_{ii}(Y-A)-a_{ii}(X-A)), \tag{37}$$

$$\frac{\Delta S^0}{R}=-\frac{1}{24}(\hbar c/k\mathrm{T})^2\sum^{3}\left(\frac{1}{m_{A'}}-\frac{1}{m_A}\right)\times(a_{ii}(Y-A)-a_{ii}(X-A)), \tag{38}$$

$$\frac{\Delta H}{RT}=-\frac{1}{12}(\hbar c/k\mathrm{T})^2\sum^{3}\left(\frac{1}{m_{A'}}-\frac{1}{m_A}\right)\times(a_{ii}(Y-A)-a_{ii}(X-A)), \tag{39}$$

$$\frac{\Delta C_p}{R}=\frac{1}{12}(\hbar c/k\mathrm{T})^2\sum^{3}\left(\frac{1}{m_{A'}}-\frac{1}{m_A}\right)\times(a_{ii}(Y-A)-a_{ii}(X-A)), \tag{40}$$

where $a_{ii}(Y-A)$ and $a_{ii}(X-A)$ are the force constants for small displacements of A along Cartesian coordinates from their respective positions adjacent to Y and X, respectively. Intercomparison of Eqs. (36) to (40) with (10) to (14) shows explicitly that, in general, the differences in the thermodynamic properties of isotopic isomers are smaller than the differences between a pair of isotopic molecules. This has been pointed out previously.[12,13]

The isotopic isomer equilibrium problem presents itself in the theory of reaction rates in dealing with intramolecular isotope effects.[13] In this case, it is significant to point out that some of the $a_{ii}(Y-A)$ and $a_{ii}(X-A)$ can be of different sign, thus partially enhancing the effect.

It is of some interest to indicate how Eq. (36) can give useful information even for systems which do not obey the $u^2/24$ law. We shall consider the isomers of N_2O whose vibrational spectrum is sufficiently well analyzed so that exact calculations have been made.[12] To illustrate the applicability of Eq. (36) we shall limit the discussion to the contributions from the stretching frequencies alone. The stretching-force constants, corresponding to atomic displacements along the internuclear axis are f_1(N−N) 18.72, f_2(N−O) 11.61, and f_{12}(NNO) 1.31 all in 10^5 dyne cm^{-1}. If we write the reaction in the form

$$\mathrm{N^{15}N^{14}O^{16}}=\mathrm{N^{14}N^{15}O^{16}}, \tag{41}$$

then

$$f_{\text{stretch}}-1=\frac{1}{24}\mathrm{N}(\hbar/k\mathrm{T})^2\left(\frac{1}{14}-\frac{1}{15}\right)\times(18.72+11.61-18.72-2.61)\times10^5. \tag{42}$$

Since the $u^2/24$ law does not hold for the stretching vibrations in N_2O, the right-hand side of Eq. (42) can be corrected approximately by multiplication by the ratio $G(u)/(u/12)$. If there were but one frequency involved the correction would be exact. However, there are the symmetric- and asymmetric-stretching frequencies, and each has a different $G(u)$ factor. For this reason, the correction, which is sizable at room temperature, cannot be exact. After applying this $12G(u)/u$ correction we find $f_{\text{stretch}}-1$ is computed by Eq. (42) to be 3.1×10^{-2} and 5.4×10^{-3} at 300° and 1000°K, respectively. This is to be compared with the exact calculations based on

$$f-1=\sum_i^2 G(u_i)\Delta u_i, \tag{43}$$

which give 2.44×10^{-2} and 5.09×10^{-3} at the corresponding temperatures. The deviations correspond to those expected for the difference between $G(u)$ and $u/12$. When the ratio of a_{ii}/T^2 is such that u is three or less, the method is a convenient and reliable one.

[12] J. Bigeleisen and L. Friedman, J. Chem. Phys. **18**, 1656 (1950).

[13] J. Bigeleisen, J. Phys. Chem. **56**, 823 (1952).

Scattering of High Velocity Neutral Particles. VI. Krypton-Krypton

I. AMDUR AND E. A. MASON*
Department of Chemistry, Massachusetts Institute of Technology, Cambridge, Massachusetts
(Received January 25, 1955)

Total collision cross sections have been measured for krypton atoms with energies between 700 and 2100 ev, scattered in room temperature krypton, to obtain potential energy information for the interaction of two krypton atoms. The potential function may be represented by

$$V(r)=2.55\times10^{-10}/r^{5.42} \text{ ergs}$$

for r between 2.42 A and 3.14 A.

The present potential appears to be consistent with potentials, valid at larger separation distances, which have been derived from measurements of gaseous compressibility, transport, and crystal properties, within the limits of uncertainty of these larger distances potentials.

THE present results are part of an extended investigation, through scattering experiments, of intermolecular forces at small distances of separation. A discussion of experimental and calculation procedures appears in a previous publication on the scattering of high-energy helium atoms in helium.[1]

Table I shows the experimental cross sections, $\bar{S}_w$ and $\bar{S}_n$, measured with a wide detector and a narrow detector (geometric apertures, 13.4 and 0.96 minutes, respectively), as a function of energy. The results have been represented, using the method of least squares, by the relations:

$$\log S_w=-0.35364\log E-1.73560, \quad (1)$$

$$\log S_n=-0.38522\log E-1.93862 \quad (2)$$

for S_w and S_n in A^2 and E, in ergs. Percentage deviations between calculated and experimental cross sections are included in the table. Figure 1 is a graphical comparison between the experimental points and the curves represented by Eqs. (1) and (2).

If the potential form is assumed to be $V(r)=K/r^s$, the parameters s and K may be obtained from the slope and intercept, respectively, of Eq. (1) or Eq. (2) as described in the helium paper. The wide detector results lead to

$$V(r)=K/r^s$$
$$=3.35\times10^{-10}/r^{5.66} \text{ ergs} (2.42 \text{ A}\leqq r\leqq 2.94 \text{ A}) \quad (3)$$

and the narrow detector results, to

$$V(r)=K/r^s$$
$$=1.94\times10^{-10}/r^{5.19} \text{ ergs} (2.61 \text{ A}\leqq r\leqq 3.14 \text{ A}). \quad (4)$$

TABLE I. Summary of collision cross-section results.

E ev	Wide detector $\bar{S}_w$ A^2	Wide detector S_w A^2	Wide detector Percent deviation	Narrow detector $\bar{S}_n$ A^2	Narrow detector S_n A^2	Narrow detector Percent deviation
700	27.08	26.89	+0.7			
800	25.90	25.65	+1.0	29.63	30.68	−3.4
900	23.98	24.60	−2.6	29.10	29.32	−0.8
1000	23.14	23.70	−2.4	28.02	28.15	−0.5
1100	23.47	22.92	+2.3	27.27	27.14	+0.5
1200	22.58	22.22	+1.6	27.14	26.24	+3.2
1300	21.71	21.60	+0.5	26.15	25.45	+2.7
1400	20.97	21.04	−0.3	25.40	24.73	+3.0
1500	20.48	20.54	−0.3	24.38	24.08	+1.2
1600	20.10	20.07	+0.1	23.76	23.49	+1.1
1700	19.44	19.65	−1.1	22.33	22.95	−2.8
1800	19.20	19.25	−0.3	22.14	22.45	−1.4
1900	18.93	18.89	+0.2	21.80	21.99	−0.9
2000	18.49	18.55	−0.3	21.14	21.56	−2.0
2100	18.36	18.23	+0.7	21.15	21.15	0.0

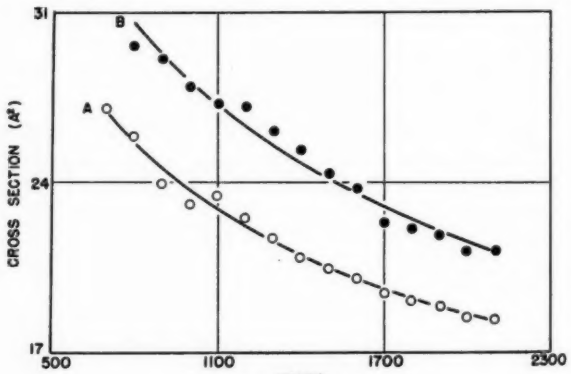

FIG. 1. Total collision cross sections: A. wide detector; B. narrow detector.

Equations (3) and (4) are shown in Fig. 2 as curves A and B, respectively. The ratio of $V(r)$ calculated from Eq. (3) to that calculated from Eq. (4) varies from 1.10 to 1.04 as r increases from 2.61 A to 2.94 A, the range of interaction distance common to the two potential functions. When these functions are extrapolated slightly to cover the maximum range, 2.42 A to 3.14 A, the above ratio ranges from 1.14 to 1.01. A relation which gives $V(r)$ values intermediate between those of Eqs. (3) and (4) and which will be taken as the potential between two krypton atoms derived from both wide and narrow detector results, may be written in the form

$$V(r)=2.55\times10^{-10}/r^{5.42} \text{ ergs} (2.42 \text{ A}\leqq r\leqq 3.14 \text{ A}). \quad (5)$$

Values of S_w calculated from Eq. (5) are between 1.5

* Present address: Institute of Molecular Physics, University of Maryland, College Park, Maryland.
[1] I. Amdur and A. L. Harkness, J. Chem. Phys. 22, 664 (1954).

and 3.1% lower than the smoothed values in Table I, and calculated values of S_n are between 1.6 and 3.1% higher than the corresponding tabulated values.

The potential between two krypton atoms appears to be less well defined than the corresponding potentials for argon, neon, and helium. For values of r between about 3.5 A and 4.1 A, Mason and Rice[2] have derived the potentials

$$V(r)=[45.7\exp(-3.03r)-1.90/r^6]\times10^{-10}\text{ ergs }(r\text{ in }A) \quad (6)$$

and

$$V(r)=(4150/r^{12}-1.91/r^6)\times10^{-10}\text{ ergs}(r\text{ in }A) \quad (7)$$

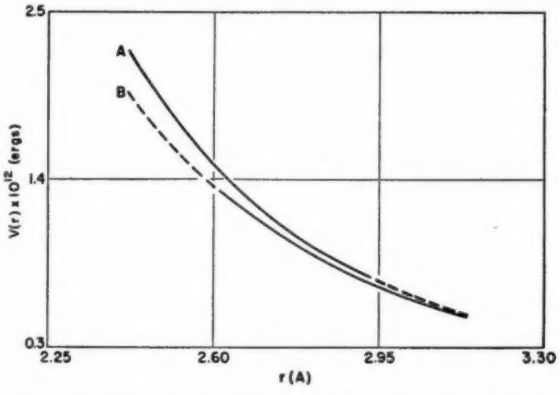

FIG. 2. Potential energy between two krypton atoms: A. wide detector results; B. narrow detector results.

from experimental results on gaseous compressibility, transport properties, and crystal data. Equation (6) seems better suited for calculating second virial coefficients than Eq. (7) which, in turn, seems better suited for calculating transport properties. Questions raised by Mason and Rice concerning the probable accuracy of the experimental results on the crystal properties and transport properties would indicate that a choice between Eqs. (6) and (7) is probably not justified. Whally and Schneider[3] have recently completed a new series of compressibility measurements on krypton in the range 273.16° to 873.16°K, and have used the derived second virial coefficients to determine the interaction potential.[4] They propose a number of

[2] E. A. Mason and W. E. Rice, J. Chem. Phys. **22**, 843 (1954).
[3] E. Whalley and W. G. Schneider, Trans. Am. Soc. Mech. Engrs. **76**, 1001 (1954).
[4] E. Whalley and W. G. Schneider (to be published).

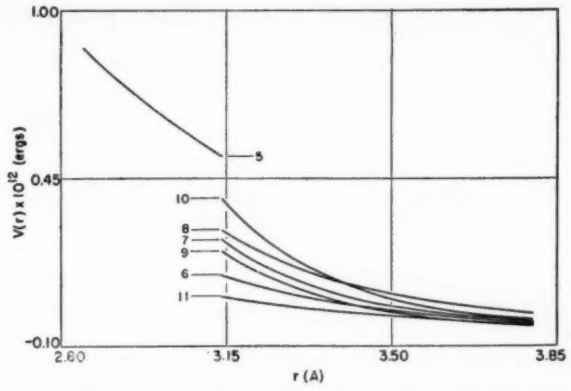

FIG. 3. Comparison of potential energy curves at small and large interaction distances. (Numbers on curves refer to equation numbers in text.)

potentials, all of which reproduce the second virial coefficients very well, and the lattice distance and heat of sublimation, both at 0°K, moderately well. Representative functions, in the range from about 3.4 A to 4.1 A, from the group they propose are:

$$V(r)=[32.6\exp(-2.76r)-2.70/r^6]\times10^{-10}\text{ ergs}(r\text{ in }A), \quad (8)$$

$$V(r)=[553\exp(-3.79r)-1.64/r^6]\times10^{-10}\text{ ergs}(r\text{ in }A), \quad (9)$$

$$V(r)=(5670/r^{12}-2.28/r^6)\times10^{-10}\text{ ergs}(r\text{ in }A), \quad (10)$$

and

$$V(r)=(79.6/r^9-1.95/r^6)\times10^{-10}\text{ ergs}(r\text{ in }A). \quad (11)$$

Figure 3 shows the terminal portion of the potential given by Eq. (5), and the initial portions extrapolated to 3.14 A, of the potentials given by Eqs. (6)–(11). It is felt that the present potential energy information at small distances agrees with that available at larger distances about as well as the potentials at the larger distances agree among themselves.

ACKNOWLEDGMENTS

The authors wish to thank the Research Corporation for its generous support of the work with grants-in-aid, and the Linde Air Products Company for its gift of pure krypton. They are also very grateful to Dr. W. G. Schneider for sending them potential energy results prior to publication, and to Luke M. Shuler for calculation assistance.

Theory of Protein Solutions. II*

TERRELL L. HILL
Naval Medical Research Institute, Bethesda, Maryland
(Received February 10, 1955)

The formal theory of the first paper of this series is extended here to include the binding of several different species of ions or molecules on a protein, aggregation in a protein solution, and solutions containing more than one type of protein molecule.

I. INTRODUCTION

IN an earlier paper,[1] a theory of protein solutions was developed, based on the McMillan-Mayer theory of solutions.[2] Aside from the restriction to solutions containing only one protein and one species of ion or molecule which can be bound to the protein, the equations of I are quite general and provide, among other things, a reliable point of departure for use with specific, approximate models of protein solutions. For example, the work of Kirkwood and Shumaker[3] on protein-protein forces is a special case of the theory presented in I.

As in I, we refer the reader elsewhere[4] for an explicit discussion of the applicability of the McMillan-Mayer theory to ionic solutions.

The purpose of the present paper is to show, without attempting to be completely general, how the treatment in I can be extended to: (a) the binding of several different species of ions or molecules on a protein (Sec. II); (b) aggregation in a protein solution (Sec. III); and (c) solutions containing more than one type of protein (Sec. IV). These are all important cases in practice.

The notation of I is carried over here as far as possible; the reader is referred to I for definitions.

II. BINDING OF SEVERAL DIFFERENT SPECIES ON A PROTEIN

The modification of I in this case is rather trivial. Let s_i be the number of molecules of species i bound on a protein molecule. The subscript $\omega(s)$ now refers to $s_1, s_2, \cdots$ molecules of the various species arranged in some particular configuration on a protein molecule. The absolute activity of species i is x_i and for x (e.g., in Eqs. (I-44) and (I-53b)) we now read $\mathbf{x}=x_1, x_2, \cdots$. We have the equilibrium relation

$$\mathfrak{z}_{\omega(s)}=x_1^{s_1}x_2^{s_2}\cdots\mathfrak{z} \tag{1}$$

so that in all equations (osmotic pressure, distribution functions, integral equations, etc.) except those having to do with the number of bound molecules the only further change in I is to replace x^s by $x^{s_1}x_2^{s_2}\cdots$.

Binding

Let $\bar{M}_i$ be the mean number of molecules of species i bound to protein. Then

$$\bar{M}_i=\Big\langle \sum_{s,\omega(s)} s_i m_{\omega(s)}\Big\rangle_{N}=x_i\left(\frac{\partial \ln e^{\Pi V/kT}}{\partial x_i}\right)_{\mathfrak{z},x_j,T,V,\gamma,W}. \tag{2}$$

In the equivalent of Eqs. (I-67) to (I-71) for $\bar{M}_i/\bar{M}_P$, we replace $E_1, E_2, \cdots$ by $E_1^{(i)}, E_2^{(i)}, \cdots$ where

$$\begin{aligned}
&E_1^{(i)}=e_1^{(i)}V, \quad e_1^{(i)}=\sum_{(s)} s_i x_1^{s_1}x_2^{s_2}\cdots H_{\omega(s)}\\
&E_2^{(i)}=\sum_{(s)}\sum_{(s')}(s_i+s_i')(x_1^{s_1}x_2^{s_2}\cdots H_{\omega(s)})\\
&\qquad\times(x_1^{s_1'}x_2^{s_2'}\cdots H_{\omega(s)'})\\
&\qquad\times\int\exp[-\mathfrak{W}^{(2)}((1_{\omega(s)}),(1_{\omega(s)'}),0)/kT]\\
&\qquad\qquad\times d(1_{\omega(s)})_x d(1_{\omega(s)'})_x,
\end{aligned} \tag{3}$$

etc. Thus, the mean number of molecules of i bound per protein molecule is

$$\frac{\bar{M}_i}{\bar{M}_P}=\frac{e_1^{(i)}}{c_1}\left[1+\frac{\rho}{c_1}\left(\frac{E_2^{(i)}}{2E_1^{(i)}}-\frac{C_2}{C_1}\right)+\cdots\right]. \tag{4}$$

In the limit $\rho\to 0$,

$$\frac{\bar{M}_i}{\bar{M}_P}=\frac{e_1^{(i)}}{c_1}=\frac{\sum_{(s)} s_i x_1^{s_1}x_2^{s_2}\cdots H_{\omega(s)}}{\sum_{(s)} x_1^{s_1}x_2^{s_2}\cdots H_{\omega(s)}}\quad(\rho=0). \tag{5}$$

Equation (5) shows how other species influence the binding of i at $\rho=0$, while Eq. (4) gives the first-order correction for finite protein concentration. Equation (5) can be rewritten formally to resemble the corresponding equation for the binding of a single species, Eq. (I-71). For example, taking $i=1$,

$$\frac{\bar{M}_1}{\bar{M}_P}=\frac{\sum_{(s_1)} s_1 x_1^{s_1}\mathfrak{J}\mathcal{C}_{\omega(s-s_1)}}{\sum_{(s_1)} x_1^{s_1}\mathfrak{J}\mathcal{C}_{\omega(s-s_1)}}\quad(\rho=0) \tag{6}$$

* The opinions expressed herein are those of the author and not necessarily those of the Navy Department.

[1] T. L. Hill, J. Chem. Phys. **23**, 623 (1955), hereafter referred to as I.

[2] W. G. McMillan and J. E. Mayer, J. Chem. Phys. **13**, 276 (1945).

[3] J. G. Kirkwood and J. B. Shumaker, Proc. Natl. Acad. Sci. **38**, 863 (1952).

[4] T. L. Hill in *Ion Transport Across Membranes* (Academic Press, Inc., New York, 1954), edited by H. T. Clarke.

where

$$\mathfrak{IC}_{\omega(s-s_1)}=\sum_{(s-s_1)} x_2^{s_2}x_3^{s_3}\cdots H_{\omega(s)} \tag{7}$$

and $s-s_1$ refers to the set $s_2, s_3, \cdots$. The effect of the binding of other species on the binding of species 1 is included here in $\mathfrak{IC}_{\omega(s-s_1)}$.

An alternative and more compact form of the expansion in Eqs. (4) and (I-70) may be obtained as follows. From Eqs. (2), (I-58) and (I-60), we have

$$\frac{\bar{M}_i}{\bar{M}_P}=-\frac{1}{\rho}\left(\frac{\partial\Pi/kT}{\partial\ln x_i}\right)_{\mathfrak{z},x_j,T,\gamma,W}$$

$$=-\frac{1}{\rho}\sum_{j\geq 1}\left[\left(\frac{\partial \mathfrak{b}_j}{\partial\ln x_i}\right)_{x_j,T,\gamma,W}(\mathfrak{z}c_1)^j+j\mathfrak{b}_j\mathfrak{z}(\mathfrak{z}c_1)^{j-1}e_1^{(i)}\right]$$

$$=\frac{e_1^{(i)}}{c_1}+\frac{1}{\rho}\sum_{j\geq 1}\frac{\partial \mathfrak{b}_j}{\partial\ln x_i}(\mathfrak{z}c_1)^j. \tag{8}$$

Now in the sum in Eq. (8) we substitute for $\mathfrak{z}c_1$ the expansion in powers of ρ, Eq. (I-61), and replace the $\mathfrak{b}_j$ by the virial coefficients $\mathfrak{B}_k$, using the inverse[5] of Eq. (I-63). The result, to terms in ρ^3, is

$$\frac{\bar{M}_i}{\bar{M}_P}=\frac{e_1^{(i)}}{c_1}-\rho\frac{\partial\mathfrak{B}_2}{\partial\ln x_i}-\tfrac{1}{2}\rho^2\frac{\partial\mathfrak{B}_3}{\partial\ln x_i}-\tfrac{1}{3}\rho^3\frac{\partial\mathfrak{B}_4}{\partial\ln x_i}-\cdots \tag{9}$$

where the derivatives are carried out with x_j, T, γ, W held constant. Equation (I-72) is a special case of this relation.

Isoelectric Point

Let z be the charge on a protein molecule when $s_1=s_2=\cdots=0$, and let z_i be the charge on a molecule or ion of species i. If species 1 refers to H^+, the isoelectric point is found (in principle) by solving the equation

$$z+\frac{\bar{M}_1}{\bar{M}_P}+\sum_{i\geq 2} z_i\frac{\bar{M}_i}{\bar{M}_P}=0 \tag{10}$$

for x_1. In the special case that the only species being bound is H^+, Eq. (10) becomes ($x_1\equiv x$)

$$\sum_{(s)}(z+s-S)x^sH_{\omega(s)}=0 \tag{11}$$

where

$$S=\rho\frac{\partial\mathfrak{B}_2}{\partial\ln x}+\tfrac{1}{2}\rho^2\frac{\partial\mathfrak{B}_3}{\partial\ln x}+\cdots.$$

[5] See also pp. 288 and 292 of J. E. Mayer and M. G. Mayer, *Statistical Mechanics* (John Wiley and Sons, Inc., New York, 1940).

Equation (11) can also be written as

$$\sum_s (z+s)x^sK_s=0 \tag{12}$$

where

$$K_s=\left(1-\frac{S}{z+s}\right)\sum_{\omega(s)}\int d'(1_{\omega(s)})_\theta H_{\omega(s)}. \tag{13}$$

Equation (12) is in the conventional form[6] for the equation determining the isoelectric point except that x is an absolute activity instead of a concentration. K_s is the statistical mechanical equivalent of the reciprocal of a product of successive apparent[6,7] dissociation constants of the protein. The dependence of K_s on, for example, ρ and x is contained in Eq. (13).

III. PROTEIN AGGREGATION

Aggregation in a protein solution, if it exists, is already treated *implicitly* in the equations of I, since all protein-protein forces, including those strong enough to lead to aggregation, are taken into account there. However, we want to introduce aggregation *explicitly* here, in much the same manner as we did for a one component monatomic gas elsewhere.[8]

For a gas,[8] we wrote down alternative expressions for Ξ, the grand partition function, with clusters explicit and clusters implicit. By comparing these expressions, we obtained formal relations between the two types of partition functions (clusters implicit and explicit) that had to be satisfied in order to provide an exact discussion of cluster equilibria.

In the present case, this same procedure can be applied to Ξ [Eq. (I-43) with $\mathbf{x}$ for x]. Or, alternatively, a formally equivalent procedure can be applied to $e^{\Pi V/kT}$ [Eq. (I-44) with $\mathbf{x}$ for x]. That is, there are here two levels (Ξ and $e^{\Pi V/kT}$) at which we can introduce aggregates explicitly and without approximation. Which level is used depends on how one wishes to define an aggregate (e.g., in terms of potential energy, or potential of average force). In the present state of development of the statistical mechanical theory of solutions, it is much more realistic to employ the $e^{\Pi V/kT}$ level, since in practice it is not possible actually to carry out the computation of $e^{\Pi V/kT}$ from Ξ, or potentials of average force $W_{\mathbf{m}}$ from $U_{\mathbf{N}}$ (Eq. (I-44) from Eq. (I-43)). In applications one always has to start with Eq. (I-44) and introduce approximations for $W_{\mathbf{m}}$. However, the particular definition of an aggregate to be emphasized below ($r<a$ criterion), leads to the same results whether introduced with Ξ or with $e^{\Pi V/kT}$.

[6] See E. J. Cohn and J. T. Edsall, *Proteins, Amino Acids and Peptides* (Reinhold Publishing Corporation, New York, 1943), p. 92.

[7] The dissociation constants would be expressed here in terms of concentrations of protein ionic species and of the hydrogen ion absolute activity.

[8] T. L. Hill, J. Chem. Phys. **23**, 617 (1955), hereafter referred to as M.

Formal Relations

An equation for $e^{\Pi V/kT}$ with aggregates implicit is Eq. (I-55) (with **x** for x, etc.),

$$e^{\Pi V/kT}=1+\zeta C_1+\frac{\zeta^2}{2!}C_2+\frac{\zeta^3}{3!}C_3+\cdots. \tag{14}$$

For explicit aggregates, we introduce the subscript notation $\omega(ns)$ to refer to an aggregate of n protein molecules with a total of $s_1, s_2, \cdots$ molecules of various species bound in some particular configuration on the aggregate. In place of Eq. (I-52), we can write here

$$e^{\Pi V/kT}=\sum_{\mathbf{m}\geq\mathbf{0}}\int d'\{\mathbf{m}\}_\theta \prod_{n,s,\omega(ns)} \times\left\{\frac{\zeta_{\omega(ns)}{}^{m_{\omega(ns)}}}{m_{\omega(ns)}!}\prod_{(m_{\omega(ns)})}H_{\omega(ns)}\right\} \times\int\exp[-\mathfrak{W}_{\mathbf{m}}(0)/kT]d\{\mathbf{m}\}_x. \tag{15}$$

In view of the equilibria existing, we have

$$\zeta_{\omega(ns)}=\zeta^n x_1{}^{s_1}x_2{}^{s_2}\cdots \tag{16}$$

where ζ is the absolute activity of a protein monomer with no bound molecules. If we substitute Eq. (16) in Eq. (15), and expand in powers of ζ, we obtain (to terms in ζ^3)

$$e^{\Pi V/kT}=1+\zeta C_{100}+\frac{\zeta^2}{2!}(C_{200}+2C_{010}) +\frac{\zeta^3}{3!}(C_{300}+6C_{110}+6C_{001})+\cdots \tag{17}$$

where

C_{100}(one monomer)$=c_{100}V$; $c_{100}=\sum_{(1s)} x_1{}^{s_1}x_2{}^{s_2}\cdots H_{\omega(1s)}$

C_{200}(two monomers)

$$=\sum_{(1s)}\sum_{(1s')}(x_1{}^{s_1}x_2{}^{s_2}\cdots H_{\omega(1s)})(x_1{}^{s_1'}x_2{}^{s_2'}\cdots H_{\omega(1s)'}) \times\int\exp[-\mathfrak{W}^{(2)}((1_{\omega(1s)}),(1_{\omega(1s)'}),0)/kT] \times d(1_{\omega(1s)})_x d(1_{\omega(1s)'})_x$$

C_{010}(one dimer)$=c_{010}V$; $c_{010}=\sum_{(2s)} x_1{}^{s_1}x_2{}^{s_2}\cdots H_{\omega(2s)}$

C_{110}(one monomer, one dimer)

$$=\sum_{(1s)}\sum_{(2s')}(x_1{}^{s_1}x_2{}^{s_2}\cdots H_{\omega(1s)})(x_1{}^{s_1'}x_2{}^{s_2'}\cdots H_{\omega(2s)'}) \times\int\exp[-\mathfrak{W}^{(2)}((1_{\omega(1s)}),(1_{\omega(2s)'}),0)/kT] \times d(1_{\omega(1s)})_x d(1_{\omega(2s)'})_x, \tag{18}$$

etc. The relations between the coefficients of Eqs. (14) and (17) are

$$\begin{aligned} C_1&=C_{100}\\ C_2&=C_{200}+2C_{010}\\ C_3&=C_{300}+6C_{110}+6C_{001}, \end{aligned} \tag{19}$$

etc. For an exact treatment, the aggregates must be defined ($H_{\omega(ns)}$, $\mathfrak{W}_{\mathbf{m}}(0)$) in such a way that Eqs. (19) are satisfied. Of course all definitions satisfying Eqs. (19) will give the same *thermodynamic* results. For example, the coefficients in the expansion of ζc_1 in powers of ρ [Eq. (I-61)] or the osmotic pressure virial coefficients [Eqs. (I-62,63)] will be independent of the definition adopted. Explicit expressions for these coefficients are found by substituting Eqs. (19) into Eq. (I-59).

To find the equilibrium number $\bar{m}_n$ of n-aggregates, we apply

$$\bar{m}_{\omega(ns)}=\zeta_{\omega(ns)}\frac{\partial \ln e^{\Pi V/kT}}{\partial\zeta_{\omega(ns)}} \tag{20}$$

to Eq. (15), substitute Eq. (16) for $\zeta_{\omega(ns)}$, and finally sum over s, $\omega(ns)$. This gives[9]

$$\begin{aligned} \bar{m}_1&=\zeta C_1+\zeta^2(C_{200}-C_{100}{}^2)+\zeta^3(\tfrac{1}{2}C_{300}+C_{110}+C_{100}{}^3 -\tfrac{3}{2}C_{100}C_{200}-C_{100}C_{010})+\cdots\\ \bar{m}_2&=\zeta^2C_{010}+\zeta^3(C_{110}-C_{100}C_{010})+\cdots\\ \bar{m}_3&=\zeta^3C_{001}+\cdots, \end{aligned} \tag{21}$$

etc. By using Eq. (I-61), we find[10] for the analogous expansions in powers of ρ,

$$\begin{aligned} \rho_1&=\frac{\bar{m}_1}{V}=\rho-\rho^2\left(\frac{2c_{010}}{c_{100}{}^2}\right)+\rho^3\left(\frac{4C_{200}c_{010}}{c_{100}{}^4V} +8\frac{c_{010}{}^2}{c_{100}{}^4}-2\frac{c_{010}V}{c_{100}{}^2}-2\frac{C_{110}}{c_{100}{}^3V}-3\frac{c_{001}}{c_{100}{}^3}\right)+\cdots\\ \rho_2&=\rho^2\frac{c_{010}}{c_{100}{}^2}+\rho^3\left(\frac{c_{010}V}{c_{100}{}^2}+\frac{C_{110}}{c_{100}{}^3V} -2\frac{C_{200}c_{010}}{c_{100}{}^4V}-4\frac{c_{010}{}^2}{c_{100}{}^4}\right)+\cdots\\ \rho_3&=\rho^3\frac{c_{001}}{c_{100}{}^3}+\cdots. \end{aligned} \tag{22}$$

The equilibrium quotient for monomers in equilibrium with n-mers is[8,9]

[9] Note that $C_{\mathbf{N}}/\Pi_k N_k!$ plays the same formal role throughout this paper that $Q_{\mathbf{N}}$ does in M.

[10] As in footnote 9, the formal connection between $C_{\mathbf{N}}$ and $Y_{\mathbf{N}}$ of M is $Y_{\mathbf{N}}\leftrightarrow N!C_{\mathbf{N}}/(\Pi_k N_k!)c_1{}^N$, where $N=\Sigma_k N_k$.

$$\frac{\rho_1^n}{\rho_n}=\frac{c_{100\cdots}{}^n}{c_{00\cdots1}}\left\{1+\frac{\rho}{c_{100\cdots}}\left[\frac{nC_{200\cdots}}{c_{100\cdots}V}-(n-1)c_{100\cdots}V-\frac{C_{100\cdots1}}{c_{00\cdots1}V}\right]+\cdots\right\}. \quad (23)$$

The (nonthermodynamic) results in Eqs. (21)–(23) clearly depend on the particular definition of an aggregate that is adopted. However, it is only worthwhile to discuss aggregates explicitly when the aggregating forces are strong, and in this case the results will be essentially the same for any physically reasonable definition.

The extent of binding of an ion or molecule to a protein which aggregates in solution is independent of the definition of an aggregate, provided that Eqs. (19) are satisfied. However, explicit expressions in terms of aggregates are easily obtained from Eqs. (4) and (9) by using Eqs. (19) to replace the C_k and the corresponding

$$\begin{aligned} E_1{}^{(i)}&=E_{100}{}^{(i)}\\ E_2{}^{(i)}&=E_{200}{}^{(i)}+2E_{010}{}^{(i)} \end{aligned} \quad (24)$$

etc., to replace the $E_k{}^{(i)}$, where the $E_{\mathbf{N}}{}^{(i)}$ follow from Eqs. (18) and

$$E_{\mathbf{N}}{}^{(i)}=x_i\left(\frac{\partial C_{\mathbf{N}}}{\partial x_i}\right)_{x_j,T,V,\gamma,W}. \quad (25)$$

Definition of an Aggregate

One procedure here is to adopt models for aggregates of different sizes, and use Eqs. (18) to calculate the $C_{\mathbf{N}}$. There remains the problem of adjusting the models to satisfy Eqs. (19), if an exact treatment is desired.

A more direct procedure which automatically satisfies Eqs. (19) is the following. We start with Eq. (I-56) for C_k. The complete translational[11] configuration space [over which the configuration integral is carried out in Eq. (I-56)] is divided into nonoverlapping subspaces which are assigned to the various $C_{\mathbf{N}}$ making up C_k in Eq. (19). This is analogous to the division of phase space into subspaces in M. Perhaps the simplest and most useful division of translational configuration space is one based on a fixed distance a between the centers of mass of each pair of protein molecules. If r is the intermolecular distance, we choose a according to some reasonable structural criterion so that for $r\leqslant a$ the two protein molecules are considered bound to each other and for $r>a$ they are considered not bound. For example, for $k=3$ we would have the division given in Table I of the translational configuration space. It should be mentioned that it is not necessary to introduce the superposition (pair) approximation in $\mathfrak{W}^{(k)}(0)$ in order to apply this criterion, although in practice it would ordinarily be employed for simplicity. If the superposition approximation is used, one can follow the u^*, $u^\ddagger$ (here w^*, $w^\ddagger$; $w\equiv\mathfrak{W}^{(2)}$) procedure in M [see Eq. (M-37)].

[11] Alternatively, the entire configuration space (rotation and translation) can be divided into subspaces if we adopt Eq. (I-46) as the starting point instead of Eq. (I-52).

TABLE I.

$r\leq a$	$r>a$		
r_{12}, r_{13}, r_{23}	...		
r_{12}, r_{13}	r_{23}	$6C_{001}$	
r_{12}, r_{23}	r_{13}		
r_{13}, r_{23}	r_{12}		
r_{12}	r_{13}, r_{23}		C_3
r_{13}	r_{12}, r_{23}	$6C_{110}$	
r_{23}	r_{12}, r_{13}		
...	r_{12}, r_{13}, r_{23}	C_{300}	

The foregoing procedure is not restricted to spherically symmetrical molecules.

IV. BINARY PROTEIN SOLUTIONS

To illustrate how the theory can be extended to solutions containing more than one protein, we consider here a binary protein solution and restrict the treatment to second-order terms, corresponding to the second virial coefficient.

Let us label the two proteins a and b. Equation (I-51) becomes, with obvious notation,

$$\begin{aligned} e^{\Pi V/kT}=\sum_{m\geqslant 0}\int d'\{\mathbf{m}\}_\theta \prod_{s,a\omega(s)} &\times\left\{\frac{\zeta_{a\omega(s)}{}^{m_{a\omega(s)}}}{m_{a\omega(s)}!}\prod_{(m_{a\omega(s)})}H_{a\omega(s)}\right\}\\ &\times\prod_{s',b\omega(s)'}\left\{\frac{\zeta_{b\omega(s)'}{}^{m_{b\omega(s)'}}}{m_{b\omega(s)'}}\prod_{(m_{b\omega(s)'})}H_{b\omega(s)'}\right\}\\ &\times\int\exp[-\mathfrak{W}_{\mathbf{m}}(0)/kT]d\{\mathbf{m}\}_x. \end{aligned} \quad (26)$$

We put

$$\begin{aligned} \zeta_{a\omega(s)}&=\zeta_a x_1{}^{s_1}x_2{}^{s_2}\cdots\\ \zeta_{b\omega(s)'}&=\zeta_b x_1{}^{s_1'}x_2{}^{s_2'}\cdots \end{aligned} \quad (27)$$

and then expand $e^{\Pi V/kT}$ in powers of ζ_a and ζ_b. We find

$$e^{\Pi V/kT}=1+\zeta_a C_{a1}+\zeta_b C_{b1}+\frac{\zeta_a{}^2}{2!}C_{a2}+\zeta_a\zeta_b C_{ab2}+\frac{\zeta_b{}^2}{2!}C_{b2}+\cdots \quad (28)$$

where C_{a1}, C_{b1}, C_{a2}, and C_{b2} are defined as in I and Sec. II for single protein species, and

$$\begin{aligned} C_{ab2}=\sum_{(as)}\sum_{(bs')}&(x_1{}^{s_1}x_2{}^{s_2}\cdots H_{a\omega(s)})(x_1{}^{s_1'}x_2{}^{s_2'}\cdots H_{b\omega(s)'})\\ &\times\int\exp[-\mathfrak{W}^{(2)}((1_{a\omega(s)}),(1_{b\omega(s)'}),0)/kT]\\ &\times d(1_{a\omega(s)})_x d(1_{b\omega(s)'})_x. \end{aligned} \quad (29)$$

We rewrite Eq. (28) as

$$e^{\Pi V/kT}=1+(\zeta_a c_{a1})V+(\zeta_b c_{b1})V+\frac{(\zeta_a c_{a1})^2}{2}\frac{C_{a2}}{c_{a1}^2}+(\zeta_a c_{a1})(\zeta_b c_{b1})\frac{C_{ab2}}{c_{a1}c_{b1}}+\frac{(\zeta_b c_{b1})^2}{2}\frac{C_{b2}}{c_{b1}^2}+\cdots$$

and take the logarithm to find

$$\frac{\Pi}{kT}=\zeta_a c_{a1}+\zeta_b c_{b1}+\mathfrak{b}_{aa}(\zeta_a c_{a1})^2+\mathfrak{b}_{ab}(\zeta_a c_{a1})(\zeta_b c_{b1})+\mathfrak{b}_{bb}(\zeta_b c_{b1})^2+\cdots \quad (30)$$

where

$$2!V\mathfrak{b}_{aa}=\frac{C_{a2}}{c_{a1}^2}-V^2$$

$$2!V\mathfrak{b}_{bb}=\frac{C_{b2}}{c_{b1}^2}-V^2 \quad (31)$$

$$1!1!V\mathfrak{b}_{ab}=\frac{C_{ab2}}{c_{a1}c_{b1}}-V^2.$$

From

$$\zeta_a\frac{\partial\Pi/kT}{\partial\zeta_a}=\rho_a \quad (32)$$

and the corresponding equation for ρ_b, we obtain series which can be inverted to give

$$\begin{aligned}\zeta_a c_{a1}&=\rho_a-2\mathfrak{b}_{aa}\rho_a^2-\mathfrak{b}_{ab}\rho_a\rho_b+\cdots\\ \zeta_b c_{b1}&=\rho_b-2\mathfrak{b}_{bb}\rho_b^2-\mathfrak{b}_{ab}\rho_a\rho_b+\cdots.\end{aligned} \quad (33)$$

Equation (30) becomes then

$$\Pi/kT=\rho_a+\rho_b-\mathfrak{b}_{aa}\rho_a^2-\mathfrak{b}_{ab}\rho_a\rho_b-\mathfrak{b}_{bb}\rho_b^2+\cdots. \quad (34)$$

If we let α be the protein mole fraction of a, and $\rho=\rho_a+\rho_b$, then

$$\Pi/kT=\rho+\mathfrak{B}_2\rho^2+\cdots \quad (35)$$

where

$$\mathfrak{B}_2=-\mathfrak{b}_{aa}\alpha^2-\mathfrak{b}_{ab}\alpha(1-\alpha)-\mathfrak{b}_{bb}(1-\alpha)^2. \quad (36)$$

The total number of species i molecules bound on both proteins is given by

$$\bar{M}_i=x_i\left(\frac{\partial\ln e^{\Pi V/kT}}{\partial x_i}\right)_{\zeta_a,\zeta_b,x_j,T,V,\gamma,W}. \quad (37)$$

As in Eq. (9), we find (after some algebra)

$$\frac{\bar{M}_i}{\bar{M}_a+\bar{M}_b}=\left(\frac{\bar{M}_i}{\bar{M}_a+\bar{M}_b}\right)_{\rho=0}-\rho\frac{\partial\mathfrak{B}_2}{\partial\ln x_i}-\cdots \quad (38)$$

where

$$\left(\frac{\bar{M}_i}{\bar{M}_a+\bar{M}_b}\right)_{\rho=0}=\frac{e_{a1}^{(i)}}{c_{a1}}\alpha+\frac{e_{b1}^{(i)}}{c_{b1}}(1-\alpha) \quad (39)$$

and

$$\begin{aligned}V\frac{\partial\mathfrak{B}_2}{\partial\ln x_i}=&\alpha^2\left(\frac{e_{a1}^{(i)}C_{a2}}{c_{a1}^3}-\frac{E_{a2}^{(i)}}{2c_{a1}^2}\right)\\&+\alpha(1-\alpha)\left(\frac{e_{a1}^{(i)}C_{ab2}}{c_{a1}^2c_{b1}}+\frac{e_{b1}^{(i)}C_{ab2}}{c_{a1}c_{b1}^2}-\frac{E_{ab2}^{(i)}}{c_{a1}c_{b1}}\right)\\&+(1-\alpha)^2\left(\frac{e_{b1}^{(i)}C_{b2}}{c_{b1}^3}-\frac{E_{b2}^{(i)}}{2c_{b1}^2}\right).\end{aligned} \quad (40)$$

Aggregation can be introduced as in Sec. III, but we omit the details.

THE JOURNAL OF CHEMICAL PHYSICS VOLUME 23, NUMBER 12 DECEMBER, 1955

Extended Interpretation of the Boltzmann-Maxwell Equation (A Theory of Nonstationary Random Processes)

TOYOKI KOGA*
Faculty of Engineering, Nagoya University, Nagoya, Japan
(Received July 12, 1954)

Usual theories of statistical mechanics of nonuniform state stand on the assumption of approximately stationary random processes. Generally speaking, this assumption is not reasonable when the state concerned deviates considerably from thermal equilibrium. For a system in such a state, it is difficult not only to define but also to observe a complete set of gross variables. In this case the deviations of the actual future values of the gross variables from their expected future values cannot be neglected.

A new method of coarse-graining is proposed as available to such a state. As a concrete example of system we take a gas. We get a coarse-grained function $\langle f \rangle_D$ by averaging the fine-grained probability function of one molecule over a series of observations made on the system on different occasions where at each observation the system is initially in a common macroscopic state as determined by our incomplete set of initial conditions. It is shown that $\langle f \rangle_D$ satisfies the Boltzmann-Maxwell equation. The equation is valid even when the state concerned deviates considerably from thermal equilibrium and the random processes are not stationary. In this situation, however, the interpretation of the equation is different from the usual one; i.e., the equation predicts not the result of an individual observation of the gas concerned but the result obtained by averaging over a series of observations made repeatedly on different occasions on the same gas under a common incomplete set of macroscopic initial conditions where, with the lapse of time from the start, the result of each observation deviates from the others even in the macroscopic sense. For the time being, the theory is given only in the sense of classical mechanics.

INTRODUCTION

THERE are a number of excellent methods of approach to problems in irreversible statistical mechanics.[1–3],† They stand, however, almost always on the assumption of stationary or nearly stationary random processes. As we can naturally presume, there is some danger that the processes are not stationary when the deviation from thermal equilibrium is large. Consequently one must be careful of the limitations of validity of the theories when the states under consideration deviate too far from thermal equilibrium. A set of systems at first manifestly similar will in the course of time assume totally different behavior patterns. For this situation, the current theories are not suitable.

We propose an alternative method of coarse-graining available for this case: that is, of averaging the processes with respect to a series of observations made on the same system repeatedly at different times under manifestly similar initial conditions. By this method we can extend the limit of the usual theories. In Part I of this article a general study is given. In Part II the result of the general study is applied to a special model, rarefied gas, obtaining the Boltzmann-Maxwell equation as the result. Here the interpretation of the equation is modified as compared with the usual one. We prove that the equation is available for wider domain of nonstationary random processes by our extended interpretation. The theory is given for the time being in the sense of classical mechanics.

PART I. NONSTATIONARY RANDOM PROCESSES

I-1. Limitations of Usual Theories‡

As is well known, according to statistical mechanics, we can describe the character of a system in uniform states in terms of a very few grossly observable variables in spite of the fact that the system is composed of many particles consequently having many degrees of freedom. This macroscopic description is obtained by coarse-graining the microscopic behavior of the system under an assumption: (a) the identification of the time averages of certain functions of the phase of a mechanical model with the values that grossly observable properties of a physical system assume after a long enough time and (b) the identification of time averages with phase space averages.

From the standpoint of statistical mechanics, many authors[1–3] have dealt with the behaviors of systems which are not uniform in time and space. Their works, whether dependent upon particular models of systems or not, have inherited a common fortune (the assumption mentioned above) from the statistical mechanics of uniform states although the inheritance is modified to some degree. Assaying the methods of coarse-graining applied in these theories we have the following three elemental coarse-grainings: (1) assigning a certain small number of particles out of a system to particular states, we average certain functions of phase of the system over all the possible states of the other particles of the system; (2) we average the behavior of a system over a period of time; and (3) we coarse-grain the behavior of a system by averaging over each small cell of the configuration space which is filled with the system. Born and Green[1] adopted the first method, while Kirkwood[2]

* Now at Jet Propulsion Center, California Institute of Technology, Pasadena, California.
[1] H. S. Green, *Molecular Theory of Fluids* (North-Holland Publishing Company, Amsterdam, 1952).
[2] J. G. Kirkwood, J. Chem. Phys. **14**, 180 (1946); **15**, 72 (1947).
[3] M. S. Green, J. Chem. Phys. **20**, 1283 (1952); **22**, 398 (1954).
† Other literatures may be found in references 1, 2, and 3.

‡ The opinions stated in this section are not necessarily new. They are given only for the purpose of clarifying the need for our own method.

used the second combining it with the first, and M. S. Green[3] combined the second with the third.

When the density of number of particles in the configuration space is not too small, and the state of the system does not deviate considerably from thermal equilibrium, the differences in the theories may not be important. However, when the density of number of particles is too small, the results of Born and Green have no measurability, because too frequent fluctuations appear. On the other hand, when the states of the system deviate too far from thermal equilibrium and, as a consequence, the nonuniformity of the state is large, Kirkwood's as well as M. S. Green's methods may lose their precise meaning. That is to say, in accepting the second method of coarse-graining as available for nonuniform phenomena, there should be a premise, as follows: The behavior of a system concerned can be readily specified as the result of superposition of two kinds of nonuniformity, one macroscopic and of low frequencies, the other microscopic and of high frequencies (random processes). The behavior of the system is easily separated into macroscopic and microscopic elements, and we can assume that the microscopic random processes are approximately stationary.[4]

We assume that it is possible to accept this premise when the states of the system concerned do not deviate far from thermal equilibrium. According to this premise, M. S. Green[3] assumed that $\langle a_i \rangle$ defined by

$$\langle a_i \rangle = \int da_1 \cdots da_s a_i T(a_i^0 t_0 / a_i t), \quad i=1, \cdots, s \qquad \text{(I-1.1)}$$

has one definite value as long as the time interval $t-t_0$ is not less than a time which is small compared to times observable by macroscopic methods. Here a_i are the grossly observable variables and T is the transition probability. The circumstances are similar to those in the case where Kirkwood[2] deals with the theory in the phase-space of n-ples of particles. If we define φ as a proper function of the phase $X(t)$ of our system and if the phase changes according to the mechanical principles as time goes on, then $\langle \varphi \rangle_t$ defined by

$$\langle \varphi \rangle_t = \frac{1}{\tau} \int_0^\tau \varphi(t+s) ds \qquad \text{(I-1.2)}$$

is a function of time t. This function is independent of τ as long as τ ranges longer (not too much longer) than a certain stretch which is small in the macroscopic sense but large in the microscopic sense. On the other hand, where the state of a system deviates considerably from thermal equilibrium and the behavior of the system is not easily separated into macroscopic and microscopic elements, the validity of the premise is not assured. This is easily shown in the following estimation: Let us expand φ in a Fourier's series between the time t_1 and t_2. Here $t_2-t_1=T$ is sufficiently large as compared with the minimum period which we can recognize by our macroscopic method.

$$\left.\begin{aligned} &\varphi = a_0 + \sum_{n=1}^{\infty} \varphi_n(t), \\ &\varphi_n = a_n \sin n \frac{2\pi}{T}\left(t - t_1 - \frac{T}{2}\right) \\ &\qquad + b_n \cos n \frac{2\pi}{T}\left(t - t_1 - \frac{T}{2}\right), \\ &t_2 - t_1 = T. \end{aligned}\right\} \qquad \text{(I-1.3)}$$

After coarse-graining φ over τ, we obtain

$$\left.\begin{aligned} &\langle \varphi \rangle_t = a_0 + \sum \langle \varphi_n(t) \rangle_t, \\ &\langle \varphi_n \rangle_t = \frac{1}{\tau} \int_0^\tau \varphi_n(t+s) ds. \end{aligned}\right\} \qquad \text{(I-1.4)}$$

Here we easily see that

(1) those terms where $T/n \ll \tau$ can be neglected, *viz.*,

$$\langle \varphi_n \rangle_t \doteqdot 0, \qquad (1)$$

(2) those terms where $T/n \gg \tau$ are approximately independent of τ, and we see that

$$\langle \varphi_n \rangle_t \doteqdot \varphi_n(t), \qquad (2)$$

(3) those terms where T/n is comparable to τ are not independent of τ nor small. (3)

The processes corresponding to the terms (1) may be called "microscopic" and those corresponding to (2) "macroscopic." When a system concerned is nearly in thermal equilibrium, the φ_n are classified easily into (1) and (2), as Kirkwood and others assume, and moreover the number of the terms assigned to (2) is very small. However, when the state of our system deviates considerably from thermal equilibrium, it is surmised that there appear many terms belonging not only to (2) but also to (3). The existence of the terms (3) makes the second method of coarse-graining a failure.§

We may hope that we can avoid the difficulty found in making time averages by treating our system in the space-like sense (the third method of coarse-graining). In general, however, the time-dependent changes of the state of a system are accompanied by space-dependent changes. When a time-dependent change is large, the accompanying space-dependent change is presumed to

[4] N. Wiener, *The Extrapolation, Interpolation, and Smoothing of Stationary Time Series* (Technology Press of M.I.T., Cambridge, Massachusetts, and John Wiley and Sons, Inc., New York, 1950).

§ In the theory of Born and Green (see reference 1, pp. 214–225), there is found a phase average but no time average which latter, according to Kirkwood (see reference 2), is essential for our observation. They seem, however, to presume the possibility of the coincidence between the two averages, as the density of the number of molecules is not too small.

be large also.‖ Thus by the space-dependent nonuniformity also we are prevented from giving precise definitions of gross variables and from making fine observations on them. This example is found in the following situation:

According to M. S. Green,[3] the gross variable which represents the density of particles is given by

$$\left.\begin{aligned}\rho(x)&=a^{-3}\sum_{i=1}^{N}\sum_{\mathbf{k}}\exp i\mathbf{k}\cdot(\mathbf{x}_i-\mathbf{x}),\\ \mathbf{k}&\equiv(2\pi l/a,2\pi m/a,2\pi n/a),\\ &\qquad |l|,|m|,|n|\leq M,\end{aligned}\right\}\quad\text{(I-1.5)}$$

where we have reduced the fineness of the description by eliminating those Fourier coefficients for which l, m, n are greater than M where M is some large integer. This has the effect of ignoring variations in the local density which take place over distances smaller than a/M, a being the side of the cube in which our fluid is assumed to be contained. If we choose M so that a/M is smaller beyond the limit of macroscopic measurability, but still large enough so that a cube of volume $(a/M)^3$ contains on the average a large number of molecules, the set of gross variables will contain all information required, but no more than is required, for a complete macroscopic description of the local density. In the same way we can define the momentum density

$$\mathbf{p}(x)=a^{-3}\sum\sum\mathbf{p}_i\exp i\mathbf{k}\cdot(\mathbf{x}_i-\mathbf{x})\qquad\text{(I-1.6)}$$

and the energy density

$$E(x)=a^{-3}\sum\sum(\mathbf{p}_i^2/2m+\sum_j V(\mathbf{x}_i-\mathbf{x}_j)/2)\times\exp i\mathbf{k}\cdot(\mathbf{x}_i-\mathbf{x}).\qquad\text{(I-1.7)}$$

As we can easily see in the procedures for deriving these expressions, they are the results of coarse-graining in a sense. Consequently by giving only values of the densities of mass, momentum, and energy defined above we cannot determine exactly the microscopic state of the system under consideration. When the state deviates slightly from thermal equilibrium, these representations will be sufficient to express the state even if M is considerably small. When the state deviates considerably from thermal equilibrium and the nonuniformity is large, however, it is expected that M must be sufficiently large to make our descriptions of ρ, $\mathbf{p}$, and E sufficiently precise. If it is difficult to make M larger, for any reason, an alternative way to make our theory precise is to take into consideration other independent variables¶ (functions of phase) in addition to the three. The present author made this attempt in his previous paper.[5] The more considerably the state deviates from thermal equilibrium, either the more precise the expression of those three variables we must make or the larger the number of the independent gross variables. It is not easy to predict the necessary and sufficient preciseness of expression of these three variables nor what are important and necessary among possible gross variables. Furthermore, we cannot deal with too many variables even if they are expressed roughly nor can we deal too precisely with the variables even if their number is small. Thus, in this situation our sets of gross variables are not complete. Consequently there is an important elimination of the preciseness in our theories and the deviation of actual future values of the gross variables from their future values expected by our macroscopic law, cannot be neglected even in the macroscopic sense. This is the second of the difficulties which we meet generally in treating states deviating considerably from thermal equilibrium. That is to say, a complete set of gross variables is not readily defined nor easily observed with respect to a system in states deviating considerably from thermal equilibrium.

In consequence of these difficulties, there is the danger which cannot be neglected that there are deviations of the actual future values of the gross variables from their expected future values. The reasons for this danger are summarized as follows: (1) The initial conditions are incomplete as given in terms of the results of observing incompletely an incomplete set of gross variables. (2) Given in terms of the incomplete set of gross variables, the law connecting the initial state and the final state is naturally incomplete. In the following section, let us consider another method of coarse-graining available for the case which is difficult to approach by usual methods.

I-2. A Method of Coarse-Graining

Let D_0 denote the region of the phase space which represents an initial state in the macroscopic sense. In the concrete, we define D_0 as follows: When the system concerned starts from a state represented by any microscopic point in D_0, the given set of macroscopic initial conditions is satisfied by the average of the behavior during the period between the initial time and the time $t=\tau$. As stated in Sec. I-1, this definition is not exact where the states concerned deviate considerably from thermal equilibrium and the random processes are not stationary, according to (1) our failure in paying ready attention to all the necessary gross variables and (2) the errors of macroscopic observation of the same kind as those which happen to occur even in the

‖ For example, when a fluid contained in a vessel changes its state as time goes on, no space-dependent uniformity can be expected, at least not near the wall of the vessel. According to our usual experiences, the larger the time-dependent change, the more remarkable the space-dependent change. It may be difficult to mention any one example which contradicts this statement.

¶ If the molecules are assumed to be mass points and M is infinitely large, there is no other gross variable independent of ρ, $\mathbf{p}$, and E. When M is finite, however, there are many other variables independent of each other.

[5] T. Koga, J. Chem. Phys. **22**, 1633 (1954).

macroscopic observation of systems in thermal equilibrium, and also (3) the dependence of our observations on τ. We assume that we select the values of τ so that the errors (3) are of a magnitude comparable to those of the errors (1) and (2).

Let a point d_{01} in D_0 be the initial starting point of the first trajectory and d_1 be the point which represents the microscopic state at the time t. The second trajectory starts from d_{02} in D_0 and reaches d_2 at t, and so on. Thus we get two sets of infinite series:

$$\begin{aligned} &d_{01}d_{02}d_{03}d_{04}\cdots, \\ &d_1d_2d_3d_4\cdots. \end{aligned} \tag{I-2.1}$$

The d_0's are always in D_0 and distributed uniformly, because d_0 is chosen at random in D_0 at the start of each observation represented by a trajectory in the phase space. Then we define $f_0^{(N)}$ and $f^{(N)}$ as follows: $f_0^{(N)}$ is a function of d_0 and is the density of number of trajectories representing experiments of different times which start at d_0. As explained above, $f_0^{(N)}$ is constant throughout D_0. In regard to**

$$f^{(N)}=f^{(N)}(\mathbf{r}_1,\mathbf{p}_1,\mathbf{r}_2,\mathbf{p}_2,\cdots,\mathbf{r}_N,\mathbf{p}_N,d_0,t), \tag{I-2.2}$$

$f^{(N)}\prod_{i=1}^{N}\delta\mathbf{r}_i\delta\mathbf{p}_i\delta D_0$ is the number of trajectories representing the behavior of the system, the microscopic initial states of which are found in δD_0 surrounding d_0 and simultaneously the states at t are found in the region of the phase space situated between

$(\mathbf{r}_1,\mathbf{p}_1)$ and $(\mathbf{r}_1+\delta\mathbf{r}_1,\ \mathbf{p}_1+\delta\mathbf{p}_1)$ of the first molecule,††
$(\mathbf{r}_2,\mathbf{p}_2)$ and $(\mathbf{r}_2+\delta\mathbf{r}_2,\ \mathbf{p}_2+\delta\mathbf{p}_2)$ of the second molecule,
. . . . . .
$(\mathbf{r}_N,\mathbf{p}_N)$ and $(\mathbf{r}_N+\delta\mathbf{r}_N,\ \mathbf{p}_N+\delta\mathbf{p}_N)$ of the nth molecule.

Consequently we see that

$$\int\int f^{(N)}\prod_{i=1}^{N}d\mathbf{r}_id\mathbf{p}_i=f_0^{(N)}. \tag{I-2.3}$$

By the relation

$$\int\int f^{(N)}\prod_{j=1}^{N}d\mathbf{r}_jd\mathbf{p}_j=f_i(\mathbf{r},\mathbf{p},d_0,t),\quad j\neq i \tag{I-2.4}$$

f_i is defined. Here $f_i\delta D_0\delta\mathbf{r}\delta\mathbf{p}$ means the number of trajectories where the initial microscopic states are found in δD_0 and simultaneously the ith molecule is found at the state between $(\mathbf{r},\mathbf{p})$ and $(\mathbf{r}+\delta\mathbf{r},\ \mathbf{p}+\delta\mathbf{p})$ at the time t. Consequently

$$\sum_{i=1}^{N}f_i\delta D_0\delta\mathbf{r}\delta\mathbf{p} \tag{I-2.5}$$

represents the sum of the number of all molecules which are found at t between $(\mathbf{r},\mathbf{p})$ and $(\mathbf{r}+\delta\mathbf{r},\ \mathbf{p}+\delta\mathbf{p})$ in regard to all the trajectories which begin in δD_0. Defined by

$$\sum_{i=1}^{N}f_i/f_0^{(N)}=f(\mathbf{r},\mathbf{p},d_0,t), \tag{I-2.6}$$

$f\delta D_0\delta\mathbf{r}\delta\mathbf{p}$ is the number of molecules between $(\mathbf{r},\mathbf{p})$ and $(\mathbf{r}+\delta\mathbf{r},\ \mathbf{p}+\delta\mathbf{p})$ at t for each trajectory which starts from D_0. Further,

$$\int_{D_0}ff_0^{(N)}dD_0\Big/\int_{D_0}f_0^{(N)}dD_0=\langle f(\mathbf{r},\mathbf{p},D_0,t)\rangle_D \tag{I-2.7}$$

denotes the mean of f over D_0.

As stated in the previous section, the law of behavior of the system concerned is described in terms of $\langle f\rangle_D$, and the observation of each trajectory is represented by $\langle f\rangle_t$ defined by

$$\langle f\rangle_t=\frac{1}{\tau}\int_0^{\tau}f(\mathbf{r},\mathbf{p},d_0,t+s)ds \tag{I-2.8}$$

which is not strictly independent of τ as stated in Sec. I-1. Kirkwood[2] gives his macroscopic distribution function $\bar{f}$ as follows:

$$\bar{f}(\mathbf{r},\mathbf{p},t)=\frac{1}{\tau}\int_0^{\tau}\frac{Nf_i(\mathbf{r},\mathbf{p},t+s)}{f_0^{(N)}}ds \tag{I-2.9}$$

by means of our notations. This is considered to be independent of the individuality of molecule i and perhaps has the same meaning as that defined in (I-2.8). Anyway, defined by (I-2.8), $\langle f\rangle_t$ is a function of d_0. In regard to any trajectory representing the behavior of the system observed on one occasion we cannot identify d_0 microscopically. We know only that d_0 is in D_0.

We define φ_t and φ_D by

$$\begin{aligned} f&=\langle f(d_0,t)\rangle_t+\varphi_t(d_0,t) \\ &=\langle f(D_0,t)\rangle_D+\varphi_D(d_0,D_0,t). \end{aligned} \tag{I-2.10}$$

According to (I-2.7) and (I-2.8), we see

$$\int_0^{\tau}\varphi_t(t+s)ds=0,\quad \int_{D_0}\varphi_DdD_0=0. \tag{I-2.11}$$

Here φ_t is a function of d_0, and φ_D is a function of d_0 and D_0. Because of the fact that D_0 is decided by an incomplete set of macroscopic conditions, so far as their microscopic random processes are concerned, any two trajectories starting from two parts, δ_1D_0 and δ_2D_0, in D_0, respectively, are not supposed to be correlated considerably with each other. Consequently, if we let φ_D' and φ_D'' denote, respectively,

$$\begin{aligned} \varphi_D'&\equiv\varphi_D(\mathbf{r},\mathbf{p}',d_0,D_0,t), \\ \varphi_D''&\equiv\varphi_D(\mathbf{r},\mathbf{p}'',d_0,D_0,t), \end{aligned}$$

the relation between

$$\varphi_D'(d_{01})\varphi_D''(d_{01})\quad\text{and}\quad\varphi_D'(d_{02})\varphi_D''(d_{02})$$

** $\mathbf{r}$ denotes the position of a particle and $\mathbf{p}$ its momentum.
†† $+\delta\mathbf{r}$ is a vector. On the other hand, $\delta\mathbf{r}$ denotes $\delta r_x\delta r_y\delta r_z$.

is supposed to be random. This means that

$$\frac{1}{D_0}\int_{D_0}\varphi_D'\varphi_D''dD_0\equiv\langle\varphi_D'\varphi_D''\rangle_D\ll\langle f'\rangle_D\langle f''\rangle_D \quad \text{(I-2.12)}$$

when $\mathbf{p}'\neq\mathbf{p}''$, even though $\langle\varphi_D'\varphi_D''\rangle_D$ does not vanish completely. Further it may be presumed that

$$\langle\langle f\rangle_t\rangle_D\doteqdot\langle\langle f\rangle_D\rangle_t\doteqdot\langle f\rangle_D. \quad \text{(I-2.13)}$$

When the gas concerned is composed of several kinds of molecules and 1st, 2nd, $\cdots$, N_1th molecules are of the first classification, (N_1+1)th, (N_1+2)th, $\cdots$, N_2th molecules of the second classification, $\cdots$, $(N_{\nu-1}+1)$th, $(N_{\nu-1}+2)$th, $\cdots$, N_νth molecules of the νth classification $(N_\nu=N)$, then we define $f_{(1)}$, $f_{(2)}$, $\cdots$, $f_{(\nu)}$ as follows:

$$f_{(g)}=\sum_{N_{g-1}+1}^{N_g} f_i/\jmath_{(0)}{}^{(N)}, \quad g=1,2,\cdots,\nu, \quad N_0=0. \quad \text{(a)}$$

Consequently

$$f=\sum_{g=1}^{\nu} f_{(g)}. \quad \text{(b)}$$

We can define

$$\langle f_{(g)}\rangle_t, \quad \langle f_{(g)}\rangle_D \quad \text{(c)}$$

in the same way as with $\langle f\rangle_t$ and $\langle f\rangle_D$.

By making use of $\langle f\rangle_D$ instead of $\langle f\rangle_t$ and f, we can describe laws and define observations. In this case the limits of the validity of the theory are considerably more extended in comparison with the usual theories. However the interpretation of both the laws and the observations is modified; a law thus described predicts not the result of observation made on an individual occasion on the system concerned but predicts the result obtained by averaging over a series of observations made repeatedly upon different occasions on the same system under manifestly similar initial conditions. The details of discussion are given in Sec. II-2 where a gas is treated concretely from our new point of view.

PART II. AN EXTENDED INTERPRETATION OF B-M EQUATION‡‡

II-1. Derivation of B-M Equation by the New Method of Coarse-Graining

Let us find the law to which $\langle f\rangle_D$ is subject under the assumption that our system is a gas. It is well established that $f^{(N)}$ satisfies the following (Liouville's) equation:

$$\frac{\partial f^{(N)}}{\partial t}+\sum_{l=1}^{N}\left[\frac{\mathbf{p}_l}{m_l}\cdot\nabla_{rl}f^{(N)}+(\mathbf{X}_l+\mathbf{F}_l)\cdot\nabla_{pl}f^{(N)}\right]=0 \quad \text{(II-1.1)}$$

where $\mathbf{X}$ is the external force and $\mathbf{F}$ is the intermolecular force. From this equation we will derive the equation to which the behavior of $\langle f\rangle_D$ is subject. In the beginning, let us assume that the density of the gas under consideration is sufficiently small and the collisions are binary.

First, as the medial process, we will see the equation which states the law of variations of the function f. This equation has already been obtained by Born and Green[1] based upon Eq. (II-1.1)§§:

$$\frac{\partial f}{\partial t}+\frac{\mathbf{p}}{m}\cdot\nabla_r f+\mathbf{X}\cdot\nabla_p f$$

$$=\int\int\int[f(\mathbf{p}^*)f(\mathbf{p}^{*\prime})-f(\mathbf{p})f(\mathbf{p}')]ud\mathbf{p}'bdbd\epsilon,$$

$$u=|\mathbf{p}-\mathbf{p}'|/m \quad \text{(II-1.2)}$$

where all the molecules are of the same type and of the mass m. Here the explanation of notations, b, ϵ, $\mathbf{p}'$, etc., is omitted as they are well known to us.||| Equation (II-1.2) is easily averaged over D_0 giving the result:

$$\frac{\partial\langle f\rangle_D}{\partial t}+\frac{\mathbf{p}}{m}\cdot\nabla_r\langle f\rangle_D+\mathbf{X}\cdot\nabla_p\langle f\rangle_D$$

$$=\int\int\int(\langle f^*\rangle_D\langle f^{*\prime}\rangle_D-\langle f\rangle_D\langle f'\rangle_D)ud\mathbf{p}'bdbd\epsilon. \quad \text{(II-1.3)}$$

This result is based upon the fact that

$$\langle\varphi_D\varphi_D'\rangle_D\ll\langle\langle f\rangle_D\langle f'\rangle_D\rangle_D=\langle f\rangle_D\langle f'\rangle_D$$

as was considered at the end of Sec. I-2, (I-2.12). Our result thus obtained is formally the same as B-M equation.

In considering gases composed of a variety of molecules we get¶¶

$$\frac{\partial f_{(g)}}{\partial t}+\frac{\mathbf{p}}{m_{(g)}}\cdot\nabla_r f_{(g)}+\mathbf{X}\cdot\nabla_p f_{(g)}$$

$$=\int\int\int(f_{(g)}{}^*f^{*\prime}-f_{(g)}f')ud\mathbf{p}'bdbd\epsilon, \quad g=1,\cdots,\nu,$$

which is averaged over D_0 resulting in

$$\frac{\partial\langle f_{(g)}\rangle_D}{\partial t}+\frac{\mathbf{p}}{m_{(g)}}\cdot\nabla_r\langle f_{(g)}\rangle_D+\mathbf{X}\cdot\nabla_p\langle f_{(g)}\rangle_D$$

$$=\int\int\int(\langle f_{(g)}{}^*\rangle_D\langle f^{*\prime}\rangle_D-\langle f_{(g)}\rangle_D\langle f'\rangle_D)ud\mathbf{p}'bdbd\epsilon.$$

‡‡ Hereafter B-M equation is the abbreviation of the Boltzmann-Maxwell equation.

§§ In deriving (II-1.2) from (II-1.1), it is not necessary to make any other assumption than that the gas is sufficiently rarefied and the collisions are binary.

||| For instance, see S. Chapman and T. G. Cowling, *The Mathematical Theory of Non-Uniform Gases* (Cambridge University Press, London, 1936), p. 60.

¶¶ See definitions (a), (b), and (c) in Sec. (I-2).

II-2. An Extended Interpretation

We have been acquainted with two representative methods of coarse-graining of distribution function, the one by Born and Green[1] and the other by Kirkwood.[2] According to Born and Green, the final distribution function of one molecule, f, is given by

$$\left.\begin{aligned} &f=Nf_i(\mathbf{r},\mathbf{p},t)=\sum^N f_i \\ &\text{where} \\ &f_i=\int\int f^{(N)}\prod_{j=1}^{N} d\mathbf{r}_j d\mathbf{p}_j, \quad j\neq i. \end{aligned}\right\} \tag{II-2.1}$$

On the other hand, according to Kirkwood, the result is given in terms of

$$\langle f\rangle_t=\frac{1}{\tau}\int_0^\tau f(\mathbf{r},\mathbf{p},t+s)ds. \tag{II-2.2}$$

In this article we have proposed a further method of coarse-graining, giving for the distribution function

$$\langle f\rangle_D=\int_{D_0} ff^{(N)}dD_0\Big/\int_{D_0} f^{(N)}dD_0. \tag{II-2.3}$$

These three functions are mutually different in meaning. Nevertheless each of them satisfies the same equation, B-M equation. In other words, B-M equation is interpreted in three different ways. However when (1) the density of the gas concerned is moderate and not too small and (2) the states under consideration deviate slightly from thermal equilibrium, it is supposed that the disagreement among the three interpretations does not result in any great difference. That is to say (1) there is the approximate identification of time average with phase average and also (2) we can easily define and observe a complete set of gross variables with sufficient accuracy. Consequently f, $\langle f\rangle_t$, and $\langle f\rangle_D$ can easily coincide with each other.

As the density of the gas becomes more considerably rarefied,*** however, the differences between f and $\langle f\rangle_t$ begin to appear. In this case both time and space-like changes of f may be strong and frequent so that one cannot observe f in any macroscopic sense. On the other hand, even in this case, $\langle f\rangle_t$ may be sufficiently stable and may remain within the limit of our macroscopic measurability. In this situation we cannot yet distinguish the difference between $\langle f\rangle_t$ and $\langle f\rangle_D$. As the state becomes deviated considerably from thermal equilibrium and the random processes become nonstationary, however, there appears the distinction between $\langle f\rangle_t$ and $\langle f\rangle_D$, and the former, $\langle f\rangle_t$, loses its preciseness of meaning (see Sec. I-1).

*** Here the deviation of the state from thermal equilibrium is assumed not too large.

In a case where the density of the gas concerned is very small and the state deviates considerably from thermal equilibrium so that the random processes are not considered stationary, the result of each individual observation does not coincide with the other observations nor with the result directly predicted by our law (B-M equation). According to our new interpretation, however, B-M equation is available for a law even in this case. That is to say, we interpret B-M equation to predict not the result of observing the behavior of a system represented by a trajectory in the phase space but the result of averaging a series of observations made repeatedly at different times on the same system (represented by many trajectories) under the macroscopic initial conditions given in terms of the incompletely observed values of an incomplete set of gross variables. Thus the validity limit of B-M equation is extended by modifying its interpretation.

SUMMARY AND CONCLUSION

When the states of system under consideration deviate considerably from thermal equilibrium, it is not plausible to assume that the microscopic processes are stationary. "A complete set of grossly observable variables"[3] is not easily defined nor readily observed as to a system in such a state.

Since our macroscopic states are determined by the incompletely observed values of variables of an incomplete set, the behaviors of similar systems which are initially in a common macroscopic state are after a time even macroscopically distinguishable from each other.

As to a gas, we define $\langle f\rangle_D$ for the distribution function in terms of which the law is given. This function is the result of averaging the fine-grained distribution function over the trajectories representing a series of observations made repeatedly on the same system at different times under a common and incomplete set of macroscopic initial conditions.

Our law thus obtained is an integro-differential equation and in form is the same as the Boltzmann-Maxwell equation. The interpretation, however, is not the usual one, and consequently the physical meaning differs. By this law we can predict the mean of a series of observations made repeatedly on the same system at different times under a manifestly same set of initial conditions.

The differences between our interpretation and the usual one grow less as the deviation of the state concerned from thermal equilibrium decreases.

In the course of preparing this paper, the author was greatly indebted to Mrs. M. L. Mayland, an American now staying in Japan, for help in overcoming linguistic difficulties. He wishes to thank her cordially.

APPENDIX

Even if the random processes are not stationary, f defined by Born and Green satisfies B-M equation under

the condition of binary collisions only. Under the same condition $\langle f \rangle_D$ also satisfies B-M equation. According to the definitions, however, f and $\langle f \rangle_D$ are different from each other; f fluctuates deviating considerably from $\langle f \rangle_D$. This fact suggests to us that even though we have obtained a function by solving B-M equation, the function does not always represent what we intend to learn. That is to say, B-M equation by itself does not completely determine the physical meaning of the functions obtained by solving the equation. We need some other assumptions or principles to give a proper physical meaning to the functions.[5]

THE JOURNAL OF CHEMICAL PHYSICS VOLUME 23, NUMBER 12 DECEMBER, 1955

Bonding in the Zinc Family Metals

W. E. WALLACE
Department of Chemistry, University of Pittsburgh, Pittsburgh, Pennsylvania
(Received March 7, 1955)

Attention is directed to the very large departures of the structures of the zinc family (IIb) metals from those produced by the close packing of spheres. This seems to indicate that cohesion in these metals differs considerably from the normal nondirectional metallic bonding. It is proposed that there is a system of covalent bonds in the basal plane resulting from bonding orbitals which are hybrids of one of the d and two of the p atomic orbitals. These absorb some of the s electrons and leave only 1.33 electrons/atom in the s band. Support for the proposed bonding scheme is provided by showing that with it one can account for many otherwise puzzling properties of the IIb metals and their alloys. The properties which are discussed in terms of the proposed scheme are (1) the abnormally large axial ratios in zinc and cadmium, (2) the effect of temperature on the axial ratios of these metals and the alloys of magnesium and cadmium, (3) the effect of alloying on the axial ratio, (4) the dependence of the axial ratio on the degree of order in $MgCd_3$, (5) the great abundance of Schottky defects in certain magnesium-cadmium alloys, (6) the asymmetry of the heats of alloying of magnesium and cadmium, (7) the structure of solid mercury, (8) electrical conductivities of the solids, (9) the positive Hall coefficient for zinc and cadmium, (10) the poor solvent power of these metals as solids, and (11) certain unusual features of the electrical conductivities of the liquid metals and the dilute amalgams.

I. INTRODUCTION

IN a metallic element which crystallizes in the face centered cubic structure each atom is equidistantly surrounded by its twelve neighbors in the first coordination shell. This is also true of the metals crystallizing in the close-packed hexagonal structure if the axial ratio c/a exactly equals $(8/3)^{\frac{1}{2}}$, or 1.633. When the axial ratio differs from 1.633, the so-called ideal value, the twelve atoms in the first coordination shell divide into two groups, six in the basal plane at a distance r_1 and the other six at a distance r_2.

From the compilation by Barrett[1] it is found that twenty-six of the solid elements, all of which are metals, occur in the *Cph* structure. For most of these c/a is smaller than the ideal value, ranging from 1.565 for lithium to 1.624 for magnesium. In only three cases does the axial ratio exceed 1.633; for calcium (1.636), and for the IIb metals zinc (1.856) and cadmium (1.886). From this it can be seen that the differences between r_1 and r_2 are considerably greater for zinc and cadmium than for any of the other metals. The uniqueness of these two elements is further emphasized by comparison with the IIa metals calcium and strontium.[2] Both metals occur in the cubic form where r_2/r_1 is of course exactly unity. Calcium occurs also in the hexagonal form with r_2/r_1 exceeding unity by only 0.1%. For beryllium and magnesium, the remaining group II metals, r_2/r_1 is less than unity by 2.6 and 0.4%, respectively. In contrast with these modest differences, for zinc and cadmium r_2 and r_1 differ by about 10%. Mercury, the other IIb metal, crystallizes in the rhombohedral system with a structure which may be regarded as a distortion of the cubic scheme for the close-packing of spheres. For mercury $r_2/r_1=0.855$. Thus one sees that the nonequivalence of the nearest neighbor distances in the IIb metals exceeds by roughly an order of magnitude that of the rest of the Group II elements.

This odd characteristic of the IIb metals has been known for many years. Studies have been made, particularly for zinc and cadmium, of the effects of alloying on their abnormally high axial ratios, in the course of which definite systematic trends have been discerned. For example, it has been found that c/a decreases as the valence electron-to-atom ratio (hereafter in this paper called Z) is reduced. Jones[3] and more recently Goodenough[4] have interpreted these findings in terms of interactions between the Fermi surface of the electron gas in the metal and certain of the Brillouin zone faces. These papers make it quite clear why, if

[1] C. S. Barrett, *Structure of Metals* (McGraw-Hill Book Company, Inc., New York, 1952), p. 646.
[2] Barium does not occur in a close-packed structure.
[3] H. Jones, Proc. Roy. Soc. (London) **A147**, 396 (1934).
[4] J. B. Goodenough, Phys. Rev. **89**, 282 (1953).

one has an axial ratio considerably in excess of the ideal value, reducing Z (by introducing some monovalent metal into the zinc or cadmium lattice) will diminish c/a. However, they offer no explanation for the initial occurrence of the abnormal ratios in the pure metals. Indeed there has as yet been no satisfactory explanation for the abnormal packing in cadmium and zinc.

In this connection Nabarro and Varley published a few years ago a paper dealing with distortions from the *Cph* structure.[5] They considered a model in which the energy of a solid is represented as the sum of two terms. The first term is the sum of the bond energies of all the nearest neighbor pairs. This energy of course depends on the bond length and is assumed to vary with the length of the bond in much the same way as with a diatomic molecule. The second term depends solely on atomic volume and is identified with the Fermi energy of the electron gas when the model is applied to metals. The volume dependent energy term decreases monotonously to zero with increasing atomic volume. For certain forms of the bond potential energy function the stable state of a system conforming to this model is the distorted *Cph* structure with $r_1 \neq r_2$.

It is clear that the Nabarro-Varley model corresponds only approximately with the situation in a real metal since (1) the Fermi energy depends on the repeat distance in three dimensions and is not uniquely determined by the atomic volume, (2) non-nearest neighbor contributions are neglected and (3) the tacit assumption is made that the bond length uniquely determines the interionic potential energy whereas in the real metal the energy depends as well on the location of the other ions which are first neighbors to the paired ions. As the difference in energies of the distorted and undistorted structures is undoubtedly quite small compared to the total energy, the effect of the approximations cited would appear to be sufficiently large to cast considerable doubt on the validity of conclusions based on the Nabarro-Varley model about the packing in real metals.[6]

The only other explanations for the abnormal packing in the zinc group metals are a few vague and fleeting references in the literature to covalency in these metals.[7] The experimental evidence cited shows clearly that the bonding in the IIb metals is atypical; it would appear to differ in a fundamental way from the bonding in the other metals of Group II. One is naturally interested in revealing and studying the special factors at work here, partly to reach a better understanding of the IIb metals but also because of the possibility that in so doing, principles may emerge of general utility in the electron theory of metals.

The remainder of this paper is devoted to a detailed presentation of a suggestion about the bonding in the IIb metals. Support for the proposed scheme of bonding will be provided by showing that with it one can account for a wide variety of properties of the IIb metals and their alloys, including the abnormal axial ratios in cadmium and zinc and some features of the structure of solid mercury. The scheme contains what is perhaps a novel idea, namely, that the cohesion in the zinc group metals is in part due to a system of covalent bonds, such as is found for example in diamond, and is in part due to the ordinary metallic binding, which is exemplified by the cohesive forces in the alkali metals. Unfortunately this scheme has not yet been developed from calculation based on quantum theory. It would be overly optomistic to hope that if and when such calculations are made, the ideas presented here will be corroborated in all respects. It is felt, however, that the two principal ideas introduced in this paper, that (1) some of the *d* electrons are involved in the bonding and (2) Z is closer to 1.33 than to 2, will be supported by proper theoretical considerations.

II. ROLE OF THE *d*-ELECTRONS

In the literature and in conversation one frequently encounters the idea that cohesion in the IIb metals involves only the *s* electrons, implying that interactions involving the core electrons make no significant contribution to the cohesive energy of the system. The reasoning appears to be somewhat as follows: In the transition metals the *d*-orbitals of adjacent atoms overlap considerably and the atomic *d*-orbitals are broadened into a band. This band is only partially filled with electrons and their energy on the average is less than in the free atom. The reduction in energy in the solid represents a substantial part of the cohesive energy of the transition metals.[8] Passing on to the copper group one finds that the *d* band is full. Consequently the *d* electrons do not contribute to cohesion, at least not in the same sense as in the transition metals. It is possible that they make an appreciable contribution to cohesion in the form of a large van der Waals type interaction between the ion cores. In the IIb metals, so continues this line of reasoning, the ion cores are widely separated so that neither exchange nor van der Waals interactions occur to any appreciable extent. There is no *d* character to the delocalized orbitals because the *d* states are too low in energy compared with the *s* band to participate in the bonding, a point of view which has received support from the x-ray emission spectra of zinc and the brasses observed by

[5] F. R. N. Nabarro and J. H. O. Varley, Proc. Cambridge Phil. Soc. 48, 316 (1952).

[6] This is not true in principle (though it may be in practice) for the scheme of bonding advanced in this paper. The several approximations involved in the Nabarro-Varley approach are avoided and the solid is discussed in such a way that an exact quantum-mechanical treatment of it as a many body problem could in principle be carried out. This does not appear to be possible using the Nabarro-Varley model.

[7] L. Pauling, *The Nature of the Chemical Bond* (Cornell University Press, Ithaca, New York, 1948), p. 412.

[8] This is the case with elements whose *d* shells are less than half full.

Bearden, Shaw, and co-workers.[9–11] Their analysis of the $K\beta$ spectra indicates that the d electrons lie 7–8 ev below those states in the conduction band corresponding to the peak intensity of the $K\beta_2$ emission line. Furthermore, on alloying copper with zinc the wavelength and width of the $K\beta_5$ line (electron transfer from the $3d$ band to a vacancy in the K shell) is observed[11] to be independent of composition, apparently indicating that the $3d$ electrons are *not* involved in the bonding. We shall return to these points below.

Resuming now discussion of the anomalous axial ratios in zinc and cadmium, Goodenough[4] has described how for certain values of Z a metal can lower its Fermi energy, and hence its free energy, by distortion from the ideal axial ratio. Is this the cause of the zinc-cadmium anomalies? If so, and if this is the sole cause, one must explain why similar distortions do not occur in magnesium and calcium. One way, which runs contrary to conventional thought, to explain these differences is to postulate that Z is not the same for the two pairs of metals. Another way, which does not necessitate differences in Z, is to postulate that for zinc and cadmium the E *vs* k (energy *vs* wave number) relationship is quite different in a direction parallel to the hexagonal axis than along a line in the basal plane. This statement requires elaboration.

In Fig. 1 we see the first Brillouin zone for the *Cph* structure. Since the zone holds less than two electrons per atom, for Z=2 some of the states lying outside the first zone must be occupied. Imagine a *Cph* arrangement of the ion cores of a divalent metal, for example magnesium, with an ideal axial ratio. We will now supply electrons to this assemblage of ion cores gradually until Z=2. The first electrons go into the lowest lying states near the center of the zone and initially the volume of occupied states is spherical. With increasing Z the Fermi surface moves outward and as it approaches the A faces, it is distorted from spherical symmetry, bulging outward toward the zone boundaries.[4] Finally at Z=2 the Fermi surface has cut the A faces and reached a position just inside the two B faces. Let us now imagine the same process for zinc. Again the Fermi surface for very small Z is spherical. Now suppose that E increases with k more rapidly in a direction normal to the A faces than it does along the hexagonal axis. Then as Z is increased, the Fermi surface will deviate from a sphere, bulging this time not toward the A faces as with magnesium, but toward the B faces. If the E *vs* k relationships differ sufficiently, the distortion of the Fermi sphere can become so severe that with further increase in Z the first overlaps occur at the B faces. Once electrons occupy states just beyond B a stress develops, as Jones[3] first pointed out, which increases the axial ratio. In this way one can explain the unusual packing in zinc (or cadmium) but only

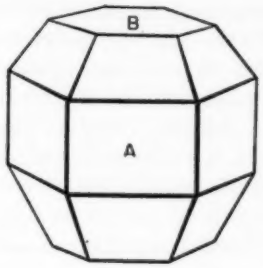

FIG. 1. First Brillouin zone for close packed hexagonal metal.

by postulating that the E *vs* k relationship varies greatly for different directions of k.[12] As the isolated zinc ion is spherically symmetrical, one expects a spherical ion in the solid if interactions involving the core electrons are negligible. The notion that E is a strong function of direction for a given value of k is not consistent with an underlying ion of spherical symmetry. Thus it appears that attempts to attribute the anomalous axial ratio in zinc and cadmium to Fermi surface-zone boundary interactions leads inevitably to the conclusion that there are interactions between the s electrons and those in the core (undoubtedly the d electrons); and furthermore since these interactions are large, they probably represent a substantial part of the cohesive energy of the IIb metals. Perhaps an elaborate quantum-mechanical treatment of these metals will reveal this type of interaction and lead naturally to an explanation of their unusual nearest neighbor relationships without need of the special postulates introduced below. At present this is only a possibility, not a certainty, which would still fail to provide explanations for (1) the peculiar dependence of the axial ratios on temperature for cadmium and certain of its alloys with magnesium or (2) the striking variation of c/a with degree of order in the $MgCd_3$ superlattice. Considering these additional crystallographic features, which are discussed in detail in a later section, one feels justified in abandoning this approach, at least until it has received the support of rigorous calculations.

Another line of reasoning is sometimes employed. The metals are pictured as being composed of ions in the shape of prolate ellipsoids with major axes parallel to the hexagonal axis. The ions are supposedly drawn together by electrostatic interaction with the conduction electrons until they come into contact. The large axial ratio is then a consequence of the nonspherical shape of the ions. There are at least three objections to this reasoning. First, as indicated above the isolated ion is spherical and one must postulate an interaction of the ion with either its neighboring ions in the solid or with the conduction electrons to give it a different shape in the crystal. This again involves the ion core electrons in the bonding. Second, in some alloys, for example the

[9] J. A. Bearden and C. H. Shaw, Phys. Rev. **48**, 18 (1935).
[10] W. W. Beeman and H. Friedman, Phys. Rev. **56**, 392 (1939).
[11] J. A. Bearden and H. Friedman, Phys. Rev. **58**, 387 (1940).

[12] The variation must be large since some of the states toward the A faces must, following this reasoning, have their energies altered by an amount at least as great as the energy discontinuity at B.

ϵ phases of the Cu–Zn or the Ag–Cd systems, $c/a < 1.633$. Thus it is necessary to suppose that in a single binary alloy system the ion behaves at some compositions like a prolate spheroid (in the terminal solid solutions) and at others like an oblate spheroid. Third, and perhaps most important, a variety of evidence[13] suggests that the IIb metals are what Hume-Rothery has called an *open* metal, that is their interatomic distances are not determined by contact between hard ion cores.

We thus see objections to simple interpretations of the anomolous packing in the IIb metals in terms of (1) Fermi surface-zone boundary interactions or (2) nonspherical ions. It is entirely possible that the ions are nonspherical, as some experimental evidence suggests,[14–16] and it is undoubtedly true that there are important interactions between the Fermi surface and the boundaries of the zone (vide infra) but these are, as it appears at present, the result of more fundamental features of the bonding in these metals.

If one asks what is the essential difference between the calcium and zinc atoms, one immediately notes that zinc has *d* electrons and *d*-orbitals whereas calcium does not. It seems logical, therefore, to seek for the difference between these two solids in terms of the *d* electrons. In the well-known octahedral complexes of the transitional elements there are covalent bonds formed by hybridization of the *d*-, *s*-, and *p*-orbitals.[17] Hybrids employing the *d*-orbitals are also involved in the square co-planar complexes,[15] e.g., in $Ni(CN)_4^-$. As pointed out above the r_1 distances in zinc and cadmium are quite small in comparison with the r_2 distances. This could result from a system of covalent bonds operating n the basal plane, supplying extra cohesion in the plane over and above that which comes from the nondirectional normal metallic bonding. It appeared from the outset that such a system of covalent bonds might result from an appropriate hybridization of the *d*-orbitals with the *s*- and/or *p*-orbitals.

The procedure suggested by Kimball[18] was used to see if it is possible to obtain a set of mutually orthogonal wave functions by hybridization of the nine $3d$-, $4s$-, and $4p$-orbitals from which six equivalent co-planar bonds can be formed. Analysis showed that this is not possible but in Kimball's paper it is pointed out that three equivalent co-planar bonds at angles of 120° can be formed using wave functions which are hybrids of one of the *d*-orbitals and two of the *p*-orbitals. The three orthonormal wave functions are

$$\psi_1 = -\frac{1}{\sqrt{3}}d_z + \frac{2}{\sqrt{6}}P_x,$$

$$\psi_2 = -\frac{1}{\sqrt{3}}d_z - \frac{1}{\sqrt{6}}P_x + \frac{1}{\sqrt{2}}P_y,$$

$$\psi_3 = -\frac{1}{\sqrt{3}}d_z - \frac{1}{\sqrt{6}}P_x - \frac{1}{\sqrt{2}}P_y.$$

The existence of these functions permits the formation of a system of covalent bonds compatible with the *Cph* lattice. However, to use them in bond formation it is necessary to change the quantization of the zinc atom. The situation is like that for carbon in which the excitation of a $2s$ electron into a $2p$ state is pecessary before carbon can act as a quadrivalent element. In carbon hydrids of the $2s$- and $2p$-orbitals are produced each containing one electron, which can then form covalent linkages with a suitable atom. In the zinc atom to form the dp^2 hybrid wave functions for subsequent use in bond formation, it is necessary to transfer two electrons into the $4p$-orbitals, one from one of the $3d$ states and one from the $4s$-orbital. Then hybridization occurs and each hybrid state contains one electron which can form a covalent bond with an adjacent atom in the basal plane. The feasibility of this process from an energy standpoint will be considered presently.

The assumed bonding scheme for the three IIb metals is as follows:

(1) There is a system of covalent bonds between the ions in the basal plane so that an ion is singly bonded to each of three neighboring ions in the plane.

(2) These covalent bonds are formed by overlapping of wave functions which are linear combinations of one *d* and two *p* atomic orbitals.

(3) The system of covalent bonds links together a hexagonal network of ions in each of the basal planes. At the center of each hexagon there is an ion core in the state $3d^{10}$ (for zinc), which is not involved in the covalent network. The covalently bonded ion cores are of course in the state $3d^8$. The fractions of the ions in the $3d^8$ and $3d^{10}$ states are $\frac{2}{3}$ and $\frac{1}{3}$, respectively.

(4) The hexagonal network drifts with time so that the three ways of fitting it into the basal plane are used equally. Thus, averaged over a period of time all ions are equivalent.

(5) The remaining *s* electrons,[19] 1.33 per atom on the average, are completely delocalized, being contained in the *s* band with energies comparable with that of

[13] W. Hume-Rothery, *Atomic Theory for Students of Metallurgy* (Institute of Metals, London, 1948), p. 249.
[14] E. O. Wollan and C. G. Harvey, Phys. Rev. **51**, 1054 (1937).
[15] G. W. Brindley, Phil. Mag. **21**, 790 (1936); Proc. Leeds Phil. Lit. Soc. **3**, 200 (1936).
[16] G. E. M. Jauncey and W. A. Bruce, Phys. Rev. **51**, 1068 (1937) and earlier papers in the series to which reference is made in this paper.
[17] Reference 7, p. 92.
[18] G. E. Kimball, J. Chem. Phys. **8**, 188 (1940).
[19] There are two kinds of valence electrons involved in the bonding, the *s* electrons and those in the covalent network. Since it is necessary to distinguish between the two, we shall call the former "The valence electrons" and the latter "the covalent electrons" or sometimes "the electrons in the covalent network."

the electrons forming the covalent linkages. The bonding by the s electrons is of the usual Wigner-Seitz type.

One may regard the bond linking adjacent ions in two ways, only one of which has been emphasized in the preceding paragraph. They may be looked upon as ordinary covalent bonds quite similar except in strength to the hybrid covalent bonds in diamond. Alternatively, they may be considered from the collective electron point of view just as the bonding in diamond can be treated using the collective electron model. From the second viewpoint the three states corresponding to ψ_1, ψ_2, and ψ_3 for the isolated atom broaden into a band as the atoms are brought together to form the solid. The high energy s electrons spill into this lower lying band until it is filled, reducing the Fermi energy of the system by an amount sufficient to more than compensate for the energy necessary to promote the d state. There are then two bands of comparable energy just as there are two such bands (from the d states and the s states) in copper.

Let us consider briefly the energetics of the proposed bonding scheme. Call E_p the energy required to promote the necessary electrons and E_b the energy released when the covalent bonds form. For the covalent network to develop, it is of course necessary that E_b exceed E_p. Since exact values of these quantities are not known, one cannot reach a clear decision about the feasibility of the proposed scheme of bonding from energy considerations. It is, however, possible to estimate E_p and E_b. We must now demonstrate that reasonable estimates of these quantities do not exclude the possibility that $E_b > E_p$ and the energy of the solid is lower with the covalent network than without it. In making these estimates, and in fact in most of the discussion which follows, it has proved simpler to employ the covalent bond terminology and mode of thinking rather than the equivalent and equally correct collective electron description.

E_p may be estimated from the observed x-ray emission spectrum of zinc.[10,11] As was indicated earlier, the atomic $3d$ states lie 7 to 8 ev below those states in the conduction band which give rise to the peak of the $K\beta_2$ line. These latter states are probably near the Fermi limit. Broadening of the atomic $4p$ states occurs as the solid forms so that the lowest $4p$ levels undoubtedly lie well below the Fermi energy. As only the lowest $\frac{1}{3}$ of the p states are used for the promoted d electrons, the average energy would perhaps be about 5 ev. The overlapping of the s and p states is such that the transfer of electrons from a full s band to a $\frac{1}{3}$ filled p band would require little if any energy. E_p can therefore be estimated as about 5 ev.

Following Pauling we may use the maximal value of the angular part of a bond orbital as a measure of the strength of the bond which can be formed from that orbital. On this scale the tetrahedral orbitals of the carbon atom have a strength of 2. The tetrahedral bonds have a strength, as measured in energy, of about 3 ev. The prior excitation of the carbon atom necessary for the formation of the tetrahedral bonds requires[20] about 4 ev so that the actual energy released when the bonds are formed is about 4 ev per bond. Therefore one can crudely equate a bond strength of 2 with 4 ev of energy. The maximal value of the angular part of the dp^2 hybrid bonds is 2.059. We might therefore expect them to form covalent bonds with a release of about 4 ev of energy. Since $\frac{3}{2}$ bonds are formed for each promoted d electron, E_b is estimated as about 6 ev.

From crude estimates of this sort one must admit the possibility that under some circumstances, perhaps exceptionally favorable circumstances, the bond energy may slightly exceed[21] the energy of promotion. We must therefore conclude that while in principle the energetics are decisive, they are in fact inconclusive due to the very considerable latitude in the possible estimates of E_p and E_b, quantities which probably differ only slightly in the first place.

Item (4) in the proposed bonding scheme merits some comment. Although this notion will be retained, since one intuitively expects all the ions in the solid to be equivalent, it is probably not essential to the arguments which follow. At present one can regard the two kinds of zinc ions in much the same fashion as Mott's picture of the nickel ions in pure nickel.[22] He has suggested that in nickel one has a mixture of ions in states $3d^9$ and $3d^{10}$, whose positions change slowly with time. Similarly in elemental zinc we can suppose that a given zinc ion changes back and forth from the $3d^8$ to the $3d^{10}$ state as the covalent network shifts about among the three equivalent positions. These changes are slow, however, compared to the motion of the electrons so that the s electrons may be regarded as moving in a field of a mixture of ions of types $3d^8$ and $3d^{10}$, having formal charges of $+1$ and $+2$, respectively. Alternatively, one might regard the three equivalent arrangements of covalent bonds as existing in a state of resonance so that the true representation is a linear combination of wave functions characterizing the three structures. This would certainly be the stable state were it not that the disposition of two of the d electrons in each of the ion cores differs among the three resonating structures. If resonance supplied sufficient energy to promote all ions to the $3d^8$ state, this alternative point of view would be correct. It appears that one cannot decide without making elaborate quantum-mechanical calculations about the stabilizing effect of resonance when the cores resonate between the $3d^8$ and $3d^{10}$ states.

As indicated in the introductory remarks, the principal support for the proposed bonding scheme comes from its effectiveness in accounting for a variety of properties of the IIb metals and their alloys. This

[20] C. A. Coulson, *Valence* (The Clarendon Press, Oxford, England, 1952), p. 196.

[21] The properties of the metals make it appear that the covalent network contributes only slightly to cohesion.

[22] N. F. Mott, Progr. Metal Phys. **3**, 76 (1952).

is the subject of the next six sections of this paper. During much of the discussion which follows, it may seem that the bonding scheme is being used as if it were an established fact. It will be appreciated, of course, that the discussion is presented in this way only for the sake of convenience. It would be awkward and tiresome to reiterate the true status of the scheme as often as perhaps one should, and remarks in this regard will be confined to an occasional reminder. Furthermore, since the arguments to follow are entirely qualitative in nature, even after it has been demonstrated that the proposed scheme of bonding is consistent with a certain body of experimental data, obviously one cannot claim to have conclusively established its validity. It can only be claimed that the scheme has been made to seem plausible and that matters have been advanced to a stage where it is in order to attempt some kind of quantitative verification.

III. CRYSTALLOGRAPHIC EFFECTS AND THE BONDING SCHEME

A. Position of the Fermi Sphere in the First Brillouin Zone

According to the bonding scheme advanced in the preceding section the anomalous axial ratios in cadmium and zinc are due to the existence of a network of covalent bonds linking together the ions in planes perpendicular to the hexagonal axis. A consequence of this concept is that Z=1.33. Since previous analyses of the effects of zone boundaries on the Fermi energy of the IIb metals and their alloys were made using Z=2, it is necessary to re-examine the situation to see what, if any, new features enter as a result of the smaller value of Z.

For reasons which will be clarified presently we should expect the axial ratios in cadmium and zinc to be even larger than those experimentally observed if there were no planes of energy discontinuity in k-space. Then the distances of the A planes from the origin, d_A, would greatly exceed d_B, the distance from the origin to the two B faces. Let us now consider the addition of the valence electrons to a Cph arrangement of ion cores with c/a greatly in excess of the ideal value. We may assume, for example, c/a to be 2.5. As the Fermi sphere grows, it encounters first the two B faces when Z is still less than unity. With further increase in Z it is energetically favorable for the crystal to undergo a distortion without volume change so that the B faces move outward while the A faces move in toward the origin.[23] By increasing d_B it is possible to avoid for the moment populating the high-energy states outside the first zone beyond the B faces. This synchronized motion of the A and B faces keeps the increment of the Fermi energy to a minimum as Z rises toward 1.33 but it does so at the expense of the energy of the covalent network; for as d_A is diminished, r_1 increases and the covalent bonds become strained. The strain energy of the covalent network will ultimately impose a limit on the increase in d_B which is favorable from an energy standpoint, a factor which appears to be of considerable importance in the mercury structure (see below).

By analogy with Newton's third law for material objects[24] when a force is exerted by the Fermi sphere on the B faces, there is an equal and opposite force exerted by the zone boundaries on the Fermi sphere. Therefore, as the B faces are pushed outward, the Fermi sphere is distorted and bulges toward the incoming A faces. Let us denote by n_A and n_B the volumes of the Fermi sphere in electrons/atom with radii equal to d_A and d_B, respectively, and by n_1 the volume of the first Brillouin zone. For zinc[25] $n_A=1.29$, $n_B=1.06$, and $n_1=1.799$. Hence for a sufficiently distorted Fermi sphere 1.33 electrons per atom can be accomodated entirely within the first zone. For Z=1.33 it seems quite clear that the Fermi surface does not cut the A faces; it is undoubtedly pushing against these faces so that for a slight distance where it is in contact with them it is flattened. There are two possibilities at the B faces—(1) slight overlap into the next zone or (2) no overlap but instead a very strong contact between the Fermi surface and the zone faces so that the surface is flattened for a considerable distance at the B faces. Simple calculations based on free electron theory indicate that unless the energy discontinuity at B is less than 1.5 ev no overlap will occur there.

Either of the two possibilities mentioned leads to the notion that the Fermi surface is in contact with the A faces. This is obviously the case for the second possibility. As regards the alternative, one can see that if there were unoccupied states between the Fermi surface and the A faces, a crystallographic distortion at constant atomic volume could occur so as to reduce the energy of the system. By simultaneously increasing d_B and reducing d_A, electrons in the second zone could be transferred to lower energy states within the first zone. This process would continue until the Fermi surface reached the A faces. Thus we see that for minimum kinetic energy of the electrons when Z=1.33, there will be mutual readjustment of the positions of the A faces and the Fermi surface until the two are brought into contact.

[23] If there is motion of the B faces alone, the volume of the zone is changed. This means that the atomic volume of the metal is being altered as a result of which E_0, the energy of the lowest level in the conduction band, is changed and the energy of the entire conduction band shifted. Goodenough (see reference 4) has emphasized the advantage from an energy standpoint of synchronized motion of the zone boundaries so as to keep the atomic volume and, therefore, E_0 constant.

[24] It is hoped that the reader will not be misled when the description is presented as if the zone boundaries and the surface of the Fermi sphere were physical entities with forces acting between them. Strictly speaking one should only say that the distortions occur so as to reduce the energy of the system. However, it facilitates discussion and thinking to translate this principle into the mechanical analog of objects with forces acting between them, which is done throughout this paper.

[25] These three quantities all depend slightly on the axial ratio and hence vary a little from metal to metal.

B. Influence of Alloying on the Axial Ratio

From the preceding discussion we see that when the Fermi surface lies inside the six A faces of the first zone, there are forces acting to pull the zone boundaries at A in and at the same time to move the Fermi surface out until contact is made. With this idea in mind one can readily see why the alloying of monovalent metals with zinc or cadmium reduces c/a. The distorted Fermi sphere shrinks as A is decreased pulling the A faces in after it. Concurrently the B faces move outward and if there are electrons beyond B, they are diminished in number. In this way one can qualitatively account for the decrease in c/a when copper is alloyed with zinc or when silver is alloyed with cadmium. It is to be noted that this explanation is in essence the same as that given by Jones and by Goodenough.

There is an extremely interesting effect in the alloys of magnesium with cadmium which cannot be given a simple interpretation in terms of the original Jones theory. Hume-Rothery and Raynor in 1938 observed[26] that there is a rapid variation of c/a when magnesium is alloyed with cadmium at 310°C. Up to 5–6% of solute[27] magnesium lowers the cadmium axial ratio about $\frac{2}{3}$ as rapidly as silver. Considering the silver-cadmium system for the moment in terms of the original notion of Jones, one postulates an initial Z value of 2 and overlaps into the second zone at the A and B faces. There are stresses associated with these overlaps and these are partially relieved when Z is reduced below 2, as monovalent silver is introduced into the lattice. The relief of stresses results in a fall of the axial ratio. This approach enables one to understand the effect of dissolved silver but does not make it at all clear why divalent magnesium dissolved in cadmium affects the axial ratio to the observed extent. The crux of the matter lies not in the zone boundary effects but in the influence of a dissolved magnesium ion on the covalent network. It has neither d electrons nor d-orbitals and hence cannot take part in the covalent bonding as can a solute atom of silver. With each added magnesium atom a part of the necessarily cooperative covalent network is destroyed and the c/a value is reduced progressively toward the ideal value 1.633. The variation with concentration would probably be even more rapid were it not for the fact that additional stress is developed at the inward moving A faces, and this tends to sustain the axial ratio at the higher value. We thus see that the proposed bonding scheme for the IIb metals provides a straightforward explanation for this otherwise puzzling feature of the magnesium-cadmium system and in addition satisfactorily accounts for the variation of the axial ratio when the monovalent Ib metals are used as solutes in zinc and cadmium. In the latter case the solute atoms can participate in the covalent network and the variation in the c/a values are exclusively a consequence of the interactions between the Fermi surface and the boundaries of the zone.

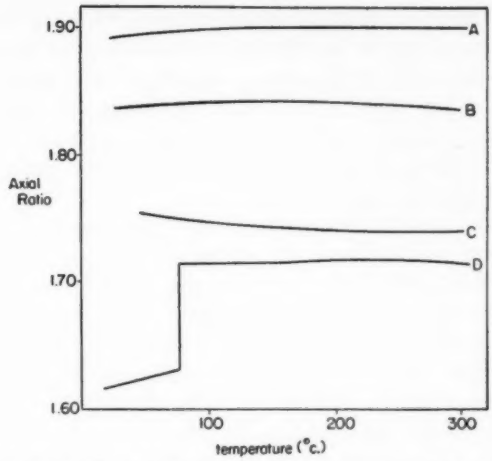

FIG. 2. Variation of axial ratio with temperature. A-Cadmium; B, C, and D-Cadmium alloyed with 9.4, 22.0, and 24.8 atomic percent magnesium, respectively.

C. Dependence of Axial Ratio on Temperature

Several years ago in this Laboratory a study was made[28] of the effects of temperature on the lattice parameters of some of the cadmium rich magnesium-cadmium alloys. Pure cadmium was also included in this study. A portion of the results obtained is shown in Fig. 2. They reveal some interesting systematic trends. The reversal of the temperature coefficient of the axial ratio for pure cadmium between 225 and 250°C, which is seen in the figure, has also been observed by Owen and Roberts.[29] Owen and Yates measured[30] c/a for zinc as a function of temperature and the trend of a plot of their results against temperature makes it appear that the axial ratio in zinc would also pass through a maximum if melting did not intervene. It looks as if the temperature at which this would occur lies 20 to 30°C above the melting point. From Fig. 2 one sees that the reversal temperature of about 250° is reduced by roughly 100° when 10% magnesium is present and with 22% magnesium the temperature coefficient of c/a is negative for all temperatures above 33°C.

In the original publication it was pointed out how these data could be interpreted by postulating that between ions in the basal plane there exists a "special" interaction whose range is short compared to the "normal" interactions. At that time there was no concrete notion about the nature of the special interaction nor was the character of the normal interactions exactly clear. These terms can now be given a precise meaning in terms of the new bonding scheme. The

[26] W. Hume-Rothery and G. V. Raynor, Proc. Roy. Soc. (London) **174A**, 471 (1940).
[27] In this paper percentages always mean atomic percentages.
[28] Edwards, Wallace, and Craig, J. Am. Chem. Soc. **74**, 5256 (1952).
[29] E. A. Owen and E. W. Roberts, Phil. Mag. **22**, 290 (1936).
[30] E. A. Owen and E. L. Yates, Phil. Mag. **17**, 113 (1934).

short-range forces are due to the covalent network and the normal interactions are a result of the usual metallic bonding of the 1.33 valence electrons. We shall now describe how the temperature coefficients of the axial ratio in cadmium and in its alloys with magnesium can be accounted for using the bonding scheme being presented in this paper.

First consider the case of pure cadmium. With increasing temperature the distances between a given central ion and all of its twelve neighbors increase. One expects r_1 to increase less rapidly than r_2, however, since there is extra cohesion in the basal plane. Consequently one anticipates an increasing axial ratio as the temperature is raised. This can, in fact, be regarded as the normal trend and in the temperature range where c/a is diminishing with increasing temperature the metal is behaving anomalously. As was pointed out earlier, the covalent network contributes only slightly to the stability of the system because of the large amount of energy required to promote one of the d electrons into a p state. The network forms only because exchange between the overlapping dp^2 hybrid orbitals of adjacent ions releases sufficient energy to compensate for this excitation energy. Therefore, *any factor which increases the separation of the ions will diminish the exchange term, upset the delicate balance between the exchange and excitation energies and hence weaken the covalent network.* We have already seen the effect of this in one instance—alloying magnesium with cadmium at a given temperature. Upon forming an alloy the number of cadmium-cadmium contacts is diminished, the covalent network is weakened and the axial ratio falls. The anomalous temperature coefficient of c/a in pure cadmium is another instance. As the temperature is raised, distances between adjacent ions in the basal plane are increased. Initially this is not serious but at sufficiently high temperatures the separation of ions increases to a point where the exchange energy can no longer compensate for the energy of excitation. With cadmium this point is apparently reached at about 225°C. Further increase in temperature steadily weakens the covalent network and the axial ratio falls toward the ideal value.

In a dilute solid solution of magnesium in cadmium the covalent network is, as indicated earlier, already weakened in comparison with pure cadmium at the same temperature. Hence one expects that with increasing temperature of the alloy the point at which exchange effects fail to supply enough energy to promote the d electron will be reached more quickly than for the pure metal. We thus expect the steady decrease of the reversal temperature with increasing magnesium content which is shown in Fig. 2.

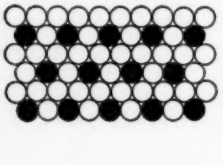

FIG. 3. Arrangement in the basal plane of the $MgCd_3$ superlattice.

D. Dependence of Axial Ratio on Order in $MgCd_3$

The magnesium-cadmium alloy containing 25% magnesium presents some interesting crystallographic features. Above 80°C the two kinds of atoms are more or less randomly distributed over the lattice sites and the alloy has the same structure as cadmium, except that its axial ratio is lower.[26] On cooling below 80°C it undergoes an order-disorder transformation. The structure of the ordered phase is hexagonal[28] and is such that all of the planes perpendicular to the hexagonal axis are identical. In Fig. 3 the arrangement of matter in one of the planes is shown. From this it can be seen that the c-spacing in the superlattice is twice the distance between adjacent basal planes as is the case with the disordered alloy. The a-spacing, on the other hand, is doubled when the superlattice forms. In the following discussion and in Fig. 2 to facilitate intercomparisons of the axial ratio in the ordered and disordered phases this doubling of the a-spacing is ignored.

First consider the large drop in the axial ratio which occurs when the superlattice forms c/a for the disordered alloy is about 1.72. On ordering the axial ratio drops[28] precipitously to 1.631, which is very close to the ideal value. Clearly the factors responsible for distortion from spherical packing have been eliminated when the superlattice develops. It appears that no explanation can be provided for this striking property of $MgCd_3$ if one retains the notion that alterations in the axial ratio are solely the result of interactions between the Fermi surface and the zone boundaries. It is true that when the superlattice appears, there develop new planes in k-space across which the energy varies discontinuously. One might attempt to relate the drop in c/a to interaction between the Fermi surface and these new planes. However, this seems to be an improbable explanation, especially if one holds to the idea of 2 valence electrons per atom. The new planes are too far within the Fermi surface to interact appreciably with it.

One can very simply account for the c/a variation in terms of the properties of the covalent network. The stability of the system of covalent bonds depends upon contacts between cadmium ions. Any sharp reduction in the number of cadmium-cadmium contacts will weaken the covalent network correspondingly. Figure 3 shows that $MgCd_3$ orders in such a way that the contacts between like ions are reduced. The number of nearest neighbor cadmium-cadmium pairs per gram atom of alloy is $(27/8)N_0$ for the random alloy and $3N_0$ for the perfectly ordered alloy, where N_0 is Avogadro's number. When the superlattice forms, the number of cadmium-cadmium contacts is abruptly reduced by roughly 10%. Apparently this is more than the tenuous covalent network can withstand and it is almost totally de-

stroyed. It seems therefore that in the ordered phase the influence of the covalent network is slight and cohesion is due almost exclusively to the normal metallic bonding of the *s* electrons. Since the covalent network has ceased to exist, there are in it 2 valence electrons per atom.

Although the disappearance of the covalent network is mainly responsible for the great change in c/a when $MgCd_3$ orders, there are also effects due to Fermi surface-zone boundary interactions. The first Brillouin zone for disordered $MgCd_3$ has the interesting geometrical characteristic that the A and B faces are almost equidistant from the origin. If c/a equalled $1.732(=\sqrt{3})$ instead of 1.72, d_A and d_B would be exactly equal. For disordered $MgCd_3$ $n_A=1.20$, $n_B=1.22$, and $n_1=1.77$ electrons/atom. If one assumes that the cadmium and magnesium atoms contribute 1.33 and 2 electrons/atom, respectively, to the conduction band, $Z=1.50$. Since this number can be accomodated entirely within the zone with little distortion of the Fermi sphere, the Fermi surface probably lies entirely within the zone. It is undoubtedly in contact with the A and B faces and exerting considerable pressure on them. The alloy is thus seen to be in a critical state. Actually the distances to the A faces are abnormally large because of the covalent network. The sudden collapse of this network when the superlattice forms draws the A faces inward increasing the pressure on the Fermi surface until it breaks through. After that the pressure at A is relieved while that at the B faces continues. The latter are pushed outward until they reach the position expected with a system of ions possessing spherically symmetrical force fields. Thus we see that the reduction in Fermi energy of the system also operates to reduce the axial ratio in $MgCd_3$ when it orders.

We shall discuss only one other characteristic of the $MgCd_3$ superlattice, the negative temperature coefficient of the a-spacing between 25 and 75°C. In this range it drops from 6.2209 to 6.2177 *kx*.[31] This drop is related to the fact that the ordering takes place over a range of temperature. Precision specific heat measurements in this Laboratory[32] have shown that in $MgCd_3$ alterations in the degree of order continue down to −80°C. Thermal measurements indicate,[33] that there is considerable improvement in the degree of order in the sample as the temperature is reduced from 75 to 25°C, during which from the above discussion the remainder of the covalent network is progressively destroyed. As the covalency disappears, the a-spacing lengthens. Thus the anomalous thermal expansivity along a is a direct consequence of the radical alteration in the bonding when the ordered alloy begins to disorder.

[31] This is the true a-spacing and not $a/2$, as has been used until now in this section.

[32] Coffer, Craig, Krier, and Wallace, J. Am. Chem. Soc. **76**, 241 (1954).

[33] Khomyakov, Kholler, and Troshkina, Vestnik. Moskov. Univ. No. 6 Ser. Fiz-Mat. i. Estestven. Nauk. No. 4, 5, 43 (1950).

IV. LATTICE DEFECTS IN THE MAGNESIUM-CADMIUM ALLOYS

Elsewhere it has been pointed out that there are extensive vacancies in the high cadmium magnesium-cadmium alloys.[28] In a pure metal at temperatures well below its melting point no more than about one lattice site per thousand is unoccupied.[34] In contrast, there exist in some of the magnesium-cadmium alloys Schottky defects to the extent of 2.0%. The composition range in which very extensive vacancies are found extends from 0 to 25% magnesium. The corresponding alloys on the magnesium end of the scale have essentially no Schottky defects.

Since the vacancies in the cadmium-rich alloys are considerably more abundant than one has become accustomed to expect, it is worthwhile to review briefly the supporting experimental evidence. There are two independent lines of approach: (1) comparison of densities measured for the bulk specimen with those computed from unit cell dimensions[28,35] and (2) comparison of the entropies of formation of the alloy with those computed,[36] assuming random mixing of the two elements. It was found that the measured entropy of formation at 270°C for the high cadmium alloys *exceeded* the random mixing entropy by as much as 15%. For $MgCd_3$ the entropy of formation was corrected[32] to absolute zero to remove any vibrational contribution. A residual entropy of about 0.2 eu/g atom was thereby found, which correlated very well with the residual entropy expected from the random distribution of about 1.7% vacancies throughout the lattice. 1.7% was the value obtained for $MgCd_3$ by the density method. The anomalously large number of Schottky defects are thus indicated by density and by entropy measurements.

We now wish to know (1) why the vacancies are so extensive in this system and (2) why the region of extensive vacancies is confined to the cadmium end of the composition scale. The answer to these questions is to be found in the drastic difference in bonding in the two pure metals and the great variation in the type of bonding that occurs as one moves along the composition scale. In magnesium and in the magnesium-rich solid solutions there is the normal metallic bonding of the *s* electrons. The covalent network cannot develop until the number of cadmium-cadmium contacts rises above some threshold value. When one introduces a cadmium ion into the magnesium lattice, it behaves like an ordinary divalent metal and conforms to the bonding scheme of the solvent. When the converse process is performed however, the solute magnesium ion cannot participate in the covalent network. It is incompatible with an essential feature of the cadmium

[34] W. Shockley, *Imperfections in Nearly Perfect Crystals* (John Wiley & Sons, Inc., New York, 1952), Chap. I by F. Seitz, p. 31.

[35] J. M. Singer and W. E. Wallace, J. Phys. Colloid Chem. **52**, 999 (1948).

[36] Trumbore, Wallace, and Craig, J. Am. Chem. Soc. **74**, 132 (1952).

FIG. 4. Heat of the reaction x Cd(s)+y Mg(s)→ alloy at 270°C; $x+y=1$.

lattice. As a consequence the forces acting on the twelve cadmium ions adjacent to a solute ion are unbalanced and they are pulled out by their neighbors on the side opposite to the dissolved ion. The incoming ion, therefore, acts as if it were larger than the cadmium ion which it has replaced in the lattice. Now, it has been shown elsewhere[37] that when a small ion is replaced by a large ion, extensive vacancies result. As an example consider the formation of a dilute KBr solid solution in a solvent of KCl. Replacement of the small chloride ion with the larger bromide ion strains the lattice. The strain energy can be lowered by the occasional omission of an ion. In a solution where the KBr mole fraction is 0.2 there are 1.9% Schottky defects.[37] In the same way the large magnesium ion strains the cadmium lattice and extensive vacancies result. No such effects are expected when cadmium is dissolved in magnesium.

V. HEATS OF ALLOYING OF MAGNESIUM AND CADMIUM

When one alloys two metals of greatly different electronegativity, one generally expects the process to be exothermal. Magnesium and cadmium are well separated in the electrochemical series, suggesting that their electronegativities differ considerably. One expects a heat evolution when they are alloyed and this has been experimentally confirmed.[36,38] The heat of alloying *versus* composition[36] is shown in Fig. 4.

The effect of electronegativity differences of the components of a binary alloy, the so-called "electronegativity factor," is frequently referred to in thermodynamic considerations of alloys but appears not to have been given a precise formulation in terms of the electron theory of metals. There is no intention here to attempt such a formulation but it appears that the electronegativity factor can be crudely interpreted along the following lines. The two types of ions in the alloy have different affinities for electrons and in the solid they will carry different charges. There will thus be an electrostatic term arising from the different charges of the ions, as in an alkali halide crystal. If the electron affinites of the ions are independent of composition, the contribution of the electronegativity factor to the cohesive energy of the system follows a simple pattern. The contribution is maximal for the equimolal alloy and is of course zero for both pure components. A plot of this electrostatic energy *versus* composition would give a curve symmetrical about mole fraction 0.5. This is also the form of the heat of alloying curve if no other factors are involved in the formation of the alloy.

Figure 4 shows that the heat of alloying of magnesium and cadmium is not symmetrical about mole fraction 0.5. There is a greater energy release when cadmium is dissolved in magnesium than for the converse process. This asymmetry is readily understandable in terms of the different kinds of bonding in the two metals. When magnesium is inserted into cadmium, energy is released due to the electronegativity factor. However, the covalent network is at the same time partly broken down with an attendant rise in energy of the system. Thus, there are two competing effects. When one introduces cadmium into magnesium, however, there is no endothermal term and the full exothermicity associated with the electronegativity factor is realized.

VI. MERCURY STRUCTURE

The discussion to this point has centered upon zinc and cadmium and their alloys, particularly those of cadmium with magnesium. We must now see what the proposed bonding scheme can indicate about the remaining IIb element, mercury. As is well known its structure is rhombohedral, a distortion of the cubic scheme of packing spheres. In contrast with zinc and cadmium, its neighbors in the basal plane are further removed from the central ion than the other six neighbors in the first coordination shell. In this section an attempt will be made to supply answers to two questions: (1) Why does mercury forsake the structure used by its congeners and crystallize in a distorted version of the cubic packing of spheres? (2) Why is the distortion so that the distances in the basal plane are longer rather than shorter than the other nearest neighbor distances?

First, consider the hypothetical *Cph* structure for mercury. Judging from the increase in axial ratio between zinc and cadmium, mercury in the *Cph* structure should have an axial ratio in excess of 1.9. Thus on proceeding from zinc to cadmium to mercury the altitude of the first Brillouin zone decreases while its cross section expands. In section IIIA we have seen how the electron gas exerts forces on the zone boundaries to increase d_B and reduce d_A. It was remarked upon then that the reduction of the distance to the A faces to diminish the Fermi energy was detrimental to the

[37] W. E. Wallace and R. A. Flinn, Nature **172**, 681 (1953).
[38] Buck, Wallace, and Rulon, J. Am. Chem. Soc. **74**, 136 (1952).

covalent network, since the covalent linkages are strained as d_A is reduced. It is clear that for minimum kinetic energy of the electron gas c/a should be only moderately in excess of the ideal value, while for minimum energy of the electrons in the covalent bonds the axial ratio should be very much in excess of the ideal value. The system, of course, seeks a minimum in its over-all energy and a compromise must be struck between these two opposing factors. An intermediate value of c/a will be adopted.

With increasing covalency the equilibrium axial ratio will be displaced to larger values and the Fermi energy of the system simultaneously raised. With Z=1.33 a rapid increase in the Fermi energy is anticipated when c/a raises above 1.91. At that axial ratio the Fermi sphere holding 1.33 electrons/atom is tangent to the A faces. For zinc and cadmium $n_A=1.29$ and 1.32, respectively and the A faces are in contact with and exerting pressure on the distorted Fermi sphere. On passing from zinc to cadmium (c/a increasing from 1.85 to 1.89) this pressure is at least partially relieved and the Fermi energy somewhat reduced. Concurrently, however, additional pressure is being developed at the inward moving B faces, the effects of which offset or more likely overbalance the energy decrease. It would appear that as c/a is increased from 1.85, the Fermi energy rises initially at a relatively slow rate. When c/a exceeds 1.91, the energy reductions due to the relaxation of pressure at the A faces either disappear or are reduced sharply so that the Fermi energy increases at an appreciably faster rate. These are the circumstances which lead a metal to seek an alternative structure in which its electrons can be accomodated at a lower energy. Since one anticipates for mercury in the *Cph* structure an axial ratio of about 1.93, its use of another structure is not surprising. Furthermore, since the bonding scheme of the IIb metals requires a close packed structure one would expect *a priori* the alternative structure to be closely related to or perhaps even identical with the cubic scheme for the close packing of spheres.

From the preceding remarks we see that it is the Fermi energy of the valence electrons which is responsible for the difference in structure between mercury and its two congeners. We shall now see that even after mercury has been forced to follow the cubic scheme of close packing, there are important consequences arising from the continued need to reduce the Fermi energy. In particular, this causes the distortions from ideal packing which preferentially lengthen the interatomic distances in the basal plane.

TABLE I. Ratios of the melting points to Debye temperatures for several elements.

Cu	4.3	Mg	3.28	Zn	2.75
Ag	5.75	Ca	4.75	Cd	3.46
Au	7.85	Sr	6.32	Hg	2.44

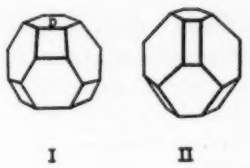

FIG. 5. Brillouin zones for the face centered cubic (I) and mercury (II) structures.

In Fig. 5 we see the first zones for the fcc and the mercury structures. The latter is a distorted version of the former. The inscribed sphere tangent to the faces marked D in the fcc zone holds 1.36 electrons/atom. When Z=1.33, the surface of the Fermi sphere is just inside the eight D faces and powerful forces act between it and these faces. The system can achieve a lower kinetic energy of the electron gas by inward motion of the eight D faces. This, however, expands the lattice and raises E_0, the energy of the lowest level in the band, which in turn increases the energy of all the valence electrons. Symmetrical inward motion of all the D faces is therefore not favorable energetically. By moving two of the faces in and the other six out so as to maintain a constant atomic volume, it is possible to keep E_0 constant and at the same time appreciably lower the Fermi energy of the system. This can also be done with a considerably greater reduction of energy by moving six faces in and two faces out. Thus we can appreciate the relationship between the two Brillouin zones shown in Fig. 5 and can understand why the distortion from ideal cubic packing is such as to lengthen rather than shorten distances in the basal plane.

It is immediately apparent that in the actual mercury structure the covalent bonds and zone boundary interactions are working in opposition just as they were in the hypothetical *Cph* structure. This, of course, results in a high energy state in both cases. Prediction as to which of the two rather unstable states will have the greater stability is obviously impossible from qualitative considerations and would probably be difficult from detailed quantum mechanical calculations since the energy differences are very likely slight.

The notion that there is competition between the covalent network and the Fermi energy suggests that cohesion in mercury should be abnormally weak. That this is the case is indicated by the data in Table I. Various investigators, including Hume-Rothery[39] and Pauling,[40] have drawn attention to the fact that the lattice energy is not an entirely satisfactory index of the strength of cohesion in a solid. The melting point is one property which has been suggested as a better criterion. It would seem that comparative melting points are meaningful only if the solids in question have nearly the same values of θ, the Debye temperature. T_m/θ appears to be a more satisfactory measure of cohesive strength when Debye temperatures vary widely. (T_m is the melting point.) This can be crudely justified in the following way. We shall take the Debye theory of the

[39] Reference 13, p. 220.
[40] L. Pauling, Phys. Rev. **54**, 899 (1938).

vibrational energy of solids as being sufficiently correct for the present purpose. In the Debye theory the vibrational energy is a function only of T/θ and consequently a series of solids at a given value of T/θ have equal vibrational energies. Since melting occurs when the vibrational excitation becomes large enough to overcome the ordering forces of cohesion, we can see that, all other things being equal, two solids which have the same value of T_m/θ, and hence the same vibrational energies at their respective melting points, have about the same cohesive strengths. When one metal has the value of T_m/θ which exceeds that of a second metal, it follows that the first metal can sustain its crystallinity up to higher vibrational energies and hence the factors responsible for cohesion in it are greater. We can thus expect a rough parallel between the strength of cohesion and T_m/θ.

In Table I we see the T_m/θ values for the zinc group elements and, for purposes of comparison, similar data for the group IIa elements and the neighboring elements of group Ib. In the latter groups T_m/θ rises as we go down the group. For the IIb metals not only are their melting points rather low compared to their Debye temperatures but the normal trend of the ratio stops with cadmium. The fall of T_m/θ on going to mercury is a marked indication of the weakened cohesion in that element.

VII. ELECTRICAL AND MAGNETIC PROPERTIES

A. Conductivities of the Solids

It is possible to discuss some aspects of the electrical and magnetic behavior of the IIb metals in terms of the bonding scheme being proposed in this paper. First consider briefly their electrical conductivities in the solid state. If there were 2 valence electrons/atom and if there were no mixing of states with the s band, the conduction band would be full, and zinc and its congeners would be insulators not metals. To explain their conductivity it has been necessary to postulate a mixing of states and overlap of electrons into the second Brillouin zone. It should be emphasized that while the new bonding scheme retains the idea that there are other states (namely d and p) with energies comparable to the s states, zone overlaps are no longer essential to account for metallic conduction in the IIb metals. With Z=1.33 the first zone is incompletely filled even when no states outside that zone are populated.

B. Conductivities of the Pure Liquids and the Dilute Amalgams

For many years the resistance increment of mercury upon fusion has been known to be exceptionally large.[41] As the resistance of the solid is not unduly small, one concludes that this unusual feature is a characteristic of mercury in the liquid state, perhaps signifying that here the covalent network persists into the liquid. With zinc and cadmium, particularly the former, the tendency to covalency is weaker and the network is largely destroyed by the fusion process. Thus, zinc[42] is found to be a normal close-packed liquid with coordination number only slightly less than 12. For mercury, however, Campbell and Hildebrand[43] and Hendus[44] have found from the scattering of x-rays by the liquid that each atom has only six close neighbors at 3.0 A, the same as in the crystal. According to Hendus the next nearest neighbors are also at the same distance from the central atom as in the crystal (3.5 A) but in this shell there are only four atoms in the liquid whereas the solid has six. One may suppose, therefore, that in zinc the normal resistance increment due to fusion is partially nullified by an increase in the number of conduction electrons (as the covalent network is destroyed) and the relaxation of zone boundary effects. In mercury, on the other hand, there is no increase in the number and freedom of the conduction electrons. On the contrary it seems likely that in addition to the normal increment there is extra resistance due to transitions from the conduction band to vacant states in the covalent network. The covalent network cannot be perfect in the liquid state; there are places where atoms are missing and at which vacancies in the bonding orbitals occur. These can act as traps for the conduction electrons and can lead to extra resistance here just as the s-d transitions lead to additional resistance in the transition metals.[45] Cadmium undoubtedly occupies an intermediate position between zinc and mercury as regards covalency in the liquid, although the evidence suggests that it lies closer to zinc.

In liquid zinc the temperature coefficient of resistance is negative, from which it appears that even here some vestiges of the covalent network probably remain. With further increase in temperature these are destroyed and the slight increase in number of conduction electrons outweighs the normal thermal effect. The situation is somewhat similar in liquid cadmium except that in this instance the remnants of the covalent network are more stable and the freeing of additional conduction electrons suffices merely to keep the resistance nearly independent of temperature. For liquid mercury there is a very large positive temperature coefficient. This is perhaps due to the fact that in addition to the normal thermal effect there is an increase in resistance due to greater imperfection in the covalent network at the higher temperatures. As the temperature is raised, more vacancies develop in the bonding orbitals and scattering of the conduction electrons by transitions into these vacancies steadily increases.

Liquid mercury possesses another odd property. Its

[41] G. Borelius, *Handbuch der Metallphysik* (1935), Vol. I, p. 182.

[42] N. S. Gingrich, Revs. Modern. Phys. **15**, 90 (1943).

[43] J. A. Campbell and J. H. Hildebrand, J. Chem. Phys. **11**, 330 (1943).

[44] H. Hendus, Z. Naturforsch. **3A**, 416 (1948).

[45] N. F. Mott and H. Jones, *Properties of Metals and Alloys* (Clarendon Press, Oxford, England, 1936), p. 267.

resistance is in many cases lowered when small amounts of other metals are dissolved in it.[41] Some of the strongly electropositive elements—cesium, rubidium, etc.—raise its resistance, probably due to the formation of nonconducting molecular compounds. Its resistance is lowered by gold, tin, lead, cadmium, etc. An explanation for this can be provided by noting that these various solutes are for one reason or another incompatible with the covalent network in mercury. As they are introduced, the system of covalent bonds is seriously weakened and the number of conduction electrons rises sufficiently to overbalance the normal resistance increment due to impurity scattering.

C. Sign of the Hall Coefficient

Both zinc and cadmium have positive Hall coefficients. In certain instances the sign of the Hall coefficient can be predicted from simple considerations. For an almost full zone and no overlaps into the second zone, it has a positive sign. When the first zone is full and there are slight overlaps into the second zone, the Hall coefficient has a negative sign. However, when there are vacancies in the first zone *and* overlaps into the second zone, one cannot be sure of the sign. When reference is made to the Hall coefficients for cadmium and zinc, it is stated without elaboration that their positive signs are due to the fact that for them the zone is nearly filled. This ignores the negative contribution of the electrons lying outside the zone. If Z=2 there are about $0.2+x$ electrons/atom in the second zone, where x is the number of "holes" in the first zone. Since the outlying electrons are more numerous, to justify the positive sign it is necessary to make the *ad hoc* assumption that a hole contributes more to the Hall effect than an electron. If Z=1.33, the electrons can all be accommodated in the first zone, in which case the Hall coefficient is necessarily positive. Overlaps into the second zone, if they occur at all, will be slight compared to the situation when Z=2. With Z=1.33 the holes are considerably more abundant and it is reasonable to suppose that the contribution from them predominates. The predominance of hole effects may also be true for 2 electrons/atom but the issue in this instance seems very much less clear.

VIII. SOLVENT POWER OF ZINC AND CADMIUM

The bonding scheme postulated for the IIb metals is sufficiently unusual in nature that we might expect few other metals to be compatible with it. For this reason we anticipate, and do in fact find, that the IIb metals are rather poor solvents. The metallic elements whose size-factors are favorable[46] for solubility are as follows: in zinc—aluminum, copper, gallium, germanium, arsenic, silver, tin, antimony, tellurium, gold plus sixteen elements in groups Vb, VIb, VIIb, and VIII; in cadmium—lithium, magnesium, aluminum, silver, indium, tin, antimony, tellurium, gold, mercury, bismuth plus eleven elements in groups Vb, VIb, VIIb, and VIII. One expects very limited solubilities of the electronegative metals such as antimony, bismuth, tellurium, and arsenic in either cadmium or zinc because of a strong tendency toward compound formation. Also, only slight solubility of gallium in zinc is anticipated in view of the unusual bonding in gallium. However, we would expect moderate solubilities for many of the remaining elements, with limitations in those cases where, as for example with the Ib metals, the solute atom is considerably different in electronegativity from the atoms of the solvent and primary solubility is restricted by tendencies toward compound formation.

TABLE II. Metallic elements exhibiting the largest solubilities in cadmium and zinc.

Zinc			Cadmium		
Element	Sol. (atomic %)	T(°C)	Element	Sol. (atomic %)	T(°C)
Ag	6	430	Mg	100	260 to 320
Au	5	420	Hg	22	190
Al	2	380	Ag	7	345
Cu	2	425	Au	4	310
Li	2	400	Zn	4	265
			Li	3	250

Listed in Table II are the maximum solubilities and the corresponding temperatures for the elements which are soluble to the greatest extent in solid zinc and cadmium.[47] These data show that there are no metals which are highly soluble in zinc and only with magnesium and mercury do the primary solid solutions cover a wide range of composition in cadmium. The paucity of metals with valences greater than 2 in Table II is noteworthy. It is true that there is some solubility of aluminum in zinc but there is some doubt that in zinc aluminum is behaving as a trivalent element; that is, one cannot be sure that it is fully ionized and contributing three electrons/atom to the system.[48]

The behavior of cadmium toward aluminum as a potential solute is interesting and significant. Despite favorable size- and electronegativity-factors, the solubility of aluminum in solid cadmium is immeasurably small.[45] Furthermore, aluminum is insoluble in liquid cadmium and even at temperatures where both metals are liquid the system consists of two nearly immiscible liquids. Zinc is not quite so hostile to aluminum as a solute but even so the solubility is not great. We may cite three more cases: zinc-tin, solubility less than 0.1%; cadmium-tin, maximum solubility 0.27%; cadmium-

[46] W. Hume-Rothery, *The Structure of Metals and Alloys* (Institute of Metals, London, England, 1950), p. 60.

[47] The data are taken from M. Hansen, *Aufbau der Zweistofflegierungen* (Julius Springer, Berlin, Germany, 1936) and *Metals Handbook* (The American Society for Metals, Cleveland, Ohio, 1948).

[48] See reference 40, p. 27.

indium,[49,50] solubility less than 1%. The atomic sizes differ by 5, 6, and 1%, respectively, in these three cases.[51]

Clearly the IIb metals have considerable reluctance to dissolve elements with a valence electron-to-atom ratio in excess of 2. This correlates with the picture presented earlier (Sec. IIIA). When Z=1.33 the Fermi sphere was shown to be in contact with the *A* faces of the first Brillouin zone and either in very strong contact with or perhaps cutting the *B* faces. In either event the Fermi energy will rise rapidly as Z is increased. Thus the dissolving of tri- or quadrivalent elements is expected to be strongly endothermal. As a consequence the free energy of formation of the alloys will be positive and solid solutions will not form.

The situation is somewhat more favorable for monovalent solutes, particularly the Ib group metals. With decreasing Z the Fermi energy of the system is diminished and this, of course, favors solubility. However, in some cases, e.g., lithium,[52] the solute atom cannot participate in the covalent network. Thus when lithium is alloyed with zinc or cadmium the energy of the system is raised and it is clear that only a limited amount of solute can be accommodated. The Ib metals *can* take part in the covalent network and hence should be somewhat more soluble than lithium. This is found to be the case in the main, although the large difference in electronegativity of the zinc and copper group metals leads, as noted above, to weak compound formation and tends to restrict their solubility.

There is another factor which tends to limit the solubility of a monovalent metal if zinc and cadmium conform to the bonding scheme under discussion in this paper. When Z is reduced too far, the most energetic electrons in the *s* band will have lower energy than the electrons which comprise the covalent network. At this point the covalent network will become energetically unstable and disappear while Z increases to 2 and the bonding reverts to that characteristic of a normal divalent metal. It seems very likely that this is what is happening at the limit of the η phase in the copper-zinc system and in the corresponding phases of the silver-cadmium, gold-cadmium, etc. systems. In the ϵ phases the number of valence electrons has been reduced to a point where the covalent network cannot be maintained and in those phases there is the normal metallic bonding. The great change in c/a between the ϵ and η phases is due mostly to the collapse of the covalent network. The departure of the axial ratio for the ϵ phase from the ideal value is on this basis entirely due to zone boundary overlap.

The large solubility of mercury in cadmium is to be expected in view of their chemical similarity. Solute mercury is of course entirely compatible with the bonding in cadmium and zinc. It is prevented from dissolving extensively in the latter only because their atomic sizes differ considerably (13%). There appears to be no simple reason why magnesium is completely miscible with cadmium. It is probable that this results merely from a fortuitous combination of factors and is of little significance with respect to general principles.

IX. CONCLUDING REMARKS

A. Valence of the IIb Metals

Prior to the Pauling theory of metals the valence of the IIb elements had always been assumed to be 2. In Pauling's treatment they are assigned[53] a valence of about 4.5. The bonding scheme proposed in this paper leads to an average valence of 3.33.

B. Extension to Other Metals

It is natural to inquire if the bonding scheme proposed here for the metals of the zinc group can also be applied to elements in the adjacent groups of the Periodic Table. It appears that it cannot for reasons which are closely related to the discussion in the preceding section. When one tries to utilize the bonding scheme with trivalent metals, the Fermi energy is too high and alternative structures having different modes of bonding are more stable. When one tries to adapt it to the Ib metals, it develops that there are insufficient electrons. As stated earlier the covalent network is probably destroyed when Z is reduced by only a small amount below 1.33. The number of valence electrons in the metals of group Ib is too small to support a covalent network. General considerations suggest and experimental evidence seems to support the notion that the special bonding postulated for zinc, cadmium, and mercury operates only in those pure metals and in dilute solid solutions based on them.

X. ACKNOWLEDGMENT

The author would like to express his appreciation to the John Simon Guggenheim Foundation for Fellowship support while this work was carried out. He would also like to thank Professor G. Borelius of the Royal Institute of Technology in Stockholm for his kindness in providing very pleasant working quarters in his Institute during the Fellowship period.

[49] C. L. Wilson and O. J. Wick, Ind. Eng. Chem. **29**, 1164 (1937).

[50] W. Betteridge, Proc. Phys. Soc. (London) **50**, 519 (1938).

[51] Taking Hume-Rothery's estimate (reference 46) of the size of fully ionized indium.

[52] The other alkali metals have unfavorable size factors and are in addition too electropositive to form extensive solid solutions.

[53] L. Pauling, Proc. Roy. Soc. (London) **A196**, 343 (1949).

Photolysis of Acetic Anhydride

HERMAN BURWASSER* AND H. AUSTIN TAYLOR
Chemistry Department, New York University, New York 53, New York
(Received March 14, 1955)

The photolysis of acetic anhydride has been studied using a hot mercury arc at temperatures from 60° to 160°C by analysis of the gaseous products. CO and C_2H_6 are produced at equal rates which are one-half the rate of production of CO_2. At 60°C, CO production is delayed initially but in time reaches the same rate as C_2H_6. Using acetone as actinometer, the quantum yield of CO_2 is two, of CO and C_2H_6, unity. The decomposition of acetic anhydride can be photosensitized by acetone. Mass-spectral analysis of the liquid residue at 160°C showed the absence of acetone, biacetyl, methyl acetate, acetylacetone, and acetonyl acetone. A fragment of mass 57, increasing in intensity with duration of reaction was present in amounts sufficient to account for a material balance. Some steps in the mechanism are discussed.

AN earlier study of the photochemical decomposition of acetic anhydride by Kandel and Taylor[1] using a mercury resonance lamp inside the reaction vessel was attributed to the absorption of 1849 A radiation. The rate of reaction measured as a pressure change was found to be first order, though studied only over a limited pressure range. There existed a possibility that the reaction may have been, at least in part, mercury sensitized and the analytical results reported represented the products only after rather extensive decomposition, while the rate of measurements were made in terms of the pressure change occurring essentially initially. It was therefore felt that a better insight into the reaction could be obtained by an alternative study. Since acetic anhydride exhibits some absorption around 2500 A, a medium pressure mercury lamp, in which the resonance lines are completely reversed, was used, and provision made to eliminate any 1849 A radiation. The reaction was followed analytically over a much larger concentration range than heretofore.

EXPERIMENTAL

Acetic anhydride, after standing over metallic sodium, was distilled through a column packed with carbon rings and a fraction boiling between 138–139°C was collected in a vessel protected from moisture by anhydrous calcium sulfate. The purity of the fraction was checked by its refractive index. Later, an analysis by a mass spectrometer, showed trace amounts of acetic acid as the only impurity, and these could be attributed to hydrolysis during sampling or by moisture in the mass spectrometer. The acetic anhydride was distilled *in vacuo* into a storage bulb immersed in liquid nitrogen and separated from the reaction vessel by a mercury cutoff.

The reaction cell of 300 cc volume was cylindrical, with plane polished ends. It was mounted in an oven, whose temperature was maintained by a bimetallic regulator. A Hanovia S.H. type quartz medium pressure mercury lamp was the source of illumination and was mounted on top of the oven about one foot above the cell. To achieve a variety of pressures of acetic anhydride vapor, the system between the cell and storage bulb was wrapped with Nichrome wire and heated. The storage bulb was heated by hot water, the temperature being determined by trial according to the vapor pressure required. The high solubility in and solvent action on stopcock grease was overcome by using mercury cutoffs wherever necessary. A conventional pumping system consisting of a two-state mercury diffusion pumped backed by an oil pump was used. The analytical system, consisting of a constant volume manometer as gas pipet and appropriate absorption pipets was similar to that used for microanalysis by Saunders and Taylor.[2]

The procedure for a run was as follows: after the system had been evacuated to 10^{-6} mm, the lamp operated for at least one-half hour to attain full intensity and the storage bulb of acetic anhydride warmed to the desired temperature, vapor was admitted to the reaction cell by lowering a mercury cutoff, the time being noted. The initial pressure to within one mm mercury, was read on a mercury cutoff functioning as a manometer, separating the cell from the analytical system. After the required exposure the reaction system was opened to a series of traps through the manometer cutoff.

The first trap was kept at −110° to −112°C using dry ice and acetone, precooled in liquid nitrogen. A second trap was maintained at −212°C using liquid nitrogen held at low pressure. The temperature was calculated from the measured vapor pressure. After standing open to the traps for at least one-half hour, noncondensables were pumped by a Toepler pump into the gas buret where the total volume was measured. Carbon monoxide was then oxidized over copper oxide at 300°C and the resulting dioxide trapped out in a cold-finger in liquid nitrogen. The remaining volume of gas was measured and the process repeated to constant volume. Only a

* Abstract from a thesis presented in partial fulfillment of the requirements for the degree of Doctor of Philosophy at New York University, March, 1954.

[1] R. J. Kandel and H. A. Taylor, J. Chem. Phys. **19**, 1250 (1951).

[2] K. W. Saunders and H. A. Taylor, J. Chem. Phys. **9**, 616 (1941).

TABLE I.

Temp. 80°C Time (min)	Initial pressure 25 mm moles ×10⁶ CO	C_2H_6	CO_2
30	3.30	3.16	9.20
40	4.00	4.14	10.1
60	6.60	6.20	15.4
70	7.78	7.30	18.2
90	10.4	9.65	22.5

very small residual gas was found, too small for further analysis and for reasons to be shown was assumed to be methane.

The cold-finger in liquid nitrogen was warmed by replacement with dry ice acetone. This enabled any carbon dioxide to vaporize but would hold back water vapor, had there been hydrogen in the noncondensable gas. The volume of the gas was measured and the gas passed into a pipet containing ascarite. In all cases complete absorption occurred indicating that the original gas was carbon monoxide. No evidence of water vapor was found showing hydrogen to be absent from the noncondensable gas. Hence, since methane is the only possible fixed gas at temperatures below the triple point of nitrogen, the traces of residual gas were assumed to be methane.

After the analysis of the noncondensable gas the liquid nitrogen trap was allowed to warm, and the gaseous products passed into the gas buret. Having shown by experiment that acetic anhydride is quantitatively trapped at −110°C, this second gaseous fraction was taken to be CO_2 and C_2 hydrocarbons. The total volume having been measured, CO_2 was absorbed over ascarite. Since no hydrogen had been found earlier, the probability of ethylene in the C_2 fraction was small, and, in general, the residual gas was taken to be ethane. Several explosion analyses, using a threefold excess of oxygen, which was found to give consistent results using pure ethane, justified the assumption.

In an attempt to characterize any liquid products from the reaction, five runs were made, each of one hour duration at 160°C and 24 mm initial pressure, and the liquid products, along with undecomposed acetic anhydride from all the runs, were collected in a cold-finger in dry ice and submitted to a mass-spectrometric analysis. A second series of runs of two-hour duration were made for the same purpose, liquid nitrogen being used instead of dry ice for the collection of products.

Some runs were made in an attempt to sensitize a decomposition of acetic anhydride using acetone. A quartz cell containing liquid acetic anhydride as a filter was placed between the lamp and the reaction vessel. Runs made using the anhydride vapor alone and acetone vapor alone showed appreciable decomposition of the acetone alone but no measurable decomposition of the anhydride alone. The difference in volatility of acetone and acetic anhydride made it almost impossible to prepare mixtures containing a known small amount of acetone. Instead, samples of solutions of acetone in acetic anhydride, of known composition, were injected through the mercury seal, the samples being small enough to insure complete volatilization. In the analysis, the trap at −111°C was replaced with a petroleum ether slush at −150°C to separate acetone and carbon dioxide.

RESULTS

A typical series of runs of different duration at 80°C and 25 mm initial pressure are reported in Table I. The amounts of product are linear functions of the time, a result observed in all cases except at 60°C and 10 mm pressure, where carbon monoxide production exhibits an induction period as seen in Table II. Plots of these data extrapolate to the origin for ethane and carbon dioxide but the carbon monoxide data extrapolate to 23 min indicating that the carbon monoxide might be produced from a secondary species rather than directly from acetic anhydride. To observe any change in the ratios after appreciable photolysis, a run of fourteen-hours duration was also made at 60°C and 10-mm initial pressure.

In an attempt to identify any liquid products of the photolysis two samples were analyzed with the mass spectrograph.[3] The first sample was collected from five, one-hour runs made at 160°C and 25 mm initial pressure, the products being trapped out with dry ice. The mass spectral range covered in the analysis did not extend beyond m/e values of 120. The only peak observed not attributable to acetic anhydride or acetic acid was at m/e of 57 and corresponded to an estimated 0.5 mole percent. A second sample, the products from five, two-hour runs under similar conditions but trapped out in liquid nitrogen, exhibited a more intense peak at the same value, 57, corresponding to an estimated one percent. It is significant that doubling the duration caused a doubling of the amount and indicates that the fragment represents a product of the reaction. A third sample, consisting of some of the acetic anhydride used for the photolysis to which 10% acetone had been added, was analyzed but showed no mass peak at 57. This precludes the possibility that the peak was due to any impurity in the starting material. Characteristic

TABLE II.

Temp. 60°C time (mm)	Initial pressure 10 mm moles ×10⁶ CO	C_2H_6	CO_2	CH_4
60	1.56	2.14	7.12	
70	2.00	2.45	7.80	
80	2.63	2.84	9.65	
90	2.72	3.16	10.5	
100	3.34	3.78	11.8	
840	29.5	28.8	60.7	3.65

[3] The analyses were obtained through the courtesy of the M. W. Kellog Company, New Jersey.

m/e values of biacetyl, acetyl-acetone, acetonyl-acetone, and methyl acetate were not observed in any of the spectra. The mass peak at 57 could correspond to the acetonyl radical and might suggest the presence of some more complex substance decomposing in the ion source.

The quantum yield of the photolysis was determined using acetone as an actinometer. Two twenty-minute runs at 160°C using acetone gave 0.138 cc carbon monoxide for an initial acetone pressure at 40 mm and 0.116 cc for an initial pressure of 36 mm. The latter gives 1.49×10^{17} molecules formed per minute; the former, 1.85×10^{17}. With unit quantum yield, these are also the numbers of quanta absorbed by the acetone per minute. Since the lamp did not emit monochromatic radiation, the calculation of the intensity of the incident radiation involved a summation over the several wavelengths present each with its spectral distribution factor and extinction coefficient. The incident intensity of the lamp estimated from the above data was found to be 4.3×10^{17} or 4.1×10^{17} quanta per minute, an average of 4.2×10^{17}.

For acetic anhydride the absorption data were taken from Ley and Arends.[4] The anhydride absorbs at 2537 and at 2652 A in the range studied giving the number of quanta absorbed per minute as 6.95×10^{16}. At 160°C and 25 mm the rate of production of carbon dioxide from acetic anhydride was 0.00565 cc min^{-1} or 15.2×10^{16} molecules per minute. The quantum yield of carbon dioxide is thus 2.2. Table III summarizes the quantum yields.

In the two runs made with the acetone-acetic anhydride mixtures, owing to the slow rate of reaction, the quantities of gas for analysis were very small and the analytical results subject to large error. It is certain, however, from a qualitative point of view, that carbon dioxide was produced and in a quantity greater than carbon monoxide.

DISCUSSION

The results in Table III show that the initial rates of formation of the gaseous products are directly proportional to the initial pressure of the acetic anhydride. In the fourteen-hour run at 60°C, reported in Table II, corresponding to about 42% decomposition, the volumes of CO and C_2H_6 are linear in time with the volumes produced after shorter irradiation, while the plot of the volumes of CO_2 falls quite appreciably. Nevertheless, the first order rate constant for CO_2 production calculated over the first 5% of reaction is 0.05 hr^{-1} while for the 42% reaction the value is 0.04 hr^{-1}. This agreement must indicate that the rate determining step in CO_2 production is approximately first order and the CO_2 may be taken as a measure of the amount of acetic anhydride decomposed. The validity of this assumption may be open to question, but it will be seen not to be inconsistent with the data. On the other hand, the continued steady production of CO and C_2H_6 even after 40% decomposition must mean that these are produced from species which have assumed a steady-state concentration.

TABLE III. Quantum yields.

Temp. °C	Press. mm	CO	C_2H_6	CO_2
60	10	0.7[a]	0.6	1.9
80	10	0.8	0.8	1.9
	20	0.8	0.8	2.0
	25	0.8	0.8	1.9
120	10	1.2	1.1	2.2
	25	0.9	0.8	1.8
160	10	1.3	0.9	2.5
	25	1.1	0.8	2.2

[a] After the induction period.

The approximately first-order rate of the acetic anhydride photolysis is most easily accounted for on the basis of the weak absorption of the light. From the extinction coefficients at 2537 and 2652 A it is calculated for the present experimental conditions that only 16% of the incident radiation is absorbed. Hence, the rate should be approximately proportional to the gas concentration. A first-order rate will, however, be an upper limit and actually on this account alone the order of the reaction should be less than unity.

The primary process may then be written as producing an excited molecule:

$$CH_3COOCOCH_3+h\nu\rightarrow CH_3COOCOCH_3.^* \quad (1)$$

Whether this molecule may be deactivated by collision with other molecules, or lose energy by fluorescence cannot be ascertained from the present work. The fate of the excited molecule presents two possibilities for consideration:

$$CH_3COOCOCH_3^*\rightarrow CH_3+CH_3COOCO \quad (2)$$

or

$$CH_3COOCOCH_3^*\rightarrow CH_3CO+CH_3COO. \quad (2')$$

There is very little direct information concerning the acetate radical. Rice[5] estimated the energy of activation of the reaction:

$$CH_3CO_2\rightarrow CH_3+CO_2$$

to be between 40 and 70 kcal which agrees with Burton's[6] interpretation of the vapor phase photolysis of acetic acid. On this basis the acetate radical should be relatively stable and the CO_2/CO ratio should be less than unity and certainly not much greater than one at temperatures around 100°C. Experimentally it is seen that the CO_2/CO ratio remains about two regardless of temperature or pressure indicating that CO_2 is produced more easily than CO which would not be expected if the acetate radical were the major source of CO_2. Further-

[4] H. Ley and B. Arends, Z. physik. Chem. **B17**, 177 (1932).

[5] F. O. Rice and K. K. Rice, *The Aliphatic Free Radicals* (Johns Hopkins Press, Baltimore, Maryland, 1935), p. 187.

[6] M. Burton, J. Am. Chem. Soc. **58**, 692, 1645 (1936).

more, owing to the acetate stability, a reaction with methyl to produce methyl acetate would be expected to occur without difficulty, whereas none was found in the mass spectrographic analyses. Finally, the rate of formation of CO_2 has a negligible temperature coefficient, quite inconsistent with its production from acetate radicals requiring 40 to 70 kcal for decomposition. Reaction (2′) is, therefore, not consistent with the experimental observations.

There remains the alternative reaction (2). To produce CO_2 in the amounts found, the CH_3COOCO radical must decompose readily leaving an acetyl radical. From the work of Herr and Noyes[7] on acetone photolysis, the acetyl radical appears to decompose readily at temperatures above 100°C as shown by the unit quantum yield for CO but at lower temperatures becomes stabilized as biacetyl with a corresponding deficiency in CO production. The results found in the 60°C run are very similar and could therefore be similarly accounted for. On the other hand, Pitts and Blacet[8] have interpreted their studies of acetone photolysis in presence of iodine to indicate that acetyl radicals are stable up to at least 175°C in presence of small concentrations of free radicals. In presenting an alternative explanation Nicholson[9] observes that it is "meaningless to compare the stabilities of free radicals in different systems unless all the rate constants of the reactions in which the radicals disappear are known." There is at least one difference between the acetyl radicals produced in the acetone and the acetic anhydride systems. The activated anhydride molecule has absorbed about 110 kcal/mole. If 80 kcal are used in breaking the C—C bond, 30 kcal remain to be divided between the two fragments and if neither is electronically excited, the CH_3COOCO radical would get no more than 5 kcal/mole. The subsequent splitting out of CO_2 should leave a very "cold" acetyl radical. In acetone photolysis the acetyl radical initially formed is much more energetic. In addition, the reactivity of acetyl radicals in an atmosphere of acetic anhydride need not necessarily be identical with that in acetone.

The quantum yield of two found for CO_2 was essentially constant over the temperature range covered. The slight increase with temperature is not inconsistent with an effect of temperature on the extinction coefficients of acetic anhydride. The quantum yield of two requires that a second molecule of the anhydride decompose to yield a molecule of CO_2 subsequently to the initial split. Two reactions appear possible:

$$CH_3+CH_3COOCOCH_3\rightarrow CO_2+\text{residue} \quad (3a)$$

$$CH_3CO+CH_3COOCOCH_3\rightarrow CO_2+\text{residue}. \quad (3b)$$

The early production of C_2H_6, observed in all the runs made, probably occurs by combination of the methyl radicals formed in reaction (2). In the 60°C run, however, the amount of C_2H_6 produced early in the reaction is only about one-third and not one-half of the CO_2 produced. There is thus a deficiency in the methyl radicals. Later in the reaction at 60°C the CO/C_2H_6 ratio approaches two just as at higher temperatures. This would not seem consistent with a removal of acetyl radicals as biacetyl at 60°C. Reactions (3a) and (3b) can thus account for both the methyl radical deficiency as ethane and for the removal of acetyl radicals. The possibility of either of these reactions was at least qualitatively established by the runs made with the anhydride-acetone mixtures where methyl or acetyl radicals from acetone photolysis produced a decomposition of the anhydride as evidenced by the production of CO_2.

The reaction of an acetyl or a methyl radical with anhydride presents a problem in accounting for the observed over-all order, approximately the first. In the absence of its decomposition the acetyl radical concentration should be proportional to the light absorbed, that is, approximately proportional to the anhydride concentration. The reaction of acetyl with anhydride would thus be approximately second order. The total rate of disappearance of acetic anhydride as measured by CO_2 production would be $k_2[A]+k_3[A]^2$, where A stands for the anhydride, with an over-all order between one and two. The maximum dependence of the concentration of methyl radicals, produced by reaction (2) and removed by recombination, on the concentration of acetic anhydride would be the square root and reaction (3a) would be three-halves order. It has already been pointed out, however, that the first-order dependence of reaction (2) is an upper limit owing to the approximation for weak absorption and hence the order approximately first, found here is not inconsistent with either reactions (3a) or (3b).

The identification of the residue of reactions (3) could not be made. A material balance, based on the assumption that CO_2 measures the acetic anhydride decomposed, carried out on the gaseous products indicates that the over-all residue unaccounted for has the empirical formula C_3H_6O. The mass-spectrographic analysis of the liquid produced a fragment of mass-to-charge ratio of 57 which could have the empirical formula C_3H_5O. Since the characteristic mass peaks of biacetyl, acetone, acetyl acetone, acetonyl acetone, and methyl acetate were not observed in any of the mass spectra, it was concluded that these substances were not present to an extent greater than 0.5 mole percent. The unidentified 57 peak was present in an amount which would lead to a material balance. Damon and Daniels[11] found that a trace of water catalytically

[7] D. S. Herr and W. A. Noyes, J. Am. Chem. Soc. **62**, 2052 (1940).
[8] J. N. Pitts and F. E. Blacet, J. Am. Chem. Soc. **74**, 6155 (1952).
[9] A. J. C. Nicholson, J. Chem. Phys. **20**, 1811 (1952).
[11] G. H. Damon and F. Daniels, J. Am. Chem. Soc. **55**, 2363 (1933).

produced a photochemical condensation of acetone, although the product was not completely identified. It could be surmised that the acetyl radical could induce some condensation or polymerization reaction with the ejection of a molecule of CO_2 from the condensate which in the mass spectrograph produces the fragment of mass 57.

At 160°C, and probably more so at higher temperatures, some methane is produced. This undoubtedly results from a hydrogen abstraction reaction of methyl radicals with acetic anhydride. The fate of the radical produced may only be speculated, but presumably it either breaks down or enters into a recombination reaction.

THE JOURNAL OF CHEMICAL PHYSICS VOLUME 23, NUMBER 12 DECEMBER, 1955

Study of Electrokinetic Effects Using Sinusoidal Pressure and Voltage*

CLAUDE E. COOKE, JR.†
Department of Physics, The University of Texas, Austin, Texas
(Received March 14, 1955)

The electrokinetic effects streaming potential, streaming current, and electro-osmotic pressure were studied by applying and measuring sinusoidal variations of hydrodynamic pressure and electrical voltage. Phenomenological relations between the effects were investigated, and an improved experimental method for measuring the electrokinetic coefficients, hence the zeta potential, was used. Saxen's law was verified within 6% at frequencies of 20, 100, and 200 cycles per second. The systems studied were restricted to glass-water and glass-salt solutions. The advantages and disadvantages of using sinusoidally varying quantities for electrokinetic measurements are discussed.

IN recent years the streaming potential has been applied in various types of pressure transducers.[1,2] Packard[3] has developed a theoretical expression for the variation of the streaming potential with frequency, and has made experimental measurements of the sinusoidal potential developed across capillaries upon application of a sinusoidal pressure. The phenomenon of electro-osmosis has been investigated extensively using a constant applied voltage. To the author's knowledge it has never been studied quantitatively before using an applied electrical voltage which varies sinusoidally with time. The advantage of using the alternating voltage to measure the magnitude of the electrokinetic potential is, of course, the possibility of alleviating difficulties which arise at the electrodes.

PHENOMENOLOGY OF THE ELECTROKINETIC EFFECTS

The electrokinetic effects which are considered here are of a class of irreversible processes which have been treated in theory.[4] The phenomenological relations between the electrokinetic effects have also been thoroughly discussed in the literature.[5,6]

The so-called phenomenological equations describing the electrokinetic effects are

$$I = L_{11}E + L_{12}P, \tag{1}$$

$$V = L_{21}E + L_{22}P. \tag{2}$$

I, electric current through the system, is taken as positive when flow is from side 1 to side 2. E, electric potential across the system, is taken as positive when side 1 is positive with respect to side 2. Similar convention is used for the hydrodynamic quantities volume flow, V, and pressure, P. The coefficients (L_{ij}) are called the phenomenological coefficients. It can be seen that L_{11} and L_{22} are the ordinary electrical and hydrodynamic conductance coefficients. L_{12} and L_{21} are the electrokinetic coefficients.

From Eqs. (1) and (2),

$$L_{12} = -L_{11}\frac{E_s}{P} + \frac{I_s}{P} \tag{3}$$

$$L_{21} = -L_{22}\frac{P_{e0}}{E} + \frac{V_{e0}}{E}. \tag{4}$$

The subscripts have been added to designate the streaming potential and streaming current, E_s and I_s, and the electro-osmotic pressure and volume flow, P_{e0} and V_{e0}.

Note that if the coefficients are positive the equations imply positive charge transport in the liquid from application of a positive pressure. If an excess of negative charges exists in the flowing liquid then the coefficients L_{12} and L_{21} are negative. In any case, the

* This paper is part of a dissertation submitted to the Graduate School of the University of Texas in partial fulfillment of the requirements for the degree of Doctor of Philosophy. The work was partially supported by a grant from Research Corporation.
† Present address: Houston Research Center, Humble Oil and Refining Company, Houston, Texas.
[1] M. Williams, Rev. Sci. Instr. **19**, 640 (1948).
[2] E. V. Hardway, Instruments **26**, 1186 (1953).
[3] R. G. Packard, J. Chem. Phys. **21**, 303 (1953).
[4] S. R. De Groot, *Thermodynamics of Irreversible Processes* (North Holland Publishing Company, Amsterdam, 1951).
[5] J. Th. G. Overbeek, J. Colloid Sci. **8**, 421 (1953).
[6] P. B. Lorenz, J. Phys. Chem. **56**, 775 (1952).

two terms in Eqs. (3) and (4) are really of the same sign. If positive charges are flowing: E_s/P is negative, I_s/P is positive, L_{11} is always positive, and therefore L_{12} is the sum of two positive terms. Similar considerations show that L_{21} is also the sum of two terms of the same sign as that of the net electrical charge in the liquid.

Now suppose that electrodes are placed in contact with each end of a capillary or porous medium filled with a liquid. The electrical conductance (L_{11}) of the system can then be measured. If there is no streaming current flow between the electrodes, $I_s=0$, then (assuming positive charge transport),

$$L_{12}=-\left(-\frac{E_s}{P}\right)L_{11}. \tag{5}$$

But if there is a finite resistance (R_e) between the electrodes and external to the capillary, then Eq. (3) becomes

$$L_{12}=-\left(-\frac{E_s'}{P}\right)\frac{1}{Rs}+\left(\frac{E_s'}{R_e}\right)\frac{1}{P}$$

$$=\frac{E_s'}{P}\left(\frac{1}{R_s}+\frac{1}{R_e}\right)=\frac{E_s'}{P}\left(\frac{1}{R_t}\right)$$

since $L_{11}=1/R_s$, where R_s is the resistance of the capillary or porous plug system, and $I_s=E_s'/R_e$. R_t is the parallel resistance of the capillary and the external resistance between the electrodes. The E_s' measured in this case is not by strict definition the streaming potential, but is measured in the same manner. It might be termed a "pseudo streaming potential." Any value of R_e can be used to make experimental measurements convenient. Experimenters in the past making measurements of the dc streaming potential have usually used a potentiometer circuit so that I_s was equal to zero. Other experimenters have measured the streaming current, I_s, when the streaming potential was negligibly small to obtain a value of the electrokinetic potential, but have had experimental difficulties in measuring such small currents. The method described above, which follows immediately from the phenomenological equations, allows one to measure a voltage across a resistance equal to that of the sample or across any desired resistance less than that of the sample obtained by a parallel combination with an external resistance. In making measurements of alternating voltages this method proved very helpful when high resistance samples were used.

The value of the other electrokinetic coefficient, L_{21}, can be measured by measuring the quantities on the right side of Eq. (4). Measurements have previously been made under conditions such that one term on the right was negligibly small. The experimental method described later consists of measuring the electro-osmotic pressure (P_{e0}) when a voltage E was applied, but the volume flow (V_{e0}) was not zero. The value of the volume flow could be determined by measuring the apparent hydrodynamic impedance of the sample when it was attached to the same system as when the electro-osmotic pressure was measured. In using sinusoidally varying quantities it was not possible to measure either the pressure or volume flow with the other negligibly small. A description of a means of measuring the electro-kinetic coefficient L_{21} will be deferred until after a description of the experimental apparatus.

EXPERIMENTAL APPARATUS AND PROCEDURE

A block diagram of the apparatus and the circuits analogous to the hydrodynamic system is shown in Fig. 1. The apparatus for producing and measuring the hydrodynamic pressure and volume flow was originally developed for acoustic measurements, and has been described in detail by Thurston.[7] In the experiments reported here a Lucite cell for holding the sample was rigidly attached to the top of the acoustic system. The cell is shown in Fig. 2. The porous diaphragms or capillaries used as samples were placed between platinum screen electrodes which were pressed tightly against the ends of the sample.

In the analogous circuits for the hydrodynamic system shown in Fig. 1 the symbols denote the following quantities: e, the sinusoidal pressure induced by the driver; i the volume flow induced by the driver in the case of measuring the streaming potential, or the electro-osmotic volume flow in the case of electro-osmosis; L_D the inductance of the driver; C_D the capacitance of the driver; C_S the shunting capacity resulting from the finite stiffness of the walls of the test chamber and compression of the liquid; L_{CH} and C_{CH} the inductance and capacitance of the capacity hydrophone; R_S and L_S the resistance and inductance of the porous diaphragm or capillary used as a sample;

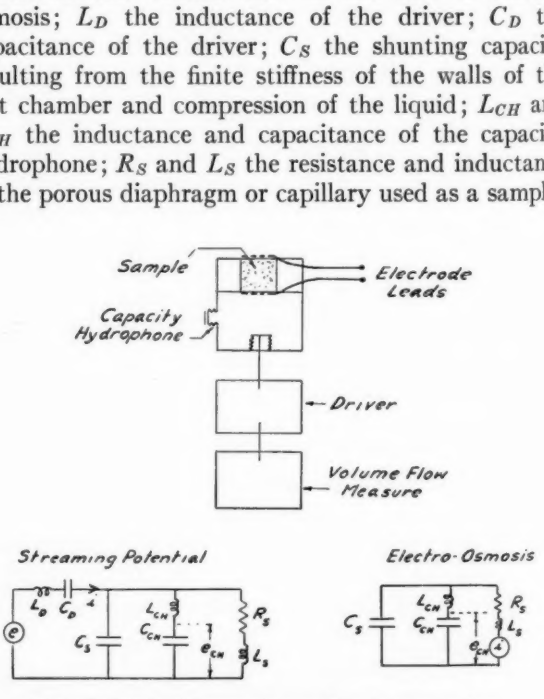

FIG. 1. Block diagram of experimental apparatus and the analogous circuits.

[7] G. B. Thurston, J. Acoust. Soc. Am. 24, 649 (1952).

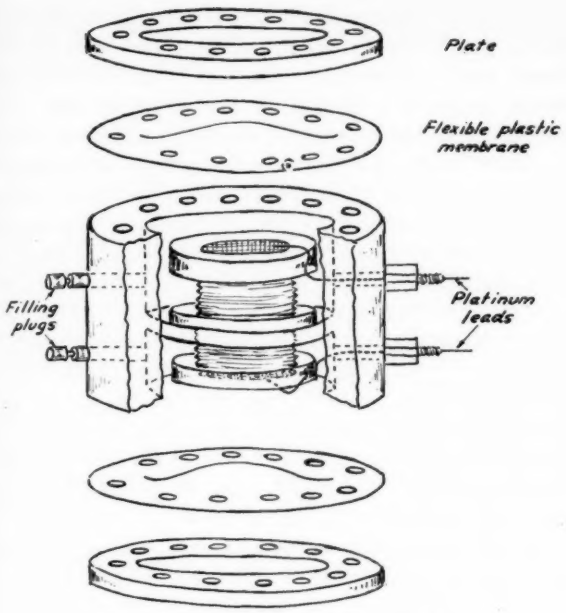

FIG. 2. Lucite cell for holding samples.

and e_{CH} the pressure exerted on the capacity hydrophone. Since the hydrophone was calibrated by hydrostatic pressure the effect of L_{C_L} must be considered, but calculations show that up to the highest frequency employed here the pressure measured across C_{CH} is not appreciably different from that across the sample impedance, R_S and L_S. The frequency limitations and other limitations to the range of acoustic variables that can be measured are discussed by Thurston.[7]

The samples used in these experiments were of either Pyrex or Vycor glass, in the form of capillaries or fritted diaphragms one inch long. The diaphragms were one inch in diameter and were of either medium or course porosity (Corning Glass Works). The glass surfaces were cleaned by extracting the samples in benzene, then alcohol, and then by pulling conductivity water through them. The samples were then put in the Lucite cell, the cell assembled, and the entire assembly was evacuated in a desiccator and filled through the filling plugs (Fig. 2) with deaerated liquid.

The liquids used were restricted to conductivity water and salt solutions. Organic liquids could not be used in the Lucite cell. The conductivity of liquids was measured using a dip cell connected in a Leeds and Northrup conductivity bridge. The "cell constant" of the diaphragms was determined by saturating them with 0.01 N KCl solution.

MEASUREMENT OF THE ELECTROKINETIC POTENTIAL

If the values of the electrokinetic coefficients L_{12} and L_{21} are known, the value of the zeta potential, or electrokinetic potential, can easily be computed. The quantity L_{12} was determined by measuring the quantities on the right side of Eq. (6) at three different frequencies. The value of E_s' was measured for several values of the pressure, P. The ratio remained constant for pressures up to the highest attainable (about 10 000 dynes/cm²-rms). The value of the parallel resistance of the sample and the external resistance (R_t) was measured with the conductivity bridge.

The quantity L_{21} can be determined by measuring the quantities on the right side of Eq. (4). However, when measuring the hydrodynamic conductivity (L_{22}) of a sample by measuring flow at the driver an erroneous value is obtained due to the shunting compliances (C_S and C_{CH}, Fig. 1). Let us call the apparent value of L_{22}, that is the ratio V_D/P found by measuring V at the driver, L_{22}'. The true hydrodynamic conductivity of the sample, L_{22}, is

$$L_{22}=\frac{V_D-V_C}{P}=L_{22}'-\frac{V_C}{P}, \tag{7}$$

where V_C is the volume flow through the shunting compliances. But

$$V_C=\frac{P}{Z_C}, \tag{8}$$

where Z_C is the acoustic impedance of the compliances. Therefore,

$$L_{22}=L_{22}'-(1/Z_C). \tag{9}$$

Now let us look at Eq. (4):

$$L_{21}=L_{22}\left(\frac{P_{e0}}{E}\right)+\frac{V}{E}$$

Both terms are of the same sign. The value of the net volume flow, V, is

$$V=P'_{e0}/Z_C. \tag{10}$$

(P_{e0}' will be used for the "pseudo electro-osmotic pressure," that is, the electro-osmotic pressure when there is a flow of liquid.) Therefore,

$$L_{21}=\left(L_{22}'-\frac{1}{Z_C}\right)\frac{P_{e0}'}{E}+\frac{P_{e0}'}{E}\frac{1}{Z_C}=L_{22}'\left(\frac{P_{e0}'}{E}\right). \tag{11}$$

Thus the value of the electrokinetic coefficient L_{21} can be measured independently of the values of the shunting compliances. The value of L_{22}' was found at each particular frequency. The ratio of P_{e0}' to E was measured for several values of applied voltage E at these frequencies. The product of the two quantities measured at the same frequency gave the value of L_{21} at that frequency. As the frequency is increased the implicit assumptions become invalid and phase differences become troublesome. Measurements could be made satisfactorily up to 200 cycles per second.

From the kinetic theory for the streaming potential and electro-osmosis,

$$\frac{E_s}{P}=-\frac{\zeta\xi}{4\pi\eta\sigma}=-\frac{V_{e0}}{I} \tag{12}$$

where ζ is the electrokinetic potential, ξ is the dielectric constant of the liquid, η is the viscosity of the liquid, and σ is the total conductivity (bulk and surface).

The resistance of a capillary or porous medium is

$$R=\frac{J}{\sigma}=\frac{1}{L_{11}} \tag{13}$$

where J is the "cell constant" of the capillary or porous medium. Since

$$L_{12}=-L_{11}\left(\frac{E_s}{P}\right),$$

then

$$L_{12}=-\frac{\zeta\xi}{4\pi\eta\sigma}=L_{21}, \tag{14}$$

since from the phenomenological equations the statement that L_{12} is equal to L_{21} can be shown equivalent to the statement

$$\frac{E_s}{P}=-\frac{V_{e0}}{I}, \tag{15}$$

which is Saxen's law. It has been verified for water, aqueous salt solutions, and for at least one organic liquid[8] using steady-state flow of liquid and electrical current.

RESULTS AND CONCLUSIONS

The observation of a sinusoidal pressure induced by electro-osmosis afforded an opportunity to observe how well the linear phenomenological equation for electro-osmosis applied. From Eq. (2),

$$P=\frac{V}{L_{22}}-\frac{L_{21}E}{L_{22}}. \tag{16}$$

To observe how well the pressure follows addition of the two terms in the equation, a pressure was induced by a volume flow V using the driver and by a voltage E across the electrodes. The output of the pressure detector was observed on an oscilloscope. For various values of pressures up to about 10 000 dynes/cm² rms, voltages up to 250 volts rms, and frequencies up to 400 cycles per second, the two pressures were found to add within the limits of accuracy afforded by measuring the pressure amplitude on an oscilloscope screen. When the two driving frequencies were made nearly the same and the pressure amplitudes due to V and E were made the same (A), then the amplitude at the beat frequency varied between the limits of zero and $2A$.

[8] P. B. Lorenz, J. Phys. Chem. **57**, 430 (1953).

The electroviscous and electro-osmotic conductance effects could not be observed in these experiments. These effects arise from the fact that electrokinetic effects make the hydrodynamic conductivity of a system dependent upon the electrical potential across the system (electroviscous effect), and the electrical conductivity of a system dependent upon the hydrodynamic pressure across the system (electro-osmotic conductance effect). To observe the effects in a system both the conductivities should be very small—smaller than it was feasible to obtain here. The effects have been detected by Lorenz[8] but are exceedingly small.

In order to verify the validity of Eq. (6), for a given run of a sample the value of the resistance shunting the sample (R_e) was changed, of course changing the value of R_t. When the value of R_e was changed by a factor of 200 the measured value of L_{12} remained the same well within experimental error.

The plots of streaming potential *versus* frequency for three porous diaphragms are shown in Fig. 3. It can be seen that the values increase to a steady value at sufficiently low frequency. The shape of the curve depends on the pore sizes of the diaphragm. The decrease of streaming potential with frequency for the diaphragms follows qualitatively the theory developed by Packard[3] for capillaries. Frequency runs made with capillaries failed to follow the theoretical curve. In using capillaries of radii about one or two millimeters in diameter and one inch long the streaming potential decreased at low frequencies below the maximum value, usually attained at about 50 or 75 cycles per second. This is an acoustic effect and could be eliminated by using smaller diameter and longer capillaries. A reasonable value of the zeta potential was calculated using the maximum value of streaming potential. In using the large diameter capillaries the hydrodynamic impedance was so low that the electro-

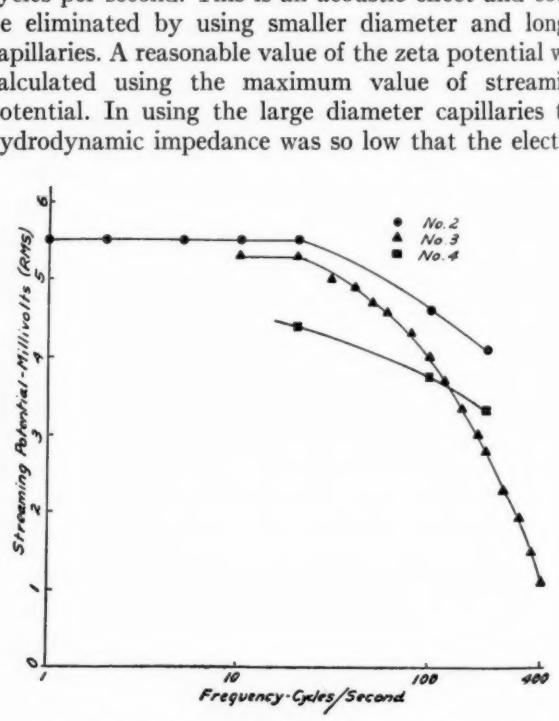

FIG. 3. Plots of streaming potential *versus* frequency for three porous diaphragms.

osmotic pressure could not be observed. The "pseudo-electro-osmotic pressure" developed by a given voltage also increases with decrease in frequency. The shape of the curve depends on the acoustic parameters of the sample and the system which measures the pressure. The greater the electro-osmotic volume flow the greater is the proportional decrease of the pressure with frequency.

To obtain useful data from the measurements of electro-kinetic effects taken at frequencies greater than zero it is necessary to extrapolate the data to zero frequency. This is usually easy in the case of the streaming potential across diaphragms because the potential becomes constant with frequency at frequencies below a certain value. If it were desired to obtain data using a concentrated electrolyte solution so that polarization occurred at these low frequencies, the shape of the curve could be determined at low concentrations where polarization did not occur. Then values at higher frequencies using the concentrated electrolyte could be reduced to the zero-frequency value.

Overbeek and Wijga[9] have shown that in the presence of surface conductance in a porous diaphragm the measured value of the zeta potential will be lower than the true value. Experimental work by Moore[10] indicates that the bulk conductivity of the liquid and the pore radii of the diaphragm must be small in order for this effect to be manifest. Recently an attempt has been made to overcome the difficulty of calculating the zeta potential from streaming potential measurements made across a diaphragm.[11]

Using the experimental technique described previously and Eqs. (6) and (11), the electrokinetic coefficients L_{12} and L_{21} were measured. The results are given in Table I. The largest deviation from the average value of the coefficients for any run was about 6%. This is within experimental uncertainty in measuring each of the coefficients. Using Eq. (14), assuming the dielectric constant of water in the double layer to be 80 and the viscosity to be 0.009 poise, the value of the zeta potentials was calculated from the average of the values of the electrokinetic coefficients measured at 20 cps and the measured value of the cell constant (J) of the diaphragms and capillaries. The results are also shown in Table I.

TABLE I. Experimental results (c.g.s.—e.s.u. except zeta).

Sample no.	Frequency	L_{12}	L_{21}	Cell constant	Bulk conductivity	Zeta potential
2	20	0.0736	0.0661	1.96	2.2×10^{-4}	59 mv
	100	0.0702	0.0700			
	200	0.0635	0.0706			
3	20	0.0560	0.0598	3.38		83
Run 1	100	0.0422	0.0424			
	200	0.0307	0.0298			
3	20	0.0580	0.0530	3.38	1.4	80
Run 2	100	0.0406	0.0416			
	200	0.0289	0.0308			
3	20	0.0578		3.38	15.6	83
KCl	100	0.0409				
Solution	200	0.0296	0.0303			
4	20	0.0726	0.0723	1.94	3.2	59
	100	0.0648	0.0723			
	200	0.0602	0.0680			
Capillary 1	40	0.00045	0.00050	399	17.0	81
Capillary 2 KCl sol.	40	0.00045		399	80.0	77

The values of the zeta potential are surprisingly consistent. Samples 2 and 4 were of lower porosity than Sample 3, which is the cause of the lower value of the zeta potential obtained, owing to the presence of surface conductance. The values agree qualitatively with values reported in the literature for this system, but there is a diversity of reported values, doubtless caused by difficulty in obtaining a clean solid surface and a pure liquid. It is not felt that the systems used here were well enough defined chemically to make more than a qualitative comparison meaningful, but there is no feature inherent in the method which would make elaborate purification procedures impractical.

The use of sinusoidally varying quantities in measuring the electrokinetic potential seems to be a satisfactory method. It eliminates the necessity of averaging the different values obtained upon reversing the polarity of direct currents and voltages, and offers the possibility of eliminating electrode difficulties encountered when using electrolyte solutions. When using either steady-state or alternating quantities the method which follows from the phenomenological equations, that of measuring the "pseudo streaming potential," or the "pseudo electro-osmotic pressure," could possibly often be used to make experimental measurements more convenient.

The author wishes to express his sincere appreciation to Dr. D. S. Hughes, Dr. Norman Hackerman, and Dr. S. Leroy Brown for their help and advice, and to Research Corporation for the financial aid furnished the project.

[9] J. Th. G. Overbeek and P. W. O. Wijga, Rec. trav. chim. **65**, 556 (1946).

[10] R. G. Moore, Master's thesis presented to the Graduate School, The University of Texas, June, 1954.

[11] Ghosh, Choudhury, and De, Trans. Faraday Soc. **50**, 955 (1954).

Variational Theory of the Radial Distribution Function*

JOHN M. RICHARDSON†
Explosives and Physical Sciences Division, Bureau of Mines, Pittsburgh, Pennsylvania
(Received June 11, 1954)

A variational approach to the calculation of the radial distribution function is presented. The approximations consist in the neglect of fourth-order correlation in the entropy and the use of a constant third-order correlation chosen to satisfy the third-order normalization condition. The average interaction energy, containing only pair terms, does not involve correlations higher than second order. Finally, one obtains approximate expression for the excess Helmholtz free energy as a function of the radial distribution function (r.d.f.) and macroscopic parameters. This free energy, when minimized with respect to the r.d.f. at constant temperature and density, yields an integral equation for the r.d.f. This theory has a simpler structure and yields thermodynamic functions in a more direct way than earlier theories. The theory has not yet been adequately tested; however, the author speculates that it will give good results for short-range forces but poor results for long-range forces.

1. INTRODUCTION

KIRKWOOD,[1] Yvon,[2] Born and Green,[3] and Mayer[4] have presented theories of the radial distribution function (r.d.f.) in liquids. All of these theories involve at some point in their development integral or integrodifferential equations containing the r.d.f. as the dependent variable. These equations can be based upon a general theorem relating the derivative of the log of the r.d.f. (with respect to some parameter) to the average force (defined by this parameter) acting upon a pair of molecules. The desired results are obtained after the average force term, involving a triplet d.f., is expressed in terms of the r.d.f. and singlet d.f. by means of the Kirkwood superposition approximation.

The purpose of this paper is presentation of a variational theory of the r.d.f. that has a logical structure entirely different from that of the earlier theories. Here we start by deriving an approximate expression for the excess Helmholtz free energy[5] as a functional of the r.d.f. The minimization of this quantity with respect to the functional form of the r.d.f. yields an integral equation similar, but not identical, to those obtained in the earlier theories. The derivation of the free-energy expression employs an approximation very similar to the superposition approximation but slightly less stringent—as a matter of fact the success of the theory rests quite heavily upon this slight deviation from the usual statement of the approximation. The present theory differs further from the others in that very close attention must be devoted to the process of letting the volume of the system become infinite. In the petit canonical ensemble, which we use here, there are some rather subtle paradoxes connected with the above limiting process. However, in the grand canonical ensemble they can be easily removed. The question will be considered further in a later paper.

In Sec. 2, we set up the variational function for the case of finite volume. We introduce certain approximations making the variational function dependent only upon the r.d.f. besides the macroscopic parameters, temperature and density. In Sec. 3, the problem of passing to the limit of infinite volume is treated. Here we obtain the final form of the variational function and the attendant constraint on the r.d.f. In Sec. 4, we express thermodynamic quantities as functions of the r.d.f., temperature, and density by a completely self-consistent procedure. In Sec. 5, we establish certain connections between the present theory on one hand and the virial expansion and the earlier r.d.f. theories on the other hand. Although no quantitative tests of the theory are yet available, we present certain speculations concerning its validity and comment on it from the methodological standpoint.

2. FORMULATION OF THE VARIATIONAL PRINCIPLE FOR A SYSTEM OF FINITE VOLUME

We consider a classical one component system of volume V containing N molecules of mass m interacting pairwise according to the potentials $\phi(s,s')$, where s and s' symbolize the coordinates (rotational as well as translational, if desired) of molecules labeled by s and s', respectively. The excess Helmholtz free energy $\bar{A}_N(\beta)$, giving the increment between the actual value and the hypothetical perfect gas value, is defined by

$$\bar{A}_N(\beta) = -\beta^{-1} \log[Z_N(\beta)/(V\omega)^N], \tag{2.1}$$

* This research, conducted at the Bureau of Mines, was sponsored by the Flight Research Laboratory, Wright Air Development Center, under Contract AF 18(600)-156.

† Physical chemist; formerly, Chief, Kinetics Section, Explosives and Physical Sciences Division, Bureau of Mines, Pittsburgh, Pennsylvania. Present address: The Ramo-Wooldridge Corporation, Los Angeles 45, California.

[1] J. G. Kirkwood, J. Chem. Phys. **3**, 300 (1935). J. G. Kirkwood and E. M. Boggs, J. Chem. Phys. **9**, 514 (1941); **10**, 394 (1942).

[2] J. Yvon, *Actualites Scientifiques et Industrielles* (Hermann et Cie, Paris, 1935), p. 203.

[3] M. Born and H. S. Green, Proc. Roy. Soc. (London) **A188**, 10 (1946).

[4] J. E. Mayer, J. Chem. Phys. **15**, 187 (1947).

[5] Strictly speaking, this variational function is the excess Helmholtz free energy when it is minimized in an appropriate manner. However, we will, on occasion, use the term to describe the variational function whether it is minimized or not.

where $Z_N(\beta)$ is the Gibbs phase integral defined by

$$Z_N(\beta)=\int\cdots\int d(1)\cdots d(N)\exp(-\beta U_N), \quad (2.2)$$

$$U_N=\sum_{\substack{s,s'=1\\ s>s'}}^{N}\phi(s,s'), \quad (2.3)$$

and where

$$V\omega=\int d(1) \quad (2.4)$$

is the volume of configuration space accessible to one molecule. In the above formulas β is, as usual, $1/kT$, and the integrations are understood to extend over all of accessible translational (and possibly rotational) configuration space.

Let us consider the variational function

$$\beta\bar{A}'_N=(V\omega)^{-N}\int\cdots\int d(1)\cdots d(N)\times P_N(\log P_N+\beta U_N), \quad (2.5)$$

in which $P_N=P_N(1,\cdots,N)$ is an arbitrary distribution function (in configuration space) to be varied under the constraints of constant β and of normalization defined by

$$(V\omega)^{-N}\int\cdots\int d(1)\cdots d(N)P_N=1. \quad (2.6)$$

It can be proved readily that the minimum value of $\bar{A}_N'$ is the excess Helmholtz free energy $\bar{A}_N'$ (defined only for equilibrium, strictly speaking) given by Eq. (2.1). It also can be proved, of course, that the form of P_N giving this minimum is, except for a modified normalization, the canonical distribution in configuration space.

Let us express P_N in the form

$$P_N=\prod_{\substack{s,s'=1\\ s>s'}}^{N}g(s,s')\prod_{\substack{s,s',s''=1\\ s>s'>s''}}^{N}g^{(3)}(s,s',s'')\cdots, \quad (2.7)$$

in which the g's of a given order are of the same functional form and are invariant to permutations of their arguments (i.e., $g(s,s')=g(s',s)$). Let us require that

$$P_1(1)=1, \quad (2.8a)$$

which is trivial, and that

$$P_2(1,2)=g(1,2), \quad (2.8b)$$

$$P_3(1,2,3)=g(1,2)g(2,3)g(3,1)g^{(3)}(1,2,3), \quad (2.8c)$$

etc. In the foregoing sequence, $P_n(1,\cdots,n)$, $n\leqslant N$, is an nth order d.f. (in the system of N molecules, not the highest order d.f. in a system of n molecules) defined by

$$P_n(1,\cdots,n)=(V\omega)^{-N+n}\int\cdots\int d(n+1)\cdots d(N)P_N(1,\cdots,N). \quad (2.9)$$

The relation (2.8b) thus requires $g(1,2)$ to be the r.d.f.[6] Later we will have occasion to use explicitly the following relations derivable from the relations immediately above:

$$(V\omega)^{-1}\int d(2)g(1,2)=1, \quad (2.10a)$$

and

$$(V\omega)^{-1}\int\int\int d(1)d(2)d(3)g(1,2)\times g(2,3)g(3,1)g^{(3)}(1,2,3)=1. \quad (2.10b)$$

Inserting Eq. (2.7) into Eq. (2.5), using the constraints expressed by Eqs. (2.8a), (2.8b), (2.8c), etc., and (2.9), and remembering the definition of U_N (Eq. (2.4)), we finally obtain

$$\beta\bar{A}'_N=\tfrac{1}{2}(C/\omega)^2\int\int d(1)d(2)g(1,2)\times[\log g(1,2)+\beta\phi(1,2)]+\tfrac{1}{6}(C/\omega)^3\times\int\int\int d(1)d(2)d(3)g(1,2)g(2,3)\times g(3,1)g^{(3)}(1,2,3)\log g^{(3)}(1,2,3)+\cdots, \quad (2.11)$$

where C is the number density N/V. Terms of the order of unity and smaller have been neglected in Eq. (2.11), since $\beta\bar{A}_N'$ is of the order of N. The result is exact in the limit of large N. It is an expansion in which correlations of order n and higher do not appear in the first $n-2$ terms.

Now let us make the approximation of setting fourth and higher order g's equal to unity. The approximation of setting the third order g also equal to unlty would be equivalent to the well-known superposition approximation of Kirkwood.[1] However, we make a slightly different approximation, namely,

$$g^{(3)}(1,2,3)=1-\gamma=\text{constant}, \quad (2.12)$$

where γ is to be determined by the third order normalization condition, Eq. (2.10b). After some manipulations involving the use of Eq. (2.10a), we find

$$\gamma=(V\omega)^{-3}\int\int\int d(1)d(2)d(3)[g(1,2)-1]\times[g(2,3)-1][g(3,1)-1], \quad (2.13)$$

neglecting terms of the order of γ^2. It is evident that γ is a very small quantity of the order of V^{-2}.

[6] To be sure, the usual definition of the radial distribution function implies a dependence only upon the scalar distance between two molecules. Here we use the term in a more general sense.

Introducing these approximations into Eq. (2.11) we obtain

$$\beta\bar{A}'_N=\tfrac{1}{2}(C/\omega)^2\int\int d(1)d(2)g(1,2)$$
$$\times[\log g(1,2)+\beta\phi(1,2)]-\tfrac{1}{6}(C/\omega)^3$$
$$\times\int\int\int d(1)d(2)d(3)[g(1,2)-1]$$
$$\times[g(2,3)-1][g(3,1)-1], \quad (2.14)$$

in which we have used the approximation $\log(1-\gamma)\simeq-\gamma$. If we require $g(1,2)$ to depend only upon the relative coordinates[7] of molecules 1 and 2, Eq. (2.14) can be recast in the form

$$\beta\bar{A}'_N/N=\tfrac{1}{2}(C/\omega)\int d(2)g(1,2)[\log g(1,2)+\beta\phi(1,2)]$$
$$-\tfrac{1}{6}(C/\omega)^2\int\int d(2)d(3)[g(1,2)-1]$$
$$\times[g(2,3)-1][g(3,1)-1], \quad (2.15)$$

where molecule 1 is held fixed at an arbitrary position (and in an arbitrary orientation, if angles are present) in the midst of the system. Equation (2.15) is to be minimized with respect to the functional form of g under the constraints (2.10a).

3. THE LIMIT OF INFINITE VOLUME

When one considers more closely the variational problem just described one encounters inconveniences associated with the finiteness of the volume V. Therefore it is desirable to go to the limit of infinite volume keeping $C=N/V$ fixed. In view of the fact that in a system of finite volume g differs from unity at large separations by an increment of the order of V^{-1}, one must proceed with caution because of the following paradox. If this increment occurs linearly in the integrand of an integral spanning the configuration space of one molecule, it will contribute a term of the order of unity to the result. If we allow the volume to become infinite first and then extend the range of integration (translational part) over the volume (now infinite) the increment will contribute nothing since it vanished when we initially let the volume become infinite. If we reverse the order of these processes, the increment will contribute a finite amount. Thus there is a paradox here which must be removed before we can obtain a meaningful expression for infinite volume. It can be removed by modifying Eq. (2.15) so that the increment occurs in each integrand to higher powers than the number of integrations over the configuration space of one molecule. This can be accomplished by subtracting from (2.15) the expression

$$\tfrac{1}{2}(C/\omega)\int d(2)[g(1,2)-1]=0. \quad (3.1)$$

We can now take the limit $V\to\infty$ with impunity with the result

$$\beta\bar{a}'=\tfrac{1}{2}(C/\omega)\int d(2)\{g(1,2)[\log g(1,2)$$
$$-1+\beta\phi(1,2)]+1\}-\tfrac{1}{6}(C/\omega)^2\int\int d(2)d(3)$$
$$\times[g(1,2)-1][g(2,3)-1][g(3,1)-1], \quad (3.2)$$

where $\bar{a}'=\lim_{V\to\infty}\bar{A}'_N/N$ (keeping $C=N/V$ fixed, of course). The normalization condition (2.10a), in which the paradox occurs, may now be dropped. All that is required now is that the integral

$$\lim_{V\to\infty}\int_V d(2)[g(1,2)-1]$$

exist. The condition for this may be expressed in the form,

$$\lim_{r_{12}\to\infty} r_{12}^3[g(1,2)-1]=0, \quad (3.3)$$

where r_{12} is the scalar distance between molecules 1 and 2.

The quantity $\bar{a}'$ when minimized with respect to g under the new constraint (3.3) is equal to $\bar{a}$, an approximation to the excess Helmholtz free energy per molecule, and the resultant g is an approximation to the r.d.f.

At a given density and temperature we could use Eq. (3.2) directly by inserting for g a trial function (satisfying (3.3)) containing a finite number of parameters which could be adjusted to give the best form of g and the best value of $\bar{a}'$. A possible example might be $g=\exp(-\beta^*\phi)$ in which β^* is the adjustable parameter whose best value could be interpreted as giving a "structure temperature" $T^*=1/k\beta^*$. This special trial function would obviously be very bad for hard spheres with no mutual attraction. However, it might conceivably give fair results (as far as the thermodynamic functions are concerned) for potentials containing attractive terms whose range is of the order of molecular diameters. It is not hard to construct more elaborate trial functions which should give more accurate results.

Alternatively, we can obtain for the variation problem a formal solution expressed by the following integral equation:

$$\log g(1,2)=-\beta\phi(1,2)-(C/\omega)$$
$$\times\int d(3)[g(1,3)-1][g(2,3)-1]. \quad (3.4)$$

[7] If angle coordinates are present, we will be concerned only with the relative angles.

We could then attempt to solve this equation by suitable approximate means.

4. THERMODYNAMIC FUNCTIONS

Unlike other theories of the r.d.f., the present theory allows the thermodynamic functions to be evaluated in a particularly simple way. First of all the minimum value of $\bar{a}'$, the variational function, is the excess Helmholtz free energy $\bar{a}$, from which all other excess thermodynamic quantities can be obtained by differentiation with respect to C or β. Thus the results are necessarily thermodynamically consistent. In obtaining mathematical expressions for these quantities we are greatly assisted by the following lemma: The derivative of $\bar{a}$ with respect to β or C is equal to the same derivative of $\bar{a}'$ holding g fixed, after which g is assigned its best functional form for the given values of β and C.

First of all, the excess Helmholtz free energy (per molecule) $\bar{a}$ is given by Eq. (3.2) after one has assigned g its best functional form. For convenience we summarize the result here:

$$\beta\bar{a}=\tfrac{1}{2}(C/\omega)\int d(2)\{g(1,2)[\log g(1,2)-1+\beta\phi(1,2)]+1\}$$
$$-\tfrac{1}{6}(C/\omega)^2\int\int d(2)d(3)[g(1,2)-1]$$
$$\times[g(2,3)-1][g(3,1)-1]. \quad (4.1)$$

To repeat, ω is the volume of the rotational part of the configuration of one molecule.[8] Next we consider other excess thermodynamic functions: The excess energy per molecule, $\bar{e}$; the excess entropy per molecule, $\bar{s}$; and finally the excess pressure, $\bar{p}$. These can be derived with the aid of the formulas

$$\bar{e}=(\partial(\beta\bar{a})/\partial\beta)_C, \quad (4.2a)$$
$$\bar{p}=C^2(\partial\bar{a}/\partial C)_\beta, \quad (4.2b)$$
$$\bar{s}=k\beta(\bar{e}-\bar{a}). \quad (4.2c)$$

We obtain

$$\bar{e}=\tfrac{1}{2}(C/\omega)\int d(2)g(1,2)\phi(1,2), \quad (4.3a)$$

$$\bar{s}/k=\tfrac{1}{2}(C/\omega)\int d(2)\{g(1,2)[\log g(1,2)-1]+1\}$$
$$-\tfrac{1}{6}(C/\omega)^2\int\int d(2)d(3)[g(1,2)-1]$$
$$\times[g(2,3)-1][g(3,1)-1], \quad (4.3b)$$

$$\beta\bar{p}/C=\tfrac{1}{2}(C/\omega)\int d(2)\{g(1,2)$$
$$\times[\log g(1,2)-1+\beta\phi(1,2)]+1\}-\tfrac{1}{3}(C/\omega)^2$$
$$\times\int\int d(2)d(3)[g(1,2)-1]$$
$$\times[g(2,3)-1][g(3,1)-1]. \quad (4.3c)$$

The total thermodynamic functions can be obtained by adding the above excess functions to the corresponding functions computed for the hypothetical perfect gas.[9]

5. DISCUSSION

Unfortunately, it is not yet possible to present quantitative tests of the present theory. In lieu of this we discuss the connection between this theory and the virial expansion in the theory of imperfect gases. Later we consider the relation between our theory and other theories of the r.d.f.

If we set $g=\exp(-\beta\phi)$ in $\bar{a}'$ given by Eq. (3.2) we obtain the virial expansion of $\bar{a}'$ correct up to (and including) the third virial coefficient. If we minimize $\bar{a}'$ for the low density case we will obtain a better answer since the above form of g is not the best possible form. It can be shown, however, that with the best form for g one still does not obtain the correct expression for the fourth virial coefficient. The present theory has this property in common with the other theories of the r.d.f.

Equation (3.4) does not exhibit any obvious connections with the integral equations derived by Kirkwood, Yvon, Born and Green, and Mayer. However, the connections can be brought out by putting the equations in integro-differential form. It is perhaps simplest to show the similarity with the Born and Green integro-differential equation. We take the gradient of Eq. (3.4) in the configuration space of molecule 1. The result can be expressed in the form

$$-\beta^{-1}\nabla_1\log g(1,2)=\nabla_1\phi(1,2)+(C/\omega)$$
$$\times\int d(3)g(1,3)g(2,3)\nabla_1 w(1,3), \quad (5.1)$$

where

$$w(1,3)=-\beta^{-1}\log g(1,3) \quad (5.2)$$

is the potential of average force acting on molecules 1 and 3, including the direct interaction between these molecules. In deriving Eq. (5.1) we used the fact that $\int d(3)g(1,3)$ is independent of the position (and orientation, if rotational coordinates are present) of molecule 1. In our notation the corresponding result of Born and Green may be written

[8] For example, if the configuration is given by a unit vector specifying orientation in addition to a vector specifying position, then $\omega=4\pi$.

[9] Precisely, the hypothetical perfect gas is obtained by letting the interaction potentials ϕ vanish in the actual system.

$$-\beta^{-1}\nabla_1 \log g(1,2)=\nabla_1\phi(1,2)+(C/\omega)$$
$$\times\int d(3)g(1,3)g(2,3)\nabla_1\phi(1,3). \quad (5.3)$$

Thus our result differs from the result of Born and Green only in the presence of $w(1,3)$ in the integrand instead of $\phi(1,3)$. This difference is not necessarily trivial, however; in the case of long-range forces the difference between ϕ and w may be quite large. The connection with the other theories can be exhibited by analogous procedures.

The author speculates that the present theory will give satisfactory results for short-range forces but rather poor results for long-range forces.

The author is indebted to Professor J. G. Kirkwood and Professor F. P. Buff for several interesting discussions.

THE JOURNAL OF CHEMICAL PHYSICS VOLUME 23, NUMBER 12 DECEMBER, 1955

Note on Theories of Time-Varying Space-Charge Polarization

J. Ross Macdonald
Texas Instruments Incorporated, 6000 Lemmon Avenue, Dallas 9, Texas
(Received March 14, 1955)

The nonlinearity of the differential equations governing space-charge buildup or decay cause the principle of superposition to be inapplicable. Thus, charging and discharging curves should differ and depend strongly on applied voltage when space-charge formation is appreciable. Two approximate theories of space-charge formation and decay are compared, and it is found that one of their main differences is that one has been partly linearized while the other has not. Finally, it is mentioned that of the several theories of the ac response of materials with space charge, only one has not been linearized; hence, it is the only one applicable for applied voltages above about kT/e.

THE partial differential equations governing space-charge polarization buildup or decay in solids and liquids are nonlinear even when some discharge of current carriers occurs at one or both electrodes.[1,2] Because of this voltage-dependent nonlinearity, the equations have not been solved exactly. Another consequence of the nonlinearity is that the principle of superposition does not hold, and differences in the temporal variation of charging and discharging currents may be expected, as well as strong nonlinear dependence on applied voltage.

There are presently available two approximate theories of transient polarization effects. The earlier[2] makes the approximation that the electric field in the medium is homogeneous. This assumption is strictly valid only in the limit of small applied voltages and represents a partial linearization of the basic differential equations. Since the equations are not completely linearized, however, their solutions for the charging and discharging currents still depend nonlinearly on applied voltage. For discharge, a method is briefly discussed of correcting the first-order solution for the originally neglected field inhomogeneity. Of the infinite number of additional terms required to correct exactly for this inhomogeneity, only the first (second-order) term is treated. Further, this correction term itself is only approximated since the field inhomogeneity is once more neglected. Such neglect means that the correction term exhibits only the same type of voltage-dependent nonlinearity as the first-order term. For these reasons, the corrected discharge solution still does not include any nonlinear voltage dependence arising from the field inhomogeneity. Unlike the theory discussed below, the earlier theory takes explicit account of a finite rate of discharge of current carriers at the electrodes.

The second approximate theory is based on somewhat different assumptions. It is possible to solve the nonlinear space-charge equations exactly for completely blocking electrodes under static conditions.[3,4] If a material containing free charges blocked at one or both electrodes is charged (or discharged) through an external resistance much greater than the effective internal resistance of the material, determined by its dimensions and the concentrations and mobilities of the free charges, the charging rate is almost entirely limited by the external resistance. In this case, charging of the material occurs in a quasistatic fashion, and the polarization buildup at any instant may be calculated to good approximation by using the exact static solution corresponding to the actual fraction of the total applied voltage which appears across the electrodes of the material at the given instant.[5] This theory yields both very strong voltage dependence and large differences between charging and discharging current curve shape, in contradistinction to the first theory.

Extensive measurements to test the applicability of

[1] J. R. Macdonald, Phys. Rev. **92**, 4 (1953).
[2] G. Jaffé and C. LeMay, J. Chem. Phys. **21**, 920 (1953).
[3] J. R. Macdonald and M. K. Brachman, J. Chem. Phys. **22**, 1314 (1954).
[4] J. R. Macdonald, J. Chem. Phys. **22**, 1317 (1954).
[5] J. R. Macdonald and M. K. Brachman, Proc. Inst. Radio Engrs. **43**, 71, 741 (1955).

the earlier theory have yielded good agreement between theory and experiment.[2,6] It should be pointed out, however, that such agreement is not a conclusive test of this theory. Curve fitting is accomplished by the adjustment of six or eight disposable constants. Several of these constants refer to the properties of slow current carriers whose presence, in addition to that of faster carriers, must be assumed to obtain agreement between theory and experiment. However, no physical reasons are given for the presence of these slow carriers. The presence of appreciable electrode discharge in these experiments prevents the appearance of very strong nonlinear voltage dependence. Such dependence as does appear is treated, however, by the trial-and-error selection of a single theoretical applied voltage for all curves, no matter what the experimentally applied voltage, and by the introduction of some dependence of the mobility and exponential decay constant of the slow carriers on applied voltage magnitude and polarity. These assumptions seem unjustifiable. In addition, the homogeneous field approximation used is only valid for applied voltages of the order of 0.02 volt or less; the voltage employed for all curve fitting is 0.2 volt, however, and the experimentally applied voltage was often as large as 380 volts.

A careful reading of the earlier theory shows that it is only applied to a thin polarization layer localized near the electrodes. The difference between the large applied voltage and the 0.2 volt assumed across the polarization layer must, therefore, appear across the ohmic bulk resistance of the material, exclusive of the polarization layer. These conclusions thus indicate that the earlier theory does not differ greatly from the second theory in some of its basic assumptions since both theories tacitly or explicitly include the effect of an ohmic resistance in series with a polarization layer, or polarization capacitance.

Although both theories are approximate, the second theory may be expected to describe nonlinear voltage dependence better than the earlier theory and with fewer *ad hoc* assumptions. On modifying the nonlinear theory to include discharge at the electrodes by putting an ohmic resistance R_p in parallel with the nonlinear capacitor, it is found that the previous results and curves[5] hold with the following modifications. First, the final voltage across the capacitor is reduced by the voltage reduction ratio $\gamma=R_p/(R_p+R_s)$, where R_s is the original series resistance. Second, the normalized time unit is changed from $\tau=t/R_sC_\infty$ to $t/\gamma R_sC_\infty$. Since γ will usually be much less than unity, this result shows that charging and discharge occur essentially γ^{-1} times as rapidly as before[7] and that the actual maximum potential across the nonlinear capacitor will usually be much smaller than the applied potential.

The above conclusions are in general qualitative agreement with the data of references 2 and 6. In particular, the large observed ratios between charging and discharging times are consistent with the small values of the final voltage appearing across the polarization layer capacitance which may be inferred by comparing experimental and theoretical charging curve shapes as a function of time and externally applied voltage. An especially satisfying feature of the theory which is observed experimentally is a progressively more rapid current decay in the initial portions of the charging curves as the applied voltage is increased.

The second theory predicts a ratio between initial and final charging currents of $(1-\gamma)^{-1}$. When γ is much less than unity, as expected in the present case, this ratio is itself near unity, in disagreement with experiment. When it is remembered that the second theory was originally developed for a system including an external ohmic resistor in series with the material showing space-charge formation, while it is here applied to such a material alone, the reason for the discrepancy is obvious. The liquid materials used in the experiments were almost insulators. Initially, they may be expected to contain an appreciable concentration of charge-carrying impurities. When an external voltage is first applied, these impurities contribute strongly to the initial current. However, as the impurities are drawn to the electrodes, their influence progressively diminishes and the final current is determined by the large bulk resistance of the intrinsic material in series with the much smaller parallel resistance R_p. Note that the charged impurities may perhaps be identified with the faster ions of the earlier theory and the slower "ions" with the intrinsic conductivity of the material.

Rather wide claims for the applicability of the Jaffé theories of ac polarization effects in electrical conduction have been made.[2,6,8,9]

These theories represented important advances in understanding at the time of their appearance. It is desirable to point out now that (a) they have since been improved by less approximate theories for blocking electrodes[1] and for electrodes with discharge,[10] and that (b) all these theories apply only in the small signal range where the applied ac voltage is less than about 25 millivolts at room temperature. No theory is available of the large signal ac response because of the difficulty of solving the governing equations when their nonlinearity is not neglected. A theory of the differential capacitance of materials exhibiting space-charge polarization in the presence of dc voltages as large as a few volts, has, however, been recently given.[11] This theory is exact and shows strong voltage nonlinearity. It includes the effect of an insulating layer between the electrodes and the bulk material; in electrolytes, the insulating layer may be an ionic hydration layer.

[6] J. A. Rider, J. Chem. Phys. **23**, 61 (1955).
[7] See reference 5 for details of the time variation of charge and discharge currents.
[8] G. Jaffé, Phys. Rev. **85**, 354 (1952).
[9] H. C. Chang and G. Jaffé, J. Chem. Phys. **20**, 1071 (1952).
[10] R. J. Friauf, J. Chem. Phys. **22**, 1329 (1954).
[11] J. R. Macdonald, J. Chem. Phys. **22**, 1857 (1954).

Pyrolysis of Acetone and the Heat of Formation of Acetyl Radicals

M. Szwarc and J. Watson Taylor
Chemistry Department, State University of New York, College of Forestry, Syracuse 10, New York
(Received February 28, 1955)

Pyrolysis of acetone in the presence of an excess of toluene has been studied. The rate of the decomposition has been followed by the rate of formation of CO, the following sequence of reactions being assumed:

$$CH_3\cdot CO\cdot CH_3 \rightarrow CH_3 + CO\cdot CH_3 \quad \text{slow}$$
$$CH_3\cdot CO \rightarrow CH_3 + CO \quad \text{fast}$$

The reactions seem to be first order and unimolecular, the rate constant of the first step being determined as $k = 2.4\cdot 10^{14} \exp(-72\,000/RT)$ sec^{-1}. It is assumed that the observed activation energy may be identified with $CH_3\cdot CO - CH_3$ bond dissociation energy and on this basis the heat of formation of acetyl radical is calculated at -10.8 kcal/mole.

The last result is compared with the findings resulting from investigation of the pyrolyses of diacetyl and of benzyl methyl ketone.

The validity of the toluene carrier technique is reviewed.

THE purpose of this investigation, carried out by using the toluene carrier technique,[1] was to obtain a value for the C—C bond dissociation energy in acetone. Since this dissociation energy is related to the heat of formation of the acetyl radical by the equation

$$D(CH_3CO-CH_3) = \Delta H_f(CH_3CO) + \Delta H_f(CH_3) - \Delta H_f(CH_3COCH_3)$$

its determination provides us with the heat of formation of this radical.

It can safely be assumed that the first step in the decomposition of acetone is its dissociation into a methyl and an acetyl radical,[2]

$$CH_3COCH_3 \rightarrow CH_3 + CH_3CO. \quad (1)$$

At high temperatures the acetyl radical decomposes rapidly into a methyl radical and carbon monoxide,[2]

$$CH_3CO \rightarrow CH_3 + CO. \quad (2)$$

Hence, two moles of methyl radicals and one mole of carbon monoxide would be produced for each mole of decomposed acetone. In the presence of an excess of toluene methyl radicals react according to Eq. (3)

$$CH_3 + PhCH_3 \rightarrow CH_4 + PhCH_2, \quad (3)$$

and it appears therefore that the rate of the initial decomposition may be determined by the rate of formation of methane or by the rate of formation of carbon monoxide. However, since the decomposition of acetone was investigated at comparatively high temperatures (1000–1100°K) a considerable amount of methane is formed by the decomposition of the toluene used as a carrier. This is a complicating feature which makes it undesirable to measure the rate of reaction (1) by the rate of formation of methane. On the other hand, carbon monoxide can result only from the decomposition of acetone, and therefore it was decided to measure the rate of the decomposition by the rate of formation of carbon monoxide.

[1] M. Szwarc, Chem. Rev. **47**, 75 (1950).
[2] E. W. R. Steacie, *Atomic and Free Radical Reactions* (Reinhold Publishing Corporation, New York, 1954), second edition.

EXPERIMENTAL

The pyrolysis of acetone was investigated over the temperature range 993–1101°K, using an apparatus which has been described previously.[3] Reagent grade acetone was fractionated, and the middle fraction was used in the pyrolysis. The toluene was purified by two prepyrolyses followed by careful fractional distillation.

The products of the pyrolysis consisted of permanent gases volatile at liquid nitrogen temperature, gas condensed by liquid nitrogen but volatile at −115°C† (C_2-fraction), and solid or semisolid material (m.p. 35–45°C) which was collected at about −15°C in a simple U-tube.‡ Fractional combustion of the permanent gases over copper oxide showed them to consist of methane and carbon monoxide together with small quantities of hydrogen. The C_2-fraction was shown to be composed of ketene and small quantities of ethane. The former gas was determined by reacting the C_2-fraction with water and titrating the resulting acetic acid, while the amount of the residual gas was taken as equal to the amount of ethane. In this way, it was estimated that the amount of ketene formed was equivalent to 10–15% of the carbon monoxide formed, and the amount of ethane was equivalent to about 3% of that of carbon monoxide.

RESULTS AND DISCUSSION

Assuming that one mole of carbon monoxide is formed for each mole of acetone decomposed we can calculate the percentage decomposition in each experiment from the amount of carbon monoxide collected. The results obtained in this way are listed in Table I and were used for calculating the first-order rate constants given in

[3] M. Szwarc, J. Chem. Phys. **17**, 431 (1949); Proc. Roy. Soc. (London) **A198**, 267 (1949).

† It was found that the volatility of acetone at −78°C is sufficiently high to cause difficulty in the quantitative determination of the "C_2"-fraction if this temperature is used.

‡ The melting point and the evidence obtained from other studies, see, e.g., Blades, Blades, and Steacie, Can. J. Chem. **32**, 298 (1954), shows that this material is composed most probably of dibenzyl and its products of decomposition and isomerization.

TABLE I. Pyrolysis of acetone.

Run	T°K	P toluene mm Hg	P acetone mm Hg	Time of contact sec	Fraction decomp.	k_{CO} sec^{-1}
24	993	11.7	0.41	0.851	0.0275	0.0328
23	994	12.1	0.24	0.778	0.0278	0.0362
26	1006	12.1	0.13	0.854	0.0470	0.0564
25	1007	11.8	0.30	0.834	0.0488	0.0600
27	1009	5.2	0.15	0.913	0.0437	0.0489
28	1009	21.0	0.10	0.813	0.0564	0.0714
8	1019	11.8	0.16	0.402	0.0352	0.0886
12	1020	18.3	0.23	0.335	0.0336	0.102
11	1022	5.7	0.15	0.667	0.0537	0.0828
9	1022	11.8	0.26	0.401	0.0377	0.0959
10	1023	12.1	0.07	0.415	0.0411	0.102
22	1039	11.9	0.15	0.394	0.0712	0.188
29	1051	12.1	0.21	0.400	0.0973	0.256
5	1054	12.1	0.19	0.397	0.112	0.299
7	1054	12.0	0.10	0.389	0.105	0.285
6	1055	12.0	0.20	0.393	0.110	0.297
20	1055	11.9	0.23	1.51	0.354	0.291
4	1058	12.1	0.29	0.400	0.122	0.325
13	1058	8.7	0.12	0.134	0.0382	0.291
16	1059	11.9	0.10	0.126	0.0414	0.335
14	1060	10.2	0.14	0.134	0.0410	0.312
15	1060	9.9	0.10	0.131	0.0403	0.314
30	1060	12.0	0.26	0.399	0.129	0.345
21	1064	12.1	0.12	0.394	0.156	0.430
2	1069	12.1	0.17	0.390	0.165	0.463
18	1100	11.8	0.09	0.120	0.133	1.19
19	1100	11.8	0.11	0.120	0.137	1.23
17	1101	12.0	0.10	0.121	0.134	1.19

the last column. It appears that the first-order rate constants are unaffected by variation of the partial pressure of acetone and of the time of contact. To show this quite clearly the relevant rate constants have been recalculated to common temperatures by short interpolations and these values are given in Table II. In addition, Table II contains similar values showing the effects resulting from variation of the pressure of toluene, and it can be seen that the first-order rate constants increase by about 45% when the pressure of toluene increases by a factor of four. We suggest tentatively that this effect is a manifestation of the inefficiency of the energy transfer process and we shall return to this phenomenon later in the discussion.

The Arrhenius plot of the first-order constants obtained from experiments at constant toluene pressure is shown in Fig. 1. The activation energy was calculated by the least square method to be 72 kcal/mole, the corresponding frequency factor being 2.4×10^{14} sec^{-1}.

At this juncture it is desirable to examine the basic assumptions of our mechanism. It was assumed that the decomposition of acetone under our experimental conditions is represented by Eqs. (1), (2), and (3). However, the presence of ketene and ethane in the products of decomposition indicates that other processes have to be taken into account. The formation of ethane could be accounted for either by reaction (4)

$$CH_3COCH_3 \rightarrow C_2H_6+CO \qquad (4)$$

or by dimerization of methyl radicals. Reaction (4) would represent another source of carbon monoxide and since the rate of formation of this product was taken to be a measure of the rate of reaction (1), the occurrence of reaction (4) would call for an appropriate correction. It is impossible at this stage to refute the occurrence of reaction (4), nevertheless our results show that the maximum error in the rate constant, k_1, resulting from this cause cannot be greater than a few percent as estimated from the amount of ethane formed.

The presence of ketene in the products can be attributed either to reaction (5)

$$CH_3COCH_3 \rightarrow CH_2{:}CO+CH_4 \qquad (5)$$

or to the induced decomposition represented by the sequence of reactions (6) and (7)

$$R+CH_3COCH_3 \rightarrow RH+CH_2COCH_3 \qquad (6)$$

$$CH_2COCH_3 \rightarrow CH_2{:}CO+CH_3, \qquad (7)$$

R denoting a benzyl or a methyl radical. We favor the latter explanation, but whichever process is responsible for the formation of ketene, its occurrence cannot significantly affect our numerical results. This conclusion follows from the fact that the amount of ketene formed amounted to only 10–15% of the carbon monoxide formed and that the total fraction of acetone decomposed was always§ less than 20%. Furthermore, the reactions involved in the formation of ketene do not yield any carbon monoxide.

The mechanism proposed demands that the ratio

TABLE II. Variation of the partial pressure of acetone.

Run	T°K	P acetone mm Hg	$k_{1022°K}$ sec^{-1}
10	1023	0.07	0.0984
8	1019	0.16	0.0984
9	1022	0.26	0.0959
			$k_{1055°K}$
7	1054	0.10	0.294
6	1055	0.20	0.297
4	1058	0.29	0.295

Variation of the time of contact

Run	T°K	Time of contact sec	$k_{1022°K}$
8	1019	0.402	0.0984
26	1006	0.854	0.0989
			$k_{1055°K}$
16	1059	0.126	0.301
6	1055	0.393	0.297
29	1051	0.400	0.292
20	1055	1.51	0.291

Variation of the partial pressure of toluene

Run	T°K	P toluene mm Hg	$k_{1009°K}$
27	1009	5.2	0.0489
26	1006	12.1	0.0626
28	1009	21.0	0.0714
			$k_{1022°K}$
11	1022	5.7	0.0828
8	1019	11.8	0.0984
12	1020	18.3	0.109

§ With the exception of one run where the fraction decomposed was 35%.

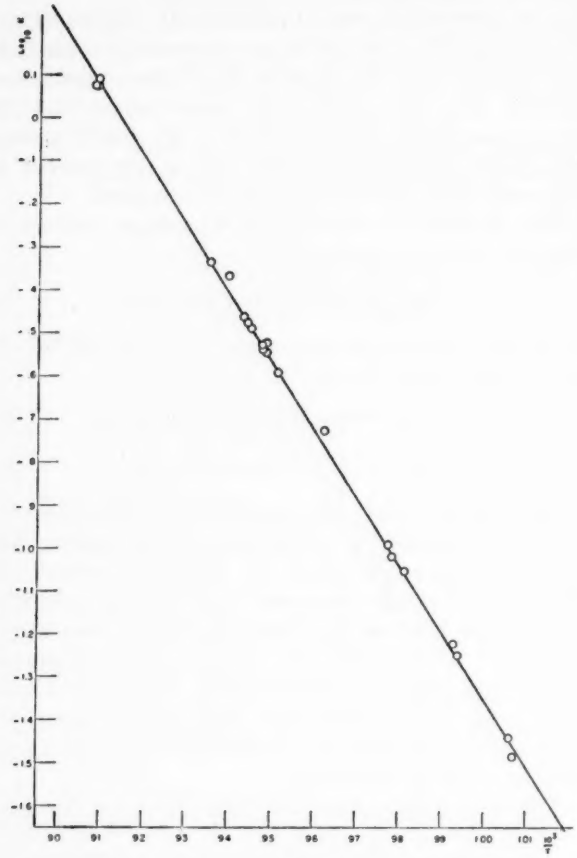

FIG. 1. Pyrolysis of acetone. Points correspond to runs at constant toulene pressure. $E=72.0$ kcal/mole. $\nu=2.4\times10^{14}$ sec^{-1}.

CH_4/CO should be greater than 2.[||] It was found, however, that this ratio was definitely less than 2, as can be seen from the examples quoted in Table III. A closer examination of the conditions prevailing in our experiments shows that methyl radicals may recombine with benzyl radicals. To illustrate this point let us calculate the stationary concentration of methyl radicals assuming that they are formed by reactions (1) and (2) and consumed only by reaction (3). Taking the results of run 5 as typical, we calculate the rate of formation of methyl radicals to be 1.9×10^{-9} moles/cc/sec. From the data of Trotman-Dickenson and Steacie[4] the rate

TABLE III.

Run	T°K	Permanent gases % CO	% H_2	% toluene blank (60% H_2)	CH_4 from acetone CO
5	1054	33.2	11.8	8.3	1.56
7	1054	28.3	17.1	14.4	1.72
21	1064	28.9	18.8	22.4	1.50
17	1101	28.6	21.4	22.1	1.44

|| Participation of the reactions (1), (2), and (3) leads to a value of 2 for this ratio while the reactions responsible for the formation of ketene would form an additional amount of methane but not carbon monoxide.

[4] A. F. Trotman-Dickenson and E. W. R. Steacie, J. Chem. Phys. 19, 329 (1951).

of reaction (3) at 1050°K is 2.5×10^{9} moles/cc/sec, and since the concentration of toluene is about 2×10^{-7} moles/cc, we calculate the stationary concentration of methyl radicals to be 3.8×10^{-12} moles/cc. Assuming that each methyl radical forms a benzyl radical according to Eq. (3), we find that the total amount of benzyl radicals formed during this particular experiment is 8×10^{-10} moles/cc, and in the absence of any reaction consuming them in the hot zone we can take their average concentration as equal to 4×10^{10} moles/cc. Assuming further that the rate constant for the recombination of methyl and benzyl radicals is 10^{12} cc/mole/sec¶ we calculate that about 1.6×10^{-9} moles/cc/sec of methyl radicals combine with benzyl radicals. The latter number, which gives only the order of magnitude, is comparable with the rate of formation of methyl radicals calculated above as 1.9×10^{-9} mole/cc/sec. We conclude, therefore, that it is reasonable to expect that under these conditions a considerable fraction of methyl radicals will be consumed by the reaction

$$CH_3+PhCH_2\rightarrow PhCH_2CH_3. \qquad (8)$$

The experimental results given in Table III show that this fraction is about 25% of originally formed methyl radicals, which implies that reaction (8) would result in a "loss" of approximately 50% of originally expected benzyl radicals. This arises from the fact that every

TABLE IV.

Run	T°K	Dibenzyl from acetone[a] CO
22	1039	0.58
20	1055	0.41

[a] The values are corrected for dibenzyl formed from the pyrolysis of toluene.

methyl radical which consumes one benzyl radical by reaction (8), is thereby no longer available to form a benzyl radical by reaction (3). The results given in Table IV do indeed show that the amount of "dibenzyl" collected was roughly only 50% of that expected, which therefore provides further support for the occurrence of reaction (8).

It seems from the foregoing discussion that we are fully justified to identify the rate of formation of carbon monoxide with the rate of reaction (1). The observed activation energy of 72 kcal/mole therefore represents the activation energy of this reaction, and probably it can be identified with the $CH_3-CO\cdot CH_3$ bond dissociation energy. However, since the calculated rate constant increases slightly with increasing total pressure (see Table II), it is possible that the rate of energy transfer is not sufficient to maintain the "true" rate of

¶ The rate constant for the recombination of a benzyl radical with a methyl radical is probably somewhat lower than that for the mutual recombination of methyl radicals and, hence, the assumed value of 10^{12} seems to be reasonable.

the unimolecular decomposition. Such an effect is observed in decompositions of comparatively small molecules,[5] and it is plausible that it might be expected in the case of acetone. If this is the case, then the true bond dissociation energy might be slightly higher than the observed value.

Taking $D(CH_3-CO\cdot CH_3)=72$ kcal/mole, we calculate the heat of formation of the acetyl radical as

$$\Delta H_f(CH_3CO)=72-\Delta H_f(CH_3)+\Delta H_f(CH_3COCH_3)$$
$$=72-31+(-51.79)=-10.8 \text{ kcal/mole.}$$

Using the data of Roberts and Skinner[6] this value gives the following values for the dissociation energies of bonds of the type CH_3CO-X.

X	C_2H_5	nC_3H_7	sec-C_3H_7	CHO	H	OH	NH_2	Cl	Br	I
$D(CH_3CO-X)$	72.7	73.0	70.0	54.6	81.0	97.7	94.1	77.2	62.5	46.5

Furthermore, using the equation

$$D(CH_3-CO)=\Delta H_f(CH_3)+\Delta H_f(CO)-\Delta H_f(CH_3\cdot CO)$$

we calculate $D(CH_3-CO)$ as about 17 kcal/mole. This would indicate that the activation energy of the reaction

$$CH_3CO\rightarrow CH_3+CO$$

is certainly higher than 20 kcal/mole. See in this connection McDowell and Thomas, J. Chem. Soc. 2208 and 2217 (1949); and Porter and Benson, J. Am. Chem. Soc. **75**, 2773 (1953).

FURTHER DISCUSSION OF THE HEAT OF FORMATION OF ACETYL RADICALS

Further information on the heat of formation of acetyl radicals may be obtained from studies of pyrolyses of diacetyl and of benzyl-methyl ketone. It is probable that diacetyl should decompose into two acetyl radicals and benzyl-methyl ketone into an acetyl and a benzyl radical.

The pyrolyses of these compounds were studied by Murawski and Szwarc and then again by Taylor and Szwarc [see, e.g., J. Watson Taylor, Ph.D. thesis, Manchester, (1953)]. It appears that the decomposition is unimolecular and that the rate of decomposition could be measured by the rate of formation of CO. However, these investigations lead to values for activation energies which seem to be too high, and also to exceedingly high-frequency factors, namely:

for diacetyl $\nu=5.10^{15}$ sec^{-1}, $E_a=66$ kcal/mole

for benzyl-methyl ketone $\nu=9.10^{15}$ sec^{-1}, $E_a=68$ kcal/mole.

On the other hand, using the values for heats of formation of diacetyl and of benzyl methyl ketone as obtained by Nicholson, Szwarc, and Taylor[7]; we derive the following values for $D(CH_3\cdot CO-CO\cdot CH_3)$ and $D(CH_3CO-CH_2\cdot C_6H_5)$ based on $\Delta H_f(CH_3CO)=-10.8$ kcal/mole.

$$D(CH_3\cdot CO-CO\cdot CH_3)=56.6 \text{ kcal/mole}$$
$$D(CH_3CO-CH_2\cdot C_6H_5)\sim 50 \text{ kcal/mole.}$$

If the foregoing values are assumed to be identical with the "correct" activation energies of the respective dissociation processes, then one deduces from the observed rate constants the following values for the respective frequency factors:

for diacetyl $\nu=5.10^{13}$ sec^{-1}

for benzyl-methyl ketone $\nu\sim 10^{12}$ sec^{-1}.

It seems to us that the latter frequency factors are more reasonable than the experimental one.

It is impossible, at this stage, to express any final opinion on these discrepancies. However, it is our feeling that the value obtained from the investigation of pyrolysis of acetone is the most reliable, and that some side reactions vitiate the activation energies obtained from investigations of the pyrolyses of diacetyl and of benzyl-methyl ketone.

VALIDITY OF TOLUENE CARRIER TECHNIQUE

It is desirable to reconsider at this stage the validity of the toluene carrier technique. Its applicability is limited to those cases for which the reaction $C_6H_5\cdot CH_3+R\rightarrow C_6H_5\cdot CH_2+RH$ proceeds very rapidly, and competes efficiently with the recombination reactions, such as $C_6H_5\cdot CH_2+R\rightarrow C_6H_5\cdot CH_2\cdot R$ or $R+R\rightarrow R_2$. Such a situation is attained when R is very reactive, toluene is present in a great excess, and the concentration of benzyl radicals is low. The last condition implies that the number of R radicals produced per cc is low as compared with the concentration of toluene.

It seems that all these conditions are essentially met in the pyrolyses of organic bromides and chlorides. It appears that reactions involving Cl or Br atoms do not demand a low steric factor (see, e.g., reference 2, pages 707–708), and since the activation energies for the reactions

$$C_6H_5\cdot CH_3+Cl\rightarrow C_6H_5\cdot CH_2+HCl$$
$$C_6H_5\cdot CH_3+Br\rightarrow C_6H_5\cdot CH_2+HBr$$

are comparatively low, the energy restriction is not too great at high temperatures of the pyrolysis.

On the other hand, the situation is very different in the case of methyl radicals. It appears (see reference 2, pages 497, 568) that the steric factor is very low for the reaction $C_6H_5\cdot CH_3+CH_3\rightarrow C_6H_5\cdot CH_2+CH_4$, and consequently, toluene is not a sufficiently effective trap for methyl radicals when the concentration of radicals

[5] See, e.g., F. Kern and W. D. Walters, Proc. Natl. Acad. Sci. 38, 937 (1952); and C. N. Hinshelwood, *The Kinetics of Chemical Change* (Oxford University Press, New York, 1940).

[6] J. S. Roberts and H. A. Skinner, Trans. Faraday Soc. **45**, 339 (1949).

[7] Nicholson, Szwarc, and Taylor, J. Chem. Soc. 2769 (1954).

present in the system is relatively high. Such a difficulty has been noted recently in a few investigations.[8,9]

However, if the primarily formed radical decomposes rapidly into a smaller radical and a stable molecule, then the toluene carrier technique can be applied profitably, since the rate of the reaction can be measured easily by the rate of formation of the stable species. Such a situation is encountered in the present work and, e.g., in the pyrolysis of *n*-butylbenzene.[8]

[8] C. H. Leigh and M. Szwarc, J. Chem. Phys. **20**, 407 (1952).
[9] M. T. Jaquiss, thesis, Manchester (1953).

ACKNOWLEDGMENTS

The financial support of this investigation by the National Science Foundation is gratefully acknowledged.

Note added in proof.—The pyrolysis of acetone has been investigated recently by D. Clark and H. O. Pritchard. Their values for activation energy and frequency factor are 71.0 kcal/mole and $1.4 \cdot 10^{14}$ sec^{-1} respectively. The agreement between our and their finding is thus very satisfactory, (D. Clark and H. O. Pritchard, unpublished results).

THE JOURNAL OF CHEMICAL PHYSICS VOLUME 23, NUMBER 12 DECEMBER, 1955

Statistical Computation of Mean Dimensions of Macromolecules. III*

F. T. WALL, L. A. HILLER, JR., AND W. F. ATCHISON
Noyes Chemical Laboratory, University of Illinois, Urbana, Illinois

(Received March 7, 1955)

Random walks subject to the excluded volume effect have been generated by means of a high-speed electronic digital computer for a number of different three-dimensional lattices and for one four-dimensional lattice. In contrast to results obtained for two-dimensional lattices discussed in an earlier article, the present results are compatible with the view that the ratio, $\langle r_n^2 \rangle_{Av}/n$, where $\langle r_n^2 \rangle_{Av}$ is the mean square length of permissible walks of n steps, converges as $n \to \infty$ for three-dimensional and four-dimensional lattices. This conclusion is obtained through an analysis of an appropriate difference equation employing the methods developed earlier.

Convergence to a limiting value of the critical ratio mentioned above appears relatively rapid for the four-dimensional lattice investigated. Possible convergence for the three-dimensional lattices that have been investigated to date appears to be very slow. Thus, it appears that the limiting behavior will not be approached experimentally for values of n within the usual range of the degrees of polymerization of real polymer molecules.

INTRODUCTION

IN two earlier publications,[1,2] we described the generation of nonintersecting random walks by means of a high-speed electronic digital computer. As noted therein, such walks can be used as models for linear coiling-type polymer molecules subject to the volume exclusion which arises because no two atoms can occupy the same site in space. The background of this problem has been discussed in the articles referred to above and has also been recently reviewed.[3]

Other recent work on the use of numerical computations to analyze the nonintersecting random walk problem includes the work of Rosenbluth and Rosenbluth,[4] King,[5] and Teramoto and Kurata.[6]

The present paper is a continuation of an investigation of the nonintersecting random walk problem using a digital computer as a quasi-experimental instrument for generating data. The object of this investigation is to determine the dependence of the mean square end-to-end separation of a polymer chain, $\langle r_n^2 \rangle_{Av}$, upon n, the number of links in the chain, with particular reference to the limiting behavior of the ratio, $\langle r_n^2 \rangle_{Av}/n$, as n becomes large. At the present time, it is not known for sure whether this ratio converges or diverges as $n \to \infty$ for the three-dimensional problem. The question concerning convergence of this ratio constitutes the heart of the problem, and the answer to this question could have an important effect on the theories used to describe the properties of linear macromolecules in solution.

In the article referred to in reference 1, random walks subject to volume exclusion in two different three-dimensional lattices—a four-choice simple cubic lattice and a three-choice tetrahedral lattice—were examined. It was found that the behavior of $\langle r_n^2 \rangle_{Av}/n$ could not be directly observed for large n because so many of the samples were lost with each successive step as a result of loop closures. The decrease in samples becomes very nearly an exponential function of n, thus making im-

* The work discussed herein was performed as a part of the research project sponsored by the Federal Facilities Corporation, Office of Synthetic Rubber, in connection with the government synthetic rubber program.
[1] Wall, Hiller, and Wheeler, J. Chem. Phys. **22**, 1036 (1954).
[2] Wall, Hiller, and Atchison, J. Chem. Phys. **23**, 913 (1955).
[3] F. T. Wall and L. A. Hiller, Jr., Ann. Rev. Phys. Chem. **5**, 267 (1954).
[4] M. N. Rosenbluth and A. W. Rosenbluth, J. Chem. Phys. **23**, 356 (1955).
[5] G. W. King, Natl. Bur. Standards, Appl. Math. Ser. AMS 12 (June 11, 1951).
[6] E. Teramoto and M. Kurata, Kyoto University, private communication.

practical the generation of sufficient samples to obtain reliable values for $\langle r_n^2\rangle_{Av}$ for n greater than about 80 to 100, depending on the lattice. Because of this, one can fit the available experimental values for $\langle r_n^2\rangle_{Av}$ with equal success to equations predicting either convergence or divergence of the ratio, $\langle r_n^2\rangle_{Av}/n$.

The number of ring closures of each size, k, was also obtained for the simple cubic lattice. Except for loops closed back to the origin, the probabilities for closure of rings of definite size were found to be quite independent of the total number of steps. These probabilities also appeared to be approximately inversely proportional to the square of the ring size.

As shown in the second reference,[2] it is possible to derive a significant difference equation for random walks subject to volume exclusion. Thus, if p^* is the probability for a walk failing, i.e., for meeting itself for the first time at the nth step, and if $\langle R_n^2\rangle_{Av}$ is the mean square length of such walks measured from the origin to this point of meeting and if $\langle r_n^2\rangle_{Av}$ is the mean square length of all successful walks, then assuming unit step lengths, the following exact difference equation can be derived whenever the sum of the trial vectors for a new step is zero:

$$p^*\langle R_n^2\rangle_{Av}+(1-p^*)\langle r_n^2\rangle_{Av}=\langle r_{n-1}^2\rangle_{Av}+1. \tag{1}$$

The probability, p^*, of failure, is the sum of probabilities, p_k^*, for ring closures of each possible size, *viz.*

$$p^*=\sum_k p_k^*. \tag{2}$$

This is correct provided the individual probabilities are mutually independent and also independent of n. We can then write:

$$p^*\langle R_n^2\rangle_{Av}=\sum_k p_k^*\langle {}_kR_n^2\rangle_{Av}, \tag{3}$$

where $\langle {}_kR_n^2\rangle_{Av}$ is the mean square length of failures resulting from ring closures of size k. Combining the above equations, we obtain the following:

$$\langle r_n^2\rangle_{Av}=\langle r_{n-1}^2\rangle_{Av}+1+\sum_k p_k^*\{\langle r_n^2\rangle_{Av}-\langle {}_kR_n^2\rangle_{Av}\}. \tag{4}$$

To use this equation we now require values for $\langle {}_kR_n^2\rangle_{Av}$. Since failure distances were not included in the results obtained from the original digital computer codes which were described in the first article,[1] it was necessary to rewrite the codes to obtain this information. At the same time, the investigation was extended to cover nonintersecting random walks for a variety of additional lattices. The following data were obtained: (a) the total number of samples, N_n, remaining after step n, (b) the mean square lengths of permissible walks, $\langle r_n^2\rangle_{Av}$, (c) the number of single ring closures of each possible size, k, at each step, n, and (d) the mean square distances of these ring closures from the point of closure back to the origin.

The results obtained in four different two-dimensional lattices were considered previously.[2] In general, these results were quite similar to those obtained earlier for three-dimensional lattices, except that the numerical values of the significant parameters were found to depend upon the lattice. In addition, however, it was possible to relate the mean square distances of single ring closures to the mean square lengths of successful walks. By plotting $\langle {}_kR_n^2\rangle_{Av}$ *versus* k, straight lines were obtained except in the region where $k=n$. When these straight lines were extrapolated to $k=0$, the limiting values so obtained agreed quite well with the mean square lengths for successful walks. It was possible, therefore, to express the relationship between $\langle {}_kR_n^2\rangle_{Av}$ and $\langle r_n^2\rangle_{Av}$ in the following way:

$$\langle {}_kR_n^2\rangle_{Av}\leqslant\langle r_n^2\rangle_{Av}[1-k/n]. \tag{5}$$

Substituting the upper limit of $\langle {}_kR_n^2\rangle_{Av}$, as given in Eq. (5), into Eq. (4), we find that

$$\langle r_n^2\rangle_{Av}=\langle r_{n-1}^2\rangle_{Av}+1+\langle r_n^2\rangle_{Av}\cdot A_n/n, \tag{6}$$

where

$$A_n=\sum_k kp_k^*. \tag{7}$$

If we assume for large n that A_n approaches a limit, A, then Eq. (6) can be converted into the following differential equation:

$$d\langle r_n^2\rangle_{Av}/dn=1+A\cdot\langle r_n^2\rangle_{Av}/n. \tag{8}$$

This equation can be readily integrated to yield the following solutions:

$$\langle r_n^2\rangle_{Av}=n/(1-A)+Cn^A, \quad (A\neq 1), \tag{9}$$

and

$$\langle r_n^2\rangle_{Av}=n\ln n+Cn, \quad (A=1), \tag{10}$$

where C is an integration constant.

It can be seen from Eqs. (9) and (10) that the parameter, A, is of critical importance in determining whether the quotient, $\langle r_n^2\rangle_{Av}/n$, converges as $n\to\infty$. If $0\leqslant A<1$, the quotient converges whereas if $1\leqslant A\leqslant 2$, the quotient diverges. A cannot exceed 2 since $\langle r_n^2\rangle_{Av}$ can never exceed n^2, the length of a completely stretched out polymer chain.

In the case of the two-dimensional lattices, we were unable to ascertain the exact dependence of p_k^* on k, so indirect methods employing attrition data were used to determine a value of A for each lattice. This parameter was found to be greater than unity for all the two-dimensional lattices investigated with the possible exception of the two-choice square lattice. This indicates that the ratio, $\langle r_n^2\rangle_{Av}/n$, as a general rule diverges in two dimensions, but it must not be supposed that the behavior of the ratio depends *only* on the number of dimensions.

Experimental data for lattices in three and four dimensions similar to the above have also been obtained with the ILLIAC digital computer. These lattices are the following: the four-choice orthogonal simple cubic lattice, the five-choice simple cubic lattice, the three-choice tetrahedral or diamond lattice, and the six-

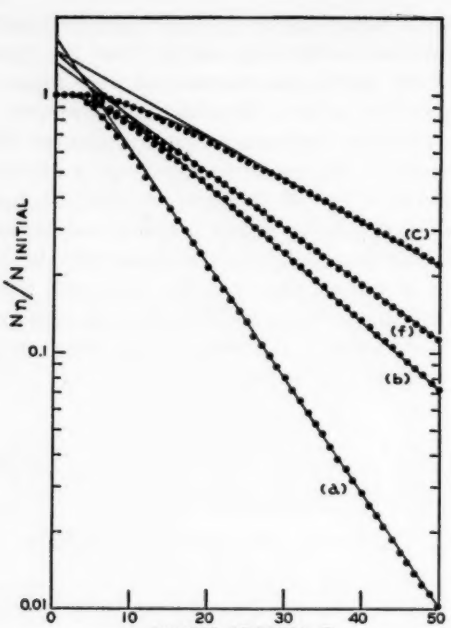

FIG. 1. Attrition in three- and four-dimensional lattices; (a) four-choice simple cubic lattice, (b) five-choice simple cubic lattice, (c) three-choice tetrahedral lattice, (f) six-choice four-dimensional 90° lattice.

choice 90° orthogonal lattice in four dimensions analogous to the four-choice orthogonal cubic lattice. As in the case of the two-dimensional lattices, at least 200 000 walks were completed in each lattice and all walks reaching the fiftieth step were terminated at that point.

In addition to the above, simplified codes were written for two somewhat more complex three-dimensional lattices, namely, the seven-choice body-centered cubic lattice and the eleven-choice face-centered cubic lattice. In the codes for these lattices, n was permitted to go as high as 100, while the calculation of the mean square lengths of ring closures was omitted, for by the time these codes were written, the relationship between failure lengths and success lengths had been adequately established.

ATTRITION AND PROBABILITIES FOR SINGLE RING CLOSURE

Except for small values of n, the attrition or sample loss resulting from the return of random walks to previously occupied lattice sites has been characterized in all lattices so far examined by the expression[1,2]

$$N_n = N_0 \exp(-\lambda n), \tag{11}$$

where N_0 is a constant. N_0 is obtained by extrapolation to $n=0$ of the straight-line portions of plots of $\log N_n$ *versus* n; it is not the same as N_{initial}, the actual number of starting samples. The parameter, λ, which we call the attrition constant, is obtained from the slopes of the aforementioned straight lines for values of n greater than about 20. In Fig. 1, there are plotted attrition results obtained from computer codes in which n was limited to a maximum value of 50. The results from the remaining computer codes are shown in Fig. 2. Significant attrition parameters are given in Table I. Values for $1-\exp(-\lambda)$ represent the fractions of samples lost at each step for walks in each lattice. The "half-walk," $n_{\frac{1}{2}}$, is the number of steps required to reduce the number of samples by one-half.

As previously noted,[2] all trial step vectors must add up to zero to render valid the simple difference equation, Eq. (1). Except for the four-choice simple cubic lattice and the six-choice four-dimensional lattice, this condition requires recognition of the possibility of trying to step backwards. The values for λ obtained from the machine data do not take into consideration this backward step, which was ruled out in the programming, but they are easily recalculated to give corrected values, λ^*. These are also given in Table I.

Experimental probabilities for single ring closures are obtained from the numbers of rings formed of k steps each. An "initial" probability, p_k^0, is observed for ring closures back to the origin; this is distinctly greater than the "limiting" probability, p_k, found for the same ring size for rings closed at lattice points other than the origin. Furthermore, it is also observed that plots of $\log p_k^0$ and $\log p_k$ against $\log k$ appear to be linear except for small values of k. Thus, if $\log p_k$ is plotted *versus* $\log k$ as shown in Fig. 3, it is seen that, except for the four-dimensional lattice, the probability for single ring closure once again appears to be proportional to the

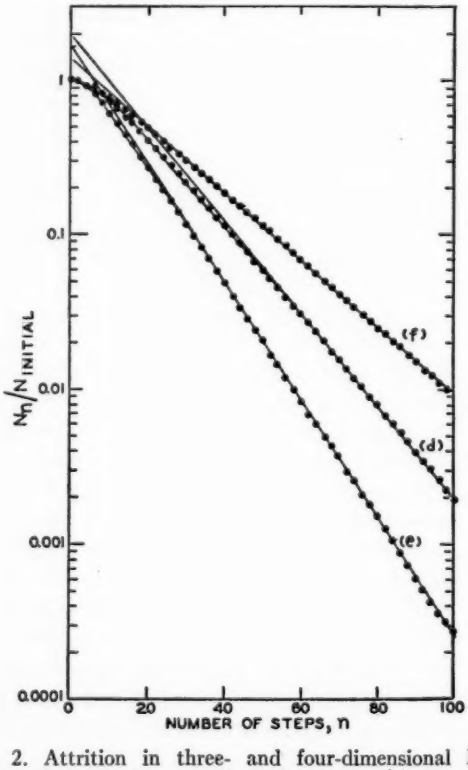

FIG. 2. Attrition in three- and four-dimensional lattices; (d) seven-choice body-centered cubic lattice, (e) eleven-choice face-centered cubic lattice, (f) six-choice four-dimensional 90° lattice.

inverse square of the ring size except for the smaller rings.† In Fig. 3, ring closure probabilities for the large rings ($k>14$) have been averaged for all the three-dimensional lattices except the eleven-choice face-centered cubic lattice in which rings of an odd as well as an even number of sides can be formed. Within the limits of experimental error, the extrapolated intercepts on the ordinate axis in Fig. 3 and for a similar plot of $\log p_k^0$ *versus* $\log k$ are found to be $c=0.35$ and $c^0=0.50$, respectively, for all the three-dimensional lattices investigated except the one already noted. For the four-dimensional lattice, $c=0.40$ and $c^0=0.53$. The ratio of these intercepts, c^0/c, is used in the calculation of A.

As in the case of attrition parameters, it is necessary to correct the experimental values for ring closure probabilities whenever the possibility of trying a backward step is required to maintain angular symmetry. For example, ring closure probabilities in the five-choice simple cubic lattice are reduced by the factor, 5/6. This gives the "corrected" probabilities, p_k^{0*} and p_k^*, required in the theoretical interpretation of nonintersecting random walks.

TABLE I. Attrition in three- and four-dimensional lattices.

Lattice	λ	$1-\exp(-\lambda)$	$n_{\frac{1}{2}}$	N_0/N_{initial}
(a) 4-choice simple cubic	0.103	0.098	6.7	1.7
(b) 5-choice simple cubic	0.061	0.059	11.4	1.5
(c) 3-choice tetrahedral	0.039	0.038	17.2	1.5
(d) 7-choice body-centered cubic	0.070	0.067	9.9	2.0
(e) 11-choice face-centered cubic	0.086	0.083	8.0	1.7
(f) 6-choice 90° four-dimensional	0.051	0.049	14.0	1.3
Attrition corrected for backward step				
	λ^*	$1-\exp(-\lambda)^*$	$n_{\frac{1}{2}}^*$	$(N_0/N_{\text{initial}})^*$
(a) 4-choice simple cubic	0.103	0.098	6.7	1.7
(b) 6-choice simple cubic	0.244	0.216	2.8	2.0
(c) 4-choice tetrahedral	0.327	0.279	2.1	2.0
(d) 8-choice body-centered cubic	0.203	0.184	3.4	2.0
(e) 12-choice face-centered cubic	0.184	0.169	3.8	2.0
(f) 6-choice 90° four-dimensional	0.051	0.049	14.0	1.3

It was pointed out previously[2] that an exact inverse dependence of ring closure probability on the square of the ring size is incompatible with the theory we have developed thus far if Eq. (5) is assumed to be valid. (If the inverse square relationship held, the limit of A_n would not merely be greater than 2; it would not exist.) As will be shown below, Eq. (5) represents an interpolation between fixed points while the results shown in Fig. 3 must be extrapolated as k increases beyond the experimental range. Since interpolation is to be preferred to extrapolation and since log-log plots are inherently poor for extrapolation, it is expedient to assume at present that either these probabilities for ring closure are inversely proportional to $k^{2+\epsilon}$, where ϵ is a

† A more detailed examination of ring closure probabilities in the two-dimensional lattices discussed in the previous article[2] indicates that the inverse square relationship also characterizes adequately all these data in the experimental range. A possible proportionality of p_k to $k^{-2.2}$ in the five-choice 60° lattice was indicated because the plot for this lattice is curved much like the plot for the eleven-choice face-centered cubic lattice shown in Fig. 3 and because acceptable values for p_k were obtained for the five-choice 60° lattice only through $k=25$.

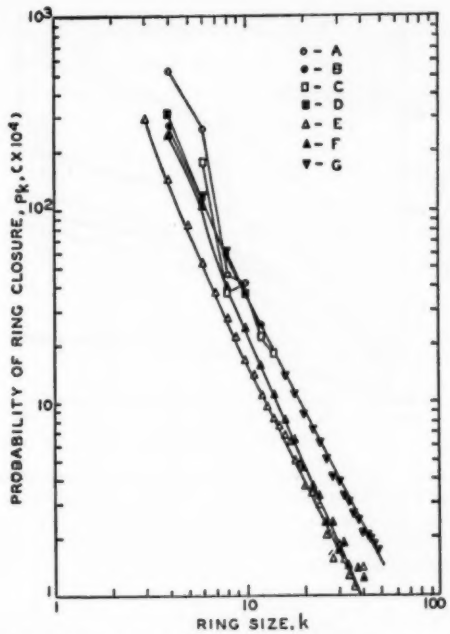

FIG. 3. Log-log plot of limiting probabilities for single ring closure versus ring size; (a) four-choice simple cubic lattice, (b) five-choice simple cubic lattice, (c) three-choice tetrahedral lattice, (d) seven-choice body-centered cubic lattice, (e) eleven-choice face-centered cubic lattice, (f) six-choice four-dimensional 90° lattice, (g) "average" values for three-dimensional lattices (a), (b), (c), and (d) for $k>14$.

positive number of such magnitude that $\sum_k^\infty k p_k^* \leqslant 2$, or that the plot of $\log p_k$ *versus* $\log k$ does not remain linear as k becomes large. The experimental data limit the determination of ring closure probabilities to $k \leqslant 48$. For these probabilities, the best approximate picture of the dependence of ring closure probability upon ring size still appears to be that shown in Fig. 3.

Finally it should be noted that the probabilities for single ring closure are related to attrition as follows:

$$\lim_{n\to\infty} \sum_k^n p_k = 1-\exp(-\lambda). \tag{12}$$

This means that Eq. (11) is really valid only when $n\to\infty$, because new terms are always being added to the summation, $\sum_k^n p_k$. The plots in Figs. 1 and 2 are not truly linear and, as will be shown, small corrections have to be applied to the experimentally determined values for λ before these values can be used in the calculation of the parameter, A.

MEAN SQUARE LENGTHS OF PERMISSIBLE RANDOM WALKS

Mean square lengths of permissible random walks are plotted through $n=50$ in the form of $\langle r_n^2\rangle_N/n$ *versus* n in Fig. 4. It is observed that the departures of $\langle r_n^2\rangle_N/n$ from unity are least in the two orthogonal lattices. This is in agreement with the observation that in various two-dimensional lattices the limit of the ratio, $\langle r_n^2\rangle_N/n$, is nearest to convergence for the two-choice square lattice.[2]

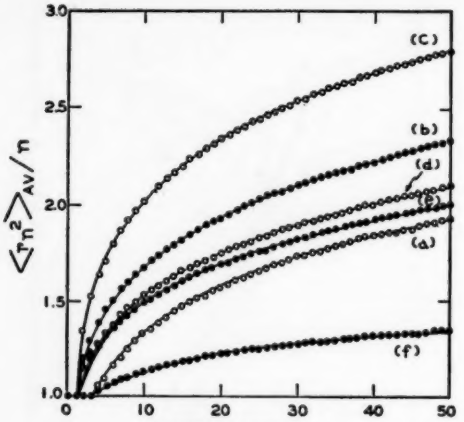

FIG. 4. Plot of $\langle r_n^2\rangle_{Av}/n$ *versus* n for three- and four-dimensional lattices; (a) four-choice simple cubic lattice, (b) five-chcice simple cubic lattice, (c) three-choice tetrahedral lattice, (d) seven-choice body-centered cubic lattice, (e) eleven-choice face-centered cubic lattice, (f) six-choice four-dimensional 90° lattice.

The plot of $\langle r_n^2\rangle_{Av}/n$ *versus* n for the six-choice four-dimensional lattice appeared fairly flat at $n=50$. Of all the lattices investigated, this four-dimensional lattice is the one in which this quotient is most likely to converge. This suggested the possibility of generating longer random walks in this particular lattice to see whether, for once, the limiting behavior of $\langle r_n^2\rangle_{Av}/n$ could be directly observed. Consequently, new data for the six-choice 90° four-dimensional lattice were collected with the ILLIAC computer. This time only values of $\langle r_n^2\rangle_{Av}$ were saved, and even though more than 200 000 walks were completed, the longest walk survived to only 235 steps. These results are shown in Fig. 5. It is seen immediately that even in this lattice, with its relatively low rate of attrition, it is not possible to generate sufficient samples to test directly for convergence of $\langle r_n^2\rangle_{Av}/n$. The results are good up to $n=90$, perhaps acceptable to $n=110$, but after that the reduction in the number of samples induces serious scattering of the data.

MEAN SQUARE LENGTHS OF RING CLOSURES

When mean square distances of ring closures are plotted *versus* ring size, straight-lines may be drawn through all points except those in the region where $k=n$. The intercepts of these lines at $k=0$ are the mean square distances for successful walks. A typical plot is shown in Fig. 6, where data for the five-choice simple cubic lattice are plotted in accord with Eq. (5).

Assuming the equality to be valid, Eq. (5) can be rearranged to the form

$$\langle {}_kR_n^2\rangle_{Av}/\langle r_n^2\rangle_{Av}=1-mk/n, \tag{13}$$

where a parameter, m, has been inserted to determine the slope of the linear portion of the curve. From Eq. (13) it is seen that straight lines should be observed if $\langle {}_kR_n^2\rangle_{Av}/\langle r_n^2\rangle_{Av}$ is plotted either against k or against $1/n$ or against their product. For example, if $\langle {}_8R_n^2\rangle_{Av}/\langle r_n^2\rangle_{Av}$ is plotted against $8/n$ for eight-sided rings in the five-choice simple cubic lattice, as in Fig. 7, it is seen that a straight line can be drawn through the experimental points from an ordinate value of unity at $8/n=0$ down toward the horizontal axis. It is advantageous to plot the data in this way because the best experimental data are available for small values of n, which correspond to

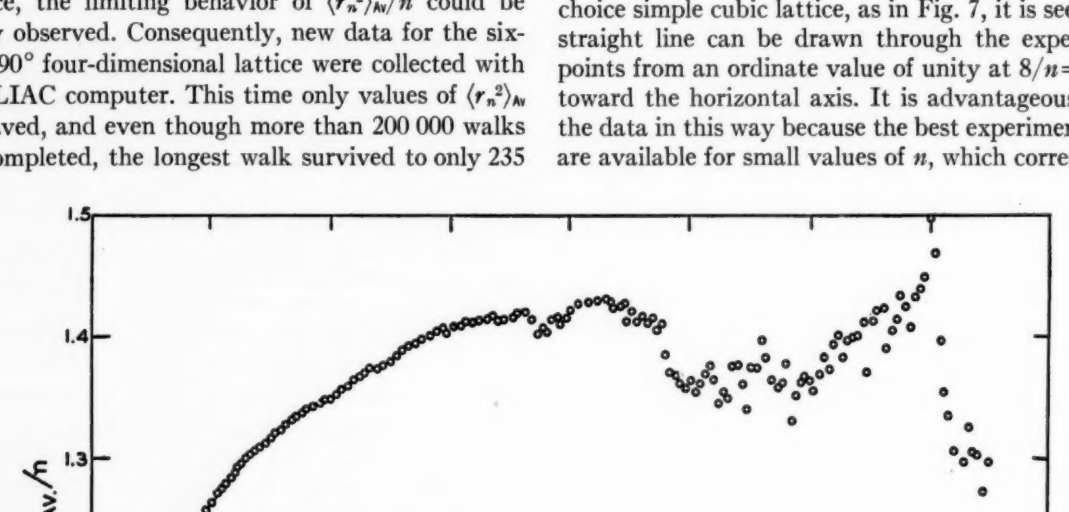

FIG. 5. Plot of $\langle r_n^2\rangle_{Av}/n$ *versus* n to large values of n for the six-choice four-dimensional 90° lattice.

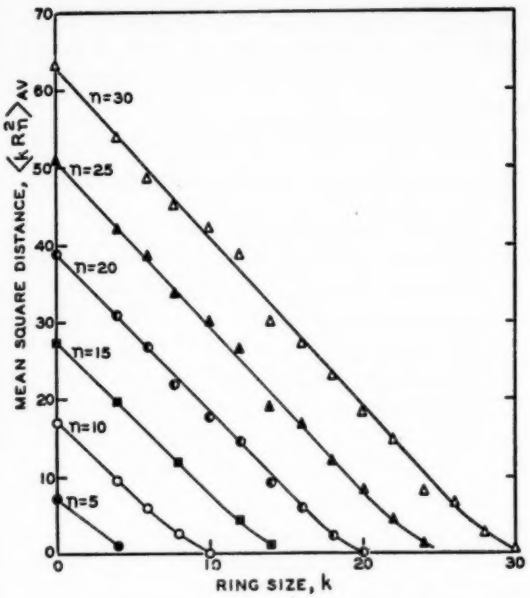

FIG. 6. Plot of mean square distances of single ring closures, $\langle {}_kR_n^2\rangle_{Av}$ *versus* ring size, k, for selected values of n. Data apply to the five-choice simple cubic lattice.

large values of the abscissa. The slopes, m, of the plots can also be determined. There is a little indication that m decreases slowly as k increases but it is impossible with the present data to determine precisely the nature of this trend. If such a trend does exist, then plots of $\langle {}_kR_n^2\rangle_{Av}/\langle r_n^2\rangle_{Av}$ *versus* k, with n held constant, cannot be perfectly linear but must curve very slightly as k is varied. This curvature, however, is too small to be detected from the present data.

In deriving Eq. (9), which relates $\langle r_n^2\rangle_{Av}$ to n, it was assumed that deviations from true linearity shown in Fig. 7 tend to become negligible or that the equality in Eq. (5) becomes exact as $n\to\infty$. This simplification tends to minimize possible divergence of the quotient, $\langle r_n^2\rangle_{Av}/n$, since it leads to the calculation of lower limiting values. If the quotient, $\langle r_n^2\rangle_{Av}/n$, appears to converge, this approximation is unsatisfactory, for under these conditions an estimate of upper, not lower, limiting values for $\langle r_n^2\rangle_{Av}$ is desired. Actually, the convergence or divergence of the ratio, $\langle r_n^2\rangle_{Av}/n$, is not very sensitive to the exact mathematical form assumed for the relationship between mean square lengths of failures and successful walks. It might, for example, be not too unreasonable to assume that $\langle {}_kR_n^2\rangle_{Av}$ is the same as $\langle r_{n-k}^2\rangle_{Av}$. This would be equivalent to saying that the mean square lengths of the failures resulting from loops of k steps after a total of n steps are the same as the mean square lengths of successful walks realized at $n-k$ steps. Our experimental findings show that $\langle {}_kR_n^2\rangle_{Av} \geqslant \langle r_{n-k}^2\rangle_{Av}$. Hence, if we assume for the failures too small values, such as $\langle r_{n-k}^2\rangle_{Av}$, we tend by reason of Eq. (4) to calculate too large values for the successes. Therefore, if we can find a condition for convergence of $\langle r_n^2\rangle_{Av}/n$ under this more drastic assumption concerning mean square lengths of failures, we can be reasonably sure that the same condition would be sufficient for convergence under the actual state of affairs. Making the assumption that $\langle {}_kR_n^2\rangle_{Av}=\langle r_{n-k}^2\rangle_{Av}$, we find that

$$p^*\langle R_n^2\rangle_{Av}=\sum_k p_k^*\langle {}_kR_n^2\rangle_{Av}=\sum_k p_k^*\langle r_{n-k}^2\rangle_{Av}. \quad (14)$$

If this relationship is substituted into the difference equation for nonintersecting random walks, Eq. (1), the following is obtained:

$$\langle r_n^2\rangle_{Av}=\{\langle r_{n-1}^2\rangle_{Av}+1-\sum_k p_k^*\langle r_{n-k}^2\rangle_{Av}\}/(1-p^*) \quad (15)$$

or:

$$\langle r_n^2\rangle_{Av}=\langle r_{n-1}^2\rangle_{Av}+\{1+\sum_k p_k^*[\langle r_{n-1}^2\rangle_{Av} -\langle r_{n-k}^2\rangle_{Av}]\}/(1-p^*). \quad (16)$$

Let us now determine the conditions under which Eq. (16) has an asymptotic solution of the following form:

$$\langle r_n^2\rangle_{Av}=Kn. \quad (17)$$

If Eq. (17) is substituted into Eq. (16), and the result rearranged, we find that such a solution exists provided

$$K=\frac{1}{1-\sum_k kp_k^*}=\frac{1}{1-A}. \quad (18)$$

This is the same solution for the $\lim_{n\to\infty}\langle r_n^2\rangle_{Av}/n$ that can be obtained from Eq. (9) for $A>1$. Hence it is evident that Eq. (9) will suffice for the calculation of $\lim_{n\to\infty}\langle r_n^2\rangle_{Av}/n$ if the limit exists.

CALCULATION OF $\Sigma_k kp_k^*$

In the previous article,[2] we described several methods for calculating the quantity, A, or more explicitly,

$$\lim_{n\to\infty}\sum_{k=2}^{n} kp_k^* \text{ (or } \lim_{n\to\infty}\sum_{n=4}^{n} kp_k$$

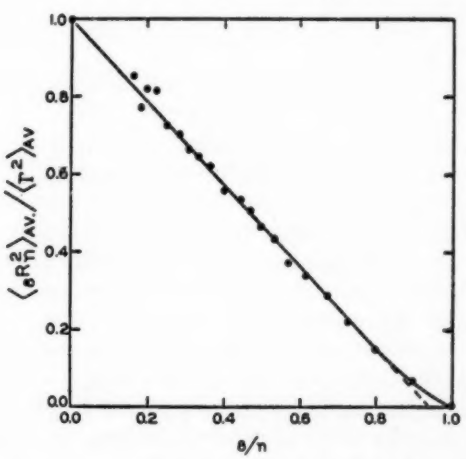

FIG. 7. Plot of $\langle {}_kR_n^2\rangle_{Av}/\langle r_n^2\rangle_{Av}$ *versus* $1/n$ with k held constant. $k=8$ in this example. Data apply to the five-choice simple cubic lattice.

TABLE II. Estimated values of A and related quantities.

Lattice	$\sum_k^{48} kp_k^*$ (Direct summation)	$\lim_{n\to\infty} \sum_k^n kp_k$ Eq. (19)	$\lim_{n\to\infty} \sum_k^n kp_k^*$ Eq. (20)	$\frac{1}{1-A}$
(a) 4-choice simple cubic	0.72	0.77	0.77	4.3
(b) 6-choice simple cubic	0.78	0.65	0.88	8.3
(c) 4-choice tetrahedral	0.83	0.59	0.94	16.7
(d) 8-choice body-centered cubic	0.74	0.72	0.88	8.3
(e) 12-choice face-centered cubic	0.66	0.51	0.63	2.7
(f) 6-choice 90° four-dimensional	0.36	0.40	0.40	1.7

in the case of orthogonal lattices). As seen in the foregoing, the calculation of a value for A makes it possible to predict whether or not $\langle r_n^2\rangle_{Av}/n$ converges. One method which directly yields a lower limit for A involves adding together experimental values for kp_k^*; if this sum ever exceeds unity, divergence of the aforementioned quotient is indicated. If this sum is less than unity, the result is inconclusive, since only a lower limit is so obtained. In a second method, the quantity A is calculated from attrition data by starting with the following equation:

$$\lim_{n\to\infty} \sum_{k=4}^{n} kp_k = \lim_{n\to\infty} \{ \sum_{i=1}^{n+1} N_i/N_{i-1} - (n+1) \times \exp(-\lambda) + c^0/c[1-\exp(-\lambda)]\}. \quad (19)$$

A is then obtained for lattices in which the backward step is involved by making the following correction:

$$A = \sum_{k=2}^{\infty} kp_k^* = 2p_2^* + (1-p_2^*) \sum_{k=4}^{\infty} kp_k. \quad (20)$$

These two methods have been used to calculate the results shown in Table II. Equation (19) was solved for $\lim_{n\to\infty} \sum_{k=4}^{n} kp_k$ for various values of $n+1$ as high as $n+1=150$. Attrition data in this wide range were available for the three-choice tetrahedral[1] and six-choice four-dimensional lattices. In addition, we have calculated $1/(1-A)$, which should be the limit of the quotient, $\langle r_n^2\rangle_{Av}/n$.

As was pointed out earlier, the attrition plots are not perfectly linear. This change is very slight but it is enough to have a profound effect on the value of A. Values of A shown in Table II were calculated by using as large a value for λ as could be derived from the experimental attrition data and yet be consistent with those data. Average values for λ were calculated over small ranges of attrition to observe possible changes throughout the experimental range. To consider one example, if the attrition is assumed to be constant for $n>40$ for the tetrahedral lattice, then $\exp(-\lambda)$ is equal to 0.962. Repeating this calculation for $n>100$, however, we find that the value of $\exp(-\lambda)$ is equal to 0.961. If this is the value of $\exp(-\lambda)$ at $n=150$, an upper limit on how much more this quantity will change as $n\to\infty$ is obtained by assuming p_k to be equal to c/k^2 and by summing c/k^2 from $k=152$ to ∞. This is so small that by assuming $\exp(-\lambda)$ to be 0.960, we have a reasonable estimate for the lower limit for $\exp(-\lambda)$ and hence the upper limit for λ.

There is another possible error in the calculation of $\lim_{n\to\infty} \sum_{n=4}^{n} kp_k$ which must also be mentioned. Equation (19), like Eq. (11), can be applied exactly only as $n\to\infty$, whereas values for N_i/N_{i-1} can be obtained, of course, only for relatively low values of n. This means that an error may accumulate if values for N_i/N_{i-1} differ from $\exp(-\lambda)$ for larger n. An examination of N_i/N_{i-1} in the range $n=50$ and up indicates that this error is probably not very large, but because the experimental values begin to scatter the error cannot be evaluated very precisely.

DISCUSSION

It will be seen from Table II that A appears to be less than unity for all of the three-dimensional lattices that were investigated. Moreover, in the case of the four-dimensional lattice, A is very much less than unity, so there seems to be relatively little doubt that the ratio, $\langle r_n^2\rangle_{Av}/n$, converges for the four-dimensional example. In three dimensions, the results are somewhat more problematical since A is fairly close to unity in several instances, indicating the possibility of divergence of $\langle r_n^2\rangle_{Av}/n$ in some three-dimensional lattices and convergence in others. The lattice for which this quotient is most likely to diverge is the four-choice tetrahedral lattice, the one most nearly resembling a real polymer chain made up of carbon atoms. Because of this result, we are currently investigating three-dimensional lattices for which it may be possible to demonstrate unequivocal divergence of the ratio. On the other hand, it seems reasonable to conclude, on the basis of the present data, that $\langle r_n^2\rangle_{Av}/n$ converges as $n\to\infty$ in at least some three-dimensional lattices. The twelve-choice face-centered cubic lattice, for which A is only around 0.63, appears to be just such an example. These results all tend to substantiate the conclusion reached previously,[2] after an examination of two-dimensional lattices, that the number of dimensions is only one factor determining the

TABLE III. Comparison of excluded areas and volumes with values for A.

Two-dimensional lattices	Relative excluded areas and volumes	A
3-choice 120°	$3\sqrt{3}/4=1.30$	1.20
4-choice square	$1=1.00$	1.15
6-choice 60°	$\sqrt{3}/2=0.87$	1.12
Three-dimensional lattices		
4-choice tetrahedral	$8/(3\sqrt{3})=1.54$	0.94
6-choice simple cubic	$1=1.00$	0.88
8-choice body-centered cubic	$4/(3\sqrt{3})=0.77$	0.88
12-choice face-centered cubic	$1/\sqrt{2}=0.71$	0.63

ultimate convergence or divergence of $\langle r_n^2\rangle_{Av}/n$ in random walks subject to area or volume exclusion.

It is also of interest to compare values of A with the volume per lattice site (or area, in the case of two-dimensional lattices). Such a volume, which is the equivalent of the volume of a bead or monomer unit of a flexible polymer molecule, is essentially the basic excluded volume that cannot be filled more than once during the course of a given random walk. Since the steps in all lattices are equal, these volumes are most conveniently calculated relative to that for the six-choice simple cubic lattice. Such relative values for excluded volumes, or excluded areas in two dimensions, are shown in Table III in conjunction with values for A. Within each group of lattices, the value of A increases in relation to size of the excluded areas of volumes; this is perfectly reasonable from a physical point of view.

In examining the results for three-dimensional lattices, it is of interest to consider what relationship between $\langle r_n^2\rangle_{Av}$ and n may be reasonably expected in the

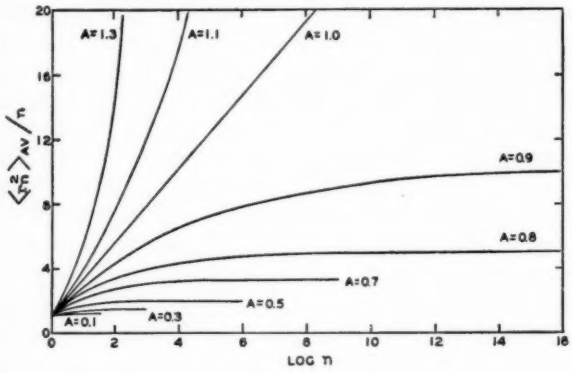

FIG. 8. Plot of values for $\langle r_n^2\rangle_{Av}/n$ *versus* log$n$ for various values of A. Data calculated by means of Eq. (21).

range of values for n equivalent to those found for real polymers. An approximate picture of what happens is obtained by calculating values for $\langle r_n^2\rangle_{Av}$ by means of Eq. (9). A value of C, the integration constant of Eq. (9), can be obtained by fitting the equation to the experimental data at $n=1$ to yield

$$\langle r_n^2\rangle_{Av}=(n-An^A)/(1-A). \tag{21}$$

Strictly speaking, this equation only applies in the limit where A is constant. Using Eq. (21), the dependence of $\langle r_n^2\rangle_{Av}/n$ on n can be determined as a function of A for large values of n.

In Fig. 8, $\langle r_n^2\rangle_{Av}/n$ is plotted *versus* log$n$ for values of A ranging from 0.1 to 1.3. In the special case of $A=1$, $\langle r_n^2\rangle_{Av}=n\ln n+n$. It is observed that if A is small, the value of $\langle r_n^2\rangle_{Av}/n$ reaches 99% of its limit by the time $n=100$ to 1000. Then as A becomes larger, greater values of n are necessary before equivalent behavior is observed. There are tabulated in Table IV values for n at which $\langle r_n^2\rangle_{Av}/n=0.99/(1-A)$ for different values of A ranging between zero and unity.

TABLE IV. Calculated limiting behavior of $\langle r_n^2\rangle_{Av}/n$.

A	$\lim_{n\to\infty}\langle r_n^2\rangle_{Av}/n$	Approximate value of n at which 99% of limit is realized
0.1	1.11	50
0.2	1.25	200
0.3	1.43	10^3
0.4	1.67	10^5
0.5	2.00	10^6
0.6	2.50	10^7
0.7	3.33	10^9
0.8	5.00	10^{16}
0.9	10.00	10^{30}
1.0	diverges	...

Three-dimensional lattices appear to have values for A in the range of 0.6 to 0.9 and perhaps higher. When $A=0.6$, the above described limiting behavior is not observed until $n=10^7$. Moreover, when $A=0.9$, this limiting behavior is not observed until $n=10^{30}$. Since even 10^7 exceeds the degree of polymerization for any ordinary polymer chains, these results indicate that the "limiting behavior" will *not* be observed experimentally, especially since the lattice most closely resembling polymer chains made up of carbon atoms is the three-choice tetrahedral lattice, for which the value of A appears to be at least 0.9. Thus the present investigation of nonintersecting random walks in three dimensions has led to the rather interesting conclusion that, in theory, the ratio, $\langle r_n^2\rangle_{Av}/n$, may converge in some three-dimensional lattices, but that in practice, this convergence will generally not be observed. For real polymers, $\langle r_n^2\rangle_{Av}$ should appear to increase somewhat more rapidly than by simple proportionality to n. Practically speaking, the actual behavior can be described with sufficient accuracy over limited ranges of n by the following simple power law expression:

$$\langle r_n^2\rangle_{Av}=an^b, \tag{22}$$

where a and b are constants. b has a value in the neighborhood of 1.22 for three-dimensional lattices and 1.11 for the four-dimensional lattice for low values of n. The range of values for n for which Eq. (22) is applicable becomes smaller as A becomes smaller.

Adsorption Studies on Clay Minerals. V. Montmorillonite-Cesium-Strontium at Several Temperatures*

GEORGE L. GAINES, JR.,† AND HENRY C. THOMAS
Sterling Chemistry Laboratory, Yale University
(Received March 14, 1955)

Ion-exchange equilibria for the pair cesium-strontium between aqueous chloride solutions and a montmorillonite clay have been studied in the temperature range 5°–75°. Data from chromatographic elution experiments have been found to be unreliable because of nonequilibrium effects, and a method independent of rate behavior has been applied. From the data obtained, equilibrium constants, solid-phase activity coefficients, heat content and entropy changes for the reaction have been evaluated.

IN this paper we report results of equilibrium studies in the system montmorillonite-cesium chloride-strontium chloride at temperatures from 5° to 75°. Investigations of the effect of temperature in ion-exchange equilibria have not been extensive and, up to the present, have been confined largely to studies involving resinous exchangers. Coleman and Harward[1] have reported measurements on the heats of neutralization of acid bentonites, but apparently no work has been reported on the temperature coefficient of the equilibrium constant, directly measured, in clay-ion systems.

In extending our studies of ion-exchange equilibria on the clay minerals to mixed charge types we have been forced to abandon the purely chromatographic technique in which isotherms are deduced from a single elution chromatogram. Corrections for nonequilibrium behavior, such as that given in the first paper of this series,[2] have proved to be inadequate. In our effort to put the treatment of these equilibria on a sound thermodynamic basis we have not wanted to leave such an uncertainty in the results, although the necessary change in method greatly curtails the amount of work which can be completed in a given time. The data of this paper have been obtained by what may be called the equilibrium column technique, in which a bed of clay mineral, dispersed on asbestos as a filter aid, is treated by passing over it a large volume of solution of fixed composition. After the bed is shown to have reached equilibrium with the solution, the bed is analyzed by appropriate isotopic exchanges, always from solutions of the original fixed chemical composition. This method is entirely independent of the effect of finite rates in the bed, of difficulties caused by channeling, of variable solvent uptake of the clay, and, in short, of all nonequilibrium effects. Since the bed is always carried to isotopic equilibrium with the flowing solutions, the shape of the elution curve is immaterial. Only the area under the elution curve is needed.

The isotopic exchange determines the total ion holdup of the column and not solely the capacity of the exchanger. It is therefore necessary to have a method for measuring the free volume of the column and this without in any way disturbing the chemical equilibrium in the system. Without isotopic tracers this appears to be an impossibility in principle. With the use of tracers, however, the measurement can be made; *viz.*: Suppose that a column containing exchanger of known total capacity q_0 has been brought to equilibrium with a solution of concentration c_A, c_B measured in equivalents of ions A and B. The column is now "eluted" with a solution of A and B of identical chemical composition carrying radioactive isotopes of *both* of its exchangeable constituents. The effluent samples are collected, weighed, and in each A is separated chemically from B before counting. Thus break-through curves for each constituent are determined. The areas above these curves will be proportional to the total holdup of the column for the species in question. If the free volume of the column is h, we have for the two areas

$$A_A = hc_A + q_A,$$
$$A_B = hc_B + q_B,$$

and also

$$q_0 = q_A + q_B.$$

Thus q_A and q_B as well as h are determined by these measurements. Some such procedure as this seems to be the only unambiguous manner in which to define the free volume of a column. Any method involving a chemical change, rather than merely isotopic displacements, necessarily gives a result influenced by a variety of factors, the most important of which will usually be changes in volume of the exchanger itself resulting from changes in its environment. The equilibrium column method is evidently capable of extension to cases involving more than two ions, provided that chemical separa-

* Contribution No. 1233 from the Sterling Chemistry Laboratory, Yale University. This paper is based in part on the dissertation presented in 1954 by George L. Gaines, Jr., to the Faculty of the Graduate School of Yale University in partial fulfillment of the requirements for the degree of Doctor of Philosophy. The work has been supported by the Department of Nuclear Engineering of Brookhaven National Laboratory, to which we wish to express our indebtedness. During 1953–54 G. L. G. held the duPont Fellowship in Chemistry at Yale, which aid contributed much to the work.

† Present address: The Research Laboratory, General Electric Company, Schenectady, New York.

[1] N. T. Coleman and M. E. Harward, J. Am. Chem. Soc. **75**, 6045 (1953).

[2] Faucher, Southworth, and Thomas, J. Chem. Phys. **20**, 157 (1952).

tions might not be necessary if adequate differential radioactive analysis can be performed. In any case the labor involved is considerable, and it is fortunate that in many cases rough estimates of free volume are entirely adequate. Such is the case when a break-through occurs at a large volume, say for dilute solutions of a strongly held constituent, in which case that part of the holdup caused by the free volume may be entirely negligible. Frequently a sufficiently accurate estimate may be obtained merely by weighing the column before and after the initial filling with solution. If this can be done, the exchangeable ion composition in the clay can be determined by an equilibrium column experiment in which only one constituent is isotopically traced.

The clay mineral used in this work was a portion of the material described by Faucher and Thomas,[3] the montmorillonite from Chambers, Arizona, designated No. 23 in the Reference Clay Mineral series of the American Petroleum Institute. The preparation of the columns has also been described.[1] In much of the present work the temperature of influent solution and clay bed was controlled by pumping thermostat water through jackets around the columns and the tubes connecting them to the solution reservoirs. In the preliminary chromatographic work flow rates were maintained constant by the use of a constant flow pump; but since constancy of flow rate is not a requirement of the equilibrium column method, simple siphons were used to feed most of the columns.

Although more recent work has shown that the apparent exchange capacity of the asbestos used as filter aid is almost certainly less than 0.01 meq/g, this value has been used in correcting the results of the experiments.

Ordinary analytical grade reagents were used without special purification. Dried samples of the cesium chloride, from A. D. Mackay Company, New York, assayed 100.0±0.2% by volumetric chloride determination. Stock solutions of cesium and barium chlorides were prepared by weight. Solutions of strontium chloride were analyzed gravimetrically for Sr.

Extent of exchange was followed throughout by means of radioactive tracers. Carrier-free Cs^{137} was taken from a stock solution containing 1 mc per liter of water, and, the cesium content being negligible, the tracer was added as a part of the distilled water used in preparing the solutions. Long-lived Sr^{90} proved to be useless in this work. In the absence of bulk yttrium the Y^{90} daughter adsorbed on clay, asbestos, and glassware and completely obscured the results. Through the courtesy of Brookhaven Laboratory we obtained an irradiated sample of strontium nitrate containing about 1.5 mc Sr^{89}. Even after conversion to the chloride via a precipitation as the carbonate it was found essential to purify the material further. (A major fraction of the activity could not be precipitated as the carbonate from the chloride solution.) Repeated precipitations as the carbonate eventually gave a satisfactory material. The purified strontium carbonate was dissolved in HCl and this solution saturated with "cold" $SrCO_3$. The resulting solution, at pH 6.8, was filtered, diluted, and analyzed gravimetrically for Sr, this analysis being taken into account when adding activity to solutions of $SrCl_2$.

Standard counting techniques were used employing jacketed Geiger-Müller solution counters. Dead time and background corrections were applied throughout.

[3] J. A. Faucher and H. C. Thomas, J. Chem. Phys. **22**, 258 (1954).

RESULTS

Since all of the results to be discussed depend on the constancy of the exchange capacity of the clay and the equivalence on the clay of the ions in the pairs considered (principally Cs, Sr/2), these facts were first established as follows. The capacity of a clay is most conveniently discussed in terms of its "backbone" weight, that portion, excluding the content of exchangeable ion, left after ignition to constant weight in air (in platinum, over a Meker blast). Portions of the natural clay were converted to the cesium, barium, and strontium forms by washing repeatedly with 0.1–0.5 N solutions of the corresponding chloride. Complete removal of calcium (the principal exchangeable ion of the natural clay) was confirmed by spot tests, and the clays were washed well with distilled water, dried at 50°, and ground to pass a 100-mesh screen. The samples were then allowed to stand in the open air (at about 25° and 50–60% relative humidity) for several days, when they were stored in tightly stoppered bottles. In Table I are given the results of the backbone determina-

TABLE I. Exchange capacity of montmorillonite API23 under various conditions. Fraction backbone: Natural clay, 0.773; Cs-clay, 0.765; Ba-clay, 0.790; Sr-clay, 0.757.

Initial clay form	Elutriant CsCl, N. Temp. 25°–27°	Capacity, meq/g backbone
Natural	0.0200	1.360
Natural	0.0500	1.360
Natural	0.0500	1.371
Natural	0.0496	1.355
Natural	0.0498	1.365
Natural	0.0498	1.363
Natural	0.200[a]	1.385
Sr	0.0500	1.359
Ba	0.0500	1.353
Cs[b]	0.0500	1.295
Cs	0.0500	1.293
	Temp. 75°, all at 0.0500 N	
Natural		1.352
Natural		1.347
Cs[b]		1.273
Cs		1.286
Cs		1.300
Cs		1.311
Cs		1.282

[a] Errors are larger at this concentration because of uncertainty in hold-up volume.
[b] Dried at 50° (see text).

TABLE II. Doubly traced isotopic exchange on equilibrium column $c_0 = c_{Cs} + c_{Sr} = 0.05000$ N; $c_{Cs}/c_0 = 0.00250$.

Sample	Vol. (ml)	Room temperature [Sr]/[Sr]$_0$	[Cs]/[Cs]$_0$	meq Sr	meq Cs
1	23.117	1.000	1.000	1.153	
2	21.427	1.000	1.000	1.068	
3	21.484	1.000	1.000	1.072	
4	20.624	0.990	1.000	1.018	0.0188
5	20.731	0.926	1.000	0.958	
6	21.407	0.707	1.000	0.755	
7	21.434	0.393	1.000	0.421	
8	21.439	0.141	0.969	0.150	0.0026
9	21.443	0.0278	0.968	0.030	0.0026
10	21.483	0.0170	0.970	0.018	0.0026
11	20.952	0.0094	0.989	0.010	0.0026
12	21.419	0.0067	0.998	0.007	0.0027
I	238.6	0.000	0.967		0.0288
II	335.5		0.617		0.0259
III	99.7		0.128		0.0016
IV	240.5		0.0226		0.0007
V	95.5		0.0055		0.0001
			Total	6.659	0.0889

$q_{Sr} + 0.04988\,h = 6.659$
$q_{Cs} = 0.000125\,h = 0.0889$
$q_{Sr} + q_{Cs} = 5.654$ (from weight of clay in column)
$h = 21.9$ ml, $q_{Sr} = 5.568$ meq, $q_{Cs} = 0.0862$ meq.

tions and the exchange capacities of these samples as found by eluting with labeled CsCl at various concentrations. It is apparent from these results that the capacity of the clay is independent of the temperature, of its initial composition, and, at least to a good approximation of the concentration of the solution. For the cesium clay there is some evidence of an irreversible loss in capacity possibly resulting from the drying at 50°. This result has been confirmed by independent work and does not seem to be due to "fixation" of cesium. The effect is relatively small and in any case has no influence on our equilibrium determinations, which in all cases started with natural clay.

In the doubly traced equilibrium column experiments the separation of cesium and strontium was accomplished through the precipitation of strontium carbonate. To aliquots of the samples containing 1–1.5 mg of Sr was added a slight excess of carbonate in the form of 0.75 N $(NH_4)_2CO_3$ in 0.75 N NH_4OH. After standing overnight the mixture was filtered, the precipitate washed by decantation and dissolved in hydrochloric acid. The procedure was checked against several known solutions containing varying proportions of cesium and strontium, both labeled with radioactive tracers. Comparison of the initial and separated activities of both ions gave a maximum discrepancy of just one percent, 0.5% on the average for ten determinations, about what one would expect from the character of the counting.

The complete data for a typical doubly traced equilibrium column are given in Table II. In this experiment large quantities of both doubly labeled and cold solutions were prepared: 0.04988 N in $SrCl_2$ and 0.000125 N in CsCl. The labeled solution was passed through the column filled with the natural clay until the counting rate of the effluent reached the value of the feed. The feed was then changed to the untraced solution and the effluent collected first in test tubes then in flasks. When the activity of the effluent had dropped to background rate, the elution was considered complete. Separations were made as indicated above and the activities of both fractions determined.

In Table III is given a comparison of the results obtained with doubly and singly traced equilibrium columns at room temperature. In two cases the columns have been run both by measuring eluted activity and on the same column by measuring uptake of activity. The results obtained in this way are certainly not in perfect agreement, differing by as much as 18%, but compared with uncertainties of 200–300% in q/q_0 in this concentration range as obtained in earlier work, we must consider the agreement satisfactory. Between the singly and doubly traced experiments the agreement is generally better than three percent and is all that could be expected. The values deduced from single chromatographic elutions are not at all in agreement with the equilibrium experiments and have not been taken into account in the thermodynamic calculations described below.

TABLE III. Comparison of double and single isotopic exchange on equilibrium columns and chromatographic data.

	$c_0 = 0.0500$ N Double isotopic		Room temperature Single isotopic (Cs traced)		Chromatographic
c_{Cs}/c_0	h (ml)	q_{Cs}/q_0	h (by wt.)	q_{Cs}/q_0	q_{Cs}/q_0
0.0025		0.015			(0.11)[a]
0.005		0.030			(0.22)[a]
0.010		0.053			(0.42)[a]
0.050	26.1	0.254	20.4	0.256	0.635
0.100	21.0	0.451	21.2	0.451	0.738
0.300	25.4	0.826	19.3	0.843	0.867
0.500	20.2	0.913	19.4	0.916	0.924
0.700	21.0	0.947	17.5	0.970	0.966

[a] Estimated from chromatographic isotherm.

In Table IV are given the results of singly traced equilibrium columns at different temperatures. In the experiments at 50° and 75° the influent solutions were preheated and the columns were equipped with extensions at the bottom to allow the effluent solutions to cool and so minimize evaporation. At 5° temperature control was not nearly so satisfactory and some difficulty was experienced in verifying the attainment

TABLE IV. Strontium-cesium equilibria on montmorillonite $c_0 = 0.0500$ N.

c_{Cs}/c_0	q_{Cs}/q_0 5°	25°	50°	75°
0.005	0.052	0.029	0.016	0.010
0.01	0.097	0.053	0.030	0.019
0.10	0.628	0.457	0.292	0.247
0.30	0.888	0.835	0.746	0.744
0.50	0.932	0.906	0.861	0.827

of isotopic equilibrium in the columns. The data at the lowest temperature are doubtless of less significance than the others. In most cases the results given represent average values for successive isotopic saturations and elutions. The effect of temperature on the exchange equilibrium is at once apparent. The clay becomes less specific for cesium as the temperature rises; in the region of low cesium concentration the effect is very marked indeed, amounting to a factor of five in the initial slope of the isotherm.

DISCUSSION

From the data of Tables III and IV the values for the stoichiometric equilibrium ratios for the reaction of strontium replacing cesium,

$$K'_c = c_0 \frac{[1-(q/q_0)](c/c_0)^2}{(q/q_0)^2[1-(c/c_0)]}$$

have been calculated. These are given in Table V, and the $\ln K'_c$ are depicted as functions of the composition

TABLE V. Equilibrium ratio K'_c for the reaction $Sr^{++}+Cs_2M \rightleftharpoons SrM+Cs^+$ in chloride solutions at $c_0=0.0500$ N.

c_{Cs}/c_0	5°	25°	50°	75°
0.005	4.41×10^{-4}	1.45×10^{-3}	4.82×10^{-3}	1.25×10^{-2}
0.010	4.85	1.70	5.44	1.37
0.100	5.24	1.44	4.61	0.69
0.300	9.15	1.52	2.94	0.30
0.500	19.5	2.87	4.70	0.63

Room temperature

c_{Cs}/c_0		c_{Cs}/c_0	
0.0025	1.38×10^{-3}	0.100	1.50×10^{-3}
0.005	1.36	0.300	1.65
0.010	1.73	0.500	2.61
0.050	1.52	0.700	4.83

of the clay in Fig. 1. The data at room temperature are indistinguishable from those at 25° and are included on the same plot. In making the extrapolations to the mono-ion clays we have as a guide little more than the very reasonable supposition that the excess free energy of the ion present in small amount is finite. On this basis we will certainly have a finite intercept for $\ln K_c'$. The experimentally well-established constant initial slope of the adsorption isotherms leads one to expect a linear variation of $\ln K_c'$ near the edges of the diagram. The curves have been approximately so drawn.

We may now calculate the thermodynamic functions for the equilibrium at the total concentration 0.05 N. Since we have no evidence that the anion participates significantly in the exchange adsorption, these computations may be carried out in the manner detailed by the present authors[4] as Case *A*. The required formulation

[4] G. L. Gaines, Jr., and H. C. Thomas, J. Chem. Phys. **21**, 715 (1953).

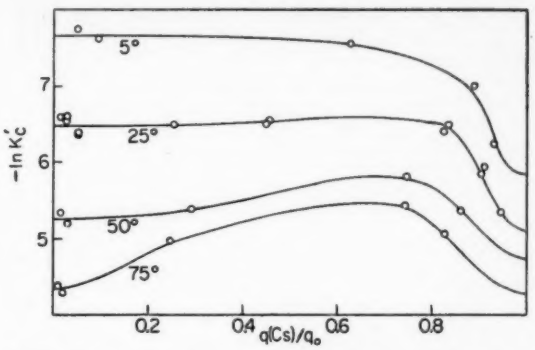

FIG. 1. Stoichiometric equilibrium ratios for the reaction $Sr^{++}+Cs_2M \rightleftharpoons SrM+2Cs^+$.

for the thermodynamic equilibrium constant is

$$\ln K+1=\ln\{f_{Sr}(0.05)/f_{Cs}^2(0.05)\}+\int_0^1 \ln K'_c \cdot d\left(\frac{q}{q_0}\right)+\int_0^1 \ln\left(\frac{\gamma_{Cs}^2}{\gamma_{Sr}}\right)\cdot d\left(\frac{q}{q_0}\right)-2\int_{Sr}^{Cs} n_{H_2O}\, d\ln a_{H_2O}.$$

The first term on the right measures the contribution to the standard free energy of the reaction due to the process of bringing the mono-ion clays from equilibrium with infinitely dilute solutions into equilibrium with solutions at 0.05 N. We shall assume that the free energy difference is the same for strontium as for cesium clay; or, what amounts numerically to the same thing, for present purposes we make the necessary shift in standard states.

The last integral on the right gives the contribution due to the change in water activity in passing from 0.05 N $SrCl_2$ to 0.05 N CsCl and may be written $-2\bar{n}_{H_2O}\ln\times[a_{H_2O}(0.05\text{ N CsCl})/a_{H_2O}(0.05\text{ N }SrCl_2)]$, $\bar{n}_{H_2O}$ being an appropriate average water content in moles per exchange equivalent of clay. In spite of the relatively large value of $\bar{n}_{H_2O}$ the contribution of this term is

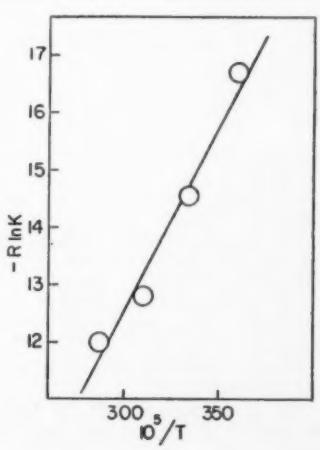

FIG. 2. Temperature dependence of K', the equilibrium constant uncorrected for aqueous solution activity coefficients.

TABLE VI. Equilibrium constants for the reaction $Sr^{++}+Cs_2M \rightleftharpoons SrM+2Cs^+$.

Temperature °C	$-\ln K'$
5	7.39
25	6.34
50	5.46
75	5.03

quite negligible in our case. Water content data are not available for the system with which we are dealing, but from the work of Mooney, Keenan, and Wood[5] we obtain a rough estimate for $\bar{n}_{H_2O}$ at 20°, namely 27 moles per exchange equivalent. Assuming all osmotic coefficients equal to unity in the dilute solutions (which leads to an error of not more than a factor of two or three), we estimate the contribution of the integral as 0.02 in $\ln K$. As is apparent the temperature coefficient of this term will be extremely small, and the water integral is therefore entirely without influence in the calculation of heat content data.

While the principal contribution to $\ln K$ is the integral involving the stoichiometric equilibrium constant, the term involving the activity coefficients in solution is not negligible with salts of mixed charge types. Since direct experimental information on the activity coefficients in mixed solutions is lacking, we may proceed as follows.[6] Plots of the activity coefficients were made, using data above 0.1 m as given by Harned and Owen[7] for $SrCl_2$ and for CsCl from Robinson and Stokes.[8] Below 0.1 m activity coefficients were calculated as described by Harned and Owen.[9] From these plots and the equation given by Glueckauf,[10] values for the activity coefficient ratio $\gamma^2_{Cs}/\gamma_{Sr}=\gamma^4_{\pm CsCl}/\gamma^3_{\pm SrCl_2}$ at 0.05 N were then calculated for different values of c/c_0. From a plot of the logarithms of these ratios against the corresponding values of q/q_0 the integral was evaluated at 25° and found to be 0.406. Combining this result with a graphical integration of the curve of Fig. 1, we find

$$Sr^{++}+Cs_2M \rightarrow SrM+2Cs^+; \quad \Delta F^\circ = 3500 \text{ cal}, \quad 25°C,$$

for standard states as detailed above.

TABLE VII. Solid-phase activity coefficients at 25°.

$q(Cs)/q_0$	$f(Sr)$	$f(Cs)$
0.015	0.98	1.55
0.030	0.96	1.51
0.053	0.93	1.66
0.254	0.78	1.45
0.451	0.65	1.26
0.826	0.45	1.07
0.913	0.28	1.05
0.947	0.17	1.02

Data are not available from which to obtain an accurate evaluation of the activity coefficient integral at other temperatures. In Table VI are given values for $\ln K'$, the constant with the activity coefficients for the solutions omitted. In order to use these data for a computation of the heat of the reaction, we must assess the temperature coefficient of the omitted integral. Again no directly applicable data are available, but we may obtain an estimate of the effect from the temperature dependence of an expression analogous to the Guggenheim-Glueckauf formula in which the temperature dependent terms of the Debye-Hückel contribution to the activity coefficient have not been suppressed. Using such a formula in conjunction with experimental values for the $\bar{L}$ in pure salt solutions,[11] we find 400 cal as an upper limit to the effect on ΔH of the neglected term.

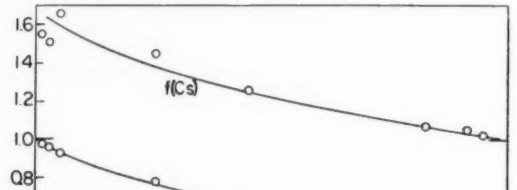

FIG. 3. Clay phase activity coefficients at 25°.

In Fig. 2 is given the plot of $\ln K'$ *vs* $1/T$. The slope of this plot corresponds to $\Delta H = 6.5$ kcal for the reaction of strontium displacing cesium and leads to the value $\Delta S = +10$ eu for the reaction. This rather large entropy increase is possibly to be explained in terms of disordering of water molecules as strontium enters the clay structure, water oriented about the divalent ion in solution being lost in the exchange for cesium.

Because of uncertainties in the values of the solution activity coefficients we have evaluated the solid phase activity coefficients at 25° only. These are given in Table VII and are shown in Fig. 3. These values are subject to the same uncertainties involved in the equilibrium constant measurements, besides which they generally represent small differences between larger experimentally determined quantities. It is apparent from Fig. 3 how differently cesium and strontium behave on the clay; we are unable, however, to undertake any detailed discussion of the nature of these differences in this complex system.

[5] Mooney, Keenan, and Wood, J. Am. Chem. Soc. **74**, 1372 (1952).

[6] We are indebted to E. Glueckauf, A.E.R.E., Harwell, England, for pointing out the necessity of this correction for salts of mixed valence types and how it can be made.

[7] H. S. Harned and B. B. Owen, *The Physical Chemistry of Electrolytic Solutions* (Reinhold Publishing Corporation, New York, 1950), p. 602.

[8] R. A. Robinson and R. H. Stokes, Trans. Faraday Soc. **45**, 612 (1949).

[9] H. S. Harned and B. B. Owen, *The Physical Chemistry of Electrolytic Solutions* (Reinhold Publishing Corporation, New York, 1950), p. 607.

[10] E. Glueckauf, Nature **163**, 415 (1949).

[11] H. S. Harned and B. B. Owen, *The Physical Chemistry of Electrolytic Solutions* (Reinhold Publishing Corporation, New York, 1950), p. 541.

THE JOURNAL OF CHEMICAL PHYSICS VOLUME 23, NUMBER 12 DECEMBER, 1955

Theory of One-Dimensional Fluid Binary Mixtures

RYOICHI KIKUCHI*
Institute for the Study of Metals, The University of Chicago, Chicago, Illinois
(Received March 9, 1955)

The rigorous solution of a one-dimensional fluid binary mixture with arbitrary interparticle potentials is obtained under the assumption that a particle interacts with its nearest neighbors, and that the system obeys classical statistical mechanics. This rigorous solution provides the interpretation of parameters used in the lattice model of binary mixtures.

1. INTRODUCTION

VARIOUS methods of deriving the rigorous equations of state of a one-dimensional system of particles obeying classical statistics and for an arbitrary interaction potential are already known.[1-4] The reason why such a hypothetical system has drawn much attention is that it can be treated rigorously and also that it can be used as a test case for any technique of statistical mechanics which is intended to be applied to three-dimensional liquid systems. The author has also contributed a method[5] to this problem, under a slight restriction for the shape of the potential, as an example of a general scheme which, in principle, can be applied to three-dimensional systems. Due to the mathematicl complexity, however, it was found hopeless to carry out the calculation of the proposed method for the three-dimensional case.

In the following sections, an alternative way of handling one-dimensional systems will be presented. This approach seems more practical than those reported previously.[1-5] As evidence for the flexibility of the technique, in the latter half of the paper, it is applied to derive the rigorous solution for binary mixtures, which, so far as the author is aware, has not yet been reported.†

The essential idea of the method was already stated in Sec. V of TCP II, and as one may easily see there, the idea was primarily conceived with the aim of applying it to the solid state. This suggests that the present method, when applied to three-dimensional systems, would be suitable to discuss the solid-liquid transition, though this is not attempted in the present paper.

2. ONE-COMPONENT SYSTEM

In the one-dimensional system we are looking at, suppose there are M particles within the length L. To make the calculation simpler we assume the periodic boundary condition so that the same configuration is repeated with the period of L, which is a macroscopic length. The average length per particle is $l=L/M$. In the system, suppose a virtual lattice with the lattice constant l. Then the number of lattice points within the length L is equal to the number of particles in the same interval, so that when any configuration[6] of the system is given, one can establish one-to-one correspondence between particles and the lattice points.

Let us number the lattice points from left to right, and use the same numbering for the lattice point and the particle attached to it. For instance the ith particle belongs to the ith lattice point. Let R_i and R_i+x_i be the coordinates of the ith lattice point and of the ith particle.[7] We establish the one-to-one correspondence under the restriction that the $(i+1)$th particle is to the right of the ith particle. This restriction is

$$-l+x_i<x_{i+1}, \tag{2.1}$$

in which the relation $R_{i+1}=R_i+l$ is taken into account.

After finishing the one-to-one correspondence, one introduces a probability function $f^{(2)}(x, x'; R_i, R_{i+1})$ which denotes the probability density of finding the ith particle at R_i+x and $(i+1)$th particle at $R_{i+1}+x'$. When the end effect is neglected, all the lattice points are equivalent to each other, so that we may hereafter drop the arguments R_i and R_{i+1} in the above function $f^{(2)}$ and may simply write it as $f^{(2)}(x,x')$ without causing any confusion. But it should always be remembered that the second argument x' is for the particle belonging to a lattice point which is a unit lattice constant l to the right of the lattice point to which the particle of the first argument x belongs. Because of the symmetry of the system, we have a relation

$$f^{(2)}(x,x')=f^{(2)}(-x',-x). \tag{2.2}$$

Next, one defines $f^{(1)}(x;R_i)$ which is the probability density of finding the ith particle at R_i+x. This is

* Present address: Armour Research Foundation of Illinois Institute of Technology, Chicago, Illinois.

[1] H. Takahasi, Proc. Phys.-Math. Soc. Japan **24**, 60 (1942).

[2] F. Gürsey, Proc. Cambridge Phil. Soc. **46**, 182 (1950).

[3] Salsburg, Zwanzig, and Kirkwood, J. Chem. Phys. **21**, 1098 (1953).

[4] Sells, Harris, and Guth, J. Chem. Phys. **21**, 1422, 1617 (1953).

[5] R. Kikuchi, J. Chem. Phys. **19**, 1230 (1951), hereafter called TCP II.

† *Note added in proof.*—Since this article was submitted, Professor I. Prigogine kindly informed the author of the following papers: I. Prigogine and S. Lafleur, Bull. classe sci. Acad. roy. Belg. **40**, 484 and 497 (1954), where the problem of linear binary mixtures was solved using a different method.

[6] In a configuration, particles are not constrained on the lattice points only, as in the lattice model, but can occupy any points on the line.

[7] This means that x_i is the coordinate of the ith particle measured from the ith lattice point.

derived from $f^{(2)}$ by the relation

$$f^{(1)}(x;R_i)=\int_{-l+x}^{L-l+x}dx'f^{(2)}(x,x';R_i,R_{i+1}). \quad (2.3)^8$$

$f^{(1)}$ is also subject to a symmetry restriction:

$$f^{(1)}(x)=f^{(1)}(-x), \quad (2.4)$$

where we have dropped the argument R_i due to the equivalence of lattice points as mentioned above. The normalization is

$$\int_{-L/2}^{L/2}dxf^{(1)}(x)=1. \quad (2.5)$$

The formula for the entropy S of the system[9] is already given in Eq. (52) of TCP II, in which $2z'$ is the coordination number. Putting $z'=1$ in it, one obtains

$$\frac{S}{kM}=\int_{-L/2}^{L/2}dxf^{(1)}(x)\ln f^{(1)}(x)$$
$$-\int_{-L/2}^{L/2}dx\int_{-l+x}^{L-l+x}dx'f^{(2)}(x,x')\ln f^{(2)}(x,x') \quad (2.6)$$

where k is the Boltzmann constant. When one assumes that the potential energy is contributed only by the nearest neighbor pairs, the energy E is

$$E=M\int_{-L/2}^{L/2}dx\int_{-l+x}^{L-l+x}dx'\varphi(x,x')f^{(2)}(x,x'), \quad (2.7)$$

where $\varphi(x,x')$ is the potential energy of a pair of particles. Actually this is a function of only the relative distance r:

$$r=x'+l-x \quad (2.8)$$

so that we may write

$$\varphi(x,x')\equiv\Phi(r). \quad (2.9)$$

Then it is clear also that $\varphi(x,x')$ is subject to the following relation:

$$\varphi(x,x')=\varphi(-x',-x). \quad (2.10)$$

Using Eqs. (2.6) and (2.7), one can easily construct the free energy. The main mathematical procedure is to minimize the free energy with respect to the functions $f^{(1)}(x)$ and $f^{(2)}(x,x')$ under the four restrictions, Eqs. (2.2) through (2.5). When the undetermined multipliers for Eqs. (2.5), (2.3), (2.4), and (2.2) are denoted as λ_1, $2\lambda_2(x)$, $\lambda_3(x)$, and $\lambda_4(x,x')$, respectively, the equations one obtains after the variation process are

$$-1-\ln f^{(1)}(x)+\lambda_1+2\lambda_2(x)+\lambda_3(x)-\lambda_3(-x)=0, \quad (2.11)$$

$$\beta\varphi(x,x')+1+\ln f^{(2)}(x,x')-2\lambda_2(x)$$
$$+\lambda_4(x,x')-\lambda_4(-x',-x)=0, \quad (2.12)$$

and one can also see that

$$\lambda_1=-F/(MkT), \quad (2.13)$$

where F is the Helmholtz free energy of the system, and T is the absolute temperature, and β in Eq. (2.12) is $(kT)^{-1}$.

Combining Eqs. (2.2) and (2.10) with Eq. (2.12), one eliminates $\lambda_4(x,x')$ to obtain

$$f^{(2)}(x,x')=\exp[\lambda_2(x)+\lambda_2(-x')-\beta\varphi(x,x')-1]. \quad (2.14)$$

Similarly, $\lambda_3(x)$ is eliminated from Eq. (2.11) using Eq. (2.4) so that

$$f^{(1)}(x)=\exp[\lambda_2(x)+\lambda_2(-x)+\lambda_1-1]. \quad (2.15)$$

Inserting Eqs. (2.14) and (2.15) into Eq. (2.3), one obtains an integral equation for $\lambda_2(x)$. As is shown in Appendix I a possible solution of the equation is

$$\lambda_2(x)=\xi x+c, \quad (2.16)$$

where ξ and c are constants. c is determined by putting Eqs. (2.15) and (2.16) into Eq. (2.5) and the results are

$$f^{(1)}(x)=L^{-1}, \quad (2.17)$$

$$f^{(2)}(x,x')=[LI(\xi)]^{-1}\exp[-\xi r-\beta\Phi(r)], \quad (2.18)$$

$$\lambda_1=-F/(MkT)=\xi l+\ln I(\xi), \quad (2.19)$$

where

$$I(\xi)=\int_0^\infty dr\exp[-\xi r-\beta\Phi(r)]. \quad (2.20)^{10}$$

The constant ξ is determined from Eq. (2.19) so that the Helmholtz free energy F becomes a minimum with respect to ξ, keeping T and l constant. The result is

$$l=-\left[\frac{\partial}{\partial\xi}\ln I(\xi)\right]_T. \quad (2.21)$$

The meaning of ξ is determined from Eq. (2.19) as follows:

$$\beta p=-\left[\frac{\partial}{\partial l}\left(\frac{F}{MkT}\right)\right]_T=\left(\frac{\partial\lambda_1}{\partial l}\right)_T=\xi, \quad (2.22)$$

where p is the pressure of the system. Equation (2.21) with the definition of ξ of Eq. (2.22) is the equation of

[8] Because of the periodic boundary condition, the integration over x' is taken for the interval of L. But as is seen from the form of $f^{(2)}$, Eq. (2.18) below, the detailed value of the upper limit is not important if it is sufficiently large.

[9] As is well known in classical statistical mechanics, the kinetic energy part of the partition function is separable from the potential energy part, and the former does not contribute to the equation of state. Therefore in the following we discuss only the potential energy part. The thermodynamic quantities, S, E, etc., we use hereafter are only of the potential part of the system.

[10] The upper limit of the integral was originally L, but was changed to ∞ in order to avoid the arbitrary length L.

state, derived already by several authors.[1-5] Equations (2.19) and (2.22) give

$$I(\xi)=\exp\left(-\frac{G}{MkT}\right)=e^{-\beta\mu}, \tag{2.23}$$

where G is the Gibbs free energy and μ the chemical potential. From Eqs. (2.7) and (2.18), the energy E is written as

$$E=Me^{\beta\mu}\int_0^\infty dr\Phi(r)\exp[-\beta pr-\beta\Phi(r)], \tag{2.24}$$

where $e^{\beta\mu}$ actually means $[I(\beta p)]^{-1}$. The average particle density $\rho(R_i+x)$ at a point R_i+x is

$$\rho(R_i+x)=\sum_{j=-M/2}^{M/2} f^{(1)}(x-jl;R_{i+j})=ML^{-1}=l^{-1} \tag{2.25}$$

as is expected.

When we started the calculation we had in mind a picture of the cell model, as we assigned one particle to each one of the lattice points. Using an analogy with the distribution of a particle near the center of a cell in the cell model, we expected to obtain a more or less Gaussian type of distribution for $f^{(1)}(x)$ around the lattice point. Therefore it is rather surprising to have ended up with a constant value (2.17) throughout the line.[11] This result seems to indicate one aspect of the limitations of the cell model.[12]

3. TWO-COMPONENT SYSTEM

When one deals with a mixture of two kinds of particles A and B, one uses the following probability functions: $f_A^{(1)}(x_A)$, $f_B^{(1)}(x_B)$, $f_{AA}^{(2)}(x_A,x_A')$, $f_{AB}^{(2)}(x_A,x_B')$, $f_{BA}^{(2)}(x_B,x_A')$, and $f_{BB}^{(2)}(x_B,x_B')$. The meaning of these functions is understandable following the analogy with $f^{(2)}(x,x')$ used in the previous section. For instance, $f_{AB}^{(2)}(x_A,x_B')$ is the probability density of finding A and B particles at R_i+x_A and $R_{i+1}+x_B'$, respectively. The symmetry requirements are

$$\begin{aligned} f_{AA}^{(2)}(x_A,x_A')&=f_{AA}^{(2)}(-x_A',-x_A),\\ f_{BB}^{(2)}(x_B,x_B')&=f_{BB}^{(2)}(-x_B',-x_B), \end{aligned} \tag{3.1}$$

and also

$$f_{AB}^{(2)}(x_A,x_B')=f_{BA}^{(2)}(-x_B',-x_A), \tag{3 2}$$

the last of which is used to derive $f_{BA}^{(2)}$ from $f_{AB}^{(2)}$. For $f^{(1)}$'s,

$$\begin{aligned} f_A^{(1)}(x_A)&=f_A^{(1)}(-x_A),\\ f_B^{(1)}(x_B)&=f_B^{(1)}(-x_B). \end{aligned} \tag{3.3}$$

Equation (2.3) is replaced by

$$\begin{aligned} f_A^{(1)}(x_A)&=\int_{-l+x_A}^{L-l+x_A} dx_A' f_{AA}^{(2)}(x_A,x_A')\\ &\quad+\int_{-l+x_A}^{L-l+x_A} dx_B' f_{AB}^{(2)}(x_A,x_B'),\\ f_B^{(1)}(x_B)&=\int_{-l+x_B}^{L-l+x_B} dx_A' f_{BA}^{(2)}(x_B,x_A')\\ &\quad+\int_{-l+x_B}^{L-l+x_B} dx_B' f_{BB}^{(2)}(x_B,x_B'). \end{aligned} \tag{3.4}$$

The normalizations are

$$\begin{aligned} \theta&=\int_{-L/2}^{L/2} dx_A f_A^{(1)}(x_A),\\ 1-\theta&=\int_{-L/2}^{L/2} dx_B f_B^{(1)}(x_B), \end{aligned} \tag{3.5}$$

in which θ is the mixing ratio of the particles. Equations (2.6) and (2.7) are generalized to give

$$\begin{aligned} \frac{S}{kM}&=\int_{-L/2}^{L/2} dx_A f_A^{(1)}(x_A)\ln f_A^{(1)}(x_A)\\ &\quad+\int_{-L/2}^{L/2} dx_B f_B^{(1)}(x_B)\ln f_B^{(1)}(x_B)\\ &\quad-\int_{-L/2}^{L/2} dx_A\int_{-l+x_A}^{L-l+x_A} dx'_A f_{AA}^{(2)}\\ &\qquad\times(x_A,x'_A)\ln f_{AA}^{(2)}(x_A,x_A')\\ &\quad-2\int_{-L/2}^{L/2} dx_A\int_{-l+x_A}^{L-l+x_A} dx_B' f_{AB}^{(2)}\\ &\qquad\times(x_A,x'_B)\ln f_{AB}^{(2)}(x_A,x_B')\\ &\quad-\int_{-L/2}^{L/2} dx_B\int_{-l+x_B}^{L-l+x_B} dx_B' f_{BB}^{(2)}\\ &\qquad\times(x_B,x'_B)\ln f_{BB}^{(2)}(x_B,x_B'), \end{aligned} \tag{3.6}$$

$$\begin{aligned} \frac{E}{M}&=\int_{-L/2}^{L/2} dx_A\int_{-l+x_A}^{L-l+x_A} dx_A'\varphi_{AA}\\ &\qquad\times(x_A,x'_A)f_{AA}^{(2)}(x_A,x_A')\\ &\quad+2\int_{-L/2}^{L/2} dx_A\int_{-l+x_A}^{L-l+x_A} dx_B'\varphi_{AB}\\ &\qquad\times(x_A,x'_B)f_{AB}^{(2)}(x_A,x_B')\\ &\quad+\int_{-L/2}^{L/2} dx_B\int_{-l+x_B}^{L-l+x_B} dx_B'\varphi_{BB}\\ &\qquad\times(x_B,x'_B)f_{BB}^{(2)}(x_B,x_B') \end{aligned} \tag{3.7}$$

[11] In private conversation, Dr. E. W. Montroll kindly informed the author that when the zeroth particle is fixed, the standard deviation of $f^{(1)}(x,R_i)$ of the ith particle is proportional to $\sqrt{i}$. The calculation of the present section corresponds to $i\to\infty$.

[12] For a critique of the cell model or the free volume theory of the liquid state, see J. G. Kirkwood, J. Chem. Phys. **18**, 380 (1950).

in which φ_{AA}, φ_{AB}, and φ_{BB} are the interaction potentials between A–A, A–B, and B–B pairs, resprectively. The free energy is made a minimum with respect to $f_A^{(1)}$, $f_B^{(1)}$, $f_{AA}^{(2)}$, $f_{AB}^{(2)}$, and $f_{BB}^{(2)}$ under the additional conditions (3.1), (3.3) to (3.5).

Using undetermined multipliers λ_1 and λ_2 for Eqs. (3.5), $2\lambda_3(x_A)$ and $2\lambda_4(x_B)$ for Eqs. (3.4), $\lambda_5(x_A)$ and $\lambda_6(x_B)$ for Eqs. (3.3), and $\lambda_7(x_A,x_A')$ and $\lambda_8(x_B,x_B')$ for Eqs. (3.1), the equations corresponding to Eqs. (2.11), (2.12) and (2.13) become

$$-1-\ln f_A^{(1)}(x_A)+\lambda_1+2\lambda_3(x_A)+\lambda_5(x_A)-\lambda_5(-x_A)=0, \quad (3.8)$$

$$-1-\ln f_B^{(1)}(x_B)+\lambda_2+2\lambda_4(x_B)+\lambda_6(x_B)-\lambda_6(-x_B)=0, \quad (3.9)$$

$$\beta\varphi_{AA}(x_A,x_A')+1+\ln f_{AA}^{(2)}(x_A,x_A')-2\lambda_3(x_A)+\lambda_7(x_A,x_A')-\lambda_7(-x_A',-x_A)=0, \quad (3.10)$$

$$\beta\varphi_{BB}(x_B,x_B')+1+\ln f_{BB}^{(2)}(x_B,x_B')-2\lambda_4(x_B)+\lambda_8(x_B,x_B')-\lambda_8(-x_B',-x_B)=0, \quad (3.11)$$

$$\beta\varphi_{AB}(x_A,x_B')+1+\ln f_{AB}^{(2)}(x_A,x_B')-\lambda_3(x_A)-\lambda_4(-x_B')=0, \quad (3.12)$$

$$-F/(MkT)=\theta\lambda_1+(1-\theta)\lambda_2. \quad (3.13)$$

Combining Eqs. (3.3) and (3.1) with Eqs. (3.8) through (3.11), one can eliminate λ_5, λ_6, λ_7, and λ_8, so that $f^{(1)}$'s and $f^{(2)}$'s are expressed using only λ_1, λ_2, λ_3, and λ_4. Following the scheme used in the previous section, as is shown in Appendix II, a possible solution of the integral equation (3.4) is the following set:

$$\lambda_3(x_A)=\xi x_A+c_3, \qquad \lambda_4(x_B)=\xi x_B+c_4, \quad (3.14)$$

ξ, c_3, and c_4 being constants. Determining c_3 and c_4 from Eq. (3.5), one obtains

$$f_{AA}^{(2)}(x_A,x_A')=\theta L^{-1}\times\exp[-\lambda_1+\xi(l-r_{AA})-\beta\Phi_{AA}(r_{AA})]$$
$$f_{BB}^{(2)}(x_B,x_B')=(1-\theta)L^{-1}\times\exp[-\lambda_2+\xi(l-r_{BB})-\beta\Phi_{BB}(r_{BB})] \quad (3.15)$$
$$f_{AB}^{(2)}(x_A,x_B')=[\theta(1-\theta)]^{\frac{1}{2}}L^{-1}\times\exp[-\tfrac{1}{2}(\lambda_1+\lambda_2)+\xi(l-r_{AB})-\beta\Phi_{AB}(r_{AB})]$$

and also

$$f_A^{(1)}(x_A)=\theta L^{-1}, \qquad f_B^{(1)}(x_B)=(1-\theta)L^{-1}. \quad (3.16)$$

In Eq. (3.15), r_{AB} etc. are the relative distance defined in analogy with Eq. (2.8). For instance

$$r_{AB}=x_B'+l-x_A. \quad (3.17)$$

$\Phi_{AB}(r_{AB})$ is identical with $\varphi_{AB}(x_A,x_B')$ written using the relative distance r_{AB}. Φ_{AA} and Φ_{BB} have similar meanings.

Inserting Eqs. (3.15) and (3.16) into Eqs. (3.4), one obtains

$$e^{-\xi l}=\exp[-\lambda_1-\beta\mu_{AA}]+\exp[-l-\tfrac{1}{2}(\lambda_1+\lambda_2)-\beta\mu_{AB}], \quad (3.18)$$

$$e^{-\xi l}=\exp[l-\tfrac{1}{2}(\lambda_1+\lambda_2)-\beta\mu_{AB}]+\exp[-\lambda_2-\beta\mu_{BB}], \quad (3.19)$$

where

$$e^{l}=[\theta/(1-\theta)]^{\frac{1}{2}} \quad (3.20)$$

and, following Eqs. (2.20) and (2.23) we have put

$$\exp[-\beta\mu_{AA}(\xi)]\equiv\int_0^\infty dr\,\exp[-\xi r-\beta\Phi_{AA}(r)]. \quad (3.21)$$

$\mu_{BB}(\xi)$ and $\mu_{AB}(\xi)$ are defined when one replaces $\Phi_{AA}(r)$ in Eq. (3.21) by $\Phi_{BB}(r)$ and $\Phi_{AB}(r)$, respectively.

Solutions of Eqs. (3.18) and (3.19) are

$$e^{-\lambda_1}=\exp[\beta\mu_{AA}-\xi l](\Gamma-1+2\theta)/(\Gamma+1), \qquad e^{-\lambda_2}=\exp[\beta\mu_{BB}-\xi l](\Gamma+1-2\theta)/(\Gamma+1), \quad (3.22)$$

where

$$\Gamma^2\equiv 1+4\theta(1-\theta)\{e^{\beta w(\xi)}-1\}, \quad (3.23)$$

and

$$w(\xi)=2\mu_{AB}(\xi)-\mu_{AA}(\xi)-\mu_{BB}(\xi). \quad (3.24)$$

Inserting Eq. (3.22) into Eq. (3.13), one obtains

$$-F/(MkT)=\xi l+\ln(\Gamma+1)-\theta[\beta\mu_{AA}+\ln(\Gamma-1+2\theta)]-(1-\theta)[\beta\mu_{BB}+\ln(\Gamma+1-2\theta)]. \quad (3.25)$$

ξ is determined from the condition that F of Eq. (3.25) is made a minimum with respect to ξ, keeping l and T constant. Then one obtains the equation of state:

$$-l=\frac{\partial}{\partial\xi}\{\ln(\Gamma+1)-\theta[\beta\mu_{AA}+\ln(\Gamma-1+2\theta)]-(1-\theta)[\beta\mu_{BB}+\ln(\Gamma+1-2\theta)]\}. \quad (3.26)$$

The same procedure as in Eq. (2.22) tells one that

$$\xi=\beta p. \quad (3.27)$$

Combining Eqs. (3.15) and (3.22), the final results for $f^{(2)}$'s are

$$f_{AA}^{(2)}(x_A,x_A')=\frac{\theta}{L}\frac{\Gamma-1+2\theta}{\Gamma+1}\times\exp[\beta\mu_{AA}-\beta pr_{AA}-\beta\Phi_{AA}(r_{AA})],$$
$$f_{BB}^{(2)}(x_B,x_B')=\frac{1-\theta}{L}\frac{\Gamma+1-2\theta}{\Gamma+1}\times\exp(\beta\mu_{BB}-\beta pr_{BB}-\beta\Phi_{BB}(r_{BB})], \quad (3.28)$$
$$f_{AB}^{(2)}(x_A,x_B')=\frac{2\theta(1-\theta)}{L(\Gamma+1)}\times\exp[\beta\mu_{AB}-\beta pr_{AB}-\beta\Phi_{AB}(r_{AB})].$$

4. THERMODYNAMIC QUANTITIES OF MIXTURE

Recalling Eq. (2.23), $\mu_{AA}(\xi)$ defined in Eq. (3.21) is the chemical potential of the pure A system, and following Eq. (2.24)

$$E_{AA}=M\int_0^\infty dr\Phi_{AA}(r)\exp[\beta\mu_{AA}-\beta pr-\beta\Phi_{AA}(r)] \quad (4.1)$$

is the energy of M particles of the pure A system. E_{BB} is analogously defined replacing μ_{AA} and $\Phi_{AA}(r)$ in Eq. (4.1) by μ_{BB} and $\Phi_{BB}(r)$ respectively. Also Eq. (2.21) gives, when multiplied by M,

$$L_{AA}=M\beta\left[\frac{\partial}{\partial\xi}\mu_{AA}(\xi)\right]_T, \quad (4.2)$$

for the equation of state of the pure A system. It is convenient in the following mathematical manipulation to imagine a system of particles interacting with the mutual potential $\Phi_{AB}(r)$. This is of course hypothetical, but let us call this system a "Φ_{AB}" system, for the sake of simplicity. Then $\mu_{AB}(\xi)$ defined from Eq. (3.21) is the chemical potential of the "Φ_{AB}" system and the energy and the equation of state of this system are

$$E_{AB}=M\int_0^\infty dr\Phi_{AB}(r)\times\exp[\beta\mu_{AB}-\beta pr-\beta\Phi_{AB}(r)], \quad (4.3)$$

$$L_{AB}=M\beta\left[\frac{\partial}{\partial\xi}\mu_{AB}(\xi)\right]_T.$$

Inserting Eq. (3.28) into Eq. (3.7), one obtains the energy of the mixture, E. The frequently quoted quantity, the energy of mixing, Δ_mE, becomes after algebraic transformations

$$\Delta_mE\equiv E-\theta E_{AA}-(1-\theta)E_{BB}=\theta(1-\theta)(2E_{AB}-E_{AA}-E_{BB})2/(\Gamma+1). \quad (4.4)$$

Equation (3.26) is simplified to

$$\Delta_mL\equiv L-\theta L_{AA}-(1-\theta)L_{BB}=\theta(1-\theta)(2L_{AB}-L_{AA}-L_{BB})2/(\Gamma+1). \quad (4.5)$$

As the heat function H is $E+pL$, Eqs. (4.4) and (4.5) give the heat of mixing Δ_mH:

$$\Delta_mH\equiv H-\theta H_{AA}-(1-\theta)H_{BB}=\theta(1-\theta)(2H_{AB}-H_{AA}-H_{BB})2/(\Gamma+1). \quad (4.6)$$

The Gibbs free energy G for the mixing is obtained from Eqs. (3.25) and (3.27), recalling that μ_{AA} and μ_{BB} are the chemical potentials of the pure systems, as

$$\Delta_mG/(MkT)\equiv[G-\theta G_{AA}-(1-\theta)G_{BB}]/(MkT)=\theta\ln(\Gamma-1+2\theta)+(1-\theta)\times\ln(\Gamma+1-2\theta)-\ln(\Gamma+1). \quad (4.7)$$

Combining Eqs. (4.6) and (4.7), the entropy of mixing becomes

$$\Delta_mS/(Mk)=-\theta\ln\theta-(1-\theta)\ln(1-\theta)-\theta\ln\frac{\Gamma+1+2\theta}{\theta(\Gamma+1)}-(1-\theta)\ln\frac{\Gamma+1-2\theta}{(1-\theta)(\Gamma+1)}+\theta(1-\theta)2(\Gamma+1)^{-1}\times(2H_{AB}-H_{AA}-H_{BB})/(MkT). \quad (4.8)$$

When $\Phi_{AA}(r)$, $\Phi_{BB}(r)$, and $\Phi_{AB}(r)$ are closely alike, so are the three μ's defined in Eq. (3.21), making w of Eq. (3.24) and $2H_{AB}-H_{AA}-H_{BB}$ of Eq. (4.6) vanish. Then Γ of Eq. (3.23) becomes unity and $\Delta_mS/(Mk)$ of Eq. (4.8) reduces to its first two terms, which are the correct forms for an ideal mixture.

5. DISCUSSION

As the formulation of this paper is valid for any shape of the interaction potentials, it includes as its special case the lattice model of regular solutions (of one-dimension) discussed, for instance, by Guggenheim.[13] It is interesting to compare the results of the previous section with his treatment of the lattice model based on the quasi-chemical method, which is rigorous for the one-dimensional system. In the process of comparison, one must remember that the concept of the pressure does not come into the lattice treatment and hence the Gibbs and the Helmholtz free energies become identical, and so are the internal energy and the heat function.

x and β in G.M. correspond to our θ and Γ, respectively, and though w, too, has the same meaning in both cases, our Eq. (3.24), combined with Eq. (3.21), gives the detailed form for w. When one defines u as in G.M. (4.27.1), one easily sees, using our notation, that

$$u=w-T\left(\frac{dw}{dT}\right)_p=(2H_{AB}-H_{AA}-H_{BB})/M. \quad (5.1)[14]$$

Inserting this relation into Eq. (4.6), one obtains

$$\Delta_mH/M=2u\theta(1-\theta)/(\Gamma+1), \quad (5.2)$$

which is identical with G.M. (4.27.8) when one notes that Δ_mU of the latter actually means Δ_mH. One also notices that G.M. (4.27.4) for Δ_mF is identical with our Eq. (4.7) for Δ_mG, as it should be. G.M. (4.12.13) for the temperature of critical mixing holds for our case also, and putting $z=2$ in it we see that there is no separation into two phases in one-dimensional binary mixtures for any shape of the interaction potentials.

[13] E. A. Guggenheim, *Mixtures* (Oxford University Press, New York, 1952), Chapter 4. Equations from this book will be quoted with G.M. attached to the number.

[14] In the simplest treatment based on the lattice model, w is assumed constant independent of T, giving $u=w$. The fact that w has the nature of a free energy and may depend on T was pointed out by Guggenheim in, for instance, Sec. 4.27 of G.M.

As Γ in Eq. (3.23) is a function of $\theta(1-\theta)$, the dependence of $\Delta_m H$ in Eq. (5.2) on θ is through the combination $\theta(1-\theta)$, and is symmetric around $\theta=\frac{1}{2}$. But in experimental data[15] of $\Delta_m H$ in three-dimensional liquid systems, $\Delta_m H$ is not necessarily symmetrical around $\theta=\frac{1}{2}$. This disagreement is due to the fact that in two- and three-dimensional problems spacial filling of two kinds of particles brings in additional cooperative volume effects which could not be taken into account in the present treatment of a one-dimensional model.

APPENDIX I. DERIVATION OF EQ. (2.16)

Inserting Eqs. (2.14) and (2.15) into Eq. (2.3), one obtains

$$\exp[\lambda_2(x)+\lambda_2(-x)+\lambda_1]=\int_{-l+x}^{L-l+x} dx' \times\exp[\lambda_2(x)+\lambda_2(-x')-\beta\varphi(x,x')]. \quad \text{(AI.1)}$$

When one changes x' into the relative coordinate r defined in Eq. (2.8), Eq. (AI.1) can be written as

$$\exp[\lambda_1]=\int_0^L dr \times\exp[-\beta\Phi(r)+\lambda_2(l-r-x)-\lambda_2(-x)]. \quad \text{(AI.2)}$$

As the left-hand side, $\exp(\lambda_1)$, does not depend on x, a sufficient condition for Eq. (AI.2) is that $\lambda_2(l-r-x)-\lambda_2(-x)$ is independent of x. If this is the case, then

$$\frac{\partial\lambda_2(l-r-x)}{\partial x}=\frac{\partial\lambda_2(-x)}{\partial x}. \quad \text{(AI.3)}$$

In order that this equation holds for any value of $l-r$, each side should be independent of x. Hence, putting

$$\frac{\partial\lambda_2(-x)}{\partial x}=-\xi, \quad \text{(AI.4)}$$

one obtains Eq. (2.16).

[15] See, for instance, Fig. 3 of O. J. Kleppa, J. Am. Chem. Soc. **71**, 3275 (1949).

APPENDIX II. DERIVATION OF EQ. (3.14)

After the elimination of λ_5 to λ_8 from Eqs. (3.1), (3.3), (3.8) through (3.11), one obtains

$$\begin{aligned}\ln f_A^{(1)}(x_A)&=\lambda_3(x_A)+\lambda_3(-x_A)+\lambda_1-1,\\ \ln f_B^{(1)}(x_B)&=\lambda_4(x_B)+\lambda_4(-x_B)+\lambda_2-1,\end{aligned} \quad \text{(AII.1)}$$

$$\begin{aligned}\ln f_{AA}^{(2)}(x_A,x_A')&=\lambda_3(x_A)+\lambda_3(-x_A')-\beta\varphi_{AA}(x_A,x_A')-1,\\ \ln f_{BB}^{(2)}(x_B,x_B')&=\lambda_4(x_B)+\lambda_4(-x_B')-\beta\varphi_{BB}(x_B,x_B')-1,\\ \ln f_{AB}^{(2)}(x_A,x_B')&=\lambda_3(x_A)+\lambda_4(-x_B')-\beta\varphi_{AB}(x_A,x_B')-1.\end{aligned} \quad \text{(AII.2)}$$

Looking back at the constance of $f^{(1)}(x)$ as is shown in Eq. (2.17), it is plausible to choose $\lambda_3(x_A)$ and $\lambda_4(x_B)$ of Eq. (AII.1) so that $f_A^{(1)}(x_A)$ and $f_B^{(1)}(x_B)$ become constant. This reasoning gives one

$$\begin{aligned}\lambda_3(x_A)&=\xi_3 x_A+c_3,\\ \lambda_4(x_B)&=\xi_4 x_B+c_4,\end{aligned} \quad \text{(AII.3)}$$

λ_3 and λ_4 not necessarily being equal.

Putting these into Eqs. (AII.2) and changing the primed coordinates into the relative ones, r_{AB} etc., using Eq. (3.17) and the associated relations, one obtains

$$\begin{aligned}\ln f_{AA}^{(2)}(x_A,x_A')&=\xi_3(l-r_{AA})+2c_3-1-\beta\Phi_{AA}(r_{AA}),\\ \ln f_{BB}^{(2)}(x_B,x_B')&=\xi_4(l-r_{BB})+2c_4-1-\beta\Phi_{BB}(r_{BB}),\\ \ln f_{AB}^{(2)}(x_A,x_B')&=\xi_4(l-r_{AB})+c_3+c_4-1-\beta\Phi_{AB}(r_{AB})+(\xi_3-\xi_4)x_A.\end{aligned} \quad \text{(AII.4)}$$

Of these three relations, $f_{AA}^{(2)}$ and $f_{BB}^{(2)}$ are functions only of the relative coordinates. Therefore it is reasonable to conclude that $f_{AB}^{(2)}(x_A,x_B')$ also depends only on the relative coordinate r_{AB}, to obtain

$$\xi_3=\xi_4=\xi. \quad \text{(AII.5)}$$

Combining Eqs. (AII.3) and (AII.5), one obtains Eq. (3.14).

Mass Spectrometric Investigation of Active Nitrogen*

D. S. JACKSON† AND H. I. SCHIFF
Department of Chemistry, McGill University, Montreal, Canada

(Received February 28, 1955)

A small, central portion of an active nitrogen stream was continuously sampled into a mass spectrometer. The ratio of ion intensities at masses 14 to 28 was found to be higher than that for normal nitrogen at the same pressure. The ionization efficiency curves at mass 28, in the presence and in the absence of the discharge were superimposable, but those at mass 14 were quite different. The difference $\Delta 14$, between these two curves was plotted against the applied electron voltage. A discontinuity in this $\Delta 14$ curve showed that it resulted from two processes. The appearance potentials for these two processes were $14.7_2 \pm 0.2_6$ ev and 16.1 ± 0.3 ev. The lower value clearly indicated the presence of ground state atoms in active nitrogen. Several processes capable of producing the higher value are discussed. The concentration of active species is estimated to be between 0.1 and 1%.

INTRODUCTION

THE intense yellow afterglow of nitrogen was first reported by E. P. Lewis in 1900.[1] The main characteristics of the afterglow are: (1) its long duration, (2) its emission spectrum which consists mainly of the first positive band of nitrogen, corresponding to the transition from the $B^3\Pi$ to the $A^3\Sigma$ state, with intensity maxima at $v'=6$ and 12, and (3) an enhanced chemical reactivity of the gas,[2] which has resulted in the use of the term, active nitrogen.

Numerous attempts have been made to explain these characteristics. Metastable molecules, N_3, ions, and atoms have each been suggested as major components of active nitrogen. However, no direct determination of its composition has been reported. In view of the recent success of the mass spectrometer in detecting free radicals[3] an attempt was made to apply this technique to the analysis of active nitrogen. A preliminary report of this work has already appeared in this journal.[4] This paper presents a more detailed account.

EXPERIMENTAL

Apparatus

The mass spectrometer was a 90° sector-type instrument, the analyzer tube of which had a 15.0 cm radius of curvature. The ion source, of the Nier design with drawing out potentials, was modified according to Lossing[5] to provide differential pumping of the filament chamber. Magnetic scanning was used, the ion accelerating potential being maintained at 2000 volts. The electronic controls were similar to those of Graham, Harkness, and Thode.[6] The slit widths were chosen to allow a mass resolution of one in two hundred. An electrometer tube dc amplifier, used in conjunction with a model *G* Speedomax recorder, provided a maximum sensitivity of 1 cm deflection per 3×10^{-14} ampere ion current. The gas flow into the instrument was through a leak punched in a quartz thimble in the manner described by Lossing.[5] The hole was 30 microns in diameter and 10 microns in depth, and was located 1.5 cm from the top slit of the ion source. Pressures of nitrogen up to 3 mm Hg could be used above this leak without any alteration of sensitivity or cracking pattern of the nitrogen spectrum.

The original discharge tube used to produce the active nitrogen was of the familiar Wood-Bonhoeffer type with the gas outlet leading to the mass spectrometer located at the center of the discharge. An electrical circuit similar to that described by Winkler and Greenblatt,[7] but without the spark-gap, produced an intermittent, dc arc, the pulse rate of which could be varied by controlling the input voltage to the power supply. This arrangement was found to interfere with the operation of the mass spectrometer. First, there was an increase in the background noise of the amplifier; this could be reduced to less than twice its normal value by appropriate shielding of the discharge power supply. There remained, however, a distinct instability when the mass spectrometer was focused on an ion peak. This was traced to interference with the high potential of the mass spectrometer. Moreover, operation of the discharge resulted in an increase in the size of the mass spectrometer leak. Both of these observations suggested that negatively charged particles were being accelerated through the quartz thimble to the top plate of the ion source, which was maintained at a potential 2000 volts above ground. An auxiliary electrode (*B*, Fig. 1) was

* This work was supported by the National Research Council (Canada) and reported to the Chemical Institute of Canada, June, 1954.

† Holder of a Canadian Industries Limited Fellowship 1952–1954. Present address: Aluminum Company of Canada, Arvida, Quebec.

[1] E. P. Lewis, Astrophys. J. **12**, 8 (1900).

[2] See for example, the systematic investigation of the reactions of active nitrogen with the hydrocarbons by C. A. Winkler and associates, Can. J. Chem. **30**, 915 (1952); **31**, 1, 346, 129 (1953); **32**, 351, 718 (1954).

[3] See for example the series by F. P. Lossing and associates, J. Chem. Phys. **20**, 907 (1952); **21**, 1135 (1953); **22**, 621, 1489 (1954), Disc. Faraday Soc. No. 14, 34 (1953); Can. J. Chem. **31**, 30 (1953).

[4] D. S. Jackson and H. I. Schiff, J. Chem. Phys. **21**, 2233 (1953).

[5] F. P. Lossing and A. W. Tickner, J. Chem. Phys. **20**, 907 (1952).

[6] Graham, Harkness, and Thode, J. Sci. Instr. **24**, 119 (1947).

[7] J. Greenblatt and C. A. Winkler, Can. J. Research **B27**, 721 (1949).

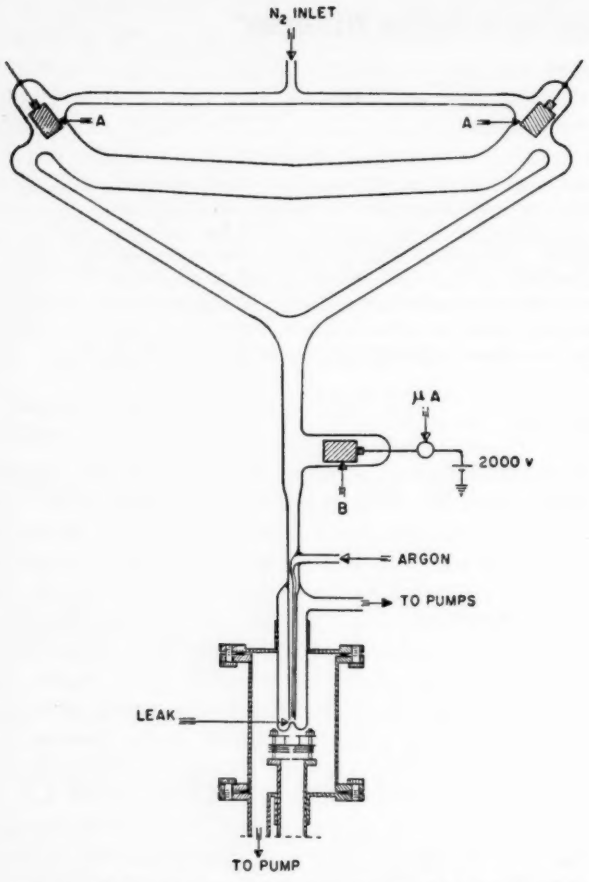

FIG. 1. Discharge tube and mass spectrometer ion source. Discharge occurs between electrodes *A*; electrode *B* acts as an electron trap.

therefore inserted between the discharge tube and the leak and connected through a microammeter (μA) to a positive 2000 volt supply. When the discharge was excited, deflections up to 20 microamperes were observed. The path length of the active nitrogen was also increased to 50 cm. These two modifications greatly reduced the interference with the high potential. Finally, various discharge tube designs were tried and that shown in Fig. 1 was found to give the least interference. It might be of interest to point out that the afterglow was as intense in the exit tube from the anode as in that from the cathode.

Procedure

Commercial, water-pumped nitrogen was drawn from a cylinder at atmospheric pressure by allowing an excess to escape through a bubbler. It was freed from oxygen by passage over copper-wool at 440°C, and from water and other "condensible" impurities by passage through several traps immersed in liquid nitrogen. The nitrogen then passed through a flow meter and a variable capillary to reduce its pressure to approximately 1 mm Hg. It entered the discharge tube as indicated in Fig. 1, flowed over the mass spectrometer leak, and thence to the rotary pumps, which were capable of maintaining a flow rate of 10.3 micromoles per second at 1 mm Hg pressure. The glass walls of that part of the apparatus shown in Fig. 1 were treated with a 10% solution of meta-phosphoric acid to decrease the loss of activity of the gas.

A small, central portion of the gas stream was continuously sampled through the leak. Since the bottom of the quartz thimble was less than 1 mm from the top slit of the mass spectrometer, most of the sampled gas entered the ion source directly. Any portion which did not, was prevented from diffusing back into the ion source by the differential pumping arrangement.

Nitrogen was allowed to flow through the system until a constant ion current at mass 28 indicated steady flow conditions. The ion currents at masses 14 and 28 were then recorded. The discharge was excited, and after steady flow conditions were re-established the ion intensities were again recorded. Finally, the discharge tube was extinguished and the ion intensities compared with the initial readings to ensure that the flow conditions had not altered during the experiment.

Normal nitrogen, at a pressure of 1 mm Hg, gave ion intensities at masses 14 and 28 in the ratio of 0.0385 to 1, when 50 volt electrons were used. When the discharge was excited the ion intensity at mass 28 decreased while that at mass 14 increased. The ratio of the intensities increased to an average value of 0.0420. This increase in ratio was found to be independent of the discharge pulse rate over the range 5 to 50 pulses per second, but was smaller outside this range. The effect of pressure on the ratio has already been reported.[4] A freshly "poisoned" vessel, or one which had recently been exposed to water vapor always produced a high ratio. When argon was introduced into the nitrogen stream through the jet (see below), no change in the ion intensity at mass 40 was observed upon excitation of the discharge; this indicated that the change in the ratio of the nitrogen peaks was not due to any temperature change of the gas which might have resulted from the discharge.

Appearance Potential Measurements

To identify the species responsible for the increase in the ion intensity at mass 14, appearance potential measurements were undertaken. A model 622 Weston microammeter, in series with either a 1 or a 3 megohm precision resistor, was used to measure the voltage applied between the midpoint of the filament and the case of the electron gun. The applied voltages could be read or reset with an accuracy of ± 0.3 volt on the 60-volt range, and ± 0.1 volt on the 20-volt range.

Argon, used as a calibrating gas, was introduced directly over the mass spectrometer leak as shown in Fig. 1. Welding grade gas, rated as 99.9% pure, was further subjected to several trap-to-trap distillations. The argon flow was regulated, by temperature control of its vapor pressure, to give an ion current at mass 40

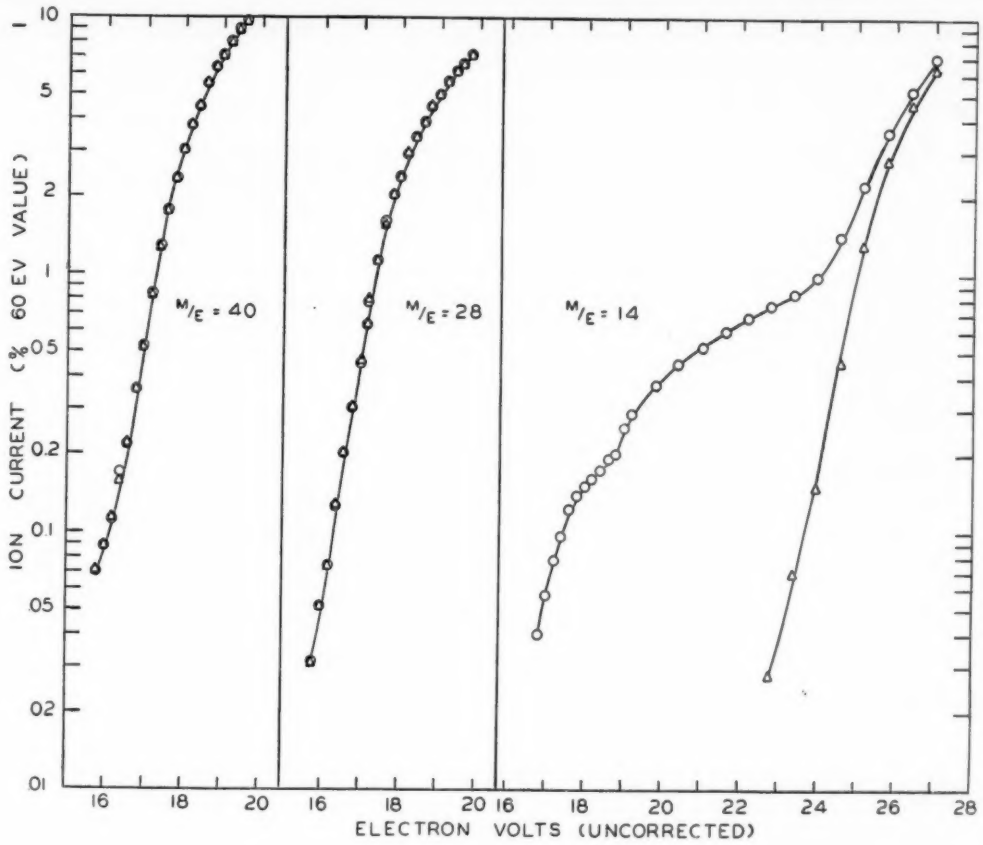

FIG. 2. Semilogarithmic ionization efficiency curves for the ions A^+, N_2^+, and N^+. The circles represent values obtained with excitation of the discharge, the triangles represent values obtained in the absence of the discharge.

commensurate with the increase in ion current at mass 14.

When steady flow of both nitrogen and argon had been achieved, the ion intensities at masses 28, 14, and 40 were recorded at an electron energy of 60 volts. The applied voltage was then decreased and the ion intensities measured at 0.2 ev intervals. The total electron emission was maintained at 70 microamperes. Finally, the electron energy was again increased to 60 ev and a check taken of the initial readings.

The same procedure was then followed with the discharge tube excited.

Figure 2 shows typical semilogarithmic curves obtained when the ion intensities are plotted, as the percentage of their 60 ev values, against the applied electron voltage. It will be seen that the curves at mass 28 are superimposable, as are those at mass 40. The curves at mass 14 however, are quite different, the inflection clearly indicating the presence of one or more new species in active nitrogen.

If the difference $\Delta 14$, between the two curves at mass 14, is plotted as a function of the applied electron voltage the curve shown in Fig. 3 is obtained. This plot should then represent the ion efficiency curve for the new species. It will be seen that the $\Delta 14$ curve is itself composite, resulting from at least two separate processes. The argon ionization efficiency curve is repeated on this nonlogarithmic plot for comparison.

Various methods for evaluating appearance potentials from ionization efficiency curves have been employed. The least ambiguous methods appear to be the "critical slope" method of Honig,[8] and the "extrapolated difference" method of McDowell and Warren,[9] or the equivalent "1% method" of Lossing.[10] These methods all require relatively large ion intensities which could not be achieved in this research. Since the $\Delta 14$ values at 60 ev are less than 1% of the mass 28 ion intensities, recourse was made to the adjusted linear extrapolation method in which the ionization efficiency curves are plotted so as to make parallel the approximately linear portions for the ion under investigation and that of the calibrating gas. This method gives reproducible results which are in agreement with those obtained by the other methods provided the ionizing process is a simple one,[9] such as the production of the molecule ion. Otherwise this method gives values which are slightly high.

The observed appearance potentials obtained in this way for the molecule ions of argon, nitrogen, ethane, and helium were plotted against the spectroscopic ionization potentials. A straight line with a slope of unity was obtained, which indicated that the use of the single calibrating gas, argon, was justified.

[8] R. E. Honig, J. Chem. Phys. **16**, 105 (1948).
[9] C. A. McDowell and J. W. Warren, Discussions Faraday Soc. No. 10, 53 (1951).
[10] Lossing, Tickner, and Bryce, J. Chem. Phys. **19**, 1254 (1951).

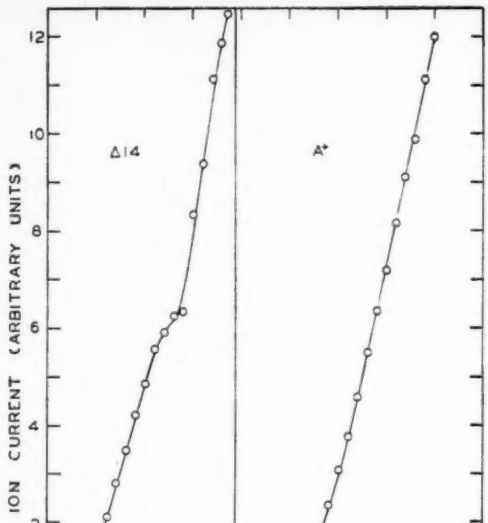

FIG. 3. Normal ionization efficiency curves at mass 14 for the new species, and at mass 40 for argon.

The two linear portions of the Δ14 curve were extrapolated to the voltage axis. The corrected appearance potentials thus obtained were $14.7_2 \pm 0.2_6$ ev, and 16.1 ± 0.3 ev. Both values represent the average of 18 separate experiments. The appearance potentials obtained by using the extrapolated difference method for several experiments agreed with these values within the limits of accuracy indicated.

Concentration of the Active Species

The two portions of the Δ14 curve are of approximately equal lengths, but the discontinuity was not sufficiently sharp to permit a good resolution into the two component curves. For this reason, the contribution of each process could not be evaluated separately. However, an upper limit can be placed on the atomic nitrogen concentration by assuming that it alone is responsible for the Δ14 curve.

Let the peak heights at masses 28 and 14 in the absence of the discharge be H and h respectively, and in the presence of the discharge, H' and h' respectively. The ratio of the partial pressure of nitrogen atoms (N), to the partial pressure of nitrogen molecules (N_2) would be:

$$\frac{(N)}{(N_2)} = \frac{(h' - hH'/H)}{H'} \cdot \frac{S_{N_2}}{S_N},$$

where S_{N_2} and S_N are the sensitivities of the mass spectrometer to nitrogen molecules and atoms respectively. This expression reduces to

$$\frac{(N)}{(N_2)} = \left(\frac{h'}{H'} - \frac{h}{H}\right) \cdot \frac{S_{N_2}}{S_N}. \tag{1}$$

The ratio of the sensitivities can readily be expressed as

$$\frac{S_{N_2}}{S_N} = \frac{2(H - H')}{(h' - hH'/H)}. \tag{2}$$

Equations (1) and (2) merely represent a separation of the obvious relation

$$\frac{(N)}{(N_2)} = \frac{2(H - H')}{H'}. \tag{3}$$

The application of Eq. (3) however, requires that the pressure remains absolutely constant during the experiment, which is a difficult condition to fulfill. Although Eq. (2) also contains the difference between peak heights, and consequently is subject to the same condition, only one carefully controlled experiment is required to determine the relative sensitivities once and for all. Equation (1) can then be used to calculate the concentrations for all other experiments, and, since it involves only the ratios of ion intensities with and without the discharge, is not nearly as sensitive to transient fluctuations in pressure.

The relative sensitivities S_{N_2}/S_N, calculated from Eq. (2) for carefully controlled experiments, was found to be 1.4. The atom concentration calculated from Eq. (1) was between 0.1 and 1%, depending on the condition of the walls of the discharge tube. This is an upper limit for the atom concentration and probably corresponds more closely to the total concentration of active species. Benson[11] estimated a concentration of active species of 0.3% from calorimetric measurements. E. Inn[12] suggested an upper limit of 2% on the atomic nitrogen concentration from vacuum ultraviolet absorption studies. These estimates are all in substantial agreement when the differences in experimental conditions and the assumptions in the calculations are considered.

DISCUSSION

The various species which have been postulated as the energetic constituent of active nitrogen will now be discussed from the point of view of the possible processes which could occur upon electron impact.

(a) Atomic Nitrogen

The spectroscopic ionization potential of the ground state ^4S atom has been reported as 14.54 ev.[13] The value of $14.7_2 \pm 0.2_6$ ev obtained for the lower of the two appearance potentials of the new species agrees with this

[11] J. M. Benson, J. Appl. Phys. **23**, 757 (1952).
[12] E. Inn, private communication.
[13] C. E. Moore, Natl. Bur. Standards Circ. 467, Vol. 1, (1949).

value within experimental error. Ionization of the ^4S atom to the ^1D excited state of the ion would require an energy of 16.43 ev, which is within the experimental error of the 16.1 ev appearance potential.

No process involving ionization of atoms in low-lying metastable states could give an appearance potential within experimental limits of the 14.7_2 ev value. Only one process—the ionization of the long-lived ^2D atom to the ^1S state of the ion—could give an appearance potential within the experimental limits of the 16.1 ev value.

(b) N_2^+ Ions

Positive ions have been strongly advocated by Mitra,[14] primarily for theoretical reasons but also because active nitrogen has been found to be an electrical conductor. This observation was confirmed during the present investigation by some experiments in which active nitrogen was passed between parallel plane electrodes, 3.5 cm in diameter and placed 1.0 cm apart. Current-voltage characteristics, typical of a cold cathode discharge of a gas containing charged particles, were obtained. However, similar curves were obtained when argon was substituted for nitrogen, which indicated that the conductivity was not necessarily due to an ionic species of active nitrogen.

An attempt was then made to determine the nature of the charged particles. When positive voltages were applied between only one of these electrodes and either ground potential or the midpoint of the voltage across the discharge, currents up to 20 microamperes were obtained. When negative voltages were applied no current readings could be obtained. Since negative nitrogen ions are unknown, these observations suggest that electrons are the only charged particles present in the nitrogen afterglow,—a conclusion also reached by Benson,[12] who used the more sensitive microwave technique. This suggestion was also supported by the observation that the negative particles could be readily deflected away from the electrode by means of a weak magnetic field. A crude calculation based on the saturation current between the parallel electrodes gave a value of about 1 electron per 10^7 nitrogen molecules, which can be compared with Benson's more accurate estimate of 1 electron per 2.5×10^8 molecules.

(c) The N_3 Molecule

Triatomic nitrogen was first suggested as a constituent of active nitrogen by Strutt,[15] and more recently by Uri and by Herzberg.[16] The possible electron impact processes for this species are

$$N_3+e^-\rightarrow N_3^++2e^-. \quad (1)$$

This process does not occur to a significant extent since no ion current corresponding to $m/e=42$ was detected.

$$N_3+e^-\rightarrow N_2^++N+2e^-. \quad (2)$$

The appearance potential for the mass 28 ion arising from this process would be

$$A(N_2^+)=I(N_2)+D(N_2-N)+E$$

where: $I(N_2)$ is the ionization potential of molecular nitrogen=15.76 ev. $D(N_2-N)$ is the strength of the N−N bond in N_3. E is the excess energy, kinetic or electronic, which the dissociation products of the process might possess.

$$N_3+e^-\rightarrow N^++N_2+2e^-. \quad (3)$$

The appearance potential of the mass 14 ion would be

$$A(N^+)=I(N)+D(N_2-N)+E.$$

This process could account for the 16.1 ev appearance potential at mass 14 if the N−N bond strength in N_3 is not greater than 1.4±0.3 ev.

(d) Metastable Nitrogen Molecule

Excited molecules (N_2^*), if present, could undergo the following processes:

$$N_2^*+e^-\rightarrow N_2^++2e^-. \quad (4)$$

The appearance potential of the mass 28 ion from this process would be lower than 15.76 ev by an amount approximately equal to the excitation energy of the metastable molecule.

$$N_2^*+e^-\rightarrow N^++N+2e^-. \quad (5)$$

The appearance potential of the mass 14 ion would be:

$$A(N^+)=I(N)+D(N-N^*)+E$$

where $D(N-N^*)$ is the energy required to dissociate the excited molecule. This process could account for the 16.1 ev appearance potential if the dissociation energy of the excited molecule is not greater than 1.4±0.3 ev.

CONCLUSIONS

There appears to be four processes capable of explaining the 16.1±0.3 ev appearance potential. These are the ionization of ^4S atoms to ^1D ions, the ionization of metastable ^2D atoms to ^1S ions, and processes (3) and (5). If ^2D atoms do exist in active nitrogen it is rather difficult to understand why they do not also form ions in the ^3P ground state, which would give an appearance potential of 12.17 ev.

The failure to find any evidence for process (4) may be taken as an argument against the occurrence of process (5), and consequently against the presence of metastable molecules. Process (4) should be readily detectable since it should occur at an appearance potential considerably lower than the ionization potential for molecular nitrogen.

On the other hand, failure to detect evidence for

[14] S. K. Mitra, *Active Nitrogen* (Indian Association for the Cultivation of Science, Calcutta, 1946).
[15] R. J. Strutt, Proc. Roy. Soc. (London) **A87**, 179 (1912).
[16] N. Uri, Discussions Faraday Soc. No. 14, 127 (1953); G. Herzberg, *ibid.*

processes (1) and (2) cannot be used as an argument against process (3). Thus, if triatomic nitrogen were present it might quite conceivably fail to give a parent ion. Moreover, process (2) would have an appearance potential greater than 15.76 ev, so that its contribution might be completely masked by the large ion intensity at mass 28. An unequivocal explanation for the 16.1-ev appearance potential can therefore not be offered.

The ionization of ^4S atoms however, is the only process capable of explaining the 14.7_2-ev appearance potential. The existence of ^4S atoms in active nitrogen is therefore established.

THE JOURNAL OF CHEMICAL PHYSICS VOLUME 23, NUMBER 12 DECEMBER, 1955

Electronic Population Analysis on LCAO-MO Molecular Wave Functions. III. Effects of Hybridization on Overlap and Gross AO Populations*

R. S. MULLIKEN
Laboratory of Molecular Structure and Spectra, Department of Physics, The University of Chicago, Chicago 37, Illinois

(Received January 6, 1955)

The effects of AO hybridization on gross AO and overlap populations for LCAO-MO electron configurations are discussed in terms of some simple examples, using equations and graphs. The validity of "gross AO populations" as true measures of the population in various AOs is critically discussed. It is shown that the degree of hybridization in the AOs of an LCAO MO does not in general give the true amount of s or p character in the MO; this is given instead by the gross s or p population in the MO. Nevertheless, "forced hybridization" among the AOs, although not contributing to gross AO populations, leads to important negative contributions to overlap populations, hence to bond energies. For example, forced $2s-2p$ hybridization has the result that the total overlap population for two pairs of electrons occupying bonding σ LCAO MOs built from $2s$ and $2p\sigma$ AOs in a homopolar diatomic molecule is actually *less* than the sum of the overlap populations which one would have if one pair could be in an MO built from pure $2s$ AOs and the other in an MO built from pure $2p\sigma$ AOs. This sort of forced hybridization with resultant loss of bond strength may explain why double bonds seldom if ever consist of two σ bonds.

1. EFFECTS OF HYBRIDIZATION ON POPULATIONS

IN a paper hereafter referred to as I, definitions and formulas applicable for LCAO-MO wave functions have been given for gross AO populations $N(r_k)$ and for overlap populations $n(k,l)$, and in a second paper (II), relations between overlap populations and covalent bonding have been examined.[1] (Atoms are denoted by k, l, etc., AOs by r, s, $\cdots$.)

Most of the analysis in these papers is based on the use of LCAO MOs ϕ_i expressed as linear combinations of pure (nonhybrid) AOs χ_{rk}, with in general several AOs χ_r per atom. However, any such pure-AO LCAO MO can be recast as a linear combination of hybrid AOs χ_k, one per atom. The basic equations of I are directly applicable for either pure-AO or hybrid-AO LCAO MOs.

While *in general* it is more convenient to work entirely with pure-AO LCAO MOs (these were used in the applications in I and II) there are some important effects of hybridization on overlap and gross-AO populations which can best be made clear by discussing a few simple examples in terms of hybrid-AO LCAO MOs. For this purpose, some selected partial configurations which occur in the electron configurations of simple homopolar diatomic molecules such as Li_2, C_2, and N_2 will be used. The $^1\Sigma^+_g$ ground state of N_2 has the configuration

$$(1\sigma_g)^2(1\sigma_u)^2(2\sigma_g)^2(2\sigma_u)^2(1\pi_u)^4(3\sigma_g)^2.$$

The $^1\Sigma^+_g$ ground state of Li_2 and a low $^1\Sigma^+_g$ (perhaps the ground) state of C_2 have configurations obtained from that of N_2 by removing the last eight or the last two electrons, respectively.

The various σ_g and σ_u MOs are all of the hybrid-AO LCAO forms

$$\left.\begin{aligned}\phi(m\sigma_g)&=[2(1+S)]^{-\frac{1}{2}}(\chi_k+\chi_l)\\ \phi(m\sigma_u)&=[2(1-S)]^{-\frac{1}{2}}(\chi_k-\chi_l)\end{aligned}\right\} \quad (1)$$

where S is $\int \chi_k\chi_l dv$. Each χ_k or χ_l is of the form

$$\chi=\mu 1s+\alpha 2s+\beta 2p\sigma+\cdots \quad (2)$$

* This work was assisted in part by the Office of Scientific Research, Air Research and Development Command, under Project R-351-40-4 of Contract AF 18(600)-471 with The University of Chicago.

[1] R. S. Mulliken, J. Chem. Phys. **23**, 1883 and 1841 (1955): I and II, respectively. In Paper I, the following additional references should have been cited. (a) The elements of the **R** matrix of P. O. Löwdin, J. Chem. Phys. **19**, 1572 (1951) are the same as the "atom" and "bond charges" of McWeeny (1951, reference 3 of Paper I) and the "net-atomic" and "overlap" populations here, whose prototypes are used in reference 2 of I. (b) The quantities here called "gross atomic populations," used by the writer in 1949 (reference 6 of I), were called "formal charges" by Chirgwin and Coulson (1950, reference 6 of I) and by McWeeny (1951, reference 3 of I). (c) For some applications, see R. McWeeny, Proc. Roy. Soc. (London) **A223**, 321 (1954); **A227**, 301 (1955); Acta Cryst. **5**, 463 (1952).

with a *different set* of hybridization coefficients μ, α, β for each different MO. However, the coefficients always conform to the relation $\mu^2+\alpha^2+\beta^2=1$, if pure AOs beyond the three explicitly indicated are neglected. It should further be noted that S is different for each different MO.

The hybrid-AO LCAO MOs described by Eqs. (1) and (2) are seen to be all of the general form

$$\phi_i=c_{ik}\chi_{ik}+c_{il}\chi_{il} \tag{3}$$

with $c_{il}=c_{ik}$ or else $c_{il}=-c_{ik}$ for all the MOs ϕ_i. When Eq. (3) is expanded in terms of pure-AO LCAO MOs, it becomes

$$\phi_i=\sum_r c_{ir_k}\chi_{r_k}+\sum_s c_{is_l}\chi_{s_l}, \tag{4}$$

with

$$\left.\begin{aligned} &c_{ir_k}=\eta_{ir_k}c_{ik};\\ &\text{in particular,}\\ &c_{i1s_k}=\mu_i c_{ik};\quad c_{i2s_k}=\alpha_i c_{ik};\quad c_{i2p\sigma_k}=\beta_i c_{ik}. \end{aligned}\right\} \tag{5}$$

For the overlap population $n(i;k,l)$ in any hybrid-AO LCAO MO ϕ_i occupied by $N(i)$ electrons, the first two of Eqs. (4) of paper I reduce to

$$n(i;k,l)=2S_iN(i)c_{ik}c_{il}, \tag{6}$$

where

$$S_i=\int\chi_{ik}\chi_{il}dv=\sum_r\sum_s\eta_{ir_k}\eta_{is_l}S_{r_ks_l}. \tag{7}$$

Besides Eq. (6), the following equation for gross pure-AO populations, based on Eqs. (6) and (7) of paper I, will be needed in the present paper:

$$N(i;r_k)=N(i)c_{ir_k}(c_{ir_k}+\sum_s c_{is_l}S_{r_ks_l}). \tag{8}$$

For the SCF (self-consistent field) LCAO MOs of a diatomic molecule, μ, α, and β of Eq. (2) are all different from zero for all occupied MOs. However, it is often more convenient to use a different orthogonal set of MOs obtainable from SCF MOs by an orthogonal transformation. This is allowable, since *any* orthogonal transformation can be made among the *occupied* MOs without changing the (antisymmetric) total wave function.[2] For instance, this can be done in such a way that $\alpha=\beta=0$ for the MOs of Eqs. (1) with $m=1$; or alternatively, so that $\mu=0$ for the MOs with $m=2$ and 3; or in other ways. It will be simplest here to choose the second alternative. The AOs χ_i (i.e. χ_{ik} or χ_{il}) in the $m\sigma_g$ and $m\sigma_u$ MOs with $m=2$ or 3 now take the simple form

$$\chi_i=\alpha_i 2s+\beta_i 2p\sigma;\quad \alpha_i^2+\beta_i^2=1.$$

[2] It is not absolutely necessary even to use orthogonal MOs, but if they are *not* used, the same consequences for molecular properties arise as if they *were* used, but arise in forms which are less convenient to deal with, and which in practice have often suggested approximations that have resulted in misleading conclusions. SCF-LCAO MOs are always mutually orthogonal.

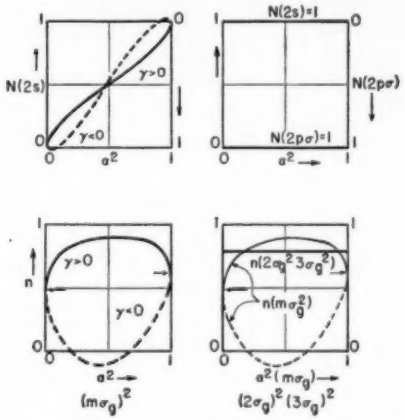

FIG. 1. Gross populations $N(2s)$ and $N(2p\sigma)$ per atom, and total overlap population n, for electron configurations $(m\sigma_g)^2$ and $(2\sigma_g)^2(3\sigma_g)^2$, plotted against amounts of $2s$ character α^2 in $m\sigma_g$. The LCAO MOs $m\sigma_g(m=2$ or 3) are assumed to be both of the form $C(\alpha 2s_k+\beta 2p\sigma_k+\beta 2\sigma\cdot_l+\alpha 2s_l)$, where $\alpha^2+\beta^2=1$, with $3\sigma_g$ orthogonal to $2\sigma_g$; γ means β/α. Normally, $\gamma>0$ for $2\sigma_g$ and $\gamma<0$ for $3\sigma_g$. Computed for N_2 at its equilibrium distance using Slater $2s$ and $2p\sigma$ AOs.

For convenience, α_i will always be taken positive, while β_i may then be either positive (χ_i a *positive hybrid*) or negative (negative hybrid).[3] It is particularly convenient to recast the equation just given in the form

$$\chi_i=\alpha_i(2s+\gamma_i 2p\sigma);\quad \alpha_i^2(1+\gamma_i^2)=1, \tag{9}$$

and to characterize any given hybrid AO by the *amount of 2s character* α_i^2 and the *sign* of γ_i for it.[3]

We are now ready to consider the gross AO populations $N(i;2s)$ and $N(i;2p\sigma)$ and the overlap population $n(i)$ for any one of the partial electron configurations $(2\sigma_g)^2$, $(2\sigma_u)^2$, $(3\sigma_g)^2$, or $(3\sigma_u)^2$. In each of these cases, $N(i)=2$ for each MO. Making use of Eq. (8) combined with Eqs. (1), (3)–(5), (7), and (9), we find, for each atom,

$$\begin{aligned} N(i;2s)&=1-N(i;2p\sigma)\\ &=\alpha_i^2[1\pm S_s\pm\gamma_i S_{s\sigma}]/(1\pm S_i). \end{aligned} \tag{10}$$

Using Eqs. (6), (3), and (1) we obtain for the total overlap population

$$n(i)=\pm 2S_i/(1\pm S_i). \tag{11}$$

In Eqs. (10) and (11), according to Eqs. (7), (5), and (9),

$$S_i=\alpha_i^2(S_s+2\gamma_i S_{s\sigma}+\gamma_i^2 S_\sigma). \tag{12}$$

S_s, $S_{s\sigma}$, and S_σ, respectively, mean $S(2s,2s)$, $S(2s,2p\sigma)$, and $S(2p\sigma,2p\sigma)$. The upper signs in Eqs. (10) and (11) apply to $(m\sigma_g)^2$, the lower to $(m\sigma_u)^2$, for $m=2$ or 3 only.

In order to illustrate how $N(2s)$, $N(2p\sigma)$, and n depend on the value of α^2 and the sign of γ, computations have been made and graphs drawn for $(m\sigma_g)^2$ and for $(m\sigma_u)^2$. These are shown in the first columns of Figs. 1 and 2, respectively. It should be noted that Figs. 1 and 2 are based on N atom AOs at the internuclear

[3] R. S. Mulliken, J. Chem. Phys. **19**, 900 (1951).

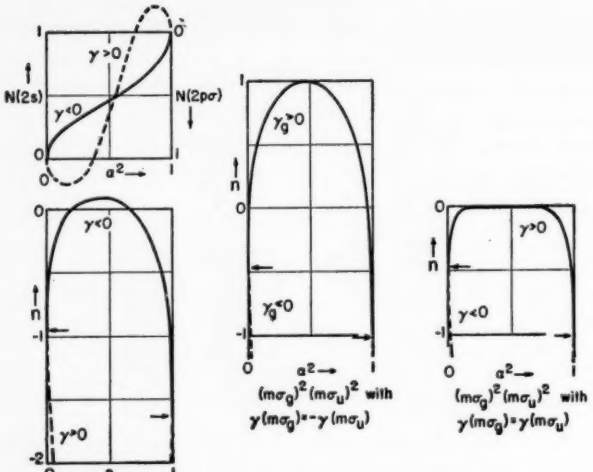

FIG. 2. Gross populations for $(m\sigma_u)^2$ and total overlap populations for $(m\sigma_u)^2$ and for $(m\sigma_g)^2(m\sigma_u)^2$ for LCAO MOs assumed to be of the form $C(\alpha 2s_k+\beta 2p\sigma_k\pm\beta 2p\sigma_l\pm\alpha 2s_l)$. The cases illustrated for $(m\sigma_g)^2(m\sigma_u)^2$ are only two examples out of an infinity of possible cases differing in the relation of $\gamma(m\sigma_u)$ to $\gamma(m\sigma_g)$. Computed for N_2 using Slater AOs.

distance which is observed in N_2, hence as applied to other molecules than N_2 they are only qualitatively illustrative.

The curves in Figs. 1 and 2 show that the gross $2s$ population $N(2s)$ in general differs considerably from being, as one might have naively expected, equal to the amount of $2s$ character α^2 in the hybrid AOs used to construct $m\sigma_g$ or $m\sigma_u$ in LCAO approximation. The n curves for $(m\sigma_g)^2$ and $(m\sigma_u)^2$ show among other things that, since one expects bonding or antibonding according as n is positive or negative (see II), the usually bonding MO $m\sigma_g$ can be slightly antibonding by a particularly unfavorable choice of $\gamma<0$, and the usually antibonding MO $m\sigma_u$ can be slightly bonding by a particularly favorable choice of $\gamma<0$.

At this point it is necessary to recognize that Eqs. (10)–(12) and the graphs in Figs. 1 and 2 really have significance only in the context of a consideration of the states of an actual molecule. The configurations $(m\sigma_g)^2$ and $(m\sigma_u)^2$ may conveniently be thought of as corresponding to states of Li_2, although it must be kept in mind that Figs. 1 and 2 are only qualitatively relevant to Li_2. *By definition*, $3\sigma_g$ is an MO of higher energy than $2\sigma_g$, and $3\sigma_u$ than $2\sigma_u$. There can be no doubt that the ground state of Li_2 is $(2\sigma_g)^2$, with $(2\sigma_u)^2$, $(3\sigma_g)^2$, and $(3\sigma_u)^2$ as excited states, almost certainly with energy increasing in the order given.[4]

The ground state of Li_2 is clearly $(2\sigma_g)^2$ with a positive γ value (see Fig. 1). The actual value of γ will be determined by that compromise which minimizes the total energy, as between *gain* in bonding energy with increase in n as α^2 falls below 1, and *cost* in promotion energy, which should increase nearly proportionally to $N(2p\sigma)$ as α^2 falls below 1 (see Fig. 1). Probably the best α^2 will lie above 0.5 but well below 1.0. In a similar way (see Fig. 2) it is seen that the excited state $(2\sigma_u)^2$ must have $\gamma<0$, with α^2 probably between 0.5 and 1. It is also fairly clear that $2\sigma_u$ will be only slightly antibonding, perhaps even slightly bonding, hence that the state $(2\sigma_u)^2$ will be only moderately high in energy.[4]

The states $(3\sigma_g)^2$ and $(3\sigma_u)^2$ may be considered next. Since every excited state of an actual molecule has to be orthogonal to other states of the same species, $(3\sigma_g)^2$ has to be orthogonal to $(2\sigma_g)^2$, and $(3\sigma_u)^2$ to $(2\sigma_u)^2$, and this requires that $3\sigma_g$ be orthogonal to $2\sigma_g$, and $3\sigma_u$ to $2\sigma_u$.[5]

In general, the γ values (say, γ_3 and γ_2) of $3\sigma_g$ and $2\sigma_g$ respectively (or of $3\sigma_u$ and $2\sigma_u$) are forced by the orthogonality requirement to be related in the following way.[6]

$$\left.\begin{array}{l}\gamma_3=-Q/R;\quad Q=A+B\gamma_2;\quad R=B+C\gamma_2\\ \text{where [if } \mu=0 \text{ as we are assuming here, —see Eq. (9)]}\\ A=1\pm S_s;\quad B=\pm S_{s\sigma};\quad C=1\pm S_\sigma.\end{array}\right\}\quad(13)$$

The upper signs apply to $m\sigma_g$, the lower to $m\sigma_u$.

From Eqs. (13) it is now seen that $\gamma<0$ for $3\sigma_g$ and $\gamma>0$ for $3\sigma_u$, making $3\sigma_g$ at most weakly bonding so that $(3\sigma_g)^2$ should be a fairly low excited state, but making $3\sigma_u$ strongly antibonding (see Figs. 1, 2) so that $(3\sigma_u)^2$ should be a high excited state.

As has been stated in I, gross AO populations are probably good measures of "true" AO populations, yet Figs. 1 and 2 show that these quantities can sometimes take on slightly unreasonable values. Thus in Fig. 1 for $(m\sigma_g)^2$, $N(2s)$ is slightly less than zero and $N(p\sigma)$ slightly greater than one, or vice versa, in certain limited ranges of *negative* γ values; while in Fig. 3 for $(m\sigma_u)^2$ similar but much worse departures occur in certain ranges of *positive* γ values. However, it will be noted that these anomalies apparently do *not* occur for the ranges of γ values which are possible for states of an actual molecule: with $\gamma>0$ in $(2\sigma_g)^2$ and $\gamma<0$ in $(2\sigma_u)^2$, $N(2s)$ and $N(2p\sigma)$ are well behaved, while in $(3\sigma_g)^2$ and $(3\sigma_u)^2$, the requirement of orthogonality to $(2\sigma_g)^2$ and $(2\sigma_u)^2$ causes those ranges of γ values where $N(2s)$ and $N(2p\sigma)$ take on unreasonable behavior to be more or less completely excluded from

[4] This statement is subject, however, to the reservation that, since all these states are of the same ($^1\Sigma_g^+$) symmetry, one must take into account strong configuration interactions among them in seeking better approximations to the actual molecular states. However, these interactions are not of interest here and will be neglected in the following discussion.

[5] All σ_u MOs are orthogonal by symmetry to all σ_g MOs, hence both states $(m\sigma_u)^2$ are automatically orthogonal to both states $(m\sigma_g)^2$.

[6] R. S. Mulliken, J. Chem. Phys. **19**, 912 (1951). For Eqs. (13) here, see Eqs. (16)-(18) there, but with the overlap terms involving 1s omitted.

real occurrence in a way which can be seen by examination of a previous paper.[7]

In passing, it may be remarked that what has been said about the 2-electron states $(2\sigma_g)^2$, $(2\sigma_u)^2$, $(3\sigma_g)^2$ is evidently equally applicable (except that configuration interaction[4] is absent) to 1-electron states $2\sigma_g$, $2\sigma_u$, $3\sigma_g$, and $3\sigma_u$, as in Li_2^+.

The ground state of Be_2, though scarcely stable, must have the configuration $(2\sigma_g)^2(2\sigma_u)^2$, while $(2\sigma_g)^2 \times (3\sigma_g)^2$ would correspond to an excited state. These same two configurations, supplemented by $(1\pi_u)^4$, must occur as stable states of C_2, $(2\sigma_g)^2(2\sigma_u)^2(1\pi_u)^4$ being a known $^1\Sigma^+_g$ state which may be the ground state. In the configuration $(2\sigma_g)^2(2\sigma_u)^2$, the total energy will be minimized with $\gamma>0$ for $2\sigma_g$ and $\gamma<0$ for $2\sigma_u$, with α^2 values probably between 0.5 and 1. It is to be expected that this will occur with somewhat unequal values of α^2 for $2\sigma_g$ and $2\sigma_u$. This case is too general to be shown graphically, but one can judge fairly well what can happen by looking at graphs in which α^2 is assumed equal for $m\sigma_g$ and $m\sigma_u$ (Fig. 2). The actual $(2\sigma_g)^2(2\sigma_u)^2$ in C_2 should correspond to a situation similar to that of a point somewhere on the right upper segment of the closed curve for n, in the middle section of Fig. 2. The lower segment of the same curve would then correspond to $(3\sigma_g)^2(3\sigma_u)^2$, and the upper and lower segments of the right-hand curve in Fig. 2 to $(2\sigma_u)^2(3\sigma_g)^2$ and $(2\sigma_g)^2(3\sigma_u)^2$ respectively.

2. FREE AND FORCED HYBRIDIZATION

The concept of *forced hybridization* was introduced in an earlier paper.[6] Its meaning and consequences can now be made clearer in terms of gross pure-AO and overlap populations. In general, forced hybridization is a consequence of the requirement[2] of orthogonality among the various LCAO MOs of any one group-theoretical species. It is affected also by the number of members in the set of pure AOs which one uses to construct the LCAO MOs of a given species. For the most important (low-energy) electronic states of a molecule, one commonly uses only those AOs (valence-shell and inner-shell AOs mainly) which are occupied in the ground and some of the low energy excited states of the atoms from which the molecule is formed. Thus for a molecule like N_2, one commonly uses a closed set[8] of three σ AOs ($1s$, $2s$, and $2p\sigma$) per atom, from which closed sets of just three σ_g MOs ($1\sigma_g$, $2\sigma_g$, and $3\sigma_g$) and three σ_u MOs ($1\sigma_u$, $2\sigma_u$, and $3\sigma_u$) can be constructed.

In the choice of the forms of the LCAO MOs of such a set there is a certain amount of freedom, if we do not insist on using SCF MOs [see paragraph following Eq. (8) above]. Since we are primarily interested in the valence-shell MOs $2\sigma_g$, $2\sigma_u$, $3\sigma_g$, $3\sigma_u$, the choice was made in Sec. 1 to treat these as built from $2s$ and $2p\sigma$ AOs alone.[9] A consequence of this choice is that, contrary to naive expectation, the $1\sigma_g$ and $1\sigma_u$ MOs, which are primarily built from $1s$ AOs, are now forced to include some $2s$ and some $2p\sigma$ in their LCAO forms.[9] This is an example of *forced hybridization*. A fundamental characteristic of forced hybridization is that the AOs which it forces into an LCAO MO appear, on the whole, with negative coefficients, and result in a *negative* contribution to the overlap population.

With the $m\sigma_g$ and $m\sigma_u$ MOs for $m=2$ and 3 chosen as just indicated, there is still some freedom of choice, or possibility of *free hybridization*, for the $2\sigma_g$ and $2\sigma_u$ MOs, in the sense that for them no constraint is placed by the orthogonality requirement[10] on the hybridization coefficients α and γ of Eq. (9). For the $3\sigma_g$ and $3\sigma_u$ MOs, however, there is then forced hybridization, with corresponding strong negative contributions to the overlap population. For further elucidation, it will be convenient to discuss some particular partial electron configurations. In each case discussed, it is assumed that the additional partial configuration $1\sigma_g^2 1\sigma_u^2$ is present.

For the configuration $(2\sigma_g)^2$ taken alone, or for $(2\sigma_u)^2$ taken alone, there is free hybridization in the sense stated above. Likewise in the configuration $(2\sigma_g)^2(2\sigma_u)^2$ there is free hybridization in both $2\sigma_g$ and $2\sigma_u$, independently. In the configurations $(3\sigma_g)^2$ and $(3\sigma_u)^2$ discussed in Sec. 1, there is forced hybridization.

In the configuration $(2\sigma_g)^2(3\sigma_g)^2$ also, there is forced hybridization. This means that, although $2\sigma_g$ may freely be based on any desired hybrid AO, the form of $3\sigma_g$ is then completely determined by the orthogonality requirement, in such a way that in general $2s$ is forced to mix with $2p\sigma$, or vice versa.[6] For example, if $2\sigma_g$ is taken to be built from pure $2s$ AOs [χ_k and χ_l both $2s$ in Eq. (1), or $\mu=0$, $\alpha=1$, $\beta=0$ in Eq. (2)], then $3\sigma_g$ is *not* built from pure $2p\sigma$ AOs, but from negative-hybrid AOs containing a considerable amount of $2s$.[11]

The configuration $(2\sigma_g)^2(3\sigma_g)^2$, occurring either alone, or as part of a more extended configuration as in N_2,

[7] See reference 6, Figs. 1 and 2. It seems possible that this exclusion of unreasonable $N(r_k)$ values may be rigorous for states of actual molecules, but an investigation and possible proof is beyond the scope of the present paper.

[8] The closure is of course an arbitrary simplification. More accurately, all possible σ AOs should be admitted, and must be admitted if one goes to excited states requiring higher MOs $4\sigma_g$, $5\sigma_g$, $\cdots$ or $4\sigma_u$, $5\sigma_u\cdots$.

[9] In the paragraph following Eq. (8), two alternative assumptions for simplifying the $m\sigma_g$ and $m\sigma_u$ MOs were discussed, of which the *second* ($\mu=0$ for $m=2$ and 3, which as a corollary requires α and β *not* zero for $m=1$) was adopted. In a previous paper,[6] the *first* alternative ($\alpha=\beta=0$ for $m=1$, which requires $\mu\neq 0$ for $m=2$ and 3) was chosen. For any given complete electron configuration, the computed effect of $1s$, $2s$ and $1s$, $2p\sigma$ forced hybridization on the overlap population is necessarily the same by either choice.

[10] They are, however, subject to the requirement that the energy of the state in which they occur shall be minimized; with the further requirement, in the case of excited states, that their wave functions shall be orthogonal to those of any lower-energy states of the same species.

[11] Here, as in general for one of any fully occupied complete closed set of MOs of a given species, there is no energy-minimization limitation on the form of $2\sigma_g$. The total energy is independent of the hybridization in $2\sigma_g$, provided only that $1\sigma_g$, $2\sigma_g$, and $3\sigma_g$ are all orthogonal.

illustrates well the phenomenon of forced hybridization and its consequences. The gross AO populations and the overlap populations are of particular interest. From a general invariance theorem[12] which is applicable whenever all of a closed set of LCAO MOs of a particular symmetry (here σ_g) which can be constructed from a given closed set of AOs are occupied, it follows that $N(2s)=N(2p\sigma)=1$ always (for each atom, of course) for the foregoing configuration, so long as $2\sigma_g$ and $3\sigma_g$ are taken orthogonal (see Fig. 1). [This result can also be verified specifically for $(2\sigma_g)^2(3\sigma_g)^2$ by taking $N(2\sigma_g;2s)+N(3\sigma_g;2s)$, using Eqs. (10) and (12), with γ called γ_2 for $N(2\sigma_g;2s)$, and with γ called γ_3 and taken from Eqs. (13) for $N(3\sigma_g;2s)$.]

In a similar way, it can be proved from a general invariance theorem[12] that $n(2\sigma_g{}^2 3\sigma_g{}^2)$ is a constant independent of the individual extents of hybridization in $2\sigma_g$ and $3\sigma_g$. This result also can be verified, and interesting formulas for n obtained, by adding expressions for $n(2\sigma_g{}^2)$ and $n(3\sigma_g{}^2)$ obtained using Eqs. (11), (12) with $\gamma_3(3\sigma_g)$ related to $\gamma_2(2\sigma_g)$ in the manner given by Eqs. (13). Carrying out the indicated operations, one arrives at

$$n(2\sigma_g{}^2 3\sigma_g{}^2)=4-2(2+S_s+S_\sigma)/[(1+S_s)(1+S_\sigma)-S_{s\sigma}{}^2] \quad (14)$$

independent of the γ's. Equation (14) can also be expressed in the interesting form

$$n(2\sigma_g{}^2 3\sigma_g{}^2)=2\left[\frac{S_s}{1+S_s}+\frac{S_\sigma}{1+S_\sigma}-\frac{(2+S_s+S_\sigma)S_{s\sigma}{}^2}{(1+S_s)(1+S_\sigma)[(1+S_s)(1+S_\sigma)-S_{s\sigma}{}^2]}\right]. \quad (15)$$

As can be seen from Fig. 1, the total n, and hence (see II) probably the bonding effect, for $(2\sigma_g)^2(3\sigma_g)^2$ is actually less than could be obtained for reasonable α^2 and γ values for $(2\sigma_g)^2$ alone.

Another interesting comparison is the following: if $2\sigma_g$ were built from pure $2s$ and $3\sigma_g$ from pure $2p\sigma$ AOs ($\alpha^2=1$ and $\alpha^2=0$, respectively), one would have

$$n(2\sigma_g{}^2)=2S_s/(1+S_s), \quad n(3\sigma_g{}^2)=2S_\sigma(1+S_\sigma).$$

As is shown by Eq. (15), $n(2\sigma_g{}^2 3\sigma_g{}^2)$ not merely shows no gain by hybridization, but is actually *less* than for the sum of the two unhybridized cases, and by a very appreciable amount, proportional to $S_{s\sigma}{}^2$. This negative contribution to the overlap population is the most important consequence of the phenomenon of forced hybridization. As we shall see in paper IV of this series, it has its counterpart in valence-bond theory in certain so-called nonbonded repulsions.

The statements of the preceding two paragraphs can be made more vivid in terms of some numerical values for the N_2 molecule at its equilibrium distance. Using Slater AOs, $S_s=0.450$, $S_\sigma=0.321$, $S_{s\sigma}=0.432$, and Eq. (15) in numerical form becomes

$$n(2\sigma_g{}^2 3\sigma_g{}^2)=2(0.310+0.244-0.156)=0.796.$$

As has been mentioned, the complete antisymmetrized wave function and its properties, including total overlap populations, are here independent of what hybrid one chooses for $2\sigma_g$ (or $3\sigma_g$). However, it is interesting to note that if one uses Scherr's SCF-LCAO form of $2\sigma_g$ as determined for N_2, which is characterized by the value 0.504 for γ (from which $\alpha^2=0.797$), then

$$n(2\sigma_g{}^2)=0.871=2(0.435)$$

using Eqs. (11), (12). Hence by difference,

$$n(3\sigma_g)^2=-0.075.$$

These individual overlap populations will be seen to be in agreement with Fig. 1 for $(2\sigma_g)^2(3\sigma_g)^2$ with $\alpha^2=0.797$ and $\gamma>0$, and with the statements in the preceding paragraph.

Brief consideration will now be given to forced hybridization in the MOs $1\sigma_g$ and $1\sigma_u$ in $(1\sigma_g)^2(2\sigma_g)^2$, $(1\sigma_g)^2(2\sigma_g)^2(3\sigma_g)^2$, $(1\sigma_u)^2(2\sigma_u)^2$, etc. This has the effect of adding small negative (antibonding) $1s$, $2s$ and $1s$, $2p\sigma$ contributions to the overlap population n in all the various cases discussed above.[9] For the N_2 molecule on the basis of Scherr's calculations,[12] the total n in $(1\sigma_g)^2(2\sigma_g)^2(3\sigma_g)^2$ is reduced thereby from 0.798 to 0.772; and in $(1\sigma_u)^2(2\sigma_u)^2$ it is reduced from -0.366 to -0.377. Although the decrease in overlap population due to 1s forced hybridization (totalling 0.037 for N_2) is small, its effect on the energy is fairly large if Eqs. (11) of II are roughly correct, since $\bar{I}_{1s,2x}$ is very much larger than $I_{2x,2x}$ (x means $2s$ or $2p\sigma$). This conclusion about the energetic importance of $1s$ forced hybridization is confirmed by calculations such as those of Ellison and Shull on H_2O (see I) and of Scherr on N_2.[12]

In the above discussion, only inner-shell and valence-shell AOs have been considered. *Free* hybridization of excited-shell AOs into all LCAO MOs should be admitted as a means of securing some further improvement even in molecules like N_2, as soon as this can be done without too exorbitant computational effort. In molecules composed of higher-row atoms, the importance of extra-valence-shell hybridization involving d AOs is well recognized.[13]

[12] C. W. Scherr, J. Chem. Phys. **23**, 569 (1955). See Appendix II for invariance theorems.

[13] As a simple example of extra-valence-shell free hybridization, that of $2p\pi$-$3d\pi$ hybridization in Cl_2 may be cited [see R. S. Mulliken, J. Am. Chem. Soc. **77**, 884 (1955)].

THE JOURNAL OF CHEMICAL PHYSICS VOLUME 23, NUMBER 12 DECEMBER, 1955

Electronic Population Analysis on LCAO-MO Molecular Wave Functions. IV. Bonding and Antibonding in LCAO and Valence-Bond Theories*

R. S. MULLIKEN
Laboratory of Molecular Structure and Spectra, Department of Physics, The University of Chicago, Chicago 37, Illinois
(Received January 6, 1955)

It is shown that there is a practically one-to-one correspondence between the occurrence, on the one hand, of positive (bonding) and negative (antibonding) overlap populations in LCAO theory and, on the other hand, of bonded attractions and nonbonded repulsions in VB (valence-bond) theory. This correspondence is discussed in terms of examples, and is traced for the N_2 molecule both for the assumed case of no $s-p$ hybridization, and for the actual case with hybridization. It is pointed out that repulsions between nonbonded atoms in VB theory (including those which give rise to steric hindrance) have their counterpart in negative overlap populations between the same atoms in LCAO theory. The π overlap populations for the various links in 1,3-butadiene are computed by LCAO theory. It is shown how they are affected by conjugation (see Table I) and the results are compared with those of VB theory.

1. INTRODUCTION

IN previous papers of this series,[1] hereafter referred to as I, II, and III, definitions of overlap populations for the link between any two atoms in a molecule have been given (I), relations between overlap populations and covalent bonding have been discussed (II), and the effects of hybridization on overlap populations have been treated (III), all on the basis of LCAO-MO wave functions. In the present paper, it will be shown that there is a practically one-to-one correspondence between positive (bonding) and negative (antibonding) overlap populations in LCAO theory, and exchange attractions and nonbonded repulsions, respectively, in AO-VB theory (valence-bond theory as developed by Heitler, London, Slater, and Pauling).

In the latter, the energy of atomization of a molecule is usually thought of as a sum of "bond energies," each made up of covalent (or "exchange"), and "Coulomb" terms; plus correction terms if polar bonds are present. If the bonds are not too strongly polar, the covalent terms are thought of as dominant, although there are indications[2] that actually the Coulomb terms may often be important.

The covalent terms include, first of all, bonded "exchange" attraction terms between electrons which are interatomically paired, but also important nonbonded "exchange" repulsion terms between electrons which while of like symmetry (e.g., both σ, or both π) are not so paired.[3] There are also some exchange attraction terms between nonpaired electrons of unlike symmetry (e.g., one σ, one π; or one π, one π') on different atoms; these, while of relatively minor importance, are not negligible.[3] In special cases, there are further attraction terms which are ascribed to "resonance" between AO configurations or between different ways of drawing bonds.

Counterparts of both the bonded attraction and the nonbonded repulsion terms of AO−VB theory can be identified[2,4] in the overlap population terms and corresponding overlap-energy terms of LCAO-MO VB theory. It seems fair to classify all such terms in either theory as covalent terms.

The strength of covalent bonding between two atoms in AO-VB theory is the *difference* between the pertinent bonded (plus nonbonded) attraction terms and the nonbonded repulsion terms. The obvious equivalent in LCAO theory is the difference of the positive and negative overlap population terms, or of their energy representatives (see II); plus allowance for some equivalent of the nonbonded attractions of AO-VB theory.

In polyatomic molecules, atom pairs, which in ordinary chemical theory are considered not to be connected by covalent bonds (e.g., the two H atoms in H_2O), show in AO-VB theory "nonbonded repulsion" but no bonded attraction terms. In LCAO-MO theory they show an excess of negative over positive overlap population terms, again indicating net antibonding. According to the LCAO point of view, one might speak of covalently bonded and covalently *antibonded* atoms in a molecule, rather than of covalently bonded atoms and *nonbonded* atoms. Steric hindrance would then be thought of as a result of covalent antibonding between atoms.

2. DISCUSSION OF EXAMPLES ASSUMING NO PROMOTION

Let us consider in more detail how the counterparts of the covalent bonding and antibonding terms of AO-VB theory appear in LCAO-VB theory, beginning

* This work was assisted in part by the Office of Scientific Research, Air Research and Development Command, under Project R-351-40-4 of Contract AF 18(600)-471 with The University of Chicago.

[1] For papers I, II, III of this series, see J. Chem. Phys. **23**, 1833, 1841, and 2338 (1955).

[2] See R. S. Mulliken, J. Phys. Chem. **56**, 295 (1952).

[3] See reference 2 for earlier references, K. S. Pitzer, J. Am. Chem. Soc. **70**, 2140 (1948) for a recent discussion, and R. S. Mulliken, reference 2 and J. Am. Chem. Soc. **72**, 4493 (1950), p. 4502, for some estimates of the magnitudes of nonbonded repulsion energies. See reference 2 for some nonbonded attraction energies.

[4] R. S. Mulliken, J. Chem. Phys. **19**, 912 (1951).

with diatomic molecules. Among the simplest typical cases are H_2^+, H_2, He_2^+, and He_2 (i.e., a pair of He atoms).[2] As is well known, the wave functions representing the 2-electron case of H_2, the prototypical case of a single bond, are distinctly different in the LCAO and VB theories; but the properly antisymmetric wave functions for the 1-, 3-, and 4-electron cases of H_2^+, He_2^+, and He_2 are identical in the two theories, provided identical $1s$ AOs are used in both. This comparison illustrates a fact which should be borne in mind in the following discussion when one seeks to establish corresponding energy terms in the two theories; namely, that there is *in general* only an approximate correspondence which, however, may become closer in some cases.

Two important types of antibonding terms may be considered in AO-VB theory: (1) the repulsion between two like closed shells on two atoms; (2) the repulsion between either a closed shell or a bonded electron on one atom and either a different kind of closed shell or a different kind of bonded electron on the other atom.

The simplest illustration of Type 1 nonbonded repulsions is the interaction of two helium atoms squeezed together so as to produce appreciable overlap. In AO-VB theory, there is an exchange repulsion between each of the two electrons on one atom and an electron of like spin on the other. In LCAO theory, the electron configuration is $(1\sigma_g)^2(1\sigma_u)^2$, with $1\sigma_g$ and $1\sigma_u$ of the forms $(1s_a \pm 1s_b)/[2(1\pm S)]^{\frac{1}{2}}$. The total overlap population is then

$$n = 2S/(1+S) - 2S/(1-S) = -4S^2/(1-S)^2.$$

It is seen that the negative population from $(1\sigma_u)^2$ outweighs the positive population from $(1\sigma_g)^2$ to give a net negative population, whose antibonding effect is obviously the LCAO counterpart of the nonbonded repulsion of VB theory. In this case, since the wave functions of the two theories are identical, the correspondence is exact.

Similar Type 1 repulsions between like closed shells of two atoms occur also for heavier diatomic molecules, but in general the correspondence between the two theories is made less sharp by hybridization. Here an examination of the N_2 molecule will be instructive. First let us consider the hypothetical case that there is no hybridization in VB theory, and the corresponding case that there is no promotion in LCAO theory. The electron configuration would then be:

$$\text{VB: } (1s_a)^2(1s_b)^2(2s_a)^2(2s_b)^2 \times (2p\sigma_a \cdot 2p\sigma_b)(2p\pi_a \cdot 2p\pi_b)(2\pi_a' \cdot 2p\pi_b') \quad (1)$$

$$\text{LCAO: } (1\sigma_g)^2(1\sigma_u)^2(2\sigma_g)^2(2\sigma_u)^2(3\sigma_g)^2(1\pi_u)^4.$$

The effective electron configuration (see I, Sec. 3) for each atom in both cases[5] is the unpromoted configuration $1s^2 2s^2 2p\sigma 2p\pi^2$, provided only that the $2\sigma_u$MO is a linear combination of pure $2s$ AOs only. It is allowable also to assume[6] that $2\sigma_g$ is built from pure $2s$ AOs.[7] With $2\sigma_g$ and $2\sigma_u$ both built from pure $2s$ AOs, the (strong) net antibonding effect of the LCAO partial configuration $2\sigma_g^2 2\sigma_u^2$ would be identical with the Type 1 nonbonded repulsion between the $(2s_a)^2$ and $(2s_b)^2$ shells in VB theory, since everything would be exactly analogous to the case of He_2 considered above. Similarly, there would be a (very small) net antibonding effect for $1\sigma_g^2 1\sigma_u^2$ in N_2 corresponding to a Type 1 nonbonded repulsion between $1s_a^2$ and $1s_b^2$.

Next, $(3\sigma_g)^2$ of LCAO theory may be compared with the bonded pair $2p\sigma_a \cdot 2p\sigma_b$ of VB theory. It should be recalled that if $2\sigma_g$ is built from pure $2s$ only, as just assumed,[6] there is necessarily a considerable amount of forced hybridization in $3\sigma_g$. According to Eqs. (11), (12) of III, $n(2\sigma_g^2)$ would be $+2S_s/(1+S_s)$, and then, from Eq. (15) of III,

$$n(3\sigma_g^2) = +2S_\sigma/(1+S_\sigma) - (4+2S_s+2S_\sigma)S^2_{s\sigma}/(1+S_s)(1+S_\sigma)[(1+S_s)(1+S_\sigma) - S^2_{s\sigma}]. \quad (2)$$

The positive first term represents the bonding overlap that would be expected if $3\sigma_g$ were built from pure $2p\sigma$, while the negative second term (which is somewhat larger in magnitude here than the positive first term) then represents antibonding overlap due to forced hybridization. Numerical values of the terms in the above equation for $n(3\sigma_g)^2$ can be obtained from the $n(m\sigma_g^2)$ and $n(2\sigma_g^2 3\sigma_g^2)$ graphs in Fig. 1 of III for $\alpha^2=1$, and the $n(m\sigma_g^2)$ graph for $\alpha^2=0$.

In VB theory, the electron-pair bond $(2p\sigma_a \cdot 2p\sigma_b)$ contributes an exchange attraction, but there are also nonbonded repulsions between $2p\sigma_a$ and $(2s_b)^2$, and between $2p\sigma_b$ and $(2s_a)^2$. The bonded attraction and nonbonded repulsion terms of VB theory here are almost perfect respective counterparts of the bonding and antibonding overlap terms in the above LCAO theory Eq. (2) for $n(3\sigma_g^2)$. Thus the effects of forced hybridization correspond to those of nonbonded repulsion between unlike AOs of types which can hybridize (here $2s$ and $2p\sigma$), and illustrate the Type 2 nonbonded repulsions referred to above.

Further examples of Type 2 repulsions are also present in N_2, namely nonbonded repulsions of $1s_a^2$ against $2s_b^2$ and $2p\sigma_b$, and of $1s_b^2$ against $2s_a^2$ and $2p\sigma_a$. These have their counterpart in LCAO theory in the existence of very appreciable negative $1s,2s$ and $1s,2p\sigma$ overlap populations which appear when $1s$ forced

[5] By reference to Fig. 1 of III it is seen that $(2\sigma_g^2(3\sigma_g)^2$ of the LCAO configuration contributes just one $2s$ and one $2p\sigma$ electron to the effective electron configuration of each atom.

[6] The assumption that $2\sigma g$ is built from pure $2s$ AOs involves no loss of generality when as, here, the total configuration contains the grouping $(2\sigma_g)^2(3\sigma_g)^2$. For, as was pointed out in III, when $2\sigma_g$ and $3\sigma_g$ are both filled, the complete wave function is invariant for any orthogonal transformation of these MOs into linear combinations. The assumption that $2\sigma_u$ in $(2\sigma_u)^2$ is built from pure 2s AOs is, however, a *real* restriction, tantamount to no hybridization in VB theory.

[7] In making these statements about pure $2s$ AOs, the fact that there is a little forced $1s$ hybridization in both $2\sigma_u$ and $2\sigma_g$ is being ignored for the moment; it will be considered below.

hybridization in the MOs $1\sigma_g$, $1\sigma_u$, $2\sigma_g$, $2\sigma_u$, and $3\sigma_g$ is taken into account.[8] The repulsion energies corresponding to these inner-shell: outer-shell interaction effects are fairly large (see reference 3, and Sec. 3 of II), and cannot be safely neglected.

3. RECONSIDERATION OF N_2 EXAMPLE ALLOWING PROMOTION

The discussion of N_2 thus far has assumed no hybridization (i.e., promotion) in VB theory, or correspondingly no free hybridization (i.e., promotion) but only forced hybridization in LCAO theory. If hybridization in VB theory is now admitted, the electron configuration of N_2 becomes

$$\left.\begin{aligned}&\text{VB}:\cdots(\text{hy}'_a\cdot\text{hy}'_b)(\text{hy}_a)^2(\text{hy}_b)^2\cdots\\&\text{LCAO}:\cdots(2\sigma_g)^2(2\sigma_u)^2(3\sigma_g)^2\cdots.\end{aligned}\right\}\qquad(3)$$

In the VB configuration, if A and B are taken as positive with $A^2+B^2=1$,

$$\text{hy}=A\ 2s-B\ 2p\sigma;\quad \text{hy}'=B\ 2s+A\ 2p\sigma.\qquad(4)$$

In Eqs. (4) the lone-pair AO hy is a negative hybrid, while the bonding AO hy′ is a positive hybrid. The effective electron configuration of each N atom is then $1s^2 2s^{(2-B^2)} 2p\sigma^{(1+B^2)} 2p\pi^2$. The corresponding wave function is a linear combination of the unpromoted configuration $1s^2 2s^2 2p\sigma 2p\pi^2$ with coefficient A and the promoted configuration $1s^2 ?s 2p\sigma^2 2p\pi^2$ with coefficient B,[9] the value of A^2 being somewhere between 1.0 (pure $2p\sigma$ bond) and 0.5 (digonal hybrid bond).

For the partial configuration $(2\sigma_g)^2(3\sigma_g)^2$ in the LCAO configuration, $N(2s)=N(2p\sigma)=1$ (as always), so that any promotion depends exclusively on the amount of $2p\sigma$ character in the hybrid AOs used to construct the $2\sigma_u$ MO. The effective electron configuration is then $1s^2 2s^{2-x} 2p\sigma^{1+x} 2p\pi^2$, with x equal to the gross $2p\sigma$ population in $(2\sigma_u)^2$, hence $X=N(2p\sigma)=[1-\alpha^2(1-S_s-\gamma S_{s\sigma})]/(1-S)$ using Eqs. (10) and (12) of III with the lower signs in Eq. (10). For the energy-minimizing hybrid, the amount of $2s$ character α^2 in the AOs used to construct $2\sigma_u$ is somewhere between 1.0 and 0.5 (see III).

It will be noted that the role of the hybridization coefficients (A and B) in VB theory is rather different from that of α and β in LCAO theory. Nevertheless, one should expect an approximate agreement in the effective electron configurations in the two theories when in each the hybridization is chosen so as to minimize the total energy. This will be true if B^2 is approximately equal to $N(2p\sigma)$ of $(2\sigma_u)^2$.

The solutions of the SCF-LCAO-MO problem[10,11] show $2\sigma_g$ to be an MO constructed from a positive hybrid AO and having a very large overlap population corresponding to very strong bonding. Hence $(2\sigma_g)^2$ may be set in correspondence with the very strong $(\text{hy}_a'\cdot\text{hy}_b')$ bond predicted in VB theory to occur between two electrons in the positive hybrid AOs hy′. In the remaining SCF-LCAO theory partial configuration $(2\sigma_u)^2(3\sigma_g)^2$, it follows from considerations presented in III that both $2\sigma_u$ and $3\sigma_g$ are built from negative hybrid AOs so that their overlap populations are small and their bonding or antibonding properties weak (as is observed).[10] This partial configuration can then be set into correspondence with the VB theory pair of closed shells $(\text{hy}_a)^2(\text{hy}_b)^2$. In the latter, hy is a negative hybrid, making the overlap of hy_a and hy_b small, so that the resulting Type 1 nonbonded repulsion is very much weaker than it would be without hybridization.

In VB theory, the admission of hybridization also decreases the $1s$ and $2s-2p\sigma$ Type 2 nonbonded repulsions (see reference 2, Table V). Similarly in LCAO theory, it decreases the antibonding effect of $1s$ forced hybridization in $(2\sigma_u)^2$—though not in $(2\sigma_g)^2(3\sigma_g)^2$.

4. POLYATOMIC MOLECULES

Now turning briefly to polyatomic molecules, an important case in AO-VB theory is that of covalent antibonding (nonbonded repulsion) between "nonbonded atoms," e.g. between the H atoms in H_2O or the F atoms in F_2O. Here the LCAO-MO counterpart is found, much the same as in covalent antibonding between two helium atoms, in the occurrence of some MOs containing bonding and others containing antibonding overlap populations between the two atoms in question, but in such a way as to give a *net negative* overlap population for the atom pair (see Table VIII of I for details in the case of H_2O).

Added 4 August, 1955

Another interesting situation is that which occurs in conjugated or mesomeric organic molecules. This may be illustrated by considering 1,3-butadiene. In LCAO theory, the four π electrons occupy two MOs of the forms

$$\left.\begin{aligned}\phi_1&=c_{1a}\chi_a+c_{1b}\chi_b+c_{1b}\chi_c+c_{1a}\chi_d\\\phi_2&=c_{2a}\chi_a+c_{2b}\chi_b-c_{2b}\chi_c-c_{2a}\chi_d.\end{aligned}\right\}\qquad(5)$$

The overlap populations in the bonds a, b (or in c, d, which is the same as in a, b) and b, c are of interest. According to the first of Eqs. (4) of I, each of these populations is given by

$$n(i;k,l)=4S_{kl}c_{ik}c_{il}\qquad(6)$$

---

[8] See next-to-last paragraph of III and, especially, references 3 and 4.

[9] See reference 2, Eq. (37), except that B and A here respectively replace α and β used there.

[10] C. W. Scherr, J. Chem. Phys. **23**, 569 (1955).

[11] In the combined grouping $(2\sigma_g)^2(3\sigma_g)^2$ there is really no free hybridization, and there is no *necessity* to use the SCF solution for $2\sigma_g$; one could equally well assume $2\sigma_g$ to be constructed from pure $2s$ AOs as in preceding paragraphs, with $3\sigma_g$ orthogonal to it (III); the combined grouping $(2\sigma_g)^2(3\sigma_g)^2$ would be completely unaffected (see reference 6). However, it is certainly always *permissible* to select the SCF form for $2\sigma_g$, and that choice is made here because it is convenient for the present comparison.

TABLE I. Overlap populations of π bonds in 1,3-butadiene.

	Case 1 No conjugation	Case 2 Conjugated
$n(1;ab)$	0.177	0.185
$n(2;ab)$	0.284	0.239
$n(ab)$	0.461	0.424
$n(1;bc)$	0.148	0.205
$n(2;bc)$	−0.238	−0.167
$n(bc)$	−0.090	+0.038
$n=2n(ab)+n(bc)$	0.832	0.886

Two C_2H_4 π bonds: $2n(ab)=0.872$.

where $i=1$ or 2, and k, l is a, b or b, c. It is of interest to compare the overlap populations computed for (1) the hypothetical case of no conjugation; (2) the actual, conjugated case. In case (1)

$$\left.\begin{aligned} c_{1a}=c_{1b}&=\tfrac{1}{2}(1+S_{ab})^{-\frac{1}{2}}(1+S_{bc})^{-\frac{1}{2}} \\ c_{2a}=c_{2b}&=\tfrac{1}{2}(1+S_{ab})^{-\frac{1}{2}}(1-S_{bc})^{-\frac{1}{2}}. \end{aligned}\right\} \quad (7)$$

In case (2),[12]

$$c_{1a}=0.3540, \quad c_{1b}=0.4687, \quad c_{2a}=0.5081, \quad c_{2b}=0.4229, \quad (8)$$

The overlap integrals are $S_{ab}=0.2785$, $S_{bc}=0.2328$.[12]

Using Eqs. (5)–(8), the partial and total π overlap populations of Table I are obtained. Taking the overlap populations as measures of bonding, it is seen that in case (1) the π bonding in the double bonds is somewhat stronger than for isolated double bonds like those in C_2H_4, but that there is considerable π antibonding across the single bond, so that the total π bonding is somewhat *less* than for two isolated double bonds. In case (2), on the other hand, the π bonding in the double bonds is a little weaker than for two isolated double bonds, but across the single bond there is some π bonding, so that now the total π bonding is a little *greater* than for two isolated double bonds.

In order to compare these results with those of VB theory, it must first be recognized that according to the latter there are always a number of (rather weak) nonbonded repulsions in action across any C−C single bond, in addition to the one exchange attraction between the two C−C bonding σ electrons on the two C atoms. This is equally true in, for example, C_2H_6 and the hypothetical case of butadiene with no conjugation, and the normal single bond length and other properties are determined (aside from hyperconjugation) by the net effect of the one dominant bonded attraction and the several small nonbonded repulsions.

In VB theory, conjugation in butadiene is attributed to resonance with π-excited (including π-ionic) VB structures. This has the result that *one* (namely the $\pi-\pi$) of the nonbonded repulsions of the hypothetical unconjugated case is weakened or perhaps changed to an attraction. This change is the VB counterpart of the effects noted in Table I for LCAO theory. If the result in VB theory parallels that in LCAO theory, it brings a small amount of positive π bonding across the single bond. In any event, there is a decrease in π, and so in the total of, nonbonded repulsions across the single bond.

In either theory, it is the decrease in π antibonding by conjugation which causes a shortening of the bond below the normal C−C bond length of 1.54 A.[13]

[12] R. G. Parr and R. S. Mulliken, J. Chem. Phys. **18**, 1338 (1950).

[13] About 0.03 A of the decrease may be attributed to the change from tetrahedral to trigonal hybridization in the σ bond, however.

Electronic Spectrum of the Cycloheptatrienyl (Tropylium) Ion

J. N. MURRELL AND H. C. LONGUET-HIGGINS
Department of Theoretical Chemistry, University of Cambridge, Cambridge, England
(Received March 9, 1955)

The $N \rightarrow V$ spectrum of the tropylium ion, $C_7H_7^+$, is studied theoretically by the self-consistent molecular orbital theory. Two transitions are anticipated, an allowed transition at 6.36 ev and a forbidden transition at 4.33 ev. The absorption band at 4.51 ev observed by von Doering and Knox is assigned to the latter transition.

1. INTRODUCTION

THE recent experimental work of von Doering and Knox[1] on the tropylium ion has aroused fresh interest in its electronic structure and stability.

As early as 1931 Hückel considered the probable stabilities of the cyclic ions $(CH)_5^+$, $(CH)_5^-$, $(CH)_7^+$, and $(CH)_7^-$.[2] He showed that the second and third should have closed shell electronic structures in their ground states, and predicted that the ion $(CH)_7^+$ should be the most stable of the four.

In this paper we shall investigate theoretically the electronic spectrum of the ion and compare it with that of benzene which it should closely resemble.

2. METHOD

If the $2p\pi$ atomic orbitals of the seven carbon atoms are denoted by $\phi_1 \cdots \phi_7$, then the molecular orbitals for the six π electrons can be written in complex form as follows:

$$\psi_0 = \sqrt{(1/7)} \sum_r \phi_r$$

$$\psi_1 = \sqrt{(1/7)} \sum_r e^{ir\theta}\phi_r \qquad \psi_{-1} = \sqrt{(1/7)} \sum_r e^{-ir\theta}\phi_r$$

$$\psi_2 = \sqrt{(1/7)} \sum_r e^{2ir\theta}\phi_r \qquad \psi_{-2} = \sqrt{(1/7)} \sum_r e^{-2ir\theta}\phi_r$$

$$\psi_3 = \sqrt{(1/7)} \sum_r e^{3ir\theta}\phi_r \qquad \psi_{-3} = \sqrt{(1/7)} \sum_r e^{-3ir\theta}\phi_r.$$

In the ground state of the molecule ψ_0, ψ_1, and ψ_{-1} contain two electrons each. We shall consider those excited states which arise from the excitation of one electron from ψ_1 or ψ_{-1} to ψ_2 or ψ_{-2}. Representing the ground state as

$$\chi_0 = |\psi_0\bar{\psi}_0\psi_1\bar{\psi}_1\psi_{-1}\bar{\psi}_{-1}|,$$

we obtain from the four singly excited configurations the following singlet states:

$$\chi_{1,2} = \sqrt{(1/2)}\{|\psi_0\bar{\psi}_0\psi_1\bar{\psi}_2\psi_{-1}\bar{\psi}_{-1}| - |\psi_0\bar{\psi}_0\bar{\psi}_1\psi_2\psi_{-1}\bar{\psi}_{-1}|\},$$

$$\chi_{-1,-2} = \sqrt{(1/2)}\{|\psi_0\bar{\psi}_0\psi_1\bar{\psi}_{-1}\psi_{-2}\bar{\psi}_{-2}| - |\psi_0\bar{\psi}_0\psi_1\bar{\psi}_1\bar{\psi}_{-1}\psi_{-2}|\},$$

$$\chi_{1,-2} = \sqrt{(1/2)}\{|\psi_0\bar{\psi}_0\psi_1\bar{\psi}_{-2}\psi_{-1}\bar{\psi}_{-1}| - |\psi_0\bar{\psi}_0\bar{\psi}_1\psi_{-2}\psi_{-1}\bar{\psi}_{-1}|\},$$

$$\chi_{-1,2} = \sqrt{(1/2)}\{|\psi_0\bar{\psi}_0\psi_1\bar{\psi}_{-1}\psi_{-1}\bar{\psi}_2| - |\psi_0\bar{\psi}_0\psi_1\bar{\psi}_1\bar{\psi}_{-1}\psi_2|\}.$$

The symmetry group of the ion is D_{7h}, whose irreducible representations are, in conventional notation:

$$A_1', A_1'', A_2', A_2'', E_1', E_1'', E_2', E_2'', E_3', E_3''.$$

It may be verified that $\chi_{1,2}$ and $\chi_{-1,-2}$ span E_1', and that $\chi_{1,-2}$ and $\chi_{-1,2}$ span E_3' so that these singlet configurations are acceptable wave functions for the electronic states under consideration.

3. SELECTION RULES

The two components of the dipole moment operator in the plane of the molecule span the representation E_1'; therefore a transition from the ground state to a state of symmetry E_1' is allowed with a moment in the plane of the ring, but a transition to a state of symmetry E_3' is forbidden. The near uv spectrum of the tropylium ion should therefore consist of two bands, one of which will be weak as it arises from a symmetry-forbidden transition. From a comparison with the spectrum of benzene we expect that the weak band should occur at a lower energy than the strong band.

4. EXCITATION ENERGIES

The energies of the singly excited configurations relative to the ground state may be calculated by the method of Pariser and Parr, who neglect atomic orbital overlap and all electron repulsion integrals except those of the form

$$\gamma_{rs} = \int\int \phi_r^2(1)\frac{1}{r_{12}}\phi_s^2(2)d\tau_1 d\tau_2.$$

Interpolating the values of γ_{rs} recommended by Pariser and Parr,[3] we have assigned the following values to the two-center integrals:

$$\gamma_{11} = 10.53 \text{ ev}$$
$$\gamma_{12} = 7.30 \text{ ev}$$
$$\gamma_{13} = 5.30 \text{ ev}$$
$$\gamma_{14} = 4.55 \text{ ev}.$$

The resonance integral $\beta_{rs} = \int \phi_r(i)H(r_i)\phi_s(i)d\tau_i$ for nearest neighbors has been given the value suggested by Pariser and Parr for benzene, namely $\beta_{12} = -2.39$ ev.

The energies of the excited electronic states (which

[1] W. von E. Doering and L. H. Knox, J. Am. Chem. Soc. **76**, 3203 (1954).
[2] E. Hückel, Z. Physik **70**, 204 (1931).
[3] R. Pariser and R. G. Parr, J. Chem. Phys. **21**, 767 (1953).

have been written in their real forms) are then as follows.

State	Excitation energy
$\sqrt{\frac{1}{2}}(\chi_{1,2}+\chi_{-1,-2})$ $i\sqrt{\frac{1}{2}}(\chi_{1,2}-\chi_{-1,-2})$	6.36 ev
$\sqrt{\frac{1}{2}}(\chi_{1,-2}+\chi_{-1,2})$ $i\sqrt{\frac{1}{2}}(\chi_{1,-2}-\chi_{-1,2})$	4.33 ev

5. COMPARISON WITH EXPERIMENT

We predict two bands in the near uv spectrum of the tropylium ion, a weak band at 4.33 ev and an intense band at 6.36 ev. Von Doering and Knox have made measurements on the lower energy band; the ion was studied in water at a low pH. They find a band with a maximum absorption at 4.51 ev ($\log\epsilon_{max}=3.64$), and a long tail down to the visible. This tail gives rise to the yellow color of the ion. No measurements are reported at higher energies than 5.02 ev, where there is a trough in the absorption.

It is interesting to compare these predictions on the tropylium ion with the known electronic spectrum of benzene. In benzene the configurations $\chi_{1,-2}$ and $\chi_{-1,2}$ do not span an irreducible representation of the group D_{6h}. The states arising from these must be represented by real wave functions $\sqrt{\frac{1}{2}}(\chi_{1,-2}+\chi_{-1,2})$ and $i\sqrt{\frac{1}{2}}(\chi_{1,-2}-\chi_{-1,2})$ which belong to different, non-degenerate representations. These two states give rise to two distinct bands in the benzene spectrum at energies 4.88 ev and 6.14 ev. Both these bands are symmetry-forbidden, but have intensities $\log\epsilon_{max}=2.04$ and 3.82, respectively. They may be compared with the single low-energy band of the tropylium ion. The next lowest energy states of benzene, however, do belong to a degenerate representation, E_{1u}, and give rise to a strong band of energy 6.7 ev and intensity $\log\epsilon_{max}=4.66$.

Our conclusions are summarized in Table I.

TABLE I.

Benzene			Tropylium ion			
Energy (ev)	$\log\epsilon_{max}$	Symmetry	Energy (ev) Obs.	Energy (ev) Calc.	$\log\epsilon_{max}$	Symmetry
4.88 6.14	2.04 3.82	B_{2u} B_{1u}	4.51	4.33	3.64	E_2'
6.74	4.66	E_{1u}	···	6.36	···	E_1'

THE JOURNAL OF CHEMICAL PHYSICS VOLUME 23, NUMBER 12 DECEMBER, 1955

Molecular Calculations. I. LCAO MO Self-Consistent Field Treatment of the Ground State of H_2O*

FRANK O. ELLISON†‡ AND HARRISON SHULL§
Department of Chemistry and Institute for Atomic Research, Iowa State College, Ames, Iowa

(Received July 1, 1954)

A theoretical study of the ground state of the water molecule utilizing the self-consistent field molecular orbital method in the linear-combination-of-atomic-orbitals approximation is reported. All 10 electrons have been explicitly included, and all integrals have been retained in the calculations. Results are listed for six different values of the bond angle from 90 to 180 degrees, but only for the experimentally observed OH distance. The effect of inner-shell outer-shell mixing is investigated and shown to have a significant effect upon the results. The electronic configuration is discussed both from the viewpoint of molecular and equivalent orbitals. The computed dipole moment is 1.51 D. The SCF ionization potentials agree well with the experimental values, their order of assignment being quite definitely established. The calculated total electronic energy is in error by about 0.75%. This energy changes by only 0.13% for a change in bond angle from 90° to 180°, however, and consequently, the treatment leads to an incorrect value for the equilibrium bond angle. The effect of configuration interaction is considered, and some investigation is made concerning the first excited electronic state.

I. INTRODUCTION

RECENTLY, C. C. J. Roothaan[1] has outlined a mathematical formulation of self-consistent-field (SCF) MO theory in which he has incorporated the approximation of using a linear combination of atomic orbitals (LCAO) for each MO. The applications of this treatment published to date have been confined to systems of very high symmetry and with few exceptions (namely, LiH[2] and N_2[3]) have involved additional approximations not inherently necessary for the method itself, but rather introduced to make the computations more tractable. Thus, for example, Parr and Mulliken[4] treated butadiene by this method but only in the π elec-

* Contribution No. 406 from the Institute for Atomic Research and Department of Chemistry, Iowa State College, Ames, Iowa. Work was supported in part by the Ames Laboratory of the U. S. Atomic Energy Commission.

† This paper is based on portions of a thesis submitted by F. O. Ellison in partial fulfillment of the requirements for the degree of Ph.D. in the Graduate College of Iowa State College.

‡ Present address: Department of Chemistry, Carnegie Institute of Technology, Pittsburgh, Pennsylvania.

§ Present address: Department of Chemistry, University of Indiana, Bloomington, Indiana.

[1] C. C. J. Roothaan, Revs. Modern Phys. **23**, 69 (1951).

[2] I. Fischer, Arkiv Fysik **5**, 349 (1952).

[3] C. W. Scherr, J. Chem. Phys. **23**, 569 (1955).

[4] R. G. Parr and R. S. Mulliken, J. Chem. Phys. **18**, 1338 (1950).

tron approximation. Mulligan[5] for CO_2 and Sahni[6] for CO neglected inner-shell outer-shell interactions. Finally, it should be noted that most of the previous uses of this method not only have been confined to cases where assumptions of this sort were made, but also were applied largely to situations in which there were available only a few experimental data for comparison. With these points in mind, it has been the primary objective of this research to secure the best LCAO SCF MO wave function for the water molecule with a very minimum of assumptions not inherent in the framework of the method itself. Consequently, all 10 electrons have been explicitly included in the treatment, and likewise all integrals necessary in the treatment have been included. Each one has been evaluated or approximated carefully to reduce to a minimum possible effects inaccuracies in these might have on the results. In order to provide an adequate comparison of the calculated results with experiment, the computations were carried through for six different values of the H—O—H bond angle from 90° to 180°, although only a single O—H distance, that experimentally observed, 0.9581 A,[7] was used throughout. Since, in the normal vibrations of the water molecule, the symmetrical bending and stretching modes are almost independent, it was hoped that the calculations would lead to comparison with experiment not only for ionization potentials, binding energy, and equilibrium bond angle, but also for the bending frequency. Thus, there is no lack of experimental data for use in judging the ability of the theory to describe the behavior of the molecule. As objectives secondary to the one already mentioned, we looked for the present investigation to provide (i) a means for a better understanding of the properties of the water molecule, (ii) a means to test the validity of the rigorous SCF LCAO MO approach, and (iii) a means for comparing the results of less complete treatments with the more complete one described in this paper.

Previous theoretical treatments of H_2O have been carried out by a number of investigators. In 1932, A. S. Coolidge performed a theoretical *VB* calculation in which all overlap integrals and multiple exchange terms were explicitly included.[8] Van Vleck and Cross[9] obtained quite successful results using semiempirical *VB* theory in which all AO's are assumed to be orthogonal. The electronic structure of H_2O was an early topic of discussion in the development of the Slater-Pauling theory of directed valency.[10,11] F. Hund[12] appears to have been the first to treat H_2O using simple LCAO MO's. Mulliken has utilized the qualitative MO approach very extensively to predict and assign spectroscopic data and to establish connections between relative electronegativities of atoms, LCAO coefficients, effective charges on atoms in partially polar molecules, and dipole moments.[13,14] Other theoretical approaches to the electronic structure of H_2O have been made by Heath and Linnett[15] and Linnett and Pöe.[16]

J. A. Pople[17] has carried out a unique treatment of H_2O using as a basis the Lennard-Jones[18] method of equivalent orbitals. These computations have recently been improved upon by A. B. F. Duncan and Pople.[19] A more detailed description of the method as well as a comparison of the results with those of the present calculations are given in Appendix I.

II. METHOD OF ATTACK

1. General

The initial problem in setting up the SCF MO calculations is the choice of AO's from which the MO's are constructed. In the past, Slater orbitals with the ordinary Slater Z's[20] have been most commonly used. Also, best Z-values for the free atoms are often employed. In these calculations, the following Slater functions were utilized:

For the oxygen atom:

$$\begin{aligned} 1s &= o = (\mu_1^3/\pi)^{-\frac{1}{2}} \exp(-\mu_1 r_0) \\ 2s' &= s' = (\mu_2^5/3\pi)^{-\frac{1}{2}} r_0 \exp(-\mu_2 r_0) \\ 2pz &= z = (\mu_2^5/\pi)^{-\frac{1}{2}} r_0 \cos\theta_0 \exp(-\mu_2 r_0) \\ 2px &= x = (\mu_2^5/\pi)^{-\frac{1}{2}} r_0 \sin\theta_0 \cos\phi_0 \exp(-\mu_2 r_0) \\ 2py &= y = (\mu_2^5/\pi)^{-\frac{1}{2}} r_0 \sin\theta_0 \sin\phi_0 \exp(-\mu_2 r_0). \end{aligned} \tag{1}$$

For the hydrogen atoms:

$$\begin{aligned} 1s_{h'} &= h' = (\mu^3/\pi)^{-\frac{1}{2}} \exp(-\mu r_{h'}) \\ 1s_{h''} &= h'' = (\mu^3/\pi)^{-\frac{1}{2}} \exp(-\mu r_{h''}). \end{aligned} \tag{2}$$

In general, μ_p is equal to Z_p/n_p, where Z_p is known as the effective nuclear charge and n_p is the effective principle quantum number of the AO. The following Slater μ values were used in this research: $\mu=1$, $\mu_1=7.7$, and $\mu_2=2.275$.[21] All of the oxygen AO's given in Eq. (1) are mutually orthogonal with the exception of $1s$ and $2s'$. Neglect of such orthogonality can cause serious

[5] J. F. Mulligan, J. Chem. Phys. **19**, 347 (1951).
[6] R. C. Sahni, Trans. Faraday Soc. **49**, 1246 (1953).
[7] B. T. Darling and D. M. Dennison, Phys. Rev. **57**, 128 (1940).
[8] A. S. Coolidge, Phys. Rev. **42**, 189 (1932).
[9] J. H. Van Vleck and P. C. Cross, J. Chem. Phys. **1**, 357 (1934).
[10] L. Pauling, J. Am. Chem. Soc. **53**, 1367 (1931); L. Pauling and J. Sherman, J. Am. Chem. Soc. **59**, 1450 (1937).
[11] J. C. Slater, Phys. Rev. **37**, 481; **38**, 1109 (1931).
[12] F. Hund, Z. Physik **73**, 1 (1931); **74**, 429 (1932).
[13] R. S. Mulliken, Phys. Rev. **40**, 55 (1932); **46**, 549 (1934); **74**, 736 (1948); J. Chem. Phys. **2**, 782 (1934); **3**, 506, 573, 586 (1935).
[14] Mulliken, Rieke, Orloff, and Orloff, J. Chem. Phys. **17**, 1248 (1949).
[15] D. F. Heath and J. W. Linnett, Trans. Faraday Soc. **46**, 556 (1948).
[16] J. W. Linnett and A. J. Pöe, Trans. Faraday Soc. **47**, 1033 (1951).
[17] J. A. Pople, Proc. Roy. Soc. (London) **A202**, 323 (1950).
[18] J. E. Lennard-Jones, Proc. Roy. Soc. (London) **A198**, 1, 14 (1949); **A202**, 155, 166 (1950).
[19] A. B. F. Duncan and J. A. Pople, Trans. Faraday Soc. **49**, 217 (1953).
[20] J. C. Slater, Phys. Rev. **36**, 57 (1930).
[21] These are in reasonable agreement with the values which give the best analytical approximations of the Hartree-Fock AO's; *viz.*, $\mu=1$, $\mu_1=7.68$, and $\mu_2=2.22$. W. E. Duncanson and C. A. Coulson, Proc. Roy. Soc. (Edinburgh) **A62**, 37 (1943).

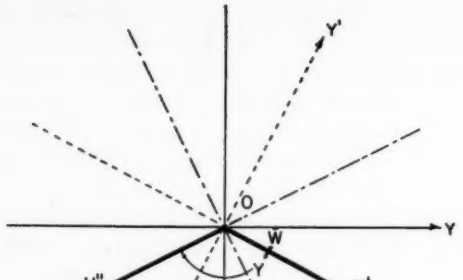

FIG. 1. Coordinates used for the H_2O calculations.

errors in the simple Hartree method which does not utilize an AP wave function.[22] No such error would occur in the present work, although some of the results of the incomplete treatments would be changed somewhat.[23] For consistency, an orthogonalized $2s$ AO was constructed from the original nodeless $2s'$ and $1s$ oxygen AO's as follows:

$$2s=s=(1-Q^2)^{-\frac{1}{2}}(2s'-Q1s), \tag{3}$$

where Q is the overlap integral $S(1s,2s')$.

The coordinate systems used in these calculations are diagrammed in Fig. 1. The x-axis, not shown, is perpendicular to the plane of the molecule. The arrows indicate the positive direction of the axes. Transformations relating these coordinate systems are determined in a straightforward manner.

The real $2p$ AO's oriented in the various directions will often be designated according to these axes; e.g., $2pz=z$, $2py'=y'$, $2pz''=z''$. It is to be noted that the $2p$ oxygen AO's based upon the various coordinate systems transform according to the same equations as the coordinate systems themselves.

The SCF calculations were carried out for 6 different values of the H—O—H bond angle: 90, 100, 105, 110, 120, and 180 degrees, for a constant value, $R=1.8103$ a.u., of the O—H distance.

In order to make maximum use of the symmetry properties of the MO's, it is convenient to introduce symmetry orbitals. These are linear combinations of AO's taken so as to belong to irreducible representations of the symmetry group of the molecule. The H_2O molecule belongs to the group C_{2v}.[24] The symmetry orbitals will be designated as follows: $\sigma_1=2^{-\frac{1}{2}}(h'+h'')$, $\sigma_2=1s_0$, $\sigma_3=2s_0$, $\sigma_4=2pz_0$, $\sigma_5=2^{-\frac{1}{2}}(h'-h'')$, $\sigma_6=2py_0$, and $\sigma_7=2px_0$. It is to be noted that σ_1 and σ_5 are not normalized.[25] The first four symmetry orbitals have A_1 symmetry, σ_5 and σ_6 have B_2 and σ_7 B_1 symmetry.

By taking linear combinations of symmetry orbitals possessing the same symmetry, a like number of MO's having that symmetry are formed. The latter are designated as follows:

$$\begin{aligned}
\phi(1a_1)&=c_{11}\sigma_1+c_{12}1s_0+c_{13}2s_0+c_{14}2pz_0,\\
\phi(2a_1)&=c_{21}\sigma_1+c_{22}1s_0+c_{23}2s_0+c_{24}2pz_0,\\
\phi(3a_1)&=c_{31}\sigma_1+c_{32}1s_0+c_{33}2s_0+c_{34}2pz_0,\\
\phi(4a_1)&=c_{41}\sigma_1+c_{42}1s_0+c_{43}2s_0+c_{44}2pz_0,\\
\phi(1b_2)&=c_{55}\sigma_5+c_{56}2py_0,\\
\phi(2b_2)&=c_{65}\sigma_5+c_{66}2py_0,\\
\phi(1b_1)&=2px_0.
\end{aligned} \tag{4}$$

The MO's are denoted by the symbol of the irreducible representation to which they belong, preceded by a running number distinguishing orbitals of identical symmetry.

2. Determination of the Best LCAO MO's

The detailed development of the procedure for determining the SCF MO wave function for the ground state of a molecule is given in Roothaan's paper on this subject.[1] A brief but convenient outline of the derivation is furnished by Mulligan[5] in conjunction with his SCF treatment of CO_2. Inasmuch as the procedure for setting up the secular equations for the H_2O problem is exactly analogous to that described by Mulligan, a detailed description will not be given here.

The secular equations were solved by the method of James and Coolidge.[26] In order to attain the self-consistent wave function, it is necessary to assume a set of coefficients c_{ip}, solve the secular equations, and compare the resulting c_{ip} with the assumed values, which are generally found to be different. To obtain self-consistency, repetition of the process is therefore required. No procedure was found which is faster than utilizing the computed c_{ip}'s as the assumed coefficients for the succeeding SCF trial.

III. RESULTS AND DISCUSSION

1. General Considerations

Utilizing the notation for MO's defined in Eqs. (4), the ground state MO electronic configuration for H_2O

[22] J. A. Van Vleck and J. Sherman, Revs. Modern Phys. **7**, 167 (1935); C. A. Coulson and W. E. Duncanson, Proc. Roy. Soc. (London) **A181**, 378 (1943).

[23] In a complete LCAO MO treatment which allows for $1s$–$2s$ mixing, it makes no difference whether one utilizes nodeless or orthogonalized $2s$ AO's; each MO may be equivalently formulated in terms of either. On the other hand, if no $1s$ mixing is explicitly allowed in the valence shells, different SCF wave functions and energies will result depending upon whether one uses $2s$ or $2s'$ AO's. It is probable that the degree of nonorthogonality among MO's resulting from the neglect of forced hybridization (see reference 27) will be lessened if one utilizes the orthogonalized $2s$ AO.

[24] R. S. Mulliken, Phys. Rev. **43**, 279 (1933).

[25] In a preliminary report of this work [F. O. Ellison and H. Shull, J. Chem. Phys. **21**, 1420 (1953)], the symbols σ_1 and σ_5 were taken to represent the normalized hydrogen symmetry orbitals. The latter are obtained from the non-normalized functions after multiplying by $[1+S(h'h'')]^{-\frac{1}{2}}$ and $[1-S(h'h'')]^{-\frac{1}{2}}$, respectively.

[26] H. James and A. Coolidge, J. Chem. Phys. **1**, 825 (1933).

may be written as follows:

$$H_2O: 1a_1)^2 2a_1)^2 1b_2)^2 3a_1)^2 1b_1)^2, \ ^1A_1. \quad (5)$$

The MO's are given in their order of increasing energy.

Two distinct SCF calculations were carried out for each bond angle. A complete treatment was made in which all electrons are assigned to MO's extending throughout the molecule. This calculation included no assumptions beyond those contained in the LCAO MO's, defined in Eqs. (4), and in the three-center integral approximations. The 7×7 secular equation reduced to one 4×4, one 2×2, and one 1×1 equations as a result of symmetry. In addition, an approximate treatment was performed which contained the conventional assumption of replacing the innermost molecular shell ($1a_1$) by an oxygen $1s$ Slater orbital, and which considered no $1s$-mixing in the outer shells, i.e., $c_{11}=c_{13}=c_{14}=c_{22}=c_{32}=0$. The secular equation was thereby simplified to one 3×3, one 2×2, and two 1×1 determinantal equations. A direct comparison of the complete and approximate treatments is of special interest inasmuch as the assumption of no inner-shell outer-shell mixing is utilized quite extensively. The general method of computation was, of course, derived under the condition that all MO's are strictly orthogonal, whereas in the approximate treatment the MO $\phi(1a_1)$ is not orthogonal to $\phi(2a_1)$ or $\phi(3a_1)$. The degree of nonorthogonality is, however, expected to be small because of the small overlap between $1s_0$ and h' or h'', and therefore, the results should be quite reliable, although they still must be interpreted with some discretion.[27]

2. Ground State MO's

In Table I are listed the best SCF LCAO coefficients for the ground state MO's as a function of the H—O—H bond angle. Also given are the coefficients for the MO's which are unoccupied in the ground-state electronic configuration. The results are tabulated for both the approximate (A) and complete (C) treatments.

A general perusal of the values, say of the 105 degree treatment, gives an indication of the nature of the MO's. The simplest MO picture of H_2O is

$$H_2O: 1s)^2 2s)^2 1b_2)^2 3a_1)^2 2px)^2, \ ^1A_1,$$

in which the bonding is attributed only to $\phi(1b_2)$ and $\phi(3a_1)$. The latter orbital must contain a negative oxygen hybrid,[28] that is, plus $2pz$ and minus $2s$ character, in order to make it orthogonal to the inner $2s$-shell.[29] This is also apparent in the approximate treatment (in which, however, bonding has been allowed also in the inner $2s$-(or $2a_1$)-shell).

The orbital $\phi(1b_2)$ is probably the most strongly bonding valence shell MO for the H—O—H bond angle of 105°. This is postulated because of the weakened $\phi(3a_1)$ bonding resulting from forced hybridization

TABLE I. LCAO SCF MO's for the ground state of H_2O.

Coefficients	H—O—H bond angle (degrees) 90 A[a]	90 C[b]	100 A	100 C	105 A	105 C
Occupied orbitals						
c_{11}	0	−0.0031	0	−0.0032	0	−0.0033
c_{12}	1	1.0002	1	1.0002	1	1.0002
c_{13}	0	0.0161	0	0.0162	0	0.0163
c_{14}	0	0.0026	0	0.0025	0	0.0024
c_{21}	0.202	0.175	0.2073	0.179	0.207	0.1781
c_{22}	0	−0.028	0	−0.029	0	−0.0286
c_{23}	0.821	0.842	0.8188	0.842	0.821	0.8450
c_{24}	0.133	0.149	0.1257	0.139	0.120	0.1328
c_{31}	0.502	0.397	0.452	0.348	0.438	0.3341
c_{32}	0	−0.031	0	−0.027	0	−0.0258
c_{33}	−0.618	−0.533	−0.569	−0.481	−0.548	−0.4601
c_{34}	0.674	0.759	0.736	0.810	0.757	0.8277
c_{55}	0.737	0.781	0.738	0.780	0.736	0.7759
c_{56}	0.618	0.585	0.587	0.554	0.575	0.5428
Unoccupied orbitals						
c_{41}		1.011		1.048		1.061
c_{42}		−0.082		−0.085		−0.086
c_{43}		−0.774		−0.819		−0.833
c_{44}		−0.741		−0.671		−0.642
c_{65}		1.300		1.247		1.230
c_{66}		−0.967		−1.000		−1.013

Coefficients	H—O—H bond angle (degrees) 110 A[a]	110 C[b]	120 A	120 C	180 A	180 C
Occupied orbitals						
c_{11}	0	−0.0033	0	−0.0035	0	−0.0038
c_{12}	1	1.0002	1	1.0002	1	1.0002
c_{13}	0	0.0163	0	0.0165	0	0.0169
c_{14}	0	0.0023	0	0.0021	0	0
c_{21}	0.204	0.175	0.204	0.1740	0.224	0.1785
c_{22}	0	−0.028	0	−0.0283	0	−0.0289
c_{23}	0.825	0.849	0.829	0.8542	0.824	0.8632
c_{24}	0.115	0.127	0.103	0.1129	0	0
c_{31}	0.426	0.322	0.386	0.2835	0	0
c_{32}	0	−0.025	0	−0.0220	0	0
c_{33}	−0.528	−0.440	−0.477	−0.3884	0	0
c_{34}	0.777	0.843	0.823	0.8802	1	1
c_{55}	0.740	0.777	0.748	0.7821	0.781	0.7863
c_{56}	0.560	0.529	0.531	0.5014	0.444	0.4378
Unoccupied orbitals						
c_{41}		1.072		1.093		1.145
c_{42}		−0.087		−0.089		−0.093
c_{43}		−0.844		−0.870		−0.955
c_{44}		−0.612		−0.541		0
c_{65}		1.213		1.185		1.147
c_{66}		−1.028		−1.055		−1.130

[a] Approximate treatment.
[b] Complete treatment.

[27] The requirement of a minimum amount of $1s$–$2s$–$2p$ mixing in order to maintain MO orthogonality has been called forced hybridization by R. S. Mulliken, J. Chem. Phys. **19**, 912 (1951). In the approximate treatment, the neglect of this type of hybridization could have been compensated for by permitting either c_{11} or c_{22} and c_{32} to take on nonzero values. In either case, the simplification of the secular equation in the approximate treatment would be lost and the computational labor becomes equal to that in the complete treatment. Therefore, the full measure of mixing was accounted for in the complete treatment, and the intermediate step of forced hybridization was omitted. The mixing introduced over and beyond the minimum requirements expressed by forced hybridization might be expected to lead only to a small improvement of the wave function. It is more likely that higher energy AO's, such as $2p$ hydrogen and $3s$ oxygen functions, would be more valuable in this respect.

[28] R. S. Mulliken, J. Chem. Phys. **19**, 900 (1951).

[29] This is relevant to Mulliken's conclusion that forced hybridization leads to a weakening of bonding MO's.[27]

and because of the more pronounced overlap which can be attained in $\phi(1b_2)$ at large bond angles.

For the angle of 105° the ratio of the LCAO coefficients in $\phi(1b_2)$ is opposite to that which is to be expected on the basis of the relative electronegativity of oxygen and hydrogen. One might expect that such a basis for predicting LCAO MO coefficients would be justified if there were one valence orbital. In the case of H_2O, the orbitals tend to correlate themselves in a manner which is governed only by the relative electronegativity in a gross sense. The $2s$–$2pz$ hybridization allows considerable charge transfer in $\phi(3a_1)$ while the electrons in $\phi(1b_2)$ tend to avoid the latter as well as go into the O—H bonding regions.

The following qualitative statements can be made with respect to the variation of the MO's with bond angle:[13] at 0° $\phi(1b_2)$ becomes a pure $2p\pi(y)$ AO on oxygen (with the real possibility of bonding with a $2p\pi$ helium AO, which is the united atom function corresponding to σ_5), and $\phi(3a_1)$ probably is quite bonding; at 180°, $\phi(1b_2)$ takes on the greatest responsibility for bonding, while $\phi(3a_1)$ becomes a pure $2p\pi(z)$ AO on oxygen.

It is seen that the differences between the approximate and complete treatments are, indeed, considerable and quite significant in some cases. The average variation of the coefficients between the two treatments in the 105 degree calculation is about 11%.

In Appendix I, the results of the present SCF MO calculation are compared with the semiempirical equivalent orbital treatment carried out by Pople and Duncan.[17,19]

The computed dipole moment is one of the important criteria for judging the accuracy of a wave function. Using the SCF MO's from the complete treatment given in Table I, the dipole moment was calculated for all bond angles and the results are listed in Table II. The integrals required in the computation are given in Appendix II. It is seen that the calculated dipole moment for the observed H—O—H bond angle is in reasonably good agreement with the experimental value of 1.84 D.

The dipole moment was also computed using the MO's from the approximate treatment. The result is 1.21 D for the 105° bond angle, a value obtained, however, by assuming, not unreasonably, that all MO's are strictly orthogonal. The improvement in the calculated dipole moment on going from the approximate to the complete treatment is remarkable, and reflects the importance of including inner-shell outer-shell mixing in its entirety.

TABLE II. The calculated dipole moment of the ground state of H_2O.

H—O—H bond angle (degrees)	Dipole moment (Debye units)
90	1.53[a]
100	1.55
105	1.52
110	1.45
120	1.32
180	0

[a] All values directed in the sense $H_2^+O^-$.

3. Ionization Energies

An SCF orbital energy should represent a good approximation to the negative of the corresponding experimental ionization potential I.[1] In Table III, orbital energies are listed for both the approximate and complete treatments for all bond angles. Also given are the observed I's as well as the SCF orbital energies for the unoccupied MO's.

There is little doubt that the lowest observed ionization potential corresponds to removal of a nonbonding $2px$ electron. The calculated value is too low because the correlation energy for the resulting H_2O^+ ion, calculated using ground-state orbitals, is less than that for the ground state itself. In other words, there is an excessive amount of electronic repulsion encountered in $(2px)^2$ in the orbital picture of H_2O because of the inability of the electrons' avoiding each other. This is not encountered in the resulting H_2O^+ ion. Quantitative justification is given for this fact by the correlation energies for the resulting dissociation products. The calculated energy of $O^+(1s^22s^22p^3, {}^4S)$ is 11.5 ev above the observed, and of $O(1s^22s^22p^4, {}^3P)$, 15.7 ev above the true energy. The appropriate valence state correlation energies are comparable to these.

It is somewhat disturbing that upon molecule formation, the valence state I of the oxygen atom, $O(1s^22s^22p^4, V_2)\rightarrow O^+(1s^22s^22p^3, V_3)$, calculated to be about 10 ev, increases in going to the corresponding molecular ionization potential to 11.8 ev. This is directly opposed in direction to that which is observed: 14.7 to 12.6 ev. The latter has generally been attributed to charge transfer effects, a phenomenon which also certainly takes place in the theoretical results, but apparently does not manifest itself in this manner. The contradiction can be explained in terms of correlation energies. The difficulty this presents reminds one of the objections voiced by Moffitt concerning the energy calculations of present orbital theories.[30] The calculated energy of H_2O^+, using H_2O SCF ground state MO's, is very poor relative to that of O^+, using Slater orthogonalized orbitals whereas the correlation energies for H_2O and O are comparable in magnitude.

It has been noted by Mulliken[31] that $\phi(1b_1)$ may be weakly bonding, as attested by the large π–π overlap; $S(2p\pi_h, 2p\pi_0)$ equals 0.19. This is also indicated experimentally in OH by the increase of internuclear distance by 0.058 A upon removal of the π electron.

There exists some question concerning the assignment of the higher ionization potentials.[32] These

[30] W. Moffitt, Proc. Roy. Soc. (London) **A210**, 224, 245 (1951).
[31] R. S. Mulliken, J. Am. Chem. Soc. **72**, 4493 (1950).
[32] W. C. Price and T. M. Sugden, Trans. Faraday Soc. **44**, 108 (1948).

TABLE III. LCAO SCF orbital energies for the ground state of H_2O (ev).

MO	H–O–H bond angle (degrees) 90 A[a]	90 C[b]	100 A	100 C	105 A	105 C	Observed
$(1a_1)$	−560.08	−558.09	−559.37	−557.52	−559.12	−557.27	
$(2a_1)$	−38.19	−36.86	−37.65	−36.40	−37.43	−36.19	
$(1b_2)$	−18.7	−17.8	−18.9	−18.3	−19.2	−18.55	−16.2±0.3[c,d]
$(3a_1)$	−15.5	−14.2	−14.6	−13.6	−14.2	−13.20	−14.5±0.3[c,e]
$(1b_1)$	−13.4	−12.2	−13.0	−11.9	−12.8	−11.79	−12.6±0.1[c,f]
$(4a_1)$		12.1		13.6		13.7	
$(2b_2)$		16.1		15.9		15.9	

MO	H–O–H bond angle (degrees) 110 A	110 C	120 A	120 C	180 A	180 C
$(1a_1)$	−558.96	−557.17	−558.58	−556.83	−556.08	−554.80
$(2a_1)$	−37.30	−36.07	−36.92	−35.75	−34.79	−34.11
$(1b_2)$	−19.5	−18.9	−19.9	−19.48	−21.0	−20.78
$(3a_1)$	−14.0	−13.0	−13.4	−12.60	−11.3	−10.80
$(1b_1)$	−12.8	−11.8	−12.5	−11.64	−11.3	−10.80
$(4a_1)$		14.0		14.5		14.4
$(2b_2)$		15.7		15.3		15.8

[a] Approximate treatment.
[b] Complete treatment.
[c] Negatives of ionization potentials obtained by electron impact; see reference 32.
[d] Spectroscopic value: 16.0±0.5 ev. H. J. Henning, Ann. Physik **13**, 599 (1932).
[e] No spectroscopic value recorded.
[f] Spectroscopic value: 12.56±0.01 ev. W. C. Price, J. Chem. Phys. **4**, 147 (1936).

calculations favor the designations as listed in Table III. The numerical agreement is not as satisfactory as one might like, although the order of assignment seems quite well determined. It is possible that the use of exact values of three-center integrals would bring about better agreement with the observed I's, but it is doubtful that the order would be reversed. A significant difference between the potentials for $\phi(1b_2)$ and $\phi(3a_1)$ exists even at 90 degrees. It is interesting to note that there is a 2 ev difference between the second and third I's of H_2S,[32] in which the equilibrium bond angle is about 92 degrees.

As was also noted in Mulligan's treatment of CO_2,[5] considerably higher I's are calculated for the nonvalence shells than those predicted by Mulliken.[13] The value for $\phi(2a_1)$ is partially explained by the fact that Mulliken took this orbital to be nonbonding (I∼32 electron volts), whereas the SCF function turns out to be quite bonding.

The variance of the computed orbital energy of $\phi(1a_1)$ from the observed K-shell x-ray absorption limit for the oxygen atom (524 ev) is due to the choice of the Slater $1s$ orbital; the calculated valence state ionization potential $O(1s^22s^22p^4,\ V_2)\rightarrow O^+(1s2s^22p^4,\ V_3)$ using Slater orbitals, is 557.1 ev, essentially identical with the computed $\phi(1a_1)$ orbital energy.

4. Total Energy and Sources of Error

The total ground state SCF electronic energies are given in Table IV as a function of bond angle for both the approximate and complete treatments. Also listed are the nuclear repulsion energies, total molecular energies, and dissociation energies. The latter are obtained by subtracting the total SCF molecular energy from the calculated total energy of the separated atoms. The electronic energy of the oxygen atom, −2027.6 ev, was computed using the same orthogonalized Slater AO's as were used for the MO calculations. Also given in Table IV are the corresponding experimental energies for H_2O.

It is seen that these calculations predict a maximum dissociation energy, and hence an equilibrium configuration, at a bond angle somewhat greater than 120°. This result, quite divergent from experiment, should probably not be considered as serious as it might first appear. The total electronic energy is the quantity

TABLE IV. Total SCF energies for the ground state of H_2O.

H–O–H bond angle (deg)	Type of treatment	Total electronic energy (ev)	Nuclear repulsion energy (ev)	Total molecular energy (ev)	Dissoc. energy (ev)
90	A[a]	−2315.0	251.06	−2063.9	9.1
	C[a]	−2313.0	251.06	−2061.9	7.1
100	A	−2314.4	250.25	−2064.1	9.3
	C	−2312.6	250.25	−2062.3	7.5
105	A	−2314.2	249.91	−2064.3	9.5
	C	-2312.4_4	249.91	-2062.5_3	7.7
105	Exp.[b]	−2330.5	249.91	−2080.6	10.06
110	A	−2314.0	249.61	−2064.4	9.6
	C	−2312.4	249.61	−2062.8	8.0
120	A	−2313.7	249.11	−2064.6	9.8
	C	-2312.1_4	249.11	-2063.0_3	8.2
180	A	−2310.6	247.95	−2062.6	7.8
	C	−2309.9	247.95	−2062.0	7.2

[a] A = approximate treatment, C = complete treatment.
[b] Atomic heat of formation, 9.49 ev, from G. Herzberg, *Molecular Spectra and Molecular Structure* (D. Van Nostrand Company, Inc., New York, 1950), second edition, Vol. I, p. 481. To this must be added the zero point energy, 0.57 ev, *ibid.*, Vol. II, p. 282. Experimental energy of the separated atoms (−2070.5 ev) from C. E. Moore, "Atomic energy levels," Natl. Bur. Standards (U.S.) Circular 467, Vol. I.

which is actually minimized by the SCF procedure. As the bond angle decreases from 180 to 90 degrees, this energy decreases by only about 0.13%. The variation of this large quantity is thus very small over this wide range of bond angle.

Moffitt's recent discussion of the inadequacies of the present orbital theories[30] with respect to energy calculations is especially relevant. It seems quite evident that a calculation of the difference between two large quantities which are in themselves almost twice as inaccurate as that difference might easily be subject to serious error.

In order to provide a test of the dependence of the total energy results on the approximate values of three-center integrals utilized a second calculation was carried out for the 105 and 120 degree bond angles. In this computation the values for two of the integrals were revised as follows:

at 105 degrees,

$$(H'':h'z)\ \ 0.1581\rightarrow 0.1337$$
$$(h''h'':h'z)\ \ 0.1400\rightarrow 0.1028;$$

and at 120 degrees,

$$(H'':h'z)\ \ 0.1319\rightarrow 0.1075$$
$$(h''h'':h'z)\ \ 0.1160\rightarrow 0.0870,$$

where values are given in atomic units. These two integrals were chosen for revision since their probable errors were considered to be relatively high. Also, it is evident that the energy as a function of bond angle must be quite dependent upon integrals involving $2pz$ and $2py$. It should be noted that the magnitude of the corrections is probably larger than can be expected from the uncertainties in the approximation process.

It was found that some significant changes in the final results were caused by using the revised integral values. The dissociation energy at 105° was increased from 9.5 to 9.8 ev, at 120° from 9.8 to 9.9 ev (the computed equilibrium bond angle moving closer to the observed value); dissociation energy calculations thus depend quite strongly on the values of three-center integrals. The computed orbital energies were changed by 0.7 ev on the average. The LCAO coefficients in $\phi(2a_1)$ and $\phi(3a_1)$ were hardly changed at all, but those in $\phi(1b_2)$ differed by about 0.04 from the original calculation.

There are several other possible causes for the divergence of the calculated equilibrium bond angle from that observed. The possibility that configuration interaction (CI) may be of importance should be considered. This question is considered with respect to the orbitals involved in the present treatment in the following section. Such CI is found to be of negligible importance in this connection. We have no way of ascertaining at this point, however, the effect of including 3-quantum orbitals on the oxygen or 2-quantum orbitals on the hydrogens in the SCF procedure itself or via configuration interaction. It is not impossible that these may be significant even in the ground state.

Another possibility is that the LCAO approximation itself is the limiting factor in this total energy calculation. One might expect the best AO's for use in an LCAO treatment to vary as a function of bond angle. In the past it has always been hoped that variation of the LCAO coefficients alone supplies sufficient flexibility to account for any required changes in the orbitals. It would be pertinent to consider in this respect both the question of better Z-values for the AO's and the inclusion of higher energy AO's.

It must also be remembered that these calculations were carried out only for a fixed value (the experimental value) of the O—H bond distance. It is not unlikely that the absolute minimum in the molecular energy for the SCF LCAO calculation lies at some other distance than the observed O—H bond distance. A slight lengthening of this distance for example might well permit the calculated minimum angle to decrease toward the observed.

Finally there is the ever-present possibility of numerical error in as long and tedious a calculation as was attempted here. Every precaution was taken to reduce these possibilities to a minimum. Once the integrals were evaluated, checked several times, and the basic calculations were set up, the very nature of the SCF procedure itself precludes the possibility of further error.

5. Configuration Interaction and Excitation Energies

In MO calculations the question of the importance of CI often arises. For low excited states, interaction of this type is expected to be quite considerable since there are likely to be many states of the same symmetry in the same energy range. For the ground state of the molecule, however, CI should be of little importance. This should be especially true of SCF calculations in which the very best combination of AO's in a single configuration is found. Some calculations were carried out, however, to test this assumption.

One must first choose which excited state wave functions are to be utilized in this calculation. Roothaan[1] has discussed this in some detail in connection with the calculation of excitation energies. It is assumed that unoccupied MO's arising from the ground state SCF calculation may be used. For H_2O, $\phi(4a_1)$ and $\phi(2b_2)$ are suitable excited state MO's. The LCAO forms of these are determined completely by the requirement of orthonormality with respect to the occupied ground state MO's.

It can be shown that the totally symmetric states differing by a single electron transfer from the ground state necessarily have zero interaction with the ground state. This is a consequence of these MO's being eigenfunctions of the SCF Hamiltonian. Two of the lowest

excited states which do interact with the ground-state function in this approximation were considered individually. These were:

$$\Phi_1\colon\ (1a_1)^2(2a_1)^2(3a_1)^2(1b_2)^2(4a_1)^2$$
$$\Phi_2\colon\ (1a_1)^2(2a_1)^2(3a_1)^2(1b_2)^2(2b_2)^2.$$

It was found that Φ_1 has zero interaction with the ground state Φ_0; i.e., mixing these two functions did not depress $E(\Phi_0)$ in the fifth significant figure. The energy of $a\Phi_0+b\Phi_2$ differs from that of Φ_0 by a negligible 0.03 ev.

Utilizing the same excited SCF function for $\phi(4a_1)$ as in the CI calculation, it is possible to compute the excitation energy as well as the corresponding oscillator strength for the lowest predicted electronic transition,

$$(1a_1)^2(2a_1)^2(1b_2)^2(3a_1)^2(1b_1)^2;\ \ {}^1A_1\rightarrow$$
$$(1a_1)^2(2a_1)^2(1b_2)^2(3a_1)^2(1b_1)(4a_1);\ \ {}^{1,3}B_1.$$

There are three absorption peaks at 1608, 1648, and 1718 A[33] which might be attributed to this transition. The energy differences between these successive bands are about 1500 cm^{-1}, which nearly equals the symmetrical bending vibration frequency.[7] The calculated energy for this transition is 96 200 cm^{-1}, corresponding to an absorption at 1040 A. This result is not expected to be very accurate since the approximation as to the nature of $\phi(4a_1)$ is probably poor. Mulliken[13] takes the excited MO to be a pure oxygen 3s AO.

Oscillator strengths for this same transition were computed using both the dipole length and dipole velocity methods. For dipole length, one obtains,

$$f=(1.085\times10^{11})\nu\left[\int(1b_1)x(4a_1)dv\right]^2$$

in which ν is given in cm^{-1} and the integral in cm. For the dipole velocity method,

$$f=(1.464\times10^{5})\left[\int(1b_1)(d/dx)(4a_1)dv\right]^2\Big/\nu$$

with ν in cm^{-1} and the integral in a.u.$^{-1}$. If one uses the theoretical value of ν one obtains 3×10^{-6} and 3.7×10^{-2} for the f-numbers by means of the length and velocity operators respectively. If one calculates semiempirical f-numbers, i.e., with the experimental ν, these become in turn 1.9×10^{-6} and 5.9×10^{-2}. The observed f-number is 3×10^{-2}.

The poor result with the dipole length procedure can certainly be attributed to the failure to include 3s character in the excited state wave function. The 3s AO with its r^2-dependence would be important at relatively large distances where the dipole length method is most sensitive. The absence of 3s character would thus be expected to result in too low a value for the computed f-number by the dipole length method.

[33] P. G. Wilkinson and H. L. Johnston, J. Chem. Phys. **18**, 190 (1950).

This is partially substantiated by some simple calculations based on the assumption that the transition is simply $(2px)\rightarrow(3s)$. If one uses Slater AO's with Z of 1.75 for the 3s AO, and the experimental ν, the dipole length method gives the more reasonable result of 0.016 whereas the dipole velocity value has increased to 0.191. It might well be that one could obtain a fairly reliable estimate of the amount of 3s character in the excited orbital by comparing the dipole length and dipole velocity results with each other and with experiment as a function of 3s character in the excited orbital, but using the SCF ground state MO. We have not, however, undertaken this project.

APPENDIX I. THE EQUIVALENT ORBITAL REPRESENTATION OF ELECTRONIC STRUCTURE OF H_2O

As was noted in the introduction, J. A. Pople has carried out a treatment of the water molecule[17] which is based upon the Lennard-Jones method of equivalent orbitals.[18] Pople's calculation began with the general LCAO formulation of the $2a_1$, $3a_1$, $1b_2$, and $1b_1$ MO's, utilizing only the 2s and 2p oxygen and 1s hydrogen AO's. The lone-pair equivalent orbitals were then obtained by a unitary transformation of the MO wave function, a step which involves no loss of rigor. Three explicit approximations were then utilized in the formation of the bond equivalent orbitals: the orbitals were assumed to be localized; the oxygen hybrids were assumed to be directed along the line of nuclei of the bonds; and the condition of orthogonality between bond equivalent orbitals was simplified. A recent refinement of the calculation has eliminated the last approximation.[19] With these assumptions, the ordinary conditions of orthonormality of the orbitals determine all but one of the LCAO coefficients. By introducing the empirical values for the dipole moment, the equivalent orbitals were determined.

The SCF MO's from the complete treatment as outlined above have been transformed rigorously to the equivalent orbital representation. These results, together with values obtained from the Duncan-Pople treatment,[19] are given in Table V. The orbitals $\phi(b_\pm)$

TABLE V. The equivalent orbitals for the ground state of H_2O.

EO	AO	90	105	105 Duncan-Pople[a]	120	180
$\phi(b_\pm)$	h'	0.607	0.577	0.58	0.557	0.482
	h''	−0.174	−0.199	0	−0.215	−0.304
	1s	−0.028	−0.026	0	−0.024	−0.020
	2s	−0.105	−0.006	0.06	0.082	0.610
	2pz	0.534	0.561	0.37	0.572	0
	2py	±0.414	±0.384	±0.49	±0.355	±0.310
$\phi(l_\pm)$	1s	−0.009	−0.009	0	−0.009	0
	2s	0.697	0.680	0.58	0.658	0
	2pz	−0.120	−0.192	−0.41	−0.258	−0.707
	2py	±0.707	±0.707	±0.71	±0.707	±0.707

[a] Adapted from results of Duncan and Pople (reference 19).

denote bond equivalent orbitals, the plus sign for the orbital directed to h', the negative sign for that directed to h''. The lone pair orbitals $\phi(l_\pm)$ are directed to the back side of the oxygen atom. They are symmetric with respect to the xz-plane, one orbital directed above the plane of the molecule, the other below the plane.

On the basis of the SCF results, complete localization of bond equivalent orbitals seems to be unjustified. Also, the assumption that these orbitals are aligned with the bond axis appears to be a restriction which is not entirely substantiated. In fact, the angle between the SCF bond functions, as indicated by the coefficients of $2pz$ and $2py$, appears to decrease as the bond angle increases. Bond localization is exact for a bond angle of zero degrees, and poorest for 180 degrees. For this reason, inspection of the variation of equivalent orbital bond properties as a function of angle is probably questionable.

Pople[34] has recently published a slightly different equivalent orbital representation of our SCF wave function for the 105 degree bond angle. Its purpose was to show that the latter calculation supports the concept of directed lone pairs. This is also exemplified in the results in Table V.

The moment arising from the lone pairs is found to be 1.69 D as compared to the value of 3.03 D found by Duncan and Pople. The latter found the total bond moment to be -6.82 D whereas our result is -5.77 D. The moment arising from the nuclei alone is $+5.60$ D.

APPENDIX II. EVALUATION OF ONE- AND TWO-CENTER INTEGRALS

The AO's utilized in the evaluation of all integrals are those defined in Eqs. (1–3). All values are given in Hartree atomic units,[35] except, of course, for overlap integrals, which are dimensionless. The various types of integrals are designated in the tables by the following symbols:

overlap integrals,

$$S(\chi_p\chi_q)=\int \chi_p{}^\mu\chi_q{}^\mu dv^\mu;$$

dipole moment integrals,

$$(\chi_p z_m\chi_q)=\int \chi_p{}^\mu z_m{}^\mu\chi_q{}^\mu dv^\mu;$$

kinetic energy integrals

$$(\chi_p T\chi_q)=\int \chi_p{}^\mu(-\tfrac{1}{2}\Delta^\mu)\chi_q{}^\mu dv^\mu;$$

nuclear attraction integrals,

$$(A:\chi_p\chi_q)=\int \chi_p{}^\mu(1/r^{\mu A})\chi_q{}^\mu dv^\mu;$$

and, electronic repulsion integrals,

$$(\chi_p\chi_q:\chi_r\chi_s)=\int \chi_p{}^\mu\chi_q{}^\mu(1/r^{\mu\nu})\chi_r{}^\nu\chi_s{}^\nu dv^\mu dv^\nu.$$

(6)

The dipole moment operator $z_m{}^\mu$ is taken along the OH′ axis, directed towards H′ with its origin at the midpoint of the internuclear axis. Other integrals arise which involve the analogous operator $y_m{}^\mu$, perpendicular to $z_m{}^\mu$.

The values of all one-center integrals are listed in Table VI. Many of these were obtained from tables published by Mulligan.[5] All others were computed using analytical expressions given by Roothaan.[36]

TABLE VI. One-center integrals over AO's.

$S(os')$	0.23345	$(oo:ss)$	1.1334
$(h'Th')$	0.5000	$(oo:zz)$	1.1297
(oTo)	29.6450	$(os:os)$	0.0703
(oTs)	−8.0885	$(os:ss)$	−0.0181
(sTs)	3.0869	$(os:zz)$	−0.0097
(zTz)	2.5878	$(oz:oz)$	0.0265
$(H':h'h')$	1.0000	$(oz:sz)$	0.0349
$(O:oo)$	7.7000	$(ss:ss)$	0.8039
$(O:os)$	−1.0505	$(ss:zz)$	0.8137
$(O:ss)$	1.2636	$(sz:sz)$	0.1750
$(O:zz)$	1.1375	$(zz:zz)$	0.8905
$(h'h':h'h')$	0.6250	$(zz:yy)$	0.7945
$(oo:oo)$	4.8125	$(zy:zy)$	0.0480
$(oo:os)$	−0.4498	(oz_mz')	0.0540
		$(s'z_mz')$	0.6345

TABLE VII. Two-center integrals over AO's involving only hydrogen AO's (a.u.).

Integral	H−O−H bond angle (degrees) 90	100	105	110	120	180
$S(h'h'')$	0.44403	0.39576	0.37459	0.35531	0.32234	0.24064
$(h'Th'')$	0.05315	0.03777	0.03174	0.02661	0.01867	0.00336
$(H':h''h'')$	0.3823	0.3553	0.3438	0.3336	0.3165	0.2753
$(H':h'h'')$	0.2752	0.2357	0.2190	0.2043	0.1798	0.1237
$(h'h':h''h'')$	0.3621	0.3407	0.3313	0.3228	0.3082	0.2715
$(h'h'':h'h'')$	0.09947	0.0770	0.06849	0.06104	0.04938	0.02621
$(h'h':h'h'')$	0.2169	0.1880	0.1757	0.1643	0.1461	0.1025

TABLE VIII. One-electron two-center integrals over AO's involving oxygen AO's.

$S(h'o)$	0.06098	$(h'Tz')$	0.2375	$(H':y'y')$	0.5043
$S(h's)$	0.4946	$(h'Ts)$	0.1342	$(O:h'h')$	0.5108
$S(h'z')$	0.3479	$(H':oo)$	0.5524	$(H':oh')$	0.0350
(oz_mh')	0.0512	$(H':os)$	−0.0005	$(H':sh')$	0.3885
$(s'z_mh')$	0.1270	$(H':oz')$	0.0165	$(H':z'h')$	0.4114
$(z'z_mh')$	−0.2847	$(H':ss)$	0.5451	$(O:oh')$	0.2353
$(y'y_mh')$	0.3561	$(H':sz')$	0.1824	$(O:sh')$	0.3924
$(h'To)$	0.0045	$(H':z'z')$	0.6279	$(O'z'h')$	0.2501

[34] J. A. Pople, J. Chem. Phys. **21**, 2234 (1953).

[35] One atomic unit (a.u.) of length equals one Bohr radius a_0 (0.5292 A); one a.u. of energy equals twice the ionization potential of the hydrogen atom, e^2/a_0 (27.204 ev).

[36] C. C. J. Roothaan, J. Chem. Phys. **19**, 1445 (1951).

TABLE IX. Two-electron two-center integrals over AO's involving oxygen AO's.

$(h'h':oo)$	0.5099	$(h'o:sz')$	0.0022
$(h'h':os)$	−0.00069	$(h'o:z'z')$	0.0643
$(h'h':oz')$	0.0112	$(h'o:y'y')$	0.0635
$(h'h':ss)$	0.4792	$(h's:oo)$	0.4005
$(h'h':sz')$	0.1078	$(h's:os)$	0.0038
$(h'h':z'z')$	0.5103	$(h's:oz')$	0.0062
$(h'h':y'y')$	0.4658	$(h'z:z'z')$	0.3525
$(h'o:h'o)$	0.00903	$(h's:ss)$	0.3425
$(h'o:h's)$	0.0261	$(h's:sz)$	0.0466
$(h'o:h'z')$	0.0202	$(h's:y'y')$	0.3400
$(h's:h's)$	0.1725	$(h'z':oo)$	0.2498
$(h's:h'z')$	0.1339	$(h'z':os)$	−0.0005
$(h'z':h'z')$	0.1331	$(h'z':oz')$	0.0154
$(h'y':h'y')$	0.02845	$(h'z':ss)$	0.2073
$(h'h':h'o)$	0.0318	$(h'z':sz')$	0.0939
$(h'h':h's)$	0.2789	$(h'z':z'z')$	0.2361
$(h'h':h'z)$	0.2599	$(h'z':y'y')$	0.2083
$(h'o:oo)$	0.1917	$(h'y':oy')$	0.0119
$(h'o:os)$	−0.0114	$(h'y':sy')$	0.0651
$(h'o:oz')$	0.0013	$(h'y':z'y')$	0.0104
$(h'o:ss)$	0.0632		

Values of all one- and two-center intervals not involving the 1*s* oxygen AO were checked with tables published by Kotani *et al.*[37]

In Table VII, the results are tabulated for all two-center integrals involving only the two 1*s* hydrogen AO's. These values depend, of course, upon the H−O−H bond angle. All were obtained using formulas published by Roothaan,[36] with the exception of $(h'h'':h'h'')$ and $(h'h':h'h'')$, which were determined using the tables of Hirschfelder and Linnett.[38]

All one-electron two-center integrals which involve oxygen AO's are listed in Table VIII, and the remaining two-center electronic repulsion integrals are given in Table IX. All integrals given in the latter two tables were evaluated using the convention that the positive z'-axis passes through the primed hydrogen (see Fig. 1). Two-center dipole moment integrals were easily evaluated in elliptical coordinates.[39] All other one-electron integrals, as well as all two-electron Coulomb repulsion integrals, were calculated using expressions listed by Roothaan.[36] Hybrid Coulomb-exchange integrals involving a spherical charge distribution were evaluated in elliptical coordinates, and the remaining hybrid integrals were computed using the method of Barnett and Coulson.[40] Exchange integrals not involving the 1*s* oxygen AO were secured by Lagrangian interpolation from the tables of Kotani.[37] The integral $(h'o:h'o)$ was calculated to five decimal place accuracy using Ruedenberg's method.[41] The two small exchange integrals $(h'o:h's)$ and $(h'o:h'z')$ were approximated.[42]

[37] M. Kotani and A. Amemiya, Proc. Phys.-Math. Soc. Japan **22**, extra number 1 (1938).
[38] J. O. Hirschfelder and J. W. Linnett, J. Chem. Phys. **18**, 130 (1950).
[39] Eyring, Walter, and Kimball, *Quantum Chemistry* (John Wiley and Sons, Inc., New York, 1944), p. 367.
[40] M. P. Barnett and C. A. Coulson, Phil. Trans. Roy. Soc. (London) **A243**, 221 (1951).

TABLE X. The series expansion of $(O:h'h'')$.

n	$T_n(0°)$	$T_n(105°)$
0	0.27715	0.27715
1	0.16114	−0.04171
2	0.05054	−0.02019
3	0.01465	0.00505
4	0.00572	0.00082
5	0.00145[a]	−0.00050
Total	0.51065[b]	0.22062

[a] By graphical extrapolation.
[b] Exact value: 0.51084.

APPENDIX III. EVALUATION OF THREE-CENTER INTEGRALS

Three of the more important three-center integrals were evaluated by exact methods. First, the nuclear attraction integral $(O:h'h'')$ was computed by utilizing the infinite series expansion of an AO on one center in terms of functions on a second center as described by Barnett and Coulson;[40] that is, the 1*s* hydrogen AO's were expanded about the oxygen nucleus, leading to the solution of $(O:h'h'')$ as an infinite series of one-center integrals:

$$(O:h'h'')=\sum_n T_n=(4\pi/R)\sum_n (2n+1)P_n(\cos\gamma) \times\int[p_n(1,r_0;R)]^2 dr_0. \quad (7)$$

The first six terms (T_n) of this series expansion are given in Table X for γ, the H′−O−H″ bond angle, equal to 0 and 105 degrees. The former case is equivalent to the two-center integral $(O:h'h')$ which has been evaluated previously in closed form by an independent method. It appears that the values thus obtained should be accurate to almost four significant figures.

The three-center integrals $(h'h'':s's')$ and $(h'h'':z'z')$ were evaluated by the Ruedenberg series expansion of the 1*s* hydrogen AO's in terms of a complete orthonormal set of oxygen AO's (see reference 42, footnote 17).

All other three-center integrals were carefully evaluated by approximate methods. Complete details and numerical results are given in reference 42.

[41] K. Ruedenberg, J. Chem. Phys. **19**, 1459 (1951).
[42] F. O. Ellison, J. Chem. Phys. **23**, 2358 (1955).

Molecular Calculations. II. Methods of Approximation of Molecular Integrals*

FRANK O. ELLISON†
Department of Chemistry and Institute for Atomic Research, Iowa State College, Ames, Iowa
(Received July 1, 1954)

A description is given of the integral approximations used in the LCAO MO self-consistent field treatment of H_2O reported in the preceding paper. The estimation of electronic repulsion integrals by replacing one of the electron charge distributions by a point charge is considered in detail and found to be reliable in certain general cases. A modification of the Sklar approximation is developed which is applicable to integrals involving $1s_a\chi_b$, in which $\mu(1s_a)$ (effective Z) is small and $\mu(\chi_b)$ is large. A method is described for securing a better "corrected" Mulliken approximation of exchange integrals. The estimation of unsymmetrical nuclear attraction integrals is carried out by using uniformly charged spheres of finite size to represent AO distributions. This method is compared with the Mulliken and Löwdin approximations.

I. INTRODUCTION

ONE of the basic problems arising in theoretical calculations dealing with molecular electronic structure is the evaluation of energy integrals involving AO's (atomic orbitals) associated with three or four different nuclear centers. It is well recognized that the neglect of such interactions can lead to very serious errors.[1–5] Therefore, it has been considered wise to include all many-center integrals even though rough approximations have had to be used in many cases. Although methods for the exact evaluation of some specific types of three- and four-center integrals have been published,[6] the actual computations tend to become extremely tedious. The comprehensive tabulation of auxiliary functions required in the more general treatments should increase their practicability.

Barker and Eyring[7] have recently pointed out the important usefulness of integral approximations in obtaining "best" values for various eigenfunction parameters. Also, they have recounted other problems in which approximate methods for evaluating integrals play a significant role. Probably the most common practice in previous molecular calculations has been to utilize quite arbitrarily a single approximation method for almost all of the integrals not computed exactly. The Mulliken,[8] the Sklar[9] and the point-charge approximations are most frequently encountered. This procedure has been quite satisfactory for the previous π electron studies in which the various any-center integrals are all quite similar. Even here, however, it has been shown[4] that care is required in choosing approximate values, since the Sklar method breaks down quite seriously for those cases in which the two charge centers approach coincidence. For the hetero-type integrals encountered in more complicated molecules, it is probable that a single method of approximation is not universally applicable. Although the general formulations have been qualitatively and theoretically[10] justified, it is necessary to reconsider the methods as applied to each individual case in order to obtain the best estimation of an integral.

This paper describes the integral approximations used in the LCAO MO self-consistent field treatment of H_2O reported in the preceding paper.[11] In the course of this work, some new methods have been evolved, and, on the basis of the experience thus gained, some qualitative criteria for the general selection and appraisal of approximations of certain types of integrals are suggested.

The notation used follows that employed in the preceding paper.[11] In this regard, Eqs. (1)–(2) defining the AO's, Fig. 1 giving the transformations relating p-orbitals, and Eqs. (7) of Appendix II defining the various integrals are especially pertinent. Atomic units of energy and length are utilized exclusively.[12]

Since H_2O was studied for various bond angles, the three-center integrals were also studied as a function of bond angle including the special cases of 0°, when these become two-center integrals, and 180°, when higher symmetry helps with the evaluation in some cases. All integrals were considered only for the O–H distance of $R=1.8103$ a.u.

* Contribution No. 407 from the Institute for Atomic Research and Department of Chemistry, Iowa State College, Ames, Iowa. This work was supported in part by the Ames Laboratory of the U. S. Atomic Energy Commission.

† Present Address: Department of Chemistry, Carnegie Institute of Technology, Pittsburgh, Pennsylvania.

[1] C. A. Coulson, Proc. Cambridge Phil. Soc. **31**, 244 (1935).

[2] R. G. Parr and B. L. Crawford, Jr., J. Chem. Phys. **16**, 526 (1948).

[3] C. C. J. Roothaan and R. G. Parr, J. Chem. Phys. **17**, 1001 (1949).

[4] H. Shull and F. O. Ellison, J. Chem. Phys. **19**, 1215 (1951).

[5] R. Taylor, Proc. Phys. Soc. (London) **A64**, 249 (1951).

[6] A. S. Coolidge, Phys. Rev. **42**, 189 (1932); Hirschfelder, Eyring, and Rosen, J. Chem. Phys. **4**, 121 (1936); C. A. Coulson, Proc. Cambridge Phil. Soc. **33**, 104 (1937); Hirschfelder, Diamond, and Eyring, J. Chem. Phys. **5**, 695 (1937); J. O. Hirschfelder and C. N. Weygandt, J. Chem. Phys. **6**, 806 (1938); S. O. Lundqvist P-O. Löwdin, Arkiv Fysik **3**, 147 (1951); R. S. Barker and H. Eyring, J. Chem. Phys. **21**, 912 (1953); **22**, 114 (1954).

[7] R. S. Barker and H. Eyring, **22**, 2072 (1954).

[8] R. S. Mulliken, J. chim. phys. **46**, 500, 521 (1949).

[9] A. L. Sklar, J. Chem. Phys. **7**, 990 (1939).

[10] K. S. Ruedenberg, J. Chem. Phys. **19**, 1433 (1951).

[11] F. O. Ellison and H. Shull, J. Chem. Phys. **23**, 2348 (1955).

[12] One atomic unit (a.u.) of energy equals twice the ionization potential of the hydrogen atom, 2×13.602 ev. One a.u. of length equals one Bohr radius, 0.5292 A.

II. POINT-CHARGE APPROXIMATION

The point-charge approximation may be regarded as the first approximation to the value of an interaction integral involving AO's. The method consists in replacing a charge distribution $\chi_a\chi_b$ by a point charge of magnitude $S(\chi_a\chi_b)$ such that the actual charge moment is obtained.[13] The extreme simplicity of the approximation should not be allowed to detract from its accuracy for certain types of integrals. On the other hand, it is probably obvious that rather serious errors can arise through indiscriminate application of the method.

The attraction of a nucleus A for a charge distribution $\chi_b\chi_c$, the center of gravity of which is located at a point P, may be estimated as follows:

$$(A:\chi_b\chi_c)\approx S(\chi_b\chi_c)/R_{AP}. \quad (1)$$

This formulation is found to be quite valid if $\chi_b\chi_c$ is point-like and if R_{AP} is large enough so that A is sufficiently outside of the main portion of $\chi_b\chi_c$. Only one of the three-center nuclear attraction integrals encountered in the H_2O problem had these characteristics, namely, $(H'':oh')$. All other nuclear attraction integrals of the type $(H'':\chi_0h')$, where χ_0 is a $2s$ or $2p$ oxygen AO, were estimated primarily by the uniformly charged sphere approximation described in section V of this paper.

Approximation of $(H'':h'o)$.—The $1s$ oxygen AO has an effective Z equal to 7.7. The electronic charge distribution formed by combining it with the relatively diffuse $1s$ hydrogen AO will be necessarily quite "concentrated" about the oxygen nucleus, i.e., point-like. It is reasonable, therefore, to replace $h'o$ by a point charge of magnitude $S(h'o)$ at its center of gravity. The latter is located at a distance $R_0=0.066$ a.u. from the oxygen nucleus.[14]

The results of this method are given in Table I. Additional discussion concerning the $h'o$ distribution is given in Sec. III in relation to a modified Sklar approximation.

Three- and four-center two-electron repulsion integrals may be reduced in an approximate manner to nuclear attraction integrals by replacing one of the electronic charge distributions by a suitable point charge:

$$(\chi_a\chi_b:\chi_c\chi_d)\approx S(\chi_a\chi_b)(P:\chi_c\chi_d). \quad (2)$$

This procedure is probably superior to replacing both charge distributions by point charges. The use of Eq. (2) presupposes, of course, that the three-center nuclear attraction integral $(P:\chi_c\chi_d)$ has been determined exactly or at least reliably estimated.

The criteria for ascertaining the validity of Eq. (2) are somewhat more extensive than those cited above for the point-charge approximation of a nuclear attraction integral. The method should be quite accurate if $\chi_a\chi_b$ is quite point-like and if P is sufficiently removed from $\chi_c\chi_d$. For more detailed consideration, it is convenient to consider separately two different cases.

TABLE I. Approximate values of integrals occurring in the H_2O calculations.

Integral[a]	H−O−H bond angle (degrees) 90	100	105	110	120	180
$(H'':h'o)$	0.0337	0.0334	0.0333	0.0332	0.0330	0.0325
$(h'h'':ss)$	0.2381	0.2180	0.2098	0.2022	0.1894	0.1530
$(h'h'':zz)$	0.241	0.221	0.211	0.203	0.190	0.150
$(h'h'':yy)$	0.239	0.219	0.211	0.204	0.192	0.158
$(h'h'':xx)$	0.230	0.211	0.203	0.195	0.183	0.150
$(h'h'':oz)$	0.0030	0.0025	0.0022	0.0020	0.0015	0
$(h'h'':sz)$	0.0275	0.0220	0.0195	0.0175	0.0135	0
$(h''h'':h'o)$	0.0315	0.0314	0.0314	0.0313	0.0313	0.0312
$(h''h'':h's)$	0.2225	0.2132	0.2101	0.2073	0.2028	0.1910
$(h''h'':h'z)$	0.1600	0.1460	0.1400	0.1320	0.1160	0
$(h''h'':h'y)$	0.0550	0.0650	0.0700	0.0740	0.0810	0.1110
$(h'h'':h'o)$	0.0155	0.0141	0.0135	0.0129	0.0119	0.0095
$(h'h'':h's)$	0.1292	0.1175	0.1123	0.1075	0.0992	0.0796
$(h'h'':h'z)$	0.0625	0.0517	0.0467	0.0422	0.0339	0
$(h'h'':h'y)$	0.0625	0.0616	0.0609	0.0602	0.0587	0.0544
$(h''o:h's)$	0.0252	0.0251	0.0250	0.0249	0.0248	0.0243
$(h''s:h'z)$	0.0841	0.0754	0.0711	0.0666	0.0577	0
$(h''s:h'y)$	0.0679	0.0727	0.0750	0.0771	0.0810	0.0927
$(h''z:h'y)$	0.0323	0.0315	0.0307	0.0298	0.0272	0
$(H'':h's)$	0.243	0.234	0.229	0.224	0.217	0.193
$(H'':h'z)$	0.1873	0.1683	0.1581	0.1497	0.1319	0
$(H'':h'y)$	0.0533	0.0622	0.0670	0.0705	0.0780	0.1065
$(h''o:h'z)$	0.0133	0.0115	0.0106	0.0096	0.0078	0
$(h''o:h'y)$	0.0086	0.0093	0.0097	0.0099	0.0103	0.0101
$(h''s:h's)$	0.1509	0.1489	0.1468	0.1458	0.1437	0.1292
$(h''z:h'z)$	0.074	0.065	0.062	0.058	0.051	0.010
$(h''y:h'y)$	−0.005	−0.011	−0.014	−0.016	−0.022	−0.038
$(h''x:h'x)$	0.019	0.018	0.018	0.017	0.016	0.010

[a] Listed in order of their discussion in the text.

A. Three-Center Hybrid Integrals

The point-charge approximation of a three-center hybrid repulsion integral may be formulated

$$(\chi_a\chi_a:\chi_b\chi_c)\approx(A:\chi_b\chi_c). \quad (3)$$

If $\chi_a\chi_a$ is, in particular, ns_ans_a (nodeless Slater AO's), the exact expression corresponding to this approximation may be written[15]

$$(ns_ans_a:\chi_b\chi_c)=(A:\chi_b\chi_c)-\pi\mu^{-3}\{(A:1s_a1s_a\chi_b\chi_c)+\mu n^{-1}\sum_{k=1}^{2n-1}(2n-k)[(2k)!]^{\frac{1}{2}}2^{-\frac{1}{2}}(k!)^{-1}\times S(1s_aks_a\chi_b\chi_c)\},^{16} \quad (4)$$

where μ is the effective charge (Z/n) in ns_a. For $n=1$, Eq. (4) becomes

$$(1s_a1s_a:\chi_b\chi_c)=(A:\chi_b\chi_c)-\pi\mu^{-3}\{(A:1s_a1s_a\chi_b\chi_c)+\mu S(1s_a1s_a\chi_b\chi_c)\}. \quad (5)$$

[13] J. F. Mulligan, J. Chem. Phys. **19**, 347 (1951), considered the best location of the point charge as being at the maximum of $\chi_a\chi_b$ measured along the internuclear axis A–B. This point corresponds closely to the charge moment result in the cases considered here.

[14] R_0 might also have been determined by the approximation of the two-center integral $(H':h'o)=0.03501\approx S(h'o)/(R-R_0)$, where R is the $O-H'$ distance. This gives $R_0=0.068$ a.u. This agreement with the above result is good evidence for the validity of the point-charge approximation of $(H'':h'o)$.

The maximum of the $h'o$ distribution measured along O−H′ is at the oxygen nucleus.

[15] In general, the potential expression for a one-center charge distribution can be shown to be equivalent to a classical pole, dipole, etc., potential decreased by an exponential factor. For large distances (i.e., small overlap of $\chi_a\chi_a$ with $\chi_b\chi_c$), the latter term may be neglected, as Mulligan[13] has done in developing his asymptotic approximation for two-center Coulomb integrals. Thus, Eq. (3) is actually an asymptotic approximation for $\chi_a\chi_a \equiv ns_ans_a$, but if p-orbitals are involved, appropriate classical multipole terms would have to be included.

[16] The latter two types of integrals are analogous to the ordinary one-electron nuclear attraction and overlap integrals; e.g., $(A:1s_a1s_a\chi_b\chi_c)=\int(1/r_{a1})1s_a(1)1s_a(1)\chi_b(1)\chi_c(1)dv(1)$.

It is quite obvious that the absolute difference between Eqs. (3) and (4) decreases as the overlap $S(\chi_a\chi_a\chi_b\chi_c)$ decreases; that is, as the angle A–B–C increases. Usually, the inequality $(ns_an s_a:\chi_b\chi_c)\leqslant(A:\chi_b\chi_c)$ is preserved, although exceptions may be shown to exist. It appears that the approximation given in Eq. (3) increases in accuracy as μ increases, that is, as $\chi_a\chi_a$ becomes more point-like.

In Table II, the point-charge estimations of two three-center hybrid integrals occurring in the H_2O calculations are compared with exact values. These integrals, $(h'h'':s's')$ and $(h'h'':z'z')$, were evaluated by the Ruedenberg expansion method, in which the hydrogen functions are expanded in terms of a complete orthogonal set of oxygen AO's.[10,17] Since the series was not carried to complete convergence, the values obtained for these integrals are accurate only to two, or possibly three significant figures. The exact values for $(O:h'h'')$ listed in the third line of Table II represent the point-charge approximation of either $(h'h'':s's')$ or $(h'h'':z'z')$. The remarkable accuracy of this approximation is rather unexpected, since $\chi_0\chi_0$ is not particularly point-like ($\mu=2.275$ for $2s$ and $2p$ oxygen AO's). On the other hand, the charge distribution $h'h''$ is quite diffuse for large H′−O−H″ bond angles, causing $S(h'h''\chi_0\chi_0)$ to become quite small. Therefore, $\chi_0\chi_0$ probably appears almost like a point-charge to the $h'h''$ cloud.

The results of two other methods for approximating $(h'h'':\chi_0\chi_0)$-type integrals are also given in Table II for the case of $(h'h'':s's')$. The first method assumes that the error of the Mulliken approximation of $(O:h'h'')$ should indicate the magnitude of error to be expected in the analogous approximations of integrals of the type $(h'h'':\chi_0\chi_0)$ (see Sec. IV). In Table II, the "corrected" approximation of $(h'h'':s's')$ secured in this manner may be compared with the results obtained by the Ruedenberg expansion method. The second method assumes that the variation of $(h'h'':\chi_0\chi_0)$ with bond angle is proportional to the variation of $S(h'h'')$ with bond angle; i.e.,

$$(h'h'':\chi_0\chi_0)\approx aS(h'h'')+b. \tag{6}$$

The parameters a and b are determined from the exact result at 0° and an assumed value at 180°. The latter may be secured by the point-charge method, for example, which should be quite reliable at 180°.

TABLE II. Comparisons of various approximations of $(h'h'':\chi_0\chi_0)$.

Integral	H−O−H bond angle (degrees) 90	100	105	110	120	180
$(h'h'':z'z')$[a]	0.2419	0.2211	0.2125	0.2049	0.1923	0.1577
$(h'h'':s's')$[a]	0.2389	0.2189	0.2104	0.2027	0.1897	0.1532
$(O:h'h'')$[b]	0.2540	0.2310	0.2207	0.2113	0.1949	0.1564
$(h'h'':s's')$[c]	0.240	0.218	0.207	0.199	0.184	0.147
$(h'h'':s's')$[d]	0.241	0.220	0.211	0.202	0.188	0.153

[a] Computed by the Ruedenberg expansion method; references 10 and 17.
[b] Exact values from reference 11; $(O:h'h'')$ represents the point-charge approximation of $(h'h'':\chi_0\chi_0)$-type integrals.
[c] Corrected Mulliken approximation obtained by assuming same percent error as for analogous approximation of $(O:h'h'')$.
[d] Values determined by Eq. (6) utilizing exact value at 0° (0.4806) and assumed value of 0.153 at 180°.

[17] This work was done as part of a quantitative investigation of the general method being undertaken as a joint program with Dr. Klaus Ruedenberg and Dr. H. Shull. The detailed results are to be published.

Approximations of $(h'h'':\chi_0\chi_0)$.—The straight point-charge approximation was used for $(h'h'':oo)$. The error for a 0° bond angle is 0.17%. In Table I, the final values for the integrals $(h'h'':ss)$, $(h'h'':zz)$, $(h'h'':yy)$ and $(h'h'':xx)$ are listed. These were determined by utilizing the results of the Ruedenberg method, the point-charge approximation and the corrected Mulliken approximation in order to secure a logical order in the values at 180°.

Since the $1s$ oxygen AO has a Z-value of 7.7, the charge distribution formed by combining it with any other oxygen AO will strongly resemble and thus be suitably represented by a point-charge. The integral involving the nodeless $2s$ oxygen AO is thus given by

$$(h'h'':os')\approx S(os')(O:h'h''), \tag{7}$$

while that involving the orthogonalized $2s$ function may be shown to be identically equal to zero in this approximation for all bond angles. The exact value of $(h'h':os)$ is −0.0007 a.u.

The integrals $(h'h'':oz)$ and $(h'h'':sz)$ vanish on account of symmetry at 180°. The exact values at 0° are 0.0112 and 0.1075, respectively. For intermediate bond angles, these integrals are therefore relatively small. The approximate results listed in Table I were secured by intuitively determining the variation between the above limits. It may be shown that these values correspond very closely to those which would be obtained using Eq. (6), which is undoubtedly quite applicable to these integrals.

Approximations of $(h''h'':h'\chi_0)$.—The point-charge approximation of $(h''h'':h'o)$ takes the form

$$(h''h'':h'o)\approx S(h'o)(P:h''h''), \tag{8}$$

where P is located at the center of gravity of $h'o$. This gives the values 0.0320 and 0.0303 a.u. for 0° and 180°, respectively. The exact result for the former is 0.0318. Slightly different values (Table I) were actually used in the H_2O calculations.

The Mulliken approximation (Sec. IV) of $(h''h'':h's')$ is in only 1.8% error for the zero-degree bond angle. At 180°, the value 0.1918 a.u. is obtained, which is in remarkable agreement with the point-charge result

$$(h''h'':h's')\approx S(h's')(P:h''h'')=0.193, \tag{9}$$

where P is located at the center of gravity of $h's'$. The Mulliken values, slightly revised, are given in Table I.

The Mulliken approximation of $(h''h'':h'z)$ and $(h''h'':h'y)$ gave very poor results. Instead, the point-charge method, using the values of $(H'':h'z)$ and $(H'':h'y)$ given in Table I, was applied. Inspection of Eq. (5) as applied to these integrals shows that $(H'':h'z)\geqslant(h''h'':h'z)$ and $(H'':h'y)\leqslant(h''h'':h'y)$.[18] The final values, given in Table I, were obtained by assuming that these inequalities become less pronounced as the bond angle increases.

The failure of the Mulliken approximation for integrals involving exchange distributions of the type $(ns)_a(n'p)_b$ is explained as follows. The Mulliken representation of $h'z'$,

$$h'z'\approx\tfrac{1}{2}S(h'z')(z'z'+h'h'), \tag{10}$$

is everywhere positive and thus contains less absolute charge than the actual distribution, which is partly negative. The amount of charge on H′ is underestimated. Thus, the Mulliken approximation of $(h'h':h'z')$ turns out to be about 24% too low. On the other hand, the approximate value of 0.124 a.u. for the three-center integral $(h''h'':h'y)$ at the bond angle of 180° is probably high.

[18] The latter inequality holds since $S(h''h''h'y)$ and $(H'':h''h''h'y)$ may be shown to be less than or equal to zero, for all bond angles.

The latter is equivalent to $(h''h'':h'z')$ at this same angle. Equation (10) places too much positive charge between H'' and O, whereas $h'z'$ is actually negative in this region.

B. Three-Center Exchange Integrals

The point-charge method applied to this type of integral takes the form

$$(\chi_a\chi_b:\chi_b\chi_c)\approx S(\chi_a\chi_b)(P:\chi_b\chi_c). \quad (11)$$

That distribution which most resembles a point charge should naturally be thus replaced. The method probably is less applicable here unless one of the distributions is considerably more diffuse than the one which is replaced by a point charge.

In the H_2O calculations, integrals of the type $(h'h'':h'\chi_0)$ were approximated by this method. These interactions are generally quite small since both electrons are exchanged. The observations which were made in connection with the point-charge approximation of $(h'h'':\chi_0\chi_0)$ seem to indicate that the absolute error in the analogous approximation of $(h'h'':h'\chi_0)$, using Eq. (11), will decrease as the bond angle increases. Since the formulation as given in Eq. (11) would give rise to a three-center nuclear attraction integral which is rather difficult to compute, the approximation was modified to give

$$(h'h'':h'\chi_0)\approx S(h'\chi_0)(\mathrm{O}:h'h''), \quad (12)$$

where $(\mathrm{O}:h'h'')$ has been evaluated exactly.[11] Therefore, Eq. (12) will tend to give a result which is higher or lower than Eq. (11) depending upon the inequality $(\mathrm{O}:h'h'')\gtrless(P:h'h'')$. For a bond angle of 0°, the lower sign is applicable, while the upper sign applies at 180 degrees. For some intermediate angle Eq. (11) and (12) give identical answers.[19]

The integrals $(h'h'':h'o)$, $(h'h'':h's)$, $(h'h'':h'z)$, and $(h'h'':h'y)$ were approximated by this method. The results are given in Table I.

III. MODIFIED SKLAR APPROXIMATION

In general, exchange integrals involving different effective nuclear charges are relatively tedious to evaluate.[20,21] Sklar[9] has given a formula for their approximation in terms of exchange integrals containing AO's of equal effective nuclear charge, which are conveniently tabulated.[22] One theoretical justification of the method depends upon suitable replacement of two-center charge distributions by one-center distributions, giving rise to simple Coulombic interactions which are then manipulated to give the following approximation formula:

$$(1s_a1s_b':1s_a1s_b')\approx\tfrac{1}{2}[S(1s_a1s_b')]^2\{(1s_a1s_b:1s_a1s_b)/[S(1s_a1s_b)]^2+(1s_a'1s_b':1s_a'1s_b')/[S(1s_a'1s_b')]^2\}. \quad (13)$$

Mulligan[13] has given a modified version of Eq. (13) which uses a geometric mean instead of an arithmetic mean.

Sklar's approximation applied to $(h'o:h'o)$ gives the value 0.0014, while Mulligan's formula yields 0.0012 and Mulliken's approximation is 0.0060 a.u. In general, the Sklar method is likely to be in error if the charge centers approach or are actually in coincidence.[4] This is exactly the situation for any symmetrical two-center exchange integral. Conversely, it should be noted here that the Sklar method (or the point-charge approximation) is undoubtedly quite reliable for four-center integrals in which the charge clouds are quite distant from each other.

In order to secure better evidence for the numerical magnitude of $(h'o:h'o)$, a different method was developed which is particularly applicable to integrals of the type $(1s_a\chi_b:\chi_b'\chi_c)$ *in which* $\mu(1s_a)$ *is small and* $\mu(\chi_b)$ *is large.* Such interactions will arise in heteronuclear molecular calculations in which inner shells are considered explicitly. Since these integrals, even in the two-center case, are rather difficult to compute exactly and since many are quite small numerically, a good method for their approximation should be very useful. The method is described for the special case in which χ_b is an s-type AO.

The charge distribution $1s_ans_b$, in which $\mu(ns_b)\gg\mu(1s_a)$, can be shown to be well-represented by a one-center charge distribution in the following approximation:

$$1s_ans_b\approx S(1s_ans_b)1s_b'ns_b'/S(1s_b'ns_b'), \quad (14)$$

where $\mu(1s_b')=\mu(ns_b')=\frac{1}{2}\mu(ns_b)$. The mononuclear overlap integral is given by the single formula

$$S(1s_b'ns_b')=(n+1)![(2n)!2]^{-\frac{1}{2}}. \quad (15)$$

The formulation given in Eq. (14) strongly resembles a Sklar-type approximation. It is different in that the one-center distribution has been fitted to the actual two-center charge distribution by a suitable adjustment of the effective nuclear charge.[23]

Formula (14) applied to the integral $(h'o:h'o)$ yields the expression

$$(h'o:h'o)\approx[S(h'o)]^2(1s_b'1s_b':1s_b'1s_b')=[S(h'o)]^25\mu(1s_b')/8, \quad (16)$$

where $\mu(1s_b')=\frac{1}{2}\mu(o)=3.85$. The result is 0.00895 a.u., which is quite close to the exact value of 0.00903 computed by the method for two-center exchange integrals

[19] More recent studies utilizing the charged sphere method described in Sec. V also indicate that Eq. (12) gives high results for large bond angles.

[20] K. Ruedenberg, J. Chem. Phys. **19**, 1459 (1951).

[21] H. Preuss, Z. Naturforsch. **8a**, 270 (1953), has described an interesting approach for determining the upper and lower limits as well as an approximation method for exchange integrals involving AO's of different effective nuclear charge.

[22] J. O. Hirschfelder and J. W. Linnett, J. Chem. Phys. **18**, 130 (1950); R. G. Parr and B. L. Crawford, Jr., J. Chem. Phys. **16**, 1049 (1948); H. J. Kopineck, Z. Naturforsch. **5a**, 420 (1950).

[23] C. Vroelant, J. chim. phys. **49**, 141 (1952), has considered more general examples of fitting one-center distributions to two-center charge clouds.

TABLE III. Examples of the modified Sklar approximation.

Integral	$\mu(1s_b)$	R (a.u.)	Approximate (a.u.)	Exact (a.u.)
		LiH and BeH^+ integrals[a]		
$(h_a1s_b:h_a1s_b)$	2.69	2.64	0.0149	0.0158
$(h_a1s_b:h_a1s_b)$	2.69	3.02	0.0075	0.0077
$(h_a1s_b:h_a1s_b)$	2.69	3.40	0.0037	0.0037
$(h_a1s_b:h_a1s_b)$	3.69	2.48	0.0106	0.0106
		H_2O integrals[b]		
$(ho:oo)$	7.7	1.8103	0.1913	0.1917
$(ho:ss)$	7.7	1.8103	0.0664	0.0649
$(O:ho)$	7.7	1.8103	0.2348	0.2353
$(H:ho)$	7.7	1.8103	0.0337	0.0350

[a] Exact values obtained from tables by I. Fischer, Arkiv. Fysik **5**, 349 (1952).
[b] Exact values from reference 11.

given by Ruedenberg.[20] An even better approximation would undoubtedly be found by approximating only one of the $h'o$ distributions using Eq. (14), giving a two-center hybrid integral. Some other numerical examples of this modified Sklar approximation are given in Table III.

This method was used also in approximating $(h'o:h''s)$ (see Sec. IV) and $(h'o:h''z)$ (see Sec. V).

Approximation of $(h'o:h''o)$.—It is seen from Table III that the modified approximation tends to give results which are too low. For *three-center* integrals of the type $(1s_an s_b:1s_cns_b)$, such as $(h'o:h''o)$, the method is independent of the angle A–B–C since the distributions are replaced by s-type functions on the center B. The formulation given in Eq. (14) has essentially taken some charge from the region between the nuclei and placed it on the backside of B. The result might be considered to be a distribution which is averaged over all bond angles, and the approximate values thus obtained should be most valid for some angle near 90°.[24]

The exact value of $(h'o:h''o)$ for a 0° bond angle is 0.00903 and the modified Sklar value of 0.00895 was assumed for 90°. Values for other angles were secured by linear extrapolation with angle.

IV. MULLIKEN APPROXIMATION

This method[8] is probably one of the most widely used formulations for obtaining approximate values of many-center integrals as well as of two-center interactions. According to this approximation, a charge distribution consisting of identical AO functions situated on two different centers may be written

$$\chi_a(1)\chi_b(1)\approx\tfrac{1}{2}S(\chi_a\chi_b)\times[\chi_a(1)\chi_a(1)+\chi_b(1)\chi_b(1)].^{25,26} \quad (17)$$

The formulation given in Eq. (17) also has been used quite often for distributions made up of different types of AO's. Löwdin[27] has proposed an extension of the Mulliken formula which is specifically designed for unsymmetrical charge distributions. This method consists in letting

$$\chi_{a\alpha}(1)\chi_{b\beta}(1)\approx\lambda_a\chi_{a\alpha}(1)\chi_{a\alpha}(1)+\lambda_b\chi_{b\beta}(1)\chi_{b\beta}(1), \quad (18)$$

where the second subscript is used to denote the type of AO as well as its effective nuclear charge. The parameters λ_a and λ_b are chosen so that the approximation yields the correct total charge and charge moment. An application of this method is described in Sec. V of this paper.

In many cases, the Mulliken approximation of an unsymmetrical charge distribution, as well as the Löwdin modification thereof, will obviously differ quite considerably from the actual distribution. A notable example was that given in Eq. (10).

Consider the ordinary Mulliken approximations of the three electronic repulsion integrals $(\chi_{a\alpha}\chi_{b\beta}:\chi_{a\alpha}\chi_{b\beta})$, $(\chi_{a\alpha}\chi_{b\beta}:\chi_{a\gamma}\chi_{b\delta})$, and $(\chi_{a\gamma}\chi_{b\delta}:\chi_{a\gamma}\chi_{b\delta})$, utilizing Eq. (17). The validity of the approximate representations of $\chi_{a\alpha}\chi_{b\beta}$ and $\chi_{a\gamma}\chi_{b\delta}$ is reflected to a certain extent by the accuracy of the Mulliken approximations of the first and third integrals, respectively. The accuracy of the approximation of the second integral might be expected to be intermediate between the accuracies of the first and third integrals.

Let E_1, E_2, and E_3 be the *percent* errors of the Mulliken approximations of the three integrals listed above. It can be shown that if E_1 and E_3 are either both positive or both negative, then $E_2\approx(E_1E_3)^{\frac{1}{2}}$ and E_2 should be of the same sign as E_1 and E_3. If E_1 and E_3 are of different sign, then $E_2\approx\frac{1}{2}(E_1+E_3)$. In this way, if the exact values for the first and third integrals are known, a corrected Mulliken approximation for the second may be written

$$(\chi_{a\alpha}\chi_{b\beta}:\chi_{a\gamma}\chi_{b\delta})\approx M_2/(1+0.01E_2), \quad (19)$$

where M_2 is the ordinary Mulliken approximation of the integral, and E_2 is appropriately approximated as described above.

This modification of the Mulliken approximation is valuable since two-center exchange integrals are usually quite tedious to compute. The extension to three- and four-center integrals should also lend itself to reducing substantially the labor of these calculations.

A rather extensive test of this method has been carried out, the results of which are listed in Table IV. The exact values of the hydride exchange integrals $(h2s:h2s)$, $(h2s:h2p\sigma)$ and $(h2p\sigma:h2p\sigma)$, as well as of the Coulomb and overlap integrals necessary for their Mulliken approximations, were obtained from tables given by Kotani and Amemiya.[28]

[24] It is interesting to note that the point-charge approximation of $(H'':h'o)$ for a bond angle of 90° (Table I), 0.0337 a.u., is exactly equal to the modified Sklar approximation (Table III). This value is probably quite accurate for this bond angle.

[25] K. Ruedenberg[10] has shown that this formulation may be derived rigorously as the first term of an infinite series expansion of the distribution $\chi_a(1)\chi_b(1)$.

[26] This approximation is, indeed, quite accurate for electronic repulsion integrals involving only 1s AO's. Application to 19 two-, three-, and four-center integrals over 1s hydrogen functions, the exact values of which have been given by R. Taylor,[5] gives an average error of about 5.7%. The Sklar approximation, on the other hand, is in 11% error on the average. If one takes the lower value as given by the two methods for each integral,[4] the average error is only 3.8%.

[27] P-O. Löwdin, J. Chem. Phys. **21**, 374 (1953).

[28] M. Kotani and A. Amemiya, Proc. Phys.-Math. Soc. Japan **22**, (1938), extra No. 1.

For the H_2O calculations, the corrected Mulliken method was utilized in securing integral approximations of $(h''o:h's)$, $(h''s:h'z)$, $(h''s:h'y)$, and $(h''z:h'y)$. The results are listed in Table I.

V. UNIFORMLY CHARGED SPHERE APPROXIMATION

A method for estimating electronic repulsion integrals over LCAO MO's involving Slater $2p\pi$ AO's has been described by R. G. Parr.[29] This treatment includes an approximation in which the atomic charge distributions are replaced by uniformly charged spheres of finite size.[30] This approximation has been extended in the present calculations to enable the estimation of a variety of integrals involving AO's.

A. Nuclear-Attraction Integrals

This approximation has been found very useful for estimating three-center attraction integrals. In Sec. II, it was noted that only $(H'':h'o)$ could be suitably approximated by the point-charge method. The estimation of the remaining integrals, $(H'':h's)$, $(H'':h'z)$ and $(H'':h'y)$, depends upon securing good representations for the charge distribution $h'\chi_0$. The Mulliken and Sklar methods are certainly not particularly applicable to the latter two integrals.

Approximation of $(H'':h's)$.—This interaction provides one of the simplest examples of the charged sphere method as used in the present calculations. The $h's'$ charge distribution is replaced by a uniformly charged sphere of radius R_1 determined by the approximation

$$(h's':h's')=0.1748\approx 6Q_1^2/(5R_1),^{31} \qquad (20)$$

where Q_1 is the total charge of $h's'$, i.e., $S(h's')$. R_1 is thus determined to be 1.777 a.u. The sphere is placed so that its center is $R_0=0.7782$ a.u. from O towards H′ (the center of gravity of $h's'$). One may test the approximation by determining the two-center integral $(H':h's')$:

$$(H':h's')\approx Q_1[3R_1^2-(R-R_0)^2]/(2R_1^3).^{32} \qquad (21)$$

This formula gives the value 0.381 a.u., whereas the exact is 0.386. The approximation of $(O:h's')$ provides a more extreme test since O is nearer to the center of gravity:

$$(O:h's')=0.437\approx Q_1(3R_1^2-R_0^2)/(2R_1^3)=0.402. \qquad (22)$$

For $(H'':h's')$ at larger bond angles, the method might be expected to be more accurate since the distance between H″ and the center of the sphere increases. For very large distances, the charged sphere result becomes equal to the point-charge value, both converging to the exact for very large distances.

One may also apply the Mulliken approximation as well as the Löwdin modification[27] thereof to this integral. The latter formulation may be written,

$$(H'':h's')=\lambda_a(H'':s's')+\lambda_b(H'':h'h'). \qquad (23)$$

The parameters $\lambda_a=0.290$ and $\lambda_b=0.219$ have been determined by fixing the total overlap and center of gravity of $\lambda_a s's'+\lambda_b h'h'$ so as to correspond to those of $h's'$. For the Mulliken method, $\lambda_a=\lambda_b=\frac{1}{2}S(h's')$.

The approximated results of $(H'':h's')$ for a 180° bond angle, $(H':h's')$ and $(O:h's')$ as obtained by the Mulliken, Löwdin and charged sphere methods are given in Table V. In Fig. 1, the magnitude of the $h's'$ charge distribution along the linear H″−O−H′ axis has been plotted exactly as well as according to the three approximations. It may be seen that the Mulliken and Löwdin methods are bound to yield high results for the 180° bond angle, since they place too much charge between H″ and O.

Since the curves in Fig. 1 merely give the electronic densities along the axis H″−O−H′, they are probably not the best representations of the over-all accuracies of the approximations. A better curve which gives some indication of the three-dimensional representation would be a plot of the total charge contained in slices of thickness Δz perpendicular to the z-axis (H″−O−H′). This is shown in Fig. 1 for the charged sphere repre-

TABLE IV. Examples of the corrected Mulliken approximation of $(h2s:h2p\sigma)$.

R a.u.	μ $(Z/2)$	Ordinary Mulliken approximation	Corrected Mulliken approximation	Exact value
1.0	3.0	0.141	0.196	0.186
	4.0	0.086	0.121	0.134
1.5	5/3	0.199	0.232	0.238
	7/3	0.141	0.180	0.177
	3.0	0.093	0.125	0.119
1.8103	2.275	0.108	0.135	0.135
2.0	1.0	0.171	0.195	0.200
	1.5	0.158	0.184	0.187
	2.0	0.110	0.135	0.135
2.5	0.6	0.093	0.113	0.114
	1.0	0.138	0.159	0.162
	1.4	0.112	0.131	0.132
3.0	2/3	0.095	0.113	0.114
	1.0	0.101	0.117	0.118

TABLE V. Approximations involving the $h's'$ distribution.

Method	$(O:h's')$	Integral $(H':h's')$	$(H'':h's')$[a]
Exact	0.437	0.386	...
Charged sphere	0.402	0.381	0.197
Mulliken	0.420	0.394	0.209
Löwdin	0.442	0.377	0.219

[a] For bond angle of 180°.

[29] R. G. Parr, J. Chem. Phys. **20**, 1499 (1952).

[30] G. F. Neumark, Ph.D. thesis, Columbia University (1951), appears to have first utilized finite uniformly charged clouds for approximating 1s orbitals in H, He, and H_2.

[31] The energy of repulsion of two superposed uniformly charged spheres of equivalent radii R_1 and total charge Q_1 (in a.u.) (see Appendix).

[32] The energy of repulsion of a point charge H′ *inside* of a charged sphere at a distance $(R-R_0)$ from its center (see Appendix). R is the O−H distance.

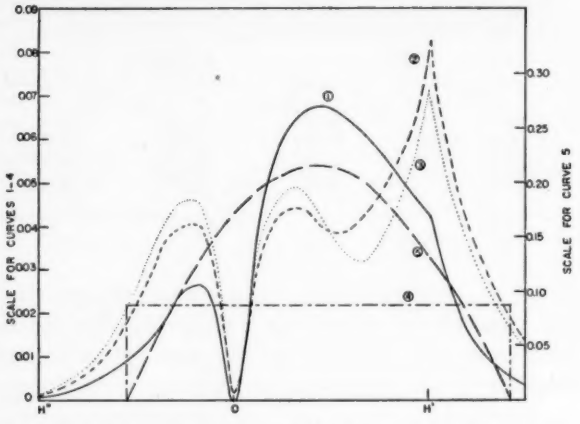

FIG. 1. (1) Exact function $h's'$ $(1s_h 2s_0)$ measured along linear H−O−H axis. (2) Mulliken approximation of (1). (3) Löwdin approximation of (1). (4) Uniformly charged sphere approximation of (1). (5) Total charge per unit length of axis in slices of the uniformly charged sphere perpendicular to the axis.

sentation.[33] The analogous curve for the exact function $h's'$ would involve rather complicated integration. Quite likely, however, it would resemble the curve for the charged sphere rather closely.

Approximation of $(H'':h'z)$ *and* $(H'':h'y)$.—The integral $(H'':h'z)$ was initially considered. The distribution $h'z'$ was replaced by a pair of tangent uniformly charged spheres of radii R_1 and R_2, and total charges $Q_1(<0)$ and $Q_2(>0)$, respectively. The following approximations were obtained by using suitable charged sphere formulas listed in the appendix:

$$(h'z':h'z')\approx 2Q_1Q_2/(R_1+R_2)+6Q_1^2/(5R_1)+6Q_2^2/(5R_2); \quad (24)$$

$$(H':h'z')\approx Q_2/(R_1-R_2)+Q_1/(R+R_1), \quad R_2<R/2; \quad (25)$$

$$(O:h'z')\approx Q_2/R_2+Q_1/R_1; \quad (26)$$

and

$$-S(h'z')=Q_1-Q_2. \quad (27)$$

For a bond angle of 180 degrees,

$$(H'':h'z')\approx Q_2/(R+R_2)+Q_1/(R-R_1), \quad R_1<R/2. \quad (28)$$

The right-hand sides of these five equations contain four unknowns: Q_1, Q_2, R_1, and R_2. If one takes R_1 and R_2 equal to the distances from O to the appropriate maxima of $h'z'$ measured along the internuclear axis (0.306 and 0.785 atomic units), then Eq. (27) and one of the first three equations may be used to determine Q_1 and Q_2. Approximations can then be obtained for the other three integrals. Table VI gives the results of these calculations.

TABLE VI. Charged sphere approximations involving the $h'z'$ distribution.

Integral	Exact value	Calculated approximate values 1	2	3	4
$(h'z':h'z')$	0.1331	(0.1331)	...	...	...
$(H':h'z')$	0.4114	0.369	0.388	(0.4114)	...
$(H'':h'z')$	...	0.117	0.107	0.092	0
$(O:h'z')$	0.2501	0.323	(0.2501)	0.15	...
$\|Q_1\|+Q_2$	...	0.469	0.540	0.642	1.30

[33] The uniform density D of charge in the whole sphere is given by $S(h's')\div(4/3)\pi R_1^3$. The total charge in a slice of thickness Δz perpendicular to the axis is thus given by $D\pi R_z^2\Delta z$, where R_z is the radius of the slice, and the total charge per unit length of axis in an infinitesimal slice at the point z is $D\pi R_z^2$.

It is seen that $(H'':h'z')$ is rather insensitive to the choice of equations used to determine the parameters. $|Q_1|+Q_2$ corresponds to the integrated *absolute* overlap between h' and z'; its value should be in the vicinity of 0.509, which is the overlap between h' and s'. It is seen that the value of zero given to $(H'':h'z')$ yields an absurd value for $|Q_1|+Q_2$.[34]

In order to approximate $(H'':h'z')$ for all bond angles, it was assumed that $|Q_1|+Q_2=0.509$, and Eqs. (25) and (26) were solved simultaneously for R_1 and R_2 giving 0.322 and 0.827 a.u., respectively. These values of the parameters should give good values for $(H'':h'z')$ for all angles.

The integral $(H'':h'y)$ vanishes on account of symmetry at 0° and is equivalent to $(H'':h'z')$ at 180° (~0.1065 a.u.). The first approximation for values at intermediate angles would be to assume that $(H'':h'y)$ is proportional to the net charge in $h'y$; i.e.,

$$(H'':h'y)\approx kS(h'y), \quad (29)$$

where k is determined by fixing the value at 180°. This method would undoubtedly give high results, since $(H'':h'y)$ decreases with decreasing bond angle not only because of the diminishing net charge in $h'y$ but also because the interaction gradually changes from $\sigma-\sigma$ (at 180°) to $\sigma-\pi$ (at 0°). The final values given in Table I were obtained by lowering the results (15% at 120°, 30% at 90°) of (41) to account for this latter effect.[35]

The integral $(H'':h'z)$ was obtained by utilizing the results of the above approximations of $(H'':h'z')$ and $(H'':h'y)$.

B. Electronic Repulsion Integrals

A number of electronic repulsion integrals were approximated by the uniformly charged sphere method. The procedure used in determining the parameters generally follows that used for the nuclear attraction integrals. Comparisons were made with other methods of approximation to insure reasonable results. The final values are given in Table I.

VI. SUMMARY

In general, good approximations of AO interaction integrals can be obtained only by securing good approximate representations of the actual charge distributions involved. The point-charge method may be regarded as the first approximation in this direction. It is applicable to only a very restricted class of nuclear attraction integrals. For two-electron interactions, the method appears to be quite reliable if only one of the charge distributions is approximated and if the overlap between distributions is small. This condition is fulfilled not only if the electrons are, on the average, far apart, but also if the distributions are close to each other and one is relatively more diffuse.

The uniformly charged sphere approximation may be considered to be the second approximation towards representing a general charge distribution. It is well suited to three-center nuclear attraction integrals.

Until better modifications of the Mulliken and Sklar approximations are developed, they should be relied upon only for interactions involving symmetrical charge distributions. Here, the best procedure is to

[34] Since H'' lies in the negative regions of $h'z'$, even the sign of the integral $(H'':h'z')$ was initially questionable.

[35] This correction has probably been overestimated. Formula (29) applies exactly to the two-center integrals $(H':h'y)$ and $(O:h'y)$. Comparison of these interactions with $(H'':h'y)$ offers little reason for the symmetry effect to be greater in the latter.

utilize the lower value as given by the two methods for each integral. In this paper, special methods have been developed for two specific types of integrals: (1) a modified Sklar approximation for integrals involving the charge distribution $(1s_a ns_b)$ where $\mu(1s_a) \ll \mu(ns_b)$ (especially applicable for heteronuclear calculations in which inner shells are considered explicitly); (2) a corrected Mulliken approximation for unsymmetrical exchange integrals.

ACKNOWLEDGMENT

The author is much indebted to Dr. H. Shull for many helpful discussions during the course of this work.

APPENDIX: UNIFORMLY CHARGED SPHERE REPULSION FORMULAS

The following equations were derived by standard integrations of the classical energy of repulsion between finite uniformly charged spheres.

(1) Repulsion of two intersecting spheres of different radii R_1 and R_2, the centers of which are at a distance R_0 apart:

$$V=[5(R_1^6+R_2^6)-R_0^6+30R_0R_1^2R_2^2(4R_1+4R_2-3R_0) -80R_2^3R_1^3-40R_0^3(R_1^3+R_2^3)-24R_0(R_1^5+R_2^5) -45R_0^2(R_1^4+R_2^4)-45R_1^2R_2^2(R_1^2+R_2^2) -15R_0^4(R_2^2+R_1^2)](160R_1^3R_2^3R_0). \quad (30)$$

This formula has been checked with a similar one given in reference 30.

(2) Special case of Eq. (30) for $R_1=R_2$:

$$V=6/(5R_1)-(80R_0^2R_1^3-30R_0^3R_1^2+R_0^5)/(160R_1^6). \quad (31)$$

(3) If $R_1<R_2$, and if the smaller sphere is contained entirely within the larger, the energy of repulsion is

$$V=[15R_2^2-3R_1^2-5R_0^2]/(10R_2^3). \quad (32)$$

The special cases of (4) $R_0=0$, $R_1<R_2$, (5) $R_0=0$, $R_1=R_2$, (6) $R_1=0$ (a point charge inside a sphere at a distance R_0 from its center), and (7) $R_1=0$, $R_0=0$, are easily derived from Eq. (32). The repulsion between two nonintersecting spheres or between a sphere and an exterior point charge is, of course, $1/R_0$.

THE JOURNAL OF CHEMICAL PHYSICS VOLUME 23, NUMBER 12 DECEMBER, 1955

Evaluation of Force Constants from Raman Effect Data. Part 1. Molecules and Radicals of the Type XY_4

K. VENKATESWARLU AND S. SUNDARAM
Annamalai University, Annamalainagar, India

(Received March 15, 1955)

The force constants of 8 radicals and 6 molecules of the type XY_4 belonging to the T_d symmetry have been calculated using Raman effect data by the Wilson's F–G matrix method. Applying Badger's and Gordy's empirical rules, the X–Y internuclear distances have been calculated and compared with the available observed data.

1. INTRODUCTION

THE most convenient method of obtaining the normal frequencies of a molecule is the one first introduced by Wilson[1] which makes use of the "symmetry coordinates." These symmetry coordinates must be such that they transform according to the characters of the vibration type concerned and also must be normalized and orthogonal. In this group-theoretical method, the elements of a matrix **F** related to the potential energy, and the elements of a matrix **G** related to the kinetic energy, are obtained. From these matrices, the equations giving the vibrational frequencies in terms of the force constants are deduced.

Though the Raman spectra of the molecules and radicals discussed in this paper have been studied by various authors,[2] it may be seen that no rigorous calculation of the force constants pertaining to these has has been made so far. The group-theoretical method of obtaining the force constants in these molecules and radicals is discussed below. The present values of the force constants in some cases are compared with those

TABLE I. Wave numbers σ in kaysers (K, cm^{-1}).

Radical	$\sigma_1(a_1)$	$\sigma_2(e)$	$\sigma_3(t_2)$	$\sigma_4(t_2)$
IO_4	795	280	840	340
SeO_4	833	335	875	432
CrO_4	858	485	875	510
SO_4	983	450	1105	611
PO_4	970	358	1080	500
MoO_4	936	220	895	365
SiO_4	800	500	1050	625
ClO_4	932	460	1110	626

TABLE II. Wave numbers in K.

Molecule	$\sigma_1(a_1)$	$\sigma_2(e)$	$\sigma_3(t_2)$	$\sigma_4(t_2)$
$TiCl_4$	385	120	496	144
$GeCl_4$	397	132	451	171
$GeBr_4$	234	78	328	111
$SnBr_4$	220	64	279	88
GeH_4	1990	833	2110	933
SiH_4	2180	970	2183	910

[1] E. B. Wilson, Jr., J. Chem. Phys. **7**, 1047 (1939); **9**, 76 (1941).

[2] Landolt-Börnstein, *Atom-Und Molekular Physik* (2 Teil, 1951 Edition).

TABLE III. Equations for the radicals.

IO_4	$f_d=5.969\times10^5$	$f_\alpha-2f_{\alpha\alpha}=0.2468\times10^5$	$1.005f_\alpha-0.3573f_{d\alpha}=0.295\times10^5$	$5.969\times10^5f_\alpha-2f_{d\alpha}^2=2.419\times10^{10}$
SeO_4	$f_d=6.551\times10^5$	$f_\alpha-2f_{\alpha\alpha}=0.3532\times10^5$	$1.159f_\alpha-0.575f_{d\alpha}=0.253\times10^5$	$6.551\times10^5f_\alpha-2f_{d\alpha}^2=3.518\times10^{10}$
CrO_4	$f_d=6.952\times10^5$	$f_\alpha-2f_{\alpha\alpha}=0.7403\times10^5$	$1.37f_\alpha-0.8728f_{d\alpha}=-0.045\times10^5$	$6.952\times10^5f_\alpha-2f_{d\alpha}^2=3.98\times10^{10}$
SO_4	$f_d=9.126\times10^5$	$f_\alpha-2f_{\alpha\alpha}=0.6374\times10^5$	$1.754f_\alpha-1.417f_{d\alpha}=-0.056\times10^5$	$9.126\times10^5f_\alpha-2f_{d\alpha}^2=5.663\times10^{10}$
PO_4	$f_d=8.886\times10^5$	$f_\alpha-2f_{\alpha\alpha}=0.4034\times10^5$	$1.789f_\alpha-1.464f_{d\alpha}=0.557\times10^5$	$8.886\times10^5f_\alpha-2f_{d\alpha}^2=4.236\times10^{10}$
MoO_4	$f_d=8.343\times10^5$	$f_\alpha-2f_{\alpha\alpha}=0.1523\times10^5$	$1.087f_\alpha-0.4733f_{d\alpha}=-0.478\times10^5$	$8.343\times10^5f_\alpha-2f_{d\alpha}^2=2.817\times10^{10}$
SiO_4	$f_d=6.043\times10^5$	$f_\alpha-2f_{\alpha\alpha}=0.787\times10^5$	$1.8964f_\alpha-1.617f_{d\alpha}=1.305\times10^5$	$6.043\times10^5f_\alpha-2f_{d\alpha}^2=5.851\times10^{10}$
ClO_4	$f_d=8.202\times10^5$	$f_\alpha-2f_{\alpha\alpha}=0.6662\times10^5$	$1.658f_\alpha-1.279f_{d\alpha}=0.828\times10^5$	$8.202\times10^5f_\alpha-2f_{d\alpha}^2=7.674\times10^{10}$

TABLE IV. Equations for the molecules.

$TiCl_4$	$f_d=3.101\times10^5$	$f_\alpha-2f_{\alpha\alpha}=0.1004\times10^5$	$1.01f_\alpha-0.9479f_{d\alpha}=-0.0985\times10^5$	$3.101\times10^5f_\alpha-2f_{d\alpha}^2=0.2819\times10^{10}$
$GeCl_4$	$f_d=3.297\times10^5$	$f_\alpha-2f_{\alpha\alpha}=0.1215\times10^5$	$0.7818f_\alpha-0.6253f_{d\alpha}=-0.0983\times10^5$	$3.297\times10^5f_\alpha-2f_{d\alpha}^2=0.4406\times10^{10}$
$GeBr_4$	$f_d=2.581\times10^5$	$f_\alpha-2f_{\alpha\alpha}=0.0956\times10^5$	$0.5929f_\alpha-0.6253f_{d\alpha}=-0.0538\times10^5$	$2.581\times10^5f_\alpha-2f_{d\alpha}^2=0.2724\times10^{10}$
$SnBr_4$	$f_d=2.281\times10^5$	$f_\alpha-2f_{\alpha\alpha}=0.06437\times10^5$	$0.4212f_\alpha-0.3824f_{d\alpha}=-0.0222\times10^5$	$2.281\times10^5f_\alpha-2f_{d\alpha}^2=0.1813\times10^{10}$
GeH_4	$f_d=2.355\times10^5$	$f_\alpha-2f_{\alpha\alpha}=0.1375\times10^5$	$12.39f_\alpha-0.6253f_{d\alpha}=4.58\times10^5$	$2.355\times10^5f_\alpha-2f_{d\alpha}^2=0.6492\times10^{10}$
SiH_4	$f_d=2.826\times10^5$	$f_\alpha-2f_{\alpha\alpha}=0.1865\times10^5$	$13.09f_\alpha-1.618f_{d\alpha}=2.18\times10^5$	$2.826\times10^5f_\alpha-2f_{d\alpha}^2=0.6101\times10^{10}$

given by Venkateswaran[3] who has obtained them by a different method. Applying the empirical rules of Badger[4] and Gordy,[5] expressing the force constants in terms of the atomic parameters like the internuclear distances and the electronegativities of the bonded atoms, the internuclear distances in these molecules and radicals are computed and compared with those obtained by other methods.

2. THEORETICAL CONSIDERATIONS

The molecules and radicals of the type XY_4 discussed in the present investigation have been proved to have the symmetry T_d. As such, it may be seen, from the relevant character table and applying the selection rules, that such a structure will give rise to 1 nondegenerate type a_1 vibration, 1 doubly degenerate type e vibration, and 2 triply degenerate type t_2 vibrations. All are allowed in the Raman spectrum. The relevant symmetry coordinates and other details have been elaborately worked out by Meister and Cleveland.[6] As the present aim is to calculate the force constants from the observed frequencies ascribed to these molecules and radicals and as there are only 4 distinct frequencies for each, only 4 force constants can be used in the expression for the potential energy. They are f_d (representing the force between the X and Y atoms), f_α (that associated with the bending), $f_{d\alpha}$ (representing that due to the interaction between bending and stretching), and $f_{\alpha\alpha}$ (that due to the interaction between bending and bending); d is the equilibrium bond distance and α is the interbond angle.

TABLE V. Force constants for the radicals.

Radical	$f_d\times10^{-5}$ dynes cm^{-1}	$f_{d\alpha}\times10^{-5}$ dynes cm^{-1}	$f_\alpha\times10^{-5}$ dynes cm^{-1}	$f_{\alpha\alpha}\times10^{-5}$ dynes cm^{-1}	d in A Badger	d in A Gordy	$f_d\times10^{-5}$
IO_4	5.969	0.3306	0.5662	0.1543	1.76	1.86	4.60
SeO_4	6.551	0.6879	0.6814	0.1641	1.64	1.76	4.22
CrO_4	6.952	1.213	0.9959	0.1278	1.62	...	4.82
SO_4	9.126	1.315	1.122	0.2443	1.49	1.46	4.57
PO_4	8.886	1.368	0.8974	0.247	1.49	1.36	5.23
MoO_4	8.343	1.388	0.8015	0.325	1.70	...	6.10
SiO_4	6.043	2.189	2.554	0.8835	1.57	1.60	...
		0.3876	1.018	0.1155			
ClO_4	8.202	2.425	2.37	0.852	1.51	1.48	...
		0.739	1.069	0.2014			

The F and G matrices corresponding to the T_d type of symmetry as worked out by Meister and Cleveland are given below:

(i) F matrix elements:

For type a_1 vibration,

$$F_{11}=f_d.$$

For type e vibration,

$$F_{11}=[d^2(f_\alpha-2f_{\alpha\alpha})]$$

and for type t_2 vibrations,

$$\begin{bmatrix}F_{11} & F_{12}\\ F_{21} & F_{22}\end{bmatrix}=\begin{bmatrix}d^2f_\alpha & \sqrt{2}df_{d\alpha}\\ \sqrt{2}df_{d\alpha} & f_d\end{bmatrix}.$$

(ii) G matrix elements:

For type a_1 vibration,

$$G_{11}=\mu_y.$$

For type e vibration,

$$G_{11}=3\mu_y/d^2$$

[3] C. S. Venkateswaran, Proc. Indian Acad. Sci. **3**, 25 (1936), **7**, 144 (1938).
[4] R. M. Badger, J. Chem. Phys. **2**, 128 (1934), **3**, 710 (1935).
[5] W. Gordy, J. Chem. Phys. **14**, 305 (1946).
[6] A. G. Meister and F. F. Cleveland, Am. J. Phys. **14**, 13 (1940).

TABLE VI. Force constants for the molecules.

Molecule	$f_d\times10^{-5}$ dynes cm^{-1}	$f_{d\alpha}\times10^{-5}$ dynes cm^{-1}	$f_\alpha\times10^{-5}$ dynes cm^{-1}	$f_{\alpha\alpha}\times10^{-5}$ dynes cm^{-1}	d in A Badger	d in A Gordy	d in A observed	$f_d\times10^{-5}$ Badger	$f_d\times10^{-5}$ Gordy
$TiCl_4$	3.101	1.214 or 0.2406	1.042 or 0.1282	0.4708 or 0.0139	2.099	2.102	2.210	2.16	2.847
$GeCl_4$	3.297	0.7415 or 0.5772	0.4674 or 0.3367	0.173 or 0.1071	2.084	2.091	2.08	3.297	3.322
$GeBr_4$	2.581	1.139 or 0.2225	1.109 or 0.1439	0.5065 or 0.0242	2.27	2.33	2.32	2.173	2.580
$SnBr_4$	2.281	0.8606 or 0.1752	0.7286 or 0.1064	0.3321 or 0.021	2.32	2.50	2.44	2.268	2.382
GeH_4	2.355	0.3634 or −0.3041	0.3879 or 0.3543	0.1252 or 0.1084	1.51	2.12			
SiH_4	2.826	0.1607	0.2342	0.0239	1.455	1.96			

and for type t_2 vibrations,

$$\begin{bmatrix} G_{11} & G_{12} \\ G_{21} & G_{22} \end{bmatrix} = \begin{bmatrix} \left(2\mu_y+\frac{16}{3}\mu_x\right)\Big/d^2 & -\frac{8\mu_x}{3d} \\ -\frac{8\mu_x}{3d} & \left(\mu_y+\frac{4}{3}\mu_x\right) \end{bmatrix}.$$

From the above matrices, the secular equations for the 3 types of vibration are:

for a_1 type,

$$\lambda_1=F_{11}G_{11}=f_d\mu_y=4\pi^2c^2\sigma_1^2,$$

for e type,

$$\lambda_2=F_{11}G_{11}=[d^2(f_\alpha-2f_{\alpha\alpha})]\frac{3\mu_y}{d^2}=4\pi^2c^2\sigma_2^2,$$

and for t_2 vibrations (in the expanded form) it is,

$$\lambda^2-\lambda[F_{11}G_{11}+2F_{12}G_{12}+F_{22}G_{22}] + \begin{vmatrix} F_{11} & F_{12} \\ F_{21} & F_{22} \end{vmatrix} \cdot \begin{vmatrix} G_{11} & G_{12} \\ G_{21} & G_{22} \end{vmatrix} = 0$$

$$\lambda^2-\lambda\left[f_\alpha\left(2\mu_y+\frac{16}{3}\mu_x\right)-\frac{16\sqrt{2}}{3}\mu_x f_{d\alpha}+f_d\left(\mu_y+\frac{4}{3}\mu_x\right)\right] + (f_d f_\alpha-2f_{d\alpha}^2)\left[\left(\mu_y+\frac{4}{3}\mu_x\right)\times\left(2\mu_y+\frac{16}{3}\mu_x\right)-\frac{64}{9}\mu_x^2\right]=0$$

where the roots are $\lambda_3=4\pi^2c^2\sigma_3^2$ and $\lambda_4=4\pi^2c^2\sigma_4^2$. Substituting the proper values of the wave numbers and masses in the above, the force constants for each radical or molecule may be obtained.

3. RESULTS

The wave numbers used[2] in the evaluation of the force constants are given in Tables I and II (Table I for radicals and Table II for molecules).

Equations involving the force constants of the various radicals, obtained from the secular equations, are given in Table III, and those of the molecules in Table IV.

The force constants of the various radicals are given in Table V, and Table VI gives the force constants for the molecules. In columns 6 and 7 of both the tables are given the values of the X–Y internuclear distances calculated from the values of f_d obtained in the present investigation using the empirical rules of Badger and Gordy, respectively. In column 8 of Table VI are given the available observed values of the internuclear distances for comparison. In the last column of Table V, the values of f_d obtained by Venkateswaran in some cases are given. The last two columns of Table VI contain the f_d values calculated from the observed d values using Badger's and Gordy's rules respectively.

It can be seen that there is good agreement between the d values calculated from the f_d values, obtained in this investigation using the empirical rules of Badger and Gordy, and the available d values. The agreement between the f_d values obtained by the present authors and the f_d values computed from observed d values using those empirical rules, is also satisfactory. While using Gordy's rule, the bond order for all these tetrahedral structures has been taken to be unity and this assumption can be seen to be fairly justifiable in all cases where observed data are available.

Evaluation of Force Constants from Raman Effect Data. Part 2. Molecules and Radicals of the Planar XY_3 Type

K. VENKATESWARLU AND S. SUNDARAM
Annamalai University, Annamalainagar, India
(Received March 15, 1955)

The force constants of 4 molecules and 5 radicals of the planar type XY_3 belonging to the point group D_{3h} have been calculated using Raman effect data by the Wilson's F–G matrix method. Applying the empirical rules of Badger and Gordy, the X–Y internuclear distances have been calculated.

INTRODUCTION

THE well-known group-theoretical method of Wilson[1] for the calculation of the normal frequencies of molecules and radicals has been employed here for the evaluation of the force constants. All the molecules and radicals discussed in this paper have been proved by electron diffraction and other experiments to have the planar symmetrical structure belonging to the point group D_{3h}. Such a structure will give rise to 1 nondegenerate a_1 type vibration and 2 doubly degenerate e type vibrations. By the usual method of obtaining the elements of the F and G matrices associated with the potential energy and kinetic energy, respectively, the following matrix elements are obtained. The force constants f_d, f_α, $f_{d\alpha}$, and $f_{\alpha\alpha}$ have their usual significance as in Part 1, and f_{dd} is the force constant between two Y atoms.

(i) F matrix elements:

For the a_1 type vibration,

$$F_{11}=f_d+2f_{dd}$$

and for the e type vibrations,

$$\begin{bmatrix} F_{11} & F_{12} \\ F_{21} & F_{22} \end{bmatrix}=\begin{bmatrix} (f_d-f_{dd}) & \frac{d}{2}f_{d\alpha} \\ \frac{d}{2}f_{d\alpha} & d^2(f_\alpha-f_{\alpha\alpha}) \end{bmatrix}.$$

TABLE I. Raman displacements in kaysers.

		$\sigma_1(a_1)$	$\sigma_2(e)$	$\sigma_3(e)$
Radicals	NO_3	1050	720	1390
	CO_3	1060	680	1415
	PO_3	946	425	1014
	SO_3	1068	653	1390
	BO_3	910	700	1445
Molecules	BCl_3	472	255	946
	BBr_3	279	151	806
	BF_3	888	480	1446
	$AlCl_3$	541	348	808

(ii) G matrix elements:

For the a_1 type vibration,

$$G_{11}=\mu_y$$

and for the e type vibrations,

$$\begin{bmatrix} G_{11} & G_{12} \\ G_{21} & G_{22} \end{bmatrix}=\begin{bmatrix} \left(\frac{3}{2}\mu_x+\mu_y\right) & -\frac{3\sqrt{3}}{4}\mu_x \\ -\frac{3\sqrt{3}}{4}\mu_x & \left(9\mu_x+\frac{7}{2}\mu_y\right) \end{bmatrix}.$$

From the above matrices, the secular equations are: For the a_1 type vibration,

$$\lambda_1=F_{11}G_{11}=(f_d+2f_{dd})\mu_y=4\pi^2c^2\sigma_1^2$$

and for the e type vibrations (in the expanded form) it is,

$$\lambda^2-\lambda[F_{11}G_{11}+2F_{12}G_{12}+F_{22}G_{22}]+\begin{vmatrix} F_{11} & F_{12} \\ F_{21} & F_{22} \end{vmatrix}\cdot\begin{vmatrix} G_{11} & G_{12} \\ G_{21} & G_{22} \end{vmatrix}=0$$

or

$$\lambda^2-\lambda\left[\left(\frac{3}{2}\mu_x+\mu_y\right)(f_d-f_{dd})-\frac{3\sqrt{3}}{4}d\mu_x f_{d\alpha}+d^2(f_\alpha-f_{\alpha\alpha})\left(9\mu_x+\frac{7}{2}\mu_y\right)\right]+d^2\left[(f_d-f_{dd})(f_\alpha-f_{\alpha\alpha})-\frac{1}{4}f_{d\alpha}^2\right]\times\left[\left(9\mu_x+\frac{7}{2}\mu_y\right)\left(\frac{3}{2}\mu_x+\mu_y\right)-\frac{27}{16}\mu_x^2\right]=0$$

where the roots are

$$\lambda_2=4\pi^2c^2\sigma_2^2 \quad \text{and} \quad \lambda_3=4\pi^2c^2\sigma_3^2.$$

RESULTS

Out of the 9 cases discussed in this paper, 4 are molecules and 5 are radicals. The observed Raman

[1] E. B. Wilson, Jr., J. Chem. Phys. **7**, 1047 (1939); **9**, 76 (1941).

TABLE II. Equations for the force constants.

NO_3	$f_d+2f_{dd}=10.41\times10^5$	$1.02(f_d-f_{dd})-0.5583df_{d\alpha}+5.18d^2(f_\alpha-f_{\alpha\alpha})=8.704\times10^5$	$d^2\left[(f_d-f_{dd})(f_\alpha-f_{\alpha\alpha})-\frac{f_{d\alpha}^2}{4}\right]=2.542\times10^{10}$
CO_3	$f_d+2f_{dd}=10.6\times10^5$	$1.129(f_d-f_{dd})-0.6516df_{d\alpha}+5.832d^2(f_\alpha-f_{\alpha\alpha})=8.754\times10^5$	$d^2\left[(f_d-f_{dd})(f_\alpha-f_{\alpha\alpha})-\frac{f_{d\alpha}^2}{4}\right]=1.896\times10^{10}$
PO_3	$f_d+2f_{dd}=8.447\times10^5$	$0.6672(f_d-f_{dd})-0.2521df_{d\alpha}+3.063d^2(f_\alpha-f_{\alpha\alpha})=4.292\times10^5$	$d^2\left[(f_d-f_{dd})(f_\alpha-f_{\alpha\alpha})-\frac{f_{d\alpha}^2}{4}\right]=1.184\times10^{10}$
SO_3	$f_d+2f_{dd}=10.72\times10^5$	$0.6579(f_d-f_{dd})-0.244df_{d\alpha}+3.007d^2(f_\alpha-f_{\alpha\alpha})=8.379\times10^5$	$d^2\left[(f_d-f_{dd})(f_\alpha-f_{\alpha\alpha})-\frac{f_{d\alpha}^2}{4}\right]=5.413\times10^{10}$
BO_3	$f_d+2f_{dd}=7.814\times10^5$	$1.211(f_d-f_{dd})-0.7227df_{d\alpha}+6.324d^2(f_\alpha-f_{\alpha\alpha})=9.158\times10^5$	$d^2\left[(f_d-f_{dd})(f_\alpha-f_{\alpha\alpha})-\frac{f_{d\alpha}^2}{4}\right]=1.809\times10^{10}$
BCl_3	$f_d+2f_{dd}=4.66\times10^5$	$1.004(f_d-f_{dd})-0.7227df_{d\alpha}+5.602d^2(f_\alpha-f_{\alpha\alpha})=3.41\times10^5$	$d^2\left[(f_d-f_{dd})(f_\alpha-f_{\alpha\alpha})-\frac{f_{d\alpha}^2}{4}\right]=0.1439\times10^{10}$
BBr_3	$f_d+2f_{dd}=3.669\times10^5$	$0.91(f_d-f_{dd})-0.7227df_{d\alpha}+5.271d^2(f_\alpha-f_{\alpha\alpha})=2.389\times10^5$	$d^2\left[(f_d-f_{dd})(f_\alpha-f_{\alpha\alpha})-\frac{f_{d\alpha}^2}{4}\right]=0.1529\times10^{10}$
BF_3	$f_d+2f_{dd}=8.841\times10^5$	$1.1514(f_d-f_{dd})-0.7227df_{d\alpha}+6.116d^2(f_\alpha-f_{\alpha\alpha})=8.245\times10^5$	$d^2\left[(f_d-f_{dd})(f_\alpha-f_{\alpha\alpha})-\frac{f_{d\alpha}^2}{4}\right]=0.9325\times10^{10}$
$AlCl_3$	$f_d+2f_{dd}=6.124\times10^5$	$0.5045(f_d-f_{dd})-0.29df_{d\alpha}+2.603d^2(f_\alpha-f_{\alpha\alpha})=2.749\times10^5$	$d^2\left[(f_d-f_{dd})(f_\alpha-f_{\alpha\alpha})-\frac{f_{d\alpha}^2}{4}\right]=0.8119\times10^{10}$

displacements were taken from *Atom-Und Molekular Physik* by Landolt-Börnstein (2 Teil, 1951 Edition) and are given in Table I.

In solving the secular equations and evaluation of the force constants, the following methods have been adopted in the present investigation. Where the internuclear distances are available from electron diffraction and other data, the values of f_d are computed using Badger's rule.[2] Knowing f_d and f_{dd} and eliminating $(f_\alpha-f_{\alpha\alpha})$ from the equations for the sum and the product of the roots of the secular equation, the quadratic in $f_{d\alpha}$ is solved, thus obtaining 2 values of $f_{d\alpha}$ and $(f_\alpha-f_{\alpha\alpha})$. Where the quadratic in $f_{d\alpha}$ has no real roots, neglecting $f_{d\alpha}$, a quadratic in (f_d-f_{dd}) is solved, thus yielding 2 sets of values for f_d, f_{dd}, and $(f_\alpha-f_{\alpha\alpha})$.

The equations involving the force constants as obtained from the secular equations for the various cases are given in Table II.

Table III gives the force constants obtained by solving the above equations. In column 6 are given the values of the internuclear distances calculated from the f_d values obtained in the present investigation and in column 7 are given the observed d values. In the case of the radicals BF_3, BCl_3, and BBr_3. Anderson, Lassettre, and Yost[3] have calculated the force constants by the normal coordinate method. Their values are not reproduced here but they are at variance from those obtained in the present investigation.

[2] R. M. Badger, J. Chem. Phys. **2**, 128 (1934); **3**, 710 (1935).
[3] Anderson, Lassettre, and Yost, J. Chem. Phys. **4**, 703 (1936).

TABLE III. Force constants.

	$f_d\times10^{-5}$ dynes cm^{-1}	$f_{dd}\times10^{-5}$ dynes cm^{-1}	$(f_\alpha-f_{\alpha\alpha})\times10^{-5}$ dynes cm^{-1}	$f_{d\alpha}\times10^{-5}$ dynes cm^{-1}	d in A Badger	d in A observed
NO_3	7.848	1.281	0.2335		1.299	1.290
	or	or	or		or	
	4.780	2.815	0.7762		1.410	
CO_3	7.641	1.475	0.1820		1.30	
	or	or	or		or	
	4.613	3.023	0.5916		1.42	
PO_3	6.438	1.004	0.0896		1.560	
	or	or	or		or	
	3.482	2.482	0.4099		1.700	
SO_3	10.47	0.1266	0.2561		1.467	1.450
	or	or	or		or	
	5.26	2.730	1.10		1.603	
BO_3	5.426	1.194	0.5204	2.239		1.38
			0.2659	−0.8368		
BCl_3	3.108	0.776	0.1436	1.071		1.73
			0.0357	−0.3755		
BBr_3	2.353	0.658	0.0968	0.6942		1.87
			0.0315	−0.1967		
BF_3	7.207	0.817	0.0864		1.269	1.30
	or	or	or		or	
	3.464	2.689	0.7117		1.433	
$AlCl_3$	5.057	0.5333	0.0516		1.865	
	or	or	or		or	
	2.659	1.732	0.2168		2.01	

The fact that the values of the internuclear X–Y distances, calculated with Badger's rule and the f_d values obtained after neglecting $f_{d\alpha}$, are in close agreement with the observed values justifies the assumption that $f_{d\alpha}$ is not of appreciable order of magnitude and may therefore be neglected as a first approximation.

Quantitative Comparison of the Approximate Dielectric Polarization Theories with an Exact One at Low Densities

A. D. BUCKINGHAM
Department of Theoretical Chemistry, University of Cambridge, Cambridge, England
(Received February 15, 1955)

The total dielectric polarization of a polar gas is expanded in inverse powers of the molar volume and the first term representing deviations from ideal gas behavior evaluated for an assembly of point polarizable dipoles, using the method developed by Buckingham and Pople. The approximate dielectric polarization equations of Debye, Onsager, Kirkwood, and Harris and Alder are expanded similarly and the corresponding coefficients of the term proportional to the first power of the density compared with the exact one. There is no term proportional to the density in the equations of Debye and of Onsager; also, to this order Kirkwood's and Harris' and Alder's theories are equivalent, both somewhat underestimating the total polarization. The use of Onsager's relationship for the dipole moment of a molecule is shown to be inappropriate for an imperfect gas.

1. INTRODUCTION

THE first successful theory relating the total dielectric polarization of a sample of material to the properties of the molecules comprising it, was that of Debye.[1] He assumed that the local field acting on a molecule was the Lorentz[2] field $\mathbf{E}+4\pi\mathbf{P}/3$, where $\mathbf{E}$ is the macroscopic field strength in the medium and $\mathbf{P}$ is the electric polarization at the point under consideration. That this field is inadequate in all cases, except that of a gas at a low pressure, has been realized for some time; it predicts electric Curie points for polar liquids and these are not found in practice.

A new approach to the problem was presented by Onsager,[3] who calculated the local field by assuming it to be the field in a cavity in a continuum whose dielectric constant is equal to the macroscopic value. He supposes that the local field is made up of two parts, the cavity field $\mathbf{G}$ and the reaction field $\mathbf{R}$. The cavity field is that part of the field existing in the cavity due to the applied electric field, and $\mathbf{R}$ is that part due to the material in the cavity polarizing the surroundings, this polarization in turn producing a field in the cavity. The field $\mathbf{R}$ has no tendency to orient the molecule. The contents of the Lorentz cavity have the macroscopic dielectric constant of the material, while in the Onsager cavity there is a single molecule of vapor moment μ_0 and polarizability α.

Another important step in the development of the theory of dielectric polarization was made by Kirkwood[4] who discussed the implications of Onsager's assumption that the immediate surroundings of a molecule have the properties of a continuum, whose dielectric constant is that of a bulk sample of the material. In a theory which is rigorous for nonpolarizable molecules, Kirkwood relates the mean moment of a spherical sample of material in the presence of an external field to the scalar product of the moment $\boldsymbol{\mu}$ of a single molecule and $\boldsymbol{\mu}^*$, the mean moment of a fixed molecule and its neighbors in a sphere in the interior of the specimen in the absence of an external field. A similar theory has been developed by Fröhlich,[5] who supposes that the contribution of the polarizabilities of the molecules of a sample to the polarization can be represented by a continuum.

The way in which the effects of the polarizability of a molecule were introduced by Kirkwood is not satisfactory and an improvement in the theory was made by Harris and Alder.[6] The effects of polarizability are twofold: firstly there is a direct contribution to the moment of a specimen due to the further polarization of the individual molecules in a particular configuration when an external field is applied. For spherically symmetrical molecules this is the only important contribution. The second effect is due to the dipole moment of one molecule inducing a moment in its neighbors, thereby altering their actual moments. Both Kirkwood's and Harris' and Alder's treatment require an assumption to be made regarding the second effect, namely that the actual moments of all molecules in the absence of an external field are independent of the configuration and equal to their average moments, fluctuations being neglected.[7]

A way of assessing the errors implicit in the above mentioned assumption of Kirkwood and Harris and Alder, namely that fluctuations in the moments of molecules are unimportant, is open to us in the case of the imperfect gas. If the total polarization is written as a power series in inverse powers of the molar volume V_m, then the volume-independent term corresponds to the approximation of noninteracting molecules and the term in $1/V_m$ to the interaction of the molecules in pairs. If we suppose that the molecules are point polarizable dipoles, it is possible to determine exactly the moments of two interacting ones, and, by integrating over all possible configurations after multiplying by the

[1] P. Debye, Physik. Z. **13**, 97 (1912).
[2] H. A. Lorentz, *Theory of Electrons* (Teubner, Leipzig, 1909).
[3] L. Onsager, J. Am. Chem. Soc. **58**, 1486 (1936).
[4] J. G. Kirkwood, J. Chem. Phys. **7**, 911 (1939).
[5] H. Fröhlich, *Theory of Dielectrics* (Oxford University Press, New York, 1949).
[6] F. E. Harris and B. J. Alder, J. Chem. Phys. **21**, 1031 (1953).
[7] F. E. Harris and B. J. Alder, J. Chem. Phys. **22**, 1806 (1954).

appropriate weighting factor, to find a precise expression for the coefficient of $1/V_m$. The assumption of negligible fluctuations requires that we replace the actual moments of the interacting pair by their average values, and this will lead to inexact conclusions. Kirkwood's and Harris' and Alder's equations are identical to the order of $1/V_m$, so that our comparison will not be capable of deciding which is the better approximation for the model we shall discuss. Harris and Alder[8] suggest that the use of Onsager's model will not be inappropriate for calculating the average moment of a molecule in a gas. However, the results of this paper show that Onsager's assumption that the surroundings of a molecule can be represented by a continuum having the macroscopic dielectric constant leads to an average moment of a molecule differing from the vapor moment by a term of the order of $1/V_m^2$, so that the use of this inexact relationship will greatly affect the term in $1/V_m$.

2. GENERAL FORMULATION

A general theory of dielectric polarization will be briefly developed in this section, thereby enabling the approximations introduced by Kirkwood[4] and Harris and Alder[6,7] to be easily understood.

Consider a large spherical specimen of volume V_m (the molar volume) containing $\mathbf{N}$ (Avogadro's number) similar molecules in a region where a uniform electric field $\mathbf{E}_0$ exists at large distances from the sphere. Then the static dielectric constant at small field strengths ϵ_s, is defined by

$$\frac{\epsilon_s-1}{\epsilon_s+2}V_m=\frac{4\pi}{3}\lim_{E_0\to 0}\left\{\frac{\partial}{\partial E_0}\langle\mathbf{M}\cdot\mathbf{e}\rangle_{Av}\right\}, \tag{1}$$

where $\langle\mathbf{M}\cdot\mathbf{e}\rangle_{Av}$ is the average value of the moment $\mathbf{M}$ of the specimen in the direction $\mathbf{e}$ of the field. Equation (1) may be shown to reduce to (see Buckingham and Pople[9])

$$\frac{\epsilon_s-1}{\epsilon_s+2}V_m=\frac{4\pi}{3}\left\langle\left(\frac{\partial\mathbf{M}}{\partial E_0}\cdot\mathbf{e}\right)\right\rangle+\frac{4\pi}{9kT}\langle M^2\rangle, \tag{2}$$

where $\langle X\rangle$ is the average value of X in the absence of an applied electric field. The validity of (2) depends only on the applicability of classical statistical mechanics. Now Kirkwood[10] showed that, for nonpolar molecules,

$$\left\langle\left(\frac{\partial\mathbf{M}}{\partial E_0}\cdot\mathbf{e}\right)\right\rangle=\mathbf{N}\alpha+\mathbf{N}0(\alpha^3), \tag{3}$$

and the same result holds for an assembly of polarizable dipoles (see the Appendix). Also,

$$\mathbf{M}=\sum_{i=1}^{\mathbf{N}}\boldsymbol{\mu}_i,$$

where $\boldsymbol{\mu}_i$ is the dipole moment of the ith molecule, so that

$$\langle M^2\rangle=\mathbf{N}\langle\boldsymbol{\mu}_i\cdot\mathbf{M}\rangle, \tag{4}$$

since all molecules are alike and Kirkwood[4] showed that the average value of $\mathbf{M}$ when a single molecule in the interior of the specimen is fixed in position and orientation does not depend on the position of the molecule unless it is near the surface, and the proportion which are near the surface can be made as small as we please simply by increasing the size of the specimen.

Hence, from (2), (3), and (4), if we neglect terms of $0(\alpha^3)$ in $\langle[(\partial\mathbf{M}/\partial E_0)\cdot\mathbf{e}]\rangle$,

$$\frac{\epsilon_s-1}{\epsilon_s+2}V_m=\frac{4\pi\mathbf{N}\alpha}{3}+\frac{4\pi\mathbf{N}}{9kT}\langle\boldsymbol{\mu}_i\cdot\mathbf{M}\rangle. \tag{5}$$

Now both Kirkwood[4] and Harris and Alder[6] replace $\langle\boldsymbol{\mu}_i\cdot\mathbf{M}\rangle$ by $\boldsymbol{\mu}_i\cdot\langle\mathbf{M}\rangle_i$, where $\langle\mathbf{M}\rangle_i$ is the average value of the moment of the sphere when the ith molecule has a fixed moment $\boldsymbol{\mu}_i$. This step is only correct when μ_i is independent of the configuration.

It is possible to express $\langle\mathbf{M}\rangle_i$ in terms of $\boldsymbol{\mu}^*_i$, the average moment of a macroscopic sphere centered upon the fixed ith molecule, when this sphere is very small in comparison to the whole specimen. Thus the surroundings of the inner sphere may be supposed to have the macroscopic dielectric constant for the purpose of relating $\mathbf{M}_i$ to $\boldsymbol{\mu}^*_i$. These two moments differ due to the fact that the surface of the specimen polarizes the whole medium. Kirkwood[4] showed that

$$\langle\mathbf{M}\rangle_i=\frac{9\epsilon_s}{(2\epsilon_s+1)(\epsilon_s+2)}\boldsymbol{\mu}^*_i=\left\{1-\frac{2(\epsilon_s-1)^2}{(2\epsilon_s+1)(\epsilon_s+2)}\right\}\boldsymbol{\mu}^*_i. \tag{6}$$

In the limit of large volumes (ϵ_s-1) is proportional to $1/V_m$, so that (6) shows that this boundary field polarization does not contribute to the term in $1/V_m$ in an expansion of the total polarization in powers of $1/V_m$.

Thus the equation of Harris and Alder[6] is

$$\frac{\epsilon_s-1}{\epsilon_s+2}V_m=\frac{4\pi\mathbf{N}\alpha}{3}+\frac{4\pi\mathbf{N}}{9kT}\boldsymbol{\mu}_K\cdot\langle\mathbf{M}\rangle_K=\frac{4\pi\mathbf{N}\alpha}{3}+\frac{4\pi\mathbf{N}}{9kT}\frac{9\epsilon_s}{(2\epsilon_s+1)(\epsilon_s+2)}\boldsymbol{\mu}_K\cdot\boldsymbol{\mu}^*_K \tag{7}$$

where μ_K is the average value of the magnitude of the moment of a molecule of the specimen in the absence of an applied field, and $\boldsymbol{\mu}^*_K$ is the average value of the moment of a small sphere in the interior of the sample which consists of molecules with moments μ_K, when the central molecule is fixed.

Kirkwood[4] employed a different value for

$$\langle[(\partial\mathbf{M}/\partial E_0)\cdot\mathbf{e}]\rangle,$$

[8] F. E. Harris and B. J. Alder, J. Chem. Phys. **21**, 1351 (1953).
[9] A. D. Buckingham and J. A. Pople, Trans. Faraday Soc. **51**, 1029 (1955).
[10] J. G. Kirkwood, J. Chem. Phys. **4**, 592 (1936).

for he supposed the local field producing this extra moment was the Onsager cavity field $9\epsilon_s\mathbf{E}_0/(2\epsilon_s+1)(\epsilon_s+2)$. He put

$$\left\langle\left(\frac{\partial\mathbf{M}}{\partial E_0}\cdot\mathbf{e}\right)\right\rangle=\frac{9\epsilon_s}{(2\epsilon_s+1)(\epsilon_s+2)}\mathbf{N}\alpha,$$

so that his equation may be written

$$\frac{\epsilon_s-1}{\epsilon_s+2}V_m=\frac{9\epsilon_s}{(2\epsilon_s+1)(\epsilon_s+2)}\frac{4\pi\mathbf{N}\alpha}{3}+\frac{4\pi\mathbf{N}}{9kT}\boldsymbol{\mu}_K\cdot\langle\mathbf{M}\rangle_K$$

$$=\frac{9\epsilon_s}{(2\epsilon_s+1)(\epsilon_s+2)}\left\{\frac{4\pi\mathbf{N}\alpha}{3}+\frac{4\pi\mathbf{N}}{9kT}\boldsymbol{\mu}_K\cdot\boldsymbol{\mu}^*_K\right\}. \quad (8)$$

Onsager's[3] equation may be put in the form

$$\frac{\epsilon_s-1}{\epsilon_s+2}V_m=\frac{9\epsilon_s}{(2\epsilon_s+1)(\epsilon_s+2)}$$

$$\times\left\{\frac{4\pi\mathbf{N}\alpha}{3\left\{1-\dfrac{2(\epsilon_s-1)\alpha}{(2\epsilon_s+1)a^3}\right\}}+\frac{4\pi\mathbf{N}}{9kT}\mu^2\right\}, \quad (9)$$

where a is the radius of Onsager's cavity of molecular dimensions, and Onsager's μ is given by

$$\mu=\frac{\mu_0}{1-\dfrac{2(\epsilon_s-1)\alpha}{(2\epsilon_s+1)a^3}}, \quad (10)$$

where μ_0 is the moment of an isolated molecule. If one uses Onsager's results $\alpha=\{(n^2-1)/(n^2+2)\}a^3$, and $4\pi\mathbf{N}a^3/3=V_m$, then his familiar equation is obtained. Since in Onsager's theory the surroundings of a molecule are supposed to be continuous, there will be no fluctuations in μ in the absence of an applied field. Also $\boldsymbol{\mu}^*$ will, on the basis of this model, be equal to $\boldsymbol{\mu}$.

Debye's equation for the total polarization may be written

$$\frac{\epsilon_s-1}{\epsilon_s+2}V_m=\frac{4\pi\mathbf{N}\alpha}{3}+\frac{4\pi\mathbf{N}\mu_0^2}{9kT}, \quad (11)$$

and is, of course, true only in the limit of very large volumes.

3. COMPARISON OF THE THEORIES APPLIED TO AN IMPERFECT GAS

(i) Exact Theory

In this section we shall write the total polarization ${}_TP$ as a power series in inverse powers of the molar volume. Such a series has been discussed by Buckingham and Pople.[9] We shall write

$${}_TP=\frac{\epsilon_s-1}{\epsilon_s+2}V_m=\mathfrak{A}+\frac{\mathfrak{B}}{V_m}+\frac{\mathfrak{C}}{V_m^2}+\cdots, \quad (12)$$

where $\mathfrak{A}$, $\mathfrak{B}$, $\mathfrak{C}$, $\cdots$, are the first, second, third, $\cdots$ *dielectric virial coefficients*. From (5) we find

$$\mathfrak{A}=\lim_{V_m\to\infty}{}_TP=\frac{4\pi\mathbf{N}\alpha}{3}+\frac{4\pi\mathbf{N}\mu_0^2}{9kT}, \quad (13)$$

and

$$\mathfrak{B}=\lim_{V_m\to\infty}\{({}_TP-\mathfrak{A})V_m\}$$

$$=\frac{4\pi\mathbf{N}}{9kT}\lim_{V_m\to\infty}\{\langle\boldsymbol{\mu}_1\cdot\mathbf{M}-\mu_0^2\rangle V_m\}+0(\alpha^3)$$

$$=\frac{4\pi\mathbf{N}}{9kT}\lim_{V_m\to\infty}\{\langle\mu_1^2-\mu_0^2+(N-1)\boldsymbol{\mu}_1\cdot\boldsymbol{\mu}_2\rangle V_m\}+0(\alpha^3) \quad (14)$$

$$=\frac{4\pi\mathbf{N}^2}{9kT\Omega}\int(\mu_1^2-\mu_0^2+\boldsymbol{\mu}_1\cdot\boldsymbol{\mu}_2)$$

$$\times\exp[-u_{12}/kT]d\tau_2+0(\alpha^3), \quad (15)$$

where the integration in (15) extends over all possible positions and orientations of molecule 2, and where u_{12} is the potential energy of interaction of molecules 1 and 2. Ω is defined by $\int d\tau_2=\Omega V_m$, so that it is the integral over the angular coordinates.

In order to compare quantitatively the several theories it will be necessary to adopt some molecular model. We shall therefore suppose that the molecules are point polarizable dipoles whose polarizabilities are such that their squares and higher powers are negligible. We shall also suppose that u_{12} is of the form

$$u_{12}=4\epsilon\left\{\left(\frac{r_0}{r}\right)^{12}-\left(\frac{r_0}{r}\right)^{6}\right\}$$

$$+\frac{\mu_0^2}{r^3}\{2\cos\theta_1\cos\theta_2+\sin\theta_1\sin\theta_2\cos(\phi_1+\phi_2)\}$$

$$-\frac{\alpha\mu_0^2}{2r^6}\{3\cos^2\theta_1+3\cos^2\theta_2-2\}, \quad (16)$$

where ϵ and r_0 are parameters having the dimensions of energy and length respectively, and r and the polar angles θ_1, ϕ_1, θ_2, ϕ_2 are as in Fig. 1. Thus we have assumed that the purely central forces are of the Lennard-Jones 6–12 variety, and the orientationally dependent terms are those corresponding to dipole-dipole and dipole-induced dipole interactions. Part of the dipole-induced dipole interaction energy is included in the term $-4\epsilon(r_0/r)^6$.

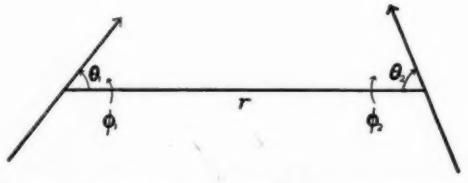

FIG. 1. Coordinates of interacting axially symmetric molecules.

Also, for this model

$$\mu_1^2=\mu_0^2\Big[1-\frac{2\alpha}{r^3}\{2\cos\theta_1\cos\theta_2+\sin\theta_1\sin\theta_2\cos(\phi_1+\phi_2)\}+0(\alpha^2)\Big] \quad (17)$$

and

$$\boldsymbol{\mu}_1\cdot\boldsymbol{\mu}_2=\mu_0^2\Big[\{\sin\theta_1\sin\theta_2\cos(\phi_1+\phi_2)-\cos\theta_1\cos\theta_2\}+\frac{\alpha}{r^3}\{3\cos^2\theta_1+3\cos^2\theta_2-2\}+0(\alpha^2). \quad (18)$$

Thus

$$\frac{\langle\mu_1^2-\mu_0^2\rangle}{\mu_0^2}=-\frac{2\mathbf{N}\alpha}{4\pi V_m}\int_0^\infty r^2dr\int_0^\pi\sin\theta_1d\theta_1\times\int_0^{2\pi}d\phi_1\int_0^\pi\sin\theta_2d\theta_2\int_0^{2\pi}d\phi_2\frac{1}{r^3}\times\{2\cos\theta_1\cos\theta_2+\sin\theta_1\sin\theta_2\cos(\phi_1+\phi_2)\}\times\exp\Big[-y^2\Big\{\Big(\frac{r_0}{r}\Big)^{12}-\Big(\frac{r_0}{r}\Big)^6\Big\}-\frac{y^2\tau r_0^3}{4r^3}\times\{2\cos\theta_1\cos\theta_2+\sin\theta_1\sin\theta_2\cos(\phi_1+\phi_2)\}\Big]+0\Big(\frac{\alpha^2}{V_m}\Big)+0\Big(\frac{\alpha}{V_m^2}\Big),$$

where

$$y=2(\epsilon/kT)^{\frac{1}{2}},\quad \tau=\mu_0^2/\epsilon r_0^3. \quad (19)$$

Hence

$$\frac{\langle\mu_1^2-\mu_0^2\rangle}{\mu_0^2}=\frac{4\pi\mathbf{N}\alpha}{3V_m}\sum_{n=1}^\infty\frac{n\{n!\}^2}{2^{2n-2}\{(2n+1)!\}^2}\times y^{4n-6}\tau^{2n-1}H_{6n}(y)\sum_{t=0}^n\frac{(2t)!}{(t!)^2}+0\Big(\frac{\alpha^2}{V_m}\Big)+0\Big(\frac{\alpha}{V_m^2}\Big) \quad (20)$$

$$=\frac{4\pi\mathbf{N}\alpha}{3V_m}\Big\{\frac{\tau}{12y^2}H_6(y)+\frac{y^2\tau^3}{800}H_{12}(y)+\frac{29y^6\tau^5}{3\,763\,200}H_{18}(y)+\cdots\Big\}+0\Big(\frac{\alpha^2}{V_m}\Big)+0\Big(\frac{\alpha}{V_m^2}\Big), \quad (21)$$

where

$$H_n(y)=y^{(27-n)/6}\sum_{P=0}^\infty\Gamma\Big(\frac{6P+n-3}{12}\Big)\frac{y^P}{P!}. \quad (22)$$

The functions $H_n(y)$ were defined by Pople[11] and have been discussed and tabulated by Buckingham and Pople.[12] Again

$$\frac{\mathbf{N}\langle\boldsymbol{\mu}_1\cdot\boldsymbol{\mu}_2\rangle}{\mu_0^2}=\frac{\mathbf{N}}{4\pi V_m}\int_0^\infty r^2dr\int_0^\pi\sin\theta_1d\theta_1\times\int_0^{2\pi}d\phi_1\int_0^\pi\sin\theta_2d\theta_2\int_0^{2\pi}d\phi_2\times\Big[\{\sin\theta_1\sin\theta_2\cos(\phi_1+\phi_2)-\cos\theta_1\cos\theta_2\}\times\Big\{1+\frac{y^2\alpha\tau r_0^3}{8r^6}(3\cos^2\theta_1+3\cos^2\theta_2-2)\Big\}+\frac{\alpha}{r^3}(3\cos^2\theta_1+3\cos^2\theta_2-2)\Big]\times\exp\Big[-y^2\Big\{\Big(\frac{r_0}{r}\Big)^{12}-\Big(\frac{r_0}{r}\Big)^6\Big\}-\frac{y^2\tau r_0^3}{4r^3}\times\{2\cos\theta_1\cos\theta_2+\sin\theta_1\sin\theta_2\cos(\phi_1+\phi_2)\}\Big]+0\Big(\frac{\alpha^2}{V_m}\Big)+0\Big(\frac{\alpha}{V_m^2}\Big)$$

$$=\frac{4\pi\mathbf{N}r_0^3}{3V_m}\Big\{\frac{y^2\tau^3}{9600}H_9(y)+\frac{y^6\tau^5}{940\,800}H_{15}(y)+\frac{y^{10}\tau^7}{216\,760\,320}H_{21}(y)+\cdots\Big\}+\frac{4\pi\mathbf{N}\alpha}{3V_m}\times\Big\{\frac{\tau^2}{120}H_9(y)+\frac{17y^4\tau^4}{134\,400}H_{15}(y)+\cdots\Big\}+0\Big(\frac{\alpha^2}{V_m}\Big)+0\Big(\frac{\alpha}{V_m^2}\Big). \quad (23)$$

From (14), (21), and (23), we find (see Buckingham and Pople[13])

$$\mathfrak{B}=\frac{\pi^2\mathbf{N}^2r_0^6}{27}\Big[\Big\{\frac{y^4\tau^4}{2400}H_9(y)+\frac{y^8\tau^6}{235\,200}H_{15}(y)+\frac{y^{12}\tau^8}{54\,190\,080}H_{21}(y)+\cdots\Big\}+\frac{\alpha}{r_0^3}\Big\{\frac{\tau^2}{3}H_6(y)+\frac{y^2\tau^3}{30}H_9(y)+\frac{y^4\tau^4}{200}H_{12}(y)+\frac{17y^6\tau^5}{33\,600}H_{15}(y)+\cdots\Big\}+0(\alpha^2)\Big]. \quad (24)$$

[11] J. A. Pople, Proc. Roy. Soc. (London) **A221**, 508 (1954).

[12] A. D. Buckingham and J. A. Pople, Trans. Faraday Soc. **51**, 1173 (1955).

[13] A. D. Buckingham and J. A. Pople, Trans. Faraday Soc. **51**, 1179 (1955).

(ii) Kirkwood's Equation

To find $\mathfrak{A}_K$ and $\mathfrak{B}_K$, that is, the coefficients of $(1/V_m)^0$ and $(1/V_m)$, in the expansion of (8) in powers of $1/V_m$, we must first write down an expression for μ_K. We shall suppose that the intermolecular energy is still represented by (16). Hence, from (20) we find

$$\mu_K^2=\mu_0^2\Big\{1+\frac{4\pi N\alpha}{3V_m}\sum_{n=1}^{\infty}\frac{n\{n!\}^2}{2^{2n-2}\{(2n+1)!\}^2}\times y^{4n-6}\tau^{2n-1}H_{6n}(y)\sum_{t=0}^{n}\frac{(2t)!}{(t!)^2}+0\Big(\frac{\alpha^2}{V_m}\Big)+0\Big(\frac{\alpha}{V_m^2}\Big)\Big\}. \quad (25)$$

From (8)

$$\mathfrak{A}_K=\frac{4\pi N\alpha}{3}+\frac{4\pi N}{9kT}\lim_{V_m\to\infty}(\boldsymbol{\mu}_K\cdot\langle\mathbf{M}\rangle_K)=\frac{4\pi N\alpha}{3}+\frac{4\pi N\mu_0^2}{9kT}=\mathfrak{A}. \quad (26)$$

Also

$$\mathfrak{B}_K=\frac{4\pi N}{9kT}\lim_{V_m\to\infty}\times\{\langle\mu_K^2-\mu_0^2+(N-1)(\boldsymbol{\mu}_{K_1}\cdot\boldsymbol{\mu}_{K_2})\rangle V_m\}+0(\alpha^3). \quad (27)$$

To the first order in α and $1/V_m$,

$$\frac{N\langle\boldsymbol{\mu}_{K_1}\cdot\boldsymbol{\mu}_{K_2}\rangle}{\mu_0^2}=\frac{N\langle\boldsymbol{\mu}_1\cdot\boldsymbol{\mu}_2\rangle}{\mu_0^2}-\frac{N}{4\pi V_m}\int_0^{\infty}r^2dr\int_0^{\pi}\sin\theta_1d\theta_1\times\int_0^{2\pi}d\phi_1\int_0^{\pi}\sin\theta_2d\theta_2\int_0^{2\pi}d\phi_2\frac{\alpha}{r^3}\times\{\sin\theta_1\sin\theta_2\cos(\phi_1+\phi_2)-\cos\theta_1\cos\theta_2\}\times\{3\cos^2\theta_1+3\cos^2\theta_2-2\}\times\exp\Big[-y^2\Big\{\Big(\frac{r_0}{r}\Big)^{12}-\Big(\frac{r_0}{r}\Big)^{6}\Big\}-\frac{y^2\tau r_0^3}{4r^3}\times\{2\cos\theta_1\cos\theta_2+\sin\theta_1\sin\theta_2\cos(\phi_1+\phi_2)\}\Big],$$

$$=\frac{N\langle\boldsymbol{\mu}_1\cdot\boldsymbol{\mu}_2\rangle}{\mu_0^2}-\frac{4\pi N\alpha}{3V_m}\times\Big\{\frac{\tau^2}{240}H_9(y)+\frac{y^4\tau^4}{16\,800}H_{15}(y)+\frac{y^8\tau^6}{3\,010\,560}H_{21}(y)+\cdots\Big\}. \quad (28)$$

From (25), (27), and (28) we find

$$\mathfrak{B}_K=\mathfrak{B}-\frac{\pi^2N^2\alpha r_0^3}{27}\Big\{\frac{\tau^2}{60}H_9(y)+\frac{y^4\tau^4}{4200}H_{15}(y)+\frac{y^8\tau^6}{752\,640}H_{21}(y)+\cdots\Big\}+0(\alpha^2). \quad (29)$$

Thus Kirkwood's equation (and also Harris' and Alder's) underestimates the total polarization of an imperfect gas of polarizable dipoles. This arises from the fact that there is a correlation between the direction of the moment induced in a molecule by a neighbor and the orientation and position of this neighbor. The replacement of the induced moment by its average value ignores this correlation and thereby causes an underestimation of $\langle\boldsymbol{\mu}_1\cdot\boldsymbol{\mu}_2\rangle$.

(iii) The Equations of Harris and Alder

Since the equations of Harris and Alder[6] and Kirkwood[4] differ only by the factor

$$\frac{9\epsilon_s}{(2\epsilon_s+1)(\epsilon_s+2)}=1-\frac{2(\epsilon_s-1)^2}{(2\epsilon_s+1)(\epsilon_s+2)},$$

in the term in $4\pi N\alpha/3$, $\mathfrak{A}_{HA}=\mathfrak{A}_K$, $\mathfrak{B}_{HA}=\mathfrak{B}_K$, and $\mathfrak{C}_{HA}\neq\mathfrak{C}_K$, where $\mathfrak{A}_{HA}$, $\mathfrak{B}_{HA}$, and $\mathfrak{C}_{HA}$ are dielectric virial coefficients according to (7).

In a paper discussing the dielectric polarization of an imperfect gas, Harris and Alder[8] suggest that μ_K might be approximated by the Onsager relationship (10). However, this leads to $\mu_K^2=\mu_0^2+0(\alpha/V_m^2)$, so that if their suggestion is adopted (as Harris and Alder[8] do in their calculations) the corresponding second dielectric virial coefficient $\mathfrak{B}_{HAO}$ is

$$\mathfrak{B}_{HAO}=\mathfrak{B}-\frac{\pi^2N^2\alpha r_0^3}{27}\Big\{\frac{\tau}{3y^2}H_6(y)+\frac{\tau^2}{60}H_9(y)+\frac{y^2\tau^3}{200}H_{12}(y)+\frac{y^4\tau^4}{4200}H_{15}(y)+\frac{29y^6\tau^5}{940\,800}H_{18}(y)+\frac{y^8\tau^6}{752\,640}H_{21}(y)+\cdots\Big\}+0(\alpha^2). \quad (30)$$

(iv) Onsager's Equation

Since both

$$\frac{9\epsilon_s}{(2\epsilon_s+1)(\epsilon_s+2)} \quad \text{and} \quad \frac{1}{1-\dfrac{2(\epsilon_s-1)\alpha}{(2\epsilon_s+1)a^3}}=\frac{1}{1-\dfrac{8\pi N(\epsilon_s-1)\alpha}{3(2\epsilon_s+1)V_m}}$$

differ from unity by terms of $0(1/V_m^2)$, the equation of

Onsager, namely (9), yields

$$\mathfrak{A}_O=\mathfrak{A}, \tag{31}$$

$$\mathfrak{B}_O=0. \tag{32}$$

(v) Debye's Equation

Debye's equation, namely (11), corresponds to

$$\mathfrak{A}_D=\mathfrak{A}, \tag{33}$$

$$\mathfrak{B}_D=0=\mathfrak{C}_D=\cdots. \tag{34}$$

(vi) Fröhlich's Equation

Fröhlich[5] employed a model for the purpose of estimating the contribution of polarizability to the total dielectric polarization. His model consisted of rigid point dipoles in a continuum of dielectric constant equal to the high-frequency dielectric constant of the material. Unfortunately this model does not enable a precise expression for $\mathfrak{B}_F$ to be evaluated.

4. NUMERICAL CALCULATIONS

For the purpose of evaluating the errors in the above approximate theories in a particular case, we shall apply the various equations to parameters corresponding roughly to those for methyl fluoride at room temperature. We shall put $\alpha=3.5\times10^{-24}$ cm^3, $y=1.6$, $r_0=3.5$ A, $\tau=3.0$. Using these figures, together with Buckingham's and Pople's[12] table for $H_n(y)$, we calculate, according to the above equations, which neglect terms of $0(\alpha^2)$,

$$\mathfrak{A}=78 \text{ cm}^3$$
$$\mathfrak{B}=7500 \text{ cm}^6 \text{ mole}^{-2}$$
$$\mathfrak{B}_K=\mathfrak{B}-\ 920 \text{ cm}^6 \text{ mole}^{-2}$$
$$\mathfrak{B}_{HA}=\mathfrak{B}-\ 920 \text{ cm}^6 \text{ mole}^{-2}$$
$$\mathfrak{B}_{HAO}=\mathfrak{B}-4600 \text{ cm}^6 \text{ mole}^{-2}$$
$$\mathfrak{B}_O=0 \text{ cm}^6 \text{ mole}^{-2}$$
$$\mathfrak{B}_D=0 \text{ cm}^6 \text{ mole}^{-2}.$$

These figures show clearly that, applied to an imperfect gas of polarizable dipoles interacting according to the potential (16), the equations of Kirkwood[4] and Harris and Alder[6] slightly underestimate the total polarization, while the use of Onsager's relationship for the ratio μ/μ_0 leads to a very much larger error in the same direction. The equation of Onsager[3] has never been claimed to be adequate for gases, Onsager himself stating that it would be absurd to apply it to this state if one uses the result $4\pi\mathbf{N}a^3/3=V_m$.

ACKNOWLEDGMENTS

The author is grateful to Dr. J. A. Pople and Dr. B. J. Alder for some valuable suggestions concerning this work, and is also indebted to the Royal Dutch Shell Group for the award of a Postgraduate Scholarship.

APPENDIX. THE EXPANSION OF $\left\langle\left(\frac{\partial M}{\partial E_0}\cdot e\right)\right\rangle$ IN POWERS OF THE POLARIZABILITY

The dipole moment of the ith molecule of the specimen may be written

$$\boldsymbol{\mu}_i=\boldsymbol{\mu}_{0i}+\alpha(\mathbf{E}_0+\mathbf{F}_i),$$

where $\mathbf{F}_i$ is the electric field strength at the center of molecule i due to all the other molecules in the sample. We shall suppose that the induced moments of all molecules behave as dipoles, that is, the α component of $\mathbf{F}_i$ can be represented by

$$F_{i\alpha}=F_{i\alpha}{}^{(0)}-\alpha\sum_{j\neq i}\epsilon_{\alpha\beta}{}^{(ij)}(E_0e_\beta+F_{j\beta}),$$

where $F_{i\alpha}{}^{(0)}$ is the field at molecule i resulting from the permanent moments of the other molecules, and where the ϵ tensors are defined by (see Pople[14])

$$\epsilon_{\alpha\beta}{}^{(ij)}=-\nabla_\alpha\nabla_\beta(1/r_{ij})$$
$$=r_{ij}{}^{-5}\{r_{ij}{}^2\delta_{\alpha\beta}-3r_{ij\alpha}r_{ij\beta}\}.$$

Thus

$$\mu_{i\alpha}=\mu_{0i\alpha}+\alpha[E_0e_\alpha+F_{i\alpha}{}^{(0)}-\alpha\sum_{j\neq i}\epsilon_{\alpha\beta}{}^{(ij)}\{E_0e_\beta+F_{j\beta}{}^{(0)}$$
$$-\alpha\sum_{k\neq j}\epsilon_{\beta\gamma}{}^{(jk)}(E_0e_\gamma+F_{k\gamma}{}^{(0)}+0(\alpha))\}],$$

whence

$$\left\langle\left(\frac{\partial\boldsymbol{\mu}_i}{\partial E_0}\cdot\mathbf{e}\right)\right\rangle=\alpha-\alpha^2\sum_{j\neq i}\langle\epsilon_{\alpha\beta}{}^{(ij)}e_\beta e_\alpha\rangle$$
$$+\alpha^3\sum_{j\neq i}\sum_{k\neq j}\langle\epsilon_{\alpha\beta}{}^{(ij)}\epsilon_{\beta\gamma}{}^{(jk)}e_\gamma e_\alpha\rangle-0(\alpha^4)$$
$$=\alpha+\frac{\alpha^3}{3}\sum_{j\neq i}\sum_{k\neq j}\langle\epsilon_{\alpha\beta}{}^{(ij)}\epsilon_{\alpha\beta}{}^{(jk)}\rangle-0(\alpha^4),$$

the term in α^2 vanishing on averaging over all directions of $\mathbf{e}$ since $\epsilon_{\alpha\alpha}{}^{(ij)}=-\nabla_\alpha\nabla_\alpha(1/r_{ij})=0$. Thus,

$$\left\langle\left(\frac{\partial\mathbf{M}}{\partial E_0}\cdot\mathbf{e}\right)\right\rangle=\mathbf{N}\left\langle\left(\frac{\partial\boldsymbol{\mu}_i}{\partial E_0}\cdot\mathbf{e}\right)\right\rangle=\mathbf{N}\alpha+\mathbf{N}0(\alpha^3).$$

This result was first proved for molecules without permanent moments by Kirkwood.[10] The above result shows that there is also no term in α^2 in the Clausius-Mossotti function for an assembly of molecules whose induced moments behave as if they were pure dipoles.

[14] J. A. Pople, Proc. Roy. Soc. (London) **A215**, 67 (1952).

Infrared Intensities in Liquid and Gas Phases*

S. R. Polo and M. Kent Wilson
Mallinckrodt Chemical Laboratories, Harvard University, Cambridge, Massachusetts
(Received March 11, 1955)

It is shown that Debye's and Onsager's theories of dielectric polarization lead to the same expression for the relation between the intensities of an infrared absorption band in the liquid and in the gas phases.

A QUESTION of considerable interest in the study of the intensities of infrared absorption bands is the relation between the values of the intensity of a given band in the gas phase and in the liquid phase. Gas phase values are required for the determination of bond moments and derivatives. Since the number of molecules for which gas phase intensities can be measured is relatively limited, the question becomes a very practical one.

Two expressions have been proposed which are at variance with each other. One of them can be deduced from Debye's[1] theory of dielectric polarization A_l, A_g

$$\frac{A_l}{A_g}=\frac{1}{n}\left(\frac{n^2+2}{3}\right)^2, \tag{1}$$

being the integrated absorption coefficients in the liquid and in the gas, respectively, and n the refractive index. The other expression

$$\frac{A_l}{A_g}=\frac{1}{n}\left(\frac{3n^2}{2n^2+1}\right)^2 \tag{2}$$

has been advanced[2] on the grounds that it corresponds to the predictions of Onsager's[3] theory of dielectric polarization. While Eq. (1) predicts an increase in intensity of the order of 30% going from gas to liquid ($n\simeq 1.4$–1.5), Eq. (2) would predict a negligible change.

This disagreement seems surprising, since one would expect that Debye's and Onsager's theories might give different results only when the molecule has a permanent dipole moment, μ_0. However, Eq. (2) does not contain μ_0 and does not reduce to Eq. (1).

Accordingly a brief discussion of the problem seems appropriate, especially since there has been some doubt as to which expression should be preferred.

The relation between A_l and A_g is given by

$$A_l/A_g=F^2/E_0^2, \tag{3}$$

where F is the "effective" field acting on the absorbing molecule in the liquid phase and E_0 is the field acting on the molecule in a vacuum.

The liquid is considered as a medium of dielectric constant $\epsilon=n^2$.† We have, in addition, the relation‡

$$E_0^2=nE^2, \tag{4}$$

where E is the field in the dielectric. F is calculated as the internal field acting at the center of a small spherical cavity of radius a in the dielectric medium.

From Debye's theory, one obtains

$$\mathbf{F}=(n^2+2)\mathbf{E}/3. \tag{5}$$

Substitution of Eqs. (4) and (5) in Eq. (3) gives Eq. (1).

Although the deduction of Eq. (2) is not given in reference 2, its form suggests that the ratio F/E has been obtained from Eq. (12) of Onsager's paper,[3] which is

$$\mathbf{F}=\mathbf{G}+\mathbf{R}=\frac{3n^2}{2n^2+1}\mathbf{E}+\frac{2(n^2-1)}{(2n^2+1)a^3}\mathbf{m}, \tag{6}$$

under the assumption that only the cavity field $\mathbf{G}$ is effective. However, there is no apparent reason for neglecting the reaction field $\mathbf{R}$. This term corresponds to the electric field acting on the molecule at the center of the cavity as a result of electric displacements induced by its own presence and has a real significance in determining the total effective field. It is true that $\mathbf{R}$ plays no role in determining the average orientation of the molecules under the applied field, but in our case no orientation effects need to be considered, as mentioned in the foregoing.

It will be noticed that $\mathbf{m}$ is the *total* electric moment of the molecule and is composed of two terms corresponding to the permanent and induced dipole moments

$$\mathbf{m}=\mu\mathbf{u}+\frac{n^2+2}{3}\alpha\mathbf{E}. \tag{7}$$

It is through the induced part of the dipole moment that the reaction field $\mathbf{R}$ still has a component in the direction of the applied field. When the value of the polarizability

$$\alpha=\frac{n^2-1}{n^2+2}a^3 \tag{8}$$

* The work was supported in whole or in part by the U. S. Air Force under contract AF18(600)-590 monitored by the Office of Scientific Research.

[1] P. Debye, *Polar Molecules* (Chemical Catalog Company, Inc., New York, 1929).

[2] R. Mecke, Discussions Faraday Soc. **9**, 161 (1950).

[3] L. Onsager, J. Am. Chem. Soc. **58**, 1486 (1936).

† For the present purpose ϵ is always identical with n^2, since for frequencies in the infrared no molecular reorientation takes place.

‡ This follows from the constancy of the magnitude of the Poynting's vector:

$$v\epsilon E^2/4\pi=cE_0^2/4\pi;\quad v=c/n.$$

is introduced in Eq. (7) and the result substituted in Eq. (6) one obtains

$$\mathbf{F}=\frac{n^2+2}{3}\mathbf{E}+\frac{2(n^2-1)}{(2n^2+1)}\frac{\mu}{a^3}\mathbf{u}, \tag{9}$$

which is Eq. (15) of Onsager's paper with $\epsilon=n^2$. The second term has the direction $\mathbf{u}$ of the permanent dipole, which can be considered fixed during the oscillation period for frequencies in the infrared. Therefore,

$$F/E=(n^2+2)/3. \tag{10}$$

This result is identical with that obtained from Debye's theory. It may be pointed out that both theories give the same answer irrespective of whether the molecule has a permanent dipole moment or not.

The validity of Eq. (1) has still to be confirmed by experiment. It is based on an extremely simplified picture and therefore a certain amount of data would be desirable in order to know to what extent its predictions are correct.

Unfortunately, there are very few experimental data, and the liquid phase values available are for solutions, for which Eq. (1) is not strictly applicable. A few measurements in our laboratory indicate that the intensity is greater in solution than in the gas phase. Also, it is found that the intensities in different solvents do not change greatly, apart from those cases where specific interactions seem to be the predominant factor. However, since the data are so few, the evidence so far is not conclusive and further measurements are required.

The authors wish to thank Dr. Frank E. Harris for helpful discussions.

THE JOURNAL OF CHEMICAL PHYSICS VOLUME 23, NUMBER 12 DECEMBER, 1955

On the Energy Dependence of Inelastic Molecular Collision Probabilities

B. WIDOM
Department of Chemistry, Cornell University, Ithaca, New York
(Received March 2, 1955)

It is pointed out that because of the uncertainty principle, cross sections for inelastic molecular collisions vanish at the threshold, in sharp distinction to their classical behavior. The dependence of the inelastic collision probability on the energy is deduced and found to be of the form

$$k^{2l+1}(a_0+a_2k^2+a_4k^4+\cdots),$$

where k and l are the wave number and the total angular momentum quantum number, respectively, which describe the incident wave in case of de-excitation or the emergent wave in case of excitation. It is shown that because of this property of inelastic collisions, the pre-exponential factor in the collision theory of bimolecular kinetics contains only non-negative integral powers of the temperature.

I

IT is the purpose of this paper to discuss a very general property of those molecular collisions in which energy is exchanged between the relative translational motion of a pair of colliding molecules, and the internal motions of these molecules, The term "inelastic collisions," as used here, is to be understood as referring only to processes of this kind. This excludes from consideration collision-induced transitions between degenerate internal states of the two-molecule system. An example of a collision of the latter kind would be the transfer of excitation energy from one molecule to another, with neither an excess nor a deficiency in the energy which is transferred, that is, the case of exact resonance.

In the collision theory of chemical reaction rates, the assumption is usually made that the probability that a collision will be inelastic increases discontinuously from zero just below the threshold to some positive value just above, and is roughly constant beyond the threshold.[1] The semiclassical theory of inelastic molecular collisions actually predicts nonvanishing cross sections at the threshold, whereas quantum mechanical theories seem consistently to yield cross sections which vanish as the threshold is approached.[2]

That the inelastic collision probability should, in fact, become zero as the threshold is approached, was inferred heuristically by Oldenberg.[3] The following considerations may perhaps be even more convincing than Oldenberg's argument.

Let k be the wave number of the relative translational motion in a collision, and let l be the corresponding quantum number of the total relative angular momentum. Then it is known[2] that the collision will be the quantum mechanical analog of a classical collision of

---

[1] R. H. Fowler and E. A. Guggenheim, *Statistical Thermodynamics* (Cambridge University Press, London, 1949), pp. 504–506.
[2] B. Widom and S. H. Bauer, J. Chem. Phys. **21**, 1670 (1953).
[3] O. Oldenberg, J. Chem. Phys. **13**, 196 (1945).

impact parameter b, where b is related to k and to l by

$$l+\tfrac{1}{2}=bk. \tag{1}$$

With each of the two waves, incoming and outgoing, is associated a set of values for l, k, b related by Eq. (1). Since

$$l\geqslant 0$$

we have as a form of the uncertainty principle

$$bk\geqslant\tfrac{1}{2}. \tag{2}$$

It is seen from Eq. (2) that k can be zero only if the impact parameter is infinite. Then in a de-excitation collision, if the relative energy is zero (which is the threshold for de-excitation), the collision takes place with an effectively infinite impact parameter. There can then be no interaction and the probability of de-excitation is zero.

The corresponding result for excitation collisions follows directly. For by the principle of detailed balance, the probability of *excitation* in a collision with relative translational energy equal to the threshold energy, is equal to the probability of *de-excitation* in a collision with vanishing relative energy. But this probability, as we have just seen, is zero.

Thus, from the inequality (2) we conclude that quantum mechanically, but not classically, *if either the relative translational energy or the impact parameter is zero, the other must be infinite.* Classical theories fail at the threshold because they allow zero-energy collisions to occur with finite impact parameters.

If by "head-on" we mean with zero impact parameter, then it is to be noted that Zener's[4] problem should not be considered a problem of head-on collisions, but rather one of S-wave scattering (i.e., $l=0$), where the collisions can become head-on only in the limit of infinite energies.

An infinite impact parameter would not in itself imply a vanishing transition probability, if the interaction potential had an infinite range, as does a Coulomb potential. This is the reason that cross sections for Coulomb scattering do not vanish at the threshold. But for ordinary intermolecular forces the situation is quite different.

From Eq. (1) it is seen that as the relative translational energy becomes zero, the impact parameter becomes infinite more rapidly the greater the value of l. Thus, the higher the value of l associated with the incoming wave in a de-excitation collision or with the outgoing wave in an excitation collision, the more rapidly will the inelastic collision cross section vanish at the threshold. This will appear quantitatively in the discussion that follows.

II

Let p be the probability of a certain transition taking place in a collision which is characterized by given initial conditions. If the transition corresponds to a de-excitation, let the incident wave be characterized by the wave number k and the usual angular momentum quantum numbers l and m_l, and let k', l',$m'_{l'}$ be the corresponding quantities in the emergent wave. If the transition is an excitation, on the other hand, let the unprimed quantities refer to the *final* relative motion and the primed quantities to the initial conditions. By definition, then,

$$k<k',$$

that is, k is the smaller of the incident and emergent wave numbers. It will be shown that the inelastic collision probability p has the asymptotic form

$$p=k^{2l+1}(a_0+a_2k^2+a_4k^4+\cdots),$$

where the constants a_i may depend on l and m_l or on l' and $m'_{l'}$.

It has been pointed out by Wigner[5] that the form of the dependence of p on k will be given correctly by any reasonable approximate solution of the scattering problem, even though the absolute magnitude of the cross section (in this case, the coefficients a_i) will certainly depend on the approximation chosen. Since we are interested at present only in the analytic form of p, we can safely assume p to be proportional to[2]

$$(kk')^{-1}\left|\int \mathfrak{R}^*_{k',l'}(k'R)Y^*_{l',m'_{l'}}(\theta,\phi)V(R,\theta,\phi)\times\mathfrak{R}_{k,l}(kR)Y_{l,m_l}(\theta,\phi)d\tau\right|^2, \tag{3}$$

where the Y's are spherical harmonics independent of k and k', the $\mathfrak{R}$'s are solutions of a differential equation to be written down presently, and V is the matrix element of the interaction potential which connects the initial and final internal states of the colliding molecules.

The function $\mathfrak{R}_{k,l}$ is the solution of the differential equation

$$d^2\mathfrak{R}/dR^2+[k^2-l(l+1)/R^2-(2\mu/\hbar^2)w(R)]\mathfrak{R}=0, \tag{4}$$

where μ is the reduced mass of the colliding particles, and $w(R)$ is a spherically symmetric interaction potential which determines the radial motion. Equation (4) is to be solved subject to the boundary conditions

$$\lim_{R\to 0} R^{-1}\mathfrak{R} \quad \text{exists}, \tag{5}$$

$$\mathfrak{R}\sim\cos(kR+\delta) \quad \text{as } R\to\infty \quad (\delta \text{ real}). \tag{6}$$

The only assumption we shall have to make about the function $w(R)$ is that

$$\lim_{R\to\infty} R^2w(R)=0, \tag{7}$$

which is certainly true of the interactions between electrically neutral molecules. Wigner[5] has already

[4] C. Zener, Phys. Rev. **37**, 556 (1931).

[5] E. P. Wigner, Phys. Rev. **73**, 1002 (1948).

noted the special properties of potentials which do not vanish faster than $1/R^2$.

If we define

$$\rho=kR$$

then Eq. (4) becomes

$$d^2\mathfrak{R}/d\rho^2+[1-l(l+1)/\rho^2-(2\mu/\hbar^2)k^{-2}w(\rho/k)]\mathfrak{R}=0.$$

Everywhere *except* in the immediate neighborhood of the origin, as $k\to 0$ the differential equation becomes

$$d^2\mathfrak{R}/d\rho^2+[1-l(l+1)/\rho^2]\mathfrak{R}=0$$

because of Eq. (7). This has the general solution

$$A\rho^{\frac{1}{2}}J_{l+\frac{1}{2}}(\rho)+B\rho^{\frac{1}{2}}J_{-l-\frac{1}{2}}(\rho).$$

To satisfy Eq. (5), it is necessary that $B=0$. Hence, as $k\to 0$,

$$\mathfrak{R}\to A\rho^{\frac{1}{2}}J_{l+\frac{1}{2}}(\rho)$$

for all $\rho>0$. *At* the origin, as $k\to 0$, $\mathfrak{R}$ is continuous, but not all of its derivatives are.

As $\rho\to\infty$, this expression for $\mathfrak{R}$ becomes

$$A(2/\pi)^{\frac{1}{2}}\cos(\rho+\delta),$$

where δ is some real number. Thus, to satisfy Eq. (6),

$$A=(\pi/2)^{\frac{1}{2}}.$$

Finally, then, as $k\to 0$,

$$\mathfrak{R}\to(\pi kR/2)^{\frac{1}{2}}J_{l+\frac{1}{2}}(kR).$$

The latter, in turn, when expanded in a power series in k, yields a constant multiple of

$$(kR)^{l+1}$$

as the first term.

But if in Eq. (4) we replace k by $-k$, the equation is unaltered, and therefore the solution which now satisfies the boundary conditions must be a constant multiple of the original $\mathfrak{R}$. It then follows by the usual argument that $\mathfrak{R}$ is either an even or an odd function of k. But we have already seen that $\mathfrak{R}\sim(kR)^{l+1}$ as $k\to 0$. Hence, $\mathfrak{R}$ must have the asymptotic form

$$\mathfrak{R}=k^{l+1}[f_0(R)+f_2(R)k^2+f_4(R)k^4+\cdots]. \quad (8)$$

The larger of the wave numbers of the incident and emergent waves, which we call k', is related to k by energy conservation:

$$k'=(k^2+k_0^2)^{\frac{1}{2}},$$

where k_0^2 is a positive constant proportional to the energy which is exchanged between the translational and internal motions during the collision. Hence, any function of k', when expanded in a power series in k, will yield a series with a nonvanishing constant term which contains only *even* powers of k. In particular, this is true of the functions $\mathfrak{R}_{k',l'}(k'R)$ and $(k')^{-1}$. Thus, from Eqs. (3) and (8), the inelastic collision probability p must have the form

$$p=k^{2l+1}(a_0+a_2k^2+a_4k^4+\cdots), \quad (9)$$

which is the desired result.

Equation (9) can be tested by the Jackson-Mott[6] solution of Zener's[4] S-wave problem. There p was found to be proportional to

$$(k'^2-k^2)^2\frac{\sinh\eta k'\sinh\eta k}{(\cosh\eta k'-\cosh\eta k)^2},$$

where η is some constant. When expanded in powers of k, with $k'=(k^2+k_0^2)^{\frac{1}{2}}$, it has precisely the form of Eq. (9) with $l=0$.

One immediate result of Eq. (9) is that near the threshold for excitation (de-excitation) those collisions with emergent (incident) S-waves are the ones which are by far the most likely to be inelastic.[7]

Note that this discussion has been based on the implicit assumption that $k\neq k'$, i.e., that the contemplated transition be between states of unequal energy. The cases which were excluded from consideration in the first paragraph of Sec. I, are precisely those in which $k=k'$.

III

Equation (9) has an interesting consequence in the collision theory of bimolecular reaction rates.

If the probability p of a certain transition taking place in a collision depended only on the initial relative translational energy ϵ and the initial impact parameter b, the average transition probability per unit time would be proportional to[2]

$$T^{-\frac{1}{2}}\int_0^\infty\int_0^\infty pe^{-\epsilon/RT}\epsilon b\,d\epsilon db, \quad (10)$$

where R is Boltzmann's constant and T the absolute temperature. The energy ϵ is related to the incident wave number κ by

$$\epsilon=\hbar^2\kappa^2/2\mu. \quad (11)$$

We wish to rewrite Eq. (10) in a quantum mechanical form. By Eq. (1), the impact parameter b, the wave number κ, and the quantum number of the initial relative angular momentum, λ, are related by

$$\lambda+\tfrac{1}{2}=b\kappa.$$

Thus, to obtain a quantum mechanical expression for the average transition probability per unit time, one must replace

$$2\int_0^\infty\cdots bdb \quad (12)$$

[6] J. M. Jackson and N. F. Mott, Proc. Roy. Soc. (London) **A137**, 703 (1932).

[7] Thus, what Oldenberg[3] calls "central collisions," which are the most effective excitation collisions near the threshold, must be emergent-S-wave collisions.

in Eq. (10) by

$$\frac{1}{\kappa^2}\sum_{\lambda=0}^{\infty}\cdots(2\lambda+1). \tag{13}$$

But even classically p does not depend only on ϵ and b, but also on a third collision parameter. Quantum mechanically, the third parameter is μ_λ, the quantum number of the component of the initial relative angular momentum along some axis fixed in space. The number μ_λ may take any of the $2\lambda+1$ integral values between $-\lambda$ and λ, inclusive. Thus, it is clear that the expressions (12) and (13) should, in turn, be replaced by

$$\frac{1}{\kappa^2}\sum_{\lambda=0}^{\infty}\sum_{\mu_\lambda=-\lambda}^{\lambda}\cdots. \tag{14}$$

Then by Eqs. (10) and (11), the average transition probability per unit time is proportional to

$$T^{-\frac{1}{2}}\sum_{\lambda=0}^{\infty}\sum_{\mu_\lambda=-\lambda}^{\lambda}\int_0^{\infty}pe^{-\epsilon/RT}d\epsilon. \tag{15}$$

Again letting k be the smaller of the incident and emergent wave numbers, we see that since p is zero below the threshold, the expression (15) is itself either proportional to

$$T^{-\frac{1}{2}}\sum_{\lambda=0}^{\infty}\sum_{\mu_\lambda=-\lambda}^{\lambda}\int_0^{\infty}p\exp(-\hbar^2k^2/2\mu RT)kdk \tag{16}$$

in the case of de-excitation, or to the expression (16) multiplied by

$$\exp(-\hbar^2k_0^2/2\mu RT) \tag{17}$$

in the case of excitation. In the latter case, the factor (17) makes up part of the factor which contains the activation energy. In *either* case, according to the collision theory, the pre-exponential factor in a bimolecular rate constant is proportional to the expression (16).

We have been using the symbol l for the angular momentum of the less energetic of the incoming and outgoing waves. In case of de-excitation, this would be the initial angular momentum, and l is then the same as λ in Eq. (16). In this case, then, the summation is over all values of l. In the case of excitation, l is the outgoing angular momentum; but any given l will in general be produced by *some* pair of initial values λ, μ_λ, so the summation in Eq. (16) is again, effectively, over all l.

It then follows from Eqs. (9) and (16) that the pre-exponential factor in a rate constant is a power series in the temperature, starting with a constant term (corresponding to $l=0$). This may be quite different from the usual $T^{\frac{1}{2}}$ temperature dependence found in the simple collision theory.

Usually the temperature dependence is found from an expression analogous to (10), where it is assumed that

$$\int_0^{\infty}pbdb$$

is zero for ϵ below the threshold, and *a positive constant* thereafter. The typical $T^{\frac{1}{2}}$ dependence then follows. We have seen, however, that the assumption of constancy is, in general, unjustified, the correct dependence on energy being that given by Eq. (9).

However, it is certainly possible that p, as given by Eq. (9), will rise very rapidly from its threshold value of zero, to some approximately constant value, as k increases. It is clear that this is more likely to be the case when k_0^2 is small than when it is large. Thus, if the rate-determining transition from reactant to product involves an energy exchange which is very small compared to RT, the power series for the pre-exponential factor might very well be given approximately by $T^{\frac{1}{2}}$ down to fairly low temperatures. At sufficiently low temperatures, however, this must break down. The implication, then, is not that the classical result is of necessity incorrect, but rather that it must be used with caution. Also, it is to be noted that these conclusions, insofar as they concern chemical reaction rates, definitely presuppose the (doubtful) applicability of the collision theory formalism.

Experiments on the Carnauba Wax Electret*

ROBERT GERSON†‡ AND J. H. ROHRBAUGH
New York University, Washington Square College, New York, New York

(Received March 8, 1954)

The strength of the applied electric field, the thickness of the slab being electrified, the time of electrification and the low temperature holding time before removing the field were varied for carnauba wax electrets. After approximately one hour the discharge current varied inversely as a power of the time since turning off the forming field, the power being close to one. The magnitude of this current depended on both the forming field strength and on the thickness of the electret. A very large discharge was obtained when the wax was electrified and discharged while not completely solid.

Dielectric constant measurements were made at temperatures between 27°C and 86°C, frequencies between 50 cps and 13 kc, and with superposed dc field strengths in the wax of zero, 3700 and 8100 volts per cm. The application of dc field was found to raise the dielectric constant at the higher temperatures.

The case for permanent dipole orientation and that for ionic space charges as the cause of the stored charge of the electret is examined, and it is shown that there are objections to each mechanism. An alternate explanation is suggested.

INTRODUCTION

THE theories of the electret effect published to date attribute the effect to two different field-producing mechanisms which are superposed in such a way that first one and then the other predominates. The most widely held theory today is that the homocharge is a real volume and surface charge distribution which is conducted into the wax from the electrodes during the electrification process. This charge is thought to be masked initially by a heterocharge which by decaying rapidly allows the homocharge to become observable. This theory is based on the experimental work of Mikola,[1] Thiessen *et al.*,[2] and, more recently, of Gross[3–5] who linked the electret with the general problem of reversible charge absorption in solid insulators.

SCOPE OF THE PRESENT INVESTIGATION

The experiments reported here were designed with a view toward obtaining further insight into the source of the heterocharge, this being perhaps the most important question still to be resolved. It has been attributed to ionic space charges within the wax[6] and also to a hindered molecular dipole rotation,[3] but neither of these ideas seems completely satisfactory.

Comparison between many of the experiments reported in the literature is unsatisfactory because various experimental conditions do not appear in sufficient detail and also because of the variety of substances used. Thus it seemed desirable to perform a reasonably complete set of experiments in a more reproducible manner and on a single substance. All of the experiments reported here were done on a single batch of the chosen substance, pure carnauba wax, and an effort is made to report the pertinent experimental procedures. It was found that reproducible data could be obtained only when an electrification procedure introduced by Gross[4] was used, i.e., electrification slightly below melting temperature.

Among the conditions varied were the forming field strength,[2] the thickness of the dielectric, the length of the high temperature electrification period, the holding time in the electric field at low temperature,[4] the temperature of discharge, and the electrode material.[5] In addition the current discharges both from electrets neutralized by iron filings and from partially liquefied electrified waxes were investigated. Experiments were also done on electrets composed of two, or three, superposed wax slabs. The complex dielectric constant of the wax used was determined over a range of temperature and of frequency for several values of applied dc electric field strength.

EXPERIMENTAL PROCEDURE

It was not found possible to make electrets reproducibly by allowing the liquid wax to solidify and cool in a mold with an electric field applied, the procedure used by early experimenters. It was found that much better reproducibility (about $\pm 10\%$) could be obtained by utilizing a single thoroughly mixed batch of the wax which had been heated to drive off occluded moisture and gas, filtered through glass wool, cast into disks and then machined to the desired size and to a good surface finish. Special care was taken during the solidification of the wax slabs to avoid inhomogeneities, internal stresses, and air bubbles. Reproducible electrets were obtained when these slabs were electrified in a well controlled oven at 71°C, a few degrees below the softening point of the wax.

The electrification procedure was:

* This work was supported in part by Air Force Cambridge Research Center, Contract AF19(604)–407 administered by L. M. Hollingsworth.

† This paper is part of a thesis submitted by Robert Gerson in partial fulfillment of the requirements for the degree of Doctor of Philosophy at New York University.

‡ Now at Erie Resistor Corporation, Erie, Pennsylvania.

[1] S. Mikola, Z. Physik **32**, 476 (1935).
[2] Thiessen, Winkel, and Herrmann, Physik. Z. **37**, 511 (1936).
[3] B. Gross, Phys. Rev. **66**, 26 (1944).
[4] B. Gross and L. F. Denard, Phys. Rev. **67**, 253 (1945).
[5] B. Gross, J. Chem. Phys. **17**, 866 (1949).
[6] A. Gemant, Phil. Mag. **20**, 929 (1935).

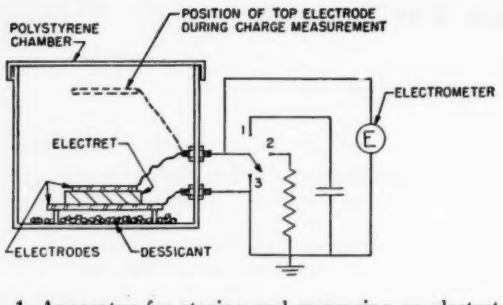

FIG. 1. Apparatus for storing and measuring an electret. The switch is in position 1 during a charge measurement, position 2 during a discharge current measurement, and position 3 during storage.

1. The wax was placed between metal plates in an air oven maintained at 71°C±0.2°C and a 45 minute period was allowed for the wax to reach thermal equilibrium.

2. The electric field was applied to the wax. In the experiments in which we were comparing electrets of different thicknesses, the temperature was then held at 71°C for five hours. This long period was used to minimize the effect of the greater thermal inertia of the thicker specimens. In experiments where only electrets of the same thickness were to be compared, a one hour period at 71°C was used. This was established experimentally as a sufficiently long electrification time.

3. The oven cooled, at a rate of 0.5°C per minute, from 71°C to 41°C and then was opened to the air at room temperature.

4. The electret was held in the electric field for several hours at room temperature and was then placed in a constant temperature box at 26.7°C±0.2°C. The forming voltage was left on for sixteen hours more.

5. The forming voltage was removed.

After electrification the electrets were stored and measured at constant temperature (26.7°C) since, as has frequently been observed by various investigators, the discharge current from an electret is extremely dependent upon its temperature, the current varying by a factor of as much as two for a temperature change of several degrees. The area electrified was 11 square centimeters.

The measurements ordinarily made on electrets are determinations of the surface field (or charge) and of the discharge current. The usual method of charge measurement[5,7] (lifting an electrode from one surface and observing the induced charge with an electrometer) has the disadvantages that it involves a temporary unshielding of the electret, a process which may affect both the charge of the electret and its subsequent behavior and that it is likely to be simply a measurement of the dielectric strength of air. Useful information can also be obtained by measuring the discharge current, this having the advantage that it does not require unshielding of the dielectric. The discharge current equals the rate of change of surface charge, the charge leakage from the wax surface to the shield being negligible as was shown by Gross[5] and confirmed by us. (Our measurements do show a possible leakage of the order of 10^{-14} ampere.) We have therefore measured the discharge current primarily, although measurements of charge were also made. The measurement procedure involved connecting the top and bottom plates of the electret shield through a high resistance (10^{9}–10^{12} ohms) and measuring the resulting potential difference, which was one volt or less, with a Lindemann electrometer (Fig. 1).

The discharge current when the wax was hot and partially liquefied was much higher than the above and was measured directly with a type *P* wall galvanometer. For such experiments the wax was held between two electrodes, one grounded and the other guarded, in a hard rubber cup.

All of the electrets made during our study had a heterocharge immediately after the forming voltage was turned off, and all developed homocharges during storage. The homocharge attained with electrets made at high voltage (10 kv per cm or more) was high enough to cause an electric field strength of at least 50 kv per cm in the air gap between the electret's surface and its shield. While some of the electrets temporarily exceeded this figure, the field after two or three months was usually within 25% of 50 kv per cm. The electrets which were made with a forming field of 5 kv per cm did not develop quite as high a homocharge as the others. The electret which developed the highest charge was the one made with the highest field strength (25 kv

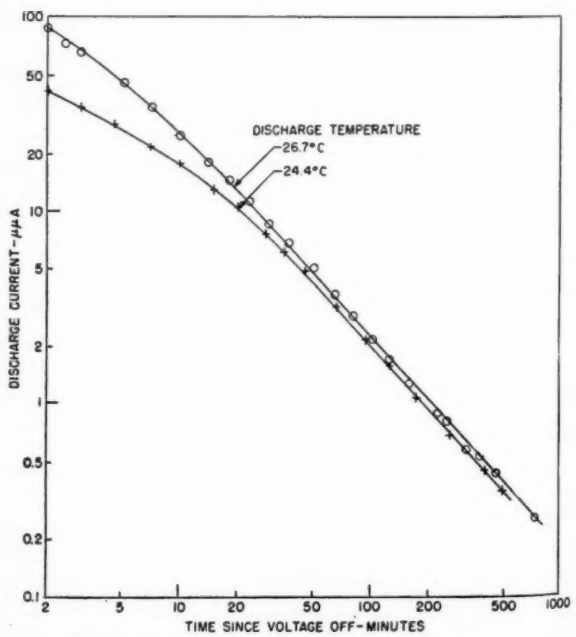

FIG. 2. The discharge currents from electrets discharged at two slightly different temperatures. The high temperature electrification was the same for both electrets. The dielectric thickness was 2 mm, and the voltage 2000 volts.

[7] F. Gutmann, Revs. Modern Phys. **20**, 457 (1948).

per cm). It developed a total charge of 74 millimicrocoulombs, corresponding to a surface field of 70 kv per cm. The field still had this value after two months of storage.

In one of our experiments the discharge temperature during the entire run was held about two degrees below the usual discharge temperature (Fig. 2). Very surprisingly the discharge was markedly decreased only for a short period of time following the removal of the forming field. After about one hour the current became almost equal to that from the usual electret at the corresponding time, and it remained so during the rest of the experiment.

THE EXPERIMENTS

1. The Discharge from Electrets Made Under Various Conditions

Curves of discharge current as a function of the time since the voltage was turned off, for electrets 2 mm thick and made at different voltages, are given in Fig. 3. It will be noted that after an initial period of an hour or less, depending upon the forming voltage, the relationship between current and time becomes the typical

$$i = C/t^n \qquad (1)$$

for discharging dielectrics, where i = discharge current, t = time, and C, n = constants.

The value of n is fairly close to unity in all cases, ranging from about 0.85 for the electret made at 25 kv per cm to 1.17 for the one made at 5 kv per cm. There is no evidence of any voltage saturation effects in these discharge currents, the use of higher forming voltages always resulting in sensibly greater discharges.

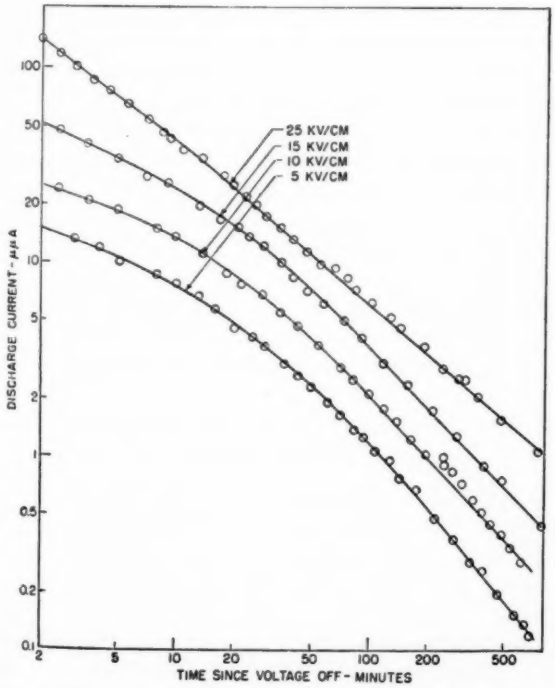

FIG. 3. The discharge currents from electrets 2 millimeters thick made with different voltages. (The discontinuity which occurred about 200 minutes after the voltage was turned off on the electret made at 10 kv per cm was due to the making of a charge measurement and is typical.)

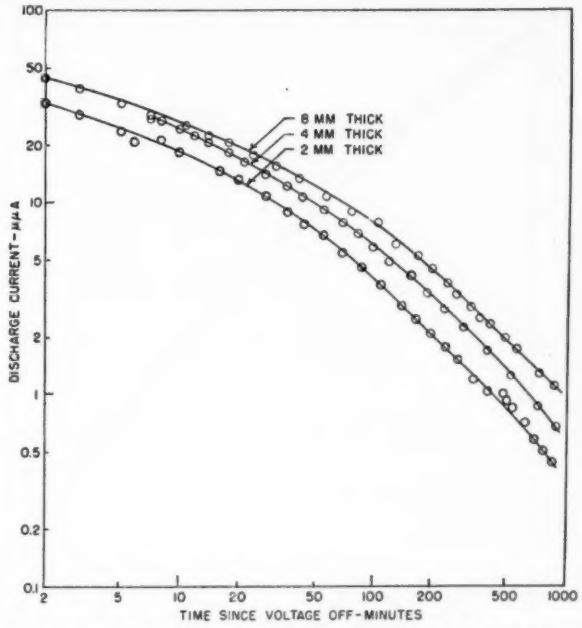

FIG. 4. The discharge currents from electrets of different thicknesses, all made at a field strength of 10 kv per cm.

Electrets of different thickness but made at the same field strength yielded significantly different discharge curves (Fig. 4). Since these measurements were made without using guard rings, larger discharge currents must be expected for the thicker electrets. The observed divergence between specimens of different thicknesses cannot be due entirely to this cause, however, because the ratio of the currents varied with time. This ratio, for example, after correcting the data for the absence of guard rings, has the predicted value of 1.3 between the 2-mm and 8-mm electrets at the first minute but the ratio rises to 2.8 in ten hours. Five hour processing schedules were used in manufacturing these electrets in order to eliminate thermal differences between thick and thin electrets. These schedules were surely more than adequate in view of the experimental measurement of a 3-minute thermal time constant for a 4 mm thick electret. It was further determined that a one-hour schedule gave almost identical results within the limits of reproducibility. Thus the curves show that there is some component of the electret's behavior which depends on its thickness. This excludes any explanation of the electret which is based completely on a uniform polarization.

It should be remarked that carnauba wax changes its properties with age. The electrets from freshly made wax slabs show a much lower initial discharge current than do electrets from aged wax slabs from the same batch of wax, although after about an hour the currents become equal and remain so. This makes it necessary to

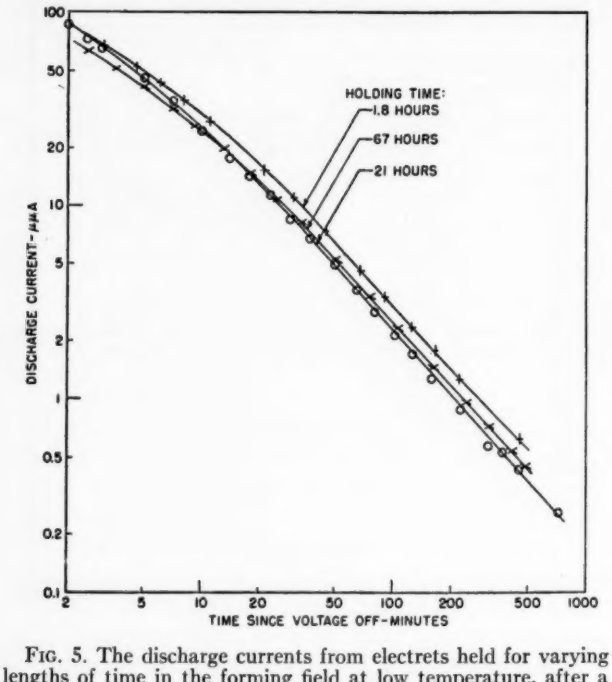

FIG. 5. The discharge currents from electrets held for varying lengths of time in the forming field at low temperature, after a high temperature electrification. The dielectric thickness was 2 mm, and the voltage 2000 volts.

run experiments on slabs of the same age if the results during the first hour or so are to be compared.

The theory of the electret put forth by Gross[3,4] assumes a volume and surface charge distribution near an electrode of the same sign as the electrode charge. It is this distribution that is assumed eventually to cause the homocharge. The forming field of course exerts a force on this charge which tends to drive it away from the electrode and thus to neutralize it. One might, on this basis, expect that an electret held in its forming field at low temperature for a long time would not show as great an eventual discharge as one discharged shortly after manufacture. This thesis was tested with three electrets whose holding periods in the forming field were significantly different (Fig. 5). The discharge from the electret with the shortest holding time was slightly but significantly stronger than that from the other two electrets. It thus appears that loss of electrification over the range of holding times studied is quite small.

One experiment was run using a gold plated set of electrodes in place of the usual brass ones. The discharge currents were initially identical but the current from the electret made with gold electrodes was slightly the larger thereafter. Other experimenters have also found that changing the electrode metal has little effect.[5]

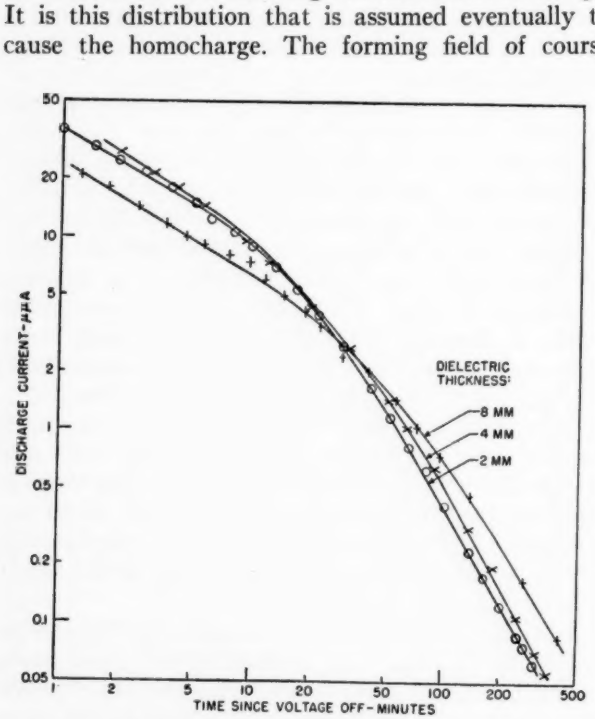

FIG. 6. The discharge currents from wax slabs of different thicknesses electrified at 27°C. The field strength used was 5 kv per cm and it was applied for one hour. Guard rings were used.

2. The Discharge from Wax Electrified at Low Temperature

A piece of wax electrified at room temperature exhibits a long-lived discharge current which corresponds, as usual, to either a decreasing heterocharge or a growing homocharge. The initial discharge current from a piece of carnauba wax electrified at room temperature is about the same as that from a thermally treated electret made at the same voltage, but the discharge from the former falls off so rapidly that it is negligible after a few hours (Fig. 6). In wax treated in this manner, it is known that whatever homocharge leaks over during electrification remains at the wax surface and consequently causes no internal electric field. The discharge current observed here should thus be entirely a heterocharge effect. The fact that the discharge curves are different for the three electret thicknesses used again indicates that the heterocharge is not due completely to a uniform polarization. As closely as can be estimated from the data, the total discharges from the 2 mm and the 8 mm slabs are equal, being about 20 millimicrocoulombs during the time of the measurement.

3. The Discharge from an Electret Neutralized by Iron Filings

An electret was removed from the usual shielding electrodes and quickly immersed in iron filings. This of course represented an interruption of the shielding but, being of only several seconds duration, it was not a sufficient interruption to change the surface charge significantly, and the filings represented a new shield. After several hours the filings were removed and the electret restored to the usual shield. Charge measurements made by the lifting electrode procedure then showed the electret's charge to be too small to measure although not quite zero. Charge measurements were

repeated at suitable intervals over the next several days and they showed a slow restoration of the surface polarization but only to about 80% of its original value. It must be pointed out that similar breaks in the continuity of shielding but with smooth electrodes, or even complete unshielding for a similar total time, show a comparatively negligible effect on the surface polarization.

In another experiment filings were applied between both surfaces of an electret and its electrodes. The electret was one month old and consequently had a very low discharge current. The electrodes were connected through a current-measuring instrument (Fig. 7) to secure an indication of the quantity of electricity associated with the depolarization. The current measured was in the same direction as, and was initially about one thousand times larger than, the ordinary electret discharge current at an age corresponding to the time of the experiment. The current variation with time was much like the discharge current from a new electret, and the total discharge from the beginning of the experiment until ten hours later was about ten millimicrocoulombs. It should be pointed out that if the iron filings had been removed from the electret and its charge measured at any time during this experiment, the measured charge would have been found to be almost zero. The measured discharge thus represents a decay of the internal (masked) polarization of the wax.

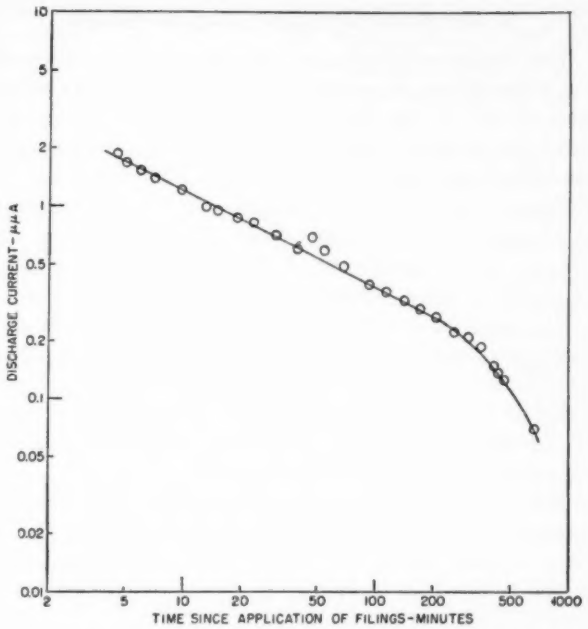

FIG. 7. The discharge current from an electret one month old when iron filings were applied to its surface.

4. The Discharge from a Partially Frozen Wax Melt

The magnitude of the discharge from electrified wax is known to depend on the temperature at which it is charged and also on that at which it is discharged. If it is both charged and discharged at the same temperature, the discharge will be greater at the higher temperatures[8] but no discharge will be observed if the temperature exceeds a temperature lying in the semimolten range. In one series of our experiments the discharges from wax in this transition range between liquid and solid were measured (Fig. 8). This was done by cooling the wax over a period of several hours in an applied field of 10 kv per cm from an initial molten state to a temperature at which the current through it was about 4% of its original value. The field was then turned off and the wax allowed to discharge through a galvanometer. The total discharge exceeded greatly any of the discharges measured from completely solid wax, being more than ten times higher than that from solid wax which was near to softening temperature and was electrified in the same field. Previous experimenters[8,9] have reported discharges of the same magnitude from electrets which were quickly heated through the melting point. The discharge under these conditions was not isothermal. On the other hand our results were substantially isothermal and yielded a discharge curve similar in form to the electret depolarization curve at low temperature. This similarity is believed to signify that similar processes occurred in both depolarizations.

It was found that the discharge under the same conditions from a melt consisting of 25% by weight of Pentalyn H§ and 75% of carnauba wax was several times larger than that from pure carnauba wax. An attempt was made to make an electret from Pentalyn H, but it was unsuccessful.

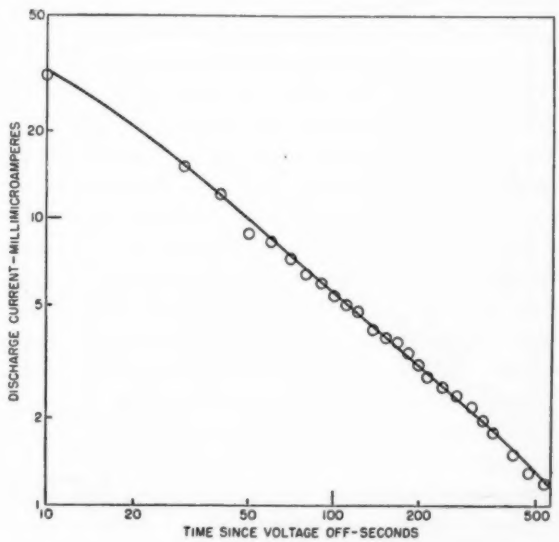

FIG. 8. The discharge current from an electrified carnauba wax melt. The electrode area was 10 square cm.

[8] H. Frei and G. Groetzinger, Physik. Z. **37**, 720 (1936).
[9] G. Groetzinger and H. Kretsch, Z. Physik **103**, 337 (1936).

§ A pentaerythritol abietate resin manufactured by the Hercules Powder Company.

5. Dielectric Constant Measurements

Two regions of dielectric absorption associated with the temperature of carnauba wax were found by Wiseman *et al.*[10] in the frequency range 0.5 kc to 30 kc. They found furthermore that the dielectric constants of electrified and unelectrified wax were not significantly different. They attribute a low (room) temperature absorption to a permanent dipole polarization and the other, high temperature (58°C) absorption to charge conduction. Both explanations are probably correct.

We have made dielectric constant measurements at various temperatures from room temperature to liquid wax, from 50 cps to 13 kc and with and without a superposed dc field of 8100 volts per cm. Where our measurements overlap those of Wiseman, the agreement is reasonable for different wax samples.

The dc field produces no observable effect on the complex dielectric constant of wax below 50°C, on an electret made in the field at high temperature and held in the field while cooling to a measurement temperature of 27°C, nor on the liquid wax. However, both the real and the imaginary parts of the dielectric constant are increased markedly by the dc field at temperatures between 50°C and the softening temperature (Fig. 9) in the frequency range for which charge conduction polarization is postulated. This result confirms the postulate of charge conduction since the dc field would be expected to create additional charge carriers.

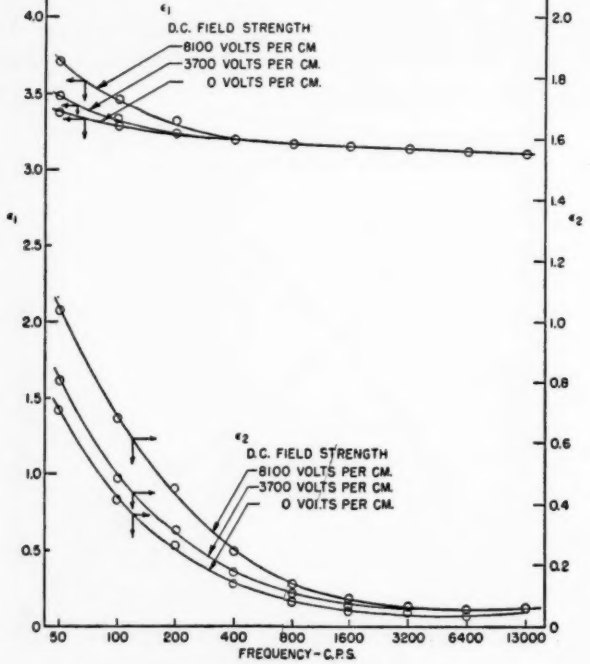

FIG. 9. The real (ϵ_1) and imaginary (ϵ_2) parts of the dielectric constant as a function of frequency at several values of dc field strength for carnauba wax at 69°C.

[10] University of Kansas, Research on Electrets, Final Report, Contract No. Da 36-039, sc 5467 (August 31, 1954).

A further series of measurements of the complex dielectric constant were made on a single wax slab at 27°C and over the above frequency range. Several runs were first made on the unelectrified wax in order to determine the internal consistency of the data. The slab was then heated to 69°C and the 8100 volts per cm field applied in order to make an electret. The electret was held in this field as the wax was slowly cooled back to 27°C. New measurements of dielectric constant, with the dc field still applied, showed no observable change in either ϵ_1 or ϵ_2 anywhere in the frequency range. The internal consistency of the data was approximately 2% for ϵ_1 and 5% for ϵ_2. This result shows that dipole orientation must be very small at this field strength, one sufficient to make an electret. The dielectric strength of the available bridge forbade extending these measurements to higher field strengths.

Large increases in dielectric constant were also reported by McMahon[11] for certain polar impregnants when below their melting temperatures. His increases disappear at approximately −5°C,[12] in apparent correspondence with our disappearance at 50°C.

6. Multilayer Electrets

Charge measurements were made on a series of electrets, each consisting of either two or three 2 mm thick slabs superposed. During forming, wax-to-wax contact was used in some cases and mica insulation between wax faces or between the electrodes and the wax in others. The charge data obtained was not consistent, due perhaps to the necessary handling of the slabs. All of the slabs became electrets, but weaker than would have been obtained for the same slabs taken one at a time and at the same field strength. No conclusions could be drawn regarding the charge distribution within the wax.

CONCLUSIONS AND DISCUSSION

The theory that the homocharge is caused by conduction into the dielectric[2,4] seems to prevail at present, being supported by many pieces of experimental evidence. According to this theory the homocharge leaks in from the electrodes as a compensating charge which partially masks the external effects of the heterocharge. The theory does not explain the nature of the large observed heterocharges.

Two plausible mechanisms have been suggested as explanations of the heterocharge. These are the hindered orientation of permanent dipoles[3] and the existence of ionic space charges.[6] It is probable that both mechanisms are operative to some extent, but the data suggest that neither is important. In regard to the first of these, and in the affirmative, it must be expected that dipole orientation of polar substances will make some contribution to a heterocharge, even if not a

[11] W. McMahon, Annual Report 1948 Conference of Electrical Insulation, 84.

[12] W. McMahon (private communication).

dominant one, and all of the substances reported as making strong and permanent electrets have been polar. The notion that the heterocharge is due mainly to dipole polarization rather than to space charges is also appealing when considered in conjunction with the theory that the homocharge is a true space charge. If the heterocharge were also a space charge, a situation would exist where two strong charges of opposite polarity and in close proximity do not move to neutralize each other, despite internal fields calculated to be in excess of 100 000 volts per cm. On the other hand, a heterocharge due to dipole polarization could coexist with a space charge.

Objections to the dipole hypothesis exist.

1. The magnitude of the currents measured while discharging the partially solidified wax indicates a polarization so large that one quarter or more of the available dipoles (an extremely high percentage) would have to be oriented in the direction of the field to account for it. This figure is based on the magnitude of the total discharge, about 2 microcoulombs, and an assumed dipole moment of 2×10^{-18} esu cm for the ester molecule.

2. The fact that the dielectric constant of an electret is about the same at room temperature as that of an unelectrified wax slab (Sec. 5) indicates that the amount of dipole alignment present in the electret is small, in sharp contrast to 1 in the foregoing.

3. The relaxation time of pure heterocharge in at least one type of experiment is about ten minutes as can be estimated from the data of Sec. 2. However, dipole orientation in ordinary solids occurs at radio-frequency rates and even in carnauba wax, which has very large molecules, it seems unlikely that the time constant would be so very high.

These objections to the dipole theory are sometimes met by postulating the existence of domains of oriented dipoles,[7] analogous to the domains in ferromagnetic effects, which act to increase both the effective dipole moment and the relaxation time. The existence of such domains has been inferred from observation of electrical pulses or small discontinuities in the discharge current from an electret, when it is heated. A considerable range of pulse sizes has been observed.[13] According to the domain theory, such pulses are due to a large number of dipoles in a domain changing their orientation simultaneously. The possibility must be pointed out, however, that the observed pulses may be caused by electrical discharges inside the wax.

Neither the dipole theory nor the space charge theory seem able to account for our observation that the discharge current from an electret is temporarily increased by several orders of magnitude following the application of iron filings to its surface (Sec. 3). This discharge and the recovery of charge that follows seem to require a very permanent internal polarization which produces a true surface charge.

Another explanation of the entire electret effect may be offered, depending on the existence of "traps" for charge carriers in electret forming substances. Simultaneously with the formation of heterocharge, electrons would move into traps and be frozen in during the cooling of the wax. Thus dipoles having little effect on the dielectric constant would be produced, as is observed, and, since the external fields of these dipoles would tend to annul the applied field, little alignment of permanent molecular dipoles would occur, as also is observed from the dielectric constant data. The rate at which electrons can go into traps must be temperature dependent so these can be produced quickly only at an elevated temperature.

The experimental observations of Chatterjee and Bhadra[14] who found a very large increase in the dielectric constant of electrified carnauba wax accompanied by a similar increase in loss tangent during the period of time between two and ninety days after electrification, are not inconsistent with the trap hypothesis. It is well known that similar phenomena occur in many trap-containing materials under conditions in which a high charge carrier density is produced.

A "sandwich" electret should be simply several electrets, and this is observed. Furthermore, mica between electrodes and the wax should reduce but not annihilate the phenomenon, and this too is observed.

An external field, if applied to a cold electret in the direction of the forming field, should produce a current in the charging direction provided that the applied field is large enough to reverse the internal field. This experiment was done and the reverse current occurs if the applied field is about half, or more, of the original forming field. The reverse current decays rapidly and reverses again after several minutes.

The above is necessarily tentative, since not enough is known of either charge conduction or trap levels in electret forming materials to allow a firm basis for such theories. It does, however, offer an explanation for a heterocharge of the observed magnitude which does not require the presence of large internal electric fields. A theory which is similar in many respects to the one proposed has recently been offered by Kallmann and Rosenberg[15] to account for polarization effects in phosphors subjected to irradiation and static electric fields. We feel that these ideas are well worth keeping in mind in the planning of future experiments such as, for example, experiments with radiation of sufficient energy and penetration to release trapped charges in carnauba wax. One such experiment would be to attempt the manufacture of an electret with intensive x-ray irradiation replacing the usual thermal treatment. The experiment could be done in a high vacuum to avoid ionization of ambient gases by the x-rays. Under

[13] N. P. Bauman and G. G. Wiseman, J. Appl. Phys. **25**, 1391 (1954).

[14] S. D. Chatterjee and T. C. Bhadra, Phys. Rev. **98**, 1728 (1955).

[15] B. Rosenberg and H. Kallmann, Phys. Rev. **97**, 1596 (1955).

these conditions the dipole hypothesis would permit the formation of only the weak room-temperature electret, while hypotheses based on charge carriers would predict the possibility of a stronger electret being made under irradiation than without it.

ACKNOWLEDGMENTS

Our thanks are due Professor Hartmut Kallmann, for many fruitful discussions and suggestions, and Mr. Richard F. Wood and Mr. Richard Chrenko for their invaluable help in performing the experiments.

THE JOURNAL OF CHEMICAL PHYSICS VOLUME 23, NUMBER 12 DECEMBER, 1955

Line Broadening and Dielectric Relaxation in Compressed Gases*

C. S. E. PHILLIPS†
Laboratory for Insulation Research, Massachusetts Institute of Technology, Cambridge, Massachusetts
(Received January 24, 1955)

An attempt is made to investigate the transition from resonance to relaxation spectrum by high-pressure research in the microwave region. Equipment has been developed for studying the dielectric constant and loss of gases and liquids in the K-band region up to 1000 atmospheres at temperatures up to 300°C. Measurements on a nearly spherical molecule of strong dipole moment ($CHClF_2$), on a linear molecule of weak dipole moment (N_2O), and on mixtures of $CHClF_2$ with nitrogen are reported and a preliminary discussion of the results is given.

IN gases, one finds resonance spectra extending from the far ultraviolet into the microwave region. By condensing gases to liquids and solids, the spectral range from microwaves to dc, previously empty, fills up with relaxation spectra. These spectra are broad and frequently hard to interpret. By observing the transition from gases to liquids with high-pressure techniques, much might be learned about the interaction of molecules leading to this change from resonance to relaxation. The Laboratory for Insulation Research is engaged in dielectric spectroscopy over the electric and optical frequency region, where this question of the transition from the gas state to the condensed phases is a key problem of molecular analysis. This is one reason why the present investigation was undertaken.

Very little is known in this field, theoretically or experimentally. At the one extreme, resonance absorption in gases at pressures up to a few centimeters of mercury is now well understood. At the other extreme, the general behavior in liquids has been a subject for research for many years but the complicated nature of liquid structure has made a detailed molecular interpretation of dielectric relaxation difficult. The second purpose of our research is therefore to investigate how far experiments on highly compressed gases and liquids lead to a better understanding of dielectric relaxation phenomena.

As far as we are aware, the only other experimental study on dielectric constant and loss to high pressures is that of David, Hamann, and Pearse[1] who measured CH_3F up to 160 atmospheres at a frequency of 1 Mc/sec. A sudden rise of the dielectric loss occurred when the critical density was reached. Above the critical temperature a smooth transition was observed from gas-like to liquid-like behavior.

EXPERIMENTAL APPROACH

For rotation spectra as well as for dielectric relaxation in liquids, the main range of interest extends from about 10 cm to 0.1 mm wavelength. The present work, intended as a preliminary study of the inherent possibilities of this type of research, has been limited to only one wavelength (1.22 cm). This wavelength was chosen as being short enough to pick up lower rotation lines, while still long enough to allow the use of standard microwave techniques and equipment. The pressure bomb, however, was designed for a possible extension to millimeter waves.

The absorption and dispersion of the gas under test was measured in a resonant cavity, completely enclosed in a pressure bomb (Fig. 1). Microwave energy from a standard klystron passed through a circular wave guide into the bomb via a glass pressure window.[2] The output signal from the resonator passed through a similar pressure window to an intermediate frequency detector. Using a swept local oscillator, an i-f signal is obtained, amplified, and displayed on a cathode ray screen. Within the limits of accuracy, the height of the pip on the oscillograph is proportional to the microwave signal amplitude.

Originally the bomb was designed for an H_{01} type cavity with the base coupling method used by Bleaney,

* Sponsored by the Office of Naval Research, the Army Signal Corps, and the Air Force under Contract N5ori-07801.

† Present address: Ministry of Supply, Radar Research Establishment, St. Andrews Road, Great Malvern, Worcestershire, England.

[1] David, Hamann, and Pearse, J. Chem. Phys. **20**, 969 (1952). See also G. Birnbaum and A. A. Maryott, Phys. Rev. **95**, 622 (1954); J. Chem. Phys. **22**, 1782 (1954) for experiments on CO_2, HCl, and HBr.

[2] T. C. Poulter, Phys. Rev. **40**, 860 (1932).

Loubser, and Penrose,[3] but this arrangment proved inflexible when adjustments had to be made. Greater accuracy and reliability in the measurements should be attainable with a suitably designed H_{10} system using base coupling. The results described here have been obtained with an H_{11} cavity having a straight-forward input and output wave guide. The apparatus is capable of measuring $\epsilon''/\epsilon_0 \equiv \kappa''$ from 0.001 to *ca* 0.03. An attempt to increase the range towards higher losses by partially filling the H_{11} cavity with Teflon proved unsuccessful because the H_{21} mode interfered. With the H_{01} cavity where side coupling is not used, this could probably be done.

The H_{11} cavity has the serious disadvantage that its mode is degenerate. Any ellipticity of the cavity barrel produces a second resonance which must be eradicated by the proper placing of a crosswire. Unfortunately, our work deals with wide ranges of dielectric constant and the positions of the crosswire and of the coupling holes may be satisfactory at one pressure but not at another. An awkward difficulty is that this disturbance of the resonance curve of the cavity is hard to distinguish from stray signal caused by direct coupling between the windows.

The resonator must be removable from the bomb, but perfectly rigid when inside it; yet, allowance must be made for small strains set up under pressure. The apparatus of Fig. 1 was designed on this basis; any strains were taken up by a sliding action of the windows. (These windows constitute roughly a low Q-tuned circuit since the glass was slightly lossy.)

Strain on the micrometer had to be avoided. This was accomplished successfully by an Oldham-type coupling which gave "finger touch" motion to the micrometer head. Since it proved to be extremely troublesome to eliminate direct coupling from input to output window, a better arrangment might have been to insert the output window in the base and to let the Oldham coupling absorb the strains which, in any case, proved less troublesome than expected. Even very efficient screening permits the output windows to pick up from elsewhere than the resonator a tiny signal which may be of the same magnitude as that coming from the cavity when gases of high loss are measured. This leakage was finally eliminated by the simultaneous use of a $\frac{3}{4}\lambda$ folded-back short circuit, beryllium-copper shorting strip, wire wool and absorbent material (carbon impregnated Teflon).

As the micrometer is completely immersed in the gas under test, there is always the possibility of corrosion. The gases and materials for our experiments were chosen with this in mind. Another problem concerns the lubrication of the micrometer spindle. Oil, even silicone oil, will be removed by gases at high pressures. Molybdenum bisulfide powder was used with some success, and the micrometer was frequently removed from the bomb and relubricated when necessary. Fortunately the gases themselves, when compressed, assist in lubrication.

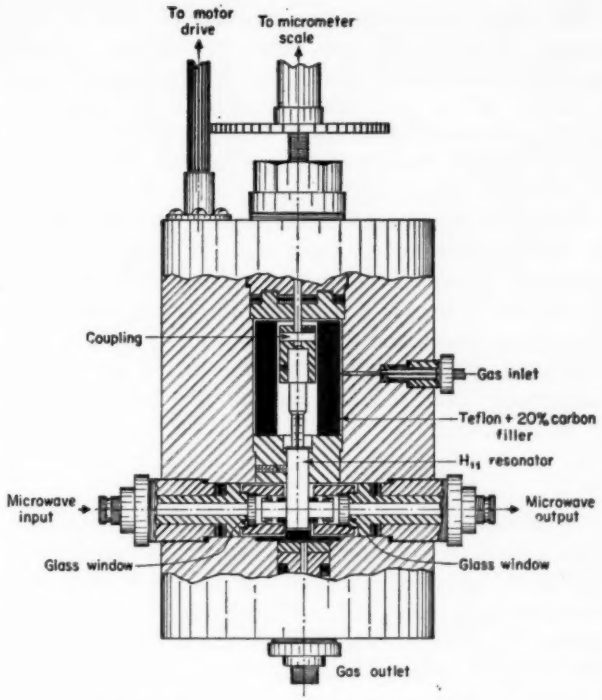

FIG. 1. Microwave absorption pressure bomb.

The micrometer was not read directly but connected via the Oldham coupling to a small rod of hardened steel which in turn was joined to a large diameter rod carrying a second micrometer thread. The latter was cut to the same pitch as the first. Any slight difference in the two threads was taken up by vertical movement in the coupling and the bomb assembled in such a way that the internal micrometer was never forced vertically. In practice, the friction on the small diameter rod proved too great at pressures above 7000 psi. The central Bridgman type seal was therefore replaced, for the experiments at high pressures, by an "O" ring. The resonator was driven by two dc motors and the micrometer drum and revolution counter read with a telescope.

The bomb was designed for 3000 atmos at temperatures up to 300°C, but the maximum pressure used in the experiments here described was 10 000 psi (680 atmos) and the maximum temperature 102°C. The main seals used silicone rubber and were of the Bridgman type. They worked satisfactorily despite the poor mechanical properties of silicone rubber. The unused space within the bomb (black area in Fig. 1) was filled with absorbent (carbon impregnated Teflon) or taken up by a hollow steel cylinder; between resonator and windows ordinary Teflon was inserted. The gas outlet, originally intended as the output window of the H_{01} system, served for flushing the bomb and as an alternative point for pressure measurements.

[3] Bleaney, Loubser, and Penrose, Proc. Phys. Soc. (London) **59**, 185 (1947).

The whole equipment was mounted in a pit in the ground (Fig. 2). Motors, gear mechanism, stirrer, mercury thermoregulator, and thermometer were mounted on a removable, heat-insulated platform which also served as the cover of the temperature bath. The silicone-oil bath was heated by two heater coils, one thermostatically and the other manually controlled.

The pressure system is shown in Fig. 3. Pressures up to 10 000 psi were obtained with an ordinary hand pump; a mercury separator prevented contamination of the gas with oil. This separator has a volume of only 50 ml compared with *ca* 150 ml for the bomb. For more compressible gases a 400 ml piston-type compressor was used, designed in this laboratory by P. W. Forsberg, Jr.

EXPERIMENTAL PROCEDURE

After the oil was heated to the desired temperature, allowance was made for the high thermal capacity of the bomb by a waiting period of several hours before measurements were taken. The results proved not greatly dependent upon temperature and the temperature control was more than sufficient. The whole pressure system was evacuated and then filled with the gas under test. At each pressure, measurements were taken of the resonance position and of the half-power points. The relative dielectric constant κ' and loss factor κ'' were then obtained from the relationship[4]:

$$\kappa' \equiv \epsilon'/\epsilon_0 = 1+\frac{\lambda^2}{\lambda_{g0}^2}\left(\frac{\lambda_{g0}^2}{\lambda_{g1}^2}-1\right)$$

$$\kappa'' \equiv \epsilon''/\epsilon_0 = \frac{2\lambda^2}{n\lambda_{g1}^3}\left[\delta l-\delta l_0\left\{\frac{1+n\lambda_{g1}^3/4a\lambda_c^2}{1+n\lambda_{g0}^3/4a\lambda_c^2}\right\}\right].$$

Here λ is the free-space wavelength (1.22 cm); λ_c the cut-off wavelength of the H_{11} resonator (1.624 cm); λ_{g0} the resonance wavelength *in vacuo* (1.867); λ_{g1} the resonance wavelength in the compressed gas; n the number of half-wavelengths in the resonator; δl and δl_0 the distance between half-power points in the gas and in vacuum, respectively; and a is the radius of the resonator. Pressures were measured by Bourdon gauges, previously calibrated against a dead-weight gauge. For gases with a critical temperature above room temperature, the gas cylinder was heated, thereby distilling the gas into the system. For gas mixtures a different procedure was required. The gases, if successively let into the bomb, will not mix properly without stirring. Since a standard amount of the polar component in each mixture was desired, the following method was used. After evacuating the whole system, with the compressor piston fully up, valve D (Fig. 4) was closed to isolate the bomb. Next, the polar gas (here $CHClF_2$) was admitted up to a standard pressure, for example, 55 psi. After closing valve F, nitrogen was admitted to mix by turbulence in the compressor, and the starting pressure of the mixture P_{mix}^0 read on the 0–2000-lb gauge. After closing valve B, the mixture was pumped into the bomb and measurements were taken at various values of P_{mix}.

As the stored energy of compressed gases can be very large, a liquid was used for initial tests of the pressure equipment. Carbon tetrachloride was selected for this purpose because the molecule is nonpolar, hence no dipole loss is to be expected in the microwave region. However, a small but noticeable loss has been observed in this and several other nonpolar liquids. Whiffen[5] has suggested that this is due to the existence of small semipermanent dipole moments created by the distortion of the chemical bonds as a result of molecular interaction. If such an effect exists it should increase with hydrostatic pressure. At pressures up to 10 000 psi we observed no significant loss increase. However, this may not be surprising as the density change amounts to only *ca* 6%, and our apparatus is not designed for measuring extremely small losses.

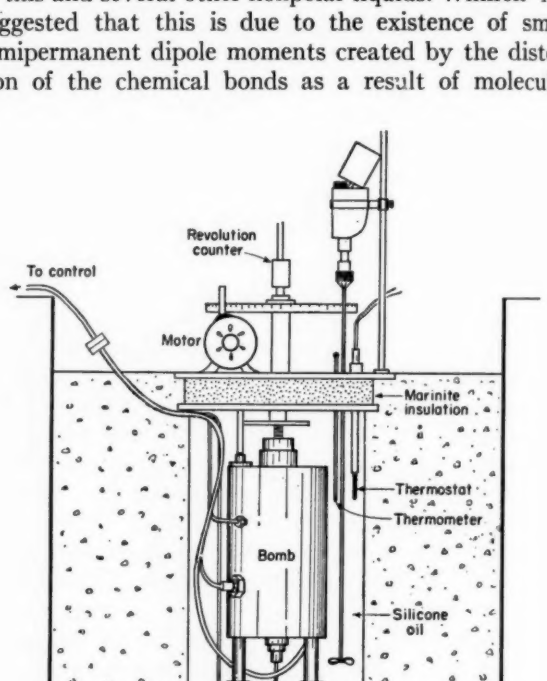

FIG. 2. Assembly of microwave absorption apparatus.

RESULTS

Since no previous measurements of microwave absorption in compressed gases and compressed liquids existed, we decided to study two polar gases of widely different molecular structure: chlorodifluoromethane ($CHClF_2$), a nearly spherical molecule with a strong dipole moment of 1.396 debye, and nitrous oxide (N_2O), a linear molecule of weak dipole moment (0.166 debye). In addition, we measured some mixtures

[4] J. Lamb *et al.*, Inst. Elec. Engrs. (London) **93**, Pt. III, 53 (1946).

[5] D. H. Whiffen, Trans. Faraday Soc. **46**, 124 (1950).

of chlorodifluoromethane in nitrogen, in analogy to the measurements of polar liquids in nonpolar solvents.

The $CHClF_2$, obtained from a commercial cylinder, was measured at three different temperatures up to the highest possible pressures (Fig. 5). A pressure limit was set by excessive losses, which cannot be measured in the microwave cavity. At 17.5° and 40°C this limit was reached by the liquefaction of the gas. Sometimes the gas did not condense on account of supercooling and higher pressures could be reached in the gas phase, as indicated in the 40°C characteristic.

For N_2O‡ the losses were low enough on account of the small dipole moment, that the measurements could be carried into the liquid range (Fig. 6). Below the critical temperature ($T_c=36.5$°C), dielectric constant and loss jump abruptly at liquefaction; above this temperature, a smooth transition is observed.

Figure 7 shows the measurements for $CHClF_2$ diluted by N_2 in various concentrations. For very small admixtures of chlorodifluoromethane, the polar molecule interacts essentially only with the nonpolar nitrogen molecules, until condensation sets in.

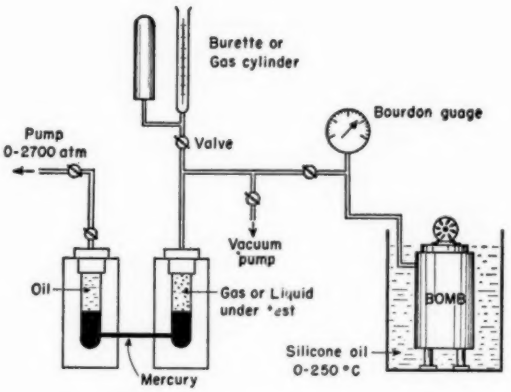

FIG. 3. High-pressure system (schematic).

DISCUSSION

The curves in Figs. 5 to 7 show widely differing shapes and a pronounced temperature dependence. This appearance is partly misleading, since the experimental variable "pressure" has been plotted as abscissa, while the more significant variable is the number of molecules per unit volume, N, that is, the density of the gas. Unfortunately, PVT data for polar gases are practically nonexistent in the literature; we hope to measure some density characteristics in the near future.

A way out of this impasse is to remove in a first approximation the factor N by replotting the loss factor κ'' as a function of the electric susceptibility $\kappa'-1\equiv\chi$. The characteristics assume now a much simpler appearance, the parameter temperature is relegated to minor importance, but still the shapes for the three cases differ significantly (Figs. 8 to 10).

‡ Commercial, Mathieson Chemical Corporation, Niagara Falls, New York.

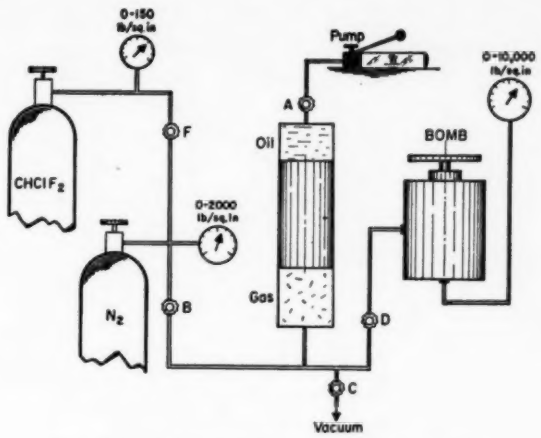

FIG. 4. High-pressure system for gas mixtures.

To proceed further in our interpretation, we should have recourse to a satisfactory general theory of collision broadening, but unfortunately such a theory does not yet exist.[6] Van Vleck and Weisskopf[7] and also

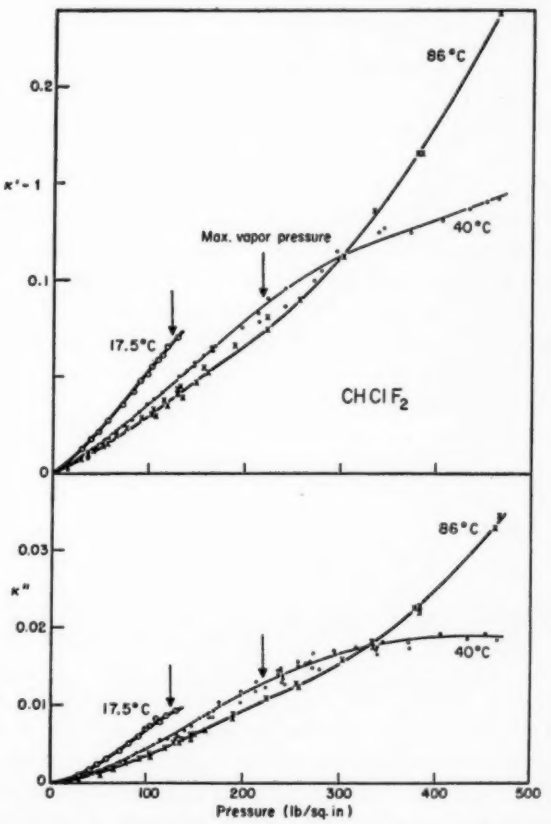

FIG. 5. $\kappa'-1$ and κ'' *vs* pressure for chlorodifluoromethane at various temperatures ($\lambda=1.22$ cm).

[6] See A. von Hippel, *Dielectrics and Waves* (John Wiley and Sons, Inc., New York, 1954), also for this formulation of the equations in the rationalized mks system.

[7] J. H. Van Vleck and V. F. Weisskopf, Revs. Modern Phys. **17**, 227 (1945).

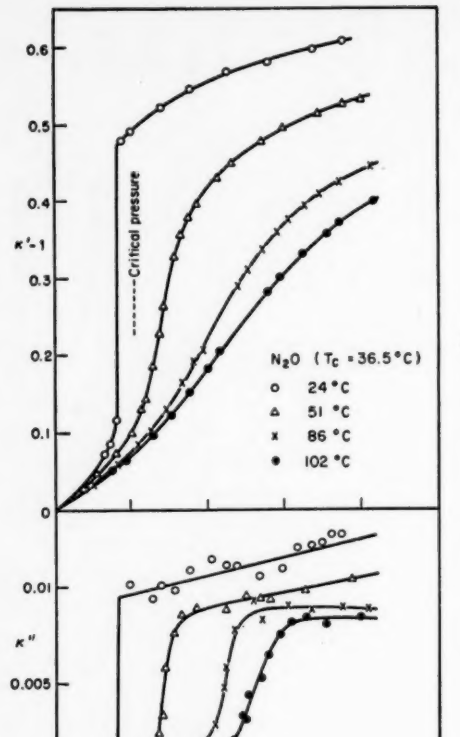

FIG. 6. $\kappa'-1$ and κ'' *vs* pressure for nitrous oxide at various temperatures ($\lambda=1.22$ cm).

Fröhlich[8] have investigated the problem, originally studied by Lorentz, of the broadening of resonance lines by collisions. Van Vleck and Weisskopf derive a line-shape formula which in the limit of zero resonant frequency transforms into the Debye relaxation equation for dilute polar liquids

$$\kappa'-1=\frac{N}{\epsilon_0}\left[(\alpha_e+\alpha_a)+\frac{\mu^2}{3kT}\frac{1}{1+\omega^2\tau^2}\right]$$
$$\kappa''=\frac{N}{\epsilon_0}\frac{\mu^2}{3kT}\frac{\omega\tau}{1+\omega^2\tau^2}. \tag{1}$$

However, in this derivation the relaxation time τ has the meaning of an average time interval between collisions and therefore decreases with increasing pressure. The τ of the Debye equation is proportional to a viscosity and increases with pressure, as has been shown, for instance, for the viscosity of glycerol, isobutyl alcohol, and eugenol up to 12 000 atmospheres by Danforth.[9] How the theory might be extrapolated from the gaseous to the liquid state, has been discussed by Gross in this laboratory.[10]

[8] H. Fröhlich, Nature **157**, 478 (1946).
[9] W. E. Danforth, Jr., Phys. Rev. **38**, 1224 (1931).
[10] E. P. Gross, Tech. Rep. 79, Lab. Ins. Res., Mass. Inst. Tech. May, 1954.

Caught in this dilemma, we will attempt a crude interpretation of our data by assuming that they can be represented in a first approximation by the simple relaxation spectrum of Eq. (1). Expressing the loss factor κ'' as function of the susceptibility $\kappa'-1$ means in this case complete elimination of N, and we obtain

$$\kappa''=b\omega\tau(\kappa'-1). \tag{2}$$

The factor b represents the ratio of orientation polarizability to total polarizability at the frequency ω:

$$b=\frac{\dfrac{\mu^2}{3kT}\dfrac{1}{(1+\omega^2\tau^2)}}{\alpha_e+\alpha_a+\dfrac{\mu^2}{3kT}\dfrac{1}{1+\omega^2\tau^2}}. \tag{3}$$

Since in our experiments the frequency is kept constant, the situation is relatively simple as long as we find ourselves not directly in the dispersion region, but, for example, appreciably below it ($\omega\tau\ll1$). Here b is a constant, if we can neglect interactions like association, which would change the dipole moment μ and the electronic and atomic polarizabilities α_e and α_a.

Returning to chlorodifluoromethane, we know that its rotational spectrum will consist of many strong resonance lines in the microwave and infrared region

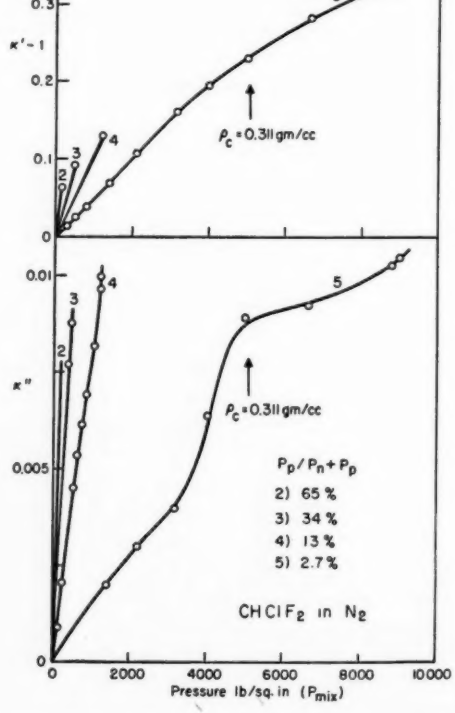

FIG. 7. $\kappa'-1$ and κ'' *vs* pressure for various mixtures of chlorodifluoromethane and nitrogen ($\lambda=1.22$ cm; T=24°C).

and that the absorption already at one atmosphere, as Hershberger[11] measured, consists of the contributions of many lines. In the plot of Fig. 8, the slope of the straightline portion is $b\omega\tau=0.14$. To obtain b and τ individually, we can return to Fig. 5 and try the following approximation:

If for $T=86°C$ the $CHClF_2$ behaves like a perfect gas ($p=NkT$), the loss factor of Eq. (1) can be rewritten

$$\kappa''=\frac{p\mu^2}{3k^2T^2}\frac{\omega\tau}{(1+\omega^2\tau^2)}. \tag{4}$$

For $\mu=1.396D$ and $\omega\tau=1$ the maximum loss factor should be

$$\kappa_{\max}''\simeq 0.0017 \text{ per atmosphere.} \tag{5}$$

Our measured loss factor is about $\kappa''\simeq 0.0005$ per atmosphere. Since

$$\frac{\kappa''}{\kappa_{\max}''}=\frac{2\omega\tau}{1+\omega^2\tau^2}, \tag{6}$$

we find $\omega\tau\simeq 0.15$ and $b\simeq 0.8$.

This result suggests that the assumption of a relaxation spectrum is not far from the truth. It says that the critical wavelength of the loss maximum lies about at 2 mm; that the major part of the polarization arises from dipole orientation (b near unity); and that the relaxation time $\tau\simeq 10^{-12}$ sec is, in the linear part of the characteristic, independent of temperature and density within the limits of accuracy of the experiment (*ca* 5%). Differently expressed: the free rotation is destroyed by collisions, but the statistical orientation time of the molecules is small as compared to $1/\omega$ and independent of pressure and temperature in the range measured. The deviation from the straight line portion at low pressures may indicate that here the separate resonance lines have not yet fully merged.

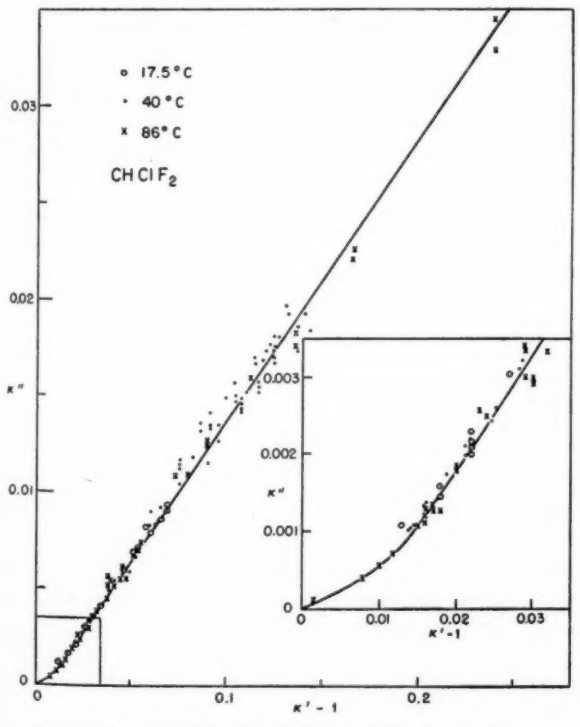

FIG. 8. κ'' *vs* $\kappa'-1$ for chlorodifluoromethane at various temperatures ($\lambda=1.22$ cm).

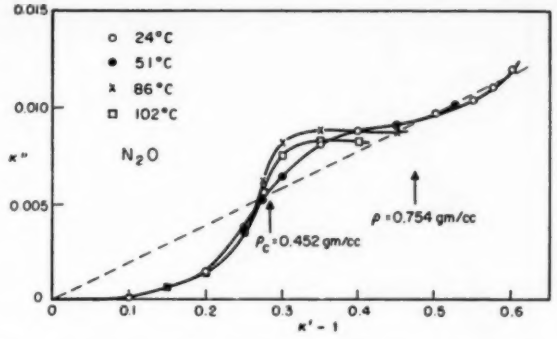

FIG. 9. κ'' *vs* $\kappa'-1$ for nitrous oxide at various temperatures ($\lambda=1.22$ cm).

For N_2O, the low-pressure rotational spectrum consists of a sequence of weak lines at 12.3, 6.2, 3.1 mm, etc.[12] The wavelength in our experiment practically coincides with the fundamental, but the absorption is too small to be detected with the present resonator. The line-broadening factor $\Delta\nu$ has been measured as 0.067 cm^{-1} per atmos,[13] hence the second line would not appreciably contribute before 200 psi are reached and even then not be measurable. Hence we are not surprised to find in Fig. 6 that the absorption is about negligible below 1000 psi. A significant loss sets in when the gas liquefies or reaches the density of the liquid (Fig. 9).

The rapid rise of the loss indicates a transition from a gas-like to a liquid-like behavior. For this latter part of the characteristic we may use the relaxation equation (1) with greater confidence. By replacing the number of molecules per unit volume, N, with $\rho N_0/M$, where ρ is the orthobaric density at 24°C ($\rho=0.754$ g/ml),[14] N_0 Avogadro's number, and M the molecular weight, we find $\kappa''_{\max}=0.0145$. According to Fig. 6, we measured $\kappa''=0.0095$; hence $\omega\tau\simeq 0.37$. The critical wavelength of maximum loss in the liquid state lies consequently for the simple relaxation spectrum at about 4.5 mm, which is in line with the known values of other polar liquids.

If the slope of the dotted line in Fig. 9 is identified with $b\omega\tau$ for the liquid state, we find $b=0.05$, that is, for N_2O the dipole polarization is only a small fraction of the total polarization. Since b is so small, it should

[11] J. E. Walter and W. D. Hershberger, J. Appl. Phys. **17**, 814 (1946).

[12] Shulman, Dailey, and Townes, Phys. Rev. **78**, 145 (1950).

[13] A. Adel and E. F. Barker, Revs. Modern Phys. **16**, 236 (1944).

[14] D. Cook, Trans. Faraday Soc. **49**, 716 (1953).

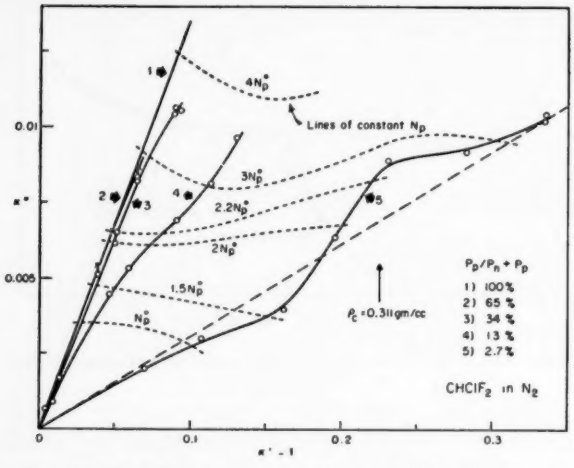

FIG. 10. κ'' *vs* $\kappa'-1$ for various mixtures of chlorodifluoromethane in nitrogen ($\lambda=1.22$ cm; $T=24°C$).

vary according to Eq. (3) approximately inversely proportional to the temperature. The range unfortunately is insufficient to check this trend. However, that b is small, can be confirmed by comparing the optical dielectric constant κ_∞', given as

$$\kappa_\infty'-1=(1-b)(\kappa'-1) \tag{7}$$

with the square of the index of refraction. From $n=1.193$[15] we obtain $n^2-1\simeq 0.43$ as compared to $\kappa_\infty'-1\simeq 0.45$ from Fig. 9 with the small b value.

In studies of the dielectric relaxation spectra of liquids and polymers it has proved useful to dissolve the polar component in nonpolar solvents. At very low concentrations the polar molecule interacts only with nonpolar molecules; the environment can be altered by changing the solvent. Furthermore, the influence of the dipolar interaction can be studied by progressively increasing the concentration of the polar constituent. The dielectric characteristics of mixtures of $CHClF_2$ in N_2 (Figs. 7 and 10) are a first installment of this type of measurement in the high-pressure gas region.

The initial pressure of the polar component P_p^0 was 55 psi; by adding a quantity of nitrogen, the pressure P_{mix}^0 is obtained and the ratio P_p^0/P_{mix}^0 is called the "concentration." The experimental characteristics show the susceptibility and loss factor as function of P_{mix}. Each curve corresponds to a constant ratio of polar to nonpolar molecules, N_p/N_n, which is approximately given as

$$N_p/N_n\simeq\frac{P_p^0}{P_{mix}^0-P_p^0}. \tag{8}$$

[15] *Handbook of Chemistry and Physics* (Chemical Rubber Publishing Company, Cleveland, 1953–1954), p. 558.

In addition to the curves of constant concentration, Fig. 10 shows lines of constant N_p obtained as follows: in every original mixture P_{mix}^0 is contained the same number of polar molecules per unit volume (equivalent to 55 psi). The susceptibilities of these mixtures are read off in Fig. 7 and translated as the N_p^0 curve into Fig. 10. By multiplying the susceptibility values with the corresponding factors 1.5, 2, 2.2, etc., the other curves are drawn.

If the relaxation equation (1) can be applied and the loss expressed as

$$\kappa''=\frac{N_p}{\epsilon_0}\frac{\mu^2}{3kT}\frac{\omega\tau}{1+\omega^2\tau^2}, \tag{9}$$

the curves of constant N_p seem to indicate that the relaxation time of the $CHClF_2$ molecules is first slightly reduced, then increased and reduced again as more and more nitrogen molecules are added. At still higher pressures, τ should increase again as the mixture assumes the properties of a dilute liquid solution.

In the very dilute mixture of 2.7% (see Fig. 10) the interaction should practically concern only the individual polar molecules with their nonpolar surroundings, hence τ should be independent of N_p and vary only with N_n. It is interesting to find that this characteristic has a similar S shape to that found for N_2O. In both cases the critical density marks approximately the point of maximum τ. The characteristic finally approaches the slope of the dotted line, represented according to Eq. (2) as $b\omega\tau=0.0305$. At this point the loss per polar molecule is about the same as in pure $CHClF_2$, hence $\omega\tau$ is almost unchanged but b, of course, is much smaller than the b of the pure material.

It is obvious that the conclusions here drawn are of a very tentative nature, as must be expected from a first foray in an unknown field.

ACKNOWLEDGMENTS

The author is greatly indebted to Professor A. von Hippel for suggesting this problem and for his continuing interest and encouragement in this work. He would like to record his gratitute to Dr. E. P. Gross for many stimulating discussions and to Professor D. J. Epstein and Dr. P. W. Forsbergh, Jr., for assistance in experimental questions. Finally, he would like to thank the Dow-Corning Corporation for the gift of silicone oil for the temperature bath.

Association and the Equation of State

ROBERT GINELL
Department of Chemistry, Brooklyn College, Brooklyn, New York
(Received February 28, 1955)

A form of the generalized gas law considering explicitly association into all possible species is derived. This law has the additional variables β_i, $\mathfrak{b}$, and ΣN_x. When β_i which is a function of the ratio of the surface of the container to the volume is neglected, as it can be at larger volumes, then the equation can be solved. Using the results derived from association theory, this gas law is developed into the form of the virial equation. The virial coefficients are functions of the equilibrium constants of association and the excluded volumes. A method of solution is indicated whereby the equilibrium constants and the excluded volumes of the individual j-mers can be obtained serially.

ATTEMPTS to make the simple gas laws apply to chemically reacting gases by inserting corrections for association were made long ago.[1,2] The basic reasons for the ordinary deviations of real gases from the perfect gas law were also recognized very early as due to the fact that molecules propagated attractive forces.[3,4] Hence it was only natural that equation-of-state problems would be attacked according to the latter line of thinking[5] rather than through a formal association theory utilizing the concept of the existence of definite 1-mers, 2-mers, 3-mers, etc. More recently, the theoretical approach has involved an analysis of gases in terms of cluster integrals,[6,7] which can be given the formal appearance of a representation in terms of association.[8] The virial coefficients, which are readily expressible in terms of the cluster integrals, are not to be confused with the coefficients in the virial equation of Kamerlingh Onnes since he omitted odd powers of the density beginning with the cubic in his virial development. There are several such semiempirical equations,[9] which have come into use for the approximate representation of actual PVT relationships for gases.

THEORY

It is understood at present that deviations from ideality are due not only to association but also in part to the fact that the molecules or particles in a gas do not have point masses, which fact alters the contributions associated with pairs, triples, quadruples, etc. Commonly in terms of occurrence of definite j-mers or clusters, the ideal gas law is modified to

$$PV/T\sum N_x = \text{a constant}, \tag{1}$$

where the $\sum N_x$ is written for the total number of particles present in units of Avogadro's number (avmoles)[10]; N_x being the number of avmoles of particles of size x in the system at equilibrium. An auxiliary equation is now needed to specify the mass of gas in the system, namely,

$$\sum xN_x = g/M^{(0)}, \tag{2}$$

where g is the weight of material in the system, $M^{(0)}$ is the weight of a 1-mer in the same units and $\sum xN_x$ is the number of empirical or formula weights present in the system (formoles).[10]

This is the form of the gas equation employed by Woolley[8] as pointed out by Kilpatrick[11] and also by Winston.[12] The equations themselves are well known.[2,7,13] One may regard these equations as providing an additional variable in the gas equation, namely $\sum N_x$. The implicit assumption in the use of these equations is that Dalton's law of partial pressures holds; namely, that

$$P=\sum p_x,$$

i.e., equivalently that particles which interact are considered to form a new species of particles.

That one should not describe the cluster representation as based on association alone can be seen from the fact that association by itself is not sufficient to account for the deviations even in the simplest of gases, helium. To demonstrate this, there is presented in Table I a calculation of $\sum N_x$ and $\sum xN_x$ for one liter of helium at various pressures at 0°C calculated from the data given by Kamerlingh Onnes and Boks.[14] As can be

[1] See, for instance, L. Boltzmann, Ann. Physik [3] **22**, 39, (1884); J. J. Thomson, Phil. Mag. [5] **18**, 233 (1884); L. Natanson, Ann. Physik [3] **38**, 288 (1889).
[2] J. Jeans, *An Introduction to the Kinetic Theory of Gases* (Cambridge University Press, New York, 1940).
[3] R. Clausius, for a summary of his work see: *Die Kinetische Theorie der Gase* (Friedrich Vierweg & Sohn, Braunschweig, Germany, 1889) Vol. 3, Chap. II.
[4] J. D. Van der Waals, Academisch Proefschrift, Leiden (1873).
[5] C. Dieterici, Ann. Physik [3] **66**, 826 (1898); [3] **69**, 685 (1899); [4] **5**, 51 (1901).
[6] B. Kahn and G. E. Uhlenbeck, Physica **5**, 399 (1938).
[7] J. E. Mayer, and M. G. Mayer, *Statistical Mechanics*, (John Wiley and Sons, Inc., New York, 1940).
[8] H. W. Woolley, J. Chem. Phys. **21**, 236 (1953).
[9] See, for instance, H. Kamerlingh Onnes, Commun. Phys. Lab. Univ. Leiden **71**, (1901), **11**, Suppl. **23**, 115 (1912); J. A. Beattie and O. C. Bridgeman, Proc. Am. Acad. Arts Sci. **63**, 229 (1928), J. Am. Chem. Soc. **49**, 1665 (1927), **50**, 3133 (1928); J. A. Beattie, Chem. Rev. **44**, 141 (1949); O. T. Bloomer and K. N. Rao, "Thermodynamic properties of nitrogen," Research Bull. **18**, Inst. Gas Tech. (1952).
[10] R. Ginell, Ann. New York Acad. Sci. **60**, 521 (1955).
[11] J. E. Kilpatrick, J. Chem. Phys. **21**, 1366 (1953).
[12] H. Winston, J. Chem. Phys. **21**, 2245 (1953).
[13] G. S. Rushbrooke, *Statistical Mechanics* (Oxford University Press, New York, 1949).
[14] J. D. A. Boks and H. Kamerlingh Onnes, Onnes Commun. No. 170a (1924) through Landolt and Börnstein, *Physikalisch Chemische Tabellen* Springer-Verlag, Berlin, Germany, (1927), fifth edition Er. I, 58.

TABLE I. Helium 0°C. $V'=1L$ at 0°C and 1 atmos; $PV/RT=\Sigma N_z$, $\Sigma xN_z=g/M^{(0)}$, $M^{(0)}=4.003$; 1 liter He=0.17846 g.

P[a]	$\frac{1}{V'}=d$[a]	ΣN_z/liter[b]	ΣxN_z/liter[c]
26.66	26.28	1.1898	1.1716
30.86	30.38	1.3767	1.3544
31.15	30.64	1.3897	1.3660
35.64	35.00	1.5900	1.5604
37.31	36.58	1.6645	1.6308
38.95	38.20	1.7376	1.7030
44.85	43.89	2.0008	1.9567
46.21	45.11	2.0615	2.0111
52.49	51.10	2.3417	2.2781
53.02	51.65	2.3653	2.3026
58.58	56.91	2.6134	2.5371

[a] Boks and Kamerlingh Onnes.[14]
[b] ΣN_z/liter $=P/RT$.
[c] ΣxN_z/liter $=g/M^{(0)}=0.17846/V'4.003$.

seen, the number of empirical weights in the system comes out to be less than the number of particles. This points definitely to the fact that we must, except at very low pressures, consider the volume of the particles. This factor, the volume of molecules, or obversely, the excluded volume of the system was first considered by Clausius to enter as a simple parameter $(V-b)$ where b was a constant factor. Weltner[15] has included it explicitly as an empirical factor which he introduced into the equation of state given by Woolley. However, because of the relation of this excluded volume to the size of the aggregates variously called clusters[7] or j-mers,[10] we should consider these two factors simultaneously and give a rational derivation for the equation containing them. In the following derivation we shall follow in principle the classical kinetic derivation of the ideal gas law.

Let us imagine that we have a box of side, l, containing a gas at equilibrium. As a consequence of our previous discussion the particles in the box are of all sizes which are multiples of $M^{(0)}$, the least size of particle of this particular gas that can exist. When the ith particle strikes the wall of the box, it undergoes a collision, and exerts pressure on the wall, and its change in momentum is $2m_iu_i$ where m_i is its mass and u_i, its velocity component normal to the wall it is striking. The number of collisions it has in unit time with the two walls in this direction is $u_i/(l-\beta_i)$ where β_i is the diameter of the ith particle. This is obvious since if the particle has a volume, and for the moment we are imagining it to be a sphere, then it cannot traverse the whole length of the box but is limited in its travels to the distance $l-\beta_i$. The change in the component of momentum/unit time in this direction is then

$$2m_iu_i\cdot\frac{u_i}{l-\beta_i}=\frac{2m_iu_i^2}{l-\beta_i}. \tag{3}$$

The area of the walls against which the ith particle strikes in this direction is necessarily $2(l-\beta_i)^2$. Hence, the pressure exerted by the ith molecule is

$$P_i=m_iu_i^2/(l-\beta_i)^3. \tag{4}$$

Since the total pressure is the sum of the pressures exerted by each particle, the total pressure is

$$P=\sum_i\frac{n_im_i\langle u_i^2\rangle_{Av}}{(l-\beta_i)^3}, \tag{5}$$

where n_i is the number of particles of size m_i in the box and $\langle u_i^2\rangle_{Av}$ is the average of the squares of the u component of the velocity of the particles of size i.

Now the prime condition of equilibrium requires that all the various species of particles be at the same temperature, and hence, that the average kinetic energy of each species be the same. Hence

$$\tfrac{1}{2}m_2\langle c_2^2\rangle_{Av}=\tfrac{1}{2}m_1\langle c_1^2\rangle_{Av}=\tfrac{1}{2}m_i\langle c_i^2\rangle_{Av}, \tag{6}$$

where $\langle c_i^2\rangle_{Av}$ is the mean square velocity of the particles of size i (species i). Since by definition $m_i=im_1$, then

$$\langle c_i^2\rangle_{Av}=\frac{\langle c_1^2\rangle_{Av}}{i}, \tag{7}$$

and since the component velocities along the three axes in space are equal

$$\langle u_i^2\rangle_{Av}=\frac{\langle c_i^2\rangle_{Av}}{3}=\frac{\langle c_1^2\rangle_{Av}}{3i}.$$

Hence

$$m_i\langle u_i^2\rangle_{Av}=\frac{m_1\langle c_1^2\rangle_{Av}}{3} \tag{8}$$

and

$$P=\frac{m_1\langle c_1^2\rangle_{Av}}{3}\sum_i\frac{n_i}{(l-\beta_i)^3}.$$

By the law of equipartition of energy

$$\frac{m_1\langle c_1^2\rangle_{Av}}{3}=kT.$$

Hence

$$P=kT\sum_i\frac{n_i}{(l-\beta_i)^3},$$

since $n_1=N_0N_1$

$$P=RT\sum_i\frac{N_i}{(l-\beta_i)^3} \tag{9}$$

where N_0=Avogadro's number, N_i=count in units of Avogadro's number (avmolity).

The term l now is the length of the box and the assumption was made that the particle must travel a distance $(l-\beta_i)$ before it could exert its pressure on the wall. Consider now that the box has a large number of particles in it and that collisions with the wall are not instantaneous and hence that there are particles attached on the wall. The distance that the ith particle

[15] Weltner, Wm., J. Chem. Phys. 22, 153 (1954).

would have to travel to exert its pressure on the wall is less by the average thickness of particles between it and the wall. On the average this will be $l=(V-\mathfrak{b})^{\frac{1}{3}}$, where V is the actual volume of the box and $\mathfrak{b}$ is the excluded volume of all the particles. This gives us the equivalent cube of free space of the particle.

Hence, our equation becomes

$$\frac{P}{RT}=\sum_i \frac{N_i}{[(V-\mathfrak{b})^{\frac{1}{3}}-\beta_i]^3} \tag{10}$$

or

$$\frac{PV}{RT}=\sum_i \frac{N_i}{\left[\left(1-\frac{\mathfrak{b}}{V}\right)^{\frac{1}{3}}-\frac{\beta_i}{V^{\frac{1}{3}}}\right]^3}. \tag{11}$$

The excluded volume $\mathfrak{b}$ is in itself a rather complex function. It certainly is not $\sum xN_x$ times the excluded volume of the 1-mer, $\mathfrak{b}_1$. This can be shown by the following calculation based on the simplest of assumptions as shown in Fig. 1. Let us assume that the 1-mer is a sphere of diameter, d, then its excluded volume is

$$\mathfrak{b}_1=(4/3)\pi d^3.$$

Similarly if we assume that the 2-mer is composed of two 1-mers in contact, i.e., assuming no shrinkage to occur, then

$$\mathfrak{b}_2=2\left(\frac{4}{3}\pi d^3\right)-2\left(\frac{5}{24}\pi d^3\right)=\frac{9}{4}\pi d^3$$

where the second term is the volume of the overlap. Similarly for a linear chain molecule of i units (a linear i-mer)

$$\mathfrak{b}_i=i\left(\frac{4}{3}\pi d^3\right)-(2i-2)\left(\frac{5}{24}\pi d^3\right)=(11i+5)\frac{\pi d^3}{12}.$$

For a particle in which the 1-mers are not packed linearly to form the i-mer, the excluded volume relationship is still more complicated and depends to a large extent upon the type of packing.

As a first approximation the excluded volume may be taken as

$$\mathfrak{b}=\mathfrak{b}_1N_1+\mathfrak{b}_2N_2+\cdots+\mathfrak{b}_mN_m=\sum_1^m \mathfrak{b}_xN_x. \tag{12}$$

This equation is approximate in the sense that the case could arise, where due to the form of packing of the j-mer, it would be possible for a 1-mer to approach closer to the j-mer than an i-mer could. This would be true if for instance the j-mer were not close-packed and hence there might be internal space where a 1-mer could go but where a 10-mer could not. For a linear molecule or for a close-packed structure the equation is probably justified.

If the volume that the gas occupies is comparatively large then β_i can probably be neglected since it is dependent on the shape of the vessel. Consequently, Eq. (11) becomes

$$\frac{PV}{RT}=\sum_i \frac{N_i}{\left(1-\frac{\mathfrak{b}}{V}\right)}$$

or

$$\frac{P(V-\mathfrak{b})}{RT}=\sum_i N_i. \tag{13}$$

However this assumption would probably not be valid for the equation of state if for instance the behavior in very narrow capillaries were considered.

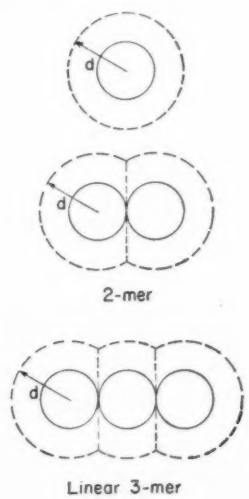

FIG. 1.

SOLUTION OF THE GAS EQUATION

To the simple ideal gas equation we have now added two additional variables which are not directly measurable, namely $\mathfrak{b}$ and $\sum N_i$. With the aid of association theory the values of these factors can be determined from measurable quantities. The pertinent equations are first Eqs. (13) and (2), and the relationships from association theory[10]

$$\sum_{x=1}^m N_x=N_1+K_2N_1^2+K_3N_1^3+K_4N_1^4\cdots K_mN_1^m, \tag{14}$$

and

$$\sum_{x=1}^m xN_x=N_1+2K_2N_1^2+3K_3N_1^3+4K_4N_1^4+\cdots mK_mN_1^m. \tag{15}$$

The best method of solving these equations is to proceed as follows: Equation (15) can be inverted to give the infinite series.

$$N_1=\sum xN_x+d_2(\sum xN_x)^2+d_3(\sum xN_x)^3+\cdots, \tag{16}$$

where

$$d_2=-2K_2$$
$$d_3=8K_2^2-3K_3$$
$$d_4=-40K_2^3+30K_2K_3-4K_4$$
$$d_5=224K_2^4-252K_2^2K_3+48K_2K_4+27K_3^2-5K_5,$$
etc.

The series for N_1 is now substituted into Eq. (14) to give

$$\sum N_x=g_1(\sum xN_x)+g_2(\sum xN_x)^2+g_3(\sum xN_x)^3+\cdots \quad (17)$$

where

$$g_1=1$$
$$g_2=-K_2$$
$$g_3=4K_2^2-2K_3$$
$$g_4=-20K_2^3+18K_2K_3-3K_4$$
$$g_5=112K_2^4-144K_2^2K_3+32K_2K_4+18K_3^2-4K_5,$$
etc.

The series in Eqs. (16) and (17) are infinite, while Eqs. (14) and (15) consist of finite series. As previously shown[10] the sole modification necessary in the infinite series is to set all coefficients greater than K_m, i.e., K_{m+1}, etc., equal to zero.

Substituting Eq. (17) into Eq. (13) we get

$$\frac{PV}{RT}=\frac{1}{1-\frac{\mathfrak{b}}{V}}[(\sum xN_x)+g_2(\sum xN_x)^2+g_3(\sum xN_x)^3+\cdots]. \quad (18)$$

Performing the indicated division on the right-hand side we have

$$\frac{PV}{RT}=[\sum xN_x+g_2(\sum xN_x)^2+g_3(\sum xN_x)^3+\cdots]\times\left[1+\frac{\mathfrak{b}}{V}+\left(\frac{\mathfrak{b}}{V}\right)^2+\cdots\right]. \quad (19)$$

Substituting the relationship from association theory

$$N_j=K_jN_1^j, \quad (20)$$

(where N_j equals the number of particles of species j in units of avmoles) into Eq. (12) we have

$$\mathfrak{b}=[\mathfrak{b}_1N_1+\mathfrak{b}_2K_2N_1^2+\mathfrak{b}_3K_3N_1^3+\cdots+\mathfrak{b}_mK_mN_1^m]. \quad (21)$$

Substituting Eq. (16) in Eq. (21) and then substituting the derived equation into Eq. (19), carrying out the indicated operations and collecting terms and inserting Eq. (2), we have

$$\frac{PV}{RT}=\left[\frac{g}{M^{(0)}}+\frac{r_2}{V}\left(\frac{g}{M^{(0)}}\right)^2+\frac{r_3}{V^2}\left(\frac{g}{M^{(0)}}\right)^3+\cdots\right], \quad (22)$$

where

$$r_2=\mathfrak{b}_1-K_2$$
$$r_3=4K_2^2-2K_3+K_2(\mathfrak{b}_2-3\mathfrak{b}_1)+\mathfrak{b}_1^2$$
$$r_4=-20K_2^3+18K_2K_3-3K_4+K_2^2(14\mathfrak{b}_1-5\mathfrak{b}_2)+K_3(\mathfrak{b}_3-5\mathfrak{b}_1)+K_2(2\mathfrak{b}_1\mathfrak{b}_2-5\mathfrak{b}_1^2)+\mathfrak{b}_1^3$$
etc.

If g is chosen so that it is equal to $M^{(0)}$ we have

$$\frac{PV}{RT}=1+\frac{r_2}{V}+\frac{r_3}{V^2}+\frac{r_4}{V^3}+\cdots. \quad (23)$$

This is a derivation of the virial equation that avoids the questions associated with negative equilibrium constants sometimes encountered.[11,12] The form and coefficients are similar to those derived by Weltner[15] in another fashion.

The value of the second virial coefficient as a function of the temperature is variously given. The van der Waals,[4] Dieterici,[5] and Keyes[16] equations of state all give the same form for r_2, namely,

$$r_2=b-(a/RT). \quad (24)$$

Berthelot's[17] equation gives

$$r_2=b-(a/RT^2) \quad (25)$$

while Beattie and Bridgeman[9] and the Benedict-Webb-Rubin[18] equations give

$$r_2=B_0-(A_0/RT)-(C/T^3). \quad (26)$$

Looking at our function r_2

$$r_2=\mathfrak{b}_1-K_2, \quad (27)$$

we see that $\mathfrak{b}_1$ which is the excluded volume of a 1-mer is not markedly dependent on temperature or at worst probably increases greatly only at rather high temperatures when the electron moves out of the ground state and large orbits are possible. On the other hand, K_2 is an equilibrium constant which is definitely a function of the temperature. This suggests that the form of the second virial coefficient might be approximated as

$$r_2=\mathfrak{b}_1-b_2(e^{-\epsilon_2/RT}-1)=(\mathfrak{b}_1+b_2)-b_2e^{-\epsilon_2/RT}, \quad (28)$$

as a particularly simplified form given by a square wall potential but suggestive of the fact that the temperature dependent parts of K_2 are a limit of a sum of many terms of the form $e^{-\epsilon_i/RT}$.

Equations (24), (25), and (26) may be seen to show a close relationship to Eq. (28) in that they are in effect obtained by empirically suppressing various terms in the expansion of these exponentials from which K_2 may be considered to be compounded.

[16] F. G. Keyes, Proc. Natl. Acad. Sci. **3**, 323 (1917).
[17] D. Berthelot, Trav. Bur. Int. Poids. Mes. **13** (1907).
[18] Benedict, Webb, and Rubin, J. Chem. Phys. **8**, 334 (1940).

Similarly, the third virial coefficient will be in the form

$$r_3=4b_2^2(e^{-\epsilon_2/RT}-1)^2-2b_3(e^{-\epsilon_3 R/T}-1)+(\mathfrak{b}_2-3\mathfrak{b}_1)b_2(e^{-\epsilon_2/RT}-1)+\mathfrak{b}_1^2,$$

or

$$r_3=4b_2^2(e^{-2\epsilon_2/RT})-2b_3e^{-\epsilon_3/RT}+[b_2(\mathfrak{b}_2-3\mathfrak{b}_1)-8b_2^2]e^{-\epsilon_2/RT}+[4b_2^2-b_2(\mathfrak{b}_2-3\mathfrak{b}_1)+\mathfrak{b}_1^2+2b_3]. \quad (29)$$

The complex form of this coefficient would account for the great variety of forms in which this virial coefficient is given. Expressions for approximating the fourth and higher virial coefficients can similarly be written.

If for a particular gas, the virial coefficients are known, values of $\mathfrak{b}_1$, b_2, and ϵ_2 producing an approximate fit of the second virial over a moderate range of temperature can be found. With these and known values of the third virial coefficient it should also be a simple matter to arrive at values for $\mathfrak{b}_2$, b_3, and ϵ_3. Thus successively all the excluded volumes $\mathfrak{b}_1$, $\mathfrak{b}_2$, $\mathfrak{b}_3$, etc., and the $K_2(T)$, $K_3(T)$, etc., can be derived. These equations can be internally checked by using the values of K_x in Eq. (17) to arrive at a value of $\sum N_x$ which when inserted into Eq. (13) will give a value for $\mathfrak{b}$. However, $\mathfrak{b}$ is also represented by Eq. (12) which may be solved in detail by the use of Eqs. (20) and (16). In turn these empirically derived values of $\mathfrak{b}_x$ can be checked by theoretical computation to arrive at the form of packing of the higher j-mer. Further work along these lines is in process.

THE JOURNAL OF CHEMICAL PHYSICS VOLUME 23, NUMBER 12 DECEMBER, 1955

Oxidation of Methane with Nitrogen Dioxide*

MARVIN L. BROMBERG AND H. AUSTIN TAYLOR
New York University, New York 53, New York

(Received March 2, 1955)

The reaction of methane with nitrogen dioxide has been studied in a flow system at temperatures from 600°–900°C with contact times of about 10^{-2} sec and in a static system from 350°–400°C and a total pressure of 250 mm. Initial rates have been related empirically and a discussion of the possible reactions occurring is presented.

SINCE as a fuel nitromethane is deficient in oxygen, studies were made of the behavior of mixtures of methane and nitrogen dioxide at various temperatures up to 900°C. The most desirable characteristic in a rocket propellant, namely, a large volume change, was not found and the work was discontinued before final conclusions could be drawn. Nevertheless some of the results are interesting and should prove worthwhile in future studies.

Under static conditions nitromethane is known to form from methane and nitrogen dioxide in the gas phase in the neighborhood of 200°C.[1] When the temperature is raised to 400°C oxidation products are found in abundance.[2] With short contact times even at temperatures above 400°C,[3] large quantities of nitromethane are formed. The decomposition of nitromethane occurs rapidly in the temperature range 400°–500°C.[4] The oxidation of methane by nitrogen dioxide has not been reported in detail although its role as a sensitizer in the slow oxidation of methane has been studied by Norrish.[5] He assumed that nitrogen dioxide supplied oxygen which initiated a methylene radical chain. The flow experiments reported here show that nitrogen dioxide is a far better oxidizing agent for methane than is oxygen. Static experiments at lower temperatures yielded an empirical rate equation leading to interesting speculations on the course of the reaction.

EXPERIMENTAL

The apparatus used in the flow runs consisted of a cylindrical fused silica reactor, one inch in diameter, with thermocouple well and a standard taper ground joint at each end. The volume of the vessel within the heated zone was 50 cc. The furnace was a Hevi Duty Electric Furnace, Type 70, with maximum temperature of 1100°C. Temperature measurements were made by means of a chromel-alumel thermocouple and pyrometer. Nitrogen dioxide was admitted through a Fischer-Porter Flowrater at 400 STP cc per min. The tube leading from the Flowrater to the reactor was wrapped with nichrome wire and maintained at 110°C. Methane was admitted through an orifice type flowmeter. Both gases were taken directly from cylinders of CP grade without further purification. The desired flow rates and tempera-

* Abstracted from a thesis presented in partial fulfillment of the requirements for the degree of Doctor of Philosophy at New York University, January, 1953.

[1] T. Urbanski and M. Slon, Compt. rend. 203, 620 (1936); 204, 870 (1937).

[2] Frohlich, Harrington, and Waitt, J. Am. Chem. Soc. **50**, 3216 (1928).

[3] O. Rideout, U. S. Pat. 2,281,345 (1943).

[4] L. J. Hillenbrand and M. L. Kilpatrick, J. Chem. Phys. **21**, 525 (1953).

[5] R. G. W. Norrish and J. Wallace, Proc. Roy. Soc. (London) **A145**, 307 (1934).

ture were adjusted while the gases were pumped through the reactor without products being collected. A steady state having been achieved the gas flow switched to a three liter collector after passing through a trap in liquid nitrogen. The pressure in the collector was allowed to rise to about 10 mm, the duration of the flow being noted. The gases in the collector were analyzed in the usual manner for methane, oxygen, and carbon monoxide. The contents of the trap was warmed to −78°C with dry ice and the resulting gases liberated were analyzed for carbon dioxide and oxygen. The residue was shown to consist mainly of nitrogen dioxide and water.

For the static runs a cylindrical quartz reaction vessel about 5 inches in length and 2.5 inches in diameter with a volume of 408 cc was used. It was located centrally in a well-insulated furnace which showed no sensible temperature variation over the seven inch length which completely included the reactor. The pressure change occurring during reaction was measured on a dibutyl phthalate manometer. Mercury manometers were used to measure pressures of nitrogen dioxide and methane admitted to a mixing vessel prior to passage into the reactor. In these manometers a layer of 10 mm of dibutyl phthalate protected the mercury surface. The dibutyl phthalate in the manometers showed no change in color or density over a period of three months and fresh liquid did not change the character of the runs. Stopcocks and ground joints were lubricated with a silicone grease. Reproducible results could only be obtained in static runs when the reactor was left for a short time prior to a run in contact with nitrogen dioxide. Thorough evacuation, especially overnight, always led to erratic results.

The dibutyl phthalate manometer in the form of a U had both arms open to the reactor while the gas mixture was admitted. After one minute one arm was closed and the subsequent pressure change was observed as a function of time. Making due allowance for the compression in the closed arm caused by the movement of the manometer fluid and for the relative density, the pressure change in mm Hg could be calculated. To relate these pressure changes to the initial pressures of nitrogen dioxide and methane, the initial rate was taken as the extrapolated pressure change occurring in the first minute. The observed pressure reading after one minute was zero. If the readings after two and three minutes are A and B, the extrapolated pressure change in the first minute, P, was taken as $P/A=A/(B-A)$. On completion of a run the reactor was evacuated through a trap in liquid nitrogen, the noncondensables being collected and analysis conducted as in the flow runs.

RESULTS

The results of the flow runs are presented in Table I. Flow rates are expressed in cc per minute at 25°C and 760 mm pressure. The NO_2 flow rate is for the $NO_2-N_2O_4$ equilibrium mixture under these conditions. The values of percent CO represent the percent CH_4 converted to CO. The percent CH_4 represents the difference between methane introduced and recovered and thus includes that converted to CO and CO_2. The quantities of CO_2 in brackets represent the whole dry ice fraction when no analysis was made. The times, t, are the duration of the run expressed in seconds during which products were collected. The pressure of the effluent gas stream was 6 mm in all cases. The results of the gas analyses are given in cc at 25°C and 760 mm.

It is apparent that the reproducibility of the data is not too good. However, in view of the rapidity of the reaction this is not surprising. Assuming that no change in the number of molecules occurs on passage through the reactor and taking the pressure as that of the effluent gases, the apparent contact time is seen to be of the order of 10^{-2} sec. This is an upper limit, but without knowledge of the actual volume change occurring and the order of the reaction, no more precise value can be calculated.

The presence of oxygen in the gases analyzed is surprising. It must be realized, however, that this does not necessarily represent free oxygen but could be oxygen liberated by decomposition of a product. Especially is this probable in view of the oxygen found from the dry ice fraction. Table II lists the amounts found from the liquid nitrogen and dry ice fractions in several runs, previously given as a total in Table I. It is doubtful that any organic peroxy acid such as those found in methane oxidation could be so unstable. Rather it ap-

TABLE I. Flow runs with NO_2 flow rate = 400 cc/min.

Run No.	Temp. °C	CH_4 rate	t sec	CH_4	O_2	CO	CO_2	N_2	%CH_4	%CO
7	600	135	72	65	16	3	(15)	14	60	1.8
8	600	125	92	74	17	3	(15)	6	61	1.6
9	600	135	80	69	9	3	(15)	23	62	1.7
10	600	145	70	70	13	2	(15)	19	59	1.2
11	600	155	63	65	19	3	(15)	22	60	1.8
18	600	90	45	...	12	1	(15)	...	...	1.5
19	600	110	40	...	12	1	(15)	...	...	1.4
1	700	115	52	30	22	12	(15)	4.2	70	12
2	700	125	51	31	17	19	(15)	39	71	18
3	700	145	51	35	20	21	(15)	38	72	17
4	700	135	51	32	23	12	(15)	39	72	10
5	700	90	60	28	26	15	(15)	37	69	17
6	700	160	56	44	21	21	(15)	30	71	14
30	700	145	45	32	12	15	(15)	40	71	14
12	800	150	41	17	38	31	30	31	84	30
13	800	125	49	22	32	31	22	18	78	30
14	800	115	34	12	42	19	18	43	81	29
15	800	135	38	16	29	28	20	35	81	32
16	800	105	46	5	51	19	19	42	94	24
17	800	160	38	14	38	34	26	34	86	34
20	800	95	41	...	18	17	...	...	...	26
21	900	125	63	...	...	56	...	...	...	43
22	900	150	60	...	...	67	...	...	...	45
23	900	100	60	...	...	45	...	...	...	45
24	900	160	38	...	...	53	...	...	...	53
31	900	145	45	0	108	49	57	40	100	45

pears probable that a nitrogen peroxide is responsible. Schwarz and Achenbach[6] report that NO_3 decomposes slowly above −14.2°C into the dioxide and oxygen.

To determine the possibility of pyrolysis of methane under the experimental conditions, runs were made at 650°, 780°, and 800°C at methane flow rates of 140 cc per minute. In all cases within the analytical precision, all the methane was recovered and no hydrogen or other products could be detected.

To compare the oxidation of methane by nitrogen dioxide with that by oxygen a series of runs were made at 700° and at 850°C using a methane flow rate of 150 and oxygen flow rate of 200 cc/min. Analysis of the noncondensables showed only methane and oxygen, in amounts which were within one percent of the quantities calculated as passing during the duration of the run. The liquid nitrogen trap contained, however, a small amount of a white solid which on fusion and treatment with Tollen's reagent gave evidence of reducing properties. It is obvious, therefore, that neither pyrolysis of methane nor oxidation of methane by oxygen produced by the decomposition of nitrogen dioxide can account for the observed results between the dioxide and methane.

TABLE II. Oxygen recovered in cc.

Run	N_2 fraction	CO_2 fraction	Total
12	18	20	38
13	15	17	32
14	19	23	42
15	9	20	29
16	26	25	51
17	17	21	38
31	11	97	108

The results of the static runs are expressed as rates of pressure increase, R, in mm mercury per minute occurring in the first minute of reaction. Table III lists a few actual data for some typical runs at 400°C and the R values calculated from them.

In Table IV are the rates found in runs made at various temperatures and proportions of the reactants. The total pressure of the initial mixture was 250 mm in all cases, nitrogen being added where necessary. Examination of these data shows that: (1) the rate of pressure change at constant methane is approximately first order in nitrogen dioxide, (2) at constant nitrogen dioxide with increasing methane the rate passes through a maximum and decreases again. Although the data are scanty, examination of this increasing and decreasing trend indicates, for the lower temperatures, that the higher the dioxide pressure, the lower is the methane pressure at which the maximum occurs. The effect of temperature is seen to be complex. When the ratio of methane to nitrogen dioxide is high a temperature increase causes an increase in R but at lower values of the ratio an increase in temperature causes R to decrease. Since R is a rate of pressure increase, the peculiarities of the effects of composition and temperature suggest that this increase is a net increase of pressure over a pressure decrease. An empirical equation was developed as a difference of two terms which could conceivably be associated with a pressure increase and a pressure decrease. This equation which was found to reproduce the observed data with respect both to composition and temperature has the form:

$$R=C_1[CH_4][NO_2]^{0.8}-C_2[CH_4]^2[NO_2].$$

The values of C_1 and C_2 are given in Table V. An extrapolation to 420°C, of the variations of C_1 and C_2 with temperature in the range 350–400°C gave the results shown in Table V. From these constants the values of R for several mixtures were calculated and then compared with observed data as shown in Table VI. The decrease in the values of C_1 and C_2 with temperature must not be taken to indicate a decrease in the rates of the reactions occurring, but merely a reflection of the general decrease with temperature of the rate of pressure increase. Further extrapolation to 500° and 600°C shows that R values calculated from the equation would be negative. In actual experiments no pressure changes could be observed. Analysis showed, however, that this was due to the rapidity of the processes involved, the over-all reaction being complete before pressure measurements could be made.

The effectiveness of oxygen in place of nitrogen dioxide was tested in several runs at 400° and at 420°C with ratios of methane to oxygen of 5:1, 3:1, 2:1, and 1:1. A slight pressure decrease was observed for the higher ratios and no pressure change for the lower ratios. The addition of nitrogen dioxide amounting to two percent of the methane-oxygen mixture caused a very slow

TABLE III. Static runs at 400°C.

Run	P_0 mm Hg CH_4	NO_2	N_2	P(mm DBT) for minute 2	3	4	5	6	7	8	9	10	R(mm Hg/min)
30S	100	50	100	25	38	46	53	60	66	72	77	81	9.4
32S	150	50	50	27	41	50	60	68	76	83	90	97	10.2
10S	150	100	···	34	51	62	73	83	92	101	110	117	13.3
33S	70	80	100	31	48	60	71	80	88	96	103	109	11.0

TABLE IV. Static rates as function of composition and temperature.

P_0 NO_2 mm	P_0 CH_4 mm	R mm/min 350°C	380°C	400°C
50	50	···	7.8	···
50	100	14.1	11.7	9.4
50	150	13.3	11.2	10.2
50	200	6.4	7.2	9.1
80	70	18.2	13.3	11.0
80	120	23.1	15.0	11.8[a]
80	170	11.2	11.2	12.7
100	50	19.6	13.3	9.8
100	100	30.6	18.4	12.4
100	150	26.8	14.9	13.3

[a] 130 mm CH_4.

[6] R. Schwarz and H. Achenbach, Ber. deut. chem. Ges. 683, 343 (1935).

TABLE V. Empirical rate coefficients.

Temp. °C	350	380	400	420
$C_1 \times 10^3$	13.5	9.64	7.16	5.5
$C_2 \times 10^5$	2.98	2.09	1.33	1.0

pressure increase and after twenty minutes about 90% of the methane was recovered unreacted.

Analyses of the reaction products were conducted in the same manner as in the flow runs. Table VII gives the data found for the amounts of unreacted methane and of carbon monoxide and carbon dioxide recovered as percentages of the methane introduced. The analyses were made after five minutes reaction except for the starred values which were obtained after twenty minutes reaction.

DISCUSSION

There can be no doubt that the pressure increase observed in the static runs is not that corresponding to any simple reaction or to a series of simple reactions each occurring with a pressure increase but must rather be a net result of pressure increases and decreases. It is necessary then, to consider which of the possible reactions are probable. At the temperatures used, nitrogen dioxide is known to dissociate giving oxygen as a product. The direct oxidation of methane by oxygen at these temperatures, it is already known and has been demonstrated in this work, is extremely slow and, in any case, this reaction is unaccompanied by any pressure change until formaldehyde has accumulated appreciably in the system and is itself decomposed or oxidized. The presence of nitrogen dioxide in small amounts reduces this induction in the pressure increase. The course of the pressure change observed here is quite different. It is well-known that methane and nitrogen dioxide at these and lower temperatures produce nitromethane although the mechanism is still uncertain. The reaction must, however, result in a decrease in pressure. Also, at these temperatures, nitromethane is unstable and decomposes thermally giving a variety of products with an over-all pressure increase. In the original study of this pyrolysis[7] the addition of oxygen was shown to enhance the rate of pressure increase and to lead to a different end point from that found in nitromethane decomposition. Thus, nitromethane is readily oxidized. The principal carbon product of this oxidation is carbon dioxide, whereas, of the pyrolysis, it is carbon monoxide. Presumably nitrogen dioxide could effect a similar oxidation both directly and indirectly through the oxygen produced dissociation.

TABLE VI. Comparison of calculated and observed R at 420°C.

P_0 NO_2 mm	P_0 CH_4 mm	R calc	Obs
50	100	6.7	6.3
50	150	0.3	4.4
80	120	9.7	9.4
80	170	8.6	7.9
100	100	11.9	11.2

[7] H. A. Taylor and V. V. Vesselovsky, J. Phys. Chem. **39**, 1095 (1935).

The production of carbon monoxide and carbon dioxide, both in the dynamic and static runs, in amounts which vary with change in the amounts of reactants taken and with change in temperature indicates a different origin for each. Thus, in the flow runs, carbon monoxide production increases more rapidly with temperature than does carbon dioxide production. At 600°C carbon dioxide production predominates while at 800° equal amounts of carbon monoxide and dioxide are found. In the oxygen-methane reaction, whether nitrogen dioxide sensitized or not, the ratio of carbon monoxide to carbon dioxide is reported to be of the order of ten to one at all stages following the induction period.

Summarizing the foregoing possibilities and undoubtedly greatly oversimplifying, it seems probable that the major reactions occurring in this study are a reaction to produce nitromethane and its oxidation by nitrogen dioxide, with a possible direct oxidation of methane by nitrogen dioxide. The production of nitromethane must involve a pressure decrease. If the second term in the empirical rate equation found to account for the static runs is assumed to represent this pressure decrease, it would require that nitromethane production at constant nitrogen dioxide was second order in methane. Some slight confirmation of this emerges from the flow runs also, if it is assumed that pyrolysis of the nitromethane is the chief source of carbon monoxide. The lack of reproducibility in the flow runs would lead one to conclude that the percentage of carbon monoxide produced was independent of the rate of flow of methane. With increasing flow of methane, however, the time of contact is correspondingly reduced and the apparent constancy of the carbon mon-

TABLE VII. Product analyses from static runs.

Temp. °C	CH_4 cc	NO_2 introduced	Percent recovered CO_2	CO	CH_4
400	10	22	20.0	40.0	35.0
	10*	22	25.0	40.0	30.0
	15	17	10.0	30.0	46.5
	15*	17	13.3	33.3	40.0
	22	10	2.3	18.2	65.6
	22*	10	4.6	22.6	63.5
	22	17	6.8	29.5	50.0
	22*	17	9.1	31.8	45.5
	33	10	3.0	19.7	66.7
	33*	10	4.6	24.2	57.5
	44	10	2.3	22.7	68.2
	44*	10	3.4	25.0	66.0
500	22	10	6.8	27.3	63.3
	22	22	13.6	38.6	40.8
600	22	10	9.1	29.5	59.0
	22	22	13.6	43.1	40.8
700	22	10	11.4	31.8	54.5
	33	22	15.1	30.3	48.5
	22	33	22.7	40.8	36.3

oxide would mean that the reaction was first order in methane. Examination of the data at 800°C, however, definitely shows a trend, with carbon monoxide increasing with increase in the methane flow, so that the ratio of carbon monoxide produced to methane flow is approximately constant. This would demand a second-order dependence on methane.

The assumption that carbon monoxide results solely from nitromethane can only be an approximation since otherwise the change in its production with temperature would be Arrhenian whereas this is not found. Taking the average percentage of carbon monoxide at each of the four temperatures of the flow runs, assuming the contact time to be inversely proportional to the temperature and correcting the percentages accordingly, one obtains the data in Table VIII where the "corrected" percentages should be proportional to the rates of production at the several temperatures. The logarithms of these rates are not linear in the reciprocals of the temperatures and the energy of activation for the three temperature intervals decreases steadily as the temperature rises. The actual values are 40, 17, and 14 kcal. Although too much significance cannot be attached to the actual values it is noteworthy that the trend is opposite to that observed by Pollard and Wyatt[8] for carbon monoxide production from nitrogen dioxide and formaldehyde, a reaction purported to occur in nitromethane pyrolysis. The observed reversed trend must mean that carbon monoxide is produced also by another reaction, not inconceivably by direct oxidation of methane or of nitromethane.

These direct oxidations should be covered by the first term in the empirical rate equation of the static runs. Norrish and Wallace[9] developed a rate expression for the disappearance of methane in the nitrogen dioxide sensitized oxidation which in its simplest terms has the form: $-d(CH_4)/dt=k(NO_2)(CH_4)/[1+k'(NO_2)]$. The term in the empirical expression is effectively of this form indicating a dependence on nitrogen dioxide corresponding to somewhat less than first order. Examination of Norrish's data shows that the pressure changes measured in his work were twenty to forty times smaller than those obtained in this work and the apparent resemblance may be illusory.

The kinetic significance of the empirical expression can be questioned also from the point of view of the decrease of the constants with increase in temperature. The sole possibility that these constants represent rate constants, since the rate of the over-all reaction does increase with temperature, is that they are complex, involving ratios of true rate constants, the denominator increasing more rapidly with temperature than the numerator. It would be impossible from the data to prove this. Since the measurements made are of a net pressure increase, the separation of this into a pressure increase and a simultaneous decrease, must always be somewhat arbitrary even if seemingly mathematically feasible. The range of the variables covered by the equation is limited and with similar limitations other empirical expressions could conceivably be equally applicable. In fact the relation $R=k(NO_2)(CH_4)/[1+k'(CH_4)^2]$ was almost as equally applicable to the observed data as the one previously used. The constant k' has a value of about 0.01 independent of temperature though the constant k still decreases with temperature rise.

TABLE VIII. Temperature coefficient of CO.

Temp. °C	% CO obs	% CO corr
500	1.5	1.5
600	14.0	15.6
700	29.0	35.7
800	45.0	60.5

A major contrast in the present results to those found in the pyrolysis of nitromethane and the oxidation of methane by oxygen lies in the relatively large amounts of carbon dioxide and of nitrogen found. The latter are probably not unconnected. Taylor and Vesselovsky found nitrogen present in appreciable amounts resulting from the decomposition of nitromethane at higher pressures in sealed tubes. Only traces of nitrogen and small amounts of carbon dioxide are found from nitromethane decomposition at lower pressures, while carbon monoxide may be as high as fifty percent of the nitromethane decomposed. The isolation of small amounts of oxygen from the products of the flow runs, already taken as indicative of the presence of higher nitrogen oxides, could provide the oxidizing atmosphere necessary to account for the decreased carbon monoxide and increased carbon dioxide and nitrogen.

It is apparent that considerably more work is necessary for any elucidation of such a complex system. Nevertheless, since at 900°C with a contact time of about 10^{-2} sec methane reacts completely in presence of excess nitrogen dioxide but without producing expected stable end products, either higher temperatures or longer contact times may be required if the desirable large volume increase is to be achieved.

[8] F. H. Pollard and R. M. H. Wyatt, Trans. Faraday Soc. 46, 281 (1950).

[9] R. W. G. Norrish and J. Wallace, Proc. Roy. Soc. (London) A145, 307 (1934).

Interaction of Rotational and Translational Diffusion

STEPHEN PRAGER
Department of Chemistry, University of Minnesota, Minneapolis 14, Minnesota
(Received March 18, 1955)

The Brownian motion of cylindrically symmetric particles is discussed, taking into account the unequal rates of diffusion parallel and perpendicular to the unique axis, as well as rotational diffusion. The problem is solved analytically for the case where the diffusing particles are initially distributed uniformly and with random orientation over a given plane. It is shown that the distribution at a later time is not strictly Gaussian, as is the case with spherically symmetric particles. On a macroscopic scale the effect is a small one.

INTRODUCTION

IN considering the Brownian motion of rod-shaped particles, it is to be expected that the frictional forces resisting the motion of a particle along its axis will be less than those opposing transverse motion, and that accordingly the longitudinal diffusion coefficient D_L will be greater than the transverse diffusion coefficient D_S. Thus a group of randomly oriented particles behaves rather like a mixture of species with different diffusion coeffients: those particles which were initially oriented parallel to their direction of motion will on the average have diffused farther in a given time interval than those which were oriented crosswise. The initially random orientation is not maintained, therefore, as the diffusion proceeds; if, for example, all the particles were to start from a common point, then at large distances from this origin we would expect radial orientation to predominate. This tendency is of course opposed by rotational diffusion, and we normally assume that this takes place with sufficient rapidity so that our particles behave as if they had just one translational diffusion coefficient given by

$$\bar{D}=\tfrac{1}{3}(2D_S+D_L). \tag{1}$$

However, as the length s of the particles increases the rotational diffusion coefficient goes down as s^{-3} while the translational diffusion coefficients go down only as s^{-1}.[1] For very long rods the assumption of an average translational diffusion coefficient should therefore be re-examined, and that is the purpose of this paper.

THE DIFFERENTIAL EQUATION

We specify the position and orientation of each particle by giving the Cartesian coordinates x, y, z of its center of mass, and the polar angles θ and ϕ of its axis. The concentration $c(x,y,z,\theta,\phi,t)$ is defined as the number of moles per unit volume per unit solid angle present in the vicinity of the point x, y, z and oriented in the direction θ, ϕ. The total concentration regardless of orientation is then given by

$$C(x,y,z,t)=\int_0^{\pi}\int_0^{2\pi} c(x,y,z,\theta,\phi,t)\sin\theta d\phi d\theta. \tag{2}$$

In writing down the diffusion equation for our problem, we must take account of the anisotropy of the translational diffusion, as well of the rotational diffusion which is occurring simultaneously. The differential equation for c becomes therefore

$$\frac{\partial c}{\partial t}=\operatorname{div}(\mathbf{D}\cdot\operatorname{grad}c)+\sigma\left[\frac{1}{\sin\theta}\frac{\partial}{\partial\theta}\left(\sin\theta\frac{\partial c}{\partial\theta}\right)+\frac{1}{\sin^2\theta}\frac{\partial^2 c}{\partial\phi^2}\right], \tag{3}$$

where σ is the rotational diffusion coefficient and $\mathbf{D}$ the translational diffusion tensor. In a co-ordinate system where the z-axis coincides with the unique axis of the molecule, the tensor $\mathbf{D}$ may be written

$$\mathbf{D}=\begin{vmatrix} D_S & 0 & 0 \\ 0 & D_S & 0 \\ 0 & 0 & D_L \end{vmatrix}; \tag{4}$$

in a frame of reference whose orientation is fixed in space, this becomes

$$\mathbf{D}=\begin{vmatrix} [D_S+(D_L-D_S)\cos^2\phi\sin^2\theta] & (D_L-D_S)\cos\phi\sin\phi\sin^2\theta & (D_L-D_S)\cos\phi\sin\theta\cos\theta \\ (D_L-D_S)\cos\phi\sin\phi\sin^2\theta & [D_S+(D_L-D_S)\sin^2\phi\sin^2\theta] & (D_L-D_S)\sin\phi\sin\theta\cos\theta \\ (D_L-D_S)\cos\phi\sin\theta\cos\theta & (D_L-D_S)\sin\phi\sin\theta\cos\theta & [D_S+(D_L-D_S)\cos^2\theta] \end{vmatrix}. \tag{5}$$

Substitution of (5) into (3) leads to

$$\frac{\partial c}{\partial t}=[D_S+[D_L-D_S]\cos^2\phi\sin^2\theta]\frac{\partial^2 c}{\partial x_z}+[D_S+[D_L-D_S]\sin^2\phi\sin^2\theta]\frac{\partial^2 c}{\partial y^2}+[D_S+[D_L-D_S]\cos^2\theta]\frac{\partial^2 c}{\partial z^2}$$
$$+2(D_L-D_S)\left[\cos\phi\sin\phi\sin^2\theta\frac{\partial^2 c}{\partial x\partial y}+\cos\phi\sin\theta\cos\theta\frac{\partial^2 c}{\partial x\partial z}+\sin\phi\sin\theta\cos\theta\frac{\partial^2 c}{\partial y\partial z}\right]+\sigma\left[\frac{1}{\sin\theta}\frac{\partial}{\partial\theta}\left[\sin\theta\frac{\partial c}{\partial\theta}\right]+\frac{1}{\sin^2\theta}\frac{\partial^2 c}{\partial\phi^2}\right]. \tag{6}$$

[1] J. J. Hermans, *Flow Properties of Disperse Systems* (North Holland Publishing Company, Amsterdam, 1953), p. 137.

To reduce Eq. (6) to manageable proportions, we restrict ourselves to cases where c is initially independent of x, y, and ϕ; for such problems the symmetry of the situation requires that c remain independent of these variables at all times, and (6) becomes

$$\frac{\partial c}{\partial t}=(D_S+[D_L-D_S]\cos^2\theta)\frac{\partial^2 c}{\partial z^2}+\frac{\sigma}{\sin\theta}\frac{\partial}{\partial\theta}\left(\sin\theta\frac{\partial c}{\partial\theta}\right). \quad (7)$$

The boundary conditions for Eq. (7) may be given by specifying the distribution of particles at $t=0$. Of particular importance is the case where the particles are initially distributed uniformly and with random orientations over the plane $z=0$:

$$c(z,\theta,0)=\frac{1}{4\pi}\delta(z). \quad (8)$$

A solution of the problem with the boundary condition (8) will enable us to handle any case of planar diffusion where the initial orientation is random.

Equations (7) and (8) may be written in dimensionless form by introducing the symbols

$$\tau=\sigma t;\quad \xi=z\left(\frac{\sigma}{\bar{D}}\right)^{\frac{1}{2}};\quad u=\cos\theta;$$
$$\varphi=4\pi\left(\frac{\bar{D}}{\sigma}\right)^{\frac{1}{2}}c;\quad \epsilon=\frac{D_L-D_S}{\bar{D}}. \quad (9)$$

In terms of these new variables we have

$$\frac{\partial\varphi}{\partial\tau}=[1+\epsilon(u^2-\tfrac{1}{3})]\frac{\partial^2\varphi}{\partial\xi^2}+\frac{\partial}{\partial u}\left[(1-u^2)\frac{\partial\varphi}{\partial u}\right] \quad (10)$$

with the boundary condition

$$\varphi(\xi,u,0)=\delta(\xi). \quad (11)$$

Equation (10) can be separated, i.e. its solutions can be expressed in the form

$$\varphi=\sum_{k,l}U_{kl}(u)e^{-(k\tau+il\xi)}, \quad (12)$$

where the U_{kl} satisfy the differential equation

$$\frac{\partial}{\partial u}\left[(1-u^2)\frac{\partial U_{kl}}{\partial u}\right]+[k-l^2(1-\epsilon(u^2-\tfrac{1}{3}))]U_{kl}=0; \quad (13)$$

unfortunately the solution of (13) is far from simple. This obvious approach to the problem seems infeasible, therefore, and we look to other methods for a solution.

THE INTEGRAL EQUATION

If we think of the quantity $\epsilon(u^2-\frac{1}{3})\partial^2\varphi/\partial\xi^2$ on the right-hand side of Eq. (10) as representing a distribution of sources, we may use a Green's function procedure to convert the differential equation to an integral equation. As our Green's function we take the solution to the equation

$$\frac{\partial\Phi_l}{\partial\tau}-\frac{\partial^2\Phi_l}{\partial\xi^2}-\frac{\partial}{\partial u}\left[(1-u^2)\frac{\partial\Phi_l}{\partial u}\right]=\delta(\xi)\delta(\tau)P_l(u) \quad (14)$$

with the boundary condition

$$\Phi_l(\xi,u,0)=0. \quad (15)$$

$P_l(u)$ is here the normalized lth order Legendre polynominal. In terms of the Φ_l we can rewrite the system of Eqs. (10) and (11) in the form of an integral equation:

$$\varphi(\xi,u,\tau)=\varphi_0(\xi,\tau)+\epsilon\sum_{l=0}^{\infty}\int_0^{\tau}\int_{-1}^{1}\int_{-\infty}^{\infty}(u'^2-\tfrac{1}{3})\times\left[\frac{\partial^2}{\partial\xi'^2}\varphi(\xi',u',\tau')\right]P_l(u')\times\Phi_l(\xi-\xi',u,\tau-\tau')d\xi'du'd\tau'. \quad (16)$$

The function φ_0 appearing in (16) is the solution when ϵ is zero; since in this case there is no interaction between translational and rotational diffusion, φ_0 will be independent of u and satisfy a simple Fick's law equation

$$\partial\varphi_0/\partial t=\partial^2\varphi_0/\partial\xi^2 \quad (17)$$

with the boundary condition (11). The solution to (17) and (11) is of course well known, and is given by

$$\varphi_0(\xi,\tau)=\frac{1}{(4\pi\tau)^{\frac{1}{2}}}\exp(-\xi^2/4\tau). \quad (18)$$

Equations (14) and (15) are also readily solved, since here again the translational diffusion coefficient is the same for all orientations. The two types of diffusion thus proceed independently and we have

$$\Phi_l(\xi,u,\tau)=\varphi_0(\xi,\tau)P_l(u)e^{-l(l+1)\tau}. \quad (19)$$

THE LIOUVILLE-NEUMANN SERIES

To solve Eq. (16) we expand φ in a power series in the parameter ϵ, following the Liouville-Neumann procedure:

$$\varphi=\varphi_0+\epsilon\varphi_1+\epsilon^2\varphi_2+\cdots. \quad (20)$$

Inserting (20) into (16) and equating coefficients of like powers of ϵ, we obtain for the nth term

$$\varphi_n(\xi,u,\tau)=\sum_l\int_0^{\tau}\int_{-1}^{1}\int_{-\infty}^{\infty}(u'^2-\tfrac{1}{3})\times\left[\frac{\partial^2}{\partial\xi'^2}\varphi_{n-1}(\xi',u',\tau')\right]P_l(u')\times\Phi_l(\xi-\xi',u,\tau-\tau')d\xi',du',d\tau'; \quad (21)$$

φ_0 is, of course, given by (18).

Substitution of the expression (19) for Φ_l into (21) and use of the identity

$$\int_{-\infty}^{\infty}\left[\frac{\partial^m}{\partial\xi'^m}\varphi_0(\xi',\tau')\right]\varphi_0(\xi-\xi',\tau-\tau')d\xi'=\frac{\partial^m}{\partial\xi^m}\varphi_0(\xi,\tau) \quad (22)$$

yields

$$\varphi_n(\xi,u,\tau)=\frac{\exp(-\xi^2/4\tau)}{\pi^{\frac{1}{2}}2^{2n+1}\tau^{n+\frac{1}{2}}}H_{2n}\left(\frac{\xi}{(4\tau)^{\frac{1}{2}}}\right)\Psi_n(u,\tau), \quad (23)$$

where $H_m(x)=(-1)^m\exp(x^2)(d^m/dx^m)\exp(-x^2)$ is the mth Hermite polynomial, and $\Psi_n(u,\tau)$ is given by the recursion formulas

$$\Psi_n(u,\tau)=\sum_l\int_0^\tau\int_{-1}^1(u'^2-\tfrac{1}{3})\Psi_{n-1}(u',\tau')\times P_l(u')P_l(u)e^{-l(l+1)(\tau-\tau')}du'd\tau' \quad (24)$$

$$\Psi_0=1.$$

Inspection of (24) readily shows that the functions Ψ_n are finite series of Legendre polynomials in u, with time dependent coefficients:

$$\Psi_n(u,\tau)=\sum_{m=0}^{n}A_{nm}(\tau)P_{2m}(u). \quad (25)$$

Inserting this into (24), and using the relation

$$\int_{-1}^1(u^2-\tfrac{1}{3})P_{2m}(u)P_{2k}(u)du=\alpha_{m-1}\delta_{m-1,k}+\beta_m\delta_{m,k}+\alpha_m\delta_{m+1,k}, \quad (26)$$

where

$$\alpha_m=\frac{2(2m+1)(m+1)}{(4m+3)(4m+1)^{\frac{1}{2}}(4m+5)^{\frac{1}{2}}},\qquad \beta_m=\frac{4m(2m+1)}{3(4m+3)(4m-1)}, \quad (27)$$

and δ_{mk} is the Kronecker delta, we get a set of recursion formulas for the $A_{nm}(\tau)$:

$$A_{nm}(\tau)=\int_0^\tau\exp[-2m(2m+1)(\tau-\tau')]\times[\alpha_{m-1}A_{n-1,m-1}(\tau')+\beta_mA_{n-1,m}(\tau')+\alpha_mA_{n-1,m+1}(\tau')]d\tau' \quad (28)$$

$$A_{00}=\sqrt{2}.$$

In Eq. (28) A_{lk} is to be taken as zero whenever k is less than zero or greater than l.

Combination of Eqs. (20), (23), and (25) leads to

$$\varphi(\xi,u,\tau)=\frac{1}{(4\pi\tau)^{\frac{1}{2}}}\exp(-\xi^2/4\tau)\times\sum_{n=0}^{\infty}\sum_{m=0}^{n}\frac{A_{nm}(\tau)P_{2m}(u)H_{2n}(\xi/(4\tau)^{\frac{1}{2}})}{2^{2n}\tau^n}\epsilon^n, \quad (29)$$

which is our complete solution. The first few A's, calculated according to (28), are

$$\begin{aligned}
A_{00}&=\sqrt{2}\\
A_{10}&=0\\
A_{11}&=\frac{1}{9}\left(\frac{2}{5}\right)^{\frac{1}{2}}(1-e^{-6\tau})\\
A_{20}&=\frac{2\sqrt{2}}{135}\left(\tau-\frac{1}{6}(1-e^{-6\tau})\right)\\
A_{21}&=\frac{4}{189}\left(\frac{2}{5}\right)^{\frac{1}{2}}\left(\frac{1}{6}[1-e^{-6\tau}]-\tau e^{-6\tau}\right)\\
A_{22}&=\frac{4\sqrt{2}}{315}\left(\frac{1}{20}-\frac{1}{14}e^{-6\tau}+\frac{3}{140}e^{-20\tau}\right)\\
A_{30}&=\frac{4\sqrt{2}}{8505}\left(\tau-\frac{1}{3}+\left(\tau+\frac{1}{3}\right)e^{-6\tau}\right).
\end{aligned} \quad (30)$$

DISCUSSION

According to (2), (9), and (29), the total concentration $C(\xi,\tau)$ is given by

$$C(\xi,\tau)=\frac{1}{2}\left(\frac{\sigma}{\bar{D}}\right)^{\frac{1}{2}}\int_{-1}^1\varphi(\xi,u,\tau)du=\left(\frac{\sigma}{4\pi\bar{D}\tau}\right)^{\frac{1}{2}}\exp(-\xi^2/4\tau)\times\sum_{n=0}^{\infty}\frac{A_{n0}(\tau)H_{2n}(\xi/4\tau)^{\frac{1}{2}})}{2^{2n+\frac{1}{2}}\tau^n}\epsilon^n. \quad (31)$$

The factor outside the summation in (31) is of course just the total concentration $C_0(\xi,\tau)$ which would be encountered for spherical particles with diffusion coefficient $\bar{D}$. The zeroth term in the summation is unity, the first term vanishes because of Eq. (30), and subsequent terms represent deviations from the simple Gaussian distribution which is to be expected in the absence of the interaction effects discussed in this paper.

As τ becomes large $A_{n0}(\tau)$ goes to infinity as $\tau^{n/2}$ for n even, or as $\tau^{(n-1)/2}$ for n odd. Thus if τ is increased while $\xi/\sqrt{\tau}$ is kept fixed, the nth term ultimately vanishes as $\tau^{-n/2}$ (n even) or $\tau^{-(n+1)/2}$ (n odd), so that for sufficiently large values of τ the series may be broken off after only a few terms even if ϵ is quite large (the largest value of ϵ which is physically possible is 0.75, corresponding to a very long rod).[1]

If the ratio ξ^2/τ is taken to be of order ten or less, as it must be if $C(\xi,\tau)$ is appreciable, then, since $\sigma/\bar{D}$ is of the same order as $1/s^2$,[1] τ must be at least of order $0.1(z/s)^2$; taking $z=10^{-1}$ cm and $s=3\times10^{-5}$ cm, we get a τ of about 10^6. For such a large τ the deviation

from a Gaussian distribution may be written

$$\frac{C-C_0}{C_0}=\frac{\epsilon^2}{1080\tau}H_4\left(\frac{\xi}{(4\tau)^{\frac{1}{2}}}\right), \tag{32}$$

which, with the values assumed in the foregoing, amounts to an entirely negligible error of at most 0.6 $\times 10^{-6}\%$. Thus the non-Gaussian terms are important only at distances comparable to the lengths of the diffusing particles.

If the initial distribution is not a δ function, then (31) must be replaced by

$$C(\xi,\tau)=\frac{1}{(4\pi\tau)^{\frac{1}{2}}}\sum_{n=0}^{\infty}\frac{A_{n0}(\tau)\epsilon^n}{2^{2n+\frac{1}{2}}\tau^n}$$
$$\times\int_{-\infty}^{\infty}C(\xi',0)H_{2n}\left(\frac{\xi-\xi'}{(4\tau)^{\frac{1}{2}}}\right)\exp\left(-\frac{(\xi-\xi')^2}{4\tau}\right)d\xi'. \tag{33}$$

If in particular $C(\xi,0)$ is a step function given by

$$C(\xi,0)=\begin{cases}a & (\xi<0)\\ 0 & (\xi>0)\end{cases}, \tag{34}$$

then (33) becomes

$$C(\xi,\tau)=a\left[\frac{1}{2}\left(1-\mathrm{erf}\frac{\xi}{(4\tau)^{\frac{1}{2}}}\right)+\frac{1}{\sqrt{\pi}}\right.$$
$$\left.\times\exp\left(-\frac{\xi^2}{4\tau}\right)\sum_{n=1}^{\infty}\epsilon^n\frac{A_{n0}(\tau)H_{2n-1}(\xi/(4\tau)^{\frac{1}{2}})}{2^{2n+\frac{1}{2}}\tau^n}\right]. \tag{35}$$

ACKNOWLEDGMENTS

The author would like to express his appreciation of the many helpful discussions he had with Professor Paul Rosenbloom concerning the convergence of the series (29).

THE JOURNAL OF CHEMICAL PHYSICS VOLUME 23, NUMBER 12 DECEMBER, 1955

Infrared Spectra of SiO_2 from 400 to 600 cm^{-1}*

J. REITZEL
Arthur D. Little, Inc., Cambridge, Massachusetts
(Received March 11, 1955)

The frequencies of the infrared bands occurring between 400 and 600 cm^{-1} in α quartz, α cristobalite, and vitreous silica have been determined by a reflection method. The observed infrared spectra are compared with published Raman data.

THE problem of the vibrational frequencies of silica in its various forms has occupied many workers in Raman and infrared spectroscopy. Part of the problem is the determination of true vibrational frequencies from observed infrared reflection bands: because of strong absorption, reflection spectra are usually the only sort obtainable, and these may be quite misleading if used without proper correction. In previous papers, Šimon[1,2] has given a method for deriving the optical constants η and κ of a substance from reflectivity measurements at two angles of incidence, and has shown that the true vibrational frequencies are located by the maxima of the quantity $\epsilon''=3\eta^2\kappa/(\eta^2+2)$.

Using this method, Šimon and McMahon[2] have studied the infrared spectra of quartz, cristobalite, and vitreous silica from 700 to 1400 cm^{-1}. The present paper reports the results of an extension of these measurements down to 400 cm^{-1}. The region 400 to 600 cm^{-1} is one of very strong Raman and infrared activity in silica, and an improved determination of the vibrational frequencies in this range is of some interest.

* This research was sponsored by the Owens-Illinois Glass Company, Toledo, Ohio.
[1] I. Šimon, J. Opt. Soc. Am. **41**, 336 (1951).
[2] I. Šimon and H. O. McMahon, J. Chem. Phys. **21**, 23 (1953).

EXPERIMENTAL METHODS AND RESULTS

Using the apparatus and methods described in reference 1, but with a CsBr prism in place of NaCl, we have measured the reflectivities of α quartz, α cristobalite, and vitreous silica at 20° and 70° incidence, in the range 400 to 600 cm^{-1}. The quantities η and κ have been deduced, and ϵ'' has been plotted to locate the actual frequencies of vibration.

The Perkin-Elmer spectrometer used was calibrated from eight bands of CO_2, 1,2,4-trichlorobenzene, and H_2O, to which a hyperboloidal curve was fitted graphically. After correction, this curve gave a calibration accurate to about $\frac{1}{4}$ cm^{-1} between 400 and 600 cm^{-1}. Slits of about 0.5 mm were used in taking the reflection spectra, giving a spectral slit width of about 8 cm^{-1} at 500 cm^{-1}.

The accuracy of the reduction procedure for deriving η and κ was checked by substituting the derived values into Fresnel's formula for reflectivity at normal incidence and comparing the results with the observed 20° reflectivities. The check points are shown as circled dots in the reflectivity plots below. While the over-all accuracy of our frequency determinations is difficult to

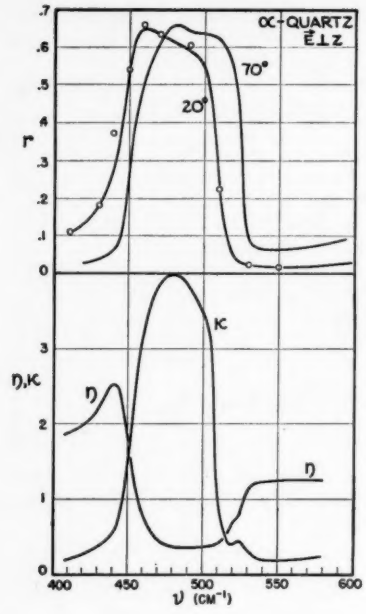

FIG. 1. Reflectivities and optical constants for α quartz with $E \perp Z$.

assess, we estimate that the final error does not exceed ± 8 cm^{-1}.

Spectra of the optically isotropic forms α cristobalite and vitreous silica were taken with unpolarized incident radiation and were corrected for spectrometer polarization. With α quartz, polarized radiation and special orientations of the optic axis Z of the sample were used to ensure the validity of the method.

The results of the work are shown in Figs. 1 to 5. Figure 1 gives the observed reflectivities r_{20} and r_{70}, and the optical constants η and κ, of α quartz, for radiation polarized with $E \perp Z$ (the O-ray). Figure 2 shows only r_{20} for α quartz with radiation polarized $E \| Z$ (the E-ray) since the measured reflectivities gave no consistent values of η and κ. In Figs. 3 and 4, r_{20}, r_{70}, η and κ are shown for α cristobalite and vitreous silica respectively. Plots of ϵ'' for the O-ray in α quartz, and for α cristobalite and vitreous silica, are given in Fig. 5, and the frequencies of the maxima, which are the vibrational eigenfrequencies, are noted.

Since the measured reflectivities for the E-ray in α quartz do not give values for η and κ, they must be somewhat in error. The 20° reflectivity is only shown here to give an idea of the intensity and general appearance of the band. We may safely associate this reflection with a vibration lying somewhere between 500 and 550 cm^{-1}, and since such a band is quite absent in the plot of ϵ'' for the O-ray (making allowance for imperfect polarization), we may also say that the band between 500 and 550 cm^{-1} is completely polarized $\| Z$. We cannot say with such certainty that the 455 cm^{-1} O-ray band has no component $\| Z$, since ϵ'' could not be found for the E-ray band. The frequency separation of the O- and E-ray 20° reflectivity bands is, however, sufficient to give support to the assumption that the 455 cm^{-1} band is completely polarized $\perp Z$.

The observed reflectivities of cristobalite may differ somewhat from true reflectivities, since the sample used was an oriented devitrified layer on a fused silica plate, rather than a polished surface. The fact that the two reflectivities are consistent, however, shows that the error so introduced must be very small. There is further possibility of error from the presence in the sample of a small percentage of tridymite.

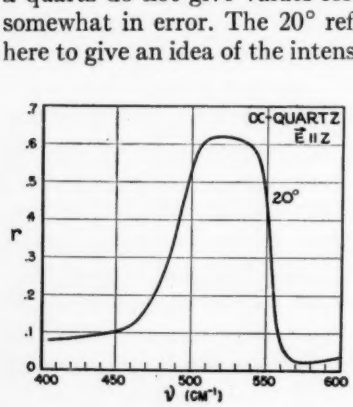

FIG. 2. Reflectivity at 20° for α quartz with $E \| Z$.

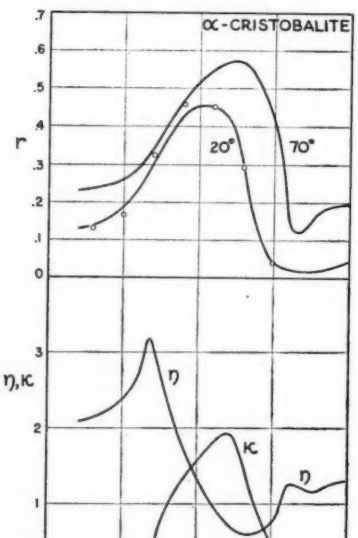

FIG. 3. Reflectivities and optical constants of α cristobalite.

An important feature of all the bands we have observed is their very great intensity. Comparison of these bands with those observed at higher frequencies by Šimon and McMahon shows that the quartz O-ray band at 455 cm^{-1} is the most intense in the quartz spectrum, while the corresponding bands in cristobalite and vitreous silica are second only to the very strong bands at about 1100 cm^{-1}.

DISCUSSION

For comparison with the infrared spectra, the Raman activity of silica in the same region may be reviewed briefly. The spectra of α quartz taken by Saksena and others, as tabulated in a paper of Saksena,[3] show a very

[3] B. D. Saksena, Proc. Indian Acad. Sci. **A12**, 93 (1940).

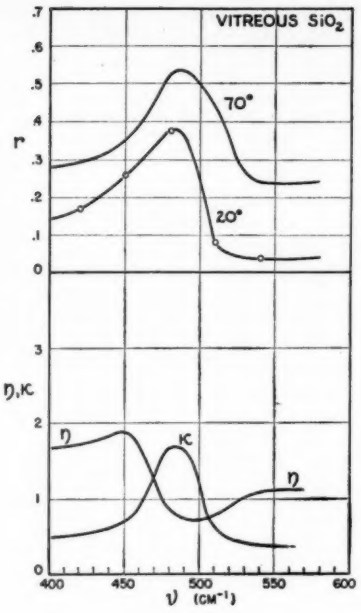

FIG. 4. Reflectivities and optical constants of vitreous silica.

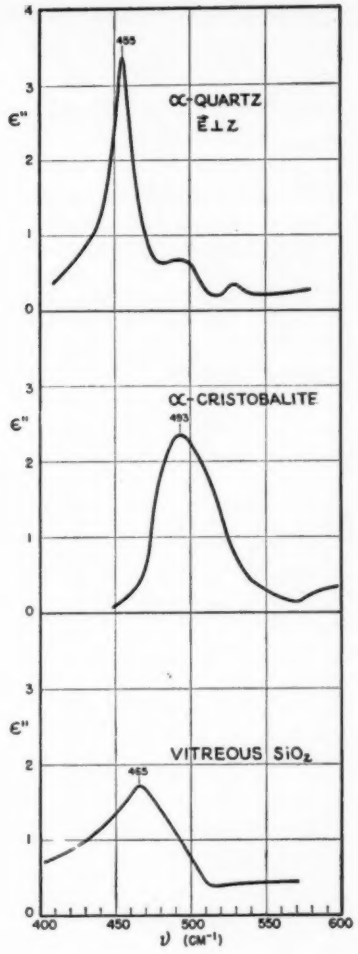

FIG. 5. ϵ'' for α quartz with $E \perp Z$, for α cristobalite, and for vitreous silica.

strong band at 466 cm^{-1}, whose polarization properties place it in the symmetric and infrared-inactive class A. There is also a weak band of the degenerate class E at 452, which clearly corresponds to the infrared O-ray band at 455 ± 8. Very weak lines appear also at 479 and 503, which are probably combination frequencies.

A Raman spectrum of α cristobalite powder has been taken by Harrand,[4] who reports great difficulty in obtaining any scattering of useful intensity. She has observed altogether a moderately sharp line at 470, and weak bands at 100 and 150 to 200. The 470 line clearly is distinct from the infrared band at 493, and is most probably infrared-inactive, though a very weak infrared companion could fail to be resolved by the reflection method.

Harrand[4] has also observed the Raman spectrum of vitreous silica, and agrees well with earlier workers in reporting strong scattering extending from about 275 up to a fairly sharp cutoff at 500 cm^{-1}. She observed that this whole band is strongly polarized, while some of the bands at higher frequencies are fully depolarized. The low-frequency band must accordingly arise from symmetric vibrations. The infrared spectrum appears to corroborate the Raman polarization data, though here again a weak infrared companion could escape detection.

It seems reasonable to assume that the Raman bands about 470 in quartz and cristobalite, and the broad vitreous silica band, are all symmetrical and infrared-inactive, and that all arise from the same type of vibration, which persists without very great alteration in all three structures. The infrared bands observed in the same region also seem to be related to one another, to judge from their similarity in frequency and intensity, and probably all come from a degenerate type of vibration, which the anisotropy of the quartz lattice splits into an antisymmetric and a degenerate vibration. Unfortunately, the Raman spectrum of cristobalite is so weak, and that of vitreous silica so diffuse, that it is probably futile at present to try to verify the degeneracy of the infrared bands in these materials by looking for Raman companions.

The assistance and advice of Dr. I. Šimon throughout this work is very gratefully acknowledged.

[4] M. Harrand, Compt. rend. **238**, 785 (1954).

Reactions of Br^{80}(18 min) Produced by Isomeric Transition of Br^{80m}(4.58 hr) with Benzene and Methylated Benzenes*

T. A. Carlson† and W. S. Koski
Department of Chemistry, The Johns Hopkins University, Baltimore, Maryland

(Received December 3, 1954)

The reactions of benzene, toluene, *para*- and *ortho*-xylene, and mesitylene with Br^{80} as a result of isomeric transition have been studied. It was found that the reactions were complex. The substitution reaction was accompanied by condensation reactions. Evidence was found that organic bromides with boiling points higher than bromobenzene were formed in appreciable yields. Hydrolysis experiments indicated that both primary and secondary bromides were included in these high boiling compounds. Scavenger experiments indicated that the substitution reactions were proceeding in the main through fast bromine atom reactions. No evidence was obtained that any appreciable amounts of the substitution reactions were proceeding through a positive bromine ion mechanism.

INTRODUCTION

Br^{80} exists in two isomeric forms. The metastable form decays with a half-life of 4.58 hours, by internal conversion, to the lower energy state which in turn decays with a half-life of 18 min, principally by beta emission to stable Kr^{80}. This internal conversion is accompanied by the Auger effect which results in an average positive charge on the bromine of +10 units.[1]

Some work has been done in recent years[2] in which investigators have interpreted their results in the light that the reactions of aromatic compounds with Br^{80} activated by the isomeric transition are influenced by rules of normal electrophilic substitution. Although the substitution of halogens on aromatic organic compounds is generally accomplished by an electrophilic attack, it would be erroneous to immediately conclude that reactions of the $+Br^{80}$ ions, produced as described above, on aromatic compounds would be affected by the factors influencing normal electrophilic substitution. The positively charged bromine ion is highly energetic and probably neutralizes itself by stripping electrons away from neighboring molecules and then reacts with the surrounding ions, radicals, or highly activated molecules it has formed. Our work on benzene, toluene, xylene, and mesitylene, which is reported below, does not support the theory of electrophilic attack but rather favors the latter notion.

EXPERIMENTAL

General Procedure

The general method for carrying out a hot atom reaction with Br^{80} consists of the preparation of the metastable Br^{80} in a form suitable for mixing intimately with the compound to be studied. The compound containing the Br^{80} is then mixed with the material whose reaction is being studied. The solution is permitted to stand until equilibrium is attained between the 4.58-hr Br^{80m} and its 18-min daughter. The Br^{80m} is then extracted and the product containing the 18-min activity is analyzed. This was accomplished by: (1) irradiating 4 to 5 kilograms of butylbromide with neutrons produced from the $Be^9(d,n)B^{10}$ reaction utilizing our electrostatic generator; (2) extracting about 1/5 of the bromide activity, produced by means of the Szilard-Chalmers effect, with an aqueous solution of LiBr; (3) refluxing the salt with acetone and bromoacetic acid to get the activity into the organic acid by exchange; (4) dissolving about ½ g of this acid with 30 g of the hydrocarbon to be studied and allowing the solution to stand for 2 hrs; (5) extracting the bromoacetic acid with water; (6) separating the bromine products remaining in the organic fraction by hydrolysis and/or distillation; and (7) counting the separated products (as well as an aliquot of the total 4.58-hr activity before extraction to determine the total Br 18-min retention) with a dip counter.

The benzene and toluene used were Mallinckrodt's Analytical Reagent Grade Chemicals. The remaining organic compounds used were Eastman Kodak's Eastman Grade Chemicals. Scavenger reactions were carried out on Br^{80} reactions with benzene, toluene, *para*-xylene, and mesitylene showing that impurities which might be present were not giving rise to erroneous results by scavenging action.

Analysis of Products

Br^{80} reactions on toluene, *para*-xylene, and mesitylene were carried out by the general procedure. Carriers for the side chain substituted bromide (about ½ g) and for the ring substituted bromide (about 2 g) of the respective hydrocarbons were added just before the extraction of bromoacetic acid with water. (A run in which the carriers were added after water extraction showed no change in the analysis.) The hydrolysis was

* Work done under the auspices of the U. S. Atomic Energy Commission.

† Abstracted in part from a thesis submitted by T. A. Carlson in partial fulfillment of the requirements for the degree of Doctor of Philosophy, The Johns Hopkins University, Baltimore, Maryland, 1954.

[1] S. Wexler, Phys. Rev. **93**, 182–7 (1954).

[2] N. Ivanoff and G. Gavoret, J. chim. phys. **50**, 524 (1953). G. Gavoret, J. chim. phys. **50**, 434 (1953); *ibid.* **50**, 183 (1953); N. Ivanoff, Bull. soc. chim. France **266** (1953); G. Gavoret and N. Ivanoff, *ibid.* **166** (1952). R. Daudel, Compt. rend. **228**, 1865 (1949).

carried out by refluxing the organic material 8 min with 10 ml of 5% alcoholic KOH. Two grams of KBr were also added to insure that none of the hydrolyzed bromide would remain with the nonhydrolyzed fraction. After hydrolysis, the organic material containing the unhydrolyzable products is separated from the KBr which contains the hydrolyzed products. The KBr is dissolved in water and both fractions counted with a dip counter.

To check the analysis, α bromoxylene was tagged with Br^{82} (36 hr) and then put through the procedure described above, including water extraction; and to within 5% all the activity from the α bromoxylene was found in the hydrolyzable fraction while <0.5% was found in the nonhydrolyzable state. The side chain and ring substituted bromides of toluene, *para*-xylene, and mesitylene were also checked for their behavior with regards to hydrolysis by use of silver nitrate titration. Less than 0.5% hydrolysis was noted for ring substituted bromides and the amount of hydrolysis of the side chain brominated compounds checked to within 5%.

Br^{80} runs were carried out on benzene and analyzed for lower boiling compounds in the following manner: (1) bromoacetic acid containing the 4.58-hr Br^{80m} was extracted with water, (2) ethyl bromide was added to the organic fraction as a lower boiling carrier, (3) the ethyl bromide was distilled off under 50 mm pressure, and (4) a hydrolyzable/nonhydrolyzable analysis was made on the remaining organic fraction.

A Br^{80} run was made on mesitylene in which methyl bromide was added as a carrier after radioactive bromoacetic acid had been in contact with mesitylene for 2 hours, and then distilled off immediately under 100 mm pressure and collected in a dry ice trap. The gas was then dissolved in alcohol. The method of distillation of methyl bromide was checked by running a blank in which the amount of methyl bromide carrier used and the amount of methyl bromide collected after distillation was measured by hydrolysis of the methyl bromide and subsequent titration with $AgNO_3$. The distillate checked to within 5% of the total carrier used.

Br^{80} reactions were carried out on benzene and the higher boiling products were analyzed as follows: after extraction of bromoacetic acid with water, a higher boiling carrier (about 1 g) and a lower boiling carrier (about 5 g) were added and the total organic solution fractionally distilled under 15 mm pressure. The lower boiling carrier (plus any compounds with boiling points lower than the low boiling carrier) were distilled away from the higher boiling compounds. The higher boiling compounds were then put through a hydrolyzable/nonhydrolyzable analysis. Experiments were also carried out in which the hydrolyzable/nonhydrolyzable analysis was carried out first, the nonhydrolyzable fraction then being fractionally distilled in the above manner. In these cases the materials composing the residue contained the higher boiling carrier and some inorganic bromides which resulted from the more stringent hydrolysis conditions during the course of the distillation. This residue was thoroughly washed with water and then dissolved in benzene and the activities in both the water and benzene portions were measured. To effect complete distillation, heat (100–200°C) was usually applied toward the end of the distillation. In the run using diphenyl as a higher boiling carrier, 50°C was applied.

Numerous checks were made to test the accuracy of the distillation. First, the weight of the distillation flask was taken before and after distillation to check whether the weight difference was compatible with the amount of carrier added and distilled off. In no case was the discrepancy greater than 10%. Radioactive bromobenzene, prepared from benzene and radioactive bromine, was mixed with mesitylene, benzene, 2 bromomesitylene, α bromomesitylene, and bromoxylene. This was put through hydrolysis and everything was distilled over except the bromomesitylene. An equal quantity of bromobenzene was taken for measurement of the activity used. Ninety-seven percent of the activity was found with the distilled products. No activity was found hydrolyzed. Five percent of the activity was found with the bromomesitylene, none of which was extracted with water. Even the small contaminant with the bromomesitylene might be partially explained by the presence of dibromobenzene (bp 220°C) which is a by-product in the synthesis of bromobenzene. The next check was the distillation of bromomesitylene under identical conditions of the hot atom experiments. The remaining products left after distillation were taken up with benzene and water as usual. The amount of hydrolysis was <1.5%. The possibility of exchange, especially under conditions of distillation, was investigated in a number of instances. This was not a complicating factor in any of the cases reported in this work.

Scavenging Experiments

Allyl bromide (about 2 mole %) was present during Br^{80} reactions on *para*-xylene, mesitylene, and benzene. After the extraction of bromoacetic acid with water, the allyl bromide was distilled from the organic fraction and collected. The remaining organic products were analyzed by separating into hydrolyzable/nonhydrolyzable fractions. The success of the allyl bromide distillation was checked by hydrolyzing the allyl bromide the next day and titrating with silver nitrate. About three-fourths of the allyl bromide was distilled over; the hydrolysis, however, offers a rather accurate correction (±5% of the correction). Only a ml or so of the 30 ml of the hydrocarbons, xylene, and mesitylene was distilled over, showing that the much higher boiling bromo compounds (200° to 240°C) such as bromoxylene or bromomesitylene were not distilled over.

Effect of Some Variables on the Br^{80} Reactions

Bromine 80 reactions were carried out on *para*-xylene in complete darkness, and under strong light

TABLE I. Results of hydrolyzable/nonhydrolyzable analysis expressed in percent of total Br^{80} reactions.

	Hydrolyzable (%)	Nonhydrolyzable (%)
Benzene	17	27
Toluene	26	20
Para-xylene	31	17
Ortho-xylene	30	15
Mesitylene	38	12

(tungsten bulb 250 watts, 1 foot distance). A hydrolyzable/nonhydrolyzable analysis was made.

Br^{80} reactions were carried out at $-8°C$ and at 23°C on toluene and mesitylene, respectively. A third reaction was carried out on *para*-xylene at 105°C. In each case, a hydrolyzable/nonhydrolyzable analysis was made.

Most Br^{80} reactions were carried out with 1.5 mole % bromoacetic acid. Reactions were also carried out as follows: *para*-xylene with 10 mole %, 3 mole %, and 0.4 mole % bromoacetic acid; mesitylene with 12% bromoacetic acid; toluene with 8% bromoacetic acid; benzene with 9%, 0.5%, and 0.05% bromoacetic acid. A hydrolyzable/nonhydrolyzable analysis was made on each of these reactions.

Besides the runs mentioned above, a Br^{80} reaction was carried out on benzene in which bromine (2.5 mole %) was used as a reaction initiator. The bromine was extracted with a NaSCN solution and the usual hydrolyzable/nonhydrolyzable analysis was made.

The activity level for the 4.58-hr bromine in the form of bromoacetic acid at time of extraction was of the order of 0.5×10^6 counts per minute. At the time of counting, the activity level for each of the bromine 18 min fractions ranged generally from 2000 to 4000 counts per minute. In calculating the probable error from the observable errors of weighing, pipetting, and errors in counting, one finds for an average run the error of the ratio of hydrolyzable to nonhydrolyzable products to be $\pm5\%$. In the hydrolyzable/nonhydrolyzable experiments, 5 runs each for benzene, toluene, *para*-xylene, and mesitylene showed an agreement to within 10%.

DISCUSSION OF RESULTS

A number of French investigators[2] have studied the reaction of Br^{80} with organic materials and they have interpreted their results in such a way as to indicate that at least a portion of such reactions proceed through the Br^+ ion and are influenced by the normal rules of electrophilic substitution. They have used hydrolysis criteria similar to the ones outlined in the experimental section to distinguish side chain substitution from ring substitution. If the radioactive organic material is readily hydrolyzed by alcoholic KOH, it was assumed to be brominated in the side chain. If it did not hydrolyze, it was assumed that the bromination took place on the ring. Therefore, if only simple substitution was present, the ratio of hydrolyzable to nonhydrolyzable activity was equal to the ratio of chain to ring substitution. We have carried out a number of experiments on benzene and related compounds and the percentage activity associated with the hydrolyzable and nonhydrolyzable organic material is tabulated in Table I. The only compound that we have studied in common with the French workers is toluene and here we get a hydrolyzable-nonhydrolyzable ratio of 1.3 which compares favorably with their value of 1.25. However, this simple criteria for chain and ring substitution is open to criticism when the results of the reaction of Br^{80} on benzene are examined. It is found that under our hydrolysis condition, 17% of the total activity could be readily hydrolyzed whereas 27% was not hydrolyzed giving a total organic retention of 44%. Why should one get a hydrolyzable organic bromine compound from benzene? It was demonstrated by using bromobenzene tagged with Br^{82} that it did not hydrolyze under our experimental conditions. Therefore, the conclusion must be reached that when Br^{80} reacts with benzene an appreciable fraction of reactions result in the formation of organic bromides other than bromobenzene. Secondary and possibly primary organic bromides must result since it is only such materials that would hydrolyze under our mild hydrolysis conditions. More discussion of this point will follow, however, we would like to at this time examine the results of some other experiments that have some bearing on these matters.

It has been noted[3] that bromine and certain unsaturated aliphatic bromides have the property of rapidly exchanging with bromine atoms. If such materials are present even in small amounts, they will "scavenge" all of the bromine atoms except those of very high energy. On the one hand, scavengers can be useful tools for determining the amount of bromine atoms present and consequently may indicate whether products of the reaction are formed from such species. On the other hand, scavengers present as impurities can be harmful by causing incorrect analyses.[4] We have run some Br^{80} reactions on benzene and related compounds in the presence of allyl bromide. These results which are tabulated in Table II have some interesting implications. Comparison of the data in Tables I and II shows that the presence of the scavenger did not alter the

TABLE II. Results of using allyl bromide during Br^{80} reactions expressed in percent of total Br^{80} reactions.

	Hydrolyzable (%)	Non-hydrolyzable (%)	Allyl bromide (%)
Benzene	17	25	37
Para-xylene	31	16	20
Mesitylene	38	10	21

[3] Roy, Williams, and Hamill, J. Am. Chem. Soc. **76**, 3274 (1954); S. Goldhaber and J. E. Willard, J. Am. Chem. Soc. **74**, 318 (1952).

[4] J. C. W. Chien and J. E. Willard, J. Am. Chem. Soc. **76**, 4735 (1954); M. S. Fox and W. F. Libby, J. Chem. Phys. **20**, 487 (1952).

total organic retention or the fraction of the activity that was present in hydrolyzable and nonhydrolyzable portions. Three conclusions can be drawn from these results. (1) The small amounts of impurities that might be present are not affecting the organic retention by scavenging. This is an important point since several authors[4] have pointed out that many of the hot atom results reported in the literature can be altered by purification of compounds used. Since oftentimes small amounts of impurities produce this effect, it is difficult to know when the materials are sufficiently pure. We have attempted to get around this difficulty, not by elaborate purification procedures, but rather by using a suitable criterion for purity. (2) Allyl bromide probably prevents HBr^{80} formation by the thermal process.[5] The residual inorganic yield in the presence of allyl bromide is presumably all the result of HBr formation by the high-energy process. (3) The reactions between the hydrocarbon and thermalized bromine atoms is negligibly small. It is of interest also to note that benzene gives almost twice as many scavengeable bromine atoms as do the methylated benzene compounds.

All of the experiments listed in Table I have been repeated in complete darkness as well as in a strong light produced by a tungsten bulb. The results in both cases were identical, indicating that ordinary light is not playing a role in these experiments.

Several of these reactions were run at −8°C, 23°C, and 105°C. The results are tabulated in Table III. It is clear that in going from −8°C to 23°C for toluene and mesitylene, there was no significant change either in the activities of the hydrolyzable or nonhydrolyzable materials indicating a zero or small activation energy for the reactions. In the case of *para*-xylene, there was no change in the activity of the nonhydrolyzable material in changing the reaction temperature from 23°C to 105°C. However, there was a change from 31% to 50% for the activity in the hydrolyzable fraction in going over this same temperature interval. The increase in the amount of hydrolyzable activity is the same as was scavenged by allyl bromide in this reaction. This suggests that the increased activity might be accounted for by thermally instigated reactions of bromine atoms with the side chain forming primary bromides.

TABLE III. Results of Br^{80} reactions at different temperatures, expressed in percent of total Br^{80} reactions.

	Temperature	Hydrolyzable (%)	Non-hydrolyzable (%)
Toluene	−8°C	27	18
Toluene	23°C	26	20
Mesitylene	−8°C	37	13
Mesitylene	23°C	38	12
Para-xylene	23°C	31	17
Para-xylene	105°C	50	16

[5] Roy, Williams, and Hamill, J. Am. Chem. Soc. **76**, 3274 (1954).

TABLE IV. Results of Br^{80} reactions at different bromoacetic acid concentrations expressed in percent of total Br^{80} reactions.

	Bromoacetic acid concentrations mole %	Hydrolyzable (%)	Non-hydrolyzable (%)
Benzene	0.05	17	29
Benzene	0.5	17	29
Benzene	9	27	24
Toluene	0.05	26	20
Toluene	8	33	18
Para-xylene	0.4	32	17
Para-xylene	3	33	17
Para-xylene	10	39	16
Mesitylene	0.05	38	12
Mesitylene	13	49	13

The effect of bromoacetic acid concentration was studied and the results are tabulated in Table IV. Bromoacetic acid was the reaction initiator in these cases. It will be noted that in going from 0.05 mole percent acid to 0.5 mole percent in the case of benzene no change in results was observed. A similar situation exists in *para*-xylene. However, in going to 9–10% bromoacetic acid, there was a noticeable increase in the activity of the hydrolyzable fraction. A similar observation was made in the case of toluene and mesitylene. On the other hand, the change was much smaller or even possibly zero in the activity of the nonhydrolyzable fraction. This effect suggests that the bromoacetic acid contains a small amount of impurities which act as scavengers for bromine atoms. In the cases of lower bromoacetic acid concentrations, the amounts of impurities are too small to cause appreciable scavenging but as the concentration is greatly increased the affect of the impurities becomes noticeable. It also has been pointed out to us that it is not impossible that the effect of high bromoacetic acid concentrations is due to a hot reaction of bromine atoms with the bromine of the bromoacetic acid and the resulting bromine molecule could then react with the hydrocarbon present. The nondependence of yield of activity in the hydrolyzable and nonhydrolyzable fractions at low reaction initiator concentration shows that free bromine molecules are not being formed by reaction of HBr^{80} or other species with the bromoacetic acid. Such free bromine molecules if produced could subsequently react with the hydrocarbon being studied and thereby offer a mechanism for the formation of various bromides.

Some reactions were performed in which free bromine was used as a reaction initiator. The results obtained were the same as reported in Table I. These observations further support our views listed above; namely, that there is no scavenging by impurities, bromoacetic acid is not involved in the Br^{80} reaction and, finally, the HBr^{80} cannot be directly involved in the reaction between Br^{80} and the hydrocarbons in question.

In view of the fact that readily hydrolyzable organic bromides are formed in the reaction between Br^{80} and various hydrocarbons studied, we carried out some experiments using methyl and ethyl bromide as carriers

TABLE V. Analysis of higher boiling compounds formed in Br^{80} reactions on benzene and methyl benzene compounds, expressed in percent of total Br^{80} reactions.

Reactant	Lower boiling compounds	Higher boiling compounds	Fraction extracted with water (%)	Fraction extracted with benzene (%)
Benzene	bromobenzene	diphenyl	9.7	4.3[b]
Benzene[a]	bromobenzene	anthracene	7.1	0.2[c]
Toluene	bromotoluene	anthracene	3.1	0.1[c]
Para-xylene	bromoxylene	anthracene	8.2	1.7[c]
Mesitylene	bromomesitylene	anthracene	6.7	0.3[c]

[a] Bromine was used as a reaction initiator in these two runs.
[b] Hydrolysis after distillation.
[c] Hydrolysis before distillation.

to see if any of the activity was in that molecular form. The results were conclusively negative, indicating that in reactions involving benzene and mesitylene no methyl or ethyl bromides were formed.

The various reactions that go on in the solutions that we are studying are radical reactions. It is therefore reasonable to suspect that some of these radicals combine to form higher boiling compounds. For this reason, low and high boiling carriers were added to the reaction solutions after the bromoacetic acid was removed and the resulting solution distilled. The higher boiling materials (in the case of benzene, these were materials boiling higher than bromobenzene) were subjected to the hydrolysis conditions outlined in the experimental section. These results are given in Table V. It is apparent that most of these high boiling bromides are hydrolyzed by alcoholic KOH, especially if the higher temperature conditions associated with the distillation are used Under these conditions, bromobenzene did not give any noticeable hydrolysis. This then suggests that the high boiling materials do not contain appreciable amounts of aromatic bromides. It is possible that these higher boiling compounds may contain materials that have been formed from aromatic radical combinations. Such materials might have a quinoid structure and if a bromine was attached to the appropriate position it would behave as a secondary bromide and have hydrolysis properties very similar to the ones observed.

Finally some Br^{80}-*ortho*-xylene reactions were studied. Macauley and Lien[6] found that the relative basicity of *ortho*-xylene to *para*-xylene was 3. Furthermore, the *ortho*-xylene should present less steric effect to ring substitution. So if either or both of these effects have any influence on the hot atom reaction, one might expect an increase in ring substitution if this process is going by means of a positive ion. Comparison of the data in Table I shows no significant difference between *ortho*- and *para*-xylene.

The various results discussed above suggest the following picture for the hot atom reactions between Br^{80m} and benzene and methylated benzenes. The bromine immediately after isomeric transition has a high positive charge and, as such, will pull electrons away from neighboring molecules producing organic ions and excited molecules. Even when the charge on the bromine is reduced to one, it does not appear likely that the ion would react with the benzene since the first ionization potential of bromine is 12.8 volts, whereas, for benzene it is 9.6 volts. Therefore, it would be expected that the bromine ion would extract an electron from a neighboring benzene molecule rather than reacting with it. If this picture were true, we would expect not to get any or at least very few reactions involving positive ions. The reactions involved would then in the main be reactions of atoms, both fast and thermal.[7] Such atoms would be expected to react with benzene, toluene, etc., to form a radical and HBr^{80} so this compound would be one of the expected products. The scavenger experiments indicate that the thermal Br atoms are not producing substitution reactions on the chains or the aromatic rings. Presumably, any substitution compounds that are formed are brought about by fast bromine atoms. The higher boiling bromine derivatives may be formed by ion radicals and radical combinations. Small amounts of bromobiphenyl might be expected and it is also a possibility that by combination of ion radicals and bromobenzene, etc., that higher boiling compounds with a quinoid structure may be obtained. The bromine then would behave like a secondary bromide and it would exhibit hydrolysis properties similar to those observed.

ACKNOWLEDGMENTS

One of the authors (T. A. Carlson) wishes to acknowledge a grant-in-aid from the Hynson, Westcott, and Dunning Research Fund.

[6] D. A. Macauley and A. P. Lien, J. Am. Chem. Soc. **73**, 2013 (1951).
[7] J. E. Willard, Ann. Rev. Nuclear Sci. **3**, 193 (1953).

On the Optical Properties of Solids

HERBERT B. ROSENSTOCK
U. S. Naval Research Laboratory, Washington, D. C.
(Received March 18, 1955)

A consistent treatment of the usual linear theory of lattice vibrations in ionic crystals without the use of the symplifying cyclic boundary conditions is shown to lead to an electric moment associated with each normal frequency which, like the frequency itself, is a quasicontinuous function of the propagation vector. As a result, a broadening of the line spectrum of elementary theory and additional absorption edges of apparently observable magnitude are predicted.

I. INTRODUCTION

THE usual elementary theory of crystal lattices[1] (henceforth called zero-order theory) predicts that an ionic crystal with n atoms per unit cell will have an infrared absorption spectrum (also reflection[1] and Raman[2] spectrum) consisting of at most $3n-3$ sharp lines. This result follows from the assumption that the atoms interact by forces which are linear in the displacements and from the use, at least implicitly, of the simplifying so-called "cyclic" boundary conditions. The more complicated spectra provided by experiment have in the past been qualitatively explained by theories properly called "second-order," as they utilize terms quadratic in the displacements, introduced into the previously linear theory either in the equations of motion[3] or in the expression for the dipole moment.[4] The purpose of the present paper is to show that a consistent treatment of the "first-order" (linear) theory with the correct boundary conditions leads, in addition to the zero-order results, to effects which should be observable and may help to explain experimental results.

II. BACKGROUND

To an often satisfactory approximation, a crystal may be viewed as a large number of point atoms which are arranged in space in a regular lattice and are moving about their respective lattice sites by small distances impelled by harmonic forces of interaction with their neighbors.[1] By a normal mode transformation, the variables (atomic displacements) may be separated and one vibrational frequency may be associated with each normal coordinate. The normal frequencies all fall into a finite range, and since their total number, equal to the number of atoms in the crystal multiplied by the number of degrees of freedom per atom, is very large, a quasicontinuous spectrum $g(\omega)d\omega$, giving the fractional number of normal frequencies in the frequency range $d\omega$, can be reasonably defined. The extent to which an oscillator will absorb (or emit) electromagnetic radiation of its resonant frequency is directly proportional to the change in the squared electric dipole moment associated with the vibration; if we want to know the absorption spectrum of the crystal we must therefore first of all calculate the dipole moment associated with each normal frequency.[5] The dipole moment however depends on the original atomic displacements; therefore to find the component of the dipole moment associated with each normal frequency we must use the inverse of the normal coordinate transformation to expand the atomic displacements in terms of the normal coordinates.

Finding the normal coordinates explicitly first requires the finding of the normal frequencies, which is a difficult problem in practice. It is done by writing down the three Newtonian equations of motion $\mathbf{F}=m\mathbf{a}$ of each of the nN^3 atoms, and assuming that all atomic displacements depend on time harmonically. n is the number of atoms per unit cell, N^3 is the number of cells in the crystal. Since F on any atom depends linearly on the displacement not only of the atom in question but also on the displacements of neighboring atoms, $3nN^3$ simultaneous linear equations result; they may be solved for the frequency. However, on account of the translational symmetry of the lattice only $3n$ of these equations are actually different. (It is this fact that makes the actual computation feasible in some few nontrivial cases.[6])

A troublesome exception to the preceding statement comes to light if we consider the atoms on the boundary of the crystal: their equations of motion will differ from those of corresponding atoms inside because the forces on them are different. In calculations of crystal frequency spectra the standard way of avoiding this difficulty is the use of the so-called "cyclic" or "Born-von Karman" boundary conditions. The recipe for this is: replace the correct equations for the boundary atoms by equations identical in form with those for interior atoms, and require in addition that all displacements of all atoms on one surface be identical with the

[1] M. Born and M. G. Mayer, *Handbuch der Physik* (Springer-Verlag, Berlin, Germany, 1933), 24/2, p. 632, Sec. II.
[2] M. Born and M. Bradburn, Proc. Roy. Soc. (London) **A188**, 161 (1947).
[3] M. Born and M. Blackman, Z. Physik **86**, 421 (1933); Barnes, Brattain, and Seitz, Phys. Rev. **48**, 582 (1935).
[4] M. Lax and E. Burstein, Phys. Rev. **97**, 39 (1955).
[5] Since classical and quantum mechanics give the same results for harmonic oscillators, formulation of this paper in classical terms entails no error. When nonlinearities are introduced, the two formulations give different results.[3,4]
[6] References to such work are given in the paper cited in footnote 16.

corresponding displacements of the corresponding atoms on the opposite surface. (This means in effect replacing the finite but large crystal by an infinite one consisting of blocks, each block the size of the original crystal and each block identical with any other block at any one time. Alternatively, one-dimensional crystals with cyclic boundary conditions may be visualized as in Fig. 2, where the ends of the ordinary crystal (Fig. 1) have been identified (tied together); the corresponding model of the two-dimensional crystal with cyclic boundary conditions would show the atoms arranged on the surface of a torus, and the corresponding model of the three-dimensional crystal with cyclic boundary conditions would show the atoms arranged on the 3-surface of a 4-torus.) This simplification was used by many workers, including the originators,[7] as a matter of course, because it seemed intuitively obvious to them that the applied boundary conditions could not affect the frequency distribution appreciably; after others objected,[8] their intuition was vindicated by a theorem proved by Lederman[9] which states: If, in a hermitian matrix the elements of r rows and their corresponding columns are modified in any way whatsoever, provided only that the matrix remains hermitian, then the number of characteristic values which lie in any interval cannot increase or decrease by more than $2r$. It follows almost at once that the frequency distribution obtained by use of the cyclic boundary conditions, $g_c(\omega)$ is related to the correct $g(\omega)$ by $g_c=g[1-0(1/N)]$ everywhere. The propriety of using the cyclic boundary conditions in problems of a statistical nature (e.g., problems of computing thermodynamic quantities by statistical mechanical methods) may therefore be considered established. However, in treating phenomena to which each individual normal mode contributes individually (e.g., optical problems) the possibility that small changes in each normal mode may have large cumulative effects is not excluded by the above argument.

In the following we propose to show that such cumulative effects do indeed occur in the calculation of the dipole moment associated with lattice frequencies, and that the use of the cyclic boundary conditions (zero-order theory[1]) in this connection has in the past led to overly simple results. We shall calculate the dipole moment of the one-dimensional diatomic lattice (which is the only model both nontrivial and easily tractable in detail) using the correct set of equations of motion; we shall find the dipole moment to be a quasicontinuous function of the wave number, and hence of the frequency, in contradiction to the zero-order result, obtained by use of the cyclic boundary conditions, that the dipole moment vanishes for all wave numbers other than zero. To be sure, a strong peak appears at the point predicted by zero-order theory. The calculation can be repeated semiquantitatively for three-dimensional crystals and the qualitatively important features of the dependence of dipole moment on frequency can be exhibited. The effects predicted are a broadening of the zero-order line spectrum and in addition several "absorption edges" at frequencies different from those of the zero-order spectrum. An estimate of the order of magnitude of these effects shows that the latter effects should be experimentally observable, though the former probably will not be.

[7] M. Born and Th. v. Karman, Physik Z. **13**, 279 (1912).
[8] C. V. Raman, Proc. Indian Acad. Sc. **A18**, 237 (1943).
[9] W. Lederman, Proc. Roy. Soc. (London) **A182**, 362 (1944).

III. CALCULATIONS FOR THE ONE-DIMENSIONAL LATTICE

We first write down the equations of motion, normal modes and frequencies for the one-dimensional diatomic lattice, indicating in detail how each is obtained from the preceding one; we do this both for the exact equations and for the equations resulting from the use of the cyclic boundary conditions. This amounts to little more than recopying work of Born's,[10] done, at a time before the appearance of Lederman's definitive theorem, with the purpose of defending the cyclic boundary conditions against the criticism to which it had been subjected. After harmonic time dependence has been assumed, the exact equations of motion become

$$(1-m_1\lambda)u_1=v_1, \quad (2-m_2\lambda)v_1=u_1+u_2, \tag{1.1}$$

$$(2-m_1\lambda)u_l=v_{l-1}+v_l,$$
$$(2-m_2\lambda)v_l=u_l+u_{l+1}\ l=2,3,\cdots N-1, \tag{1.l}$$

$$(2-m_1\lambda)u_N=v_{N-1}+v_N, \quad (1-m_2\lambda)v_N=u_N. \tag{1.N}$$

Here the longitudinal displacements of successive atoms are called $u_1, v_1, u_2, v_2, \cdots u_N, v_N$, (Fig. 1) so that there are $2N$ atoms in all; the u and v atoms have mass m_1 and m_2, respectively, $\lambda\equiv\omega^2/2\alpha$ is proportional to the squared frequency, and α is the force constant for nearest neighbor interaction, other interactions being, without loss of generality for present purposes, assumed absent. As the inverse normal mode transformation one assumes

$$u_l=\sum_j (A_{1j}\cos l\phi_j+A_{2j}\sin l\phi_j)\sin\omega_j t$$
$$v_l=\sum_j (B_{1j}\cos l\phi_j+B_{2j}\sin l\phi_j)\sin\omega_j t \tag{2}$$

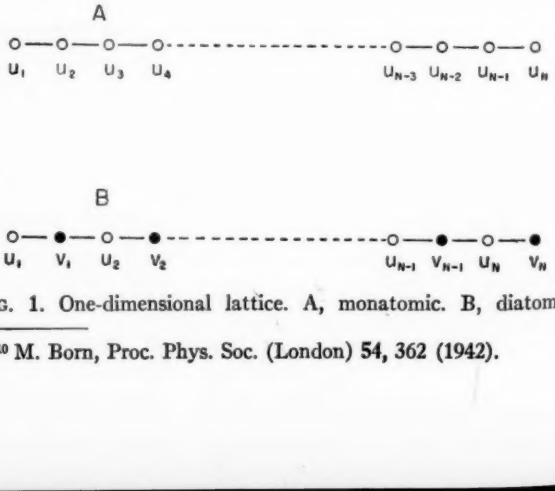

FIG. 1. One-dimensional lattice. A, monatomic. B, diatomic.

[10] M. Born, Proc. Phys. Soc. (London) **54**, 362 (1942).

with the A, B, and ϕ undetermined at this point. Putting (2) into (1.l) enables us[11] to solve for λ:

$$\lambda_{j\pm}=[(m_1+m_2)/m_1m_2]\{1\pm[\cos^2(\phi_j/2)+((m_1-m_2)/m_1m_2)^2\sin^2(\phi_j/2)]^{\frac{1}{2}}\}. \quad (3)$$

We then put (2) into (1.1) and (1.N) and obtain as compatibility conditions for these equations the permitted values of the ratios A_{1j}/A_{2j}, B_{1j}/B_{2j}, A_{1j}/B_{1j}, and of ϕ_j; for the latter we find explicitly

$$\sin N\phi_j=0, \quad (4)$$

from which follows

$$\phi_j=j\pi/N, \quad j \text{ an integer}. \quad (5)$$

The ratios between the A's and B's depend on λ and are thus rather complicated expressions even for this simple crystal model. However once they have been found explicitly, the dipole moment

$$P=e_u\sum_{l=1}^{N}u_l+e_v\sum_{l=1}^{N}v_l \quad (6)$$

can be calculated.

In searching for a nontrivial problem so simple that (6) can be evaluated explicitly, we notice that λ simplifies substantially if $m_1=m_2$ ("one-dimensional KCl lattice"). This case however can be treated even more easily if we use the equations for the monatomic lattice.[12] The equations of motion after insertion of harmonic time dependence, are in that case

$$(1-m\lambda)u_1=u_1, \quad (7.1)$$

$$(2-m\lambda)u_l=u_{l-1}+u_{l+1}, \quad l=2, 3, \cdots, N-1, \quad (7.l)$$

$$(1-m\lambda)u_N=u_{N-1}, \quad (7.N)$$

where again $\lambda\equiv\omega^2/2\alpha$. One again assumes a solution

$$u_l=\sum_j (A_{1j}\cos l\phi_j+A_{2j}\sin l\phi_j)\sin\omega_j t \quad (8)$$

and finds,[10] as may be verified by the same methods as above,

$$m\lambda=2(1-\cos\phi_j)=4\sin^2\phi_j/2 \quad (9)$$

and the A are such that (8) may be written

$$u_l=\sum_j U_j\cos(l-\tfrac{1}{2})\phi_j \quad (10)$$

with

$$\phi_j=j\pi/N, \quad j \text{ an integer}.$$

The range of j can be restricted 0, 1, 2, $\cdots$, N, because in that range λ, as given by (9), takes on every possible value once. Furthermore, $j=N$ can be eliminated because then (10) leads to the trivial solution $u_l=0$ for all l. Therefore the N nontrivial solutions that this system of N degrees of freedom must have are obtained by taking $j=0, 1, 2, \cdots, N-1$. We now assume that even atoms have charge $+e$ and odd ones have charge $-e$, and also that the total number N of atoms is even. The dipole moment (6) then becomes

$$P=e\sum_{l=1}^{N}(-1)^l u_l \quad (11)$$

and with (10)

$$P=e\sum_{j=0}^{N-1}(U_j\sin\omega_j t)p_j, \quad (12)$$

where p_j, the dipole moment associated with the jth mode and the corresponding frequency, is given by

$$p_j=\sum_{l=1}^{N}(-)^l\cos(l-\tfrac{1}{2})\phi_j,$$

which is found in Appendix I to be

$$p_j=-1/\cos(\phi_j/2) \quad \text{if } j \text{ is odd, zero otherwise.} \quad (13)$$

The largest dipole moment is associated with $j=N-1$,

$$p_{N-1}=-1/\cos[(N-1)\pi/2N]\cong-2N/\pi \quad (14)$$

corresponding to the frequency $m\lambda_{N-1}=4\sin^2(N-1)\pi/2N\cong 4$. We see that the dipole moment is a quasi-continuous function of the wave number just as the frequency itself is.

The same result may be obtained in a much more complicated fashion by using Eqs. (1) through (5) for the diatomic lattice and setting $m_1=m_2$. The maximum moment occurs at the same frequency but corresponds to wave number $j=1$ of the + branch in that notation. In terms of this, the normal, way of labeling wave numbers we should then say that our crystal has the largest moment corresponding to the long wavelength frequencies of the "optical" branch. Again half the frequencies in each branch have nonzero moments. We write down, for future reference, the result[13] for the dipole moment:

$$p_j=\begin{cases}\sin(\phi_j/4)/\sin(\phi_j/2) & \text{for the } -\text{branch}\\ \cos(\phi_j/4)/\sin(\phi_j/2) & \text{for the } +\text{branch}\end{cases} \quad (15)$$

for odd j, and $p_j=0$ for even j.

To get physically interpretable results for the one-dimensional KCl lattice, we first eliminate the wave number from Eqs. (13) and (9) and get $p_j=[1-m\omega_j^2/8\alpha]^{-\frac{1}{2}}$ for the dipole moment associated with normal frequency ω_j; the quantity of interest in

[11] The defining equation for the quantity μ in reference 10 should read

$$\mu=(m_1-m_2)/(m_1+m_2).$$

[12] If the masses of the positively and negatively charged atoms is the same, then the lattice will be monatomic from the dynamical standpoint; a given atom does not know whether it is attracted to its neighbor because the neighbor is positive and it is negative itself, or vice versa. This has been pointed out by M. Smollett, Proc. Phys. Soc. **A65**, 109 (1952).

[13] An easy way to satisfy oneself that (15) is equivalent to (13) is to eliminate j from (15) and (3); the result for either branch is $p=(1-m\omega^2/8\alpha)^{-\frac{1}{2}}$, the same as is obtained in the text by eliminating j from (13) and (9).

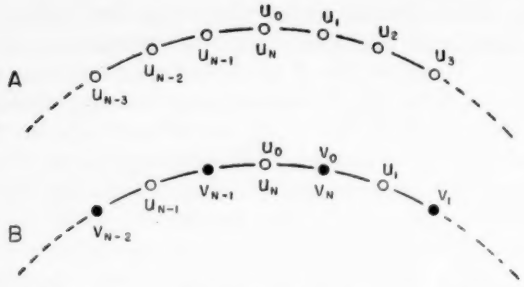

FIG. 2. One-dimensional lattice with cyclic boundary conditions. A, monatomic. B, diatomic.

absorption calculations would be p_j^2, and to get the squared dipole moment associated with frequency interval $d\omega$ we multiply by the frequency distribution[14] $G(\omega)d\omega=[1-m\omega^2/8\alpha]^{-\frac{1}{2}}$ to obtain

$$\pi^2(\omega)d\omega=[1-m\omega^2/8\alpha]^{-\frac{1}{2}}d\omega. \tag{16}$$

For purposes of comparison we now solve the same problem with the use of the cyclic boundary conditions, in order to get the result of zero-order theory. The computational simplification is so great that the diatomic case is almost as easily worked out as the monatomic one; we therefore use the diatomic formulation. Using the cyclic boundary conditions means replacing the system of Eqs. (1.1) (1.l), (1.N) by (1.l) with l=1, 2, $\cdots$, N−1 and requiring in addition $u_0=u_N$, $v_0=v_N$. As a solution we take, instead of (2)

$$\left.\begin{aligned} u_l&=\sum_j (A_{1j}e^{il\phi_j}+A_{2j}e^{-il\phi_j})\sin\omega_j t\\ v_l&=\sum_j (B_{1j}e^{il\phi_j}+B_{2j}e^{-il\phi_j})\sin\omega_j t\\ \phi_j&=2\pi_j/N,\quad j=0,1,\cdots,N/2 \end{aligned}\right\} \tag{17}$$

where the factor 2 appears in ϕ_j in order to assure that $u_0=u_N$, $v_0=v_N$. (17) gives four linearly independent normal coordinates (A_{1j}, A_{j2}, B_{1j}, B_{2j}) for $j=1, 2, \cdots$, $(N/2)-1$, and two each for $j=0$ and $j=N/2$, so that the total number of normal coordinates is $2N$, equal to the total number of original coordinates u_l and v_l, as it should. The dipole moment, given by (6) with $e_u=-e_v=e$ is evaluated in Appendix II and found to be proportional to N for $j=0$ in the + branch and identically 0 for all other j. In terms of frequency, this becomes

$$(\Pi^c)^2(\omega)\alpha\omega=\text{const}\ N^2\delta[\omega-(8\alpha/m)^{\frac{1}{2}}]d\omega.$$

We are now also able to understand intuitively, by direct reference to Figs. 1 and 2, how the difference between zero-order theory and present first-order theory is brought about by the use of the cyclic boundary conditions in zero-order theory. In the cyclic crystal, Fig. 2, it seems clear that there will exist a mode in which each white atom is displaced clockwise the same amount (at any one particular instant) and each black atom counterclockwise the same amount, and if it does exist then each cell will have a large dipole moment and the dipole moments of the individual cells will add. It also seems reasonable that for the other possible vibrations the moments will cancel by interference. In the rigorous case, Fig. 1, this exceptional "totally symmetrical" vibration can no longer exist because at the end points the symmetry has been destroyed, and as a result a more smeared-out distribution of dipole moments can be expected for the other modes as well.

[14] F. Seitz, *The Modern Theory of Solids*, (McGraw-Hill Book Company, Inc., New York, 1940), p. 121.

IV. EXTENSION TO THREE-DIMENSIONAL CRYSTALS

In zero-order theory, the use of the cyclic boundary conditions makes the calculation of the dipole moment for the general three-dimensional crystal with n atoms per unit cell just as easy as it is for the one-dimensional crystal, as examination of Appendix II will reveal. Born and Mayer[1] do this calculation in detail. The result is that for all $\omega_\mathbf{j}$ except possibly ω_0 ("limiting free quencies") the dipole moment vanishes. (We abbreviat-(j_1,j_2,j_3) by $\mathbf{j}$ and (l_1,l_2,l_3) by $\mathbf{l}$). For the acoustical branches ω_0 is 0 (translation), and no dipole moment is associated with it. The zero order spectrum of a crystal with n atoms per unit cell will therefore consist $3n-3$ sharp lines, or fewer if for reasons of symmetry several of the limiting frequencies coincide.

In first-order theory the calculation of the dipole moment for the general three-dimensional crystal with n atoms per unit cell is substantially more difficult than it is for the one-dimensional crystal. It is not possible to carry the first order theory out in all detail, but we can establish many of the important features. The inverse normal mode transformation, comparable to (2), is

$$u_{k\mathbf{l}}{}^\alpha=\sum_\mathbf{j} U_{k\mathbf{j}}{}^\alpha S_{\mathbf{lj}}\sin\omega_\mathbf{j} t. \tag{18}$$

Here the left-hand side means the displacement in the α direction ($\alpha=1,2,3$) of the kth atom ($k=1,2,\cdots,n$) in cell $\mathbf{l}$ ($(l_1,l_2,l_3=1,2,\cdots,N)$. The α component of dipole moment is $P^\alpha=\sum_{\mathbf{l}k}e_k u_{k\mathbf{l}}{}^\alpha$ where e_k is the charge on the kth atom. With (18) this can be put in the form

$$P^\alpha=\sum_\mathbf{j}\Psi_\mathbf{j}[\sum_k e_k U_{k\mathbf{j}}{}^\alpha]\sin\omega_\mathbf{j} t, \tag{19}$$

where $\Psi_\mathbf{j}\equiv\sum_\mathbf{l}S_{\mathbf{lj}}$. This formula is to be compared with (12).

For $S_{\mathbf{lj}}$ we may take

$$S_{\mathbf{lj}}=\cos(l_1\phi_{j1}+l_2\phi_{j2}+l_3\phi_{j3}+\theta_\mathbf{j}), \tag{20}$$

where the $\phi_{j\beta}$ will be linear functions of the j_β ($\beta=1,2,3$). Fortunately we may proceed without explicit knowledge of the phases $\theta_\mathbf{j}$ and the exact permitted values of the $\phi_\mathbf{j}$; finding them explicitly would, as in the one-dimensional case, involve the equations of motion and the

frequencies explicitly. (19) with (20) gives

$$2\Psi_j=\sum_{\mathbf{l}} \exp i(\mathbf{l}\cdot\boldsymbol{\phi}_j+\theta_j) \text{ +complex conjugate}$$

or

$$2\Psi_j=\sum \exp i\theta_j g_N(y_1)g_N(y_2)g_N(y_3) \text{ +complex conjugate}$$

in the notation of Appendix I with $y_\beta=\exp(i\phi_{j\beta})$. Using (A.4) for $g(y)$ we find

$$\Psi_{jk}'=\frac{(\sin N\phi_{j1}/2)(\sin N\phi_{j2}/2)(\sin N\phi_{j3}/2)}{(\sin\phi_{j1}/2)(\sin\phi_{j2}/2)(\sin\phi_{j3}/2)}\times\cos[\tfrac{1}{2}(1+N)(\phi_{j1}+\phi_{j2}+\phi_{j3})+\theta_j]. \quad (21)$$

The index k' ($k'=1,2,\cdots,n$) has been put in because θ_j (and ω_j) is an n-valued function of the wave numbers (n "branches" or solutions of the nth order secular equation). Formula (21) should be compared with (15). If again $\phi_{j\beta}=\pi j_\beta/N$, then the three sin terms in the numerator would again be 1 or 0 depending on whether j is even or odd, but we have not established this precise relationship between j and ϕ_j. The important feature of (21) is the denominator which becomes large when any one $\phi\to 0$. For physical reasons we expect that in case of the three acoustical branches the cos term in the numerator will be such as to cancel this divergence, as happens in (15). Only wave numbers or frequencies with which large dipole moments are associated will concern us henceforth; we therefore exclude the acoustical branches and write (19) as

$$P=\sum_{\mathbf{j}} V_{\mathbf{j}}(\sin\omega_{\mathbf{j}}t)/\phi_{j1}\phi_{j2}\phi_{j3}, \quad (22)$$

where factors essentially constant in the range we are interested in have been lumped into the coefficient V_j, or

$$p(\boldsymbol{\phi})=1/\phi_1\phi_2\phi_3 \quad (23)$$

for the component of dipole moment associated with mode $\mathbf{j}$. We abbreviate $\boldsymbol{\phi}$ for ϕ_j, ϕ_β for $\phi_{j\beta}$. The smallest value each ϕ_β will take on will be $\sim 1/N$; hence $p(\boldsymbol{\phi})$ will approach N whenever one ϕ_β becomes small (near three faces of the cube $0<\phi_1,\phi_2,\phi_3<\pi$); N^2 when two ϕ_β become small (near three edges of that cube); and N^3 when all three ϕ_β become small (near one corner of that cube).

To understand the physical content of the foregoing, we must again express P as a function of frequency, not of wave number. Let

$$\omega=f(\boldsymbol{\phi}) \quad (24)$$

be the expression for the frequency in terms of wave number. Then the squared dipole moment in terms of frequency will be

$$\Pi^2(\omega)=\int_{f(\boldsymbol{\phi})=\omega} p^2(\boldsymbol{\phi})d\boldsymbol{\phi}$$

TABLE I. Leading term of $\Pi^2(\tilde{\omega})$, the squared dipole moment as a function of frequency, obtained by evaluating (25) near a corner of the cube. $\tilde{\omega}\equiv\omega-\omega_c$, is the frequency at the corner, and ω_1 is the frequency closest to ω_c that is actually taken on.

$f(\boldsymbol{\phi})$	$p(\boldsymbol{\phi})$	$\Pi^2(\tilde{\omega})$ $\tilde{\omega}<0$	$\tilde{\omega}>0$	$\Pi^2(\tilde{\omega}_1)$
$\phi_1^2+\phi_2^2+\phi_3^2$	$1/\phi_1\phi_2\phi_3$	const	$\tilde{\omega}^{-3/2}$	N^6
	$1/\phi_2\phi_3$	const	$\tilde{\omega}^{-1/2}$	N^4
	$1/\phi_3$	const	$\tilde{\omega}^{-1/2}$	N^6
$\phi_1^2+\phi_2^2-\phi_3^2$	$1/\phi_1\phi_2\phi_3$	$(-\tilde{\omega})^{-9/4}$	const	N^6
	$1/\phi_2\phi_3$	const	$\tilde{\omega}^{-1}$	N^4
	$1/\phi_1\phi_2$	$(-\tilde{\omega})^{-3/2}$	const	N^4
	$1/\phi_3$	$(-\tilde{\omega})^{-1/2}$	const	N^2
	$1/\phi_2$	const	$\tilde{\omega}^{-1}$	N^2

or

$$\Pi^2(\omega)=\int_{\text{all}\boldsymbol{\phi}} p^2(\boldsymbol{\phi})\delta[f(\boldsymbol{\phi})-\omega]d\boldsymbol{\phi}. \quad (25)$$

In case of the one-dimensional KCl lattice we knew (24) explicitly [Eq. (9)] and (25) could therefore be evaluated [resulting in (16)], but for the general three-dimensional crystal the expression (24) is not usually explicitly available. However, enough is known about it to enable us to use (25) to deduce some interesting features of Π^2: it is known that[15] $f(\boldsymbol{\phi})$ has critical points (i.e., maxima, minima, and saddle points, or, analytically speaking, points about which the Taylor expansion of $f(\boldsymbol{\phi})$ contains no linear terms) and that[16] most of these critical points occur at the corners of the cube $0<\phi_1\phi_2\phi_3<\pi$. Near the corners of the cube, the quantities in (25) can therefore take the following forms: $p(\boldsymbol{\phi})=1/\phi_1\phi_2\phi_3$ or $1/\phi_2\phi_3$ or $1/\phi_3$, and $f(\boldsymbol{\phi})=\omega_c\pm\phi_1^2\pm\phi_2^2\pm\phi_3^2$ where ω_c is the frequency at the corner; coefficients of ϕ_β^2 have been omitted for simplicity. With these functions the first two integrations in (25) can be done in closed form and the leading term resulting from the third integration can be found. The results are given in Table I. The first row in Table I corresponds to the "sharp line" of zero-order theory; it is seen to be slightly broadened on one side according to $|\omega-\omega_c|^{-\frac{1}{2}}$. The fifth and sixth row of Table I give the most important new effect predicted by present first-order theory: $\Pi^2(\omega)$ is constant on one side of ω_c and decreases (increases) rapidly on the other: an "edge" type effect in the absorption spectrum. (The situation described by rows 2, 3, 4 is not likely to arise in practice.)

These new effects are seen to be proportional to N^4 (the squared surface) rather than N^6 (the squared volume) as is the main absorption line. In view of the fact that present theory differs from zero-order theory only in our refusal to ignore the proper boundary (surface) conditions, this is not surprising. Note, however, that in contrast to other frequently encountered "surface effects," the present effects do not

[15] L. vanHove, Phys. Rev. **89**, 1189 (1953).
[16] H. B. Rosenstock, Phys. Rev. **97**, 290 (1955).

vanish as the crystal becomes infinitely large: they are not modifications or perturbations of the zero-order effects, but appear at frequencies different from the zero-order effects, hence are not directly affected by them, and as the crystal increases in size, their importance will increase as $(N^2)^2=$ (surface)^2, not decrease as $(N^2/N^3)^2=$ (surface/volume)^2.

Will these effects be observable experimentally? This might be done by infrared or Raman spectroscopy; let us confine ourselves to the former. For the broadening of the main absorption line, the answer is probably no, because the slight broadening predicted is likely to be masked by larger effects such as the poor resolution of infrared spectrometer in that region of the spectrum (at 30 microns, a resolution of 0.1 micron may be expected). For the "edge" effects the answer might, however, be yes, even though the peak intensity near the edge is down by a factor of N^2 from the maximum of the zero line. The number N should be taken as only $\sim 10^3$ rather than the usual 10^8 because for observation of the zero order line, thin films (about 0.1 microns thick[17]) are used as crystal specimen on account of their extreme opacity there; weak effects in other regions might therefore be intensified by using thicker crystals. Also, the apparent difference in intensity between the line and the edge will be decreased by the instrumental smearing out of the line (Appendix III). Finally, observe that the other effects that the present ones must compete with and which have in the past been used to explain experimental results are of second order (in the sense of Sec. I), hence also small. The comparative ease with which the present first-order theory might be pushed to the point of giving quantitative results should therefore make detailed computations worthwhile.

Infrared spectra of solids have also been discussed theoretically from a different viewpoint by Winston and Halford[18] and by Hornig.[19] They treat solids as aggregations of molecules to which they then apply group theoretic analysis, in contrast to the Born-von Karman approach[1,7] which treats the solid as one giant molecule. Their zero-order results agree with zero-order theory, and as their treatments either utilize cyclic boundary conditions[18] or ignores boundaries entirely by taking the crystal as rigorously infinite,[19] is equally subject to the present criticism. The same is true for the accepted theory of the Raman effect,[2] where sums identical in form to Ψ are evaluated, in connection with computation of the polarizability, with the use of the cyclic boundary contitions.

This paper has benefited greatly from both constructive and destructive criticism of Professor W. A. Bowers. Various aspects of it have also been discussed with Dr. C. A. Beck, Mr. E. Burstein, Dr. F. E. Geiger, Jr., Dr. J. Karle, Dr. C. C. Klick, Professor M. Lax, Dr. J. A. Sanderson, and Dr. J. H. Taylor.

[17] R. B. Barnes, Z. Physik **75**, 732 (1932); R. B. Barnes and M. Czerny, Z. Physik **72**, 447 (1931); Barnes, Brattain, and Seitz, footnote 3.
[18] H. Winston and R. S. Halford, J. Chem. Phys. **17**, 607 (1949).
[19] D. F. Hornig, J. Chem. **16**, 1063 (1948).

APPENDIX I

We are to evaluate

$$p_j=\sum_{l=1}^{N}(-1)^l\cos(l-\tfrac{1}{2})\phi_j, \tag{A.1}$$

with $\phi_j=j\pi/N$, $j=0, 1, \cdots, N-1$. Using $-1=\exp(i\pi)=\exp(-i\pi)$ and $\cos(l-\frac{1}{2})\phi_j=\frac{1}{2}[\exp i(l-\frac{1}{2})\phi_j+\text{compl. conj.}]$ and writing $\exp i(\phi_j+\pi)=z_j$, we obtain

$$\begin{aligned}-2p_j&=\exp(-i\phi_j/2)\sum_{l=1}^{N}z_j{}^l+\text{compl. conj.}\\&=\exp(-i\phi_j/2)g_N(z_j)+\text{compl. conj.},\end{aligned} \tag{A.2}$$

where the auxiliary quantity

$$g_k(x)=\sum_{l=1}^{k}x^l \tag{A.3}$$

is evaluated as

$$\begin{aligned}g_k(x)&=x\sum_{l=0}^{k-1}x^l\\&=x(1-x^k)/(1-x)\quad\text{if } x\neq 1.\end{aligned} \tag{A.4}$$

In the present case, N being even, $z_j{}^N$ is 1 or -1 according as j is even or odd, hence

$$1-z_j{}^N=\begin{cases}0 & j \text{ even}\\ 2 & j \text{ odd.}\end{cases} \tag{A.5}$$

Substituting (A.5) and (A.4) into (A.3) then gives

$$p_j=-\sin\tfrac{1}{2}\pi/\sin\tfrac{1}{2}(\phi_j+\pi) \text{ provided } j \text{ is odd}, \tag{A.6}$$

that is,

$$p_j=-1/\cos\tfrac{1}{2}\phi_j \quad \text{provided } j \text{ is odd}. \tag{A.7}$$

This derivation is not valid for $z_j=1$ (meaning $j=0$), but (A.7) is correct in that case as well, as may be verified by direct evaluation of (A.1).

(As a check, we can use this method to compute the moment of a crystal all of whose atoms have the same charge. p_j for that case is given by (A.1) without the factor $(-1)^l$, and $p_0=N$ follows from direct evaluation. For $j\neq 0$, we merely replace π by 0 in the calculation, and get $p_j=0$, in agreement with physical expectation: the translation $j=0$, being macroscopic motion of a charged body, has a dipole moment, but none of the true vibrations do.)

APPENDIX II

We want to evaluate

$$P=e\sum_l u_l-e\sum_l v_l$$

or

$$P/e=q_u-q_v,$$

where

$$q_u \equiv \sum_l u_l \quad \text{is, by (17)}$$

$$q_u = \sum_j \sin\omega_j l [A_{1j} \sum_{l=1}^{N} e^{il\phi} + A_{2j} \sum_{l=1}^{N} e^{-il\phi}] \qquad \text{(A.8)}$$

$$q_u = \sum_j \omega_j l [A_{1j} g_N(y_c) + A_{2j} g_N(y_c^{-1})$$

in the notation of Appendix I, with $y_c = e^{i\phi} = e^{2\pi i j/N}$. Hence by (A.4) $q_N(y_c) = 0$ unless $1-y=0$, i.e., unless $j=0$. The other sums are similarly evaluated, yielding 0 for P/e unless $j=0$. For $j=0$, each sum over l in (A.8) evaluates to N, leading to

$$P/e = N[A_{10} - A_{20} - B_{10} - B_{20}].$$

The equation of motions yield $A_{10} = \pm B_{10}$, $A_{20} = \pm B_{20}$ for the $\pm$ branch of frequencies. Hence a nonvanishing dipole moment, $P/e[A_{10} - A_{20}] = 2N$ is associated with and only with the $j=0$ frequency of the $+$ branch.

APPENDIX III

If $\Delta\Lambda$ is the resolution of the spectrometer at wave length Λ, the approximate relation $I_L/I_E = \Lambda_c/\Delta\Lambda$ may be established between the absorption intensity I_E at the "edges" and the apparent (observed) absorption intensity I_L at the main absorption line, as follows:

A rough measure of the absorption intensity is $\Pi^2(\omega)$. Hence $I_E \sim N^4$. Since the sharp absorption line will be broadened for various reasons, its apparent peak intensity will be roughly given by $A_L = I_L \Delta\omega$, A_L being the theoretically computed area under the unbroadened line, and $\Delta\omega$ the frequency range over which this area will be smeared out on account of lattice defects, instrumental broadening or any other cause. If ω_1 is the frequency closest to ω_c that is actually taken on, then Table 1 gives

$$A_L = \int_{\omega_1}^{\omega_2} \Pi^2(\tilde{\omega}) d\tilde{\omega} = \int_{\omega_1}^{\omega_2} (K/\tilde{\omega})^{+\frac{1}{3}} d\tilde{\omega}$$
$$= \tfrac{1}{2} K^{\frac{1}{3}} \omega_1^{-\frac{1}{3}} = \tfrac{1}{2} \Pi^2(\omega_1) \omega_1,$$

the contribution from the upper limit being negligible. But (Table I) $\Pi^2(\omega_1) = N^6$; hence $A_L = \frac{1}{2} N^6 \omega_1$, $I_L = \frac{1}{2} N^6 \omega_1/\Delta\omega$, and $I_L/I_E \cong N^2 \omega_1/\Delta\omega$. To estimate ω_1, we note that near ω_c the frequency distribution is given by[15,16] $g(\omega) = \xi(\omega_c - \omega)^{\frac{1}{2}}$ and since the precise behavior far away from ω_c, is irrelevant for present purposes, we may take this expression as valid for all ω. The normalization constant ξ is fixed by

$$\int_0^{\omega_c} g(\omega) d\omega = N^3$$

and ω_1 is determined by

$$\int_{\omega_c - \omega_1}^{\omega_c} g(\omega) d\omega = 1.$$

From these relations we find $\omega_1 = N^{-2}\omega_c$. Hence $I_L/I_E = \omega_c/\Delta\omega$ or, in terms of wavelength, $I_L/I_E = \Lambda/\Delta\Lambda$. I.e., for a given size crystal, the ratio of apparent intensities depends on the resolution only. Poor resolution may, of course, result not only from instrumental imperfections, but also from effects due to the crystal itself, such as second-order interactions, lattice defects (of which large numbers may be expected in evaporated crystals), etc.

Examination of the main absorption lines in the absorption spectra of alkali halides given by Barnes *et al.*,[17,20] suggests that in his case $\Lambda/\Delta\Lambda$ is somewhere between 3 and 10. The intensity of the subsidiary "lines" in those spectra runs from about $\frac{1}{2}$ to $\frac{1}{10}$ of the peak intensity of the main line. Although in the absence of quantitative calculations of the position and intensity of the "edges" it would be rash to identify Barnes' "subsidiary lines" with poorly resolved "edges," we can conclude that the edges should provide effects of an approximately observable magnitude, and that an experimental study of these or other substances, using purer crystals and presently available instruments of greater resolution ($\Lambda/\Delta\Lambda \cong 300$ at $\Lambda = 30$ microns), together with theoretical work leading towards quantitative predictions, should be worthwhile.

[20] Note particularly Fig. 1 of Barnes, Brattain, and Seitz, footnote 3.

Spectroscopy of Gaseous Carbonyls. I. Infrared Spectra and Thermodynamic Properties of Chromium and Molybdenum Hexacarbonyls

N. J. Hawkins, H. C. Mattraw, W. W. Sabol, and D. R. Carpenter
Knolls Atomic Power Laboratory, Schenectady, New York*

(Received March 11, 1955)

Infrared spectra of gaseous chromium and molybdenum hexacarbonyls were obtained. The spectra could be interpreted as resulting from an $X(YZ)_6$-type molecule of O_h-symmetry. Of the thirteen fundamental vibration frequencies possible, all but three are fairly well established. The fundamentals are shown to be of two distinct types: (1) those which are typical of a heavy outer atom octahedral molecule and (2) those which are typical of the carbon and oxygen moving in opposition to each other. Thermodynamic properties are computed for the ideal gases for various temperatures to 600°K.

INTRODUCTION

At the present time, except for some electron diffraction studies, very little information exists on the fundamental structure and thermodynamics of gaseous carbonyls. Only in the case of $Ni(CO)_4$ has a nearly complete study of the vibrational spectrum been made.[1,2] Of the hexacarbonyls only $W(CO)_6$ had been investigated, and this investigation was conducted on the solid.[3] Investigations in this laboratory on the infrared spectra of volatile hexafluorides and other molecules[4–6] led to the development of techniques by which the infrared spectra of the vapors of materials of comparatively low vapor pressure at room temperature could be observed by elevating the temperature when a sufficient amount of the condensed material was present. When it became apparent in the case of $Mo(CO)_6$ that it was possible to obtain a number of infrared bands by this technique, studies were undertaken on $Cr(CO)_6$, $Mo(CO)_6$, and $W(CO)_6$ to determine if a reasonable interpretation of the rather complex spectra could be made from which thermodynamic properties could be calculated. In this section are presented the results on the chromium and molybdenum carbonyls. For lack of a sufficient amount of sample, the results on $W(CO)_6$ are incomplete and will be presented later. In tungsten carbonyl, however, it can be stated that the incomplete preliminary spectra are very similar to the more complete results obtained on the chromium and molybdenum hexacarbonyls.

TYPE $X(YZ)_6$ MOLECULES WITH O_h SYMMETRY

A representation of the thirty-three normal vibrational modes of the $X(YZ)_6$ type molecule with O_h symmetry is reduced to thirteen by $\Gamma=2A_{1g}+2E_g+F_{1g}+4F_{1u}+2F_{2g}+2F_{2u}$ since there is one atom, X, on all elements of symmetry and two sets of atoms, Y and Z, on fourfold axes.[7] The reduced representation for the simple type XY_6 with O_h symmetry is $\Gamma=A_{1g}+E_g+2F_{1u}+F_{2g}+F_{2u}$. It is to be noted that there are just twice as many fundamentals of each species for $X(YZ)_6$ than for XY_6 and the one additional "clutch" frequency with symmetry F_{1g} which becomes a simple rotation in XY_6. Diagrams for the normal vibrations in $X(YZ)_6$ are shown in Fig. 1. It is to be noted that the form of the ν_2, ν_4, ν_8, ν_9, ν_{11}, and ν_{13} are exactly the same as the normal XY_6 vibrations shown by Herzberg[8] if Y and Z move as if they were one atom. (In this study, these fundamentals are designated as Type A frequencies.) The frequencies ν_1, ν_3, ν_6, ν_7, ν_{10}, ν_{12} are then simply obtained by changing the direction of either all the Y-atoms or all the Z-atoms by 180° (type Type B frequencies). When this operation is performed on ν_5, it is seen that a simple rotation would be obtained. As with all molecules of O_h symmetry, the F_{1u}-component in the total symmetry is required for infrared activity, and A_{1g}, E_g, or F_{2g} is required for Raman activity.[9] The numbering system for the fundamentals is given in Table I. All of the binary combination bands allowed in the infrared are summarized in Table II and, for convenience, are diagrammatically represented in Fig. 2.

EXPERIMENTAL DETAILS

Samples of the chromium and molybdenum carbonyls were prepared by Dallas T. Hurd of the General Electric Research Laboratory. Since they are solids of only a few microns vapor pressure, they were introduced into the infrared gas cells through a window. The reassembled cells were surrounded with dry ice and pumped to a high vacuum for several hours. The cells were constructed of threaded copper pipe; windows were sealed to the body by means of caps tightened against Teflon gaskets. One type of cell used was 5 cm long and 3 cm i.d.; the other type was 10 cm long and 5 cm i.d.

* The Knolls Atomic Power Laboratory is operated by the General Electric Company for the U. S. Atomic Energy Commission. The work reported here was carried out under contract No. W-31-109 Eng-52.

[1] B. Crawford and P. C. Cross, J. Chem. Phys. **6**, 525 (1938).
[2] B. Crawford and W. Horowitz, J. Chem. Phys. **16**, 147 (1948).
[3] R. K. Sheline, J. Am. Chem. Soc. **72**, 5761 (1950).
[4] H. C. Mattraw: J. Appl. Spect. (to be published).
[5] Hawkins, Mattraw, and Carpenter, KAPL 1041 (February 1, 1954).
[6] Mattraw, Hawkins, Carpenter, and Sabol, J. Chem. Phys. **23**, 985 (1955).
[7] G. Herzberg, *Molecular Spectra and Molecular Structure: II. Infrared and Raman Spectra of Polyatomic Molecules* (D. Van Nostrand Company, Inc., New York, 1945), p. 139.
[8] Reference 7, p. 122.
[9] Reference 7, p. 253.

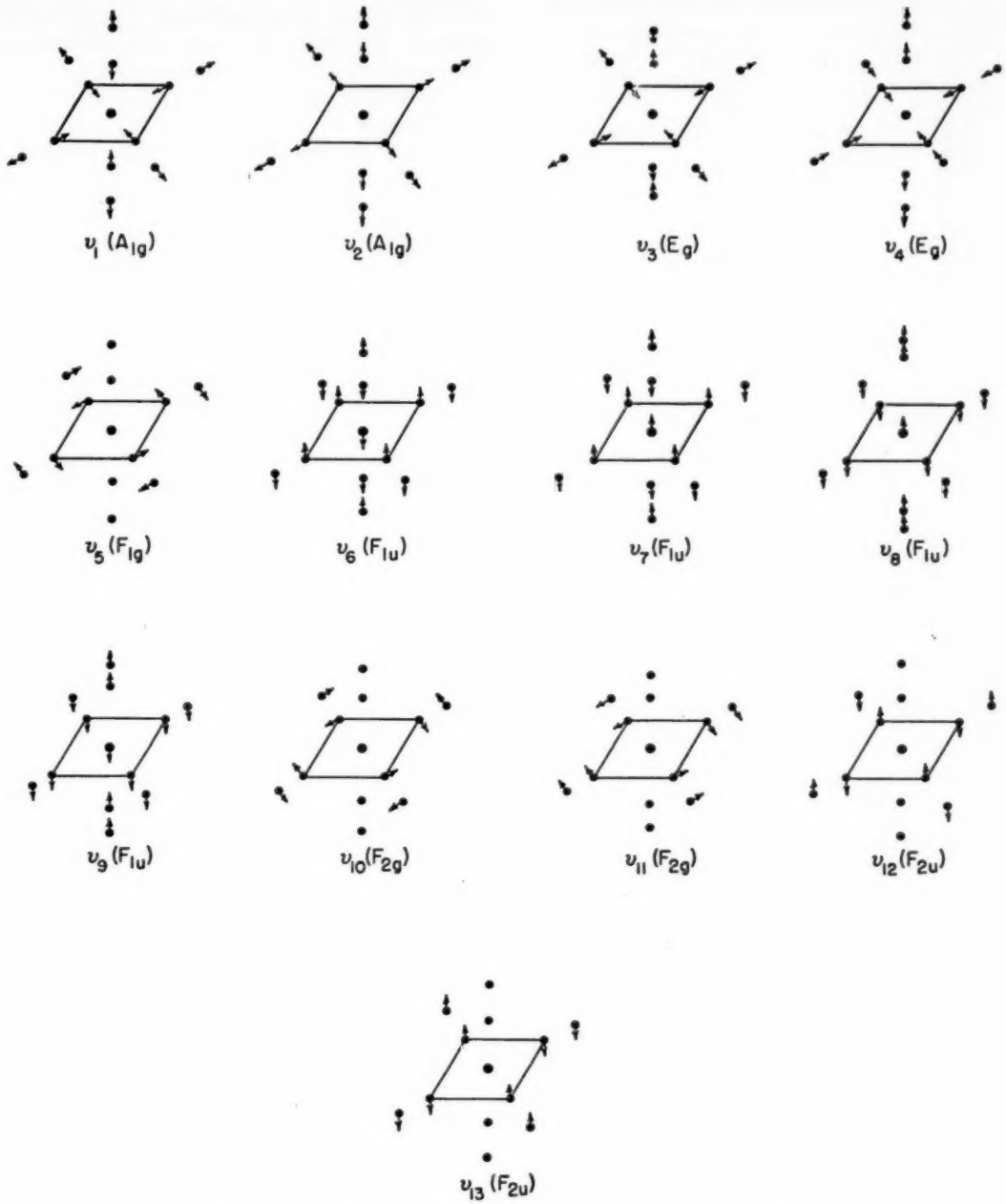

FIG. 1. Normal vibrations of a type $X(YZ)_6$ molecule of O_h-symmetry.

Windows of AgCl and KRS-5 were used. The cell body and vacuum valve (which was attached to a stem five inches from the cell body) were heated by means of Briskeat flexible heating tape to obtain the spectra of the gases at the elevated temperatures.

Spectra were obtained in the NaCl and KBr regions on the KAPL Baird double beam spectrometer. $Cr(CO)_6$ was examined in the CaF_2 region on a different Baird double beam instrument located at the G. E. Materials and Processing Laboratory.† The ν_8 fundamental vibration frequencies of both molecules were observed on a Perkin Elmer single beam spectrometer utilizing a KRS-5 prism.‡ In the latter case the cells equipped with KRS-5 windows were heated until the strong fundamentals appeared. The reported fundamentals were the only strong bands observed at the temperatures studied over the region from 250 to 450 cm^{-1}.

† Mr. Donald Harms kindly made his instrument available for this study.

‡ The spectra in the KRS-5 region were obtained through the cooperation of Dr. R. S. McDonald, of the General Electric Research Laboratory, who had borrowed the prism through the generosity of Dr. R. C. Lord of M.I.T.

TABLE I. Fundamental frequencies of $Cr(CO)_6$ and $Mo(CO)_6$.

Fundamental	Species	Activity	$Cr(CO)_6$	$Mo(CO)_6$
1	A_{1g}	Raman	2108 cm^{-1}	2131 cm^{-1}
2	A_{1g}	Raman	393	379
3	E_g	Raman	2019	2022
4	E_g	Raman	373	334
5	F_{1g}	Inactive	539	477
6	F_{1u}	I.R.	2000	2000
7	F_{1u}	I.R.	661	595
8	F_{1u}	I.R.	436	368
9	F_{1u}	I.R.	102	80
10	F_{2g}	Raman	213	230
11	F_{2g}	Raman	90	80
12	F_{2u}	Inactive	310	327
13	F_{2u}	Inactive	80	70

In addition to the infrared spectra obtained of the vapors, attempts were made to obtain the Raman spectra and the infrared spectra of the molecules in condensed states.

In the case of $Mo(CO)_6$, a KBr pressed pellet of the material revealed broad bands at 5μ, and 17μ, and some of the bands which appeared strong in the vapor, appeared weakly in the 9–12 micron region. A saturated solution in CS_2 gave essentially the same result. Other solvents were tried, but none with satisfactory optical properties was found to dissolve enough of the carbonyl to prove to be as useful as heating the solid material in a gas cell.

Raman data were obtained at Rensselaer Polytechnic Institute through the generous loan of Hilger equipment by Professor Stephen E. Wiberley. The very limited solubility of molybdendum carbonyl in such solvents as carbon disulfide, carbon tetrachloride, diethyl ether, and butyl alcohol was one handicap while the gradual photodecomposition of the carbonyl was another difficulty. Various exposure times were tried, but the two difficulties were approximately equal; longer exposures overcome limited solubility but are offset by photodecomposition.

Two Raman lines out of the six possible were observed for molybdenum carbonyl. The stronger line was measured to be 2034 cm^{-1} and the weaker line was measured to be 380 cm^{-1}. These two lines compare favorably with the values of ν_3 and ν_2 calculated from infrared combination bands.

TABLE II. Infrared allowed binary combination bands for $X(YZ)_6$ molecules of the O_h-point group and comparative data for $Cr(CO)_6$ and $Mo(CO)_6$.

Combination	$Cr(CO)_6$ Calc	$Cr(CO)_6$ obs	$Cr(CO)_6$ Intensity	$Mo(CO)_6$ Calc	$Mo(CO)_6$ obs	$Mo(CO)_6$ Intensity
$\nu_1+\nu_6$	4108	4098	medium	4131	4150	medium
$\nu_1+\nu_7$	2769	not present		2726	not present	
$\nu_1+\nu_8$	2544	2544	weak	2499	2480	weak
$\nu_1+\nu_9$	2210	2212	weak	2211	2210	medium
$\nu_2+\nu_6$	2393	2392	strong	2379	2380	strong
$\nu_2+\nu_7$	1054	1055	questionable	974	980	strong
$\nu_2+\nu_8$	829	811	questionable	747	740	medium
$\nu_2+\nu_9$	495	not present		459	not observed	
$\nu_3+\nu_6$	4019	4000	medium	4022	4050	medium
$\nu_3+\nu_7$	2680	2688	weak	2617	2600	weak
$\nu_3+\nu_8$	2455	2466	medium	2390	2380	strong
$\nu_3+\nu_9$	2121	2121	strong	2102	2115	strong
$\nu_3+\nu_{12}$	2329	2336	questionable	2349	questionable	
$\nu_3+\nu_{13}$	2099	2090	questionable	2092	2085	questionable
$\nu_4+\nu_6$	2373	2336	questionable	2334	2330	weak
$\nu_4+\nu_7$	1034	1032	strong	929	929	strong
$\nu_4+\nu_8$	808	811	strong	702	705	medium
$\nu_4+\nu_9$	475	477	medium	414	not observed	
$\nu_4+\nu_{12}$	683	673	questionable	661	661	weak
$\nu_4+\nu_{13}$	453	449	weak	404	not observed	
$\nu_5+\nu_6$	2539	2554	weak	2477	2480	weak
$\nu_5+\nu_7$	1200	1196	strong	1072	1070	strong
$\nu_5+\nu_8$	975	963	medium	845	845	strong
$\nu_5+\nu_9$	619	635	strong	557	563	strong
$\nu_5+\nu_{12}$	849	not present		804	not present	
$\nu_5+\nu_{13}$	619	blocked		547	blocked	
$\nu_6+\nu_{10}$	2213	2212	weak	2230	2210	medium
$\nu_6+\nu_{11}$	2090	2090	strong	2080	2085	strong
$\nu_7+\nu_{10}$	874	875	strong	825	845	strong
$\nu_7+\nu_{11}$	753	755	medium	675	670	medium
$\nu_8+\nu_{10}$	649	blocked		598	blocked	
$\nu_8+\nu_{11}$	526	522	medium	448	not observed	
$\nu_9+\nu_{10}$	315	not observed		310	not observed	
$\nu_9+\nu_{11}$	192	not observed		160	not observed	
$\nu_{10}+\nu_{12}$	523	522	medium	557	563	strong
$\nu_{10}+\nu_{13}$	293	not observed		300	not observed	
$\nu_{11}+\nu_{12}$	400	not observed		407	not observed	
$\nu_{11}+\nu_{13}$	170	not observed		150	not observed	

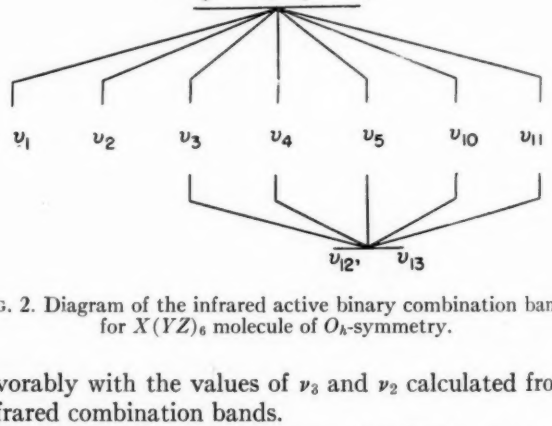

FIG. 2. Diagram of the infrared active binary combination bands for $X(YZ)_6$ molecule of O_h-symmetry.

Representative infrared spectra of $Cr(CO)_6$ are shown in Fig. 3 and of $Mo(CO)_6$ in Fig. 4. The temperatures are to be regarded as approximate.

The measured values of the frequencies, relative intensities, and assignments are summarized in Table III for $Cr(CO)_6$ and Table IV for $Mo(CO)_6$.

DISCUSSION OF THE ASSIGNMENTS

It is possible to observe only four; i.e., those of symmetry F_{1u}, of the thirteen fundamental vibration frequencies directly by means of infrared spectroscopy. Of the four, ν_9 is beyond the cutoff of presently available prisms. The other three fundamentals for both molecules were directly observed and are summarized in Table I. The values of ν_6 are the least certain because of the high frequency and are considered to be known within 10 cm^{-1}; the errors in ν_7 and ν_8 are about 2 cm^{-1}.

The next most certain frequencies are those that are obtainable from the binary combination bands with ν_6, ν_7, ν_8; namely, ν_1, ν_2, ν_3, ν_4, ν_5, ν_{10}, and ν_{11}. A band

difference matching procedure for determining these frequencies proved to be useful. The values of ν_6, ν_7, ν_8 were subtracted from all of the observed bands and arranged in three columns and the differences matched. Where discrepancies existed the values of these fundamentals were weighted more on the side of the values for ν_7 and ν_8. In making the assignments, consideration was also given to (1) the vibration diagrams (Fig. 1); (2) the nature of the vibrations in XY_6 octahedral molecules for the Type A vibrations; (3) the nature of $Ni(CO)_4$ vibrations, where applicable, for the Type B vibrations; and (4) in both molecules, comparable intensities for particular combination bands strongly influenced the final choice in assignments. (Table II.) Thus it is stated emphatically that since both molecules were studied together, any error in the interpretation of the infrared spectrum of one molecule will undoubtedly lead to the same error in the other molecule.

We shall first consider the Type A stretching frequencies; namely, ν_2, ν_4, and ν_8, the last of which was directly observed in both carbonyls. In MoF_6,[10] the comparable frequencies are ν_1, ν_2, and ν_3, respectively, and it was found that ν_1 is about equal to ν_3 with ν_2 somewhat less. For ν_2 of $Mo(CO)_6$, the average value from the combinations with ν_6, ν_7, and ν_8 was taken. For $Cr(CO)_6$, the average from the ν_6 and ν_7 combinations was used; the combination with ν_8 is evidently present with $\nu_4+\nu_8$ at 811 cm^{-1}. For $Mo(CO)_6$, ν_4 was taken as the average found from the combination bands with ν_6, ν_7, and ν_8. For $Cr(CO)_6$, ν_4 was taken as the average from the ν_7 and ν_8 combination bands. The combination with ν_6 is not clear cut. As expected, all of these fundamentals are higher in chromium than in molybdenum; furthermore, ν_2 is comparable in value to ν_8 with ν_4 somewhat less (this is particularly true for molybdenum).

Next, the Type B frequencies comparable to ν_2, ν_4, and ν_8; namely, ν_1, ν_3, and ν_6 will be considered. A study of the extant carbonyl information led to the expectation that ν_1 and ν_6 would be high frequencies of the order of 2000 cm^{-1} (1,3); however, nothing comparable to ν_3 had ever been observed. It was noted that in both carbonyl gases, after sufficient heating, two bands appeared of about equal intensity in the 4000 cm^{-1} region (this is also true of our incomplete results on the infrared spectrum of tungsten carbonyl). This is similar to the situation in heavy metal hexafluorides where it is always found that the $\nu_1+\nu_3$ and $\nu_2+\nu_3$ combination bands are of almost equal intensity. Furthermore, a study of the vibration diagrams leads to the result that ν_3 should be about the same order of magnitude as ν_1 although somewhat less (since $\nu_4<\nu_2$). Thus ν_3 was also expected to be about 2000 cm^{-1}.

In both carbonyls ν_1 was obtained as the average from the binary combinations with ν_6 and ν_8. It is curious that in both molecules the combination with ν_7 was not observed at the temperatures studied. This is also similar to the situation in heavy metal hexafluorides where it is found that $\nu_1+\nu_4$ is very much less intense than $\nu_1+\nu_3$. In both molecules, ν_3 is the average from the combination bands with ν_6, ν_7, and ν_8. ν_6 was directly observed.

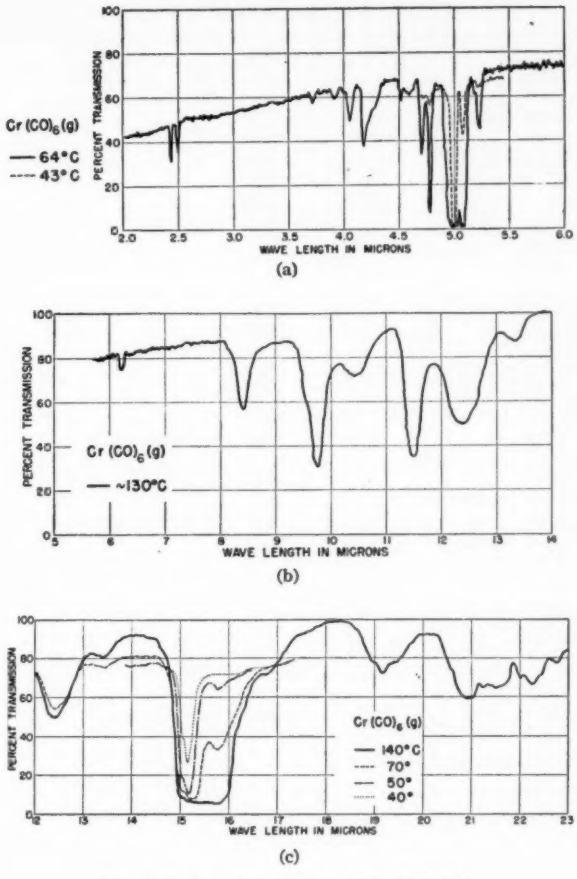

FIG. 3. Infrared spectrum of $Cr(CO)_6(g)$.

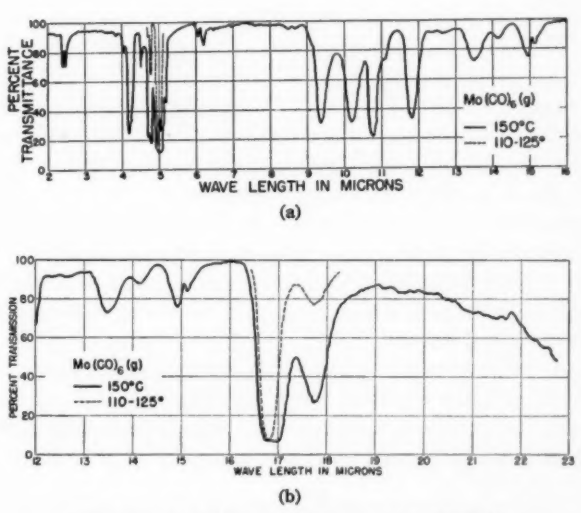

FIG. 4 (a, b). Infrared spectrum of $Mo(CO)_6(g)$.

[10] Burke, Smith, and Nielsen, J. Chem. Phys. **20**, 447 (1952).

TABLE III. Infrared bands of $Cr(CO)_6(g)$.

Frequency (cm^{-1})	Intensity	Assignment	Calc (cm^{-1})	Remarks
4098	medium	$\nu_1+\nu_6$	4108	
4000	medium	$\nu_3+\nu_6$	4019	
2688	weak	$\nu_3+\nu_7$	2680	
2554	weak	$\nu_1+\nu_8$; $\nu_5+\nu_6$	2544, 2539	
2466	medium	$\nu_3+\nu_8$	2455	
2392	strong	$\nu_2+\nu_6$		
2336		$\nu_4+\nu_6$; $\nu_3+\nu_{12}$	2373, 2329	shoulder of 2392
2212	weak	$\nu_6+\nu_{10}$; $\nu_1+\nu_9$	2213, 2210	
2174	weak			questionable band
2121	strong	$\nu_3+\nu_9$	2121	
2090	strong	$\nu_6+\nu_{11}$; $\nu_3+\nu_{13}$	2090 (2090)	
2033		$\nu_1-\nu_9$	2006	shoulder of 2000
2000	very strong	ν_6		
1970		$3\nu_7$	1983	shoulder of 2000
1912	medium	$\nu_3+\nu_9$	1917	
1631	weak	$\nu_6+\nu_4$	1627	questionable band
1196	strong	$\nu_5+\nu_7$	1200	
1055		$\nu_2+\nu_7$	1054	shoulder of 1032
1032	strong	$\nu_4+\nu_7$	1034	
963	medium	$\nu_5+\nu_8$	975	
875	strong	$\nu_7+\nu_{10}$	874	
811	strong	$\nu_4+\nu_8$; $\nu_2+\nu_8$	809, 829	
755	medium	$\nu_7+\nu_{11}$	751	
673		$\nu_4+\nu_{12}$	683	shoulder of 661
661	very strong	ν_7		
635	strong	$\nu_5+\nu_9$		shoulder of 661
595				shoulder of 661; questionable band
522	medium	$\nu_8+\nu_{11}$; $\nu_{10}+\nu_{12}$	526 523	broad; intensity questionable
513	medium	$\nu_2+\nu_9$	495	broad; intensity questionable
477	medium	$\nu_4+\nu_9$	475	broad; intensity questionable
465	weak			broad; questionable band
449	weak	$\nu_4+\nu_{13}$	453	broad; questionable band
436	strong	ν_8		

In general the results are that ν_1, ν_3, and ν_6 are typical stretching frequencies of the carbonyl group and are, within experimental error, independent of the central atom in the case of these two hexacarbonyls.

Next to be considered is the optically inactive "clutch" frequency, ν_5, the nongenuine vibration frequency in XY_6 molecules. The comparable frequency in $Ni(CO)_4$ was found[1] to be 420 cm^{-1} from the combination bands, a value which is higher than any of the Type A frequencies of nickel carbonyl. Since, in the hexacarbonyls, this vibration has to perform in a bond angle of 90° rather than 108°, it might be expected to be higher than that found in nickel with chromium higher than molybdenum because of the shorter metal to carbon distance.[11]

Accordingly in the band difference matches for both molecules, the highest frequency below ν_1 and ν_3, was assigned as ν_5 and taken as the average from combinations with ν_6, ν_7, and ν_8. It was noted in both molecules that the combination bands with ν_6 were weak while the combinations with ν_7, ν_8, and ν_9 were strong. The combination with ν_{12} in both cases was not present.

Next to be considered are the Type A bending vibrations; namely, ν_9, ν_{11}, and ν_{13} which are analogous to ν_4, ν_5, and ν_6, respectively, in XY_6 molecules. All of these fundamentals are expected to be quite low, of the order of half the corresponding hexafluoride frequencies with higher values in $Cr(CO)_6$ than in $Mo(CO)_6$. In $Cr(CO)_6$ there was a good match of 90 cm^{-1} in the band differences from ν_6, ν_7, and ν_8, and this was designated the ν_{11}. For $Mo(CO)_6$ there was a band match at 80 cm^{-1} from the combinations with ν_6 and ν_7. The comparable combination band with ν_8 could not be observed with the Baird instrument.

In both molecules ν_9 is expected in combination with ν_1, ν_3, and ν_5, in addition, in $Cr(CO)_6$, combinations with ν_2 and ν_4 might be observed. Experience with hexafluorides indicates that the combination bands with ν_2 and ν_4 are less intense than the comparable combinations with ν_8. The combination bands of ν_8 with ν_1, ν_3, and ν_5 were all observed, the latter two of which were fairly intense. Accordingly, the strong bands in $Cr(CO)_6$ at 2121 cm^{-1} and in $Mo(CO)_6$ at 2115 cm^{-1} were assigned as $\nu_3+\nu_9$ resulting in values of ν_9 which indicated that the strong band of $Cr(CO)_6$ at 635 cm^{-1} and $Mo(CO)_6$ at 563 cm^{-1} were the $\nu_5+\nu_9$ combinations. In $Cr(CO)_6$, the combinations of ν_9 with ν_2 and ν_4 are observable and found to be less intense than the corresponding combinations with ν_8.

In the case of the inactive frequency ν_{13}, it was necessary to make reasonable assumptions about the magni-

TABLE IV. Infrared bands of $Mo(CO)_6(g)$.

Frequency (cm^{-1})	Intensity	Assignment	Calc (cm^{-1})	Remarks
4150	medium	$\nu_1+\nu_6$	4131	
4050	medium	$\nu_3+\nu_6$	4022	
2600	weak	$\nu_3+\nu_7$	2617	
2480	weak	$\nu_1+\nu_8$; $\nu_5+\nu_6$	2499, 2477	
2380	strong	$\nu_3+\nu_8$; $\nu_2+\nu_6$	2390, 2379	broad
2330	weak	$\nu_4+\nu_6$	2334	
2210	medium	$\nu_6+\nu_{10}$	2230	
2115	strong	$\nu_3+\nu_9$	2102	
2085	strong	$\nu_6+\nu_{11}$; $\nu_3+\nu_{13}$	2080, 2092	
2000	very strong	ν_6		
1985				shoulder of ν_6
1955	medium	$\nu_3-\nu_{13}$	1952	shoulder of ν_6
1925	medium	$\nu_3-\nu_9$; $\nu_6-\nu_{11}$	1942, 1920	shoulder of ν_6
1650	weak	$\nu_3-\nu_8$	1654	
1615	weak	$\nu_6-\nu_2$	1621	
1070	strong	$\nu_5+\nu_7$	1072	
980	strong	$\nu_2+\nu_7$	974	
927	strong	$\nu_4+\nu_7$	929	
905	weak			questionable
845	strong	$\nu_5+\nu_8$; $\nu_7+\nu_{10}$	845, 825	
740	medium	$\nu_2+\nu_8$	747	
705	medium	$\nu_4+\nu_8$	702	
670	medium	$\nu_7+\nu_{11}$	675	
661	weak	$\nu_4+\nu_{12}$	661	
595	very strong	ν_7		
563	strong	$\nu_5+\nu_9$; $\nu_{10}+\nu_{12}$	557, 557	
386	strong	ν_8		

[11] Brockway, Ewens, and Lister, Trans. Faraday Soc. **34**, 1350 (1938).

tude and then confirm the plausibility of the choice from the allowed combination bands available. At the temperatures required to observe the bands, only those with ν_3 and ν_5 are possible in both molecules and possibly the ν_4 combination in the case of $Cr(CO)_6$. The corresponding band, $\nu_2+\nu_6$, is always observed in hexafluorides, and (ν_6) is always found to be less than the other bending frequencies (ν_4 and ν_5).

In the case of $Cr(CO)_6$ a value of 80 ± 10 cm^{-1} is not unreasonable for ν_{13}. The weak band at 449 cm^{-1} is then assigned as $\nu_4+\nu_{13}$ (the unassigned band at 465 cm^{-1}, if due to $\nu_4+\nu_{13}$ would lead to a ν_{13} of 96 cm^{-1}, which is unreasonably higher than ν_{11} from hexafluoride experience). The calculated $\nu_5+\nu_{13}$ would be certainly blocked by ν_7 and the calculated value of 2099 cm^{-1} for $\nu_3+\nu_{13}$ is not unreasonably included in the strong band found at 2090 cm^{-1}.

In $Mo(CO)_6$, ν_{13} was arbitrarily taken to be 70 cm^{-1}, 10 cm^{-1} less than the ν_{13}, not too satisfactorily found, in $Cr(CO)_6$. The resulting $\nu_4+\nu_{13}$ could not be observed for optical reasons; $\nu_5+\nu_{13}$ (547 cm^{-1}–calc) is certainly blocked by ν_7 and $\nu_3+\nu_{13}$ (2092 cm^{-1}–calc) is not unreasonably included in the band at 2085 cm^{-1}.

Finally ν_7, ν_{10}, and ν_{12}, the Type B bending vibrations, are considered. The ν_7 in both molecules was directly observed. ν_{10} was found by band difference matching from the combinations with ν_6, ν_7, and ν_8; in the case of $Cr(CO)_6$, $\nu_8+\nu_{10}$, is blocked by ν_7.

The ν_{12} is the least well-known of the thirteen fundamental vibration frequencies because there is no analogy for it in XY_6 molecules and because it does not combine with the observed fundamentals ν_6, ν_7, and ν_8. It is expected that its value will be almost the same for both molecules. A study of the vibration diagrams indicates that it is probably not less than 200 cm^{-1} and not greater than 500 cm^{-1} (the value of ν_5). Values of 310 cm^{-1} for $Cr(CO)_6$ and 327 cm^{-1} for $Mo(CO)_6$ were selected because they could explain the bands at 673 cm^{-1} and 661 cm^{-1}, respectively, as the combinations with ν_4. In the case of $Cr(CO)_6$, the broadness of the band at 522 cm^{-1} could be accounted for as the $\nu_{10}+\nu_{12}$; and $\nu_3+\nu_{12}$ (2329 cm^{-1}–calc) may be present. In $Mo(CO)_6$, $\nu_{10}+\nu_{12}$ (calc at 557) could be present at 563 cm^{-1} and $\nu_3+\nu_{12}$ (calc 2349) cannot be shown as not being present. It was noted in both molecules that the $\nu_5+\nu_{12}$ is definitely not present for the values of ν_{12} assumed. Because of the poor evidence for the values of ν_{12}, an error of 100 cm^{-1} would be not at all unreasonable.

TABLE V. Thermodynamic properties of $Cr(CO)_6(g)$ and $Mo(CO)_6(g)$.

Temp. °K	$Cr(CO)_6(g)$ C_p^0	S^0	$-(F^0-E_0^0)/T$	$Mo(CO)_6(g)$ C_p^0	S^0	$-(F^0-E_0^0)/T$
	(all in cal/deg/mole at one atmosphere)					
100	29.14	72.65	54.56	30.14	75.60	56.96
150	37.88	86.36	63.17	38.70	89.47	65.72
200	43.35	97.67	70.22	45.00	101.56	73.35
250	47.83	107.86	76.74	49.37	112.07	80.17
298	50.97	116.53	82.46	52.34	121.07	86.15
350	53.48	124.93	88.17	54.64	129.61	92.03
400	55.38	132.22	93.21	56.34	137.03	97.28
450	56.92	138.83	97.94	57.76	143.78	102.16
500	58.29	145.03	102.39	58.97	149.92	106.67
550	59.47	150.49	106.46	60.08	155.67	110.99
600	60.60	155.77	110.38	61.08	160.89	114.94

The foregoing discussion of the assignments leads to the conclusions that in addition to the three directly observed fundamentals, the values of ν_1, ν_2, ν_3, ν_4, ν_5, ν_{10}, ν_{11} are probably fairly well established from the allowed infrared binary combination bands. The values of ν_9 and ν_{13} are less well-known, and the value of ν_{12} least well-known. The Type B frequencies are almost independent of the central atom in the case of the stretching frequencies, although some variation in ν_5 and ν_7 indicates that there may be more dependence on the central atom in the "clutch" and deformation frequencies. The Type A frequencies follow the pattern of a heavy outer atom octahedral molecule.

THERMODYNAMIC PROPERTIES

The thermodynamic properties C_p^0, S^0, and $-(F^0-E_0^0)/T$ were calculated for one mole of the perfect gas at one atmosphere pressure at various temperatures to 600°K using the rigid rotor-harmonic oscillator approximation. Moments of inertia were computed from the electron diffraction data of Brockway, Ewens, and Lister.[11] Assumed in the calculations were a symmetry number of 24, singlet ground electronic states and chemical atomic weights. Neglected in the calculations were the contributions due to isotope mixing, anharmonicity, centrifugal distortion, and nuclear spins. In view of the uncertainties in some of the deformation frequencies the calculations were only carried to the second decimal place. The results are summarized in Table V.

Shape of the Coexistence Curve in the Perfluoromethylcyclohexane-Carbon Tetrachloride System*

RAM GOPAL† AND O. K. RICE
Department of Chemistry, University of North Carolina, Chapel Hill, North Carolina
(Received March 8, 1955)

Transition temperatures for the transition from the one-phase to the two-phase condition have been observed for the perfluoromethylcyclohexane-carbon tetrachloride system. It is found that $(T_c-T+0.001°)^{\frac{1}{3}}$ (where T_c, which is equal to 28.623°, is the observed critical temperature) is a linear function of the molecular fraction of carbon tetrachloride. As is indicated by the form of this function there appears to be a flat horizontal portion at the top of the coexistence curve, which extends from 0.5375 to 0.5625 volume fraction CCl_4. It involves such a small temperature range as to be almost unobservable and the flat top is much less marked than in the cyclohexane-aniline system.

The melting point of perfluoromethylcyclohexane has been found to be −41.72°C.

INTRODUCTION

THE nature and the shape of the coexistence curve in binary liquid systems near the critical point have been subjects of some quite painstaking investigations during recent years. According to the theories of Mayer,[1] Mayer and Harrison,[2] McMillan and Mayer,[3] and of Rice,[4] the curve is expected to have a finite horizontal top. The experimental data of Rice and coworkers[5] on the cyclohexane-aniline system and of Mason, Naldrett, and Maass[6] on ethane and ethylene seem to support this result of the above authors. On the other hand the experimental results of Zimm[7] on the perfluoromethylcyclohexane-carbon tetrachloride system and of Lorentzen[8] on vapor-liquid equilibrium in carbon dioxide show, in the belief of these authors, that in these systems a finite horizontal top is missing, and that the curve has a rounded top near the critical point.[9] Since Zimm's system was not protected from air and atmospheric moisture, his temperature control only ±0.002°, and since he did not investigate the range of concentrations where a flat portion might be expected to occur, his conclusions are open to doubt. It is obviously desirable to reinvestigate the system more carefully under a better temperature control and with a more minute scanning of the critical range of concentrations.

EXPERIMENTAL

The sample of perfluoromethylcyclohexane was obtained from E. I. du Pont De Nemours and Company, and was subjected to fractional distillation a number of times, the middle fraction being collected each time and fractionated through a column. The total fraction boiling between 76.4° and 76.5° was collected. An attempt was made to test the purity of the sample by determining its melting curve. A determination using a platinum resistence thermometer showed it to melt at about −41.72°, but before the compound froze some turbidity appeared about 0.3° to 0.5° above the melting point. The turbidity in this temperature range also remained after melting. Different fractions obtained by fractional crystallization showed the same behavior and melted, as nearly as could be observed, at the same temperature. It was suspected that the turbidity was due to traces of moisture, but use of an atmosphere of dry nitrogen effected no improvement, so this method of testing was abandoned.

It was then decided to take infrared spectrograms of different distillates. After taking the infrared spectrogram of the fraction boiling between 76.4° and 76.5°, it was redistilled and the spectrogram of the new middle fraction taken. When the two successive middle distillates gave identical spectrograms, they were mixed together and used for making up the mixtures for the study of the coexistence curve. About 25% of the original 76.4–5° fraction was then used.

B and A analytical grade carbon tetrachloride was subjected to careful and repeated fractional distillations. The fraction boiling at 76.8° was again distilled and the infrared spectrogram of the middle fraction was taken as above. Two successive distillates having identical spectrograms were used for making up the mixtures.

Solutions of different compositions were made by adding together the required volumes of the two components at 20°C with the help of calibrated micropipettes in an atmosphere of dry nitrogen. The liquid was dropped into a tube surrounded by a dry-ice-acetone mixture so that no evaporation would occur. The mix-

* Work supported by the Office of Ordnance Research, U. S. Army.
† On leave from Lucknow University, Lucknow, India.
[1] J. E. Mayer, J. Chem. Phys. **5**, 67 (1937).
[2] J. E. Mayer and S. F. Harrison, J. Chem. Phys. **6**, 87, 101 (1938).
[3] W. G. McMillan, Jr., and J. E. Mayer, J. Chem. Phys. **13**, 276 (1945).
[4] O. K. Rice, J. Phys. & Colloid Chem. **54**, 1293 (1950); J. Chem. Phys. **15**, 314 (1947).
[5] R. W. Rowden and O. K. Rice, J. Chem. Phys. **19**, 1453 (1951); *Changements de Phases* (Soc. Chim. Phys., Paris, 1952), p. 78. D. Atack and O. K. Rice, Discussions Faraday Soc. **15**, 210 (1953); J. Chem. Phys. **22**, 382 (1954).
[6] Mason, Naldrett, and Maass, Can. J. Research **B18**, 103, 118 (1940).
[7] B. H. Zimm, J. Phys. & Colloid Chem. **54**, 1306 (1950).
[8] H. L. Lorentzen, Acta Chem. Scand. **7**, 1335 (1953).
[9] However, O. K. Rice, J. Chem. Phys. **23**, 164 (1955), does not agree with Lorentzen's conclusions in this respect.

tures so prepared were transferred in vacuum and were dried over freshly ignited calcium oxide, following the method previously described.[5] They were finally transferred in vacuum to the experimental tube containing a magnetic stirrer and the tube was sealed off from the rest of the vacuum assembly.

Ten experimental tubes at a time containing mixtures of different compositions were placed in a rotating rack and lowered into the thermostat, which was controlled to $\pm 0.001°$ and whose temperature was measured by a Bureau-of-Standards-certified platinum resistence thermometer and Mueller Bridge assembly, and also more roughly by a Beckmann thermometer.

The tubes were heated and stirred until they became completely homogeneous. Then, following the technique previously used,[5] they were slowly cooled and a rough estimate of the temperature of separation was made. Then the tubes were heated again to get a homogeneous solution and slowly cooled to get a heavy opalescence. Temperature of the bath was fixed a few thousandths of a degree above the rough temperature of separation. The tubes were allowed to remain at this temperature from half an hour to one hour. After this the bath was heated slightly for the heavy opalescence in the tube to clear. If a line of separation had not been formed, the temperature of the thermostat was fixed at 0.001° below the previous one, the tubes were stirred and the rehomogenized tubes were allowed to stand in the bath again for an hour, and the method of observation for the boundary of separation, as given above, was repeated. This process was repeated, every time lowering the temperature by 0.001° further until a line of demarcation was visible. This was checked by heating the tube, separated into two layers, without stirring, to a fixed temperature, keeping the temperature constant for an hour. The tube was then heated sufficiently to clear the opalescence, so the meniscus could be observed. If the fixed temperature was 0.001° above the previous temperature of appearance of the meniscus, it was found that the meniscus disappeared after an hour's standing. Because of the effect of gravity, this could not mean complete homogenization of the unstirred mixture, but indicated that diffusion of the layers into each other was beginning.

The method of observation of the meniscus which we have described was particularly necessary close to the critical composition, where the temperature at which deep opalescence or "wet fog" appeared on cooling was several thousandths of a degree above T_c. For other mixtures, at which the separation of phases occurred at a lower temperature, the deep opalescence (which was not quite so deep) and the separation of phases occurred together.

The first lot of tubes gave the results shown in Table I, first series. From Table I it may be noted that the two tubes with volume fractions 0.5475 and 0.5500 separated at 28.624° but the rest of the tubes with volume fractions from 0.5375 to 0.5625 separated at 28.623°. It was thought the two tubes with the highest temperature of separation might be slightly contaminated and it was decided to purify them afresh and to redetermine the phase separation temperature in these tubes. They were taken out of the bath, washed thoroughly with soap, acid, water, and then finally with alcohol. They were then fixed to the vacuum line and evacuated. The break seal was then broken and the contents transferred to the drying tubes where the mixture remained overnight on freshly ignited calcium oxide. The contents were finally transferred to a fresh tube in vacuum. A redetermination of the transition temperature, however, gave very disappointing results as the transition temperatures rose to 28.628° and 28.626° respectively. Another transfer over silica gel did not lower the transition temperature. However, a more careful washing and evacuation of the rest of the tubes with subsequent redrying over calcium oxide and transfer to new tubes gave no abnormal results, the temperature of transition remaining unchanged in every case. It was, therefore, concluded that perhaps some volatile impurity (probably traces of alcohol which was used in washing) had been introduced in the tubes due possibly to incomplete evacuation of the systems before breaking the break seal. The only recourse left open, to make a fresh lot of tubes, was followed in order to be able to decide whether the two tubes were really free or contaminated with some impurity. A number of tubes in the critical concentration range were made as before and the phase separation temperature determined. The results are given in Table I, second series. These samples were also redried and transferred to new tubes without change in the transition temperature. One of the earlier observations of the sample at volume fraction 0.5550 gave 28.624°, but this could not be repeated and after transfer it remained at 28.623°. We speculated that the one higher observation could have been due to faulty stirring.

We were thus led to conclude that the two high tubes in the previous set were in error.

TABLE I. Coexistence curve.

First series				Second series	
Vol. fract.[a] CCl_4	Temp. of separation	Vol. fract.[a] CCl_4	Temp. of separation	Vol. fract.[a] CCl_4	Temp. of separation
0.5000	28.572	0.5525	28.623	0.5375	28.623
0.5075	28.586	0.5575	28.623	0.5425	28.623
0.5125	28.599	0.5625	28.623	0.5450	28.623
0.5250	28.616	0.5675	28.622	0.5500	28.623
0.5300	28.619	0.5700	28.621	0.5550	28.623
0.5375	28.623	0.5750	28.618	0.5625	28.623
0.5425	28.623	0.5875	28.605	0.5700	28.621
0.5475	28.624	0.6000	28.584	0.5357	28.622
0.5500	28.624				

[a] Before mixing.

DISCUSSION

It is commonly found that a coexistence curve, i.e., any physical property of the coexistent phases against

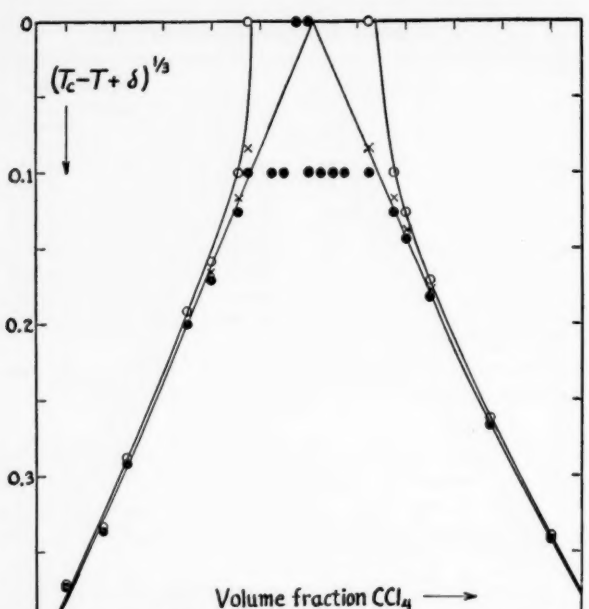

FIG. 1. Coexistence curve, perfluoromethylcyclohexane-carbon tetrachloride system. Open circles, $\delta=0$; filled circles $\delta=0.001°$; crosses, $\delta=0.0006°$.

concentration, is approximately cubic in nature.[7,8,10] However it is not strictly true in some cases, e.g., aniline-cyclohexane.[5] In the present case the plot of $(T_c-T)^{\frac{1}{3}}$ against concentration (Fig. 1) does not give the straight line which would be expected if the coexistence curve were exactly cubic. The two branches are curved lines meeting the concentration axis and cutting off between them a part of it equal to the flat part of the coexistence curve. However, if we plot, instead, $(T_c-T+0.001)^{\frac{1}{3}}$ against the concentration of CCl_4, two curves are obtained (Fig. 1), the upper portions of which are straight lines meeting at 0.551 volume fraction of carbon tetrachloride, which corresponds to the critical concentration given by Zimm.[7] The results are compared with those of Zimm in Fig. 2.

It appears to us from our data that the experimental curve is a cubic curve with a flattened top. However, the flattening occurs only about 0.001° below the expected maximum of the cubic curve, and this is about equal to the limit of fluctuation of the temperature of the bath. The question of the reality of the flattening, therefore, deserves some special consideration, especially in view of the fact that in the original observations of Table I we found two tubes very near the critical composition for which the transition temperature was 0.001° higher than it was for the rest of the tubes in this range.

In the first place we may note that, as is easily seen from Fig. 1, all the tubes between 0.5450 and 0.5575 volume fraction of CCl_4 should, if the curve were strictly cubic, have transition points lying within 0.00013° of each other. Altogether there were five tubes within this range with transition points at 28.623° as against the two which we believe to be in error and which showed the transition temperature 28.624°. In addition the two tubes with volume fraction 0.5425, and having transition temperatures at 28.623°, should lie about 0.0003 from the top of a cubic curve. A total of seven tubes in this range showed transitions at 28.623°. We feel, therefore, that the temperature of the top of the coexistence curve is pretty well fixed at 28.623°. On the other hand, a tube with volume fraction 0.5375 should, if the curve is cubic, have its transition point 0.0011° lower than one in the middle of the critical range, while one with volume fraction 0.5625 should have its transition point 0.0006° lower. Furthermore, a distinct difference was observed between tubes recorded in the tables as having differences of 0.001°. In view of the fact that we always observed ten tubes simultaneously, these often including tubes from both series, and that the results were repeatedly unchanged, with the one doubtful exception at volume fraction 0.5550, we believe that we would have noted the difference, predicted by a cubic coexistence curve, between the tubes with volume fraction 0.5375 and probably those with volume fraction 0.5625 on the one hand and those toward the center of the range between them on the other hand, had a difference existed.

We conclude that the preponderance of evidence favors the view that between these concentrations the curve is flatter than cubic, and we believe that simultaneous observation of the tubes gives a comparison which is slightly better than might be anticipated from the temperature control. The difference from an exactly cubic curve is, however, extremely slight and observations with better temperature control certainly would be extremely desirable.

We should also remark that it was observed that the meniscus always appeared within the confines of the tubes with volume fractions from 0.5375 to 0.5625. In tubes with 0.5357 or less, the meniscus appeared to fall from the top, while in tubes with 0.5675 or more it appeared to rise from the bottom. This lends further substance to the view that there is a horizontal portion

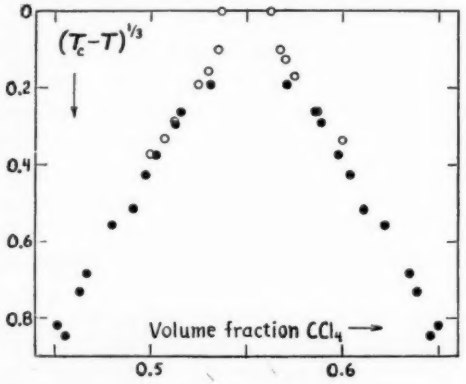

FIG. 2. Comparison of present results (open circles) with Zimm's results (filled circles).

[10] E. A. Guggenheim, J. Chem. Phys. **13**, 253 (1945).

of the coexistence curve extending from volume fraction 0.5375 to 0.5625.

The flatness in the present case is not nearly as marked as it is in the aniline-cyclohexane system, where the cubic coexistence curve appears to be flattened about 0.005° below the otherwise expected highest point. Hildebrand has suggested (private communication) that a system with two nonpolar components, like the perfluoromethylcyclohexane-carbon tetrachloride system, might be expected to be simpler than a system with one polar constituent, and perhaps would not exhibit the complexity of a flat top to the coexistence curve. We have certainly observed that the completely nonpolar system has a less marked flat top. Just as in the case of the vapor-liquid equilibrium of a nonpolar substance, like carbon dioxide, the flat portion of the coexistence curve (assuming that it exists, as we believe) involves such a small temperature range as to be barely observable. A clearer elucidation of the reason for this difference between the solutions containing a polar component and those which are entirely nonpolar would be of considerable theoretical interest.

THE JOURNAL OF CHEMICAL PHYSICS VOLUME 23, NUMBER 12 DECEMBER, 1955

Specific Heat of Lamellar Crystals*

GORDON F. NEWELL
Division of Applied Mathematics, Brown University, Providence 12, Rhode Island
(February 28, 1955)

The theoretical basis for expecting the specific heat of lamellar crystals to be proportional to T^2, at least over a sizeable range of temperatures, is re-examined and criticized in a qualitative way starting from the Born-von Kármán model of lattice vibrations. Arguments are presented to indicate that such a behavior implies special properties of the molecular forces other than those to be expected simply because of the lamellar structure. Numerous possible hypotheses are considered along with their consequences. From this, it seems doubtful that there is any simple semiphenomenological law that will fit specific heat data for all lamellar crystals in a manner comparable to the Debye law for nearly isotropic materials.

1. INTRODUCTION

SOME recent theoretical studies of the lattice vibrations of lamellar crystals,[1–6] particularly graphite, have predicted that the specific heat of these crystals would be proportional to T^2, at least over a certain range of moderately low temperatures. Experimental data on several materials[7–9] at first seemed also to give consistently a T^2 law over a sizeable range of low temperatures. More recently, however, deviations and experimental inconsistencies[10,11] have given almost as many contradictions of this rule as confirmations.

The purpose of this report is to point out that the theoretical basis for expecting a T^2 law is also not beyond question and that two derivations of this were actually based upon assumptions which are almost extreme opposites of each other. Since so many assumptions have gone into the derivations made by various investigators, some conflicting and others just borrowed from previous studies, we shall start from a completely general Born-von Kármán model and try to trace through and analyze all the various assumptions that seem necessary to arrive at any final conclusions regarding the properties of these lamellar type crystals.

The Born-von Kármán model[12] is itself based upon the assumption that the specific heat is caused by vibrations of the atoms in the lattice and that the total energy of the system can be approximated by a constant plus some function quadratic in the displacements of the nuclei from their equilibrium position. It is, of course, well known that this is only an approximation; there are other ways for the system to absorb energy and the various forms of energy are not entirely independent of each other. We shall, however, not attempt to reexamine the various arguments upon which the Born-von Kármán model is based but take this as out starting point.

We write the potential energy measured from its equilibrium value, in the form of

$$V=\sum_{j,k,l,m} x_j{}^l A_{jk}{}^{lm} x_k{}^m, \qquad (1)$$

* This work was supported by the Office of Naval Research.

[1] V. V. Tarassov, Compt. rend. URSS **46**, 20, 110 (1945); Doklady Akad. Nauk. SSSR **84**, 321 (1952); and several others with dates between these two, all in Russian.

[2] R. W. Gurney, Phys. Rev. **88**, 465 (1952).

[3] J. P. Hobson and W. A. Nierenberg, Phys. Rev. **89**, 662 (1953).

[4] H. Rosenstock, J. Chem. Phys. **21**, 2064 (1953).

[5] K. Komatsu and T. Nagimiya, J. Phys. Soc. (Japan) **6**, 438 (1951) designated here by *K–N*.

[6] J. Krumhansl and H. Brooks, J. Chem. Phys. **21**, 1663 (1953) designated here by KB.

[7] W. De Sorbo and W. W. Tyler, J. Chem. Phys. **21**, 1660 (1953).

[8] W. De Sorbo, J. Chem. Phys. **21**, 168 (1953).

[9] Dworkin, Sasmor, and Van Artsdalen, J. Chem. Phys. **22**, 837 (1954).

[10] Bergenlid, Hill, Webb, and Wilks, Phil. Mag. **45**, 851 (1954).

[11] E. F. Westrum, Jr., and J. J. McBride, Bull. Am. Phys. Soc. **29**, No. 8, 22 (1954).

[12] F. Seitz, *The Modern Theory of Solids* (McGraw-Hill Book Company, Inc., New York, 1940), Chap. III.

in which x_j^l denotes the lth component ($l=1, 2, 3$) of the displacement of the jth particle from its equilibrium position and the $A_{jk}{}^{lm}$ are the various force constants for the system. Because of the translational symmetry of the crystal, the A values will depend only on the relative positions of particles j and k in the lattice.

Any further assumptions beyond this, however, must be based upon certain special properties of the particular system in question. For one thing, it is certainly to be expected that, for any reasonable physical system, the constants $A_{jk}{}^{lm}$ will decrease in size as j and k are taken to represent particles further and further apart in the lattice. Except possibly for some ionic crystals, one can obtain good approximations by including only the interactions between the nearest few neighbors to any given particle. We shall, in fact, include in the discussions here, no more interactions than would seem necessary to give a complete qualitative picture of the vibrational energies at all temperatures. This will, however, require consideration of more than just the usual central forces between nearest neighbors.

There are certainly some physical properties that are peculiar to lamellar crystals. The most significant feature is that the forces between particles in the same layer are much stronger than those between particles in different layers, and we should not need to consider interactions between particles that are not either in the same layer or in adjacent layers. The distance between layers is also much larger (about $2\frac{1}{2}$ times larger for graphite) than the distance between nearest particles in the layers.

One of the first assumptions usually made in the analysis of lamellar crystals is that the normal modes can be separated into those for which the displacements of the particles are either in the plane of the crystal or perpendicular to the plane of the crystal. The justification for this is, with certain qualifications, fairly good. One way of verifying this is to consider the various types of forces, one by one in the order of their expected smallness until one finds something that would give a coupling between the two directions of displacement. Before doing this, we shall assume, however, that the system in consideration is one in which the layers are absolutely planar in their equilibrium state and that the crystal has symmetry with respect to reflections through any such plane.

With this restriction, we can immediately rule out any coupling of these directions of vibration due to any interactions involving particles in the same plane. If we let x_j^1 be the displacement of the jth particle in the direction perpendicular to the plane, then the terms of V arising from interactions between particles in the same layer must be invariant to changing simultaneously all x_j^1 to $-x_j^1$. There can be no terms in V of the form $x_j^1 x_k^2$ or $x_j^1 x_k^3$ (which would give rise to a coupling between the 1 and 2, 3 directions) at least from these interactions.

Any coupling between x^1 displacements and x^2, x^3 displacements must come from the interaction between layers. We consider next the nearest neighbors in adjacent layers, assuming that the line joining the centers of the nearest neighbors is directed exactly perpendicular to the planes. By essentially the same argument as the foregoing, we can say that these forces have no cross terms in the 1 and 2, 3 directions either. The first interactions in the sequence of more and more distant neighbors that can cause a coupling between the verticle and horizontal displacements are those between second nearest neighbors in adjacent layers (or the first nearest neighbors if the line of centers is not exactly perpendicular to the plane).

There are several things that must be taken into consideration in estimating the effects of such forces. The size of these forces are influenced by the facts that (1) the forces in question are expected to be of the van der Waal type which decrease very rapidly with distance, (2) since the distance between layers is much larger than the distance between particles in the same layer, the second nearest neighbors are only slightly further apart than the first nearest neighbors, and (3) there are usually many more second nearest neighbors than first. The coupling between the verticle and horizontal displacements is also strongly influenced by the fact that the line of centers joining these particles is nearly perpendicular to the plane and so one of the principle axes for these stresses is expected to be very nearly in the 1 direction giving a relatively small coefficient to the coupling term.

By including neighbors further and further away, one can produce increases in the coupling due to increases in the angles of the principle axes of interaction from the 1 direction but this will be more than compensated by the rapid decrease in the strength of the forces themselves as the distance increases. It seems safe to say that the forces causing any coupling of the displacements in the plane with those out of the plane are quite weak compared with some of the other types of forces. This, however, does not in itself necessarily mean that their effects will be unnoticed.

To carry this argument a little further, let us imagine that all the relevant force constants are known. By employing the usual technique of taking the amplitudes of various waves as new displacement coordinates, the normal mode problem, Eq. (1), can immediately be reduced to the solution of an eigenvalue equation of finite (three times the number of particles per unit cell in the crystal) dimension, the elements of which are functions of the wave vector. The roots of the secular equation give the energies of the various normal modes corresponding to each wave vector and each eigenvector of the matrix in question gives the directions of the displacements of all the particles in a unit cell for a wave of this wave vector that is a normal mode of the complete system. The coupling terms discussed in the foregoing will enter into the matrix equation as off diagonal elements connecting waves having displace-

ments in the 1 direction with waves of the same wave vector but having displacements in the 2, 3 directions.

Suppose that this secular equation could be solved completely neglecting these small coupling terms. One-third of all the normal modes could then be chosen such as to include displacements only in the 1 direction and the other two-thirds of all normal modes to include displacements only in the 2, 3 directions, i.e., the modes could be rigorously decomposed into vibrations perpendicular to the plane and vibrations in the plane.

To find the effect of the small coupling terms, we can use ordinary perturbation theory to compute the perturbed normal modes and their corresponding energies. We would take the approximate normal modes obtained above as a new set of coordinates and derive the corresponding complete matrix equation in this representation. This matrix would consist of two parts; the diagonal elements would be exactly equal to the unperturbed energies obtained above while in addition there would also be some off diagonal terms from the coupling forces which give an interaction only between the approximate normal modes with displacements in the 1 direction and those of the same wave vector but displacements in the 2, 3 directions.

As long as there is no degeneracy or near degeneracy (energy differences of the order of the off diagonal term linking the two modes) in the energies of approximate normal modes linked by the above coupling terms, the perturbations of the normal modes themselves due to this coupling will be first order in the coupling strength whereas the energies will be perturbed only in *second* order. If, however, the modes linked by the perturbation are nearly degenerate, the perturbation will have a much stronger effect. The displacement directions for these normal modes can be completely distorted by the perturbation even though the energies of the modes can be perturbed at most by a term of first order in the coupling strength and, in fact, at most by the actual value of the appropriate off diagonal matrix element.

We see then that if the properties of the system that we eventually wish to determine were sensitive to the actual directions of the normal modes, we would not be entirely justified in *a priori* decomposing the "normal modes" into either in the plane or out of the plane modes, because at least a certain small fraction of the modes are not even approximately of this type. Fortunately, the physical properties of primary interest do not depend directly on the displacements of the various normal modes but only the energies of these modes which are relatively much less sensitive to any such coupling as the above. Furthermore, the physical properties are computed by evaluating averages of certain functions of the energies over all normal modes of the system. Assuming that the functions in question are not such as to selectively pick out in some way contributions only from modes with an abnormally high percentage of degeneracies, we do not expect that the degenerate modes will contribute much to the values of the functions because the nearly degenerate modes represent only a small fraction of the total number of modes of the system. The effect of any coupling of the modes on the value of a function of this type should be even weaker than first order in the coupling strength (although generally slightly stronger than second order).

The properties of a system at very low temperatures are determined primarily by modes of the system having energies below some preassigned small energy E. It is natural to question here whether or not the states with very low energy are of necessity ones that are nearly degenerate. Except in very rare situations, this is not the case. Very low energies generally imply very small wave numbers, and it so happens that the coupling terms as well as the energies themselves are quadratic functions of the wave numbers for sufficiently small values. By selecting very low energies, we thereby select modes with nearly the same energy, but as the energies become small so also do the coupling terms become proportionately smaller and for most such modes the coupling terms remain small compared with the differences in energies of the modes which they couple.

For a more detailed analysis of the effects of perturbations on the energy spectrum and related questions[13] where similar arguments are considered in more detail as they apply to a special example of a slightly different type but with quite similar conclusions.

From the arguments above we thus conclude that although the decomposition of modes into those vibrating in the planes of the lattice and those vibrating perpendicular to the planes is not always acceptable if taken literally, the consequences of neglecting any coupling between these directions is not expected to have much effect on the thermodynamic properties. In the following, we shall assume that this is the case for the materials in question here and we shall as a matter of convenience refer to modes as "in the plane" or "out of the plane" neglecting the effects of the coupling. One should not, however, construe the above arguments to imply the neglect of all forces between second or more distant neighbors in adjacent layers, for we shall see later that these forces may be quite important.

As a consequence of the foregoing, we can consider separately in-the-plane and out-of-the-plane modes. The energy spectrum and all linear functions of it such as the total energy, specific heat, etc., are additive functions of the contributions from each type of vibration.

2. VIBRATIONS IN THE PLANE

Regarding the specific heat, it is understood that the Born-von Kármán theory of vibrations does not give a T^2 law at arbitrarily low temperatures no matter how great the anisotropy. As already noted by KB[6] and

[13] G. F. Newell, J. Chem. Phys. **21**, 1877 (1953).

Stockmayer and Hecht,[14] there is always a certain temperature range around $T=0$ over which the specific heat due to the lattice vibrations increases as T^3. This temperature range about $T=0$ may, however, in some cases be very short and in such cases may either be below the temperatures of present experiments or the specific heat so low as to be obscured by other effects. When the temperature is raised above this first region, one might argue that the thermal energy is high enough to decouple the effects of the weak interaction between layers of the crystal, with the result that the layers vibrate nearly independently of each other and so the system behaves essentially like a two-dimensional rather than a three-dimensional one. This argument has been used primarily in connection with those vibrations perpendicular to the crystal planes, but it is probably appropriate, without extensive qualifications, only for the modes vibrating in the planes of the lattice.

These in the plane modes have frequently been neglected in low-temperature studies because the large restoring forces for displacements in the planes of the crystal give rise to high frequencies for most such modes and they can be excited appreciably only at relatively high temperatures compared with the modes vibrating perpendicular to the planes.

The specific heat of these modes should itself obey a T^3 law at sufficiently low temperatures, but one can give rather strong argument for an early transition to a T^2 dependence. The arguments follow almost exactly those used by KB in considering the vibrations out of the plane. The key assumption that led them to this prediction was that the restoring forces owing to interactions between particles in the same layer were large compared with the restoring forces owing to the interaction between planes, for particle displacements out of the plane. To arrive at the corresponding conclusions for vibrations in the plane, we need only justify the corresponding assumptions for displacements in the plane. The actual analysis of the spectrum and other details would then follow in an obvious way as that discussed by KB.

The forces resisting displacements in the plane due to interactions between particles in the same plane include the forces between nearest neighbors particularly the strong central components of the force which resist displacements in the direction of the line joining the centers of the particles. In addition, there are expected to be noncentral components of the force between nearest neighbors resisting displacements in the plane but perpendicular to the line joining the particles, central forces between second nearest neighbors in the plane, and valence forces resisting a distortion of the bond angles in the plane.

The forces resisting displacements in the layer owing to the interaction between layers include the noncentral part of the forces between nearest neighbors and the forces between second and more distant neighbors in adjacent layers resisting displacements almost perpendicular to the line of centers. Which of these two types of forces between layers is larger is not obvious from naive considerations, but it is clear that we cannot *a priori* neglect the more distant interactions even though we have neglected already that part of the interaction that gives the coupling of the in-the-plane and out-of-the-plane modes. The important point here is not so much the actual size of the neglected forces as it is the fact that we do not expect the energy spectrum to be very sensitive to the coupling of the two types of modes, but it is expected to be sensitive to the existence of even a weak interaction between the modes of one layer and those of another layer. The reason for this is due primarily to the fact that the latter forces appear in the diagonal elements of the secular equation and contribute a first-order effect whereas the former appear only in off-diagonal elements and usually causes only a second-order effect.

There is also a possibility of additional forces resulting from distortion of angles between the lines joining various particles in adjacent layers, but this seems rather unlikely to be of much significance because of the nature of the forces involved.

The foregoing undoubtedly includes more forces than would usually be necessary to explain the behavior of a system in a qualitative way. One would probably tentatively neglect in a first approximation all forces between particles in the same layer, except the central forces between nearest neighbors. In some cases this will, however, give ridiculous results because it may lead to a sizeable fraction of the vibrations having no energy at all from these forces. This actually happens in the case of graphite as shown in some unpublished calculations. This means that there is a branch of the spectrum with energies arising entirely from forces other than these central forces.

The reason for expecting the specific heat contribution from the in-the-plane modes to change from a T^3 dependence to a T^2 dependence at a temperature still very low compared with any effective Debye temperatures for these modes is that the forces discussed above between particles in the same layer are large compared with those between layers. This would seem to be true beyond any reasonable doubt. Even if some branches of the spectrum are not influenced by the very strong nearest neighbor central forces in the plane, one would still feel certain that the other relevant forces (next nearest neighbor forces for example) in the planes would be large compared with the relevant forces between layers. These latter forces seem, in fact, certain to be the weakest forces that could have any significant influence at all on the spectrum. The weakness of these forces is also closely connected with the fact that one can very easily force one plane of the lattice to actually slide over another giving for example the very fine lubricating properties of graphite.

[14] W. H. Stockmayer and C. E. Hecht, J. Chem. Phys. **21**, 1954 (1953).

The temperature at which the transition from a T^3 to a T^2 law takes place is, in appropriate units, determined by the square root of the shear stiffness between layers. For graphite, an order-of-magnitude estimate would place it in the vicinity of perhaps 10°. The transition is, of course, not a sudden abrupt change but a quite gradual one. The estimate of 10° is thus the temperature in the vicinity of which the specific heat would be neither proportional to T^3 or T^2 but probably something intermediate.

After having passed this region of anomalous behavior, the part of the specific heat due to the in-the-plane vibrations should be determined primarily by just the forces in the plane and will show the general characteristics of a collection of independent two-dimensional crystals. Whether or not the high temperature specific heat can now be approximated by a two-dimensional Debye law or not depends to some extent on the geometry of the lattice. In the case of graphite, one-fourth of all the modes vibrating in the plane have low energies determined primarily by forces other than the nearest neighbor central forces. Another one-fourth of all modes have nearly the same frequency very close to the maximum possible frequency. The other half of the modes are reasonably well behaved. This minor catastrophe serves at least to indicate that a single two-dimensional Debye approximation may in some cases be an oversimplification. For graphite, one can probably do much better with two Debye temperatures and a relatively high-frequency Einstein distribution.

3. VIBRATIONS OUT OF THE PLANE

For the vibrations perpendicular to the crystal planes, the situation is quite different. The restoring forces for these displacements are expected to arise again from two sources; first, the forces between various neighboring particles in the same layer, resisting displacements in a direction perpendicular to the line joining the centers of the neighboring particles, and second, the forces between particles in adjacent layers resisting displacements in the direction or nearly in the direction of the line joining centers.

In the latter case, one can assume that the forces are central if for no other reason than the fact that the displacements in question are nearly along the line of centers anyway, but one probably should consider not only the first nearest neighbors in adjacent layers but also some of the others which are expected to be of comparable size.

Of those forces of the first type, between particles in the same layer, we shall consider two varieties which would seem to be of primary importance. First, there is a restoring force proportional to the component of the relative displacement of two particles in a direction perpendicular to the line joining the centers of the particles. This is the type of force that is usually implied by the designation noncentral. It would seem to be sufficient, at least as a first approximation, to consider only the forces of this type due to the nearest neighbors and neglect those due to more distant pairs of particles. Forces of this type can be obtained even if one assumes that the total potential energy is the sum of the potential energies due to pairs of particles. Although these forces are expected to be weak compared with the central forces discussed in the last section, we shall see that they may be important to the present discussion.

The second type of force is that resisting any distortion of the bond angles. In those cases in which a particle has just three nearest neighbors in the crystal plane, as in graphite or BN, this force is proportional to the displacements of the particles from the plane defined by the exact position of these three neighbors or, in other words, proportional to the displacement relative to the average of the displacements perpendicular to the crystal plane of the three neighbors. Although this type of force has been used extensively in models of planar molecules, very few attempts have been made to include them in the Born-von Kármán theory. These forces differ fundamentally from those of the first type in that they cannot be derived from a potential energy that is a sum of energies between pairs of particles.

The vibration spectra that would result from forces of only the first type or only the second type are also quite different from each other particularly for the waves of very long wavelength. In the first case, the potential energy is proportional to the square of the wave number (inversely proportional to the square of the wavelength) whereas in the second case, the potential energy of the wave is proportional to the fourth power of the wave number. In a continuum approximation, the two types of forces would give modes of vibration analogous, respectively, to the transverse vibrations of a plate under tension but having no rigidity and transverse vibrations of a plate under no tension but with rigidity.

To determine the behavior of the vibration spectrum and specific heat for the out of the plane vibrations, one must know the relative size of the three types of forces, (1) the central forces between layers and the two types of forces in the layers which for simplicity we shall denote as (2) noncentral forces, and (3) valence forces, respectively. Since these sizes are not too well established, we might consider the behavior of a few extreme cases.

If only forces of type (1) exist, and if, in addition, we neglect all forces of this type except those between particles whose line of centers is exactly perpendicular to the crystal planes, then for the out-of-the-plane modes, we will have interactions only between particles lying on the same line. Assuming that this does not already lead to the impossible situation of having numerous energy free displacements, it will give all the characteristics of independent one-dimensional chains.

As soon as one allows second nearest neighbor interactions between adjacent planes, which would seem necessary in any case for the reasons previously given, this whole picture changes. The second neighbor interactions give a coupling between the chains, a coupling whose strength is expected to be comparable to that within the chains themselves. The spectrum should no longer even approximately resemble that of a one-dimensional system but should be quite typically three-dimensional. The specific heat would probably even fit a three-dimensional Debye curve reasonably well.

If only the noncentral, (2), forces exist, then the system behaves strictly like a two-dimensional lattice since there is no coupling between layers. This gives a specific heat proportional to T^2 and corresponds to the model used by several people[2-4] to explain the behavior of graphite.

If only the valence forces, (3), exist, the system is also two-dimensional but the wave energy is proportional to the fourth power of the wave number instead of the square, for small wave numbers. Because of this, the spectrum of this system for low energies actually resembles that of a one-dimensional system and gives a specific heat proportional to T instead of T^2.

By including in the model only combinations of two of the three types of forces one can produce the following results.

Forces (1) alone and so also (1) and (2) together will give a T^3 law at low temperatures. Unless the (2) forces are large compared with the (1) forces, nothing very unusual will happen. The (2) forces will only help to strengthen the coupling between the chains perpendicular to the planes. This will distort the spectrum somewhat but not in any spectacular way since these chains are already coupled by the second nearest neighbor forces between planes. If, on the other hand, the (2) forces are very large compared with those between layers, we have a situation paralleling that for the vibrations in the plane. This is, in fact, precisely the type of model considered by KB for graphite. The specific heat starts as T^3 but soon changes to a T^2 dependence.

If only (1) and (3) forces are considered and forces (3) are not large compared with (1), the spectrum is again quite typically three-dimensional. If, however, (3) forces are large compared with (1) forces, one has a situation quite similar to that considered by Komatsu and Nagamiya for graphite, except that they used a continuum model throughout. Because of an additional approximation, they actually obtained a specific heat proportional to T^2 even at very low temperatures instead of the required T^3. The complete picture is a rather curious one. If the ratio of these forces is very large, the specific heat starts as T^3, changes over to T^2 and then finally to the linear dependence characteristic of (3) forces alone. The first transition results when the valence forces overpower the second nearest neighbor forces between layers and the second transition takes place when the interaction energy between layers is too weak to compete with the high energies in the valence forces. Even if one assumes that the first and second nearest neighbor forces between adjacent planes are of nearly the same strength, the valence forces will overpower the latter forces at a much lower temperature. The order of magnitude of these temperatures in this case will be such that the ratio of the first transition temperature to the second transition temperature is roughly the same as the ratio of the second temperature to the final Debye temperature determined by the maximum frequency possible for these modes.

To establish the validity of the foregoing statements, let us assume that the normal mode frequencies are given qualitatively by an expression of the type†

$$\nu^2=\alpha\theta_1^2+\beta(\theta_2^2+\theta_3^2)+\gamma(\theta_2^2+\theta_3^2)^2, \qquad (2)$$

in which θ_1, θ_2, and θ_3 are the components of the wave vector in the 1, 2, and 3 directions, respectively, chosen in appropriate units so that $|\theta_j|<1$. α, β, and γ are constants with α being a measure of the strength of essentially all the forces between layers, β of primarily just the second nearest neighbors forces between layers, and γ of the valence forces. We also assume that α and β are of approximately the same order of magnitude but that $\alpha, \beta \ll \gamma$.

For very small energies it is necessary that $\theta_1, \theta_2, \theta_3 \ll 1$ in which case the surfaces of constant frequency in the $\theta_1, \theta_2, \theta_3$ space are nearly spherical (spheroidal for $\alpha \neq \beta$). For larger energies, however, two types of distortions of the sphere will occur. For $(\theta_2^2+\theta_3^2)>\beta/\gamma$, the valence forces from the γ term begin to overpower the β term. Thus for $\nu^2>2\beta^2/\gamma$, the valence forces become important as compared with the second neighbor forces between layers.

The effect of the α term is limited by the condition $\theta_1<1$. This term begins to loose its influence on the spectrum for $\nu^2>\alpha$. The maximum energy mode possible is limited primarily by θ_2, $\theta_3<1$ giving a maximum ν of order $2\gamma^{\frac{1}{2}}$.

The two transition temperatures and the Debye temperature mentioned above are thus roughly determined by the frequencies $(2\beta^2/\gamma)^{\frac{1}{2}}$, $\alpha^{\frac{1}{2}}$, and $2\gamma^{\frac{1}{2}}$, respectively. The ratio of the first two temperatures is of order $(\beta^2/\alpha\gamma)^{\frac{1}{2}}$ while the ratio of the last two temperatures if of order $(\alpha/\gamma)^{\frac{1}{2}}$, being the same if β and α are of about the same size.

If finally only (2) and (3) forces are considered, the system is still two-dimensional. In all cases the (2) forces predominate over the (3) forces at sufficiently low temperatures because the energy of the wave due to these forces is proportional to only the square of the wave number. If the (3) forces are weak, they will never contribute much, but if they are large compared

† It is not suggested that this expression be used for quantitative calculations. It is not periodic in θ_j; it implies rotational symmetry in the planes; and it has other faults, but it is good enough for the present argument.

with the (2) forces, they will determine the features of the higher temperature behavior.

Eventually one must put all the pieces together and decide which, if any, of the forces can be neglected. The general features of the system are still roughly determined by an equation of the form of Eq. (2), as used to explain the consequences of having only forces of type (1) and (3). The effect of including also forces of type (2) is to give additional strength to the value of β in Eq. (2).

It is impossible to neglect forces of type (1), for only by including them can we obtain the required T^3 law at low temperatures. We do not recommend neglect of the forces of type (3) because there is some evidence for believing that these are the strongest forces of all.

Two reasons for believing this are the fact that they are very important in the analysis of the spectra of planar molecules, in fact they are usually weak only as compared with the strong central forces between near neighbors, and secondly, we shall see that the inclusion of these forces can remedy at least in a qualitative way some of the failures of the KB attempt to explain the specific heat of graphite.

As for the forces of type (2), there is not much information upon which to base any judgment, but there is certainly considerable advantage to including them. They give an extra degree of freedom which allows us to make $\beta \gg \alpha$, if necessary and justified. With this freedom, we can shift almost at will the relative positions of the transitions from the T^3 to T^2 to T specific heat laws and even force them close enough together as to completely obscure any well-defined T^2 region, assuming here, of course, that $\alpha \ll \gamma$.

4. COMPARISONS WITH EXPERIMENT

It is indeed unfortunate that the experimentalist can measure only the total specific heat of a material. He cannot separate the various kinds of motion and analyze them individually. Comparison with experiment then becomes somewhat of a game in which the theoretician, by including enough parameters in the theory, should be able to fit any data.

To make any quantitative comparison, we must include both the in-the-plane and out-of-the-plane modes by adding together their specific heats. For low temperatures, it is generally expected that the out-of-the-plane modes will predominate because of their lower frequencies. At sufficiently high temperatures, however, the in-the-plane modes will give about twice the specific heat of the out-of-the-plane modes because they have twice as many degrees of freedom.

At very low temperatures, their exists an interesting possibility. Both specific heats separately and together give a T^3 law, but the part from the in-the-plane vibrations seems certain to change to a T^2 law for T still very small. It is likely that the part from the out-of-the-plane modes will, at this temperature, still be in an approximate T^3 region and for a certain range of T, the specific heat will be given by a T^2+bT^3 for appropriate constants a and b. It could be that this behavior will obtain for T sufficiently low that the T^2 term overpowers the T^3 term. This means that despite the difficulty of exciting the modes in the plane, they may contribute significantly to the specific heat at some very low temperatures as well as at the very high temperatures because of the higher degree of anisotropy for these modes.

With this possible exception, however, the out-of-the-plane modes are expected to give probably 90% of the specific heat at low temperatures, enough at least so as to determine the qualitative behavior there.

There are several lamellar type crystals for which experimental data is available but only recently have measurements been made much below 50°. Although low temperature measurements have been made on molybdenite,[11] gallium,[8] boron nitride,[9,11] and a few other materials, graphite has been the subject of the greatest controversies and is the material of primary concern here. BN, however, has a very similar structure and has been the cause of similar controversies.

For graphite there exist two sets of data in the low temperature ranges, one set by De Sorbo and Tyler[7] from 13° to 300° and a set by Bergenlid *et al.*,[10] from 1.5° to 90°. The agreement between the two sets is not any too good between about 13° and 30°, but this much at least seems to be clearly indicated. If one plots the specific heat on a log-log scale, the slope of the curve is larger than 2 at the lowest temperatures so far obtained; according to Bergenlid *et al.*, the curve has a slope of about 2.4 over a certain range at the lowest temperatures they could obtain. Somewhere around $T=40°$, the slope has decreased to about 2 and, for higher temperatures, the slope gradually decreases to considerably less than 2. Above about 30°, all data is reasonably self-consistent both quantitatively and qualitatively.

For BN there is a similar situation with two sets of data, one by Dworkin *et al.*[9] from 20° to 300° and the other by Westrum and McBride[11] from 5° to 300°. The former data appears to give a T^2 dependence in the range 20° to 60°. The latter data gives a slope of about 2 on a log-log scale for T in the vicinity of about 30° to 60° but, over a wider range of temperatures, it shows a gradual monotone decrease in slope from about 3 at $T=5°$ to 10° to a value approaching 1 in the range $100°<T<300°$.

There are a few other pieces of information that are of some use. The effective Debye temperature for the modes in the planes of graphite is of the order of 2500° and that for the modes in the plane of the order of 1000°. Neither of these can be taken too seriously because the definitions may be misleading but they at least indicate relative size. From compressibility data, one can infer the approximate size of the forces between layers. These forces correspond to a temperature of the order of 100°. If we accept the model of the last

section which includes only forces of type (1) and (3), this would seem to place the first transition temperature from a T^3 to a T^2 law at around 10° and the second from a T^2 to a T law at around 100°. In view of the fact that the theory does not really expect these to be sharp transitions or these laws to be strict ones (except the T^3 part), even this simple model has some satisfactory features. If, in addition, one includes the (2) forces of the last section, the 10° temperature can be increased to give an even better qualitative agreement with the data which does not consistently show any very pronounced T^2 region at all but rather a more or less gradual change in the exponent.

The foregoing indicates in a qualitative way that this model may have some possibilities. A more detailed study of graphite is presently in progress to try to make a quantitative comparison as well. The fact that so many parameters are known only very roughly, if at all, makes this especially difficult, however, and it is doubtful if any good quantitative comparisons will be possible for some time.

The present model at least corrects some of the major deficiencies of earlier attempts. The theory of KN fails principally because it does not give a T^3 law although they have recently modified[15] it so as to give one. Neither does it include anything equivalent to the forces of type (2), which may or may not be important. From a quantitative point of view, the continuum model may also be inadequate. The criticisms of their theory made by KB are, however, not all justified.

The failures of the KB theory are less obvious but quite genuine. The Bergenlin data was not available to them at the time, and they did not have a good check on their prediction of a transition to a T^3 law which this data seems to now indicate at least better than the higher temperature data of De Sorbo and Tyler. The failures of the theory, however, pertain to the predictions in the region from about 40° to 200°. Their theory predicts a monotone decrease in the two-dimensional effective Debye temperature with temperature, leveling off to a constant value or for the log-log curve a monotone decrease in slope from 3 to 2, and eventually a decrease to lower values at temperatures comparable with the Debye temperature. The data show a minimum of this effective Debye temperature at about 40°. Although they conjectured that a minimum might be expected from a more careful analysis of their model, owing to the logarithmic singularity in spectrum found by Hobson and Nierenberg[3] and Rosenstock[4] for a strictly two-dimensional model, this prediction cannot come true. This minimum, if it exists at all, would have to occur at temperatures no lower than about 100°. A more detailed analysis of the KB model would show a monotone decrease in the effective Debye temperature up to about this temperature. The KB theory cannot possibly explain a decrease in the slope of the log-log plot below slope 2 at such a low temperature as that shown by the data.

The data on lamellar crystals seem at present to indicate that if there is any semi-imperial rule that will fit all specific heat data, as suggested by Tarassov,[1] the rule must include several adjustable parameters. The present model seems to indicate that one will need at least about five constants to determine the spectra even qualitatively. That a good imperial fit can be obtained with only two or three parameters seems rather doubtful. If this suspicion is correct, it means that a simple classification of specific heat data for these crystals may be quite difficult. On the other hand, it would also mean that the specific heat data may, by proper interpretation, give significant information about the forces in anisotropic crystals, information that is very difficult to obtain by more direct means. For nearly isotropic substances, it has always been very difficult to obtain any significant information about the molecular forces from specific heat data because of the fact that almost all data can be fitted rather well to a Debye curve having only one parameter. Even this one parameter gives very little information that cannot be obtained from elasticity measurements. Continued effort in this direction may therefore yield more than just a catalog of data.

[15] T. Nagamiya and K. Komatsu, J. Chem. Phys. **22**, 1457 (1954).

5. ACKNOWLEDGMENTS

The author is indebted to Warren De Sorbo of the General Electric Company Research Laboratory, Edward Westrum, Jr., of the University of Michigan, and J. Wilks of the Clarendon Laboratory for keeping him generously supplied with experimental data other than that which has already been published by them and their colleagues, and to James Krumhansl and Herbert Rosenstock for several discussions on the theoretical problems.

Letters to the Editor

THIS section will accept reports of new work, provided these are terse and contain few figures, and especially few half-tone cuts. The Editorial Board will not hold itself responsible for opinions expressed by the correspondents. Contributions to this section should not exceed 600 words in length and must reach the office of the Editor not later than the 15th of the second month preceding that of the issue in which the Letter is to appear. No proof will be sent to the authors. The publication charge for Letters is $25 per page, with a minimum of $25 per Letter. If honored, the Institution will be entitled to 100 reprints without covers.

Raman Spectrum of Frozen Solution of CS_2 in Methyl Cyclohexane

S. C. SIRKAR AND G. S. KASTHA
Indian Association for the Cultivation of Science, Optics Department, Jadavpur, Calcutta, India
(Received August 2, 1955)

THE Raman spectrum of carbon disulfide in the solid state was first studied by one of us[1] and two new lines at 70 cm^{-1} and 81 cm^{-1} were observed. The line 70 cm^{-1} is almost twice as intense as the strongest line 653 cm^{-1} of carbon disulfide molecule. These two new lines were attributed tentatively to vibrations in groups of associated molecules. More recently, Majundar[2] studied the Raman spectra of carbon disulfide in the liquid state at 20°C and −100°C and in the solid state at −125°C and −183°C. He observed a new broad band at 45 cm^{-1} in the case of the liquid at −100°C and two new lines 59 cm^{-1} and 70 cm^{-1} in the case of the frozen mass at −125°C. These two lines were observed to shift at 69 cm^{-1} and 80 cm^{-1}, respectively, when the temperature was lowered to −183°C. He attributed these two new lines to dimers assumed to be present in the solid mass.

In order to find out whether the intensity and positions of the two new lines depend on the environment in which the molecules are placed, the Raman spectra of frozen solutions of carbon disulfide in methyl cyclohexane have been investigated at −180°C. It is observed, as shown in Fig. 1(a), that in the case of the 50% solution, which appeared to be inhomogeneous, the new Raman lines 70 cm^{-1} and 81 cm^{-1} persist with almost undiminished intensity, the former being more intense than the line 653 cm^{-1}. Figure 1(b) shows, however, that in the case of the 20% solution at −180°C the lines 70 cm^{-1} and 81 cm^{-1} are totally absent, although the line 653 cm^{-1} appears in the spectrogram with moderate intensity. The absence of the new lines in the case of the 20% (by volume) solution at −180°C indicates that when the molecules are dispersed in a homogeneous medium the oscillations giving rise to these two lines do not take place. Two alternative explanations can be offered for the absence of these oscillations. First, the lines may be due to lattice oscillations and as the lattice is not formed when the dilute solution is frozen such oscillations are absent. Secondly, the lines may be due to oscillations in small groups of molecules which break up into single molecules when the 20% solution is made in methyl cyclohexane. There is some difficulty however, in accepting the first explanation. The carbon disulfide molecule has a center of symmetry and as the unit cell also possesses such a symmetry the only modes of lattice oscillation which are allowed in the Raman effect are the rotational oscillations on the molecules about two of its axes. Such oscillations can also take place when the molecules are dispersed in a second medium, although the frequency may be different. Since there is no indication of the presence of any new line anywhere in the Raman spectrum of the frozen solution of strength 20% the new lines observed in the case of the pure substance in the solid state cannot be due to such angular oscillations in the lattice. Further, as the new lines do not diminish in intensity at lower temperatures, it is hardly probable that they are due to any mode of angular oscillation of the molecules in the lattice. Hence it appears that these lines are due to oscillations in associated groups of molecules as suggested earlier.[1]

Investigations with other substances are being continued.

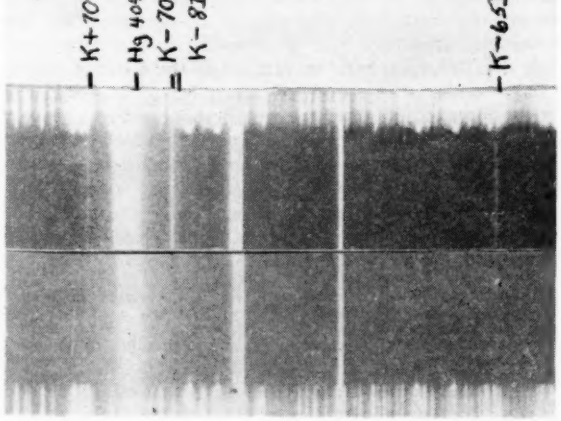

FIG. 1.

[1] S. C. Sirkar, Indian J. Phys. **10**, 189 (1936).
[2] N. C. Majumdar, Indian J. Phys. **23**, 253 (1949).

Nitric Oxide Catalyzed *Cis-Trans* Isomerization of Dideuteroethylene

B. S. RABINOVITCH AND F. S. LOONEY
Department of Chemistry, University of Washington, Seattle, Washington
(Received August 8, 1955)

RECENTLY, we reported on the thermal *cis-trans* isomerization of dideuteroethylene.[1] In that work, the height of the singlet barrier in perpendicular ethylene, $E_{N'}$, was found to be 65 kcal, while the energy of the lowest triplet state for perpendicular ethylene, $E_{T'}$, was deduced as ~52 kcal. It is a matter of considerable worth to obtain further reliable information regarding $E_{T'}$. In our previous work, marked acceleration of isomerization of dideuteroethylene by nitric oxide was observed. Harman and Eyring[2] and McConnell[3] have given different interpretations of the catalysis of olefin isomerization by paramagnetic and/or "nonsinglet" substances, respectively. The argument given by McConnell appears cogent, but in any case both mechanisms permit identification of the observed activation energy of the catalyzed isomerization reaction as an upper bound to the value of $E_{T'}$ in the case of weak catalyst-substrate interaction (physical catalysis). The examination of the nitric oxide catalysis of thermal isomerization of *trans*-ethylene, d_2, apart from kinetic aspects, is of interest for this reason.

We have studied the catalysis reaction in a quartz vessel in the interval 290–410°C, at ethylene pressures from 1.6 to 11 cm, and nitric oxide pressures from 1.0 to 63 cm. In a seasoned vessel the reaction is homogeneous, as shown by packed bulb studies, while the rate is quite reproducible, although sensitive to oxygen impurity. No exchange or polymerization is detectable by the mass-spectrograph. The first-order rate constants are independent of ethylene concentration and vary linearly with nitric oxide concentration; the second-order constants are suitably constant. Addition of inert gas, nitrogen or methane, is without effect on the rate. The activation energies obtained from the plots of $\ln k/T^{\frac{1}{2}}$ *vs* $1/T$ are independent of nitric oxide concentration and average 27.5 kcal. For k expressed in cc $moles^{-1}$ sec^{-1}, $\Delta S^{\ddagger}$ is −11 eu.

There are two possible interpretations of the observed activation energy. First, if the considerations of the first paragraph apply, then although various detailed kinetic mechanism schemes which fit the kinetics may be formulated, one concludes that the observed activation energy is closely related to the true energy of "crossing" of the N and T states of ethylene; so that, in any case, $E_{T'}<30$ kcal (1.3 ev). This number is appreciably less than that deduced from the various estimates and calculations of the difference, $E_{N'}-E_{T'}$, which have been given (<15 kcal).[4]

A second possibility is that there is strong ($\gg kT$) catalyst-substrate interaction[3] (chemical catalysis); in fact, in conventional chemical terms, it is quite probable that the mechanism of isomerization involves addition to the double bond with formation of an intermediate unstable radical. The energetics of such a process, so far as known, are consistent with the measured activation energy, while this mechanism yields a calculated entropy factor in reasonable agreement with experiment. In this case, no direct information is gained from our experiments regarding $E_{T'}$.

In the most meticulously studied cases in the literature of catalytic *cis-trans* isomerization of olefins, namely iodine (bromine) atom catalysis,[5] there seems little doubt from the magnitudes of the experimental parameters that very strong atom-substrate interaction is also involved,[3] in short, addition to the double bond. It may be remarked that it is doubtful whether physical catalysis of *cis-trans* isomerization has ever been demonstrated experimentally.[6]

It is hoped to extend this work to other olefins and catalytic agents.

This research was supported by a grant from the National Science Foundation. We thank Mr. E. Schlag for assistance with the experiments.

[1] Douglas, Rabinovitch, and Looney, J. Chem. Phys. **23**, 315 (1955).
[2] R. A. Harman and H. Eyring, J. Chem. Phys. **10**, 557 (1942).
[3] H. McConnell, J. Chem. Phys. **20**, 1043 (1952).
[4] See reference 1 for summary; also W. J. Potts, J. Chem. Phys. **23**, 65 (1955) and private communication from P. O. Lowdin quoted therein.
[5] Dickenson *et al.* J. Am. Chem. Soc. **59**, 472 (1937); **61**, 3259 (1939); **71**, 1238 (1949); H. Steinmetz and R. M. Noyes, *ibid.* **74**, 4141 (1952).
[6] Y. Urushibara and O. Simamura, Bull. Chem. Soc. Japan **12**, 507 (1937); B. Tamamushi, *ibid.* **19**, 148 (1944); E. Gelles and K. S. Pitzer, J. Am. Chem. Soc. **77**, 1974 (1955).

Remarks on Nitric Oxide Catalyzed *Cis-Trans* Isomerization of Dideuteroethylene

HARDEN M. MCCONNELL
Shell Development Company, Emeryville, California
(Received September 15, 1955)

IN the preceeding letter Rabinovitch and Looney[1] (RL) report an experimental activation energy, $E_e=27.5$ kcal mole^{-1}, for the NO catalyzed isomerization of *trans*-ethylene-d_2. An earlier study[2] yielded a value of 65 kcal mole^{-1} for the noncatalyzed activation energy which is identified with the lowest singlet state energy of *perp.*-ethylene, $E_{N'}$. RL have also cited various theoretical estimates[3] that the lowest triplet state energy of *perp.*-ethylene, $E_{T'}$, is $\gtrsim 50$ kcal mole^{-1}.

We proposed earlier[4] that the Magee, Shand, and Eyring[5] (low-energy)-(low-frequency factor) singlet-triplet isomerization mechanism could be catalyzed by "paramagnetic substances" even though the catalyst-isomer interaction energies were small. This "first-order" theory would put $E_e \approx E_{T'}$. The experimental results and arguments put forth by RL, together with the older studies on iodine catalyzed olefin isomerization, do suggest that many similar catalyst-olefin interactions will involve energies much larger than the lower limits ($\gtrsim kT$) considered earlier[4] as being *adequate* to circumvent the singlet-triplet interconversion problem. Nevertheless, our general energy level scheme,[4] and especially the quantum-mechanical repulsion of the two doublet states, D and D', retain their validity for describing and interpreting the course of isomerization catalysis irrespective of the strength of the catalyst-isomer interaction. However, for strong interactions, the $D-D'$ repulsion may amount to, say, 20 kcal mole^{-1} and may be regarded as effectively "breaking" the carbon-carbon double bond. This seems to be the case for the NO catalysis.

We also wish to use the present note to clarify, and modify, other possibly confusing points in connection with our earlier proposal. First, it must be emphasized that the proposed catalytic mechanism requires the repulsion of two doublet electronic states, D and D', and that, in turn, this repulsion requires electron exchange coupling (i.e., bonding) between catalyst and olefin. Isomerization might also be brought about by strong "ionic" catalysts but the mechanism would be entirely different from that considered here—in the ionic case, singlets and triplets would still be distinct. One of the basic requirements invoked for the catalyst is a nonzero electron spin multiplicity and not paramagnetism. Accordingly, both magnetic and nonmagnetic NO molecules ($^2\pi_{\frac{1}{2}}$ and $^2\pi_{\frac{3}{2}}$ states) are probably almost equally efficient isomerization catalysts. It must also be recognized that substances in singlet states could serve similarly as catalysts if they have low-lying electronic states of higher multiplicity.

[1] B. S. Rabinovitch and F. S. Looney, J. Chem. Phys. **23**, 2439 (1955).
[2] Douglas, Rabinovitch, and Looney, J. Chem. Phys. **23**, 315 (1955).
[3] See reference 1 for other references.
[4] H. M. McConnell, J. Chem. Phys. **20**, 1043 (1952).
[5] Magee, Shand, and Eyring, J. Am. Chem. Soc. **63**, 677 (1941).

Ozone Theory in the Troposphere*

F. N. FRENKIEL
Applied Physics Laboratory, The Johns Hopkins University, Silver Spring, Maryland
(Received October 6, 1955)

PRESENT theories of ozone formation are based on a photochemical production of ozone in the stratosphere. The resulting vertical ozone distributions agree in general with those measured in the stratosphere but do not agree with ozone measurements in the troposphere. It can be shown that in addition to the ozone produced in the stratosphere large amounts of ozone are also produced in the troposphere and more particularly near the ground. Measured ozone distributions are, therefore, the result of the added effects of stratospheric and tropospheric ozone sources.

It has been shown[1] that ozone can be produced photochemically in an atmosphere with small concentrations of nitrogen dioxide and hydrocarbons. Using mathematical models of urban pollution[2] one can determine the ozone concentrations produced in an industrial area. Under certain meteorological conditions a cloud of ozone can accumulate over a large area and then move with the wind. The total vertical amount of ozone accumulated in such a cloud, e.g. Los Angeles County, reaches 0.05 mm (SPT) of ozone and more. Tropospheric ozone may be formed by various sources including natural and industrial sources. The world production of tropospheric ozone can be evaluated and the resulting vertical ozone distribution estimated. The ozone concentrations at ground levels due to tropospheric sources are of the order of magnitude of those measured in the lower troposphere. The vertical ozone distribution resulting from the contributions of *tropospheric ozone* and of *stratospheric ozone* have been estimated for various general meteorological conditions. Several former inconsistencies between experimental and theoretical results in the troposphere seem to be explained. The latitudinal and seasonal ozone variations were reexamined and the correlation between meteorological conditions and ozone measurements justified.

* Abstract of a paper presented as a part of the lecture on "Fluid Dynamics Problems in Geophysical Sciences." American Physical Society Meeting in Mexico City, August 29, 1955. These results were not available in time to have the abstract included in the program of the meeting. This work was supported by the Bureau of Ordnance, Department of the Navy, under Contract NOrd 7386.

[1] A. J. Haagen-Smit, Ind. Eng. Chem. **44**, 1342 (1952).
[2] F. N. Frenkiel, "Mathematical analysis of atmospheric pollution in an urban area," National Academy of Sciences Meeting, April, 1955 [see abstract in Science **121**, 623 (1955)].

Electron Spin Resonance of Semiquinones*

JOHN E. WERTZ AND JUANA L. VIVO
School of Chemistry, University of Minnesota, Minneapolis 14, Minnesota
(Received August 16, 1955)

SEMIQUINONE free radical intermediates in the reduction of quinones or the oxidation of hydroquinones were demonstrated first by magnetic susceptibility and by potentiometric measurements.[1] The electron spin resonance (ESR) absorption of semiquinone ions in the oxidation of hydroquinone and methyl-substituted hydroquinones[2,3] was shown to be a more sensitive means of detecting them. The spectroscopic splitting factor g (defined by the resonance relation $h\nu = g\mu_B H$) and the appearance of hyperfine structure due to interactions with protons give additional evidence about the extent of delocalization of the unpaired electron. Additionally, these radicals form desirably simple systems for the interpretation of hyperfine spectra, for in the spectrum of the triphenyl methyl radical it would be possible in principle to have 192 lines[4] if there were no overlapping and if all of the hydrogens acted as if they were equivalent.

We have been studying both the oxidation of hydroquinones and the reduction of quinones with varying numbers and positions of substituents, and in most cases find the expected number of hyperfine lines. Assuming n equivalent protons, this number will be $2nI+1$, where I $(=\frac{1}{2})$ is the nuclear spin. The appearance of extra lines in some cases is being further studied. Figure 1 shows the derivative of ESR absorption lines for the semiquinone ions of benzoquinone, chloroquinone, 2,3 dichloroquinone, trichloroquinone, and tetrachloroquinone. Relative line intensities from integrated curves are mostly in rough agreement with expectation, with the exception of trichloroquinone. The other two dichloro compounds each give a pair of additional ESR lines. Line widths of individual components are seen to be small enough relative to their separation to allow nearly complete resolution. There is no difficulty in resolving the components either in alcoholic or in aqueous solution,[5] since the component line width (distance between points of maximum slope) is less than 0.4 gauss. Both the line widths and the separation of components show small variations from one compound to the next.

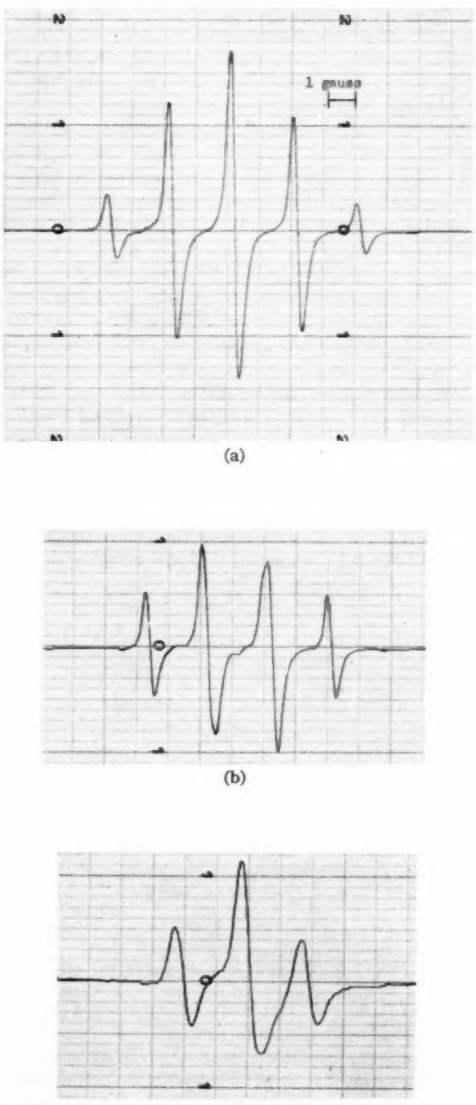

FIG. 1. Electron spin resonance absorption lines for semiquinone ions derived from the reduction by glucose in sodium ethylate solutions of a series of quinones. (a) *p*-benzoquinone. (b) Monochloroquinone. (c) 2.3-di-chloroquinone. (d) Trichloroquinone. (e) Tetrachloroquinone.

No hyperfine splitting due to the chlorine nucleus is observed in any of the chloro-substituted compounds. This is not surprising, since μ/I, the ratio of nuclear magnetic moment to spin is 5.58 for the proton, while it is 0.547 for Cl^{35}. The much smaller splitting by Cl^{35} would hardly be discernible.

For phenylbenzosemiquinone ion the splitting is qualitatively what one would expect for an inert group in place of the phenyl, thus indicating that the density of the wave function of the unpaired electron at the protons in this group is far smaller than for the protons of the principal ring. One concludes that the unpaired electron spends little time in the substituent ring system. We are extending our studies to all of the other phenyl-substituted quinones and to naphthaquinones.

Observed as a function of time, the hyperfine splitting pattern of some of these semiquinones changes markedly. This gives the appearance of several radicals being formed in succession. Studies with flow reactors will help to clarify this behavior.

The g-factors of the radicals in Fig. 1 are 2.0054 for the dichloroquinone and 2.0058 for the rest. The latter figure applies to hydroquinone in water also, the remaining values referring to alcoholic solution. Since there is no authenticated free-radical g-factor value which differs by as much as 3 parts per 1000 from the free-electron value of 2.0023, it is not informative to state that it is ". . . essentially equal to 2."[5] Further details will be published at a later date.

We have also found semiquinone-type radicals in the one-electron reduction of nitrogen compounds such as riboflavin, and theirs is a fascinating study. This technique holds great promise as a means of elucidating the kinetics of slow radical reactions.

* This work was supported in part by the United States Air Force under Contract AF 18(600)-479, monitored by the Office of Scientific Research, Air Research and Development Command.

[1] Michaelis, Schubert, Reber, Kuck, and Granick, J. Am. Chem. Soc. **60**, 1678 (1938).

[2] B. Venkataraman and G. K. Fraenkel, Abstracts Am. Chem. Soc. Meeting, September, 1954, p. 22R.

[3] B. Venkataraman and G. K. Fraenkel, J. Chem. Phys. **23**, 588 (1955).

[4] H. S. Jarrett and G. J. Sloan, J. Chem. Phys. **22**, 1783 (1954).

[5] S. Blois, J. Chem. Phys. **23**, 1351 (1955).

Mass Spectra of CuCl, CuBr, and CuI†

H. M. Rosenstock, J. R. Sites, J. R. Walton, and Russell Baldock
Stable Isotope Research and Production Division, Oak Ridge National Laboratory, Oak Ridge, Tennessee

(Received October 13, 1955)

THERMOCHEMICAL studies of cuprous chloride and bromide indicate unusually low values for the entropy of vaporization.[1] Brewer and Lofgren[2] found that the behavior of these systems could be accounted for by the existence of polymers in the gas phase. They demonstrated the existence of Cu_3Cl_3 trimers as the major species in cuprous chloride and found evidence for polymers of undetermined structure in cuprous bromide and cuprous iodide.

We would like to report here the results of some mass spectrometric studies of these compounds. The compounds were prepared by standard methods.[3] The mass spectrometer was a six-inch radius 60° sector all metal spectrometer especially designed for the study of solids. The accelerating voltage was 900 v, and the ion current was measured by a vibrating reed electrometer connected to an L- and N-recorder. The samples were placed on resistance heated platinum filaments and heated until a sufficiently rapid rate of vaporization was attained. The temperatures required were estimated to be about 150, 300, and 500°C for the chloride, bromide, and iodide, respectively. The vapor was ionized with 75 volt electrons. The mass spectra so obtained are shown in Table I. The identification of the ions was facilitated by their isotopic structure and the relative abundances were computed by summing all isotopic peaks corresponding to one species. Since the various peak heights were quite sensitive to small temperature fluctuations, the relative abundances must be regarded as only approximate.

TABLE I. Relative abundance of ions in the cuprous halide mass spectra.

	CuCl	CuBr	CuI
Cu^+	30	10	30
CuX^+	5	15	30
Cu_2^+	25	10	30
Cu_2X^+	60	50	50
$Cu_2X_2^+$	15	10	7
$Cu_2X_3^+$	...	1	...
Cu_3^+	2	1	5
Cu_3X^+	2	2	...
$Cu_3X_2^+$	40	65	90
$Cu_3X_3^+$	100	100	100
$Cu_3X_4^+$	1	...	...
Cu_4^+	...	...	...
Cu_4X^+	...	...	...
$Cu_4X_2^+$	1	...	...
$Cu_4X_3^+$	2	2	...
$Cu_4X_4^+$	15	1	...

The results indicate that the predominant vapor species in all three compounds is the trimer. The $Cu_2Cl_2^+$ intensities are not inconsistent with Brewer's[2] conclusion that the dimeric neutral species is a negligibly small constituent of the vapor. A considerable fraction of the $CuCl^+$ and $Cu_2Cl_2^+$ intensity may be due to fragment ions from the higher polymers. A preliminary study of the ionization efficiency curves of Cu^+, $CuCl^+$, and $Cu_2Cl_2^+$ indicate that several processes contribute to the ion intensities. It should also be mentioned that the nonequilibrium mode of vaporization may somewhat affect the interpretation of the relative intensities.[4] The presence of tetrameric ions is rather striking.

During one experiment a sample of CuBr was vaporized from a new filament in a source which had previously been exposed to CuCl. Besides the CuBr mass spectrum, a number of mixed halide ions were detected: $Cu_4Br_3Cl^+$, $Cu_3Br_2Cl^+$, $Cu_3BrCl_2^+$, Cu_3BrCl^+, Cu_2BrCl^+.

The mass spectrum of CuCl is also of interest in connection with the molecular structure of the trimer. Both the low entropy of vaporization and the results of electron diffraction favor a six membered ring rather than a chain structure.[2,5] The formation of Cu_3Cl^+ and Cu_3^+ in the mass spectrometer require rearrangement of the excited molecule ions before decomposition. It may be significant here that the ring structure suggested by Wong and Schomaker[5] requires a very large amplitude symmetric bending vibration of the ring.

A number of metastable transitions have been observed and will be reported on at a later date.

We are indebted to Professor L. Brewer and Professor V. H. Schomaker for helpful discussions and comments.

† This document is based on work performed at the Oak Ridge National Laboratory for the U. S. Atomic Energy Commission.

[1] L. Brewer, Paper 7, National Nuclear Energy Series, Vol. 19B, edited by L. L. Quill, (McGraw-Hill Book Company, Inc., New York, 1950).

[2] L. Brewer and N. L. Lofgren, J. Am. Chem. Soc. **72**, 3038 (1950).

[3] W. C. Fernelius, editor, *Inorganic Syntheses* (McGraw-Hill Book Company, Inc., New York, 1946), Vol. II.

[4] L. Brewer and J. J. Kane, J. Phys. Chem. **59**, 105 (1955).

[5] C.-h. Wong and V. H. Schomaker, Am. Crystallographic Assoc., Summer Meeting, Pasadena, June 27, 1955.

Vapor Pressure of HT†

Jacob Bigeleisen,‡ *Chemistry Department, Brookhaven National Laboratory Upton, Long Island, New York*
and
Eugene C. Kerr, *University of California, Los Alamos Scientific Laboratory Los Alamos, New Mexico*

(Received October 6, 1955)

A STATISTICAL-MECHANICAL treatment of the differences in the thermodynamic properties of isotopic molecules in terms of the first quantum correction ($U^2/24$ law) shows that the ratio of the vapor pressures of isotopic molecules should be a function of the reciprocal masses of the atoms in the molecule and not the total molecular weight.[1] The functional dependence on the reciprocal of the masses of the atoms provides a theoretical

TABLE I. Distribution of HT between liquid and vapor at 20.3±0.2° K. Mole ratio $HT/H_2 \sim 10^{-8}$.

Ptotal $= P_{H_2}$ in mm	Specific activity of vapor (counts/min/cc) of gas corrected to 273°K and 760 mm	$R = \frac{\text{Specific activity of liquid}^a}{\text{Specific activity of vapor}}$	$P_{H_2}-e/P_{HT}$[b] (theor.)	$P_{H_2}-n/P_{HT}$[b] (theor.)	$P_{H_2}-e/P_{D_2}-e$[b]
769.8	2.63×10^4	1.94			
755.8	2.55×10^4	2.06	2.10 (Ref. 1)	2.03 (Ref. 1)	2.89
758.4	2.55×10^4	2.06			
743.7	2.53×10^4	2.02			
(799[c])	(3.40×10^4)	(1.5)			

[a] Specific activity of liquid is constant for the series of measurements and was determined to be 5.10×10^4 counts/min/cc of uncondensed gas (corrected to 273°K and 760 mm).
[b] Corrected to the gas density and molal volume of $e-H_2$ at 20.3°K.
[c] This measurement was made after the vapor was in pressure equilibrium with the liquid for 20 hours but prior to circulation of the vapor through the liquid for isotopic equilibration.

proof of the rule of the geometric mean for vapor pressures, e.g., $P_{HD}=(P_{H_2}P_{D_2})^{\frac{1}{2}}$. On the other hand the application of quantum corrections to the law of corresponding states[2] in terms of $\Lambda^*=h/\sigma(m\epsilon)^{\frac{1}{2}}$, where m is the molecular weight, does not lead to the rule of the geometric mean, which has been established experimentally. The rule of the geometric mean and the theory of the vapor pressures in terms of the atomic masses[1] predict an appreciable difference in the vapor pressures of HT and D_2. This is in contradiction to the Raleigh distillation experiments of Libby and Barter,[3] the quantum correction treatment in terms of Λ^{*2}, and an empirical treatment of the vapor pressures of the isotopic hydrogen molecules.[4]

We have, therefore, carried out a series of experiments to look for a difference in the vapor pressures of HT and D_2. Inasmuch as HT is thermodynamically unstable with respect to disproportionation into H_2 and T_2 at 20°K, and since the equilibrium may be established by the beta activity of tritium, the work was done with dilute solutions of HT in H_2 (mole ratio $\sim10^{-8}$). Measurements were made of the specific activity of the gas in equilibrium with approximately 120 cc of liquid. The liquid was condensed from gas which had been prepared by dilution of T_2 in H_2 and then purified and equilibrated through a palladium valve at 550°C. The specific activity of the liquid was determined by measurements on the uncondensed gas. Isotopic equilibrium between the gas in thermal equilibrium with the liquid was achieved by circulation of the gas through the liquid with a piston pump. Reflux of the vapor above the liquid was avoided by maintaining the block through which the gas leads passed to the liquid container at 15°K above the liquid temperature. Assuming that the solutions obey Raoult's law and using the virial equation of state for the gas, then the ratio of the specific activity of liquid to that of the gas, defined as R, is equal to P_{H_2}/P_{HT}. The ratio of P_{H_2}/P_{D_2} is known.[5] Prior to the withdrawal of samples of the vapor for isotopic analysis, the liquid stood in contact for 20 hours with a catalyst to convert the liquid to equilibrium hydrogen (99.8% $p-H_2$). No direct measurements of the percent of ortho hydrogen in the liquid were made. The results of the experiments and comparison with theoretical predictions are given in Table I.

The data in Table I show conclusively that the vapor pressure of HT is greater than that of D_2 at 20°K. They provide additional confirmation of the theory of the vapor pressures of isotopic molecules.[1] When combined with Grilly's[6] measurements of the vapor pressure of T_2, they show that the rule of the geometric mean is valid for the sequence H_2-HT-T_2.

Additional measurements are in progress, and a complete description of the present experiments will be published after completion of the work. Similar measurements on solutions of DT in D_2 are planned.

† Research carried out under contracts between Brookhaven National Laboratory and the University of California, Los Alamos Scientific Laboratory with the U. S. Atomic Energy Commission.
‡ Consultant to the University of California, Los Alamos Scientific Laboratory.

[1] J. Bigeleisen, BNL 2190 and Phys. Rev. 99, 638(A) (1955).
[2] J. de Boer, Physica 14, 139 (1948).
[3] W. F. Libby and C. A. Barter, J. Chem. Phys. 10, 184 (1942).
[4] Friedman, White, and Johnston, J. Chem. Phys. 19, 126 (1951).
[5] H. J. Hoge and R. D. Arnold, J. Research Natl. Bur. Standards 47, 63 (1951).
[6] E. R. Grilly, J. Am. Chem. Soc. 73, 843 (1951).

Short-Lived Species from the Photolysis of Aqueous Alkali Halide and Halogen Solutions

L. I. GROSSWEINER AND M. S. MATHESON
Chemistry Division, Argonne National Laboratory, Lemont, Illinois
(Received September 28, 1955)

PREVIOUSLY unreported bands in the absorption spectra of air-free water solutions of alkali halides or halogens were detected within 30 μsec after irradiation with an intense light flash. Helium-swept solutions were irradiated in a quartz cell using a 40-μsec, 1550 joule flash from a xenon lamp. The spectra were taken with the Gaertner L 234–150 spectrograph using a 20-μsec flash as a light source. The absorption data shown are the differences in photographic density on the same plate for a 60-sec delay between flashes and for a short (30- to 300-μsec) delay.[1]

Spectrometric analysis of the final solutions showed photochemical production of the halogens[2] with a quantum yield of about 10^{-2}. The spectra of alkali halide solutions taken approximately 30 μsec after irradiation are shown in Fig. 1. The mean

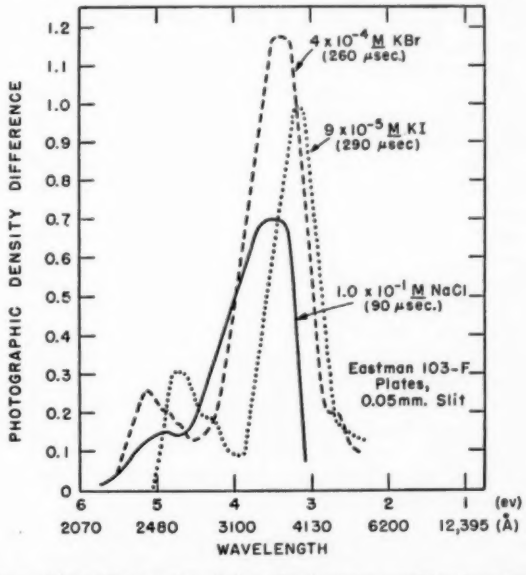

FIG. 1. Absorption spectra of short-lived species resulting from irradiation of helium-saturated solutions of alkali halides in water. Concentrations of absorbing species not equal.

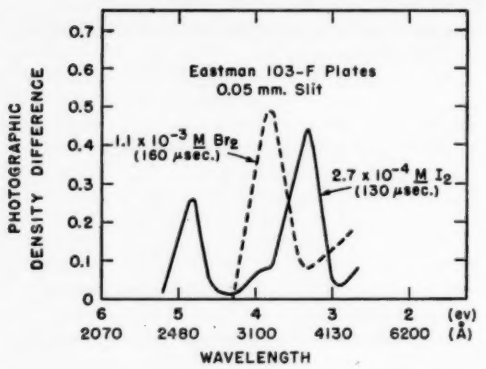

FIG. 2. Absorption spectra of short-lived species resulting from irradiation of helium-saturated solutions of halogens in water. Concentrations of absorbing species not equal.

lifetime (bracketed quantity in the figures) was determined from the rate of decrease in the main peak height with delay time, assuming first-order decay.

In further investigations, freshly prepared water solutions of the halogens were irradiated, using only light above 310 mμ, which eliminated possible absorption by halide ions if present. The results for I_2 and Br_2 are shown in Fig. 2; 1×10^{-3} M Cl_2 gave detectable transient absorption, but of insufficient intensity to resolve the bands. It appears that the main absorption band found with a given halide ion is present with the corresponding halogen. Irradiation of 2×10^{-4} M I_2 in methylcyclohexane, 4×10^{-4} M I_2 in CCl_4 and 0.1 M KOH (aq.) showed no detectable transient absorption from 225 to 750 mμ.

The possible primary products of halide ion irradiation are excited ions, solvated halogen atoms or solvated electrons. There is evidence that the absorption of the latter occurs near 400 and 1000 mμ,[3] which might account for the main absorption band found here. However, the halogen results and the absence of similar bands from irradiated OH^- argue against the solvated electron. The assignment of the bands to the solvated halogen atom is doubtful, in view of the high extinction coefficient required and the occurrence of the lowest allowed optical transitions of the gaseous halogen atoms in the vacuum ultraviolet.[4] The most likely primary product is the excited halide ion whose lifetime in solution cannot appreciably exceed 10^{-11} sec,[5] and the species measured here after 10^{-5} sec is a secondary product. A species suggested as an intermediate in the photolysis of trihalide ion[6] and whose near ultraviolet absorption is consistent with existing theory[7] is the dihalide ion. It might be possible to obtain the dihalide ion from the photolysis of aqueous halogens, but not from "violet solutions," if there is appreciable $H_2O^+\cdots X_2^-$ in the former.[8] The rupture of the $O^+\cdots X^-$ bond gives the dihalide ion directly with immediate recombination prevented by the rapid discussion of H_2O^+ in water.

A simple calculation shows our conditions can produce detectable dihalide ion by reaction of excited with normal halide ion. The estimated light intensity in the halide ion absorption region is 15 einsteins/l-sec,[9] giving for a mean lifetime of 10^{-11} sec an equilibrium yield of excited ion during the flash of 10^{-10} M. For 10^{-3} M halide ion, the maximum accumulated dihalide ion yield, from the bimolecular collision equation,[10] is 3×10^{-6} M, which is ten times the estimated detectable concentration, assuming an extinction coefficient of 10^4.

It is a pleasure to thank Mr. Jay R. Wolff for invaluable assistance in the design of the electronic equipment, and Miss Lois C. Ceterberg for technical assistance.

[1] For linear characteristics, this compensates for the spectral sensitivity of the emulsion and the output of the spectroflash lamp. The optical density difference in the cell equals the photographic density difference of the plate divided by "gamma."

[2] For at least the I^- case, some of the reacted halide ion does not appear as I_2 and I_3^-, probably a result of reactions with the solvent.

[3] J. Jortner and G. Stein, Nature **175**, 893 (1955).

[4] National Bureau of Standards Report No. 467, Vol. I, p. 195; Vol. II, p. 159.

[5] R. Platzman and J. Franck, Z. Physik **138**, 411 (1954).

[6] Roy, Hamill, and Williams, J. Am. Chem. Soc. **77**, 2953 (1955).

[7] The formula: $h\nu \cong A + H_{ion} - 0.9$ ev (reference 5) assuming possible values for A of 3/2 ev and for H_{ion} of 3 ev gives a near ultraviolet absorption for dihalide ions.

[8] R. S. Mulliken, J. Am. Chem. Soc. **72**, 600 (1950).

[9] A uranyl oxalate filter analysis showed that there were 5×10^{19} incident photons per flash between the quartz cutoff and 310 mμ of which 24% were below 225 mμ.

[10] E. A. Moelwyn-Hughes, *The Kinetics of Reactions in Solution* (Oxford University Press, New York, 1947), second edition, p. 9, Eq. (21).

Effect of Initial Temperature on Minimum Spark-Ignition Energy*

I. R. KING AND H. F. CALCOTE
Experiment Incorporated, Richmond 2, Virginia
(Received June 22, 1955)

IN a previous paper[1] the effect of molecular structure on minimum spark-ignition energy was reported. It is the purpose of this letter to report data on the effect of the initial fuel-air temperature on ignition energy employing similar capacitance sparks. If the spark volume is small compared to the volume of the minimum flame just capable of self-propagation and the energy of the spark has degraded to thermal equilibrium before conception of the flame, the effect of initial mixture temperature on ignition energy should be predictable. This gives one method of testing the concept of "ignition energy," a concept which necessarily assumes thermal equilibrium. The effect of initial temperature on minimum spark-ignition energy has been studied between −50°C and +250°C for several hydrocarbons, propylene oxide, hydrogen, and carbon disulfide. The experimental procedure was identical with that previously employed except that provision was made for controlling the temperature of the ignition bomb. This was accomplished by circulating either cooling or heating liquids from a constant-temperature bath through coils embedded in the bomb walls. A flanged cathode was used.

Figure 1 contains a faimily of curves showing the temperature effect on the minimum spark-ignition energy of *n*-pentane-air flames at varying equivalence ratios (stoichiometric air-fuel ratio divided by actual air-fuel ratio). The temperature was not carried

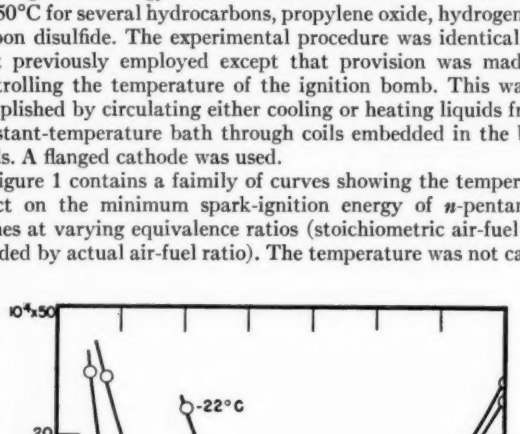

FIG. 1. Effect of initial temperature on minimum spark-ignition energy for *n*-pentane-air mixtures.

beyond 250°C because there was evidence of preignition reactions at this temperature, and the results became inconsistent. These graphs show that the equivalence ratio at which the minimum in the ignition-energy curve occurs moves toward leaner mixtures and extends over a broader range of equivalence ratios as the initial temperature is increased. An equivalent shift in the maximum burning-velocity curve with increasing initial temperature has also been observed in this laboratory and elsewhere. In Table I the minimum spark-ignition energy for stoichiometric mixtures with air of a number of fuels is summarized at 0, 25, and 100°C.

TABLE I. Minimum spark-ignition energy for stoichiometric mixtures with air.

Fuel	Ignition energy (10^{-4} joule) 0°	25°	100°C
Hydrogen	0.315	0.28	0.18
Acetylene	0.30	0.29	0.21
Methane	···	7.5	4.6
Propane	6.7	5.5	3.5
n-Pentane	10.2	7.8	4.2
n-Heptane	···	14.5	6.7
Iso-octane	···	27.	11.
Propylene oxide	···	2.4	1.5
Carbon disulfide[a]	0.86	0.70	0.49

[a] Data obtained at 1/2 atmosphere.

It has been found that the logarithm of the ignition energy is inversely proportional to the temperature except in the low temperature range (−30 to −50°C) where for some fuels a rapid increase in energy is observed with reduction in initial temperature. The possibility that this is due to fuel vapor condensing on the walls of the bomb giving leaner mixtures has been considered and rejected. All of the fuels had sufficient vapor pressure at the temperatures explored not to expect condensation. To insure against adsorption of fuel on the bomb walls, the bomb was flushed several times before each experiment with the fuel-air mixture so that the walls were saturated. Some difficulty was experienced with carbon disulfide because of its low ignition temperature and low minimum spark-ignition energy; hence it was run at 1/2 atmosphere. Even then the fuel-air mixture ignited spontaneously when placed in the bomb at approximately 175°C with an ignition delay of roughly 10 seconds.

A fuller account of this work will be presented in a forthcoming paper.

* This research was conducted under the auspices of Project SQUID, jointly sponsored by the Office of Naval Research, Department of the Navy, Office of Scientific Research, Department of the Air Force, and Office of Ordnance Research, Department of the Army.

[1] Calcote, Gregory, Barnett, and Gilmer, Ind. Eng. Chem. **44**, 2656 (1952).

Displacement of the Maximum in the Concentration-Time Diagram of Two First-Order Consecutive Reactions*

M. TALÂT-ERBEN
Faculty of Mining Engineering, Technical University of Istanbul, Istanbul, Turkey

(Received October 6, 1955)

THE known consecutive reactions in which an intermediate with a measurable mean life is produced are very few. If the two reactions are not of a very similar type the difference in their activation energies is appreciable, and a small change in temperature causes a huge displacement of the maximum in the concentration-time diagram, making the experimental determination of the new position practically impossible. This explains why none of the published papers on consecutive reactions contains a statement concerning the displacement of the maximum with temperature.

Recently, Talât-Erben and Bywater[1] have observed two apparently first-order consecutive reactions of a very similar type having practically equal activation energies. This closeness in activation energies made it possible to study experimentally the displacement of the maximum over a wide range of temperature (70 to 105°C), and to state the two empirical relations: (1) The ratio of the maximum concentration of intermediate to the initial concentration of the mother substance is independent of temperature; (2) The time required to reach the maximum concentration of intermediate is proportional to the mean life (k_1^{-1}) of mother molecules.

It is the purpose of the present note to give a theoretical interpretation of these empirical relations, and to establish their general validity.

Let us consider the sequence $A \xrightarrow{k_1} B \xrightarrow{k_2} C$. It can easily be shown that the coördinates t_{max}, $[B]_{max}$ of the maximum are given by

$$k_1 t_{max} = \frac{\ln\alpha - (\Delta E/RT)}{\alpha \exp\left(-\frac{\Delta E}{RT}\right) - 1},$$

$$\frac{[B]_{max}}{[A]_0} = \left[\alpha \exp\left(-\frac{\Delta E}{RT}\right)\right]^{\alpha \exp[-(\Delta E/RT)]/\{1-\alpha \exp[-(\Delta E/RT)]\}}$$

where $\alpha = A_2/A_1$ and $\Delta E = E_2 - E_1$. The A's and E's are the frequency factors and activation energies, respectively.

The values of $k_1 t_{max}$ and $[B]_{max}/[A]_0$ are given in Fig. 1 and Fig. 2 as functions of ΔE. It would not be far wrong to assume that both steps have frequency factors of comparable magnitudes. However, this assumption would be strictly correct if both reactions were "normal" or had equal activation entropies. Figure 2 shows that the reactions produce an *observable* intermediate, in other words, the maximum t_{max}, $[B]_{max}$ exists only if $|\Delta E|$ is very small ($|\Delta E| < 2$ kcal/mole). This property is a necessary condition for the observability of consecutive reactions. The full curves refer to 50°C and the dotted ones to 100°C. It is seen that, surprisingly, the product $k_1 t_{max}$ and the ratio $[B]_{max}/[A]_0$ are both insensitive to even such a large change in temperature. This

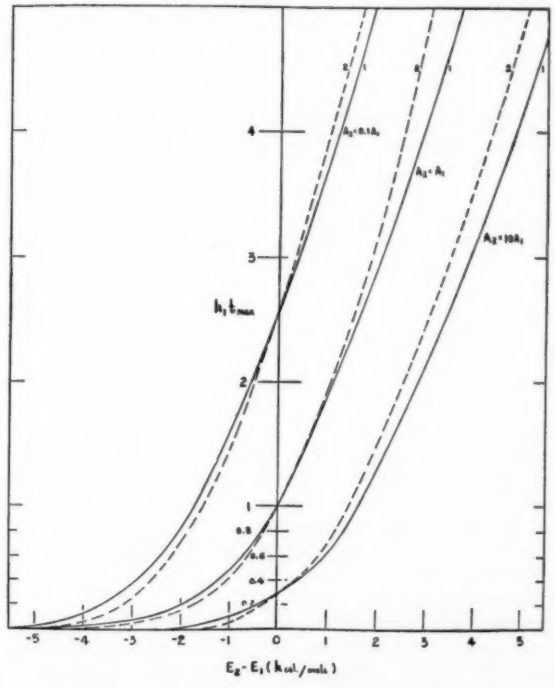

FIG. 1. For different values of the ratio $\alpha = A_2/A_1$, $k_1 \cdot t_{max}$ as function of ΔE is shown at 50°C (full curves) and at 100°C (dotted curves).

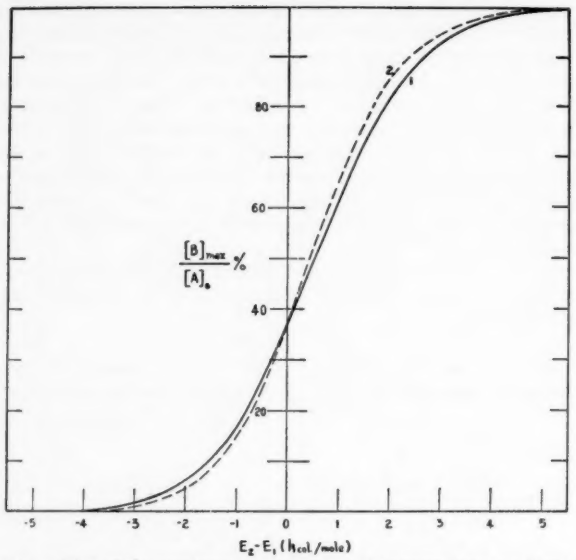

FIG. 2. Plot of the maximum concentration of intermediate as a fraction of the initial concentration of the mother, *versus* ΔE, assuming $\alpha = A_2/A_1 = 1$, at 50°C (full curves) and at 100°C (dotted curves).

insensitiveness explains the empirical displacement rules observed by Talât-Erben and Bywater[1] in the thermal decomposition of 2,2′-azo-bis isobutyronitrile in toluene solution.

Another experimental example which can be used to check the foregoing results is the mutarotation of aluminum benzoyl-camphor in CCl_4, studied by Lowry and Traill.[2] In spite of the fact that both steps are limited by the inverse transformations in this case, it is found that E_1 (21.2 kcal/mole) is only slightly different from E_2 (23.2 kcal/mole), and that $m_1 \cdot t_{max}$ is practically constant in the whole range 12.5 to 25°C, in agreement with the theoretical evidence presented above.

* This work was done while the author was holder of a National Research Council of Canada Post-doctoral Research Fellowship.

[1] M. Talât-Erben and S. Bywater, J. Am. Chem. Soc. **77**, 712 (1955).

[2] T. M. Lowry and R. C. Traill, Proc. Roy. Soc. (London) **132**, 416 (1931).

Temperature Dependence of Viscosity and Its Relation to Vapor Pressure for Associated Liquids

L. A. GIRIFALCO

Lewis Flight Propulsion Laboratory, National Advisory Committee for Aeronautics, Cleveland, Ohio

(Received October 17, 1955)

THE logarithmic expression for the temperature dependence of viscosity,

$$\ln\eta = A + \frac{E^*}{RT}, \tag{1}$$

satisfactorily describes the behavior of a large number of normal liquids but fails when applied to associated liquids. Litovitz[1] has suggested that Eq. (1) can be modified to fit associated liquids by assuming that the activation energy E^* varies inversely as the square of the absolute temperature. The resulting empirical expression fits the data for a number of associated liquids but fails for others and Litovitz found it difficult to derive any theoretical significance from the equation.

A theoretical equation for the viscosity-temperature relation can be obtained in the following way. Assume that a molecule consists of two types of force centers, one of which involves dipole interactions, and the other dispersion forces. The attractive potential associated with the pairwise interaction of these centers is given by the usual inverse sixth power law $E_a = -\frac{a}{Tr_a^6}$ for the dipole center and $E_b = -\frac{b}{r_b^6}$ for the dispersion center where a and b are constants, r_a = distance between two dipole centers, and r_b = distance between two dispersion centers. The potential energy of a molecule in a liquid is then obtained by integrating the potential energy functions over all the molecules in the liquid.

Let $W_a(r_a,\theta,\varphi)$ and $W_b(r_b,\theta,\varphi)$ be the microscopic density functions associated with the centers a and b. Then the potential energy of a molecule in an equilibrium position is

$$\epsilon_1 = -\frac{a}{T}\int W_a(r_a,\theta,\varphi)\frac{\sin\theta}{r_a^4}dr_a d\theta d\varphi - b\int W_b(r_b,\theta,\varphi)\frac{\sin\theta}{r_b^4}dr_b d\theta d\varphi. \tag{2}$$

In the activated state for viscous flow, the molecule is not in an equilibrium position so that the microscopic density functions will have other forms $W_a'(r_a,\theta,\varphi)$ and $W_b'(r_b,\theta,\varphi)$. The energy in the activated state, ϵ_2, has the same form as Eq. (2) with W_a and W_b replaced by W_a' and W_b'. The activation energy $E^* = \epsilon_2 - \epsilon_1$, therefore has the form

$$E^* = \frac{A'}{T} + B \tag{3}$$

where A' and B are constants. Inserting this in (1) gives

$$\log\eta = \frac{\alpha}{T^2} + \frac{\beta}{T} + \gamma \tag{4}$$

α, β, and γ are constants for nonpolar liquids $\alpha = 0$ and (4) reduces to (1).

This equation correctly represents the data for a large number of associated liquids. Values of the constants calculated from literature data are given in Table I.

TABLE I. Values of the constants in Eq. (4) for several liquid viscosity in c.p.

Liquid	$\alpha \times 10^{-4}$	$\beta \times 10^{-2}$	γ
Water	23.611	−6.8922	−0.3908
Methyl alcohol	3.428	2.750	−1.567
Ethyl alcohol	−1.145	7.807	−2.459
n-Propyl alcohol	9.259	3.353	−1.875
n-Butyl alcohol	0.5588	9.615	−2.878
Formic acid	12.819	−0.7629	−0.9759
Acetic acid	−15.759	15.965	−3.521
Butyric acid	6.589	2.205	−1.323
Sulfuric acid	26.37	−4.690	−0.09771
Ethylene glycol	32.036	−5.860	−0.4312
Glycerine	145.78	−72.23	10.873
Ethyl acetate	5.871	0.09764	−1.0590
Aniline	38.52	−13.287	0.7008

Mitra and Chakravarty[2] have considered the related problem of the relation between viscosity and vapor pressure. By combining the vapor pressure and viscosity formulas for normal liquids they found that

$$n \equiv \frac{\log P - \log P_0}{\log\eta_0 - \log\eta} \tag{5}$$

where n is constant for normal liquids but varies for associated liquids.

Equation (2) is essentially the heat of vaporization (neglecting RT). Using the Clapeyron equation, Eq. (2) leads to

$$\log P = -\frac{C_1}{T^2} - \frac{C_2}{T} + C_3. \tag{6}$$

Combining (6) and (4) gives

$$n = kX + m + \frac{J}{\log\frac{\eta_0}{\eta}} \tag{7}$$

where n is defined by (5), $X = \left(\frac{1}{T_0} - \frac{1}{T}\right)\Big/\log\frac{\eta_0}{\eta}$ and k, m, and J are

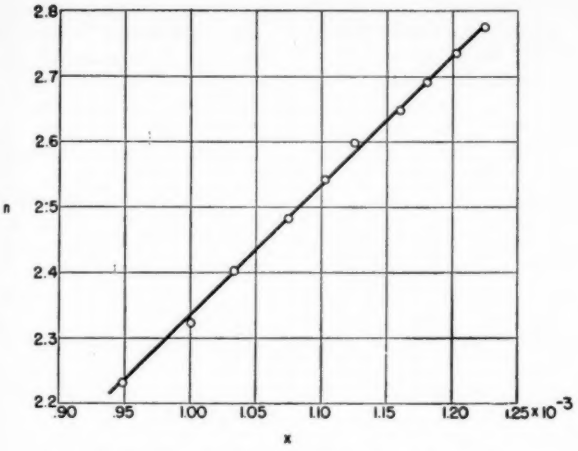

FIG. 1. The viscosity vapor pressure relation for water.

constants. The plot of n against X for water (shown in Fig. 1) is linear indicating that for water $J/\log\frac{\eta_0}{\eta}$ does not contribute appreciably to the variation of n. A similar plot for ethyl alcohol shows a slight curvature.

In this derivation, the assumption has been made that the molecules are always far enough apart so that the expression $-\frac{a}{Tr^6}$ is valid for the dipole-dipole interactions. Also the microscopic density functions are assumed to be constant with temperature. Obviously, these are only first approximations and a rigorous treatment of the subject would require a more refined model. The resulting equations, however, satisfactorily represent the experimental data. The present model can, therefore, be used to advantage and certain anomalies concerning associated liquids can be obviated.

[1] T. A. Litovitz, J. Chem. Phys. **20**, 1088 (1952).
[2] S. S. Mitra and D. N. Chakravarty, J. Chem. Phys. **22**, 1775 (1954).

Mechanism of the Conversion of *Cis-* to *Trans-* Modifications of the Unsaturated Higher Fatty Acid Esters by Nitrogen Dioxide

N. A. KHAN
Department of Physiology, University of Minnesota, Minneapolis, Minnesota
(Received September 27, 1955)

THE oxides of nitrogen have been employed for isomerizing fatty acids and esters over a long period of time. Extensive studies have been made by various investigators on different phases of this problem.[1-3] No information is yet available as to the efficiency of each individual oxide (N_2O, NO, and NO_2) in affecting isomerization. The present paper deals with this aspect and describes some experimental evidence for the mechanism of *cis-*, *trans-*conversion.

The pure nitrous oxide was obtained from a commercial source. The nitric oxide was prepared by the second method described by Farkas and Melville.[4] Nitrogen dioxide was prepared by mixing nitric oxide with pure oxygen. Methyl oleate (iodine value, 86.8) was prepared from the methyl esters of olive oil, by a combination of low-temperature crystallization and fractional distillation at reduced pressure.[5] Methyl linolenate (iodine value, 259.4) was prepared by the usual bromination and debromination procedures.[6]

The initial reactions were carried out with about 25–30 g of methyl oleate in a cylinder (1 in.×10 in.) at room temperature by bubbling the gases through a Corning gas dispersion tube for half an hour. The results from infrared analyses through absorption bands at 10.32μ for isolated *trans* bonds and through those at 6.11 and 6.44μ for nitrogen derivatives are shown in Table I. As

TABLE I.

Oxides of nitrogen	Percent *trans*-isomer	Presence of nitrogen derivatives
N_2O	none	none
NO	none	considerable
NO_2	45–51	considerable

may be seen in Table I, nitrogen dioxide is the potent isomerizing agent.

One peculiar characteristic of nitrogen dioxide is its exothermic reaction with unsaturated compounds, which is not exhibited by nitric oxide. It raises the temperature of the reacting products to 90°C within a few minutes. Under the above conditions, nitrogen dioxide polymerizes methyl linolenate in a period of 2 hours. However, in the case of methyl linolenate, in 10–15 minutes, it causes formation of the *trans*-isomer (10.32μ) which disappears under vacuum. Of course, the nitrogen derivatives (6.44μ) do not change under vacuum. This led to the studies under milder conditions for further information on the formation of this unstable *trans*-isomer of methyl linolenate in the processes of isomerization.

A thin layer of methyl linolenate (1.0–2.0 mm in thickness) in a crystallizing dish (4-in. diam) was placed inside a desiccator that was filled with NO_2 gas by flushing for some time. The course of the reaction was followed by infrared and ultraviolet absorption analyses, 5 min, 10 min, 15 min, 30 min, and 1 hr after the initiation of the reaction. From 10 minutes onward the reaction mixture showed a maximum at 301 millimicrons and no presence of *trans*-isomer (10.32 microns). This maximum at 301 mμ disappeared after 1 hour while appreciable amounts of *trans*-isomer were found to be formed. The application of high vacuum destroyed the majority of these *trans*-isomers. The ultraviolet maximum was most prominent at 30 minutes, and the general absorption by the products is shown by Fig. 1. There was no diene or triene conjugation.

From these findings, the following concepts (Fig. 2) on the mechanism of *cis-*, *trans*-isomerism have been proposed. At the initial state, the NO_2 molecule by virtue of polarization of the double bond may partially draw the π electrons (I) towards itself (II)[7] forming a molecular complex and allow the *cis*-molecule the free rotation about the activated C—C bonds (III) until it comes to the position of greatest stability. Under these latter circumstances, the molecule in the stabilized position may tend to pull back its π electrons (IV)[8] and revert to the stable *trans*-form (V)

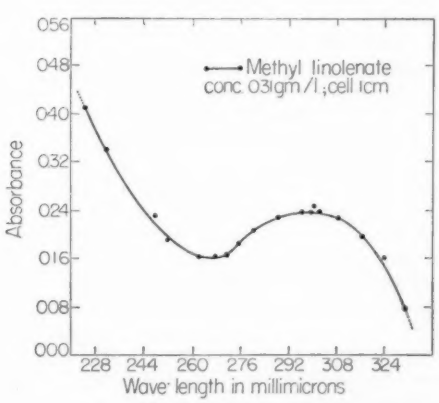

FIG. 1. Initial reactions of nitrogen dioxide.

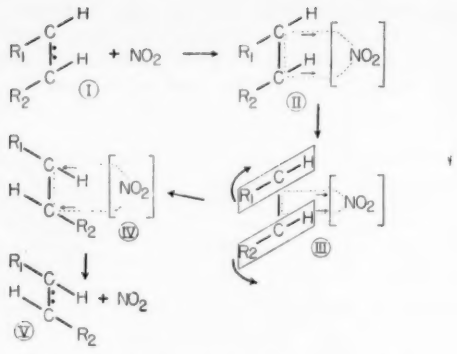

FIG. 2. Mechanism of the conversion of *cis-* to *trans*-isomer by nitrogen dioxide.

liberating NO_2. The success in these processes determines the amounts of free *trans*-isomer (V), while the failure of the activated carbon atoms of the double bond to retrieve their π electrons determines the amounts of nitrogen derivatives formed (Table I).

[1] Griffiths and Hilditch, J. Chem. Soc., 2315 (1932).
[2] Bertram, Chem. Weekblad. **33**, 3, 216 (1936).
[3] Kass and Burr, J. Am. Chem. Soc. **61**, 1062 (1939); **63**, 1060 (1941).
[4] Farkas and Melville, *Experimental Method in Gas Reactions* (MacMillan and Company, Ltd., London, 1939), p. 164.
[5] Foreman and Brown, Oil and Soap **21**, 183 (1944).
[6] McCutcheon, Org. Syntheses **22**, 82 (1942).
[7] This complex may be responsible for ultraviolet absorption at 301 millimicrons.
[8] The molecular complex may have regained enough *trans* double-bond character to give rise to absorption at 10.32 microns in the infrared region.

Infrared Spectrum of $Ni(CO)_4$ Vapor*

LLEWELLYN H. JONES
Los Alamos Scientific Laboratory, University of California, Los Alamos, New Mexico
(Received October 3, 1955)

CRAWFORD and Cross[1] investigated the infrared spectrum of nickel tetracarbonyl vapor rather thoroughly in 1938. The Raman spectrum of the liquid was reported by Duncan and Murray[2] and later by Crawford and Horwitz.[3] Crawford and Cross[1] made assignments for all of the fundamental frequencies and carried out a normal coordinate treatment of the molecule to determine its force constants. This letter is to report some recent observations on the infrared spectrum of nickel tetracarbonyl vapor which require a change in some of the fundamental frequency assignments. With the equipment available to them in 1938, Crawford and Cross could not observe the infrared spectrum below about 450 cm^{-1}. On the basis of combination frequencies they assigned 300 cm^{-1} to the asymmetric Ni—C stretching frequency, ν_6 (F_2 symmetry)[4] and 420 cm^{-1} to the inactive Ni—C—O bending frequency, ν_9 (F_1 symmetry). Using CsBr, NaCl, and LiF prisms in a Perkin-Elmer, single-beam, double-pass spectrometer, we have observed the spectrum of $Ni(CO)_4$ vapor from 270–10 000 cm^{-1} using path lengths up to 10 cm and pressures up to 300 mm Hg. A very strong band appears at 422 ± 1 cm^{-1} (second in intensity only to the C—O stretching frequency). Its absorption coefficient is 0.04 $cm^{-1}p^{-1}$ (p=mm Hg). No absorption at all was observed from 270–400 cm^{-1}. An absorption coefficient of 10^{-5} would have been observed. A band at 459 cm^{-1} was observed having an absorption coefficient of 0.002 $cm^{-1}p^{-1}$. Otherwise, the spectrum is similar to that reported by Crawford and Cross.[1]

In view of the above considerations, we feel it necessary to assign 422 cm^{-1} to the asymmetric Ni—C stretching vibration (F_2 symmetry) which should be strongly infrared active. The assignment at 459 ± 1 cm^{-1} still is uncertain. The assignment of the inactive frequency ν_9 (F_1 symmetry) cannot be made at this time. A normal coordinate treatment, using Wilson's $F-G$ matrix method, is in process. The constant for interaction between neighboring Ni—C and C—O bonds (neglected by Crawford and Cross) will be included. The results should yield an assignment for ν_9 and will be reported when completed.

The high-frequency region of the spectrum was also investigated (using an LiF prism). The asymmetric C—O stretching vibration called ν_8 by Crawford and Cross[1] shows P, Q, and R branches with the Q branch maximum at 2057 ± 1 cm^{-1}. Also, there is a much weaker band of similar structure at 2018 ± 1 cm^{-1}. The approximate absorption coefficients are 0.270 $cm^{-1}p^{-1}$ and 0.0066 $cm^{-1}p^{-1}$, respectively. This band at 2018 must be the C^{13}—O stretching frequency of the isotopic species, $Ni(C^{12}O)_3(C^{13}O)$, which is normally present to the extent of a little over 4%. The intensity ratio is about right, especially considering that for $Ni(C^{12}O)_4$ the peak at 2057 is triple degenerate while the C^{13}—O peak of the mono-C^{13} species will not be degenerate. Furthermore, a simple calculation shows that for the hypothetical linear molecule O—C—Ni—Ċ—O, when C^{13} is substituted for C^{12} the asymmetric C—O stretching frequency should be decreased by a factor of about 0.981 (using the force constants of Crawford and Cross).[1] The observed decrease, 2057→2018, is by a factor 0.981. In an article on the spectra and structures of cobalt carbonyls, Friedel and co-workers[5] report combination bands for $HCo(CO)_4$ (gas), $(Co)_2(CO)_8$ (gas), $Fe(CO)_5$ (gas), $Ni(CO)_4$ (gas), and $(Co)_4(CO)_{12}$ (heptane solution) at 2010, 2000, 1976, 2022, and 1996, respectively. These correspond to shifts from the lowest asymmetric C—O stretching frequencies of each species by factors of 0.981, 0.982, 0.982, 0.982, and 0.983, respectively. Thus, these weak bands probably arise from the mono-C^{13} species, rather than from combination transitions as indicated by Friedel and co-workers.[5]

* This work was sponsored by the U. S. Atomic Energy Commission.
[1] B. L. Crawford and P. C. Cross, J. Chem. Phys. **6**, 525 (1938).
[2] A. B. F. Duncan and J. W. Murray, J. Chem. Phys. **2**, 636 (1934).
[3] B. L. Crawford and W. Horwitz, J. Chem. Phys. **16**, 147 (1947).
[4] The numbering of the vibrational frequencies is that of Crawford and Cross.
[5] Friedel, Wender, Shufler, and Sternberg, J. Am. Chem. Soc. **77**, 3951 (1955).

Quantum Yield of a Cadmium Sulfide Photovoltaic Cell

R. E. MARBURGER,* D. C. REYNOLDS, L. L. ANTES, AND R. S. HOGAN
Aeronautical Research Laboratory, Wright Air Development Center, Air Research and Development Command, United States Air Force, Wright-Patterson Air Force Base, Ohio
(Received September 21, 1955)

IN his article on the photovoltaic effect, Lehovec[1] derives the equation

$$E=\rho_0(Je/h\nu)\cdot\alpha\cdot A\cdot\rho_0 I, \tag{1}$$

which holds for low light intensities ($kT/e\gg E$) where, E=photovoltage or external voltage, J=light intensity, α=quantum yield, A=correction factor for absorption, ρ_0=barrier layer resistance of unilluminated photoelement, and I=photocurrent.

With the development of the cadmium sulfide photovoltaic cell,[2] all the quantities (except α) in Eq. (1) are experimentally measurable and the equation may be solved for α.

When transposed, (1) becomes

$$\alpha=\frac{E/\rho_0 e+(I/e)}{(J/h\nu)\cdot A}. \tag{2}$$

When I=short-circuit current, E=0 and (2) becomes

$$\alpha=\frac{I/e}{(J/h\nu)\cdot A}, \tag{3}$$

which is simply the number of electrons per second appearing in the external circuit divided by the number of absorbed light quanta incident upon the crystal times an absorption factor.

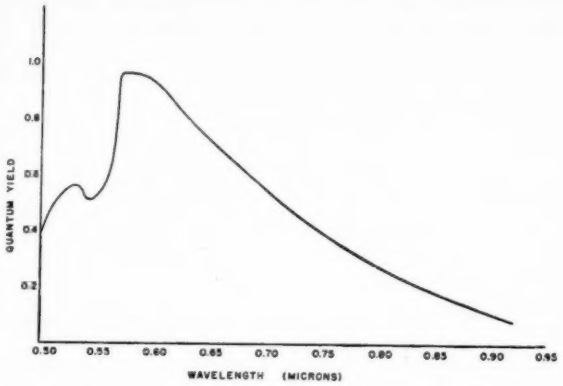

FIG. 1. Quantum yield of Cds photovoltaic cell.

A is a number representing the fraction of incident photons contributing to the photovoltaic effect and it can have a value no greater than unity. Thus, α would appear to assume its lower limit if it is assumed that every incident photon not reflected contributes to the effect, thus making $A=1$. Inserting this value of A in (3) gives the quantum yield plotted as a function of wavelength in Fig. 1 (corrected only for reflection at the crystal surface).

The cell used was a rear-wall cell made from a CdS single crystal 2 mm thick. The front electrode consisted of a band of indium deposited around the perimeter, thus leaving a clear window in the center. The barrier layer was located at the rear of the crystal and was coated with silver paint. The crystal was mounted 1 mm in front of the exit slit of a Gaertner monochromator. The slit was 4 mm long and 0.75 mm wide.

Only the central area of the crystal was illuminated. The indium band was unilluminated. The monochromator dispersion ranged from 295 A/mm at one micron to 34 A/mm at 0.4 micron. The intensity of incident radiation was measured by a Ag-Bi thermopile. The short-circuit current was measured on a Leeds and Northrup galvanometer with a sensitivity of 0.00617 μamp/mm.

It might be pointed out that since the cell was 2 mm thick, the only way an incident photon could contribute to the photovoltaic effect would be in one of two ways: (1) The photons could traverse the 2-mm thickness and thus arrive at the sensitive layer; or (2) The photon could be absorbed somewhere within the 2-mm thickness with the resulting creation of a hole-electron pair. It is reasonable to assume that some recombination takes place which would make A less than unity and would correspondingly increase quantum yield.

* Research physicist, Research Staff, General Motors Corporation, Detroit 2, Michigan.
[1] K. Lehovec, Phys. Rev. **74**, 463 (1948).
[2] Reynolds, Leies, Antes, and Marburger, Phys. Rev. **96**, 533 (1954).

Emission and Two-Body Recombination in Bromine*

HOWARD B. PALMER†
Metcalf Research Laboratory, Brown University, Providence, Rhode Island
(Received October 10, 1955)

RECENT observation in this laboratory of emission from bromine, heated to temperatures between about 1400°K and 2250°K, has yielded convincing evidence that the emission is almost entirely due to 2-body atom recombinations. The study of emission was an outgrowth of experiments using light absorption to measure the rate of dissociation of Br_2 at high temperatures produced by moderately strong shock waves.[1] It was found that emission from these hot shocks was intense enough to be easily detectable with a photomultiplier, and even to be studied at various wavelengths (3650 A, 4390 A, and 5950 A) with the aid of interference filters. Spectra of the emission[2] showed it to be essentially continuous. The shocks were not hot enough to excite appreciable impurity emission, so it was assumed that recombination of Br atoms was responsible for the continuum,[3] and that the emission intensity was proportional to the rate of recombination.

Runs were made in which the emission was recorded as a function of time as the shock traveled past a slit system at one point of the shock tube. The emission intensity rose from zero at the shock front to an equilibrium value, at which it remained until the arrival of the contact region. The equilibrium Br atom concentration was calculated for a series of shocks covering as wide an equilibrium temperature range as possible. Concentration products corresponding to 2-body and 3-body recombination, divided into the equilibrium emission height on the record, yielded what were termed "emission rate constants," k_{em}. A plot of these *versus* $1/T_{abs}$ showed the k_{em} for the 2-body case to be behaving like a true rate constant, whereas the 3-body results showed severe scatter.

Activation energies calculated on the basis of simple collision theory for the 2-body case were 29.1 kcal/mole at 3650 A, 17.7 kcal/mole at 4390 A, and 0.85 kcal/mole at 5950 A. These numbers were readily interpretable in terms of the potential diagram for Br_2. No physical meaning could be attached to an activation energy estimated from the 3-body results. It was concluded that although most atom recombinations are 3-body, it is the 2-body ones that produce virtually all the emission. That is, a molecule of Br_2 which is produced *via* a 3-body atom recombination is almost never left in an excited state.

The work described here will be presented in detail in a forthcoming publication.

* Work supported by the Office of Naval Research.
† Present address: Department of Fuel Technology, Pennsylvania State University, University Park, Pennsylvania.
[1] H. B. Palmer and D. F. Hornig (to be published).
[2] The cooperation of Dr. E. F. Greene in taking the spectra is gratefully acknowledged.
[3] G. Herzberg, *Spectra of Diatomic Molecules* (D. Van Nostrand Company, Inc., New York, 1950), *Molecular Spectra and Molecular Structure*, Vol. I.

Stereochemical Consequences of Intramolecular Attractive Forces

G. J. SZASZ
U. S. Office of Naval Research, London, England
(Received October 3, 1955)

REPULSIVE forces provide a satisfactory qualitative explanation for the well-known energy differences between rotational isomers in the simplest hydrocarbons and their derivatives. Thus in the case of *n*-butane the *trans*-configuration is favored by 800 cal/mole, while in 1,2-dichloro ethane vapor the corresponding energy difference is 1100 cal/mole, and in the dibromo ethane it is 1500 cal/mole. In marked contrast with these observations, the energy difference between the *trans*- and *gauche*-rotational isomers in *n*-propyl chloride and bromide vapor is zero.[1] A plausible explanation may be that electrostatic attraction between the halogen atom and the methyl group becomes a significant factor in the *gauche*-configuration of the *n*-propyl halides.[2] If correct, this hypothesis would predict greatly increased stability for configurations of a number of other halogen substituted hydrocarbons, which are generally considered to be highly unstable on steric grounds.

The most striking experimental data supporting this prediction relate to the isobutyl halides; the two possible rotational isomers are shown in Fig. 1 (X=halogen). On purely steric grounds form *a* would be the predominantly stable isomer; it will be recalled that in isopentane and in 1,1,2-trichloroethane the corresponding rotational isomers are favored by several kilocalories in each case.[3,4] Available Raman spectra[5] of the liquid isobutyl halides clearly indicate however that both forms are present and that the energy

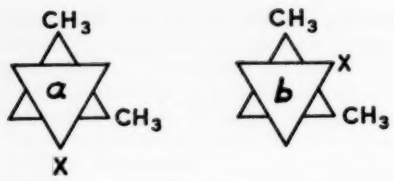

FIG. 1.

difference between them must be close to zero, for all three isobutyl halides. The location and (relative) intensities of the carbon-halogen stretching frequencies (cm^{-1}) are as follows:

isobutyl chloride	689(6)	726(10)
isobutyl bromide	621(6)	653(10)
isobutyl iodide	582(6)	602(9).

Preliminary infrared spectroscopic results recently obtained for the bromide are in good agreement with these relative intensities. The assignment of the higher of these two frequencies to form *a* (statistical weight = 2) has been recently discussed.[6] It should be noted that energy differences determined in the liquid phase are expected to be applicable to the isolated molecules in the gas, not only for nonpolar substances, but also for polar molecules such as these whose net dipole moment is only slightly dependent on the angle of internal rotation.[1]

The *sec*-butyl halides present another, somewhat more complicated, case in point. The Raman spectra[5] clearly indicate the coexistence of appreciable quantities of all three possible rotational isomers, while purely repulsive forces would preclude the presence of one of these at ordinary temperatures. The 1,2-dihalo propanes and the 1,1-dihalo propanes are other simple cases where available data can be most readily interpreted along these lines.

The author is indebted to Dr. N. Sheppard for stimulating discussions and for the opportunity to obtain some preliminary infrared spectra of isobutyl bromide; and to Dr. I. Miyagawa for information about work on the *n*-propyl halides.

[1] Komaki *et al.*, Bull. Chem. Soc. Japan **28**, 330 (1955).
[2] Goubeau and Pajenkamp, Acta. Phys. Austriaca **3**, 283 (1949).
[3] Scott *et al.*, J. Am. Chem. Soc. **73**, 1707 (1951).
[4] DiGiacomo and Smyth, J. Am. Chem. Soc. **77**, 1361 (1955).
[5] Kohlrausch, *Ramanspektren* (Akademische Verlagsgesllschaft, Leipzig, 1943), pp. 241, 242.
[6] Brown and Sheppard, Trans. Faraday Soc. **50**, 1164 (1954).

Microwave Spectrum of Propiolactone*

NOWHAN KWAK, J. W. SIMMONS, AND J. H. GOLDSTEIN
Emory University, Emory University, Georgia
(Received September 27, 1955)

CONSIDERABLE interest has been exhibited in the properties of strained four-membered ring compounds, of which propiolactone, OCH_2CH_2CO, is an example.[1-3] We have studied the rotational spectrum of this molecule in the 18–34 kmc region. Eight low-J R-type transitions have been identified and fitted in the rigid rotor approximation, as shown in Table I.

TABLE I. Rotational spectrum of propiolactone.

	Transition	Obs freq. Mc[a]	Calc freq. Mc
1	$1_{01}\rightarrow 2_{02}$	18 047.49	18 047.53
2	$1_{10}\rightarrow 2_{11}$	19 602.54	19 602.39
3	$2_{12}\rightarrow 3_{13}$	25 172.11	25 172.17
4	$2_{02}\rightarrow 3_{03}$	26 641.64	26 641.64
5	$2_{21}\rightarrow 3_{22}$	27 340.69	27 340.77
6	$2_{20}\rightarrow 3_{21}$	28 039.96	28 039.89
7	$2_{11}\rightarrow 3_{12}$	29 282.90	29 282.96
8	$3_{13}\rightarrow 4_{14}$	33 384.4	33 384.86

[a] Estimated experimental uncertainty 0.1 Mc, except for line No. 8, 0.2 Mc.

The rotational constants derived from the spectrum and the corresponding moments of inertia are presented in Table II.

For purposes of comparison we have also calculated the moments of inertia using the following structural parameters selected from the ranges reported by Bregman and Bauer[2]: C–O = 1.44 A, C–C = 1.52 A, C=O = 1.19 A; angles COC = 90°, CCO (external) = 143°; and a planar ring configuration assumed. The resulting values are 41.03, 96.62, and 130.46 a.m.u.-A,[2] in quite close agreement with the experimental values of Table II. It can be concluded, then, that the rotational spectrum is consistent with the electron diffraction results of Bregman and Bauer.

TABLE II. Spectroscopic parameters for propiolactone.

a	12 408.76 Mc	I_a	40.74 a.m.u.-A^2
b	5 244.39	I_b	96.39
c	3 869.19	I_c	130.66

$\kappa = -0.677923$

Quantitative Stark-effect studies are in progress in order to determine the value and orientation of the dipole moment and consequently resolve the question of ring planarity. The complete results of our investigation will be reported in the near future.

* This work was sponsored by the Office of Ordnance Research, U. S. Army.
[1] Gresham, Jansen, Shaver *et al.*, J. Am. Chem. Soc. **70**, 998 (1948).
[2] J. Bregman and S. H. Bauer, J. Am. Chem. Soc. **77**, 1955 (1955).
[3] L. Friedman and F. A. Long, J. Am. Chem. Soc. **75**, 2832 (1953).

Concerning Hydrogen Positions in Aquo-Complexes—$CuCl_2 \cdot 2H_2O$†

R. E. RUNDLE, KAZUO NAKAMOTO,* AND JAMES W. RICHARDSON
Department of Chemistry and Institute for Atomic Research, Iowa State College, Ames, Iowa
(Received September 19, 1955)

IT is uncertain whether water is predominately ionically or covalently bonded to transition metal ions in aquo-complexes. If ionically (ion-dipole), the water dipole should point at the metal ion, Fig. 1(a); if covalently, approximately tetrahedral MOH angles are expected, Fig. 1(b). Model A is usually assumed in crystal field theory even where covalency is indicated by other evidence.

Hydrogen positions can sometimes be inferred from hydrogen bonding,[1] determined by neutron diffraction, or, in favorable cases,

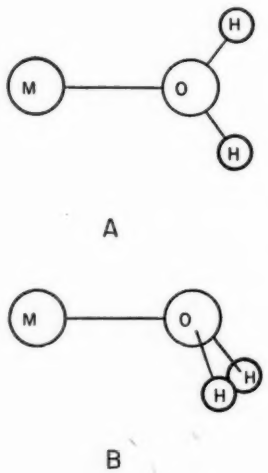

FIG. 1. Possible orientations of a water molecule in aquo-complexes.

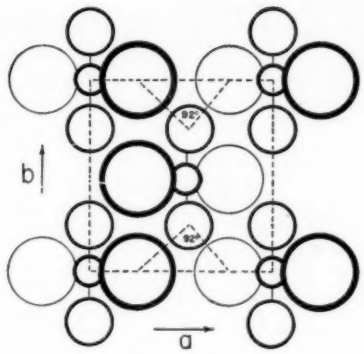

FIG. 2. Structure of $CuCl_2 \cdot 2H_2O$ after Harker. Needle axis, c, is normal to a and b.

located by nuclear magnetic resonance[2] or infrared spectra. $CuCl_2 \cdot 2H_2O$ is structurally favorable for infrared study (Fig. 2).[3] (A proton resonance determination of hydrogen positions[4] in $CuCl_2 \cdot 2H_2O$ is quite incompatible with the geometry of the H_2O molecules.)

Polarized infrared spectra of single crystals of $CuCl_2 \cdot 2H_2O$ have been examined using a Perkin-Elmer infrared microscope, a P.E. Model 112 spectrograph and AgCl polarizer. The crystals examined grew with c as the needle axis, and (110) as the principal face. Light was directed along [110] polarized with the electric vector parallel and perpendicular to c.

As can be seen in Fig. 2, Model A requires the HOH bending mode to be polarized with no component along c. The bending band at $\sim 1550\ cm^{-1}$ (Fig. 3) is, indeed, polarized, but the dichroic ratio (roughly 2.5) is incompatible with complete polarization.

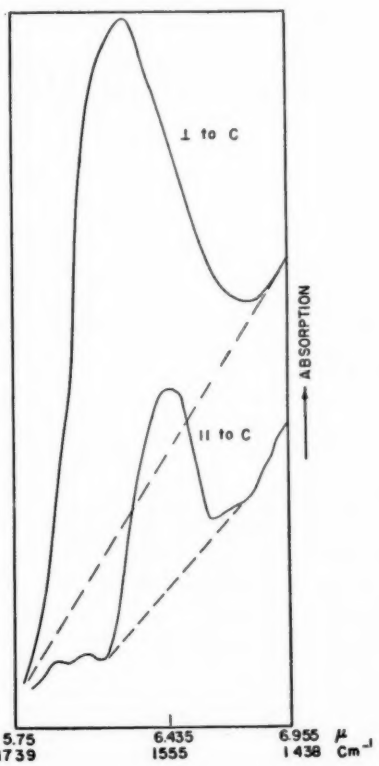

FIG. 3. Polarized infrared spectra of $CuCl_2 \cdot 2H_2O$ single crystal, with electric vector parallel and perpendicular to needle axis, c.

Since our optics give a very high dichroic ratio in other cases of complete polarization, we feel our results eliminate Model A, and, though not quantitative, are consistent with a model like, but not so extreme as (B).

Pake's nuclear magnetic resonance study of gypsum, $CaSO_4 \cdot 2H_2O$,[2] strongly suggests placing hydrogens on the short (2.7 A) $O_{water}-O_{sulfate}$ ligands in the crystal, as had been expected. In this more ionic crystal the water dipole does not point toward Ca^{++}, but is bent away by $\sim 34°$. This distortion is, however, almost surely due to hydrogen bond formation.

In $CuCl_2 \cdot 2H_2O$ the shortest O···Cl distances (3.05 A) are related in pairs about the b axis of the crystal, with the Cl−O−Cl angle $= 92°$ (Fig. 2). Thus, hydrogen bonding, O−H···Cl, should also encourage the water dipole to point along b toward the copper ion. The distortion toward tetrahedral angles must, then, be ascribed to the covalent character of the $Cu-OH_2$ bond.

As judged by the low OH stretching frequency ($\sim 3300\ cm^{-1}$) hydrogen bonding is important in $CuCl_2 \cdot 2H_2O$, but this frequency may be materially lowered by Cu−O bond formation, analogous to the effect on amines suggested by Kobayashi and Fujita.[5] (Conversely, the effects reported by Kobayashi and Fujita may be influenced by N−H···Cl bonding.) Consequently, it is reasonable to suggest, but not certain, that tetrahedral angles (Model B) are distorted toward Model A by hydrogen bonding.

Covalency of the Cu−O bonds makes unattractive crystalline field treatments of $CuCl_2-2H_2O$, which assume that an unpaired $3d$-electron of copper is responsible for the para- and anti-ferromagnetic behavior. This covalency is more compatible with the Slater-Pauling theory of directed valence which, for the observed square configuration, would place the unpaired electron in a $4p$-orbital of copper. However, a molecular orbital treatment of the complex would allow partial mixing of the metal orbitals as well as delocalization of the odd electron. Knowledge of the covalent character of the complex and approximate hybrid character of the oxygen ligand orbital should permit a more detailed MO treatment.

Thanks are due to the Corn Industries Research Foundation for a Fellowship for K. N.

† Contribution No. 400. Work was performed in the Ames Laboratory of the U. S. Atomic Energy Commission.

* Present address: Department of Chemistry, Osaka University, Osaka, Japan.

[1] See, for example, A. F. Wells, *Structural Inorganic Chemistry* (Oxford University Press, New York, 1950), second edition, pp. 436–453, and Quart. Rev. **8**, 380 (1954).
[2] G. E. Pake, J. Chem. Phys. **16**, 327 (1948).
[3] D. Harker, Z. Krist. **93**, 136 (1936).
[4] N. J. Poulis and G. E. G. Hardeman, Physica **18**, 201, 315 (1952); J. chim. phys. **50**, 110 (1953).
[5] M. Kobayashi and J. Fujita, J. Chem. Phys. **23**, 1354 (1955).

Calculated Fundamental Vibrational Frequencies for Bromosilanes

HIROMU MURATA AND KIYOYASU KAWAI
Osaka Municipal Technical Research Institute, Osaka, Japan
(Received September 19, 1955)

RAMAN and infrared spectral data for bromosilanes have been obtained by several investigators.[1–3] Using the method[4] and potential constants[5] (Table I) given by Shimanouchi, the fundamental vibrational frequencies of these molecules were calculated. All bond angles were assumed tetrahedral; i.e., 109°28′ and the equilibrium values of the bond distances were taken as Si−H

TABLE I. Potential constants for SiH_nBr_{4-n} (10^5 dynes/cm).

	K		H	F	κ
Si−H	2.65	H−(Si)−H	0.179	0.049	0.117×10^{-16} cm²
Si−Br	2.02	Br−(Si)−Br	0.051	0.230	
		H−(Si)−Br	0.087	0.140	

TABLE II. Comparison of calculated and observed frequencies for bromosilanes.

Description	$SiBr_4$ Obs		$SiBr_3H$ Obs[a]	$SiBr_3H$ Calc		$SiBr_2H_2$ Obs[b]	$SiBr_2H_2$ Calc		$SiBrH_3$ Obs[c]	$SiBrH_3$ Calc		SiH_4 Obs
δ(Br−Si−Br)	$\nu_2(e)$ 90 $\nu_4(f_2)$ 137	$\nu_6(e)$ $\nu_3(a_1)$	113 168	112 164	$\nu_4(a_1)$	122	127		...	...		...
ν(Si−Br)	$\nu_1(a_1)$ 249 $\nu_3(f_2)$ 487	$\nu_2(a_1)$ $\nu_5(e)$	360 470	347 466	$\nu_3(a_1)$ $\nu_9(b_2)$	393 456	389 456	$\nu_3(a_1)$	... 428	... 421		... ...
δ(H−Si−Br)	... ...	$\nu_4(e)$	767 ...	776 ...	$\nu_7(b_1)$ $\nu_5(a_2)$	556[c] 688	534 689	$\nu_6(e)$	... 629	... 610		... ...
δ(H−Si−H)	... ...		... ...	... ...	$\nu_8(b_2)$ $\nu_2(a_1)$	828 925	840 962	$\nu_2(a_1)$ $\nu_5(e)$	927 946	969 960	$\nu_2(e)$ $\nu_4(f_2)$	910 978
ν(Si−H)	... ...	$\nu_1(a_1)$	2234 ...	2228 ...	$\nu_1(a_1)$ $\nu_6(b_1)$	2206 2232	2215 2213	$\nu_4(e)$ $\nu_1(a_1)$	2200 2200	2199 2202	$\nu_3(f_2)$ $\nu_1(a_1)$	2183 2187

[a] See references 1 and 2. [b] See reference 2. [c] See reference 3.

$=1.48$ and Si−Br$=2.17$ A. The calculated frequencies are in good agreement with the observed as shown in Table II. Although all the potential constants were taken from the normal vibrations of SiH_4 and $SiBr_4$, except for H(H−Si−Br) which was calculated from the type a_2 frequency of $SiBr_2H_2$ molecule, the calculated fundamentals were within 4.53% (mean 1.71%) of the observed values.

[1] J. M. Delfosse and R. Goovaertts, Bull. classe sci. Acad. roy. Belg. **21**, 410 (1935).
[2] F. Francois and M. Buisset, Compt. rend. **230**, 1946 (1950).
[3] Mayo, Opitz, and Peake, J. Chem. Phys. **23**, 1344 (1955).
[4] T. Shimanouchi, J. Chem. Phys. **17**, 245 (1949).
[5] T. Shimanouchi, J. Chem. Soc. Japan, Pure Chem. Sect. **74**, 266 (1953).

Infrared Spectrum of LiH

WILLIAM KLEMPERER
Department of Chemistry, Harvard University, Cambridge 38, Massachusetts
(Received October 7, 1955)

THE infrared spectrum of the molecule LiH has been observed in emission in the frequency region 1500 to 970 cm^{-1} using a Perkin-Elmer double-pass monochromator with sodium chloride optics. Lithium hydride was prepared by heating lithium metal in an atmosphere of hydrogen in a steel tube. The temperature at which the spectrum was observed was not greater than 1400°K. The experimental details are similar to those used in the study of aluminum chloride.[1]

Lines in the P-branch of the 0–1 vibrational transition from $J=0$ to $J=21$ and those in the R-branch from $J=1$ to $J=12$ were resolved. Seventeen lines of the 1–2 transition were resolved. The difference in frequencies between the lines observed and calculated from the constants of Crawford and Jorgenson[2] was within the experimental error (3 cm^{-1}).

In view of the insensitivity of infrared spectroscopy to small amounts of substances a considerable pressure of LiH must exist under the conditions described. The path length is not well defined but probably does not exceed the length of the furnace which is 20 cm. Estimation of the minimum LiH pressure as 10 mm and assuming the maximum Li pressure possible at 1400°K yields an equilibrium constant of 1/200 atmospheres for the reaction

$$2Li+H_2=2LiH.$$

Using the harmonic oscillator rigid rotor approximation $D_0^0{}_{LiH}\geq 56$ kcal/mole is obtained. Gaydon[3] lists a value of 58 ± 5 kcal/mole for D_0^0.

Further work on the intensities of the transitions of this molecule is in progress. The Research Corporation has generously supported this research.

[1] W. Klemperer, J. Chem. Phys. (to be published).
[2] G. Herzberg, *The Spectra of Diatomic Molecules* (D. Van Nostrand Company, Inc., New York, 1950), p. 546.
[3] A. G. Gaydon, *Dissociation Energies* (Dover Publications, New York, 1950).

Series Solutions for the Rate Equations of Complex Reaction Mechanisms

J. C. MORROW
Department of Chemistry, University of North Carolina, Chapel Hill, North Carolina
(Received October 6, 1955)

IN analysis of the kinetics of complex chemical reactions, most problems of solving simultaneous nonlinear differential equations are handled by approximation of the real rate expressions with differential equations which are easily solved. An alternative procedure, that of keeping the original differential equations intact but obtaining an approximate solution, has been little exploited. It is important to note that series solutions for many nonlinear complex systems can easily be obtained without integration. Rate expressions yield directly the functions dt/dA_i, where t is the time and A_i is the concentration of the ith species, and differentiation produces higher derivatives of time with respect to A_i. The availability of these derivatives suggests the use of a Taylor's series representing time as a function of concentration:

$$t=t_0+\sum_{i=1}^{\infty}(d^it/dA^i)_{A=A_0}(i!)^{-1}(A-A_0)^i.$$

Consider, as an example, the competitive, consecutive second-order reactions for saponification of esters of dibasic acids:

$$A+B\xrightarrow{k_1}C+E$$
$$A+C\xrightarrow{k_2}D+E$$

$$dA/dt=-k_1AB-k_2AC;\quad dB/dt=-k_1AB;$$
$$dC/dt=k_1AB-k_2AC;\quad dD/dt=k_2AC.$$

Let $A_0=B_0$ and $C_0=D_0=E_0=0$ be the concentrations at $t=0$. From the first rate equation, $(dt/dA)_0=(-k_1A_0^2)^{-1}$, directly giving the first series coefficient. The second derivative may be obtained as follows: $d^2t/dA^2=d[(-k_1AB-k_2AC)^{-1}]/dA$. The quantities dB/dA and dC/dA are $(dB/dt)/(dA/dt)$ and $(dC/dt)/(dA/dt)$, which come directly from the rate equations. Successive differentiation produces the higher derivatives, all simple to evaluate at $t=0$. In the above example, the first few terms in the expansion are:

$$t=(k_1A_0^2)^{-1}(A_0-A)+(1-r/2)(k_1A_0^3)^{-1}(A_0-A)^2$$
$$+(1-7r/6+2r^2/3)(k_1A_0^4)^{-1}(A_0-A)^3$$
$$+(1-47r/24+7r^2/3-13r^3/12)(k_1A_0^5)^{-1}(A_0-A)^4+\cdots,$$

where $r=k_2/k_1$. For the specific saponification kinetics mentioned, the equivalent of the first three terms has been used as an approximate solution by Ingold,[1] who obtained it by an approximate integration scheme. Since differentiation is usually much less laborious than integration, and since the first derivatives are always readily available from the rate equations, the Taylor's series method illustrated above suggests itself as a useful and powerful tool in the analysis of complex systems where arbitrary relative values of the rate constants must be considered.

[1] C. K. Ingold, J. Chem. Soc. 2170 (1931).

Intermolecular Potential Energy of Dipolar Gases from Heat Capacity Data*

D. R. Douslin and Guy Waddington
Petroleum Experiment Station, Bureau of Mines, Bartlesville, Oklahoma
(Received September 28, 1955)

STOCKMAYER'S[1,2] equation for the second virial coefficient of dipolar gases has three variables: E, the depth of the potential well; σ, the collision diameter; and μ, the dipole moment. It is derived from the complete expression of B given by statistical mechanics and is often written in its simplified form

$$B=b_0F(\tau,t), \tag{1}$$

where,

$$b_0=2/3\pi\sigma^3, \tag{2}$$

$$\tau=T/\theta, \tag{3}$$

$$\theta=E/k, \tag{4}$$

and

$$t=(\mu^2/E\sigma^3)/\sqrt{8}. \tag{5}$$

A tabulation of the computed values of the second virial coefficient function, $F(\tau,t)$, for a Stockmayer (6–12) potential, covering the range $0.3<\tau<400$ and $0<t<1.5$, has been prepared by Rowlinson.[3,4]

If vapor heat capacity data are used to determine the potential energy, it is convenient to express the limiting pressure dependence

$$\lim_{p\to 0}(\partial C_p/\partial p)_T=-b_0/T\partial^2F(\tau,t)/\partial T^2 \tag{6}$$

in terms of the same parameters used for the second virial coefficient. A tabulation of the heat capacity function $\partial^2F(\tau,t)/\partial T^2$ over the range $0.5<\tau<3$ and $0<t<1.6$ is given in Table I as

TABLE I. The heat capacity function for the Stockmayer (6–12) potential. $\log_{10}\partial^2F(\tau,t)/\partial T^2$.

τ \ t	0	0.1	0.2	0.3	0.4	0.5	0.6	0.7	0.8
0.50	1.7585	1.8085	1.9475	2.1518	2.4036	2.6825	2.9871		
0.60	1.5431	1.5814	1.6890	1.8499	2.0503	2.2768	2.5271	2.7970	
0.70	1.3814	1.4121	1.4991	1.6306	1.7952	1.9831	2.1904	2.4142	
0.80	1.2539	1.2794	1.3521	1.4638	1.6023	1.7622	1.9387	2.1292	2.3317
0.90	1.1497	1.1715	1.2337	1.3292	1.4501	1.5893	1.7431	1.9087	2.0842
1.00	1.0622	1.0811	1.1355	1.2194	1.3261	1.4495	1.5855	1.7324	1.8879
1.20	0.9215	0.9365	0.9799	1.0474	1.1339	1.2347	1.3461	1.4660	1.5927
1.40	0.8114	0.8239	0.8599	0.9165	0.9894	1.0749	1.1697	1.2718	1.3795
1.60	0.7214	0.7320	0.7629	0.8116	0.8748	0.9492	1.0322	1.1215	1.2157
1.80	0.6454	0.6547	0.6817	0.7246	0.7805	0.8466	0.9206	1.0003	1.0846
2.00	0.5798	0.5880	0.6121	0.6504	0.7006	0.7603	0.8273	0.8997	0.9761
2.20	0.5220	0.5294	0.5512	0.5859	0.6316	0.6860	0.7473	0.8138	0.8841
2.40	0.4704	0.4771	0.4971	0.5288	0.5708	0.6210	0.6776	0.7392	0.8046
2.60	0.4238	0.4301	0.4484	0.4777	0.5165	0.5620	0.6159	0.6734	0.7345
2.80	0.3813	0.3871	0.4041	0.4313	0.4675	0.5111	0.5606	0.6146	0.6721
3.00	0.3423	0.3476	0.3635	0.3890	0.4229	0.4639	0.5105	0.5616	0.6159

τ \ t	0.9	1.0	1.1	1.2	1.3	1.4	1.5	1.6
0.50								
0.60								
0.70								
0.80	2.5459							
0.90	2.2701	2.4651	2.6681					
1.00	2.0516	2.2229	2.4021	2.5887	2.7827	2.9771		
1.20	1.7256	1.8642	2.0083	2.1579	2.3125	2.4718	2.6433	
1.40	1.4920	1.6089	1.7299	1.8550	1.9842	2.1174	2.2552	2.3978
1.60	1.3139	1.4156	1.5203	1.6285	1.7396	1.8539	1.9714	2.0923
1.80	1.1722	1.2628	1.3559	1.4516	1.5495	1.6498	1.7526	1.8579
2.00	1.0557	1.1379	1.2218	1.3084	1.3965	1.4864	1.5783	1.6721
2.20	0.9573	1.0328	1.1099	1.1890	1.2694	1.3513	1.4346	1.5194
2.40	0.8724	0.9425	1.0141	1.0873	1.1616	1.2372	1.3136	1.3914
2.60	0.7981	0.8638	0.9308	0.9992	1.0686	1.1388	1.2100	1.2821
2.80	0.7321	0.7939	0.8572	0.9216	0.9868	1.0528	1.1196	1.1870
3.00	0.6728	0.7314	0.7914	0.8524	0.9142	0.9767	1.0397	1.1033

$\log_{10}\partial^2F(\tau,t)/\partial T^2$. To evaluate the parameters b_0,θ and t from vapor heat capacity data, a plot of $\log_{10}[T\lim_{p\to 0}(\partial C_p/\partial P)_T]$ *versus* $\log_{10}T$ on semitransparent paper is matched to one of the family of curves generated by plotting the tabular values of $\log_{10}\partial^2F(\tau,t)/\partial T^2$ against $\log T/\theta$. Then by inserting the numerical values of the matched coordinates into the relationships

$$\log_{10}[T\lim_{p\to 0}(\partial Cp/\partial p)_T]=\log_{10}b_0+\log_{10}\partial^2F(\tau,t)/\partial T^2 \tag{7}$$

and

$$\log_{10}(T/\theta)=\log_{10}T-\log_{10}\theta, \tag{8}$$

a solution for θ and b_0 can be obtained.

In practice, curve matching is not a sensitive method for determining intermolecular potential energy parameters if the experimental temperature range is limited. A "unique" set of three parameters cannot be deduced from the second virial[1] coefficient data or the vapor heat capacity data alone. However, the isothermal pressure derivative of vapor heat capacity can often be used in conjunction with the second virial coefficient to obtain a

TABLE II. Second virial coefficient of nitromethane $-B$, liters mole^{-1}.

T°K	Calc	Obs
318.30	3.193	3.102
334.80	2.443	2.463
353.36	1.936	1.931
374.44	1.524	1.499
406.56	1.116	...
464.64	0.712	...
522.72	0.498	...
580.80	0.368	...

Isothermal pressure derivative of the vapor heat capacity $\lim_{p\to 0}(\partial Cp/\partial P)_T$ cal deg^{-1} mole^{-1} atmos^{-1}.

T°K	Calc	Obs
348.48	4.126	...
363.20	3.053	3.02
383.25	2.044	2.07
413.25	1.219	1.21
442.25	0.779	0.800
483.25	0.468	0.493
523.25	0.302	0.321

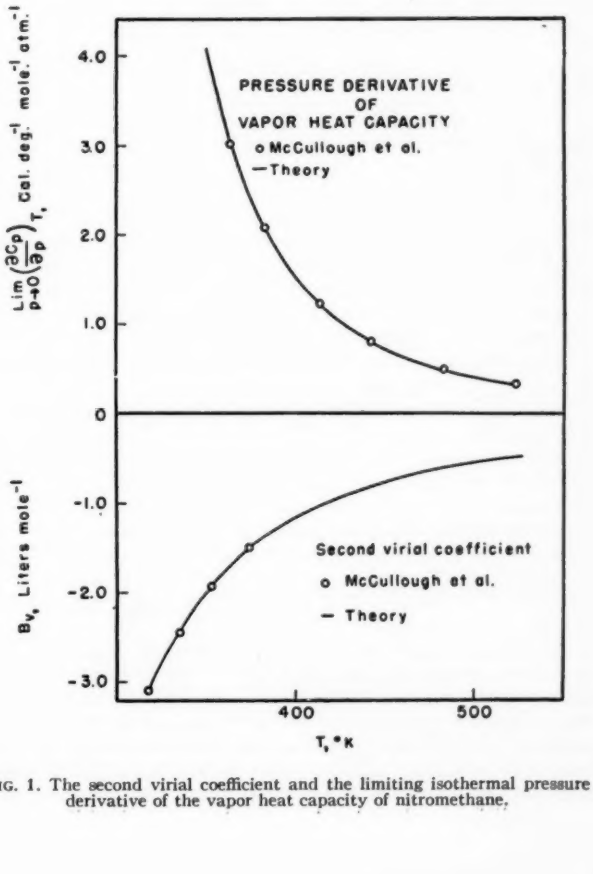

FIG. 1. The second virial coefficient and the limiting isothermal pressure derivative of the vapor heat capacity of nitromethane.

single set of parameters that will accurately represent both kinds of data.

A recent publication on nitromethane[5] contains accurate values for vapor heat capacity, vapor pressure, heats of vaporization, and derived second virial coefficients. The temperature range of these data (Table II) are greater than 200°C if the heat capacities and the second virial coefficients are used together for parameter evaluation. By trial and error, matching each set of data with its respective theoretical family of curves, it was possible to select one set of values of the three parameters of nitromethane. These values are:

$$\theta = 290.4°,$$
$$b_0 = 0.09078,$$

and

$$t = 1.6.$$

The agreement shown in Fig. 1 between the Stockmayer theory and the experimental data is remarkably good. A calculated dipole moment of 3.61 Debye units was obtained by using the above parametric values in Eqs. (4) and (5). This calculated value of the dipole moment agrees well with the experimental values of 3.50 determined by Wiswall and Smyth[6] and 3.54 determined by Smyth.[7]

* Contribution No. 52 from the Thermodynamics Laboratory, Petroleum Experiment Station, Bureau of Mines, Bartlesville, Oklahoma.

[1] W. H. Stockmayer, J. Chem. Phys. **9**, 398 (1941).
[2] H. S. Taylor and S. Glasstone, "Treatise on Physical Chemistry," Vol. 11, Chap. 11, J. A. Beattie and W. H. Stockmayer, *The Thermodynamics and Statistical Mechanics of Real Gases* (D. Van Nostrand Company, Inc., New York, 1951).
[3] J. S. Rowlinson, Trans. Faraday Soc. **54**, 974 (1949).
[4] See Table 11-A, Herschfelder, Curtis, and Bird, *Molecular Theory of Gases and Liquids* (John Wiley and Sons, Inc., New York, 1954).
[5] McCullough, Scott, Pennington, Hossenlopp, and Waddington, J. Am. Chem. Soc. **76**, 4791 (1954).
[6] R. H. Wiswall and C. P. Smyth, J. Chem. Phys. **9**, 356 (1941).
[7] C. P. Smyth, J. Am. Chem. Soc. **63**, 57 (1941).

Dirac Vector Model for Electron Coupled Nuclear Spin Interactions

HARDEN M. MCCONNELL
Shell Development Company, Emeryville, California
(Received September 28, 1955)

MOLECULAR orbital theory has been used elsewhere[1,2] to approximate the electron coupled interactions between nuclear spins that give rise to "spin-spin" multiplets in high-resolution nuclear magnetic resonance spectroscopy. Gutowsky, McCall and Slichter,[3] and Ramsey and Purcell,[4] have used valence bond (VB) theory to account for observed nuclear spin couplings in cases where the magnetic nuclei are directly bound to one another in a molecule. As shown below "long-range" nuclear spin couplings, i.e., couplings between nuclei separated by two or more bonds, are also easily understood with VB theory when use is made of the Dirac vector model.[5]

For simplicity we treat only contact[6] hyperfine contributions to the coupling of nuclei N and N' in a molecule (^1A state) considered to have one electron each in orthogonal atomic orbitals $\varphi_1, \varphi_2, \cdots \varphi_N, \varphi_{N'}, \cdots$. (This approximation is adequate for proton-proton couplings.[2]) In this case Ramsey's general equation[7] for the contact contribution to the nuclear coupling, $J_{NN'}{}^{(3)}$, can be written in the form, in standard notation,

$$J_{NN'}{}^{(3)} = -(2/3h)(16\pi\beta\hbar/3)^2\gamma_N\gamma_{N'}(1/\Delta E) \times|\varphi_N(0)|^2|\varphi_{N'}(0)|^2\langle 0|\mathbf{S}_N\cdot\mathbf{S}_{N'}|0\rangle \quad (2)$$

where $hJ_{NN'}\mathbf{I}_N\cdot\mathbf{I}_{N'}$ is the energy of the nuclear coupling, ΔE is an average electronic triplet excitation energy and where S_N and $S_{N'}$ are the electron spin angular momentum vector operators "associated with atoms N and N'" in the sense of the Dirac vector method. The essential question is then: How can there be an electron spin coupling corresponding to $\langle 0|S_N\cdot S_{N'}|0\rangle\neq 0$ when nuclei N and N' are not directly bound to one another?

Write the molecular Hamiltonian in the Dirac form,

$$\mathcal{H} = \text{const} - (\tfrac{1}{2})\sum_{j>i} K_{ij}(1+4S_i\cdot S_j) \quad (2)$$

where S_i and S_j are the electron spins associated with orbitals i and j and where K_{ij} is the two-electron exchange integral. We take $K_{ij}=0$ unless orbitals i and j are on adjacent (bonded) atoms and overlap, or are centered on the same atom. In general if $K_{ij}\neq 0$, then $\langle 0|S_i\cdot S_j|0\rangle\neq 0$ but $K_{NN'}=0$ does not imply $\langle 0|S_N\cdot S_{N'}|0\rangle = 0$. Consider, for example, three orbits, φ_N, φ_i, $\varphi_{N'}$ such that $K_{Ni}, K_{N'i}\neq 0$, $K_{NN'}=0$. Spins S_N and $S_{N'}$ will both try to couple with S_i consistent with over-all parity, and this mutual interaction with S_i will usually lead to an effective coupling of S_N and $S_{N'}$, $\langle 0|S_N\cdot S_{N'}|0\rangle\neq 0$; nuclei N and N' can then be coupled by (1). The argument can be extended to include cases where S_N and $S_{N'}$ are effectively coupled together by a chain of spins.

As a final example, consider the proton-proton coupling in a 4-electron, 4-orbital system H—C—H where the H—C—H angle is taken equal to 90° and where two 1s orbitals (s and s') are used on the hydrogen atoms and two p orbitals (p and p') on the carbon atom. For this system let us take

$$K_{ss'}=K_{sp}=K_{s'p}=0, \quad |K_{sp}|=|K_{s'p'}|\gg|K_{pp'}|, \quad K_{sp}$$

negative and $K_{pp'}$ positive. When $-2K_{pp'}S_p\cdot S_{p'}$ is treated as a first-order perturbation [relative to the K_{sp} terms in (2)] and $s-p$ overlaps are neglected, then one can easily show $\langle 0|S_H\cdot S_{H'}|0\rangle = -(3/16)(K_{pp'}/K_{sp})$. This result means the electron spins on H and H' have a slight tendency to be parallel (triplet configuration). For reasonable orders of magnitude, $\Delta E\sim 10$ ev and $(K_{pp}/K_{sp})\approx -0.1$, one obtains $J_{HH'}{}^{(3)}\approx 40$ c/sec. This result is within an order of magnitude of observed couplings between protons separated by one carbon atom in hydrocarbons.

The Dirac vector model might also be used to discuss the indirect hyperfine interactions between aromatic π electrons and in-plane aromatic protons which give rise to multiplets in the paramagnetic resonance spectra of aromatic free radicals.[2]

[1] H. M. McConnell, J. Chem. Phys. **23**, 760 (1955).
[2] H. M. McConnell, J. Chem. Phys. (to be published).
[3] Gutowsky, McCall, and Slichter, J. Chem. Phys. **21**, 279 (1953).
[4] N. F. Ramsey and E. M. Purcell, Phys. Rev. **85**, 143 (1952).
[5] P. A. M. Dirac, Proc. Roy. Soc. (London) **A123**, 714 (1929); J. H. Van Vleck, Phys. Rev. **45**, 405 (1934).
[6] E. Fermi, Z. Physik **60**, 320 (1930).
[7] N. F. Ramsey, Phys. Rev. **91**, 303 (1953).

Variation of Surface Tension and Heat of Vaporization with Temperature

S. T. BOWDEN
Department of Chemistry, University College, Cardiff, Wales
(Received September 19, 1955)

VARIOUS methods of expressing the variation of orthobaric density difference with the temperature of liquid/vapor systems have been discussed by Scott and Dillon.[1] It may be shown that similar power laws apply to the variation of surface tension and heat of vaporization and that the utility of these equations may be further extended by expressing the critical temperature in terms of more readily determined constants.

For nonassociated liquids the variation of surface tension with temperature may be expressed by

$$\gamma = \gamma_0(1-T/T_c)^{6/5} \quad (1)$$

where γ is the surface tension, T/T_c is the van der Waals reduced temperature, and γ_0 is a specific constant corresponding to the surface tension at 0°K.[2] For the liquid at its normal boiling point

$$\gamma_b = \gamma_0(1-T_b/T_c)^{6/5} \quad (2)$$

and dividing (1) by (2), we have

$$\gamma = \gamma_b\left(\frac{T_c-T}{T_c-T_b}\right)^{6/5}. \quad (3)$$

Equation (3) may be converted into a more generally applicable form by the use of the relation $T_c=3PT/4V_b$, where P is the parachor and V_b is the molar volume of the liquid at the boiling point.[3] The density of the vapor at the boiling point may be regarded as negligible in comparison with that of the liquid, so that Eq. (3) becomes

$$\gamma=\left(\frac{P}{V_b}\right)^4\left(\frac{3PT_b-4V_bT}{3PT_b-4V_bT_b}\right)^{6/5}. \tag{4}$$

Since the values of P and V_b may be computed from atom and bond constants, Eq. (4) permits the calculation of the surface tension at any temperature from a knowledge of the boiling point of the liquid. The data for benzene are given in Table I.

TABLE I. Surface tension of benzene in dynes per cm ($P=205.7$; $V_b=95.9$; $T_b=353.3$).

Temp. °C	γ_{obs}	$\gamma_{Eq.\ (4)}$	Temp. °C	γ_{obs}	$\gamma_{Eq.\ (4)}$
20	29.0	28.5	100	18.2	18.9
40	26.3	26.1	120	16.3	16.6
60	23.6	23.7	160	9.4	10.0
80	21.2	21.2	200	7.3	7.8

The temperature variation of internal heat of vaporization[4] may be represented by

$$\lambda=\lambda_b\left(\frac{T_c-T}{T_c-T_b}\right)^{1/7} \tag{5}$$

and since the true lyoparachor[5] is approximately given by $V_b\lambda^{1/4}$, we have

$$\lambda=\left(\frac{\Lambda}{V_b}\right)^{4/3}\left(\frac{3PT_b-4V_bT}{3PT_b-4V_bT_b}\right)^{1/7} \tag{6}$$

where Λ is the true lyoparachor. The data for n-pentane in Table II show that Eq. (6) holds reasonably well from 0°C to about 50° above the normal boiling point of the liquid.

TABLE II. Internal heat of vaporization of n-pentane (cal/g) ($\Lambda=3100$; $V_b=118.2$; $P=231.8$; $T_b=309.3$).

Temp. °C	λ_{obs}	$\lambda_{Eq.\ (6)}$	Temp. °C	λ_{obs}	$\lambda_{Eq.\ (6)}$
0	85.9	85.7	80	66.9	66.8
40	76.2	77.1	100	61.6	60.9
60	71.7	72.2	120	56.3	54.0

The total heat of vaporization varies with the temperature in accordance with the equation

$$l=l_b\left(\frac{T_c-T}{T_c-T_b}\right)^{2/5} \tag{7}$$

and if M is the molecular weight of the substance, multiplication of both sides by M/T_b gives

$$\Delta H=\Delta S_bT_b\left(\frac{3PT_b-4V_bT}{3PT_b-4V_bT_b}\right)^{2/5} \tag{8}$$

where ΔH is the molar heat of vaporization at the temperature T, and ΔS_b is the entropy of vaporization (Trouton ratio) at the boiling point. As shown in Table III there is close concordance between the values of ΔS_b obtained by application of the Clausius-Clapeyron equation to the specific volume and vapor pressure data and those calculated from Eq. (8).

A further simplification may be introduced by assuming conformity with Guldberg's rule ($T_c=3T_b/2$), so that Eq. (7) becomes

$$\Delta H=\Delta S_bT_b^{3/5}(3T_b-2T)^{2/5} \tag{9}$$

which reproduces the experimental results for the liquids listed in Table III with departures generally less than 1%. For non-associated liquids of this type the relation

$$\Delta H=21T_b^{3/5}(3T_b-2T)^{2/5} \tag{10}$$

furnishes a rough estimate of the heat of vaporization.

TABLE III Entropy of vaporization (cal/mole degree).

Substance	T_b	ΔH_{25}	P	V_b	ΔS_b	ΔS_b Eq. (8)	ΔS_b Eq. (9)
Methyl formate	305.0	6918	137.7	62.9	22.35	22.48	22.28
Ethyl ether	307.6	6415	211.2	106.5	20.37	20.34	20.35
n-Hexane	341.8	7540	270.4	140.9	20.17	19.94	20.14
Carbon tetrachloride	349.9	7721	219.8	104.1	20.29	20.22	19.90
Ethyl acetate	350.3	8516	215.7	106.8	21.82	21.94	21.89
Benzene	353.3	8090	205.7	95.9	20.96	20.89	20.53
n-Heptane	371.5	8735	310.8	164.1	20.38	20.15	20.58
n-Octane	398.8	9915	351.0	187.8	20.96	20.45	21.11
Ethylbenzene	409.3	10100	284.0	137.6	21.01	21.15	20.76
m-Xylene	412.2	10200	284.0	138.0	21.10	20.98	20.74

[1] A. F. Scott and R. Dillon, J. Chem. Phys. **17**, 1179 (1949).
[2] A. Ferguson, Phil. Mag. **31**, 37 (1916); S. Sugden, J. Chem. Soc. **125**, 1167 (1924).
[3] S. T. Bowden, Nature **174**, 613 (1954).
[4] W. J. Jones and S. T. Bowden, Phil. Mag. **37**, 480 (1946).
[5] S. T. Bowden and W. J. Jones, Phil. Mag. **39**, 155 (1948).

On Dielectric Properties of Solid Hydrogen and Deuterium Halides*

S. HAVRILIAK, JR., AND R. H. COLE
Metcalf Chemical Laboratories, Brown University, Providence, Rhode Island
(Received October 6, 1955)

PREVIOUS work on dielectric properties of the solid phases of hydrogen chloride[1] and hydrogen bromide[2] has been extended to hydrogen iodide, and to deuterium bromide and iodide. The measurements, over the range 20 cy/sec to 500 kc/sec from 63°K to the melting points, have revealed significant similarities and differences in behavior.

The present results give the most interesting information in the regions of partially ordered phases and phase transitions lying between 70°K and 130°K. All four bromides and iodides show lambda-type dielectric constant curves near the lowest observed transitions, and with adequate precautions against void formation, large peak values are observed: ϵ_0(HBr,89°K)=200, ϵ_0(DBr,93°K)=210, ϵ_0(HI,70°K)=28, ϵ_0(DI,76°K)=23.

There are significant differences in dispersion behavior near these transitions. Below the transition, deuterium bromide is like hydrogen bromide in exhibiting two dispersion regions which conform to circular arc loci. The center frequencies f_c are lower by factors 3 and 2 in DBr, and activation energies of 3.59 and 3.08 kcal from the temperature dependence are similar to those for HBr.

Above the transition, two distinct changes occur in the bromides. The relaxation in DBr is shifted to higher frequencies, but is slower than in HBr by a factor 50 or more. As surmised for HBr from very limited data,[2] *the frequency dependence is described by a Debye-type dispersion above the transition rather than the broader circular arc loci below it.*

The hydrogen and deuterium iodide results give evidence for only one dispersion in the low temperature phase. For both, this dispersion is fitted by a depressed circular arc locus, and appears to be the analog of the faster and smaller dispersion in the bromides. Above the transition, Debye-type dispersions again replace circular arc behavior, as shown in Fig. 1 for HI at 70.5°K and 62.5°K.

The marked specific differences indicate delicate balances of several factors which will presumably require rather detailed molecular explanation. Other observations supporting this view are the extra solid phase between 113°K and 117°K in HBr which has no counterpart in DBr[3] and the conclusion from x-ray studies[4] that the orthorhombic unit cell of the low temperature phases in

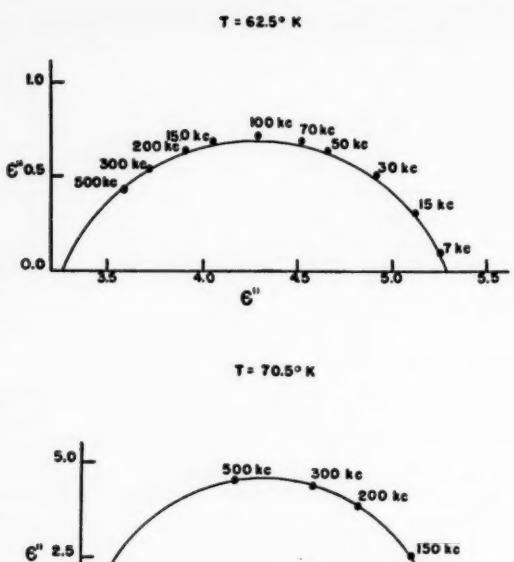

FIG. 1. Complex plane plots of hydrogen iodide. Above the phase transition (70.5°K) the dispersion can best be represented by a semicircle, below the transition (62.5°K) the dispersion can be represented by a circular arc.

HBr is tetragonal or nearly so in HI. These differences may well correspond to the difference between HBr and DBr relaxation frequencies above 100°K, and the existence of two dispersion regions in the bromides rather than the one in the iodides.

The common feature that circular arc dispersion changes to single relaxation time behavior may well be significant for relaxation theory. Circular arc dispersions formally characterized by a distribution of relaxation times are found for many dielectrics, and are so far without real molecular explanation. In the present systems, dispersions of this kind are replaced by simple Debye-type frequency dependence as a consequence of structural changes in solids composed of simple molecules. Both dielectric and structural behavior should be important for understanding the underlylng molecular interactions, and the relation among them may well aid in elucidating the origins of complex dispersion behavior in other dielectrics.

* This work was supported by the Office of Ordnance Research.
[1] R. W. Swenson and R. H. Cole, J. Chem. Phys. **22**, 284 (1954).
[2] N. L. Brown and R. H. Cole, J. Chem. Phys. **21**, 1920 (1953).
[3] Clausius and Wolf, Z. Naturforsch. **9**, 495 (1947); J. G. Powles, Compt. rend. **230**, 836 (1950).
[4] G. Natta, Nature **127**, 235 (1931).

Rayleigh's Ratio (Absolute Turbidity Levels) for Benzene and Carbon Tetrachloride. II. Corrections

ROBERT F. STAMM AND PETER A. BUTTON*
Stamford Laboratories, Research Division, American Cyanamid Company, Stamford, Connecticut
(Received September 19, 1955)

IN July, 1953[1] the writers published a note which gave values of Rayleigh's ratio (R_{90}) for several liquids thought to be suitable for use as turbidity standards. These results agreed well with those values obtained previously by the photographic method, but were 30% low with respect to values measured photoelectrically in recent years in this country and to those reported subsequently.[2-4] (One additional, direct photoelectric measurement[5] of R_{90} for benzene yielded a value of 28×10^{-6} at 4358 A, 25°C, in agreement with the results obtained photographically.)

Because of the pressure induced by these new findings, our original apparatus was rebuilt. This time, the RCA 1P21 detector was placed in an off-set housing in order to widen the aperture of the beam admitted to the photocathode. The experimental results obtained with the rebuilt apparatus checked those reported[1] earlier within the limits of error specified.

At this time, two publications[6,7] dealing with photocathode uniformity and spatial variations of response in photomultipliers of the type employed in our experiments appeared. The results of these authors were similar to those published[8] earlier, but, being newly presented, caused us to re-examine this question. Our measurements of the relative amounts of flux in the scattered and reference beams had been made without any diffusing screen in front of the detector. In addition, the sizes of the two beams were quite different although all the flux in each of the beams was picked up by the cathode.

The responses of the detector to square images of differing size but constant flux were measured. The results indicated that even though all the flux was received by the cathode, the response to an image 7 mm square was only 60% of that achieved with an image 0.75 mm square, both beams containing the same total flux. By employing two plano-convex lenses in the beam of scattered light and a plano-convex (spherical) lens plus a plano-convex (cylindrical) lens in the reference beam, both images could be made the same size (0.4 mm high×4.0 mm wide) and shape at the cathode. Under these conditions, values of $R_{90}\cong15.3\times10^{-6}$ cm^{-1} (25°C, 5461 A) were obtained for benzene. (Our previous value was 10.37×10^{-6} cm^{-1}.) The detector was employed with the long dimension of the cathode either in the vertical or horizontal directions; the reproducibility was unsatisfactory, and the positioning of the tube was quite critical.

A change was then made to a ten-stage, end-window photomultiplier (DuMont type 6291). Employing constant flux and making certain that all the flux was caught by the cathode, the response varied less than 1% in changing the image from 1×1 to 12×12 mm.[2] By using a thin (0.04 in.) plate of glass (ground on both sides with No. 600 mesh carborundum) directly in front of the cathode, the response was found to be constant over these limits of image size. The values of R_{90} measured by means of beam weakener (a)[1] under these last conditions[9] are to be found in Table I.

TABLE I. Experimental values for Rayleigh's ratio, 25.0(±0.5)°C.

Substance	$R_u\times10^6$ (cm^{-1})[a] 4358.35 A[c]	5460.74 A[c]	$R_v\times10^6$ (cm^{-1})[b] 4358.35 A[c]	5460.74 A[c]
CCl_4	15.40±0.54	5.79±0.22	29.90±1.05	11.36±0.34
C_6H_6	46.02±1.38	16.89±0.44	67.50±1.97	23.76±0.62

[a] Unpolarized, parallel incident light.
[b] Incident parallel light plane-polarized by Glan-Thompson calcite prism mounted in graduated head.
[c] New filters employed consisted of multilayer interference filters plus colored glasses and colored solutions to remove side bands. An A-H3 mercury arc fed from an auto transformer and a Sorensen voltage regulator was used as a source.

An examination of the magnitude of all the errors likely to be encountered in all the quantities having any bearing on the numerical evaluation of Rayleigh's ratio by the method employed leads to the probable error given in Table I. In the light of our present knowledge, we believe the accuracy to be about 3%. We regret very much the confusion generated by the results published by us in 1953.[1] These erroneous results were caused by an unfortunate experimental artifact.

Unanimity in this field requires agreement among direct measurements made by visual, photographic, and photoelectric methods. The present authors contemplated photographic meas-

urements with beam weakener (a)[1] but are now working in different fields and cannot attempt this.

* Now with Associated Engineers, Inc., Agawam, Massachusetts.
[1] R. F. Stamm and P. A. Button, J. Chem. Phys. **21**, 1304 (1953).
[2] H. J. L. Trap and J. J. Hermans, Rec. Trav. Chim. **73**, 167–187 (1954); ("Ludox" standard).
[3] S. H. Maron and R. L. H. Lou, J. Polymer Sci. **14**, 273–280 (1954); ("Ludox" standard).
[4] B. Sedlacek, Collection Czechoslov. Chem. Commun. **19**, 202–208 (1954); (direct visual measurement).
[5] M. Harrand, Ann. phys. **8**, 646–652 (1953).
[6] T. F. Godlove and W. G. Wadey, Rev. Sci. Instr. **25**, 1–4 (1954).
[7] H. Edels and W. A. Gambling, J. Sci. Instr. **31**, 121 (1954).
[8] K. G. Kessler and R. A. Wolfe, J. Opt. Soc. Am. **37**, 433–444 (1947).
[9] Potential divider arranged with 200 000 Ω on first state, 100 000 Ω on stages 2 to 9, inclusive, and 22 000 Ω on the last stage; total potential applied was 1000 v.

Calculation of Interaction Potentials from Scattering Cross Sections

EDWARD A. MASON
Institute of Molecular Physics, University of Maryland, College Park, Maryland
(Received September 28, 1955)

A METHOD for calculating total scattering cross sections for particles which interact according to a potential of the Lennard-Jones ($2n-n$) type has recently been given by Myers.[1] It is the purpose of this note to show how this method can be improved to yield accurate potential parameters, without introducing the large errors inherent in Myers' original treatment. Our treatment parallels that of Kells[2] for scattering by a single term inverse power potential law, which yielded parameters accurate to within one percent for the apparatus geometry of Simons and co-workers.[3]

For a potential with both attraction and repulsion, the total cross section, averaged over a scattering path of length l, is

$$\bar{S}=(\pi/l)\int_0^l b_1^2dx+(\pi/l)\int_0^{x_0}(b_3^2-b_2^2)dx, \qquad (1)$$

where b is the impact parameter necessary to cause a beam particle to just miss a detector of radius a when scattering occurs at a point x along the scattering path. The smallest value of b, denoted as b_1 above, arises from repulsive forces, whereas b_2 and b_3 arise from attractive forces and are complex for $x>x_0$. The distance of closest approach, r_c, is related to b by[4]: $b^2=r_c^2[1-(m_1/\mu W)V(r_c)]$, where m_1 is the mass of a beam particle, μ is the reduced mass of a colliding pair, W is the initial beam energy, and $V(r_c)$ is the potential energy of beam and scattering particle at the distance r_c. Substitution into Eq. (1) then gives $\bar{S}$ in terms of r_c. Myers neglected the terms arising from $V(r_c)$. The present scheme includes these terms, since they do not seriously complicate the situation and they greatly affect the accuracy of the results.

Finally, the "miss" value of r_c is found as a function of x and the indicated integrations performed. The relation between r_c and x is approximately[5]

$$\pm Wa/(l-x)=\epsilon[C_2(r_m/r_c)^{2n}-2C_1(r_m/r_c)^n], \qquad (2)$$

where ϵ and r_m denote the depth and position, respectively, of the minimum of $V(r)$, $C_1=\pi^{\frac{1}{2}}\Gamma(\frac{1}{2}n+\frac{1}{2})/\Gamma(\frac{1}{2}n)$, and $C_2=\pi^{\frac{1}{2}}\Gamma(n+\frac{1}{2})/\Gamma(n)$. The positive sign corresponds to repulsive, and the negative to attractive, scattering. There are three physically significant roots to Eq. (2), one corresponding to the positive sign and the other two to the negative sign.[1] The upper limit of the second term of Eq. (1) is then found to be: $x_0/l=1-C_2W^*a/C_1^2l$, where W^* is W/ϵ. For values of $W^*>C_1^2l/C_2a$, the attractive scattering contributes nothing to the observed cross section.

As an example we have considered H^+ scattered in He.[6] This is a favorable case for two reasons: (1) the values of ϵ and r_m are known independently of the scattering measurements from quantum-mechanical calculations[7,8]; (2) the best value of n obtained by neglecting repulsion[6] is close to $n=2$, for which all the integrations

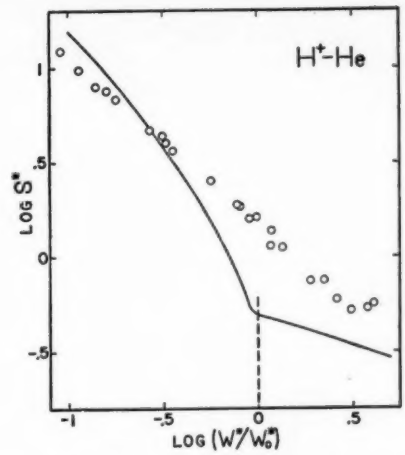

FIG. 1. Comparison of calculated and measured total cross sections for the scattering of protons by helium.

can be performed analytically. The results of these calculations are compared with the experimental measurements in Fig. 1, in terms of the reduced quantities $S^*=\bar{S}/\pi r_m^2$ and W^*/W_0^*, where W_0^* is that value of W^* above which the attractive scattering makes no contribution to S^*, and we have taken $\epsilon=2.12$ volts and $r_m=0.76$ A.[8] In the present case, $W_0^*=\pi l/3a$, corresponding to a W of about 28 volts. It is thus incorrect to interpret the scattering up to energies of over 100 volts as caused by a purely attractive potential.[6] The agreement seems quite reasonable in view of the approximation made and the fact that ϵ and r_m were not treated as disposable parameters, and indicates that the scattering results are in accord with the quantum-mechanical calculations. Substantial improvement could be obtained by varying the value of n, but at a corresponding complication in the calculations. The potential used here is quite different at small values of r from one obtained by neglect of repulsion[6]; at 0.76 A their ratio is 1.7.

[1] V. W. Myers, J. Chem. Phys. **23**, 755 (1955).
[2] M. C. Kels, J. Chem. Phys. **16**, 1174 (1948).
[3] Simons, Francis, Fontana, and Jackson, Rev. Sci. Instr. **13**, 419 (1942).
[4] E. H. Kennard, *Kinetic Theory of Gases* (McGraw-Hill Book Company, Inc., New York, 1938), pp. 117, 122.
[5] Simons, Fontana, Muschlitz, and Jackson, J. Chem. Phys. **11**, 307 (1943); see also reference 4, pp. 119–120.
[6] Simons, Muschlitz, and Unger, J. Chem. Phys. **11**, 322 (1943).
[7] C. A. Coulson and W. E. Duncanson, Proc. Roy. Soc. (London) **A165**, 90 (1938).
[8] A. A. Evett, J. Chem. Phys. **23**, 1169 (1955).

Organic Radiation Reactions with Dissolved Radioactive Iodine

WARREN W. MILLER, EDWARD P. RACK, ELLIOT BURRELL, AND CONRAD N. TRUMBORE
Department of Chemistry, The Pennsylvania State University, University Park, Pennsylvania
(Received September 12, 1955)

WE are reporting the results of some preliminary experiments on the use of dissolved radioactive substances as the source of radiation for the investigation of organic radiation chemical reactions in the liquid phase. We have investigated the reactions between molecular iodine and several organic liquids in which it is dissolved, using I^{131} as the source of the reaction promoting radiations. The radiation energy delivered to the substrate from moderate amounts of dissolved radioactive substance is sufficient to cause a readily detectable chemical effect. If one millicurie per milliliter of I^{131} decays to half-value in a substrate such as cyclohexane the dose received due to the β and γ rays is approximately 1.0×10^5 rep. The dose is readily calculated for the

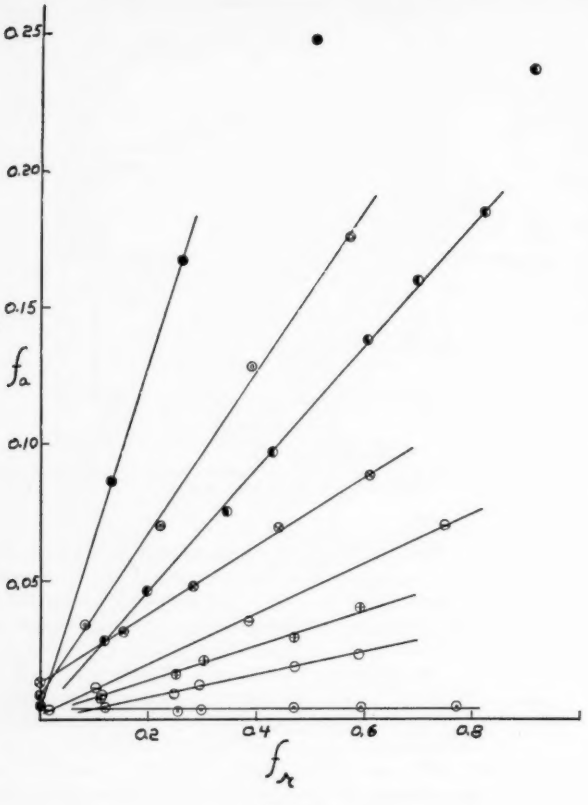

FIG. 1.

simple geometrical cases and is nearly constant throughout the volume.

Figure 1 presents the results obtained with molecular iodine containing I^{131} dissolved in cyclohexane, ethyl iodide, carbon tetrachloride, and carbon disulfide. The fraction of the activity not extractable from the solvent with dilute bisulfite solution, f_a, represents iodine that has been organically bound by the solvent in a not readily hydrolyzable form and f_r, called the radiation fraction and equal to $1-e^{-It}$, is the fraction of the total radiation that could be obtained by complete decay of the activity. Table I lists the initial conditions for these runs. Solution volumes were 5–10 ml. Iodine concentrations were determined photometrically. Absolute activities were obtained by comparison with National Bureau of Standards absolute I^{131} standards. Except for the ethyl iodide runs, oxygen was excluded by sweeping with an inert gas.

From the slopes f_a/f_r one can obtain the reaction rates as

$$\frac{\text{mg } I_2/\text{ml}}{\text{mc } I^{131} \text{ decayed/ml}}.$$

It then appears that the rate of the reaction of iodine with cyclohexane is not sensitive to the iodine concentration and is probably zero order in iodine, as also would be indicated by the persistence of the straight line over an appreciable change in iodine concentration. In the carbon tetrachloride case, dividing the reaction rates by the respective iodine concentrations gives an almost constant value, indicating that this reaction is first order in the iodine concentration with a rate constant equal to 0.059 (mc decay/ml)$^{-1}$. In the ethyl iodide reaction there is a concomitant increase in the iodine concentration and these data do not indicate any simple dependency of the rate on the iodine concentration.

There appears to be no accepted convention for rate constant units for reactions of this type. Seeking logical units that have numerical values neither very large nor very small we find from estimation of the energy absorbed in the system that the rate constant for this reaction between iodine and carbon tetrachloride may be quoted as 0.18 ml/cal.

The radiation resistance of carbon disulfide has been noted before.[1] The apparent lack of any chemical reaction in this case suggests the use of carbon bisulfide as a radiation resistant solvent for radiation chemical studies.

The results of more detailed studies in the systems I_2-cyclohexane, and I_2-ethyl iodide will be reported later. The authors gratefully acknowledge support by the U. S. Atomic Energy Commission, Contract No. (40-1)-1444.

TABLE I.

Reaction	Data symbol	I_2 conc. mg/ml	I^{131} activity mc/ml	Reaction rates f_a/f_r	Reaction rates mg I_2 / mc decay
CCL_4 I	⊖	0.91	1.53	0.091	0.054
CCl_4 II	⊕	0.167	1.36	0.076	0.0095
CCl_4 III	○	0.223	0.60	0.037	0.0137
C_6H_{12} I	◐	0.085	0.38	0.224	0.050
C_6H_{12} II	●	0.0194	0.31	0.63	0.040
EtI I	⊗	0.082	0.229	0.127	0.046
EtI II	◎	0.124	1.38	0.295	0.0268
CS_2	⊙	0.25	3.0	0	0

[1] Provost-Barnas, Chapiro, Cousin, Landler, and Magat, Disc. Faraday Soc. No. 12 (1952).

Hydrogen Peroxide Photocatalyzed Reaction of Hydrogen and Oxygen

DAVID H. VOLMAN
Department of Chemistry, University of California, Davis, California
(Received October 17, 1955)

THE products of the photochemical reaction of oxygen and hydrogen at 1849 A are ozone, hydrogen peroxide, and water. In a recent paper[1] it was postulated that thermal chains could not account for the high yields of water at room temperature, and that the yields could be explained by a photocatalyzed reaction of hydrogen and oxygen in the presence of the product hydrogen peroxide. The mechanism proposed was:

$$H_2O+h\nu\rightarrow 2OH \quad (1)$$

$$OH+H_2\rightarrow H_2O+H \quad (2)$$

$$H+O_2+M\rightarrow HO_2+M \quad (3)$$

$$HO_2+HO_2\rightarrow H_2O_2+O_2. \quad (4)$$

The net reaction is then solely the formation of water from hydrogen and oxygen.

To test this proposal, photochemical flow experiments were carried out in a manner described previously.[2] Gaseous mixtures were passed through a Vycor reaction vessel transparent to the 2537 A radiation but not to the 1849 A radiation of a mercury-rare gas discharge. Absorption of light was thus limited to hydrogen peroxide. The results are shown in the table for a mixture of H_2O_2, O_2 and N_2 and for a mixture of H_2O_2, O_2, and H_2. The pressure of H_2O_2 was 0.5 mm while the other gases were each 0.5 atmos.

Mixture	Moles $min^{-1} \times 10^6$ H_2O_2 decomposed	H_2O formed
H_2O_2, O_2, N_2	2.8	2.8
H_2O_2, O_2, N_2	0.4	3.6

In the absence of hydrogen, the mechanism for the photodecomposition of hydrogen peroxide[3] is (1) followed by

$$OH+H_2O_2\rightarrow H_2O+HO_2 \quad (5)$$

and reaction (4). Thus except for OH radicals which may be removed by

$$OH+OH\rightarrow H_2O_2 \quad (6)$$

each OH formed yields a water molecule. The discrepancy in the water formed in the two mixtures may be accounted for by (6) occurring in the absence of hydrogen and also by the somewhat greater total light absorbed in the presence of hydrogen since the peroxide concentration changes only slightly whereas the change in concentration in the absence of hydrogen was appreciable.

Photodecomposition of a mixture of H_2O_2, 0.5 mm, and N_2, 1 atmos, in a quartz reaction tube so that 1849 A radiation was not excluded yielded a decomposition rate about 3 times that at 2537 A and about equivalent to the rate of ozone production in a mixture of O_2, 0.5 atmos, and N_2, 0.5 atmos. Thus the absorption of 1839 A light is about the same for H_2O_2 at 0.5 mm as for O_2 at 0.5 atmos. This result is to be expected from the absorption coefficients reported for H_2O_2[4] and for O_2.[5]

The photocatalytic formation of water can, therefore, explain not only the results at 1849 A for the O_2-H_2 reaction but may also account for the high yields of water obtained at 1720 A in earlier studies.[6]

The author wishes to thank the Institute of Geophysics of the University of California for financial assistance.

[1] D. H. Volman, J. Chem. Phys. (to be published).
[2] D. H. Volman, J. Am. Chem. Soc. **73**, 1018 (1951).
[3] D. H. Volman, J. Chem. Phys. **17**, 947 (1949).
[4] Holt, McLane, and Oldenberg, J. Chem. Phys. **16**, 225 (1948).
[5] Watanabe, Inn, and Zelikoff, J. Chem. Phys. **21**, 1026 (1953).
[6] H. A. Smith and N. Naprovnik, J. Am. Chem. Soc. **62**, 385 (1940).

Single Crystals of the Oxides of the Transition Elements by the Flame Fusion Method

E. J. Scott
U. S. Naval Ordnance Laboratory, White Oak, Maryland
(Received October 12, 1955)

CURRENT interest in certain nonmetallic ferrimagnetic and antiferromagnetic compounds has created a need for the preparation of single crystal specimens.

The success of the flame fusion method[1] depends primarily upon the preparation of suitable feed powders in which the oxides are obtained as fluffy powders characterized by a loose metastable crystal structure. Such powders were prepared by calcining the co-crystallized alums of the metals[2] in zirconia boats at temperatures around 1000°C.

Single crystals were grown in boules obtained by fusing the powders in the oxy-hydrogen flame of a tri-cone burner. This differs from the conventional Verneuil arrangement in that it utilizes small orifices with high gas velocities to produce a very sharp directionalized flame; the surrounding refractory brick wall has but very slight influence on the temperature of the boule. The sharp flame limits the diameter of the boules to about 8 mm. The lengths varied from 2 to 5 cm. The temperature of the molten top of the boule was monitored by means of a Leeds and Northrup optical pyrometer of the disappearing-filament type. The readings were of brightness temperature and not true temperature.

The single crystals which I have grown by this method are listed in Table I. They include the single oxides, binary systems of the divalent metal oxides, ferrites, and aluminates. The starting composition listed indicates the ratio of the metal atoms in the co-crystallize alums. Nickel, cobalt, and manganese were divalent; iron, chromium, and aluminum were trivalent. The singleness of crystal orientation was checked by back reflection Laue x-ray photographs and, where possible, by cleavage. The structure was determined by x-ray powder methods using pulverized portions of the crystal.

With the exception of aluminum oxide, all of the specimens showed deviations from the stoichiometry of the perfect crystal structures. For example, cobalt oxide had the stoichiometry of $Co_{0.9}O$. These deviations correspond to vacant sites in the metal sublattices. The structure and defects of the crystals of these oxides may be understood in terms of variations in the divalent metal sublattice of the perfect rocksalt structure.[3]

TABLE I. Single crystals by flame fusion.

Starting composition	Crystal structure	Chemical designation
Ni	rocksalt	nickel(ous) oxide
7 Ni, 1 Co through 1 Ni, 7 Co	rocksalt	nickel(ous)-cobalt(ous) oxide
Co	rocksalt	cobalt(ous) oxide
6 Co, 1 Mn through 1 Co, 2 Mn	rocksalt	cobalt(ous)-manganous oxide
Mn	hausmannite	manganous-manganic oxide (manganese manganite)
1 Ni, 1 Mn through 6 Ni, 1 Mn	rocksalt	nickel(ous)-manganous oxide
Fe	spinel	ferrous-ferric oxide (ferrous ferrite or magnetite)
1 Ni, 2 Fe	spinel	nickel ferrite
1 Co, 2 Fe	spinel	cobalt ferrite
1 Mn, 2 Fe	spinel	manganese ferrite
3 Fe, 1 Al	spinel	ferrous ferrite-aluminate
1 Ni, 2 Al	spinel	nickel aluminate
1 Co, 2 Al	spinel	cobalt aluminate
1 Mn, 2 Al	spinel	manganese aluminate
Al	corundum	aluminum oxide
Cr	corundum	chromium sesquioxide

The attempts to grow single crystals of the chromites of nickel, cobalt, manganese, and iron have been unsuccessful. The difficulty seems to lie in the inability to prepare suitable powders.

Measurements of the magnetic susceptibility and microwave resonance absorption of the chromium sesquioxide (Cr_2O_3) single crystal have already been reported.[4]

[1] A. Verneuil, Compt. rend. **135**, 791 (1902).
[2] Crystallized nickel ammonium sulfate, ferric ammonium sulfate, etc., each with numerous waters of crystallization.
[3] A. F. Wells, *Structural Inorganic Chemistry* (Oxford University Press, London, 1950), p. 381.
[4] McGuire, Scott, and Grannis, Phys. Rev. **98**, 1562 (1955).

Effect of Sorbed Water Vapor upon the Electrical Conductivity of Conditioned Chromium Films

Jerrold M. Seehof and Hans J. Trurnit*
Physicochemical Branch, Toxicology Division, Medical Laboratories, Army Chemical Center, Maryland
(Received September 19, 1955)

PREVIOUS investigations[1,2] indicate that the sorption of gases upon thin metallic films is irreversible for pressures above 10^{-4} mm Hg and causes of decrease in resistance of the film. It was felt that a film with resistivity sensitive to sorbed gases and having reversible properties with respect to them might be of great utility as a detection instrument.

Because of high stability and ease of film preparation, chromium was chosen as the basic material. The chromium was vacuum evaporated upon clean glass microscope slides which were placed metal downwards upon a pair of parallel troughs filled with mercury. The resistance was measured between these troughs with a high precision Wheatstone bridge. The amount of metal deposited varied from 0.002 to 0.05 mg Cr/cm² slide surface and all slides were found to have negative temperature coefficients of resistance. Resistances measured between the troughs (50 mm), for a slide 25 mm in width, varied from 10 megohms to 80 ohms. Resistances were found to increase irreversibly upon exposure to air or water vapor for periods of over a week even when the air had been initially evacuated from the system to speed up diffusion of water vapor.

To eliminate the slow irreversible increase in resistance due to water vapor, and possibly air, a slide of thickness 0.0045 mg Cr/cm² was placed for two hours in boiling distilled water. Upon removal and drying, it was found to reach resistance equilibrium

in vacuum within one hour. This equilibration time is attributed to the slide slowly settling upon the mercury in the troughs. The resistance *in vacuo* of the slide was 190 000 ohms and the *increase* in resistance after the admission of water vapor was 1.4% at 6 mm, 2.0% at 12 mm, and 3.0% at 18 mm Hg. This equilibrium was established within five minutes and consisted of a rapid rise during the first twenty seconds (physical adsorption) followed by a slow rise during the subsequent period (probably dissipation of heat of sorption). This process is completely reversible as demonstrated by repeated cycles of adsorption-desorption with identical results. No effect upon resistance is obtained by admitting one atmosphere of *dry* air.

Work is in progress with other gases and other methods of film conditioning and a complete discussion of results will soon be published elsewhere.

* With the technical assistance of Willie Mae Lawson.
[1] N. Mostevetch, Compt. rend. **228**, 1702 (1949).
[2] N. Mostevich, Ann. phys. **8**, 61 (1953).

Role of Water in Oxidation-Reduction Reactions

W. L. Reynolds and R. W. Lumry*
Department of Chemistry, University of Minnesota, Minneapolis, Minnesota
(Received October 11, 1955)

ELECTRONS may move between reactants in redox reactions through strong chemical bonds, by quantum-mechanical leakage through potential barriers between oxidant and reductant in the transition state,[1] or they may be ferried between reactants as part of other atoms or ions which may be present. In the case of the oxidations of ferrous ion in aqueous solution the evidence presented in Table I indicates that the reactants do not approach closely

Table I.

Reaction	ΔH^* kcal	ΔS^* cal/deg	ΔF^* kcal
$Fe^{++}+Fe^{+++}$	9.9	−25	17
$Fe^{++}+FeCl^{++}$	8.8	−24	16
$Fe^{++}+FeCl_2^{+}$	10	−20	16
$Fe^{++}+FeF^{++}$	9.1	−21	15
$Fe^{++}+FeF_2^{+}$	9.5	−22	16
$Fe^{++}+Fe(OH)^{++}$	7.4	−20	13
$Fe^{++}+Ce(IV)$	7.0	−22	14
$Fe^{++}+H_2O_2$[a]	10	−15	15
$Fe^{++}+(CH_3)_3COOH$	9.2	−22	16
$Fe^{++}+p$-$CH_3C_6H_{10}C(CH_3)_2OOH$[a]	7.7	−27	16
$Fe^{++}+C_6H_5C(CH_3)_2OOH$ (in H_2O)[a]	9.97	−18.4	15.8
(in D_2O)	10.8	−17.6	16.0
$Fe^{++}+S_2O_8^{=}$	12	−8.3	15
$FeY^{-}+C_6H_5C(CH_3)_2OOH$[b]	10	−10	13
$Fe(OH)Y^{-3}+C_6H_5C(CH_3)_2OOH$	10	−10	13
$Fe(OH)_2Y^{-4}+C_6H_5C(CH_3)_2OOH$	10	−10	13
$Fe(II)P+C_6H_5C(CH_3)_2OOH$ (pH 4.8)[c]	8.2	−21	14
(pH 6.8)	8.9	−16	14
(pH 8.8)	8.4	−17	13
$Ce(III)+Ce(IV)$	7.7	−25	15
$V(OH)^{++}+VO^{++}$	11	−24	18

[a] These values measured in this laboratory. Other slightly different values exist in the literature.
[b] Y denotes the ethylenediaminetetraacetate ion.
[c] Fe(II)P denotes the ferrous pyrophosphate complex.

since the activation energies for hydroperoxide oxidants and for charged oxidants differ but slightly. Thus, if we may assume, as seems probable, that the slow steps to which the activation quantities of Table I apply are those for the actual electron transfer step, then electrostatic interaction plays no important part. On the basis of the requirements for the resonance condition in the electron tunnelling mechanism Platzman and Franck[2] have rejected this path for electron migration. The data of Table I are also inconsistent with such a mechanism because the wide variation expected in the energy requirements for resonance with different

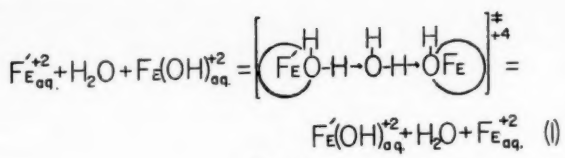

Fig. 1.

oxidants is not observed. We are thus left with some group-transfer mechanism. In particular the mechanism shown in Eqs. (1) and (2) may be suggested for ferrous-ion oxidations in aqueous solution and very likely for the other reactions of Table I since the similarity of activation parameters for all these reactions suggests a common mechanism.

Hydrogen atoms migrate by a process reminiscent of Grothus conduction down a chain of oriented water molecules to supplement the simultaneous rearrangement of electrons in the terminal reactants and thus complete the transfer step. Only inner shell water molecules are sufficiently strongly associated with reactants to exchange electrons at the bridge ends. The activation enthalpy is primarily due to stretching of O−H bonds and the apparent activation entropy arises from water orientation and electronic contributions to the transmission coefficient.

Our evidence for the postulated mechanism is fourfold. First the similarity of the activation quantities in Table I suggests that the slow steps involve the common component of these reactions, the solvent water. Second, there is a contra-indication for close approach of reactants. Only water is generally available to connect separated reactants. Third, there appears to be a requirement that at least one inner shell ligand of the reducing complex be a water molecule or one of its ions. For example, a CN^- ligand must be replaced by water in the ferrocyanide complex before ferrocyanide can be oxidized by hydroperoxides.[3] Similarly the electrolytic reduction of $Cd(CN)_4^{-2}$ proceeds through the aquotricyano complex rather than directly.[4] Fourth, on replacing H_2O by D_2O we observed an increase in $\Delta H^{\ddagger}$ of 0.8 kcal for hydroperoxide oxidation of aquo ferrous ion. The presence of the isotope effect suggests the participation of a bond containing hydrogen in the rate-determining step and the magnitude of the effect appears to be consistent with the above proposed mechanism.

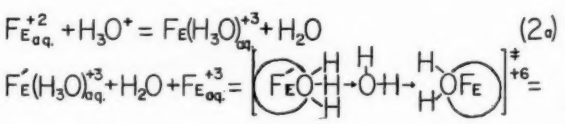

Fig. 2.

The particular sequences of steps chosen in the diagrams above have been selected on the basis of the principle of detailed balancing. In particular the exchange between aquo ferrous and aquo ferric ions, neither containing an ion of water in the inner hydration shell, should be a very poor reaction. This prediction is consistent with the published data.

The proposed mechanism would appear to have some importance for electrode reactions and biological redox reactions such as the transfer of electrons from cytochrome to cytochrome in oxidative metabolism as well as for reactions of the type exemplified in Table I.

* Presented at the 128th meeting of the American Chemical Society at Minneapolis, Minnesota. This work was in part supported by a grant from the National Science Foundation.
[1] Marcus, Zwolinski, and Eyring, J. Phys. Chem. **58**, 432 (1954).
[2] R. Platzman and J. Franck, Z. Physik **138**, 411 (1954).
[3] B. B. Lal, Proc. Indian Acad. Sci. **38A**, 522 (1953); W. L. Reynolds, thesis, University of Minnesota.
[4] H. Gerischer, Z. physik. Chem. **2**, 79 (1954).

Hydrogen-Bromine Reaction in a Nonsteady State*

DOYLE BRITTON AND NORMAN DAVIDSON
Gates and Crellin Laboratories of Chemistry, California Institute of Technology, Pasadena, California
(Received September 27, 1955)

THE elementary steps in the hydrogen-bromine reaction are:

$$\begin{array}{lll} & \rightarrow & \leftarrow \\ M+Br_2 \rightleftarrows M+Br+Br & (1) & (2) \\ & \rightarrow & \leftarrow \\ Br+H_2 \rightleftarrows HBr+H & (3) & (4) \\ & \rightarrow & \leftarrow \\ H+Br_2 \rightleftarrows HBr+Br & (5) & (6) \end{array}$$

In the classical investigations[1,2] of the slow thermal reaction at 500°K, a steady-state concentration of bromine atoms is maintained according to reactions (1) and (2). We have made a preliminary investigation of the hydrogen-bromine reaction when a shock wave is used to rapidly heat an argon-hydrogen-bromine mixture to temperatures of 1000–1500°K. Under these circumstances, a steady-state concentration of bromine atoms is not established. Reaction (3) proceeds at an increasing rate as bromine atoms are created by reaction (1); the rate of (2) is negligible. In both kinds of experiments, (5) is fast compared to (3) and (6) is unimportant.

The shock tube and experimental technique have been described.[3] Table I presents the results of the two best experiments

TABLE I.

			k_2 from 1% H_2, 1% Br_2, 98% A			
Expt.	T°K	t μsec	$\left(\frac{d(Br_2)}{dt}\right)_1$ mole liter^{-1} sec^{-1}	$\left(\frac{d(Br_2)}{dt}\right)_3$ mole liter^{-1} sec^{-1}	k_2 exp liter mole^{-1} sec$^{-1}\times10^{-8}$	k_3 calc
1	1396	40	0.144	0.164	0.89	2.0
		100	0.122	0.228	1.03	
2	1441	40	0.202	0.205	0.91	2.4
		100	0.153	0.366	0.79	

in 98% A, 1% H_2, 1% Br_2. The data have been analyzed numerically by computing the bromine atom concentration at time t expected from reaction (1) using our direct measurements of the rate of (1).[4] From the observed values of $-d(Br_2)/dt$, we subtract the computed contribution due to reaction (1), $(d(Br_2)/dt)_1$, and assert that the difference, $(d(Br_2)/dt)_3$, is due to the contribution of the chain cycle (3) and (5). The experimental values of k_3 are computed from $(-d(Br_2)/dt)_3 = k_3 \exp(Br)(H_2)$. It is compared to the values from the equation,

$$k_{3\text{calc}} = 4.56\times10^9 T^{\frac{1}{2}} \exp(-18\,780/rT) \qquad (7)$$

derived from the experimental data at 500–600° K.[2]

Photoelectric observations were made at $\lambda = 487$ mμ where the extinction coefficients of Br_2 are approximately independent of temperature.[5] Temperature changes due to the heats of reaction were small because of compensating contributions from endothermic (1) and exothermic (3) plus (5). Bromine concentrations in the unshocked gas for all experiments were *ca* 6×10^{-5} mole liter^{-1}.

In general the experimental results for k_3 are about $\frac{1}{3}$ of $k_{3\text{calc}}$. A single experiment with 2% HBr, 1% Br_2, 1% H_2, gave $k_5/k_4 = 5-15$, in agreement with the low-temperature value of 10.

There is no reason to expect Eq. (7) to be valid for extrapolation over such a large temperature range, but we do not feel that our preliminary results are sufficiently accurate to justify its revision.

The best results for the rate of reaction (1) with $M = Br_2$ were obtained for several shocks in 80% Br_2, 20% H_2 mixtures at $T = 1500$°K. Assuming a value of k_3 of 10^8 liter mole^{-1} sec^{-1}, the data were analyzed to give $k(2)_{Br_2} = 3.4\times10^8$ and 7×10^8 liter^2 mole^{-2} sec^{-1}. The value for argon is 3.4×10^8. By direct measurement, H. B. Palmer[5] has recently obtained ratios of $k(2)_{Br_2}/k(2)_A$ of 3–3.5 at 1250°K and 2–2.5 at 1667°K. Thus the present measurements confirm Palmer's result that Br_2 is not much more effective than argon as M at high temperatures for reactions (1) and (2). The same appears to be true for iodine at high temperatures, whereas iodine is a remarkably efficient catalyst for the recombination of iodine atoms at room temperature.[6,7]

Some of the shocks in 80% Br_2, 20% H_2 mixtures at 1300–1500° were not entirely steady. It can be shown that a long run-up distance is necessary in a shock tube to obtain steady shocks in a mixture capable of exothermic reaction because the initial shock strength after the membrane bursts is less than the shock strength at the steady state. It is expected that better measurements of $k(2)_{Br_2}$ and of k_3 can be made when a longer tube is constructed.

Support by the Office of Naval Research is gratefully acknowledged.

* Contribution No. 2037.
[1] Bodenstein and Lind, Z. physik. Chem. **57**, 168 (1907).
[2] For a thorough survey, see R. N. Pease, *Equilibrium and Kinetics of Gas Reactions* (Princeton University Press, Princeton, 1942), pp. 112–121.
[3] Britton, Davidson, and Schott, Discussions, Faraday Soc. **17**, 58 (1954).
[4] D. Britton and N. Davidson, (to be published).
[5] H. P. Palmer and D. F. Hornig (private communication).
[6] Britton, Davidson, Gehman, Schott (to be published).
[7] Christie, Norrish, and Porter, Discussions Faraday Soc. **17**, 107 (1954).

Paramagnetic Resonance in Solutions of Oxidized Pyrogallol

R. H. HOSKINS AND B. R. LOY
The Dow Chemical Company, Midland, Michigan
(Received October 13, 1955)

IT is well known that pyrogallol (1-, 2-, 3-benzenetriol) is a powerful organic reducing agent and that alkaline solutions of pyrogallol readily absorb oxygen, turning a deep brown color. Little is known about the way the reaction proceeds except that it is complex and that several end products can be formed.[1]

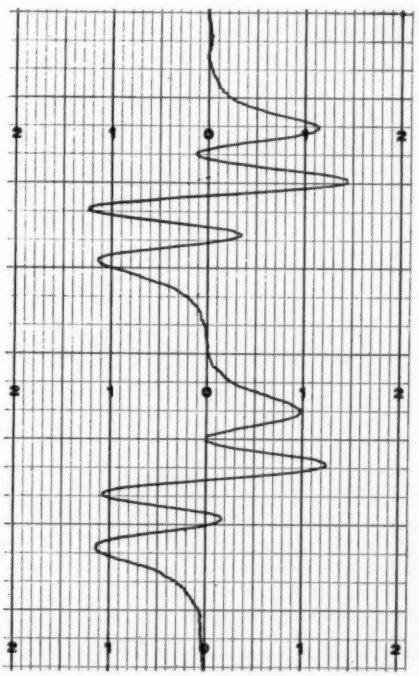

FIG. 1. Derivative of the paramagnetic resonance spectrum of an air oxidized solution of pyrogallol in alkaline alcohol at 0°C.

We have investigated by the method of paramagnetic resonance alkaline solutions of pyrogallol in both water and alcohol which had been exposed to air oxidation. The measurements were carried out at a frequency of about 9000 mc/sec at room temperature in the case of the water solution and at 0°C and −78°C in the case of the alcohol solutions. We found that a relatively stable free radical is formed as one of the oxidation steps. The lifetime of this radical increases markedly with decreasing temperature, being of the order of several minutes at room temperature and a few days at −78°C. The spectroscopic splitting factor was observed to be $g=2.005\pm0.001$.

The derivative of the absorption curve of an air oxidized solution of pyrogallol in alkaline alcohol at 0°C is shown in Fig. 1. The same structure was observed in water solution. The structure is believed to arise from hyperfine interaction of protons on the benzene ring with the unpaired electron spin. The spectrum is seen to consist of two groups of three lines each, the separation between groups amounting to 5 oersteds. The triplet structure is not resolved at −78°C. The restricted rotation of the molecules in the viscous solvent at this temperature prevents a complete averaging out of the dipolar portion of the hyperfine interaction.[2]

We propose a semiquinone type structure for the free radical. The resonance forms of this structure would then make the protons at positions 4 and 6 equivalent. The observed splitting of the line then follows from a doubling due to the proton at position 5 followed by a tripling of each of these two lines by the remaining equivalent protons at positions 4 and 6. The predicted intensity ratio would be (1,2,1), (1,2,1) which is what is observed.

[1] See, for example, Dyson, *A Manual of Organic Chemistry* (Longmans Green and Company, New York, 1950), Vol. 1, p. 326.
[2] S. I. Weissman, J. Chem. Phys. **22**, 1378 (1954).

Ion-Atom Interchange in Air

R. F. POTTER
National Bureau of Standards, Washington, D. C.
(Received October 3, 1955)

IN a recent article Bates[1] points out that ion-atom interchange could possibly play a large role in the molecular processes occurring in the ionosphere. Such a reaction

$$A^+ + BC \rightarrow AB^+ + C$$

might have a very large reaction coefficient (Bates suggests that the coefficient is of the order of 10^{-10} cm³/sec). Stevenson and Schissler observed with a mass spectrometer some reactions of this type, and reported the coefficients.[2]

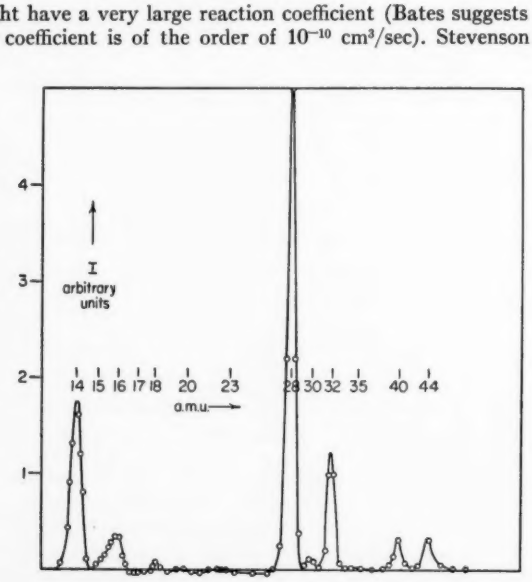

FIG. 1. Mass spectrum of laboratory air taken at a total pressure (ionization gauge) of 4×10^{-5} mm Hg. Electron energy was 50 volts, the electron current was 1.5 ma.

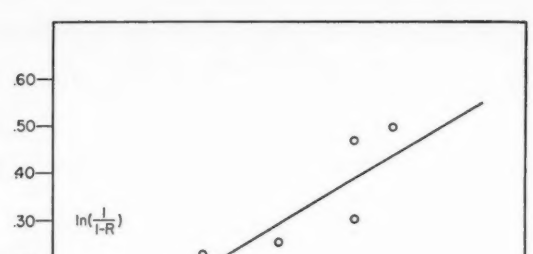

FIG. 2. Plot of experimental data from which α was estimated.

During the course of some unpublished work[3] on the development of the radio-frequency mass spectrometer,[4] an ion having a mass of 30 a.m.u. was observed in the spectrum of air (see Fig. 1). This ion does not appear in the spectra of air given by conventional spectrometers which sweep the ions into the analyzer with an applied electric field. In the light of the above-mentioned works, it is felt that this could be interpreted as being the NO^+ ion arising from the reaction

$$O^+ + N_2 \rightarrow NO^+ + N$$

taking place in the ionization chamber. An additional indication that the reaction is the one proposed, is that the appearance potential for the mass 30 ion peak was approximately the ionization potential for atomic oxygen and not that of NO. As the air was exposed to the hot filament in the spectrometer, an appreciable amount of molecular gas was dissociated.

Designating the reaction coefficient by α, and the concentration (number per cc) by n, one has

$$\frac{dn_{NO^+}}{dt}=\alpha n_{N_2} n_{O^+}$$

which can be written in terms of the ratio R of the ion currents observed:

$$R=\frac{I_{NO^+}}{I_{O^+}+I_{NO^+}}=\frac{n_{NO^+}}{n_{O^+}+n_{NO^+}}=1-e^{-\alpha n}N_2 t\sim\alpha n_{N_2} t,$$

where t will be the time duration that the O^+ ion spends in the reaction chamber, i.e., $t=s/v$, where s is the dimension of the ion chamber and v is the average velocity of the ion. An estimate of the time t is based upon the fact that the ionization takes place in an essentially field-free region with linear dimensions of approximately 3 cm and the assumption that the ion has only thermal energy corresponding to 400°K. The thermal velocity of O^+ is nearly 6×10^4 cm/sec, giving a value for t of $\sim5\times10^{-5}$ sec. (Any effects of a field present would decrease the time t.) Using this value we can calculate an α from the following expression with the partial pressure P of N_2 given in mm of Hg:

$$\alpha=\frac{7.6\times10^{-13}\ln(1/1-R)}{P}\frac{\text{cm}^3}{\text{sec}}\approx\frac{7.6\times10^{-13}R}{P}\frac{\text{cm}^3}{\text{sec}}.$$

Figure 1 is representative of the spectra used to determine R, while Fig. 2 is a plot of the several experimental points available. Using the slope of this line to evaluate α, we get

$$\alpha=(1.0\pm0.25)\times10^{-8}\text{ cm}^3/\text{sec}.$$

This reaction coefficient is two orders of magnitude larger than that suggested by Bates and approaches in value those found by Stevenson and Schissler for the reactions they studied.

Such a large reaction rate need not necessarily mean a low activation energy for the process. Glasstone, Laidler, and Eyring make a point of this fact[5] and write the specific reaction rate in the form $\alpha=(kT/h)(e^{-\Delta F^*/RT})$ where ΔF^* is the standard free energy change of the activation process at unit concentration. ΔF^* for this reaction is of the order of 38 kcal/mole or 1.6 ev/molecule.

More work of the type and quality indicated in reference 2 is desirable and necessary; however, the large coefficient estimated here gives strong support to the suggested possibility of ion-atom interchange in the ionosphere.

[1] D. R. Bates, Proc. Phys. Soc. (London) **A68**, 344 (1955).
[2] D. P. Stevenson and D. O. Schissler, J. Chem. Phys. **23**, 1353 (1955).
[3] R. F. Potter, thesis, University of Maryland (1951) (unpublished).
[4] W. H. Bennett, J. Appl. Phys. **21**, 143 (1950).
[5] Glasstone, Laidler, and Eyring, *The Theory of Rate Processes* (McGraw-Hill Book Company, Inc., New York, 1941).

Vibrational Assignment for Sodium Acetate

K. J. WILMSHURST
Chemistry Department, Auckland University College, Auckland, New Zealand
(Received October 6, 1955)

THE Raman spectrum of sodium acetate has been obtained, together with qualitative depolarization values of some of the lines, using the method of Edsall and Wilson.[1] The infrared spectrum has also been obtained from 4000–700 cm^{-1}, using a Beckman IR-2 Spectrophotometer equipped with lithium fluoride and sodium chloride prisms for their respective regions and from 700–400 cm^{-1}, using a Perkin Elmer model 21 spectrophotometer equipped with a potassium bromide prism.

Strictly, the acetate ion has only one plane of symmetry, but it has been shown[2] that if the force constants relating to interactions between the methyl and carboxyl groups are ignored, the secular equation can be factorized as if the molecule possessed symmetry C_{2v}, when assignments can be made as follows:

	CH_3 sym. stretch	2941	2933
	CO_2^- sym. stretch	1422	1408
A_1	CH_3 sym. bend	1341	1425
	C−C stretch	923	924
	CO_2^- sym. bend	651	645
A_2	Torsion about C−C	...	...
	CH_3 unsym. stretch	3006	2999
	CO_2 unsym. stretch	1575	1578
B_1	CH_3 unsym. bend	1407	1440
	CH_3 rocking	1014	1012
	CO_2^- rocking	463	465
	CH_3 unsym. stretch	3006	2999
	CH_3 unsym. bend	1438	1488
B_2	CH_3 rocking	1040	1045
	CO_2 rocking	620	615

These assignments are, for the most part, identical with those of Jones and McLaren,[3] which are given in column 2 for comparison, the only major differences occurring in the 1300–1500 cm^{-1} region.

A medium strength, polarized band at 1348 cm^{-1} in the Raman, 1341 cm^{-1} in the infrared, was assigned to the CH_3 symmetrical bending mode, on analogy with methyl chloride,[4] while of the three bands around 1420 cm^{-1} in the infrared, the strongest at 1422 cm^{-1} is assigned to the C−O symmetrical stretching. These three bands occur as one strong partly polarized band at 1416 cm^{-1} in the Raman. The other two bands in this region, at 1407 and 1438 cm^{-1}, are assigned to the B_1 and B_2 CH_3 unsymmetrical bending modes, respectively. All the class A_1 vibrations occurred in the Raman as polarized lines, thus confirming these assignments.

From consideration of the methyl halides,[5] it can be seen that of the frequencies due to the methyl group, those corresponding to the rocking and symmetrical bending modes are the most affected by the halide atom and it is interesting to compare them with the corresponding frequencies in sodium acetate and nitromethane.

	CH_3F	CH_3NO_2[6]	$CH_3CO_2^-$	CH_3Cl
		1097	1014	
CH_3 rocking	1196			1015
		1153	1046	
CH_3 sym. bend	1475	1413	1341	1355

The CH_3 rocking frequencies in sodium acetate, have decreased to a value comparable with methyl chloride and on the assignment presented here, the CH_3 symmetrical bending frequency has also decreased to a value again comparable with that in methyl chloride, while on Jones and McLaren's assignment, it would have increased beyond that in nitromethane.

This is good confirmation of the present assignment and is in further agreement with the decrease in the contribution that the structure

$$H^+CH_2=C\begin{matrix}O-\\O-\end{matrix}$$

would make to the resonance hybrid of sodium acetate, as compared to the greater contribution of a similar structure in nitromethane.

Of the other bands around 1400 cm^{-1}, the assignment as suggested here is to be preferred to that of Jones and McLaren, since as the 1341 cm^{-1} band has now been assigned to the CH_3 symmetrical bending mode, one of their bands around 1400 cm^{-1} must then be a combination band. The only combination falling in this region is 1012+465=1477, indicating that their 1488 cm^{-1} band is probably due to this combination. Thus, assuming a reasonable splitting of the B_1 and B_2 CH_3 unsymmetrical bending modes, the assignment as presented here is obtained.

I wish to acknowledge the University of New Zealand for a Research Fund Fellowship, the University Grants Committee for a grant to build a Raman light source, the Dominion Physical Laboratory for the loan of a Hilger constant deviation spectrograph, and the Dominion Laboratory for the use of their Perkin Elmer model 21 spectrophotometer. I also wish to thank Dr. H. Bloom of this department for his very kind assistance.

[1] J. T. Edsall and E. B. Wilson, Jr., J. Chem. Phys. **6**, 124 (1938).
[2] B. L. Crawford Jr., and E. B. Wilson Jr., J. Chem. Phys. **9**, 323 (1941).
[3] L. H. Jones and E. McLaren, J. Chem. Phys. **22**, 1796 (1954).
[4] G. Herzberg, *Molecular Spectra and Molecular Structure* (D. Van Nostrand Company, Inc., New York, 1945), Vol. 2, p. 313, Table 84.
[5] See reference 4, p. 315, Table 85.
[6] A. J. Wells and E. B. Wilson Jr., J. Chem. Phys. **9**, 314 (1941).

Ionization and Dissociation Processes in the Vapors of Lithium Chloride, Sodium Chloride, and Potassium Chloride

ROBERT M. HOBSON*
Department of Physics, Queen's University, Belfast, Northern Ireland
(Received August 29, 1955)

POSITIVE and negative atomic and molecular ions resulting from electron bombardment of lithium chloride vapor have been analyzed in a 180° mass spectrometer. Some preliminary results have also been obtained in the case of sodium chloride and potassium chloride vapors. The main ions detected (see Table I) are not inconsistent with those reported by Dukelsky, Zandberg, and Ionov[1] and by Friedman.[2]

Molecular ions of lower mass numbers showed a striking peak structure with peak heights in the ratio of the different combinations of the isotopes of lithium and chlorine. $Li_2Cl_2^+$, $Li_2Cl_3^-$, and

TABLE I.

Lithium chloride				Sodium chloride		Potassium chloride	
Positive ions		Negative ions		Negative ions		Negative ions	
m/e	Ion	m/e	Ion	m/e	Ion	m/e	Ion
6	$^6Li^+$	6	$^6Li^-$	23	$^{23}Na^-$	35	$^{35}Cl^-$
7	$^7Li^+$	7	$^7Li^-$	35	$^{35}Cl^-$	37	$^{37}Cl^-$
35	$^{35}Cl^+$	35	$^{35}Cl^-$	37	$^{37}Cl^-$	39	$^{39}K^-$
37	$^{37}Cl^+$	37	$^{37}Cl^-$	58	$^{23}Na\ ^{35}Cl^-$	41	$^{41}K^-$
41	$^6Li\ ^{35}Cl^+$	41	$^6Li\ ^{35}Cl^-$	60	$^{23}Na\ ^{37}Cl^-$	74	$^{39}K\ ^{35}Cl^-$
42	$^7Li\ ^{35}Cl^+$	42	$^7Li\ ^{35}Cl^-$	81	$^{23}Na_2\ ^{35}Cl^-$	76	$^{39}K\ ^{37}Cl^-$
43	$^6Li\ ^{37}Cl^+$	43	$^6Li\ ^{37}Cl^-$	83	$^{23}Na_2\ ^{37}Cl^-$	76	$^{41}K\ ^{35}Cl^-$
44	$^7Li\ ^{37}Cl^+$	44	$^7Li\ ^{37}Cl^-$	93	$^{23}Na\ ^{35}Cl_2^-$	78	$^{41}K\ ^{35}Cl^-$
47	$^6Li_2\ ^{35}Cl^+$	47	$^6Li_2\ ^{35}Cl^-$	95	$^{23}Na\ ^{35}Cl\ ^{37}Cl^-$	108	KCl_2^-[a] and
48	$^6Li\ ^7Li\ ^{35}Cl^+$	48	$^6Li\ ^7Li\ ^{35}Cl^-$	97	$^{23}Na\ ^{37}Cl_2^-$	115	K_2Cl^-[a]
49	$^7Li_2\ ^{35}Cl^+$	49	$^7Li_2\ ^{35}Cl^-$				
49	$^6Li_2\ ^{37}Cl^+$	49	$^6Li_2\ ^{37}Cl^-$				
50	$^6Li\ ^7Li\ ^{37}Cl^+$	50	$^6Li\ ^7Li\ ^{37}Cl^-$				
51	$^7Li_2\ ^{37}Cl^+$	51	$^7Li_2\ ^{37}Cl^-$				
91	$^7Li_3\ ^{35}Cl_2^+$[a]	70	$^{35}Cl_2^-$				
93	$^7Li_3\ ^{35}Cl\ ^{37}Cl^+$[a]	72	$^{35}Cl\ ^{37}Cl^-$				
		74	$^{37}Cl_2^-$				
		76	$^6Li\ ^{35}Cl_2^-$				
		77	$^7Li\ ^{35}Cl_2^-$				
		78	$^6Li\ ^{35}Cl\ ^{37}Cl^-$				
		79	$^7Li\ ^{35}Cl\ ^{37}Cl^-$				
		80	$^6Li\ ^{37}Cl_2^-$				
		81	$^7Li\ ^{37}Cl_2^-$				
		119	$Li_2\ Cl_3^-$[a]				
		160	$Li_2\ Cl_4^-$[a]				

[a] Tentative identification of incompletely resolved peak groups.

$Li_3Cl_4^-$ possessed an over-all peak shape consistent with this identification, but experimental conditions did not enable the detection of fine structure apparent in the other cases. No peaks that could be associated with $LiCl_2^+$ were detected under any operating conditions.

Retarding potential runs on the more abundant positive and negative ions indicated that these ions were formed with no measurable initial kinetic energy, and after magnetic analysis possessed energy consistent with that which they would be expected to have acquired during acceleration in the applied accelerating electric fields. This evidence, considered together with the fact that no ions were detected at nonintegral mass numbers, indicates that the complex molecular ions here considered are stable under the normal operating conditions of a mass spectrometer.

In the case of the more prominent peaks in the mass spectra, measurements were carried out on the variation of the ion current to the collector as the bombarding electron energy was altered in the range 0 to 40 ev. These measurements indicate that the complex positive and negative ions detected may be formed by a clustering process in which a diatomic LiCl molecule is in the first instance associated with an atomic ion, and then at a later state a further diatomic molecule clusters on the molecular ion. In the negative ion case this may be represented by

$$\mathrm{Li\,Cl}+e \longrightarrow \mathrm{Li\,Cl}^-,$$

$$\mathrm{Li\,Cl}+e \longrightarrow \mathrm{Li}^-+\mathrm{Cl},$$

$$\mathrm{Li}^-+\mathrm{Li\,Cl} \xrightarrow[\text{cluster}]{} \mathrm{Li_2\,Cl}^-,$$

$$\mathrm{Cl}^-+\mathrm{Li\,Cl} \xrightarrow[\text{cluster}]{} \mathrm{Li\,Cl_2}^-.$$

This is consistent with the tentative mechanism proposed by Dukelsky *et al.* However this simple clustering process does not explain all the features of the curves obtained, and in the case of $Li\,Cl_2^-$ part of the curve may be associated with a process of the type $Li\,Cl^-+Cl \rightarrow Li\,Cl_2^-$. Furthermore, it appears likely that $Li\,Cl^-$ may be formed in an ionization process involving a neutral molecule of the type $Li_m\,Cl_n$ and this is consistent with the evidence of Kusch *et al.*[3,4] concerning the existence of polymers of diatomic molecules in sodium chloride vapor. In the case of the positive ions, the rate of ionization curves are in general of the type that might well be expected of the processes

$$\mathrm{Li\,Cl}+e \longrightarrow \mathrm{Li}^++\mathrm{Cl}+2e,$$

$$\mathrm{Li\,Cl}+e \longrightarrow \mathrm{Li}+\mathrm{Cl}^++2e,$$

$$\mathrm{Li\,Cl}+e \longrightarrow \mathrm{Li\,Cl}^++2e,$$

$$\mathrm{Li\,Cl}+\mathrm{Li}^+ \xrightarrow[\text{cluster}]{} \mathrm{Li_2\,Cl}^+,$$

$$\mathrm{Li_2\,Cl}^++\mathrm{Li\,Cl} \xrightarrow[\text{cluster}]{} \mathrm{Li_3\,Cl_2}^+.$$

However there are indications that processes other than these may be at least partly responsible for these complex positive ions.

The curves indicated that under the source operating conditions used in these experiments the process $(Li\,Cl)_2+e \rightarrow Li\,Cl^++Li\,Cl+e$ was not responsible for the diatomic ions detected.

A more detailed account of these experiments will be published elsewhere. The author is indebted to Dr. R. H. Sloane for his unfailing interest and support in this work.

* Now Warren Research Fellow, Department of Physics, University College, London, England.

[1] Dukelsky, Zandberg, and Ionov, J. Exptl. Theoret. Phys. (U.S.S.R.) **20**, 877 (1950).
[2] L. Friedman, J. Chem. Phys. **23**, 477 (1955).
[3] Ochs, Cote, and Kusch, J. Chem. Phys. **21**, 459 (1953).
[4] P. Kusch, J. Chem. Phys. **21**, 1424 (1953).

Excluded Volume Effect on Light Scattering of the Coiled Linear Macromolecule*

ANTON PETERLIN†
Department of Chemistry, Wayne University, Detroit, Michigan
(Received October 5, 1955)

As a consequence of the excluded volume effect and the interaction between the solvent and the solute the mean square of the end-to-end distance R^2 of the free macromolecule increases more than linearly with the degree of polymerization. In many cases the relationship between R and M can be written as follows

$$R^2=K\cdot M^\alpha=K\cdot M^{1+\epsilon}=K'Z^{1+\epsilon} \tag{1}$$

with $\epsilon>0$ and Z number of independent segments. Hence, such a coil is less dense as in the case $\epsilon=0$. Consequently, for a given R, the decrease in scattered intensity with increasing angle will be less than for a coil with $\epsilon=0$. Therefore the radius determined from light scttering is too low when no correction is made for the change due to $\epsilon>0$.

Assuming that Eq. (1) applies also to the distance between any two chain elements,

$$R_{jk}^2=K'|j-k|^{1+\epsilon}=K'm^{1+\epsilon}=R_m^2=R^2(m/Z)^{1+\epsilon}, \tag{2}$$

and assuming a Gaussian distribution of the distances between the segments

$$\Phi(r_m)=(\mu_m/\pi)^{\frac{3}{2}}\exp(-\mu_m r^2) \tag{3}$$

where $\mu_m=3/2R_m^2$, the angular distribution of the scattered light is with

$$P(s)=2\int_0^1(1-x)\exp(-ux^{1+\epsilon})dx \tag{4}$$

where $x=m/Z$ and $u=k^2s^2R^2/6$. For determining R only the behavior of P for small values of s is required,

$$P(s)=1-\frac{2u}{(2+\epsilon)(3+\epsilon)}+\cdots=1-\frac{u}{3}\cdot\frac{1}{1+5\epsilon/6+\epsilon^2/6}+\cdots. \tag{5}$$

The result transforms to the well-known expression

$$P(s)+1-u/3+\cdots \tag{6}$$

for $\epsilon=0$.

Denoting by R_0 the radius determined according to Eq. (6) and by R the correcter value from Eq. (5) one has

$$R=R_0(1+5\epsilon/6+\epsilon^2/6)^{\frac{1}{2}}. \tag{7}$$

The correction factor in Eq. (7) has a value 1.10 in the case of polymethylmethacrylate (PMMA) in acetone, corresponding to $\epsilon=0.25$. That means that all radii determined from light scattering[1] have to be increased by 10%. This correction brings about a much better agreement with the radii as determined from viscosity and sedimentation[2] (Table I).

TABLE I. Radii of PMMA from light scattering and from viscosity and sedimentation ($R_{\eta s}$).

M	R_0	R	$R_{\eta s}$
$7.44\cdot10^6$	2950 A	3245 A	3307 A
4.59	2510	2761	2443
3.25	1710	1881	1968
2.02	1310	1441	1463
1.42	1050	1155	1174
1.01	850	935	950
0.525	610	671	633

Since ϵ is not known in advance, the radii must first be determined from light scattering according to Eq. (6). A plot of $\log R_0$ against $\log M$ yields the slope $(1+\epsilon)/2$ and hence the correction factor. Although Eqs. (2) and (3) contain simplifying assumptions, the resulting errors partially compensate with the result that R as obtained from Eq. (7) is closer to the true R than is R_0.

* This work was sponsored by the Office of Ordnance Research U. S. Army.

† On leave from J. Stefan Institute, Ljubljana, Yugoslavia.

[1] G. V. Schulz and G. Meyerhoff, J. Polymer Sci. **10**, 79 (1953).

[2] A. Peterlin, J. Colloid Sci. (to be published).

On the Calculation of the Characteristic Values and Vectors for Vibrational Secular Equations

TAKEHIKO SHIMANOUCHI
Chemical Laboratory, Faculty of Science, Tokyo University, Tokyo, Japan
(Received September 19, 1955)

THERE are many methods of solving the vibrational secular equation.[1] When the order n of the equation is large, however, the indirect expansion method due to the Hamilton-Cayley theorem[1] is preferable because it includes multiplications proportional to n^2 instead of n^3.

The problem in this method is how to choose the first vector $\mathbf{V}$. The author has noticed that the vector $(h_{11},h_{22},\cdots h_{nn})$ is preferable in order to obtain the characteristic values all of which have the same order of accuracy, where h_{ii} is the roughly estimated value of $a_{ii}^{-(n/2)}$, a_{ii} being the ith diagonal element of the secular matrix $\mathbf{a}$.

This method gives also a simple and accurate procedure for calculating the forms of normal modes, i.e., the characteristic vector $\mathbf{l}_\lambda$, a column of $\mathbf{L}$-matrix, which is related to a characteristic value λ. With the use of the coefficients of the characteristic equation, $c_1, c_2, \cdots c_n$, and n column vectors, $\mathbf{V}$, $\mathbf{aV}$, $\mathbf{a}^2\mathbf{V}$, $\cdots\mathbf{a}^{n-1}\mathbf{V}$, all values of which are calculated in the course of the present method, $\mathbf{l}_\lambda$ can be obtained from the formula

$$\mathbf{l}_\lambda=N_\lambda\{(\lambda^{n-1}+c_1\lambda^{n-2}+\cdots+c_{n-1})\mathbf{V}+(\lambda^{n-2}+c_1\lambda^{n-3}+\cdots+c_{n-2})\mathbf{aV}+\cdots+(\lambda+c_1)\mathbf{a}^{n-2}\mathbf{V}+\mathbf{a}^{n-1}\mathbf{V}\}$$

where N_λ is the normalization factor. The coefficients $\lambda^{n-1}+c_1\lambda^{n-2}+\cdots+c_{n-1}$ etc. are also obtained straightforwardly by the procedure which is ordinarily used in solving the algebraic equation numerically. The rows of $\mathbf{L}^{-1}$ matrix are also calculated from the n row vectors, $\mathbf{V}'$, $\mathbf{V}'\mathbf{a}$, $\mathbf{V}'^2\mathbf{a}$, $\cdots\mathbf{V}'^{n-1}\mathbf{a}$ by the same procedure.

The author wishes to express his thanks to Professor San-ichiro Mizushima for his interest in this work and to Mr. I. Nakagawa and Miss A. Yamaguchi for their kind discussion.

[1] Wilson, Decius, and Cross, *Molecular Vibrations* (McGraw-Hill Book Company, Inc., New York, 1955).

Potential Energy Surface of the System of Three Atoms

SHIN SATO
Laboratory of Physical Chemistry, Tokyo Institute of Technology, Ookayama, Meguro-ku, Tokyo, Japan
(Received October 6, 1955)

IN a previous paper[1] the present author devised and proposed a new semiempirical method (method (b)) of drawing the potential energy surface of the system of three atoms and compared it with Eyring's method[2] (method (a)). Then, as an example, the activation energy of hydrogen atom-molecule reaction was calculated. The present paper contains several other examples which will show that the new method is as useful in the calculation of the potential energy surface as method (a), though the results from the two methods differ considerably in several points of interest.

First, the activation energies of the reactions of the type $H+HX=H_2+X$, are calculated on the assumption of the linear configuration of three atoms in reacting. In this case, $\mathbf{k}$, which corresponds to the square of overlap-integral and is the only parameter in method (b),[1] is assumed as 0.18, which was adopted in calculating the activation energy of hydrogen atom-molecule reaction. The results of the calculation, together with experimental data[3] and the values estimated by method (a),[4] are shown in Table I, in which it is easily found that method (b) is preferable to method (a). If, with method (a), one wishes to obtain the more suitable values, the Coulomb fraction ρ, which is a parameter in method (a), must be varied to each reaction. Figure 1 shows the potential energy surface of the system H−H−Cl, calculated by method (b). The appearance of this diagram is kept even when F, Br, or I is put in place of Cl. But the diagram differs considerably from that of method (a). The main difference is that the so-called "basin" does not appear on the method (b) diagram. The same situation has already been found in the calculation of H_3 potential energy surface and discussed previously.

TABLE I (kcal/mole).

Reaction	Experimental	Calculated[a] Eyring ($\rho=0.14$)	Calculated[a] Present ($\mathbf{k}=0.18$)
$H+H_2\rightarrow H_2+H$	5∼7	7.9	5.4
$H+HCl\rightarrow H_2+Cl$	4.5	11.4	4.7
$H+HBr\rightarrow H_2+Br$	1.2	10.4	0.7
$H+HI\rightarrow H_2+I$	1.5	7.7	0.3
$F+H_2\rightarrow HF+H$	7.5	6.3	0.5

[a] Without allowing for the zero-point energy.

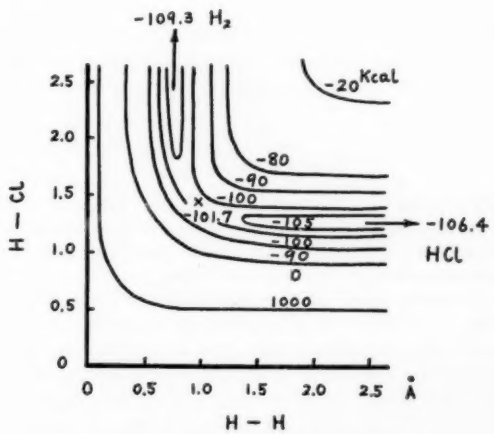

FIG. 1. Potential energy surface of H−H−Cl.

In connection with the semiempirical method, there has been an interesting discussion[4] of the problem "whether the molecules of the type X_3 exist or not?", which is not yet resolved. When using method (a) for the linear complex X_3, a deep minimum in the diagram is found, as column 2 in Table II shows. This result

TABLE II (kcal/mole).

Molecule	Eyring ($\rho=0.14$) E_m	Eyring ($\rho=0.14$) E_a	Present ($k=0.18$) E_m	Present ($k=0.18$) E_a
H_3	−1.5	10	...	5.4
F_3	−6.6	7.7	−2.0	0
Cl_3	−6.7	5.3	−2.4	0
Br_3	−5.7	3.6	−2.1	0
I_3	−4.6	2.5	−2.0	0

E_m; The potential energy at the minimum point.
E_a: The activation energy of the reaction $X+X_2\rightarrow X_2+X$, without allowing for the zero-point energy.

appears to suggest that for all the halogens the molecules of the type X_3 are stable at room temperature.[4] At the same time, the activation energies of the reactions of the type $X+X_2=X_2+X$ are found to be several kcal/mole (column 3).

On the other hand, if method (b) is used with the assumption of $k=0.18$, only a shallow "basin" is found and the so-called "saddle point" does not appear, as columns 4 and 5 show. These results suggest that the molecules X_3 do not exist* and the activation energies of the reactions $X+X_2=X_2+X$ are almost zero for all the halogens. Of course, if **k** is varied, the appearance of the surface changes somewhat and the conclusions just described will also change slightly. However, as long as method (b) is used, the so-called "basin" and "saddle point" do not appear simultaneously.

Thus, it may be concluded that, insofar as the only parameter, which is ρ in method (a) and **k** in method (b), is kept as a constant, method (b) gives more plausible results in many examples than method (a).

The author wishes to express his sincere thanks to Professor S. Shida for his interest and advice.

[1] S. Sato, J. Chem. Phys. **23**, 592 (1955).
[2] Glasstone, Laidler, and Eyring, *The Theory of Rate Processes* (McGraw-Hill Book Company, Inc., New York and London, 1941), p. 85.
[3] H. J. Schumacher, *Chemische Gasreaktionen* (Theodor Steinkopff, Dresden, 1938), p. 352; A. Farkas and L. Farkas, Proc. Roy. Soc. (London) **A152**, 124 (1935); K. H. Geib and P. Harteck, Z. physik. chem. (Bodenstein Festband) 849 (1931); M. Bodenstein and Jockusch, Z. anorg. u. allgem. Chem. **57**, 168 (1907).
[4] N. Sasaki and T. Li, *The Proceeding of Quantum Physics* (in Japanese) (Kyoritsu Book Company, Tokyo, 1944), Vol. 1, p. 560; H. Eyring and G. K. Rollefson, J. Am. Chem. Soc. **54**, 170 (1932).
* The nonexistence of the molecule I_3 is estimated experimentally in recent work [Christie, Norrish, and Porter, Proc. Roy. Soc. (London) **A216**, 161 (1953)].

Examination of the Expression, $T(dP/dT)_v+B=f(v)$, for a Number of High Purity Liquid Hydrocarbons

W. G. CUTLER,* W. WEBB, AND R. W. SCHIESSLER
The Pennsylvania State University, University Park, Pennsylvania
(Received October 3, 1955)

THE failure of the pressure coefficient, $(dP/dT)_v$, of liquids to be a function of volume alone invalidates the use of an equation of state of the Van der Waals type for liquids. A number of investigators have attempted to find a quantity that is a function of volume only. Gibson and Loeffler[1,2] have proposed the quantity $T(dP/dT)_v+B$, where B is the Tait equation[3] parameter B, and their examination of this quantity for benzene and benzene derivatives has shown it to be a function of volume alone. Eduljee, Newitt, and Weale[4] have verified that the above quantity is a function of volume only for a number of normal paraffins of low molecular weight.

TABLE VI. Values of $T(dP/dT)_v+B$ (expressed in kilobars).

Temp. (°F)	Volumes (cc/mole)				
	n-Pentadecane				
	288.9	280.4	271.9	267.6	263.4
140°		4.33	4.82		
175		4.23	4.70	4.98	5.26
210	3.80	4.33	4.75	5.00	5.25
239	3.78	4.21	4.77	4.86	5.33
Average	3.79	4.28	4.76	4.95	5.28
	n-Octadecane				
	333.4	323.2	318.1	307.9	
175	4.13	4.77	5.20		
210	4.11	4.69	5.02	5.94	
239	4.13	4.60	4.19	5.78	
Average	4.12	4.69	5.04	5.86	
	1-α-Naphthylpentadecane				
	386.1	379.3	372.6	365.8	
175		5.28	5.88	6.15	
210	5.10	5.35	5.82	6.24	
239	5.05	5.35	5.83	6.31	
Average	5.08	5.33	5.84	6.24	
	9(2-Phenylethyl)heptadecane				
	410.0	396.3	382.5	368.7	354.9
140		5.42	6.44	7.17	7.79
175	4.75	5.46	6.34	6.99	7.90
210	4.76	5.47	6.36	6.95	8.13
239	4.76	5.50	6.06	6.86	8.27
Average	4.76	5.46	6.31	6.99	8.02

Volume-pressure data to 10 kilobars for a series of structurally related hydrocarbons of high purity have been determined by the High Pressure Laboratory[5] of The Pennsylvania State University. These high purity hydrocarbons are synthetically produced by the Hydrocarbon Laboratory[5] of the Pennsylvania State University. The experimental data have been smoothed graphically and the Tait equation has been fitted to the resulting smooth curve. The values of $(dP/dT)_v$ were obtained by measuring the slopes of isochores drawn from the smooth curve volume-pressure data.

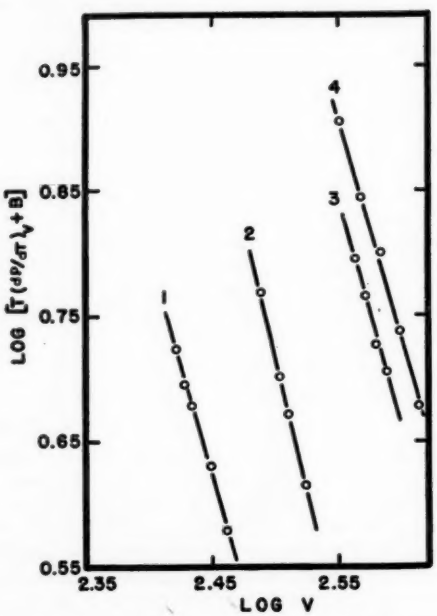

FIG. 1. Log$[T(dP/dT)_v+B]$ *versus* log$v$. Line 1: *n*-Pentadecane, Line 2: *n*-Octadecane, Line 3: 1-α-Naphthylpentadecane, Line 4: 9(2-Phenylethyl) heptadecane.

Resulting values of $T(dP/dT)_v+B$ for representative compounds and volumes are shown in Table I. Although the quantity in question is not exactly constant for a given volume the deviations are believed to be within the experimental error and the data therefore support the proposal that $T(dP/dT)_v+B$ is a function of volume only.

If one plots $\log[T(dP/dT)_v+B]$ *versus* $\log v$, straight lines are obtained. Figure 1 shows such a plot for four hydrocarbons. For the compounds examined, including normal paraffins, cycloparaffins, aromatics, and fused-ring compounds, and encompassing a molecular weight range of 170 to 351, the average value obtained for the slope was −3.89.

* Present address: Department of Physics, Mankato State Teachers College, Mankato, Minnesota.

[1] R. E. Gibson, and O. H. Loeffler, J. Am. Chem. Soc. **61**, 2515 (1939).
[2] R. E. Gibson, and O. H. Loeffler, Ann. N. Y. Acad. Sci. **51**, 727 (1948).
[3] An empirical equation for liquids proposed by P. G. Tait in 1888. This equation states: $v_0-v=C\log(1+P/B)$, where v_0 is the specific volume at atmospheric pressure, v is the volume at pressure P, and C and B are constants for a given liquid and temperature.
[4] Eduljee, Newitt, and Weale, J. Chem. Soc. (London) Part IV, 3086 (1951).
[5] Partly supported by the American Petroleum Institute and jointly known as American Petroleum Institute Research Project 42.

On the Inhibition of the NO-NO_2O_5 Reaction by NO_2†*

I. C. Hisatsune, A. P. McHale, R. E. Nightingale, D. L. Rotenberg, and Bryce Crawford, Jr.
School of Chemistry, University of Minnesota, Minneapolis 14, Minnesota
(Received October 5, 1955)

THE mechanism of Smith and Daniels[1] for the relatively fast reaction

$$NO+N_2O_5\rightarrow 3NO_2$$

has been substantiated by numerous investigators[2] in recent years. The reaction steps involved in this mechanism are

$$N_2O_5 \underset{k_2}{\overset{k_1}{\rightleftharpoons}} NO_2+NO_3$$

$$NO+NO_3 \xrightarrow{k_6} 2NO_2,$$

and the steady-state approximation leads to the rate equation

$$-d(N_2O_5)/dt=k_1(N_2O_5)[1+k_2(NO_2)/k_6(NO)]^{-1}.$$

This rate equation suggests that increasing concentration of NO_2 should inhibit the over-all reaction. While extensive work has been reported on the value of k_1, none could be found on this inhibition constant k_2/k_6. Recently, we have been able to make a quantitative estimate of this ratio and have obtained also an approximate Arrhenius activation energy associated with this ratio.

The experimental technique, which involves the use of our fast-scanning infrared spectrometer, and the method of treatment of the data have already been described elsewhere.[3] Briefly, the time variation of the concentrations of both NO_2 and N_2O_5 were followed spectroscopically. The Pyrex absorption cell into which the nitrogen-diluted reactants were expanded had silver chloride windows sealed with Halocarbon wax. The volume of the cell was approximately 162 ml. Experimentally determined concentrations of NO_2 and N_2O_5 were substituted into the integrated form of the rate equation given below.

$$y=-k'(1-3k')^{-1}w+k_1(1-3k')^{-1}$$

where

$$k'=k_2/k_6,$$
$$y=(t-t_0)^{-1}\ln[(N_2O_5)_0/(N_2O_5)]$$

and

$$w=(t-t_0)^{-1}[(NO_2)_\infty/(N_2O_5)_\infty]\ln[(NO)_0(N_2O_5)/(NO)(N_2O_5)_0].$$

The subscripts 0 and ∞ denote pressures at some initial time t_0 and at the end of the reaction, respectively. The pressure of NO was calculated from the relation

$$(NO)=(N_2O_5)-(N_2O_5)_\infty$$

since an excess of (N_2O_5) over (NO) was used in every experimental run. The average values of the calculated inhibition constants k_2/k_6 for different total pressures are given in Table I. The errors listed are computed "probably errors" with all runs weighted equally. For runs made at 22°C, the largest and the smallest value in any set of measurements differed by a factor less than approximately 3. However, in runs made at 30 and 40°C, the extreme values differed in some cases by a factor as large as 10 because of increased experimental difficulties. The Arrhenius activation energy from the results at both 400 and 57 mm total pressure was approximately 2 kcal/mole.

TABLE I. Inhibition rate constant k_2/k_6.

Total pressure (mm)	Number of runs	Temperature (°C) 22	30	40
423	3	0.098 ±0.001	...	...
400	8, 7, 10	0.088 ±0.005	0.082±0.015	0.11±0.01
286	4	0.057 ±0.003	...	...
171	4	0.047 ±0.005	...	...
57	7, 7, 10	0.0045±0.004	0.043±0.005	0.057±0.007

From our present data values of k_1 were also obtained. These were in order-of-magnitude agreement with the results of Johnston and his co-workers,[2] but in general much lower. Furthermore, the Arrhenius activation energy calculated from the temperature dependence of k_1 was found to be anomalously low. In spite of these anomalies which are yet to be cleared, we feel that the values of k_2/K_6 obtained so far are of sufficient importance to warrant this preliminary note. Work is still in progress on this reaction and complete results will be reported in the near future.

† This work was supported by the U. S. Navy, Bureau of Ordnance, through contract with the University of Minnesota.
* Presented in part at the 127th American Chemical Society meeting, Cincinnati, Ohio, April 6, 1955.
[1] J. H. Smith and F. Daniels, J. Am. Chem. Soc. **49**, 1257 (1927).
[2] R. L. Mills and H. S. Johnston, J. Am. Chem. Soc. **73**, 938 (1951); H. S. Johnston and R. L. Perrine, *ibid.* **73**, 4782 (1951); H. S. Johnston, *ibid.* **75**, 1567 (1953); D. J. Wilson and H. S. Johnston, *ibid.* **75**, 5763 (1953); R. A. Ogg, Jr., J. Chem. Phys. **18**, 572 (1950); Ogg, Richardson, and Wilson, *ibid.* **18**, 573 (1950).
[3] Cowan, Rotenberg, Downie, Crawford, and Ogg, J. Chem. Phys. **21**, 1397 (1953); Cowan, Vincent, and Crawford, J. Opt. Soc. Am. **43**, 710 (1953).

Relation of Stability Ratios to Pauling Electronegativities

R. T. Sanderson
Department of Chemistry, State University of Iowa, Iowa City, Iowa
(Received October 10, 1955)

THE relative average electronic densities of the atoms of the elements have recently been used successfully as measures of electronegativity, in a wide variety of applications.[1] The relative density has been determined as the ratio of the average electronic density of an atom to that of a hypothetical, isoelectronic inert atom, the latter value being obtained by interpolation between values for the actual inert elements. This ratio has been termed the "stability ratio" (SR).[2] The relation of stability ratios to Pauling electronegativities[3] has previously been presented graphically,[2] but the numerical dissimilarity has made difficult a precise quantitative comparison. Accordingly, a simple conversion from SR values to the arbitrary units of Pauling's electronegativity is presented here.

An empirical mathematical relationship is:

$$X^{\frac{1}{2}}=0.21\mathrm{SR}+0.77$$

where X is the Pauling electronegativity. Table I gives a comparison of the electronegativity values reported by Pauling[3] with those determined as SR values and converted to the Pauling units by means of the above equation.

TABLE I. Comparison of Pauling and Sanderson electronegativities.

Element	Pauling	Sanderson[a]	Element	Pauling	Sanderson[a]
H	2.1	2.31	Sc	1.3	1.35
Li	1.0	0.86	Ti	1.6	1.56
Be	1.5	1.37	Ge	1.7	2.31
B	2.0	1.88	As	2.0	2.53
C	2.5	2.47	Se	2.4	2.76
N	3.0	2.93	Br	2.8	2.96
O	3.5	3.46	Rb	0.8	0.77
F	4.0	3.92	Sr	1.0	1.00
Na	0.9	0.85	Y	1.3	1.30
Mg	1.2	1.21	Zr	1.6	1.56
Al	1.5	1.39	Sn	1.7	2.02
Si	1.8	1.74	Sb	1.8	2.19
P	2.1	2.16	Te	2.1	2.34
S	2.5	2.66	I	2.5	2.50
Cl	3.0	3.28	Cs	0.7	0.76
K	0.8	0.80	Ba	0.9	0.96
Ca	1.0	1.06			

[a] Calculated from SR values.

It will be observed that the only major disagreements are in the values for germanium, arsenic, antimony, and perhaps selenium. Chemical support for the newer values has previously been presented.[4] Reinforcement, for the germanium value, has been provided more recently by the work of West[5] and of Rochow and Allred.[6] In view of these arguments and of the excellent agreement for most of the other elements, there seems little reason to question the use of SR values as measures of electronegativity. Furthermore, it is evident that the fundamental ideas behind the SR values deserve very careful consideration.

[1] R. T. Sanderson, papers since 1951.
[2] R. T. Sanderson, J. Chem. Educ. **29**, 539 (1952).
[3] L. Pauling, *The Nature of the Chemical Bond* (Cornell University Press, Ithaca, New York, 1940), second edition, p. 64.
[4] R. T. Sanderson, J. Am. Chem. Soc. **74**, 4792 (1952).
[5] R. West, J. Am. Chem. Soc. **75**, 6080 (1953).
[6] E. G. Rochow and A. L. Allred, J. Am. Chem. Soc. **77**, 4489 (1955).

Ultraviolet Absorption Spectrum of Benzene in *N*-Hexane at Pressures to 6000 Bars*

W. W. ROBERTSON AND F. A. MATSEN
Departments of Physics and Chemistry, The University of Texas, Austin, Texas
(Received September 27, 1955)

A HIGH-PRESSURE system has been constructed for the purpose of observing pressures effects on absorption spectra in the visible and ultraviolet regions.[1] Pressures to 6000 bars are obtainable in an absorption cell having a path length of 1 cm. In Fig. 1 is reproduced a microphotometer tracing of the benzene spectrum in *n*-hexane at one bar and at 5500 bars. A plot of the wavelength of the 0+520 band *versus* pressure is given in Fig. 2.

The change in the spectrum on increasing pressure to 6000 bars is similar to the change obtained in going from vapor to solution with respect to the broadening, and the magnitude and the direction of the wavelength shift.

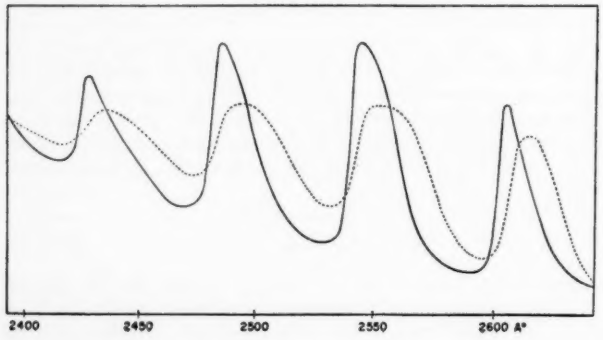

FIG. 1.

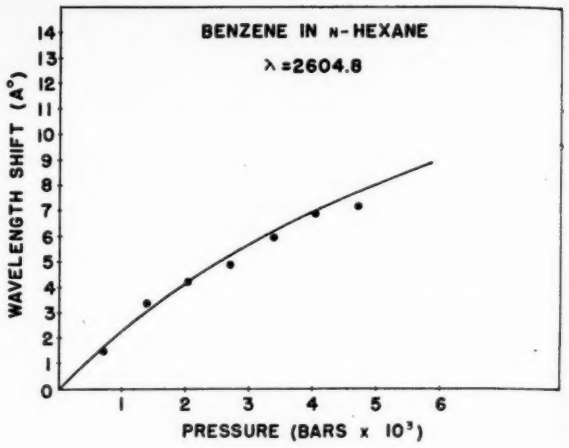

FIG. 2.

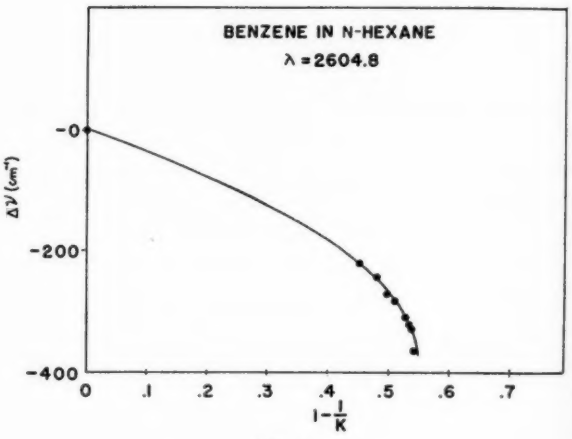

FIG. 3.

To a first approximation the increase in pressure may be regarded as affecting an increase in dielectric constant. If the excitation process is thought of as a charge separation, one may expect the Born equation to apply.[2-4]

$$\Delta = -a(1-1/K).$$

In Fig. 3, Δ is plotted against $1-1/K$.[5] The plot is not linear but it does appear to be continuous from liquid to vapor.

* This research was supported by the United States Air Force, through the Office of Scientific Research of the Air Research and Development Command.
[1] D. S. Hughes and W. W. Robertson, submitted to J. Opt. Soc. Am.
[2] S. F. Sheppard, Revs. Modern Phys. **14**, 303 (1942).
[3] A. L. LeRosen and C. A. Reid, J. Chem. Phys. **20**, 233 (1952).
[4] This is not the case for $n-\pi$ transitions, H. McConnell, J. Chem. Phys. **20**, 700 (1952) or for systems with strong solute solvent interaction.
[5] The dielectric constant as a function of pressure is for pentane and was taken from W. Danforth, Phys. Rev. **38**, 1224 (1931).

Erratum: Active Nitrogen in the Rare Gases and Its Excitation of Metal Vapors

[J. Chem. Phys. **23**, 1555 (1955)]
CARL KENTY
Lamp Division of the General Electric Company, Advanced Lamp Development Laboratory, Nela Park, Cleveland, Ohio

THE second reference 5 in the text should refer to: Yoshio Tanaka and Murray Zelikoff, J. Opt. Soc. Am. **44**, 254 (1954); Phys. Rev. **93**, 933 (1954); C. Kenty, Phys. Rev. **93**, 651 (1954).

Erratum: Solution of the Wave Equation for Internal Rotation of Two Completely Asymmetric Molecules

[J. Chem. Phys. 23, 1405 (1955)]

DONALD G. BURKHARD AND JOHN C. IRVIN
Department of Physics, University of Colorado, Boulder, Colorado

THE caption of Fig. 2 should read: $\phi=\phi_1$ for group A; $\phi=\phi_2$ for group B.

Erratum: On the Fluorescence of Self-Activated Zinc Sulfide

[J. Chem. Phys. 23, 1541 (1955)]

ARRIGO ADDAMIANO
Advanced Lamp Development Laboratory, Lamp Division, General Electric Company, Nela Park, Cleveland, Ohio

NOTE marked by asterisk (*) should read:
* To avoid oxidation! Bube fired the ZnS in air.

N. S. Khan 2445
Geraldine H. Fuller 2445
Howard B. Palmer 2449
G. J. Stone 2449
2450
2455
2456
2457
Ewald H. Velsen 2458
2459
2460
2461
2463
Robert M. Hobson 2463
2464
2465
2466
2467
2468
Carl Kenty 2468
2469

CONTENTS

Vol. 23, No. 12 December, 1955

Alfons Weber and Salvador M. Perigio 2209

Hiromu Ashio and Taizo Sasaki 2210

Solomon Zwerdling and Ralph S. Halford 2215

Solomon Zwerdling and Ralph S. Halford 2221

G. C. Hood, O. Redlich, and C. A. Reilly 2229

Daniel Kivelson 2230

Daniel Kivelson 2236

S. S. Penner and H. Aroeste 2244

J. R. White 2247

A. H. Emery, Jr., and H. G. Drickamer 2252

R. E. Skochdopole, Maurice Griffel, and F. H. Spedding 2258

Jacob Bigeleisen 2264

I. Amdur and E. A. Mason 2268

Terrell L. Hill 2270

Toyoki Koga 2275

W. E. Wallace 2281

Herman Burwasser and H. Austin Taylor 2295

Claude E. Cooke, Jr. 2299

John M. Richardson 2304

J. Ross MacDonald 2308

M. Szwarc and J. Watson Taylor 2310

F. T. Wall, L. A. Hiller, Jr., and W. F. Atchison 2314

George L. Gaines, Jr., and Henry C. Thomas 2322

Ryoichi Kikuchi 2327

D. S. Jackson and H. I. Schiff 2333

R. S. Mulliken 2338

R. S. Mulliken 2343

J. N. Murrell and H. C. Longuet-Higgins 2347

Frank O. Ellison and Harrison Shull 2348

Frank O. Ellison 2358

K. Venkateswarlu and S. Sundaram 2365

K. Venkateswarlu and S. Sundaram 2368

A. D. Buckingham 2370

S. R. Polo and M. Kent Wilson 2376

B. Widom 2377

Robert Gerson and J. H. Rohrbaugh 2381

C. S. E. Phillips 2388

Robert Ginell 2395

Marvin L. Bromberg and H. Austin Taylor 2399

Stephen Prager 2404

J. Reitsel 2407

T. A. Carlson and W. S. Koski 2410

Herbert B. Rosenstock 2415

N. J. Hawkins, H. C. Mattraw, W. W. Sabol, and D. R. Carpenter 2422

Ram Gopal and O. K. Rice 2428

Gordon F. Newell 2431

(continued on cover three)

LANCASTER PRESS, INC., LANCASTER, PA.